

A11104 589983

NIST
PUBLICATIONS

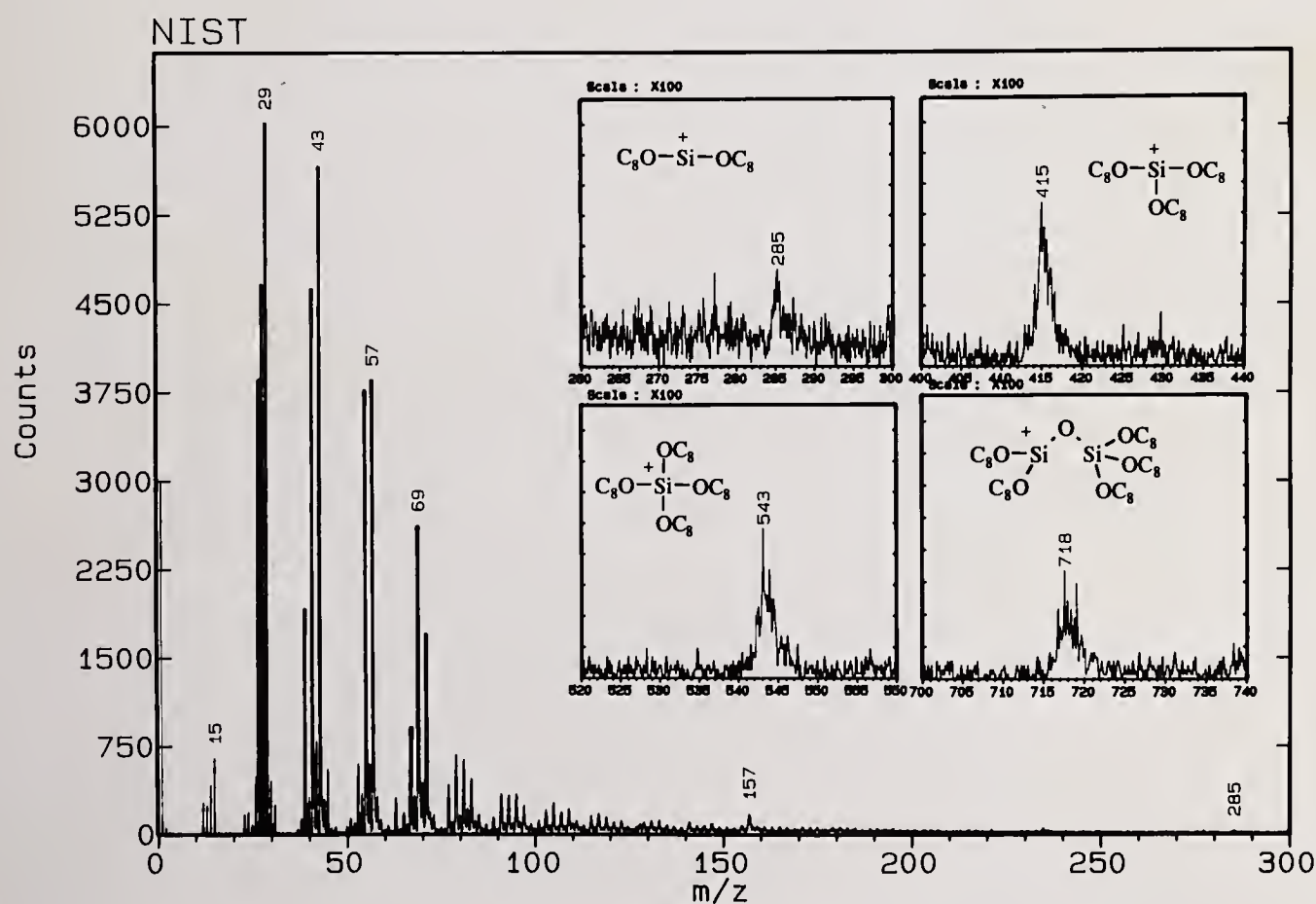
NIST

United States Department of Commerce
Technology Administration
National Institute of Standards and Technology

NIST Special Publication 876

Boundary Lubrication of Silicon Nitride

Richard S. Gates and Stephen M. Hsu



QC
100
U57
R0.876
1995

The National Institute of Standards and Technology was established in 1988 by Congress to “assist industry in the development of technology . . . needed to improve product quality, to modernize manufacturing processes, to ensure product reliability . . . and to facilitate rapid commercialization . . . of products based on new scientific discoveries.”

NIST, originally founded as the National Bureau of Standards in 1901, works to strengthen U.S. industry’s competitiveness; advance science and engineering; and improve public health, safety, and the environment. One of the agency’s basic functions is to develop, maintain, and retain custody of the national standards of measurement, and provide the means and methods for comparing standards used in science, engineering, manufacturing, commerce, industry, and education with the standards adopted or recognized by the Federal Government.

As an agency of the U.S. Commerce Department’s Technology Administration, NIST conducts basic and applied research in the physical sciences and engineering, and develops measurement techniques, test methods, standards, and related services. The Institute does generic and precompetitive work on new and advanced technologies. NIST’s research facilities are located at Gaithersburg, MD 20899, and at Boulder, CO 80303. Major technical operating units and their principal activities are listed below. For more information contact the Public Inquiries Desk, 301-975-3058.

Office of the Director

- Advanced Technology Program
- Quality Programs
- International and Academic Affairs

Technology Services

- Manufacturing Extension Partnership
- Standards Services
- Technology Commercialization
- Measurement Services
- Technology Evaluation and Assessment
- Information Services

Materials Science and Engineering Laboratory

- Intelligent Processing of Materials
- Ceramics
- Materials Reliability¹
- Polymers
- Metallurgy
- Reactor Radiation

Chemical Science and Technology Laboratory

- Biotechnology
- Chemical Kinetics and Thermodynamics
- Analytical Chemical Research
- Process Measurements²
- Surface and Microanalysis Science
- Thermophysics²

Physics Laboratory

- Electron and Optical Physics
- Atomic Physics
- Molecular Physics
- Radiometric Physics
- Quantum Metrology
- Ionizing Radiation
- Time and Frequency¹
- Quantum Physics¹

Manufacturing Engineering Laboratory

- Precision Engineering
- Automated Production Technology
- Intelligent Systems
- Manufacturing Systems Integration
- Fabrication Technology

Electronics and Electrical Engineering Laboratory

- Microelectronics
- Law Enforcement Standards
- Electricity
- Semiconductor Electronics
- Electromagnetic Fields¹
- Electromagnetic Technology¹
- Optoelectronics¹

Building and Fire Research Laboratory

- Structures
- Building Materials
- Building Environment
- Fire Safety
- Fire Science

Computer Systems Laboratory

- Office of Enterprise Integration
- Information Systems Engineering
- Systems and Software Technology
- Computer Security
- Systems and Network Architecture
- Advanced Systems

Computing and Applied Mathematics Laboratory

- Applied and Computational Mathematics²
- Statistical Engineering²
- Scientific Computing Environments²
- Computer Services
- Computer Systems and Communications²
- Information Systems

¹At Boulder, CO 80303.

²Some elements at Boulder, CO 80303.

NIST Special Publication 876

Boundary Lubrication of Silicon Nitride

Richard S. Gates
and Stephen M. Hsu

Material Science and Engineering Laboratory
National Institute of Standards and Technology
Gaithersburg, MD 20899-0001

February 1995



U.S. Department of Commerce
Ronald H. Brown, Secretary

Technology Administration
Mary L. Good, Under Secretary for Technology

National Institute of Standards and Technology
Arati Prabhakar, Director

National Institute of Standards
and Technology
Special Publication 876
Natl. Inst. Stand. Technol.
Spec. Publ. 876
387 pages (Feb. 1995)
CODEN: NSPUE2

U.S. Government Printing Office
Washington: 1995

For sale by the Superintendent
of Documents
U.S. Government Printing Office
Washington, DC 20402-9325

PREFACE

This report was born out of a cooperative program between the Chemical Engineering Department of The Pennsylvania State University and the Surface Properties Group in the Ceramics Division, Materials Science and Engineering Laboratory, NIST. The intent of the program is to assist in the education of young scientists and engineers and at the same time fulfill the mission of NIST. The program is also supported by the Department of Energy, Office of Transportation Technologies, Office of Transportation Materials through the Tribology Program. Under the program, young graduate students, after they had finished course work, come to NIST to conduct their thesis research under joint University and NIST staff supervision. While at NIST, the students are supported through the graduate cooperative program and receive regular salary for their work. At the conclusion of their research, they write the thesis and defend their work in the Department. Either an abridged or an expanded version of the thesis is published as a NIST Special Publication (SP). This is one of the reports.

This kind of cooperative program provides additional resources to the University in their training of scientists and engineers, and at the same time, provides a steady stream of high caliber young people who are interested in pursuing research to work at NIST and experience research lives first hand. NIST often not only benefits directly from the results of their labor but also gains an advantage at recruiting the best and the brightest to come to NIST.

I would like to acknowledge the efforts of Professors Larry Duda and Erwin Klaus in their tireless assistance and counseling of the students in the program, Mrs. Barbara Bush in the handling of the various administrative details at Penn State, and Carolyn Sladic and Fay Raginski here at NIST. The financial support of DOE is gratefully acknowledged.

Stephen M. Hsu
Group Leader
Surface Properties Group
Ceramics Division
Materials Sciences and Engineering Laboratory

ABSTRACT

Successful use of advanced ceramics in many tribological applications requires an understanding of the physical, chemical, and mechanical properties of the material. Physical and mechanical data are relatively abundant for most ceramics; however, information on the surface chemical interactions between ceramics and lubricants is lacking.

This report describes a systematic study to investigate the effects of selected organic chemical compounds on the friction and wear of silicon nitride under boundary lubrication conditions. A broad range of chemistries were investigated. Results are grouped according to predominant chemical compound class as oxygen, phosphorus, halogen, sulfur, and nitrogen-containing chemistries.

A Ball-on-Three-Flat (BTF) wear tester was used to evaluate many different organic compounds under boundary lubrication conditions. Tests were conducted using one weight percent of chemical compounds in paraffin oil, and the test results were compared to a base case of paraffin oil without additive. Results indicated that some compounds could provide significant improvement of friction and wear characteristics. Friction coefficients varied from + 30 % to - 45 % compared with the base case. Wear was measured as the wear increase above the elastic contact diameter (Hertzian diameter). Relative to the base case, wear changes ranged from + 61% to - 96 %. Successful wear reduction was obtained by phosphorus-containing compounds, several glycol compounds, oleic acid, sulfonates, a salicylate, an imidazoline, and a phenate and was generally associated with the formation of a film in the contact region. Additional wear tests conducted using neat compounds indicated that acids and alcohols could provide significantly better friction and wear behavior than neat paraffin oil. In the case of some short chain (C_6 - C_{10}) primary linear alcohols, very low coefficient of friction ($\mu=0.05$) and unique wear scar morphology suggested strong chemical interactions and a possible elastohydrodynamic lubrication contribution.

More in-depth study of reaction product films from alcohol-lubricated silicon nitride wear tests showed that organic compounds containing alcohol functional groups can react with the surface of silicon nitride to form high molecular weight silicon-containing organic compound films with lubricating capability. A series of static and dynamic reactions were conducted to elucidate the reaction sequence. Based on these results, a reaction mechanism is proposed in which alcohols react with the silicon nitride surface to form bonded alkoxides. Subsequent reactions in the high temperature, high shear, environment of a wearing contact result in the formation of the high molecular weight silicon alkoxide films which can lubricate.

TABLE OF CONTENTS

	Page
PREFACE	iii
ABSTRACT	v
LIST OF TABLES	xii
LIST OF FIGURES	xv
 Chapter 1. INTRODUCTION	 1
 Chapter 2. BACKGROUND AND LITERATURE SURVEY	 3
2.1. Lubrication of Materials	3
2.2. Structure of Si_3N_4	7
2.3. Properties of Si_3N_4	10
2.4. General Comparison of Wear Mechanisms of Metals vs Ceramics	12
2.5. Wear of Si_3N_4 under Unlubricated Conditions	13
2.6. Lubricated Si_3N_4 Studies	16
2.7. Technical Approach	20
2.7.1. Reactivity and Bond Strength	20
 Chapter 3. MATERIAL CHARACTERIZATION	 27
3.1. Monolithic Si_3N_4	27
3.1.1. Manufacturers Literature	28
3.1.2. Chemical Composition	29
3.1.3. X-Ray Diffraction	32
3.1.4. Raman Spectroscopy	32
3.1.5. Ceramography/Fractography	37
3.1.6. ESCA and Auger Analysis	41
3.1.7. A Surface Model for Si_3N_4	45
3.2. Si_3N_4 Powders	51

3.3.	Model Chemical Compounds	52
Chapter 4.	EXPERIMENTAL APPARATUS AND OPERATING CONDITIONS	53
4.1.	Dynamic Tests	53
4.1.1.	Wear Tester	53
4.1.2.	Specimen Preparation	58
4.1.3.	Operating Procedure	59
4.1.4.	Friction and Wear Measurement	61
4.1.5.	Selection of Wear Test Conditions	63
4.1.6.	Test Repeatability and Measurement Uncertainties	66
4.2.	Static Tests	69
4.2.1.	Batch Reactor	70
4.2.2.	Procedures	70
Chapter 5.	BASELINE WEAR STUDY	75
5.1.	Paraffin Oil Lubrication	75
5.2.	PPO Load Capacity Study	83
5.3.	Speculated PPO Lubrication Mechanism for Si_3N_4	92
5.4.	Effect of Iron Impurities	93
5.5.	Friction Trace Types Observed in this Study	94
Chapter 6.	SURVEY OF OXYGEN-CONTAINING CHEMISTRIES	99
6.1.	Wear Tests Results of 1% Oxygenates in PPO	99
6.2.	Wear Test Results of Neat Compounds	115
6.3.	Wear Tests on C_8 Compounds	120
Chapter 7.	ALCOHOL LUBRICATION	125
7.1.	Effect of Alcohol Chain Length on Wear and Friction	125
7.2.	Wedge-Shaped Feature Analysis	130
7.3.	Effect of Water on Lubrication of Si_3N_4 by Alcohols	147
7.4.	Alcohol Lubricated Micro Sample Wear Tests on Si_3N_4	148
7.5.	Analysis of Worn Si_3N_4 Specimens	149

7.5.1. FTIR Analysis of Octanol Lubrication Reaction Products	151
7.5.2. Evidence for Organo-Silicon Reaction Product Formation as Demonstrated by GPC-GFAA	153
Chapter 8. STATIC REACTION STUDY	159
8.1. TGA Analysis Method	159
8.2. Surface Reactions of Alcohols with Si_3N_4 Powder	163
8.3. Evidence of the Chemical Structure of Alcohol- Si_3N_4 Powder Reaction Products	165
8.4. Discussion on the Nature of the Alcohol- Si_3N_4 Surface Reaction	169
Chapter 9. MECHANISTIC MODEL FOR ALCOHOL LUBRICATION	177
9.1. SIMS Analysis of the 6 μl BTF Reaction Products	177
9.2. Evaluation of Lubrication Effectiveness Using the Two-Ball Collision Test	183
9.3. Tetra-Alkoxide Heating Experiments	186
9.4. Proposed Mechanism for Alcohol and Acid Lubricated Si_3N_4	188
Chapter 10. SURVEY OF PHOSPORUS CHEMISTRIES	199
10.1. 1% Compounds in PPO	199
10.2. Pure Compound BTF Tests	210
10.3. EXD Analysis of Wear Products	215
10.4. Auger Analysis of Wear Products	225
10.5. FTIR Analysis of TCP Wear Product	230
10.6. Load Capacity Plot for 1% TCP in PPO	231
10.7. Effect of [TCP] on Wear of Si_3N_4	238
10.8. Powder Adsorption Studies	240
10.9. Effect of Iron Impurities	242
10.10. Pin-On-Disc Wear Tests	243
10.11. Powder Reaction Studies	252
10.12. Proposed Reaction Mechanism between Si_3N_4 and Phosphates	253
Chapter 11. SURVEY OF HALOGEN CHEMISTRIES	263
11.1. Chlorinated Compounds	263
11.2. Chlorosilanes	268
11.3. Fluorine-Containing Compounds	276

11.4. Summary	280
Chapter 12. SURVEY OF SULFUR CHEMISTRIES	283
12.1. Sulfur Containing Compounds	286
12.2. Mo-S Containing Compounds	287
12.3. Sulfur Containing Detergent Type Compounds	291
12.3.1. Load Capacity Plot for 1% Mg Sulfonate in PPO	301
12.4. BTF Wear Tests at 200°C	301
12.5. Summary and Discussion	304
Chapter 13. SURVEY OF NITROGEN CHEMISTRIES	307
13.1. Dispersant Type Compounds	310
13.2. Imidazoline	310
Chapter 14. SUMMARY AND CONCLUSIONS	315
Chapter 15. RECOMMENDATIONS FOR FUTURE WORK	321
REFERENCES	323
APPENDIX A An Estimate of the Hertzian Contact Diameter for the Four-Ball Contact Geometry	347
APPENDIX B. An Estimate of the Hertzian Contact Diameter for the Ball-on-Three- Flat Contact Geometry	349
APPENDIX C. An Estimate of the Hertzian Contact Diameter for the Pin-on-Disk Contact Geometry	351
APPENDIX D. Silicon Nitride Flat Specimen Preparation Procedure	353
APPENDIX E. Cleaning Procedure for Si ₃ N ₄ Wear Testing	357

APPENDIX F.	Calculation of Wear Scar Depth and Wear Volumes for the BTF, POD, & Four-Ball Wear Test Geometries	359
APPENDIX G.	Description of Analytical Techniques	363
APPENDIX H.	PPO Wear Test Data on Other Si ₃ N ₄ Batches	367
APPENDIX I.	Temperature Calculations for the Ball-on-Three-Flat Contact Geometry	371
APPENDIX J.	Auger Analysis Data for Alcohol-Lubricated BTF Test Flats	373
APPENDIX K.	Hamrock and Dowson Minimum Film Thickness Calculation for BTF EHL Contacts	377
APPENDIX L.	Glossary	379

A superscript numerical format is used in this publication to denote references. The numbered references, provided after Chapter 15, are also in alphabetical order; therefore, the numbering sequence is not the sequence in which the references appear in the text.

NOTE: Certain commercial equipment, instruments, or materials are identified in this report to adequately specify the experimental procedure. Such Identification does nor imply recommendation or endorsement by the National Institute of Standards and Technology, nor does it imply that the material or equipment identified are necessarily the best available for the purpose.

LIST OF TABLES

2.1.	Lines of Defence Against Wear and Friction	6
2.2.	Wear Mechanisms for Metals and Ceramics	12
2.3.	Reference Summary for Unlubricated Si_3N_4 Wear Testing	14
2.4.	Reference Summary for Lubricated Si_3N_4 Wear Testing	18
2.5.	Reference Summary for Si_3N_4 Reactivity	22
2.6.	Bond Dissociation Energies for Selected Silicon Bonds (Source: Dean ⁶⁸) .	24
3.1.	Properties of Si_3N_4 Materials Used	29
3.2.	Manufacturers Chemical Composition Data for Typical NC132 and NBD100 Si_3N_4	30
3.3.	Neutron Activation Analysis of Si_3N_4 Samples	30
3.4.	Chemical Composition of Stark LC 12-N Si_3N_4	51
4.1.	Repeatability Data on PPO Lubricated Si_3N_4 CER024 Batch of NC132 Flats	68
5.1.	Auger Analysis of Worn Surface of PPO-Lubricated Si_3N_4 (Values are Atomic %)	80
5.2.	Characteristic Features of the Five Wear Regions for PPO-Lubricated Si_3N_4	83
6.1	Friction and Wear Data on Selected Oxygen-Containing Model Compounds	101
6.2	Summary of Neat Oxygen-Containing Compound BTF Wear Test Data . .	116
6.3	Summary of Neat C_8 Series Oxygen-Containing Compound BTF Wear Test Data	121
7.1	Summary of Neat Octylaryl Polyether-Based Alcohol BTF Wear Test Data	126
7.2	BTF Wear Test Results on Primary Linear Alcohols	126

7.3	Effect of Water on Lubrication of Si_3N_4 by Octanol	148
7.4	Comparison of 1.5 ml and 6 μl BTF Wear Test Results on Primary Alcohols	149
8.1	Solubility of Silica in Alcohols (Source: Iler ¹³⁸ p. 62)	169
9.1	SIMS Mass Spectral Data for Octanol Lubricated Si_3N_4 Wear Test Products	180
9.2	SIMS Mass Spectral Data for Decanol Lubricated Si_3N_4 Wear Test Products	182
10.1	Friction and Wear Test Data on Selected Phosphorus-Containing Model Compounds	201
10.2	Summary of 200°C BTF Data on 1% Phosphorus-Containing Compounds in PPO	208
10.3	Summary of Pure Phosphorus-Containing Compound BBTF Wear Test Data	210
10.4	EDX Analysis Data on ZDP Reaction Product Films	219
10.5	Auger Analysis Results on 1% ZDP in PPO Lubricated Si_3N_4	227
10.6	Auger Analysis Results on 1% TCP Lubricated Si_3N_4	230
10.7	Wear Test Results for POD Tests on fused Silica	248
11.1	Friction and Wear Data on Selected Chlorine-Containing Model Compounds	265
11.2	BTF Test Results on Neat Chlorine-Containing Compounds	267
11.3	BTF Test Results on Neat Fluorine-Containing Compounds	280
12.1	Friction and Wear Data on Selected Sulfur-Containing Model Compounds	285
13.1	Friction and Wear Data on Selected Nitrogen-Containing Model Compounds	309

D.1	Summary Si_3N_4 Flat Preparation Procedure	354
H.1	Repeatability Data on PPO Lubricated Si_3N_4 CER038 Batch of NC132 Flats	367
H.2	Repeatability Data on PPO Lubricated Si_3N_4 CER028 Batch of NBD100 Flats	369

LIST OF FIGURES

2.1	Lubrication Regimes Encountered under Different Contact Severities	4
2.2	Unit Layers of α and β Si_3N_4 . Filled and unfilled symbols represent different planes of atoms. (from Saito ²¹⁶).	7
2.3	Phase Diagram for Si-O-N System (from Somiya ²²⁶)	9
2.4	Bond Strengths and Effective Ranges for Different Bond Types (from Gutkowski ¹⁰⁵)	10
3.1	X-Ray Diffraction Pattern for NC132 Hot Pressed Si_3N_4	33
3.2	X-Ray Diffraction Pattern for NBD100 HIP'd Si_3N_4	34
3.3	X-Ray Diffraction Pattern for Rutgers Hot Pressed Si_3N_4	35
3.4	Raman Spectrum for NC132 Hot Pressed Si_3N_4	36
3.5	Raman Spectrum for NBD100 HIP'd Si_3N_4	36
3.6	SEM Photomicrograph of NC132 Hot Pressed Si_3N_4 Fracture Surface . . .	39
3.7	SEM Photomicrograph of NC132 Hot Pressed Si_3N_4 Polished/Etched Surface	39
3.8	SEM Photomicrograph of NBD100 HIP'd Si_3N_4 Fracture Surface	40
3.9	SEM Photomicrograph of NBD100 HIP'd Si_3N_4 Polished/Etched Surface	40
3.10	ESCA Survey Scan of Si_3N_4 Surface	42
3.11	ESCA O 1s Scan for Si_3N_4 Surface	42
3.12	ESCA Si KLL Scan for Si_3N_4 Surface	43
3.13	ESCA N 1s Scan for Si_3N_4 Surface	43
3.14	Auger Depth Profile for Si_3N_4 Surface	44
3.15	Surface Model for Silicon Nitride	46

3.16	Structure of Crystalline Silica	47
3.17	Different States of Silica as a Function of Temperature	50
4.1	NIST-Modified Four-Ball Apparatus Design	54
4.2	Four-Ball and Ball-on-Three-Flat Contact Geometries	56
4.3	Pin-on-Disk Test	57
4.4	Three-Dimensional Surface Analysis of Polished Si_3N_4	60
4.5	Load Capacity Plot for PPO Lubricated Si_3N_4	64
4.6	Friction Traces for PPO Lubricated Si_3N_4 at Several Loads	65
4.7	Wear-in Data for PPO Lubricated Si_3N_4	67
4.8	Micro-Reactor Thermal History: a) Heating, b) Cooling	72
5.1	PPO Lubricated BTF Test at 60 kg: a) Optical Photomicrograph, b) Friction Trace	76
5.2	SEM Photomicrographs of PPO Lubricated Si_3N_4 Wear Scar: a) Low Magnification, b) High Magnification (within Scar)	78
5.3	High Magnification SEM Photomicrographs of Exit Region Outside Wear Scar of PPO Lubricated Si_3N_4 Wear Test	79
5.4	Auger Depth Profile of Region within Wear Scar for PPO Lubricated Si_3N_4 Wear Test at 60 kg	82
5.5	Load Capacity Plot for PPO Lubricated Si_3N_4 Detailing Different Wear Regimes	84
5.6	PPO Lubricated Si_3N_4 BTF Test at 20 kg: a) Optical Photomicrograph, b) Friction Trace	86
5.7	PPO Lubricated Si_3N_4 BTF Test at 40 kg: a) Optical Photomicrograph, b) Friction Trace	87
5.8	PPO Lubricated Si_3N_4 BTF Test at 80 kg: a) Optical Photomicrograph, b) Friction Trace	89

5.9	PPO Lubricated Si_3N_4 BTF Test at 210 kg: a) Optical Photomicrograph, b) Friction Trace	90
5.10	PPO Lubricated Si_3N_4 BTF Test at 270 kg: a) Optical Photomicrograph, b) Friction Trace	91
5.11	POD Test Results for Rutgers Low Fe Si_3N_4 Lubricated by PPO	95
5.12	Different Friction Trace Types Encountered: a) Types I, II, and IV, b) Type III	96
6.1	Summary Friction and Wear Data for Si_3N_4 BTF Tests on 1% Oxygen-Containing Compounds in PPO	100
6.2	1% Mg Salicylate in PPO Lubricated Si_3N_4 BTF Test at 60 kg: a) Optical Photomicrograph, b) Friction Trace	103
6.3	SEM Photomicrographs for 1% Mg Salicylate in PPO Lubricated Si_3N_4 BTF Test at 60 kg: a) Secondary Electron Image, b) EDX Image (Mg)	104
6.4	EDX Spectrum for Surface inside Wear Scar for 1% Mg Salicylate (Ca Overbased) in PPO Lubricated Si_3N_4 BTF Test at 60 kg	105
6.5	1% Polypropylene Glycol Triol [600 MW] in PPO Lubricated Si_3N_4 BTF Test at 60 kg: a) Optical Photomicrograph, b) Friction Trace	107
6.6	1% Polypropylene Glycol Diol [400 MW] in PPO Lubricated Si_3N_4 BTF Test at 60 kg: a) Optical Photomicrograph, b) Friction Trace	108
6.7	1% Mannich Product in PPO Lubricated Si_3N_4 BTF Test at 60 kg: a) Optical Photomicrograph, b) Friction Trace	110
6.8	1% 3-n-Pentadecyl Phenol in PPO Lubricated Si_3N_4 BTF Test at 60 kg: a) Optical Photomicrograph, b) Friction Trace	112
6.9	1% Ethyl Stearate in PPO Lubricated Si_3N_4 BTF Test at 60 kg: a) Optical Photomicrograph, b) Friction Trace	113
6.10	Neat HMW Diacid Lubricated Si_3N_4 BTF Test at 60 kg: a) Optical Photomicrograph, b) Friction Trace	117
6.11	Neat Oleic Acid Lubricated Si_3N_4 BTF Test at 60 kg: a) Optical Photomicrograph, b) Friction Trace	119

6.12	Neat Octanol Lubricated Si_3N_4 BTF Test at 60 kg: a) Optical Photomicrograph, b) Friction Trace	122
6.13	Neat C_8 Compound Lubricated Si_3N_4 BTF Test Friction Traces: a) 2-Octanol, b) Octanoic Acid	123
7.1	Neat Octylaryl Polyether Alcohol Lubricated Si_3N_4 BTF Test at 60 kg: a) Optical Photomicrograph, b) Friction Trace	127
7.2	Neat Decanol Lubricated Si_3N_4 BTF Test at 60 kg: a) Optical Photomicrograph, b) Friction Trace	128
7.3	Neat Hexanol Lubricated Si_3N_4 BTF Test at 60 kg: a) Optical Photomicrograph, b) Friction Trace	129
7.4	Load Capacity Plots for Neat Linear Alcohols (C_6 , C_8 , C_{10})	131
7.5	Neat Hexanol Lubricated Si_3N_4 BTF Test at 20 kg: a) Optical Photomicrograph, b) Friction Trace	132
7.6	Neat Hexanol Lubricated Si_3N_4 BTF Test at 40 kg: a) Optical Photomicrograph, b) Friction Trace	133
7.7	Neat Hexanol Lubricated Si_3N_4 BTF Test at 80 kg: a) Optical Photomicrograph, b) Friction Trace	134
7.8	Neat Hexanol Lubricated Si_3N_4 BTF Test at 90 kg: a) Optical Photomicrograph, b) Friction Trace	136
7.9	SEM Photomicrographs of Neat Decanol Lubricated Si_3N_4 BTF Tests: a) 60 kg Load, b) 80 kg Load	137
7.10	SEM Photomicrographs of Neat 1-Octanol Lubricated Si_3N_4 BTF Test (Direction of Sliding is from Left to Right)	139
7.11	Surface Profile of Wear Scar from Neat 1-Octanol Lubricated Si_3N_4 BTF Test (Compared to Expected Surface Profile)	140
7.12	Wear Scar from Neat 1-Octanol Lubricated Si_3N_4 BTF Test: a) Optical Photomicrograph, b) Interferometric Photomicrograph	141
7.13	Optical Photomicrographs of Neat 1-Octanol Lubricated Si_3N_4 BTF Tests: a) 18 Second Duration, b) 180 Second Duration	143

7.14	Surface Profile of Wear Scar from Neat 1-Octanol Lubricated Si_3N_4 BTF Test (Compared to Original Surface)	145
7.15	Comparison of Wear Contact Morphologies: a) Neat Oleil Alcohol Lubricated Si_3N_4 Wear Scar, b) General EHL Contact Interferometry . .	146
7.16	6 μl Neat Octanol Lubricated Si_3N_4 BTF Test at 60 kg: a) Optical Photomicrograph, b) Friction Trace	150
7.17	Optical Photomicrographs of 6 μl Neat Octanol Lubricated Si_3N_4 BTF Test at 60 kg: a) Low Magnification, b) High Magnification	152
7.18	FTIR Spectrum of Film in Wear Scar for Octanol-Lubricated Si_3N_4	153
7.19	GPC-GFAA Analysis of Reaction Product from 6 μl Neat Octanol Lubricated Si_3N_4 BTF Test	155
7.20	GPC-GFAA Analysis of Reaction Product from 6 μl Neat Decanol Lubricated Si_3N_4 BTF Test	156
7.21	GPC-GFAA Analysis of Reaction Product from 6 μl neat Octylaryl Polyether Alcohol Lubricated Si_3N_4 BTF Test	157
8.1	TGA Analysis of Si_3N_4 Powder	161
8.2	TGA Analysis of Neat Octanol	162
8.3	TGA Analysis of Si_3N_4 Powder Reacted with Octanol at 100°C for 48 Hours Immediately After Solvent Extraction	164
8.4	FTIR Spectrum of Si_3N_4 Powder Reacted with Octanol at 100°C for 48 Hours	166
8.5	PDSC Analysis of Si_3N_4 Powder Reacted with Octanol at 100°C for 48 Hours	167
8.6	CO_2 and H_2O Mass Spectral Analysis of TGA Gases from Si_3N_4 Powder Reacted with Octanol at 100°C for 48 Hours.	168
8.7	TGA Analysis of the Same Powder 1 Day After Solvent Extraction	171
8.8	TGA Analysis of Si_3N_4 Powder Exposed to Octanol Vapor	173

8.9	TGA Analysis of Si_3N_4 Powder Reacted with Octanol at 100°C for 48 Hours as a Function of Time Since Solvent Extraction	174
8.10	TGA Analysis of Si_3N_4 Powder Reacted with Octanol at 100°C for 1, 4, and 48 Hours	176
9.1	SIMS Analysis of Residue from 6 μL Neat Octanol Lubricated Si_3N_4 BTF Test	179
9.2	SIMS Analysis of Residue from 6 μL Neat Decanol Lubricated Si_3N_4 BTF Test	181
9.3	Two-Ball Collision Test Geometry	183
9.4	Two-Ball Collision Test Results for Unlubricated and Lubricated Si_3N_4 . .	185
9.5	GPC-GFAA Analysis of Neat Tetra (C_6) Si Alkoxide	187
9.6	GPC-GFAA Analysis of Neat Tetra(C_6) Si Alkoxide Heated at 200°C for 5 Hours	189
9.7	Two-Ball Collision Test Results for Heated Neat Tetra(C_6) Si Alkoxide Reaction Product	190
9.8	Neat 6 μl PPO Lubricated Si_3N_4 BTF Test at 60 kg: a) Optical Photomicrograph, b) Friction Trace	195
9.9	GPC-GFAA Analysis of Reaction Product from 6 μl PPO Lubricated Si_3N_4 BTF Test	196
10.1	Summary Friction and Wear Data for Si_3N_4 BTF Tests on 1% Phosphorus-Containing Compounds in PPO	200
10.2	1% Oxymolybdenum Dithiophosphate in PPO Lubricated Si_3N_4 BTF Test at 60 kg: a) Optical Photomicrograph, b) Friction Trace	203
10.3	1% 2-Ethylhexyl ZDP in PPO Lubricated Si_3N_4 BTF Test at 60 kg: a) Optical Photomicrograph, b) Friction Trace	204
10.4	SEM Photomicrographs of Reaction Product Film from 1% 2-Ethylhexyl ZDP in PPO Lubricated Si_3N_4 BTF Test at 60 kg: a) Film inside Wear Scar, b) Flake Outside Entrance	205

10.5	1% TCP in PPO Lubricated Si_3N_4 BTF Test at 60 kg: a) Optical Photomicrograph, b) Friction Trace	207
10.6	Neat Zn Diaryl DP Lubricated Si_3N_4 BTF Test at 60 kg: a) Optical Photomicrograph, b) Friction Trace	212
10.7	Neat 2-Ethylhexyl ZDP Lubricated Si_3N_4 BTF Test at 60 kg: a) Optical Photomicrograph, b) Friction Trace	213
10.8	Neat TBP Lubricated Si_3N_4 BTF Test at 60 kg: a) Optical Photomicrograph, b) Friction Trace	214
10.9	SEM Photomicrographs of Regions within Wear Scar for Neat TCP Lubricated Si_3N_4 BTF Test at 60 kg	216
10.10	EDX Analysis of Flake within Wear Scar for Neat TCP Lubricated Si_3N_4 BTF Test at 60 kg	217
10.11	EDX Analysis of Wear Particles (on Teflon Filter) from Neat TCP Lubricated Si_3N_4 BTF Test at 60 kg	218
10.12	EDX Analysis of Flake outside Wear Scar for 1% Isodecyl ZDP in PPO Lubricated Si_3N_4 BTF Test at 60 kg	220
10.13	SEM Photomicrographs of Wear Scar from 1% TCP in PPO Lubricated Si_3N_4 BTF Test at 60 kg: a) Zero Tilt Angle, b) 75° Tilt Angle	221
10.14	SEM Photomicrograph of Entrance Deposit for 1% TCP in PPO Lubricated Si_3N_4 BTF Test at 60 kg: a) Bubble Formed from Electron Beam Spot Damage, b) Same Region after Bubble has Popped	223
10.15	EDX Analysis of Entrance Deposit from 1% TCP in PPO Lubricated Si_3N_4 BTF Test at 60 kg	224
10.16	EDX of FePO_4 Model Compound	226
10.17	Auger Depth Profile for Region Within Wear Scar of 1% ZDP in PPO Lubricated Si_3N_4 BTF Test at 60 kg	228
10.18	Auger Depth Profile for Region Within Wear Scar of 1% TCP in PPO Lubricated Si_3N_4 BTF Test at 60 kg	229
10.19	FTIR Analysis of Reaction Product from 1% TCP in PPO Lubricated Si_3N_4 BTF Test at 60 kg	232

10.20	Friction Traces for 1% TCP in PPO Lubricated Si_3N_4 BTF Tests	233
10.21	Load Capacity Plot for 1% TCP in PPO Lubricated Si_3N_4 BTF Tests (Compared to Pure PPO Data)	234
10.22	Friction as a Function of Test Temperature for 1% TCP in PPO Lubricated Si_3N_4 BTF Test at 60 kg	236
10.23	Wear Versus TCP Concentration for Si_3N_4	239
10.24	FTIR Spectra for TCP Adsorption on Si_3N_4 Powder Experiment	241
10.25	1% TCP + 0.1% Fe Naphthenate in PPO Lubricated Si_3N_4 BTF Test at 60 kg: a) Optical Photomicrograph, b) Friction Trace	244
10.26	PPO Lubricated POD Test on Fused Silica: a) Optical Photomicrograph, b) Friction Trace	246
10.27	SEM Photomicrograph of Wear Scar on Pin from PPO Lubricated POD Test on Fused Silica: a) Wear Scar, b) Higher Magnification of Radial and Tensile Cracks outside Wear Scar	247
10.28	SEM Photomicrographs of Pin Wear Scars from POD Tests on Fused Silica: a) 1% TCP in PPO, b) 1% TCP + 0.1% Fe Naphthenate in PPO	249
10.29	Load Capacity Plot for 1% TCP in PPO Lubricated Si_3N_4 (Low Iron Impurity) POD Test	251
10.30	TGA Analysis of Reaction Product on Surface of Si_3N_4 Powder After Reaction with TOP	254
10.31	TGA Analysis of Reaction Product on Surface of Si_3N_4 Powder After Reaction with TCP	255
10.32	Phase Diagram for $\text{SiO}_2\text{-P}_2\text{O}_5$ System	258
10.33	6 μl 5% TCP in PPO Lubricated Si_3N_4 BTF Test at 60 kg: a) Optical Photomicrograph, b) Friction Trace	259
10.34	GPC-GFAA Analysis of Reaction Product from 5% TCP in PPO Lubricated Si_3N_4 BTF Test at 60 kg	261

10.35	GPC-GFAA of Second Extraction (with Ultrasonic) of Same Reaction Product	262
11.1	Summary Friction and Wear Data for Si_3N_4 BTF Tests on 1% Chlorine-Containing Compounds in PPO	264
11.2	Optical Photomicrographs 1% Chlorine-Containing Compounds in PPO Lubricated Si_3N_4 BTF Tests at 60 kg: a) Chlorinated Paraffin, b) Chlorinated Fatty Acid	266
11.3	1% Dimethy-n-Octadecylchlorosilane in PPO Lubricated Si_3N_4 BTF Test at 60 kg: a) Optical Photomicrograph, b) Friction Trace	271
11.4	1% Methyl-n-Octadecyldichlorosilane in PPO Lubricated Si_3N_4 BTF Test at 60 kg: a) Optical Photomicrograph, b) Friction Trace	272
11.5	1% n-Octadecyltrichlorosilane in PPO Lubricated Si_3N_4 BTF Test at 60 kg: a) Optical Photomicrograph, b) Friction Trace	273
11.6	1% (p-t-butylphenethyl)dimethylchlorosilane in PPO Lubricated Si_3N_4 BTF Test at 60 kg: a) Optical Photomicrograph, b) Friction Trace	274
11.7	75° Tilt SEM Photomicrographs of Flat from 1% Dimethy-n-Octadecylchlorosilane in PPO Lubricated Si_3N_4 BTF Test at 60 kg: a) Wear Scar, b) Entrance Region	275
11.8	75° Tilt SEM Photomicrographs of Flat from 1% Dimethy-n-Octadecylchlorosilane in PPO Lubricated Si_3N_4 BTF Test at 60 kg: a) Exit Region, b) Exit Region (Higher Magnification)	277
11.9	0° Tilt SEM Photomicrographs of Flat from 1% Dimethy-n-Octadecylchlorosilane in PPO Lubricated Si_3N_4 BTF Test at 60 kg: a) Exit Region, b) Exit Region (Higher Magnification)	278
11.10	Neat n-Octadecyltrichlorosilane Lubricated Si_3N_4 BTF Test at 60 kg: a) Optical Photomicrograph, b) Friction Trace	279
12.1	Summary Friction and Wear Data for Si_3N_4 BTF Tests on 1% Sulfur-Containing Compounds in PPO	284
12.2	1% Benzyl Disulfide in PPO Lubricated Si_3N_4 BTF Test at 60 kg: a) Optical Photomicrograph, b) Friction Trace	288

12.3	1% Octadecyl Disulfide in PPO Lubricated Si_3N_4 BTF Test at 60 kg: a) Optical Photomicrograph, b) Friction Trace	289
12.4	1% Sulfur-Molybdenum Compound in PPO Lubricated Si_3N_4 BTF Test at 60 kg: a) Optical Photomicrograph, b) Friction Trace	290
12.5	1% Calcium Phenate in PPO Lubricated Si_3N_4 BTF Test at 60 kg: a) Optical Photomicrograph, b) SEM Photomicrograph at 75° Tilt	292
12.6	EDX Analysis of Film Inside Wear Scar for 1% Ca Phenate in PPO Lubricated Si_3N_4 BTF Test	294
12.7	1% Mg Sulfonate in PPO Lubricated Si_3N_4 BTF Test at 60 kg: a) Optical Photomicrograph, b) Friction Trace	295
12.8	SEM Photomicrographs of 1% Mg Sulfonate in PPO Lubricated Si_3N_4 BTF Test at 60 kg: a) Wear Scar, b) Film Within Wear Scar	297
12.9	SEM Photomicrographs of 1% Mg Sulfonate in PPO Lubricated Si_3N_4 BTF Test at 60 kg: a) Entrance Region, b) Exit Region	298
12.10	EDX Analysis of Film Inside Wear Scar from 1% Mg Sulfonate in PPO Lubricated Si_3N_4 BTF Test at 60 kg	299
12.11	Load Capacity Plot for 1% Mg Sulfonate in PPO Lubricated Si_3N_4 BTF Tests (Compared to PPO)	302
12.12	1% Mg Sulfonate in PPO Lubricated Si_3N_4 BTF Test at 200°C: a) Optical Photomicrograph, b) Friction Trace	303
12.13	1% Sulfurized Hydrocarbon in PPO Lubricated Si_3N_4 BTF Test at 200°C: a) Optical Photomicrograph, b) Friction Trace	305
13.1	Summary Friction and Wear Data for Si_3N_4 BTF Tests on 1% Nitrogen-Containing Compounds in PPO	308
13.2	1% Succinimide in PPO Lubricated Si_3N_4 BTF Test at 60 kg: a) Optical Photomicrograph, b) Friction Trace	311
13.3	1% HMW Substituted Imidazoline in PPO Lubricated Si_3N_4 BTF Test at 60 kg: a) Optical Photomicrograph, b) Friction Trace	312
F.1	Ball-on-Three-Flat Wear Geometry	359

F.2	Four-Ball Wear Geometry	360
H.1	Graphical Comparison of PPO Lubricated Friction and Wear Data for the Three Commercial Si_3N_4 's used in this Study	368
H.2	Average PPO Lubricated Friction and Wear Data Used for the Wear versus Friction Plots	370
J.1	Auger Depth Profile of Triangular-Shaped Region within the Wear Scar for 6 μl Neat Octanol Lubricated Si_3N_4 BTF Test	374
J.2	Auger Depth Profile of Deposit Region Outside the Wear Scar for 6 μl Neat Octanol Lubricated Si_3N_4 BTF Test	375

Chapter 1

INTRODUCTION

We are in the midst of a materials revolution. Many new materials have been developed and many materials are being modified to achieve specific properties to meet the requirements of new technologies. Advanced ceramics is such a class of new materials. They possess high strength, hardness, light weight, wear resistance, and corrosion resistance. They have been considered for many applications in advanced engine designs for their strength at high temperatures necessary for improved thermodynamic efficiency. A variety of ceramic engine components are being considered including valve lifters, piston caps, cylinder liners, valve seats, valve stems, and exhaust-port liners.

Si_3N_4 is the leading ceramic candidate for engine applications. The combination of high strength and toughness makes it well suited for such application. However, under engine operating conditions, wear and fatigue of the components may lead to premature failures. The lack of proper lubrication technology to protect the ceramic components has become a technology barrier for such application.

This study examines the surface interaction of Si_3N_4 with a wide variety of chemical compounds under boundary lubrication conditions. Different chemistries are discussed by chapter, grouped by predominant atomic composition of the active functional group (oxygen, phosphorus, sulfur, halogen, and nitrogen). A ball-on-three-flat (BTF) wear tester is used to

initially evaluate the boundary lubricating ability of these different chemical compounds with Si_3N_4 . Surface chemistry of the tribological surfaces and the nature of the boundary lubricating films are also studied. Where appropriate, mechanisms are proposed to describe how the compounds function.

Chapter 2

BACKGROUND AND LITERATURE SURVEY

2.1. Lubrication of Materials

Lubrication can be defined as the science and technology associated with the control of friction and wear between two surfaces, under load, in relative motion. Lubricants then are the means to accomplish such control. A lubricant may be a gas, a liquid, or a solid. For liquid lubrication, the lubrication process can be classified into several regimes which are dependant on the operating conditions, as depicted in Figure 2.1.

The dependence of the lubrication mechanism on the operating conditions is complex and is a function of many variables. These variables include not only the operating parameters, but also material attributes such as surface morphology, and physical and mechanical properties. This functional dependence may be generalized in terms of the severity of the contact conditions, as suggested by the scale in Figure 2.1. The severity of contact can be used to describe the complex interactions among several operating parameters such as load, speed, and viscosity. For example, increasing contact severity can be caused by either increasing load, decreasing speed, decreasing fluid viscosity, or a combination of these parameters. There are also other indirect, or secondary parameters that can affect the contact severity. For example, the increase in surface roughness caused by fracture of the surface or introduction of wear debris will increase the asperity pressure, hence the contact

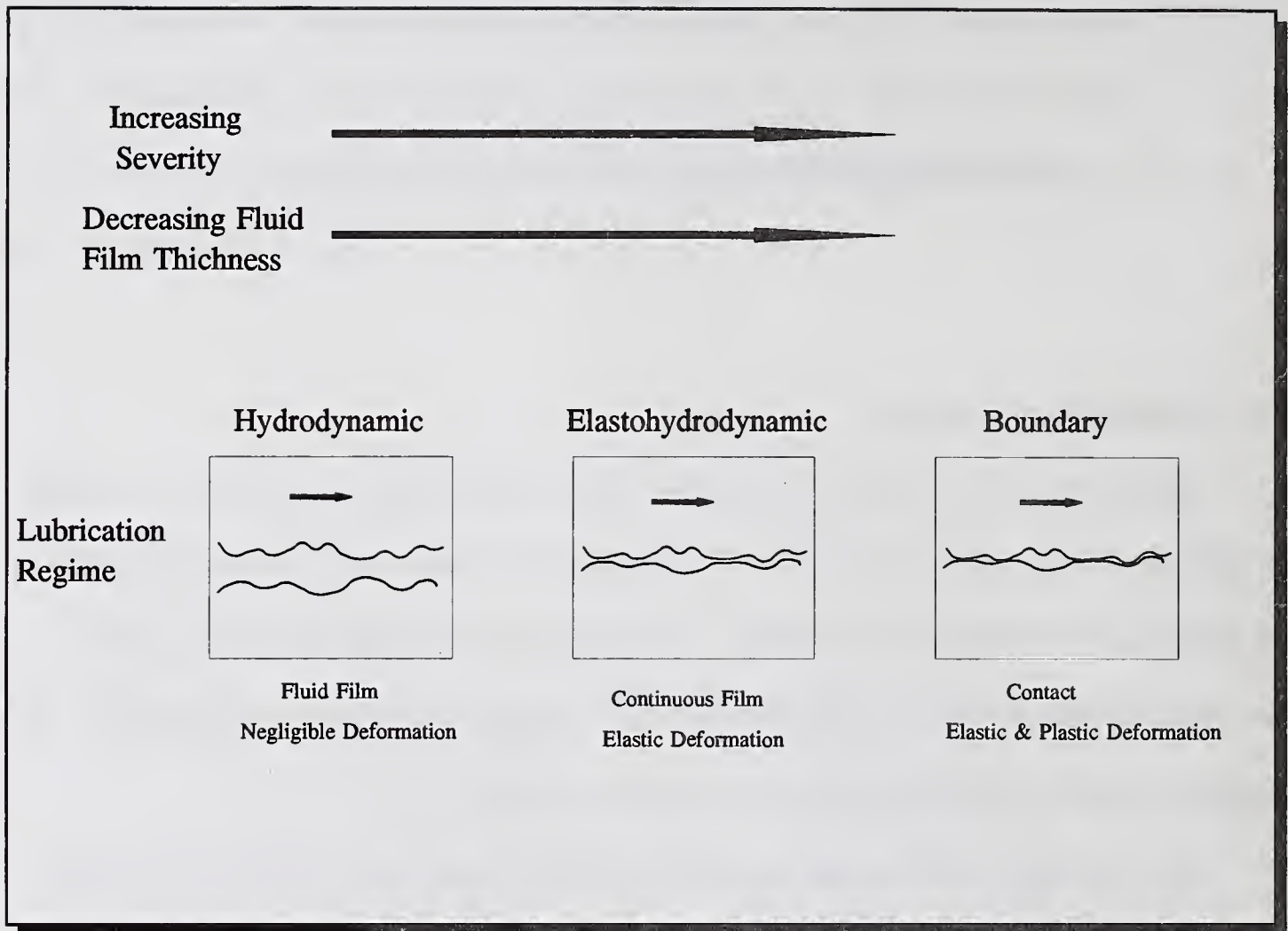


Figure 2.1 Lubrication Regimes Encountered Under Different Contact Severities

severity. As the severity increases, the lubrication mechanism moves from one regime to the next. Under mild contact conditions, the contact surfaces are completely separated by a continuous fluid film and the forces that keep the surfaces apart are described by the Reynolds Equations. This is the hydrodynamic lubrication regime. It is dominated by the fluid properties of the lubricant, especially the viscosity.

Under more severe conditions, the surfaces in the contact region are stressed to such a degree that they begin to elastically deform. There is still a continuous fluid film separating the surfaces; however, the film is very thin (slightly larger than the composite

surface roughness). This contact condition can still be described by the Reynolds Equations with the addition of elastic Hertzian surface deformation contributions. This region is generally referred to as the elastohydrodynamic lubrication regime.

Under still higher severity, the asperities on the surfaces begin to deform plastically and contact. The fluid film thickness that separates the two surfaces is often smaller than the composite surface roughness of the surfaces. Under such conditions high temperatures are generated at the tips of the contacting asperities, and chemical reactions take place between the surface and the lubricant. The contact conditions now are very complicated. Fluid mechanics still play a role but the result of the lubrication processes often is controlled by the chemical reactions and the plastic deformation processes. This is generally referred to as the boundary lubrication regime.

It should be recognized that in actual practice, mixtures of lubrication regimes are often encountered. Boundary lubrication involves asperity interactions, and elastohydrodynamic lubrication theory describes elastic deformation of a surface without contact. The pressure distribution within a contact, coupled with the distribution in asperity heights, produces a distribution of severity within the wearing contact. This means that some severity conditions may provide contacting (boundary) and non-contacting (elastohydrodynamic) conditions resulting in a "mixed" mode of lubrication.

Another convenient way to think of these different types of lubrication is as "lines of defense"¹²⁷ against friction and wear (Table 2-1).

In this context, different means or tools are used to defend against wear. Hydrodynamics can be used as the first line of defense. It depends mainly on the bulk fluid properties of the

Table 2.1
Lines of Defense Against Wear and Friction

<u>Lubrication Regime</u>	<u>Important Property Types</u>	<u>Examples</u>
Hydrodynamic	Fluid	μ
Elastohydrodynamic	Fluid Material Bulk Material Surface	μ E, ν Roughness
Boundary	Surface Chemical	Reactivity

lubricant, especially viscosity (μ). As the severity increases, the second line of defense (elastohydrodynamics or EHD) is utilized and the macroscopic material properties become more important, especially elasticity. Under still higher severity, contact between the surfaces takes place and boundary lubrication is encountered. Here the chemical properties of the surface and lubricant are important for protecting the surface. It is the chemistry in the boundary lubrication regime that will be addressed in this study.

The significance of chemistry in boundary lubrication is demonstrated by concepts of how lubrication may occur in this regime. One way in which chemistry may function to reduce wear is through the formation of lubricious oxides. It is felt that the formation of oxides of iron, for example, reduces the possibilities for bare metal-metal contact that may lead to welding together of the surfaces, galling, scuffing, and other high deformation, high wear processes^{201, 202, 231, 232}. Another important chemical reaction is the formation of inorganic compounds such as that observed with tricresyl phosphate (TCP) a common

antiwear additive. FePO_4 has been identified in the wear debris from iron-containing surfaces lubricated with TCP^{157a}. A third important chemical reaction involves the formation of organic compounds through oxidation and degradation reactions. These reactions often involve the metal surface as a catalyst to produce high molecular weight (HMW) compounds that may reduce wear and friction, form sludge, or produce varnish^{157b, 58a}. Metals from the surface can also become incorporated into the HMW compounds formed⁹².

2.2. Structure of Si_3N_4

Silicon Nitride is the ceramic compound formed from Si and N in the stoichiometric ratio of 3 silicon atoms for every 4 nitrogen atoms. The crystallographic structure and the phase diagram relationship of Si_3N_4 have been extensively studied^{226, 108, 216}. There are two major crystallographic forms, alpha (α), and beta (β). Both are classified crystallographically as hexagonal; however, their unit cells are different in structure and size. Both forms are

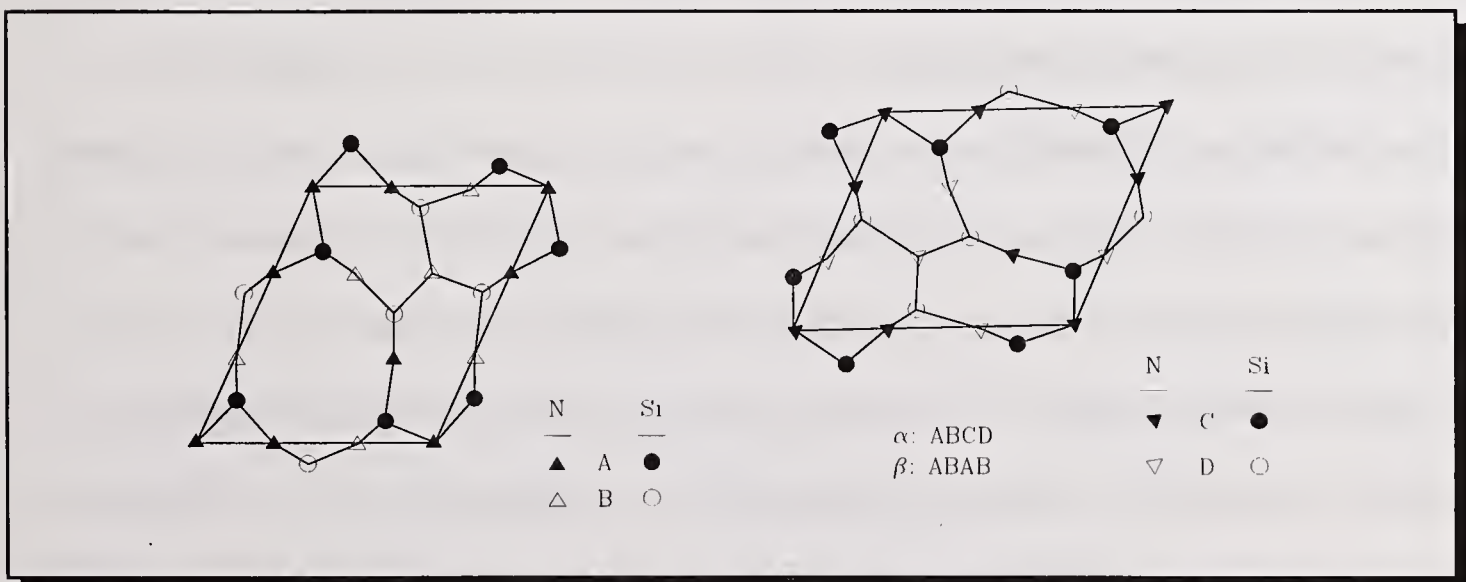


Figure 2.2. Unit layers of α and β Si_3N_4 . Filled and unfilled symbols represent different planes of atoms. (from Saito²¹⁶)

composed of unit layers as shown in the basal plane projections of Figure 2.2. Each silicon is bonded to four nitrogen atoms and each nitrogen atom is bonded to three silicon atoms. Some of the bonds in Figure 2.2. (into and out of the paper) have been omitted for clarity of presentation. The filled symbols represent atoms that exist on one layer of the structure, while the unfilled symbols represent atoms on another, parallel, layer.

According to Figure 2.2., there are two layer types, AB and CD. β - Si_3N_4 is composed solely of the first type of layer (AB) and repeats as ABAB. This results in macroscopic structure that appears quite columnar - a distinguishing feature of β - Si_3N_4 grains in the monolithic material. The second layer type (CD) is actually a mirror image of the first (AB) layer type. α - Si_3N_4 is composed of layers of ABCD. The resulting macroscopic α - Si_3N_4 grains appear much more equiaxed than those of β - Si_3N_4 . It is generally recognized that the α - Si_3N_4 phase actually contains a small amount of oxygen, making the stoichiometry $\text{Si}_{23}\text{N}_{30}\text{O}$. It is not known exactly how the oxygen is incorporated into the structure.

Si_3N_4 does not melt, but decomposes at $\approx 1871^\circ\text{C}$ to yield Si and N_2 . For this reason, high sintering temperatures are avoided in the fabrication of monolithic Si_3N_4 . Below the decomposition temperature, there are several important silicon containing phases relevant to the Si_3N_4 system. The thermodynamic phase equilibria relationships between these different forms are usually expressed in terms of partial pressures of oxygen and nitrogen as shown in Figure 2.3. Looking at the higher temperature data (solid lines - 1800°K), at low partial pressures of nitrogen, silicon and silica (SiO_2) are the stable phases, with silica being favored at higher oxygen partial pressures. At higher nitrogen partial pressures, the nitrogen containing phases of β - Si_3N_4 , and $\text{Si}_2\text{N}_2\text{O}$ (silicon oxynitride) become

stable, with β - Si_3N_4 favored at lower oxygen partial pressures. According to this figure, α - Si_3N_4 is not stable at high temperatures at any combination of partial pressures of oxygen and nitrogen. When the temperature is lowered (to 1600°K - dotted line of Figure 2.3.) formation of α - Si_3N_4 is possible at oxygen partial pressures intermediate to those required of $\text{Si}_2\text{N}_2\text{O}$ and β - Si_3N_4 . Because of these observations, α - Si_3N_4 is generally regarded as

the low temperature form of Si_3N_4 while β - Si_3N_4 is thought of as the high temperature form.

Monolithic ceramics are produced by a thermal densification process known as sintering. It is necessary to densify ceramics because open spaces known as pores can act as structural defects, resulting in fracture under relatively low stress. In sintering, powders are heated until the surfaces of the powders fuse together. This can occur through a variety of mechanisms such as evaporation-condensation, solution-reprecipitation, and diffusion (surface, boundary, or lattice). Because Si_3N_4 decomposes instead of melting, it is very difficult to achieve densification through sintering without the use of sintering aids. Metal oxides such as MgO , Al_2O_3 , and Y_2O_3 are used, to allow lower melting liquid phases (eutectics) to form with silicon nitride and silica and allow fully dense Si_3N_4 to be made. During sintering, most of the sintering aids tend to concentrate in the glassy phase that binds

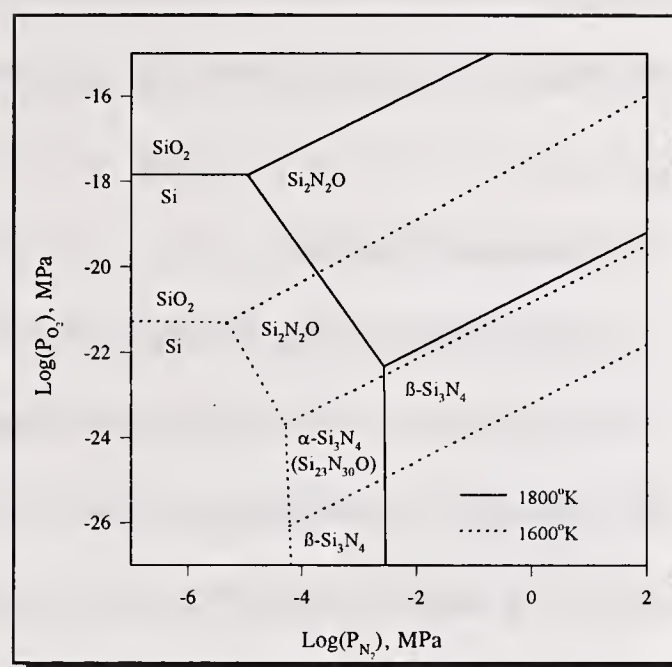


Figure 2.3. Phase Diagram for Si-O-N System (from Somiya²²⁶)

the individual grains of the ceramic together. This glassy phase also tends to collect the impurities that may be present in the original fine powder.

2.3. Properties of Si_3N_4

The fundamental difference in the nature of interatomic bonding between atoms in ceramics and atoms in metals leads to differences in physical and chemical properties. The five basic types of bonds (ionic, covalent, metallic, hydrogen, and Van der Waals) are described in detail in many references such as Kingery¹⁵⁰, Gutowski¹⁰⁵, or Richerson²¹⁰.

Figure 2.4 demonstrates a graphical method used by Gutowski to compare the different bond strengths and effective ranges.

Covalent bonds are strong bonds that are formed when electrons are shared between atoms of similar electronegativity. Ionic bonds result when complete electron transfer takes place between atoms of different electronegativity. Coulombic attraction between the resulting charged ions result in strong bonds. Bond energies are similar in magnitude to covalent bonds. Both ionic and covalent bonds act over relatively short intermolecular distances.

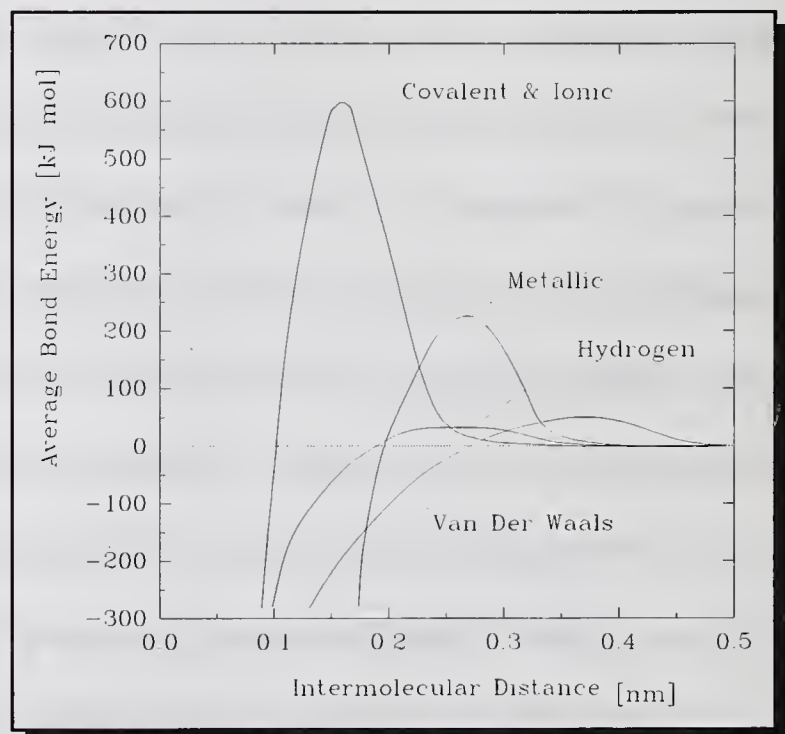


Figure 2.4 Bond Strengths and Effective Ranges for Different Bond Types (from Gutowski¹⁰⁵)

Metallic bonds are moderate in strength. These bonds are the result of attractive (coulombic) forces between positive metallic atoms with commonly shared free negative electrons. These bonds are not as directional in nature as either covalent or ionic bonds, and are effective over a longer range as shown in Figure 2.4. Two characteristics of the high electron mobility of metallic bonds are high electrical and thermal conductivity, properties which are used to classify solids as having metallic character.

Hydrogen bonds are relatively weak bonds formed when hydrogen acts as a bridge between its primary bond to an electronegative atom (such as in O-H) and another electronegative atom such as O, F, or N.

The fifth type of bonds between atoms are Van der Waals bonds. These bonds arise from dipole-dipole interactions between atoms and result in weak bond strengths; however, Van der Waals bonds act over a relatively long range, as shown in Figure 2.4.

In ceramics, interatomic bonding consists of a combination of ionic, covalent, Van Der Waals, and hydrogen bonding, with ionic and covalent being the most important¹⁵⁰. One significant feature of these types of bonding is that electrons are localized to specific atoms or shared between pairs of atoms. As a result, bonding tends to be somewhat directional in nature. Many ceramics contain bonding with mixed covalent and ionic character. The degree of covalent versus ionic character for a material depends on the difference in electronegativity between the atoms as described by Richerson²¹⁰. For example, SiO_2 is considered to be approximately 50% ionic and 50% covalent. Si_3N_4 is 70% covalent in character and 30% ionic.

One manifestation of the difference in properties between ceramics and metals can be demonstrated by the stress-strain relationships, as detailed in several references ^{91, 150, 210}. Metals exhibit a linear (elastic) response to stress up to a certain point when the material begins to plastically deform and yield. Ceramics typically exhibit a much steeper stress-strain relationship (i.e. less strain for a given stress). In addition, instead of yielding plastically, most ceramics fail by brittle fracture. This basic difference of the ductility of metals and the fracture of ceramics leads to fundamental differences in the wear mechanisms for these two classes of materials.

2.4. General Comparison of Wear Mechanisms of Metals vs Ceramics

The dominant wear mechanisms for metal systems have been described by adhesion, abrasion, corrosion, plastic deformation, fatigue, and delamination, as summarized in Table

2.2. Adhesion and abrasion are the most

common mechanisms cited. Experiments

performed in vacuum have shown that clean

metal surfaces, brought together, will adhere

strongly to each other⁴². This adhesion can

cause high wear and friction. Therefore, one

of the lubrication concepts for metals is to

provide surface barrier films to reduce or

prevent adhesion. This can be accomplished through adsorbed and reacted surface chemical layers.

Table 2.2
Wear Mechanisms for Metals and Ceramics

Metals:	Adhesion Abrasion Corrosion Fatigue Delamination
Ceramics:	Brittle Fracture 3rd body Abrasion

The dominant wear mechanisms for ceramics are different forms of brittle fracture. This has been seen at both the microscopic scale, and as gross fracture of the material. Fracture has been observed to take place both inside the grains (intragranular or intraparticle), and between the grains (intergranular or interparticle). When interparticle fracture occurs, the entire grain may be removed from the surface due to preferential fracture along the grain boundary. This is commonly referred to as grain pullout. Brittle fracture can occur because of high localized (point) stresses that can originate from a variety of sources such as asperity tips, exposed edges of grains, or trapped particles (debris). Adsorbed layers of molecules or reacted surface chemical layers may not be sufficient to modify the stress distribution enough to mitigate fracture.

2.5. Wear of Si_3N_4 under Unlubricated Conditions

Several studies have been conducted on the tribological properties of Si_3N_4 . Some studies focused on the unlubricated wear of Si_3N_4 for material evaluation purposes. Table 2.3 summarizes the unlubricated wear studies conducted on Si_3N_4 . Most of the tests were conducted under relatively light loads, with contact pressures in the range of 1 to 100 MPa. Environments ranged from high vacuum to inert gas (nitrogen, argon) and dry air. A wide range of speeds and temperatures have been covered. Despite the range of operating conditions and different Si_3N_4 materials, specific wear rates for unlubricated Si_3N_4 are fairly consistent at 10^{-3} to 10^{-5} mm^3/Nm . Enomoto⁷⁵ calculates wear rates of only 10^{-7} mm^3/Nm for his very slow speed, light load tests. Coefficients of friction of from 0.5 to 1.0 are common for unlubricated Si_3N_4 . In general, wear rates are highest in vacuum, and inert gas (argon,

Table 2.3
Reference Summary for Unlubricated Si_3N_4 Wear Testing

Reference	Year	Contact Geometry	Speed (m/s)	Load (GPa)	Temperature (°C)	Wear Rate mm^3/Nm	COF	Comments
Cranmer	1985	Flat-on-Flat	0.5-5.5	0.3	RT	10^{-4}	0.2-0.5	Observed plastic deformation, plowing, and oxide film formation.
Sutor	1985	Dual Rub Shoe	0.2	0.002	RT, 500	10^{-3}	0.5-1.0	Cracking/delamination, adhesion observed. Glassy phase surface oxide
Tomizawa	1985	Pin-on-Plate	0.001-0.01	1	150-800	NR	0.8/0.2	Fracture, oxide film in air. Lower friction in humid air below 800°C.
Tsuya	1985	Ring on Block	0.0004	NR	RT-700	10^{-4}	0.5-1.0	Ground surface had higher wear than polished surface
Akazawa	1986 1988	Rolling Rolling-Sliding	NR	1-2	RT	10^{-9} 10^{-4}	NR	Pure Rolling. Glassy film observed. Surface rich in oxygen (SiO_2 ?)
Enomoto	1987	annular	0.0008	0.001-0.003	RT	10^{-7}	0.5 ± 0.2	Wear higher in N_2 , lower in humid air. Surface oxide observed in air.
Yust	1988	Pin-On-Disk	0.3	1	RT-425	10^{-4} - 10^{-5}	0.7-1.0	Many ceramic/ Si_3N_4 couples
Cranmer	1988	Flat-on-Flat	0.5-5.5	0.3	RT	10^{-4}	0.2-0.5	Oxidized Si_3N_4 found in wear debris.
Ajavi	1990	Cylinder on flat	0.25	0.002-0.004	RT	10^{-5}	0.8	Room air. Observed transfer film
Sasaki	1989	Pin-On-Disk	0.1	1	RT	10^{-5}	0.8	Wear rate 10^{-7} under nitrogen
Boch	1990	several	0.1-1.0	0.0025	0, 1000	NR	0.8	Velocity accommodation model.
Mizutani	1990	Plate-on-Plate	0.2	0.0001	RT-1000	10^{-3} - 10^{-4}	0.8	Initial COF ≈ 1.3
Ura	1990	Pin-On-Disk	0.0013	1-2	RT	10^{-5}	0.4-0.6	In vacuum, or under argon

NR = Not Reported, RT = Room Temperature

N₂). When air with different trace levels of water is introduced, specific wear rates are usually observed to drop by an order of magnitude. The wear rate drops further when water vapor concentration is increased.

Observations of the worn surfaces include plastic deformation, fracture, and formation of compacted debris. When air is present, transfer films rich in oxygen are sometimes observed. The presence of water in the air seems to enhance the formation of these transfer films.

Tomizawa²³⁶ found that the wear of Si₃N₄ in argon or air was dominated by fracture over the temperature range from room temperature to 800°C. The coefficient of friction was 0.8. In humid air, he found that the friction coefficient dropped to 0.2, and a soft film was formed that protected the surface from gross fracture. These films were only successful within a window of temperature (150°C to 650°C) and film failure within these temperatures could be induced by increasing speed and load. Higher temperatures required higher loads for film failure. Auger analysis of the worn surface after a test in humid argon found an increase in surface oxygen.

Akazawa^{5,6} looked at rolling contact of Si₃N₄. Using energy dispersive x-ray analysis, he determined that the surface had become rich in oxygen at the end of the test. He noted that a glassy film had formed on the surface that contained some crystalline material. Infrared spectrometry indicated the presence of SiO₂ surface groups.

Enomoto⁷⁵ looked at plane contact (sliding) of Si₃N₄ to find that air decreased wear rates over dry nitrogen. He attributed the effect to oxidation of the Si₃N₄ surface. He also

noted OH absorbance peaks in the infrared spectra of wear products that he ascribed to adsorbed water and/or silanol (SiOH). Ura²⁴⁶, Tsuya²⁴³, and Sasaki²¹⁸ also showed that the water in the atmosphere affected the wear of Si_3N_4 as well as other ceramics (SiC, alumina, and zirconia).

Boch²⁹ et al studied the wear mechanisms of SiC and Si_3N_4 under a variety of (mostly unlubricated) conditions. Their observations were described in the context of what they termed velocity accommodation mechanisms (VAM's). Simply put, this approach classifies a tribological interface into five regions or sites known as accommodation sites. Each interface contains two surface sites (S1 and S5) and two boundary layers (S2 and S4), and an interlayer (S3). There are four different accommodation modes (M1-M4) of elastic, rupture, shearing, and rolling respectively. These terms then serve as a kind of tribological shorthand to describe the location and mode of the various wear mechanisms under different conditions. For example, using this shorthand, a third body roll formation observed for Si_3N_4 (usually associated with higher temperatures and humid air as found by Tomizawa²³⁶) would be characterized as VAM S3M4.

2.6. Lubricated Si_3N_4 Wear Studies

Lubricated ceramic friction and wear studies have been conducted on a wide variety of Si_3N_4 materials under many different conditions. Table 2.4 summarizes the representative studies. The lubricants used are mainly mineral oils, conventional automotive lubricants, water, and alcohols.

Enomoto⁷⁵ in 1987 first noted a "zero wear" regime for Si_3N_4 lubricated by a white oil under very light load. Habeeb¹⁰⁶ examined the wear Si_3N_4 using a base oil, oxidized species such acids and peroxides, and zinc dithiophosphate (ZDP) in base oil. He found that the addition of 0.4% lauric acid or 1% t-butyl hydroperoxide increased the wear of Si_3N_4 . The use of 1% ZDP in base oil decreased the wear. Jahanmir¹⁴³ found that both cetane and cetane + 0.5% stearic acid gave relatively high wear. The stearic acid was shown to reduce friction slightly (μ dropped from 0.12 to 0.10).

The effect of water on the wear of Si_3N_4 was pioneered by Sugita²³⁰ who suspected that the surface was reacting with water to produce a hydrated amorphous silica which was removed by rubbing. This silica was soluble in the water and could be found in the water after the test. A series of papers published between 1987 and 1990 by Tsunai,²⁴¹ Tomizawa,²³⁷ Hibi,¹²⁰ Mizutani,¹⁷⁸ and Ura²⁴⁶ expanded on the water lubricated Si_3N_4 work. In these tests, wear and friction were high and the proposed explanation was the reaction between Si_3N_4 and water to form a hydrated silica species. The proposed reaction was:



Tomizawa,²³⁷ and Mizutani,¹⁷⁸ both found extremely low friction after wear-in that they interpreted as elastohydrodynamic lubrication achieved through tribochemical reaction of water on the surface of Si_3N_4 and subsequent dissolution of the silicic acid $[\text{Si}(\text{OH})_4]$ in water. Essentially, the water reacts with the surface to chemically polish down the asperities and result in mirror finish surfaces that can then support EHD lubrication. Mizutani et al. also investigated the effect of different concentrations of sulfuric acid on the wear of Si_3N_4 .

Table 2.4
Reference Summary for Lubricated Si_3N_4 Wear Testing

Reference	Year	Contact Geometry	Speed (m/s)	Load (GPa)	Lubricant	Wear Rate (mm^3/Nm)	COF	Comments
Sugita	1985	Disk-on-Plate	0.25	NC	Water	10^{-3}	NR	Smooth surfaces. Soluble silica species in water after test. Hydrated silica?
Jahanmir	1986	Pin-On-Disk	0.001	1	Cetane, Cetane + Stearic acid	10^{-6} 10^{-6}	0.12 0.10	Hypothesized Si_3N_4 reacts with water in fluids to form amorphous silicon dioxide.
Enomoto	1988	Annular	0.0008	0.001-0.003	White Oil	"zero wear"	0.15	Surface oxide films observed.
Habeeb	1988	Four-Ball	0.12-0.46	2-3	150 N Base oil, Additives	10^{-8} - 10^{-9}	0.07-0.12	ZDP showed antiwear effect and surface film.
Tomizawa	1988	Pin-On-Disk	< 0.06 0.06-0.1	1	Water	10^{-5} "0"	0.5-0.7 0.02	Very smooth surfaces. EHD lubrication by tribochemistry postulated.
Tsunai	1988	Ball-on-Block	0.002	1	Alcohols	10^{-6} - 10^{-7}	0.09-0.15	Hypothesize tribochemical reaction with surface of Si_3N_4 to form Si esters. Films.
Tsunai	1989	Ball-on-Block	0.002	2	Water n-Alcohols	10^{-5} 10^{-7}	0.09-0.78	Wear in water very high. Wear in alcohols lower. Longer alcohols had lower wear. Hypothesized rxn \rightarrow Si esters. Films.
Hibi	1990	Ball-on-Block	0.002	2	Water n-Alcohols	10^{-5} 10^{-7}	0.7 0.1-0.2	Proposed water and lower alcohol \rightarrow silica and silica esters by tribochemical reaction.
Hibi	1990	Ball-on-Disk	0.2	1	Silane Coupling agents	10^{-6}	<0.01	Proposed agent: alkoxy groups \rightarrow silanol \rightarrow surface siloxane. Viscous film observed.
Mizutani	1990	Pin-on-Disk	0.01-0.3	0.006	Water H_2SO_4	NR	<0.05 0.3	Low friction in water \rightarrow silicon hydroxide? High wear rate in 20% H_2SO_4 (corrosion?).
Ura	1990	Pin-On-Disk	0.00013	1-2	Water	10^{-6}	0.2	Hypothesized formation of silicon hydroxides on the surface.
Gates	1990	BTF	0.23	2	Mineral Oil, Additives	10^{-8} - 10^{-9}	0.06-0.15	Low Wear with P, some acids, alcohols, detergent and dispersant compounds. Films observed.
Klaus	1990	Four-Ball BTF	0.23	1-2	Mineral Oil, Additives Form. Oil, Glycol, Ester	10^{-8} - 10^{-9}	0.05	No surface catalysis or reaction. Addition of metal salts can influence lubrication.

He noted that 20% H_2SO_4 had the highest level of wear and attributed this to grain boundary corrosion.

Tsunai,^{240, 241} and Hibi¹²⁰ conducted a series of wear tests on Si_3N_4 using alcohols and found that they reduced friction and wear below that of the unlubricated case. Longer chain alcohols ($> \text{C}_5$) gave lowered friction and wear more than shorter chains. They proposed a tribochemical reaction mechanism of surface esterification of the alcohols and subsequent dissolution of the esters by alcohol. Short-chain alcohols were thought to have higher wear than long-chain alcohols because they react with the surface at faster rate and corrosive wear might have resulted. The authors, however, did not provide any direct chemical evidence to support this hypothesis. Hibi¹¹⁹ also conducted tests using aqueous solutions of amine silane coupling agents to find reduction in friction and wear below that of the water case. Very low friction coefficients of less than 0.01 were observed; however wear rates of 10^{-6} were still present. Viscous films were observed in the wear scar that he attributed to the formation of siloxane polymers on the surface. He attributed the low friction to EHD or mixed lubrication from the viscous surface film. Lower wear was attributed to the prevention of hydrolysis of Si_3N_4 by water.

In summary, the literature provides incomplete and sometimes conflicting information on what will lubricate Si_3N_4 . Some key reactions were identified: surface oxidation, hydrolysis, and lubricant polymerization. For example, oxidation of Si_3N_4 plays a major role in the lubrication of Si_3N_4 . Along with oxidation, hydrolysis by water is another key reaction, although it is not always clear whether hydrolysis is beneficial or detrimental. Alcohols appear promising as potential lubricant under a very limited condition, but their

mechanisms are not clear. Base oils seem to provide good lubrication at low loads, and some additives seem to show lubrication improvements within certain conditions. What is needed is a systematic approach to investigating the boundary lubrication of Si_3N_4 to address the elementary questions of what works, under what conditions, and how.

2.7. Technical Approach

The approach to understand the lubrication mechanism of Si_3N_4 is best described within a framework of boundary lubrication mechanism hypothesized for this material. In a very simplistic representation, boundary lubrication of Si_3N_4 takes place through a chemical reaction on the surface. This can be represented in terms of a generalized chemical reaction as:



where "A*" represents a chemical compound which is capable of reacting with the Si_3N_4 surface to provide a lubricating product. This is a very simplistic "idealized" representation of the system; however, it emphasizes the importance of the two key concepts of chemical reaction and lubrication.

2.7.1. Reactivity and Bond Strength

As mentioned previously, the literature is relatively sparse on detailed information on what will chemically react to boundary lubricate Si_3N_4 . One approach to developing concepts on what reactions might be successful involves looking at the more general notions of

reactivity of Si_3N_4 and bond strengths for different silicon compounds. Some of the references for reactivity of Si_3N_4 are summarized in Table 2.5.

We know that Si_3N_4 will decompose (in inert atmosphere) at 1870°C . In the presence of oxygen, Si_3N_4 will oxidize significantly at temperatures above 1000°C . Oxidation rate decreases with increasing oxide film thickness that is described by a parabolic rate expression²²³.

There is also significant evidence for reaction with water^{224, 106, 111}, mostly derived from observations of ammonia gas evolution, and the presence of silica. The proposed reaction sequence is:



This reactivity with water is also consistent with wear test results on the effect of humidity on wear of Si_3N_4 ²³⁶ as well as wear test results conducted in liquid water.^{230, 237, 241, 178}

Evidence for reaction of Si_3N_4 with alcohols is provided by Hattori et al.¹¹¹ who conducted reactions between short-chain alcohols (methanol to propanol) and Si_3N_4 and found that ammonia and amines were produced. They proposed the following reaction took place on Si_3N_4 .



They also speculated that more complex chemical reactions were occurring to form Si-OR groups on the surface; however, no direct evidence of these reactions were given. No wear tests were conducted in their study.

Table 2.5
Reference Summary for Si_3N_4 Reactivity

Reference	Year	Chemistry	Temperature	Comments
Kiehle	1975	O_2	600-1450°C	SiO_2 surface layer on hot pressed Si_3N_4 observed by XRD.
Battelle	1976	O_2 , HF, Molten metals	Varied	Si_3N_4 surface oxidized easily above 1100°C. "Hot" HF "not compatible".
Singhal	1976	O_2	1000-1400°C	SiO_2 , MgSiO_3 surface oxide film observed on hot pressed Si_3N_4 .
Singhal	1976	Water	1200-1400°C	Presence of water vapor accelerates oxidation of Si_3N_4 .
Lay	1983	Many	Varied	Literature data summary
Habeeb	1987	Water	100°C	Si_3N_4 hydrolysis and dissolution. NH_3 product detected.
Sato	1987	Carbonates Sulfates	700-1000°C	Surface corrosion observed with dissolution into the melts.
Fox	1988	Na Carbonate	1000°C	Formation of Na_2SiO_3 . Rapid surface oxidation.
Hattori	1988	Water $\text{C}_1\text{-C}_3$ Alcohols	150-200°C	Formation of SiO_2 and NH_3 . Formation of SiO_2 , NH_3 , and amines (R_3N ?).
Jacobson	1988	Na Sulfate	1000°C	Surface corrosion noted.

High temperature corrosion studies have indicated that Si_3N_4 is chemically attacked by chlorine¹⁶⁴, sulfates^{220, 142}, and carbonates^{220, 84}. While the temperatures used for these corrosion studies may be too high to be directly applicable to temperatures found in a lubricated ceramic contact, they at least point to some form of surface reactivity that may be exploited. Sato²²⁰ studied the corrosion behavior of Si_3N_4 exposed to alkali sulfates and carbonates under nitrogen and air environments at temperatures in excess of 700°C . He found that the Si_3N_4 actually dissolved into the melts due to chemical reactions on the surface that could be described by a shrinking core kinetic model. Si_3N_4 is also known to react with molten hydroxides (NaOH, KOH) at elevated temperatures ($> 300^\circ\text{C}$). In fact, molten hydroxides (NaOH, KOH) are commonly used as etchants to expose the grain boundaries of Si_3N_4 . The only drawback of using this method is that these hydroxides are so aggressive that it begins to dissolve the grains themselves. Si_3N_4 does not appear to be readily attacked by any organic or inorganic acids, including HF. Lay¹⁶⁴ ascribes HF with the ability to react with Si_3N_4 , but long exposure times (days) are necessary.

Bond dissociation energies can be used to estimate relative bond strengths for different silicon bonds. Since the bond dissociation energies are related thermodynamically through ΔH_f , comparison of their values can give an approximation of the ease of forming particular bonds. Bond dissociation energies for several silicon-based bonds are summarized in Table 2.6.

The bond energy for Si-N is listed as 439 kJ/mol. The data indicates that Si-O has a bond energy of 770 kJ/mol, significantly higher than Si-N, suggesting that oxygen-containing compounds are good candidates for this study. The data also suggest that sulfur and halogen

chemistries may also be successful. For this reason, we selected compounds based on oxygen, sulfur and halogens (chlorine). Some fluorinated compounds were also used, but because of solubility limitations in paraffin oil, they were tested neat.

In addition to corrosion and bond strength inference, there are certain compounds that have the ability to modify the network structure of glasses. Since the surface of Si_3N_4 is apparently oxidized, it was felt that these network modifiers might beneficially alter the surface oxide film to reduce friction and wear. Phosphorus is a known network

modifier for silica and was selected for study based on this concept.

Table 2.6
Bond Dissociation Energies for Selected Silicon Bonds (Source: Dean⁶⁸)

<u>Bond</u>	<u>Dissociation Energy</u>			
	(kJ/mol)		(kcal/mol)	
	<u>Mean</u>	$\pm 1\sigma$	<u>Mean</u>	$\pm 1\sigma$
Si-H	297	4	71	1
Si-Si	318	21	76	5
Si-Br	343	50	82	12
Si-C	435	21	104	5
Si-N	439	38	105	9
Si-Cl	439	50	105	12
Si-F	485	50	116	12
Si-S	619	13	148	3
Si-O	770	13	184	3

The experimental plan for this study was formed in order to systematically address the important issues outlined above. Different chemistries were chosen, loosely based on the concepts of reactivity outlined previously. The basic sequence of investigation consisted of initial wear test screening of candidate compounds to determine successful chemistries. This was followed by an expanded study of the composition and morphology of the reaction product films. In the case of alcohols and phosphorus-containing compounds, additional experiments were conducted to try to reveal the nature of the surface interactions. An in-depth examination of the mechanism of lubrication of Si_3N_4 by alcohols was launched when it

became apparent that this class of compounds had a significant and potentially identifiable reactivity with the Si_3N_4 surface under boundary lubrication conditions.

Chapter 3

MATERIAL CHARACTERIZATION

The materials used in this study are a combination of commercially available and experimental research materials. The monolithic silicon nitrides used for the survey of chemistries have been commercially available for many years and represent some of the most tested Si_3N_4 materials. An experimental, low iron, Si_3N_4 was specifically developed for use in this study to explore a particular aspect of Si_3N_4 surface reactivity. This material was made by Ajoy Zutshi at Rutgers University.²⁷¹ The Si_3N_4 powder used for reactivity studies was selected not only because of its high purity, but also because of its high surface area. The chemical compounds studied were obtained from commercial sources in as pure a form as possible.

3.1. Monolithic Si_3N_4

The monolithic Si_3N_4 materials used in this study were primarily commercially available magnesia sintered materials manufactured by Norton Company and known as NC132 and NBD100. These two materials start from the same powder processing step but differ in their heat treatment to form the final dense Si_3N_4 . NC132 is hot pressed. That is to say, it is uniaxially compressed in a graphite die as it is heated. The result is a fully dense Si_3N_4 with some grain orientation due to the orientation of the pressing. The NBD100 Si_3N_4

is Hot Isostatically Pressed (HIP), which means it is encapsulated and pressurized while it is heated. Pressurizing the sample isostatically during heating allows the material to sinter more uniformly since the pressing force is in all directions inward on the sample. The result is a fully dense Si_3N_4 without the orientation of grains seen in the hot pressed material. Since both Si_3N_4 's start from the same powder specifications, they have essentially the same bulk chemical composition; however, because of the difference in processing technique and conditions, the microstructure and microscopic chemistry (i.e. glassy phase composition etc) are different.

In the course of this research, it was found that the commercially available Si_3N_4 materials have an iron content of approximately 0.2% (2,000 ppm) Fe, which might catalyze some reactions and affect the surface reactivity. A low-iron content Si_3N_4 material was obtained from Rutgers University to study the tribochemical intercalations of Si_3N_4 and selected chemistries in the absence of Fe.

3.1.1. Manufacturers Literature

Typical properties of the monolithic Si_3N_4 used in this study are presented in Table 3.1. The values given for the commercial material were provided by the manufacturer. There is no discernable mechanical or thermal property difference between the two commercial materials.

The data indicate that all three of the Si_3N_4 materials used are similar in physical and mechanical properties. The densities are close to the theoretical density, indicating a low level of porosity. In the case of NC132, the porosity has been estimated to be less than 0.1%⁵².

Table 3.1
Properties of Si_3N_4 Materials Used

<u>Property</u>	<u>Units</u>	<u>Commercial^a</u>	<u>Rutgers</u>
Density	g/cm ³	3.2	3.2
Hardness	kg/mm ²	2000	1700
Strength	Flexural	GPa	1.0
(@20°C)	Compressive	GPa	3.0
	Hertz Compressive	GPa	10.0
Fracture Toughness	MPam ^{1/2}	5.4	5.5
Young's Modulus	GPa	310	325
Poissons ratio		0.28	0.28
Thermal Expansion Coeff.	10 ⁻⁶ /°C	3.5	-
Thermal Conductivity	W/m°K	32	-

a Data supplied by manufacturer for NC132 and NBD100 Silicon Nitride.

3.1.2. Chemical Composition

Since we are primarily interested in the surface chemical reactivity of these materials, the chemical composition is important. The manufacturers data on the typical chemical composition of NC132 and NBD100 Si_3N_4 are given in Table 3.2. Both commercial products start with the same powders and have MgO and Al_2O_3 added as sintering aids. The main impurities are oxygen, tungsten, and iron. Some of the oxygen comes from the magnesia and alumina which are intentionally added; however, some of it comes from the oxidized silicon layer that exists on the surface of all Si_3N_4 powders used as starting materials. Tungsten (W) probably is from the tungsten carbide grinding media commonly used to produce these powders. The values given by the manufacturers are only approximate. The actual concentrations of elements (especially metal impurities) was

considered so important that Neutron

Activation Analysis (NAA) was carried out

on representative samples of all of the

Si_3N_4 used in wear testing. The data are

presented in Table 3.3 in order of

decreasing abundance (for CER024 hot

pressed Si_3N_4).

The neutron activation analysis data

agree in large part with the manufacturers

data. For example, NAA found 2.25%

Table 3.2
Manufacturers Chemical Composition Data
for Typical NC132 and NBD100 Si_3N_4

Component	Approximate %	Max. Allowed %
Si_3N_4	93.3	
O	3.0	
W	1.8	3.0
Mg	0.8	1.0
Fe	0.3	0.75
Al	0.2	0.5
Mn	0.05	
Ca	0.01	

Table 3.3
Neutron Activation Analysis of Si_3N_4 Samples

Element	[element] in Silicon Nitride, ppm				
	CER024 ¹	CER038 ¹	CER028 ²	CER043 ³	CER044 ⁴
W	22500 ± 1	32000 ± 1	18500 ± 1	--	--
Mg	5500 ± 2	7760 ± 1	6200 ± 2	600 ± 7	250 ± 8
Fe	1900 ± 24	3790 ± 16	2000 ± 20	< 10	< 10
Al	1500 ± 1	2250 ± 1	1400 ± 1	24900 ± 1	21000 ± 1
Co	1400 ± 1	2000 ± 1	1300 ± 1	1	1
Ta	380 ± 1	730 ± 1	330 ± 1	--	--
Ti	221 ± 15	265 ± 12	163 ± 20	< 10	< 10
Na	220 ± 19	617 ± 14	690 ± 9	39 ± 25	36 ± 19
Mo	100 ± 9	39 ± 32	90 ± 8	--	--
Mn	75 ± 1	89 ± 1	95 ± 1	--	--
Cr	48 ± 15	39 ± 21	48 ± 12	5	4

All confidence limits are given as a percentage ($\pm 1\sigma$) of the [].

¹ Norton NC132 Hot Pressed Si_3N_4
² Norton NBD100 HIPPED Si_3N_4
³ Rutgers 10% Sintering Aid Hot Pressed Si_3N_4 (5% Al_2O_3 , 5% Y_2O_3)
⁴ Rutgers 7% Sintering Aid Hot Pressed Si_3N_4 (5% Al_2O_3 , 2% Y_2O_3)
 -- Indicates [] is below detectable limits

(22 500 ppm) W in CER024, and 3.2% (32 000 ppm) in CER038 while the manufacturers literature estimates 1.8%. One impurity that showed up in the commercial material that was not mentioned in their literature was cobalt. This was present at 1.4% in CER024, 2.0% in CER038, and 1.3% in CER028. The ratio of W:Co is fairly constant for the three samples and seems to suggest that these two metals are associated. Since cobalt is used as part of the binder matrix in tungsten carbide materials, both tungsten and cobalt probably come from wear of the tungsten carbide grinding media used to mill the powders. Titanium and tantalum may also come from the tungsten carbide. There is a variation of concentration of impurities in the commercial materials from sample to sample. For example, the concentration of iron in NC132 varies from a low of 0.19% to a high of 0.38%, an increase of 100%.

The experimental Rutgers Si_3N_4 materials were essentially free of any iron contaminants. They also did not contain any tungsten or cobalt, since the powders from which they were produced were not ball milled with tungsten carbide balls. Aluminum is present in high concentration because it is one of the two sintering aids added to the Si_3N_4 powder to aid densification (Y_2O_3 was the other). The only other impurities observed at any appreciable concentration was magnesium. The observation in the Rutgers samples that the 2% Y_2O_3 sample had 250 ppm Mg and the 5% Y_2O_3 sample had 600 ppm Mg suggests that the Mg is an impurity in the Y_2O_3 added to aid densification of these samples during sintering. The NAA technique used was not able to quantify yttrium, carbon, silicon, or oxygen.

3.1.3. X-Ray Diffraction

X-ray diffraction (XRD) was used to identify the major crystalline phases present in the Si_3N_4 samples used in this study. The sampling depth for this technique is approximately 100 μm for Si_3N_4 therefore this can essentially be considered a bulk technique. According to the data obtained, the hot pressed and HIP'd Si_3N_4 were composed of different phases.

Hot pressed Si_3N_4 NC132 (Figure 3.1) had two identifiable phases. Most of the sample consisted of $\beta\text{-Si}_3\text{N}_4$, with a small amount of silicon oxynitride ($\text{Si}_2\text{N}_2\text{O}$) also detected. The other peaks in the spectra were not identified.

HIP'd Si_3N_4 NBD100 had three identifiable phases (Figure 3.2). Most of the NBD100 consists of a mixture of $\alpha\text{-Si}_3\text{N}_4$ and $\beta\text{-Si}_3\text{N}_4$, with small amounts of tungsten carbide (WC) also present.

$\beta\text{-Si}_3\text{N}_4$ was the only crystalline phase detected in the Rutgers Si_3N_4 sample (Figure 3.3).

3.1.4. Raman Spectroscopy

Raman spectroscopy was performed on polished samples of the commercial Si_3N_4 's to further characterize them. The sampling depth for the μ -Raman technique used is on the order of 50 nm (500 Å) so it is still a relatively "bulk" technique, but it is certainly more surface sensitive than x-ray diffraction. NC132 hot pressed Si_3N_4 exhibited only one set of raman peaks (Figure 3.4). These peaks were associated with the $\beta\text{-Si}_3\text{N}_4$ phase. NBD100 HIP'd Si_3N_4 was observed to give two sets of peaks (Figure 3.5); one set was associated with $\beta\text{-Si}_3\text{N}_4$ and the other set with $\alpha\text{-Si}_3\text{N}_4$. Both of these sets of Raman peak

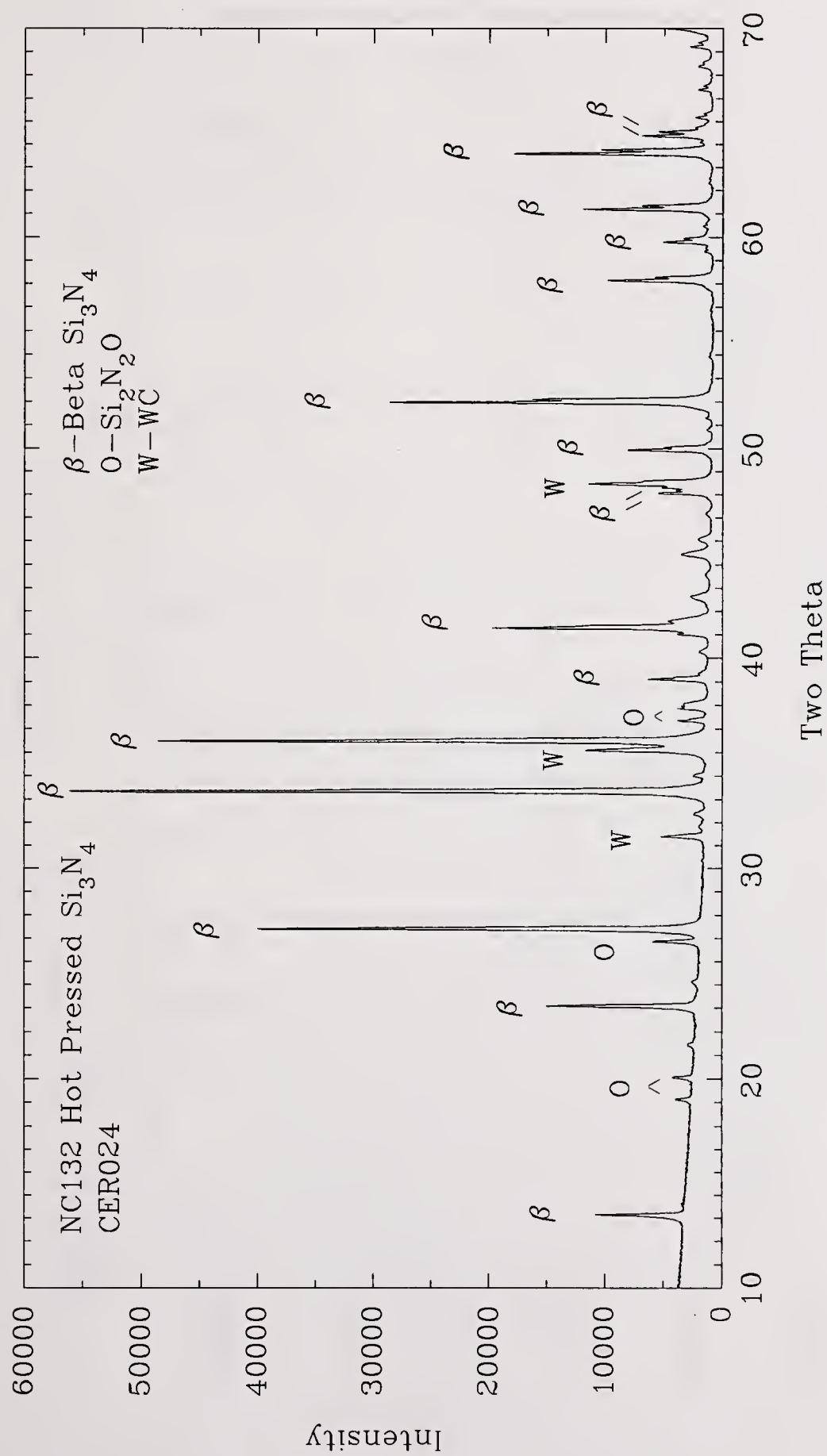


Figure 3.1 X-Ray Diffraction Pattern for NC132 Hot Pressed Si_3N_4

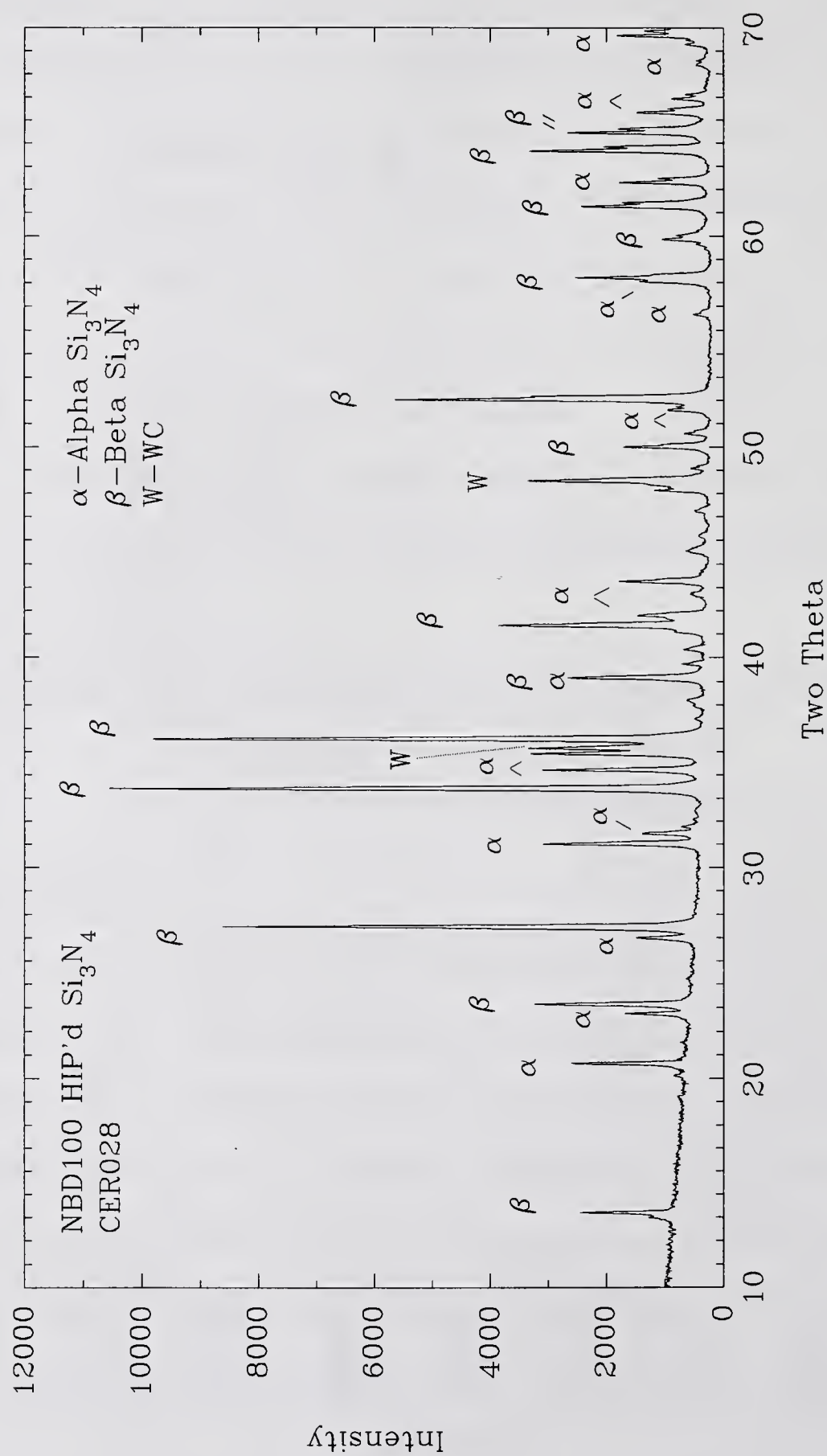


Figure 3.2 X-Ray Diffraction Pattern for NBD100 HIP'd Si_3N_4

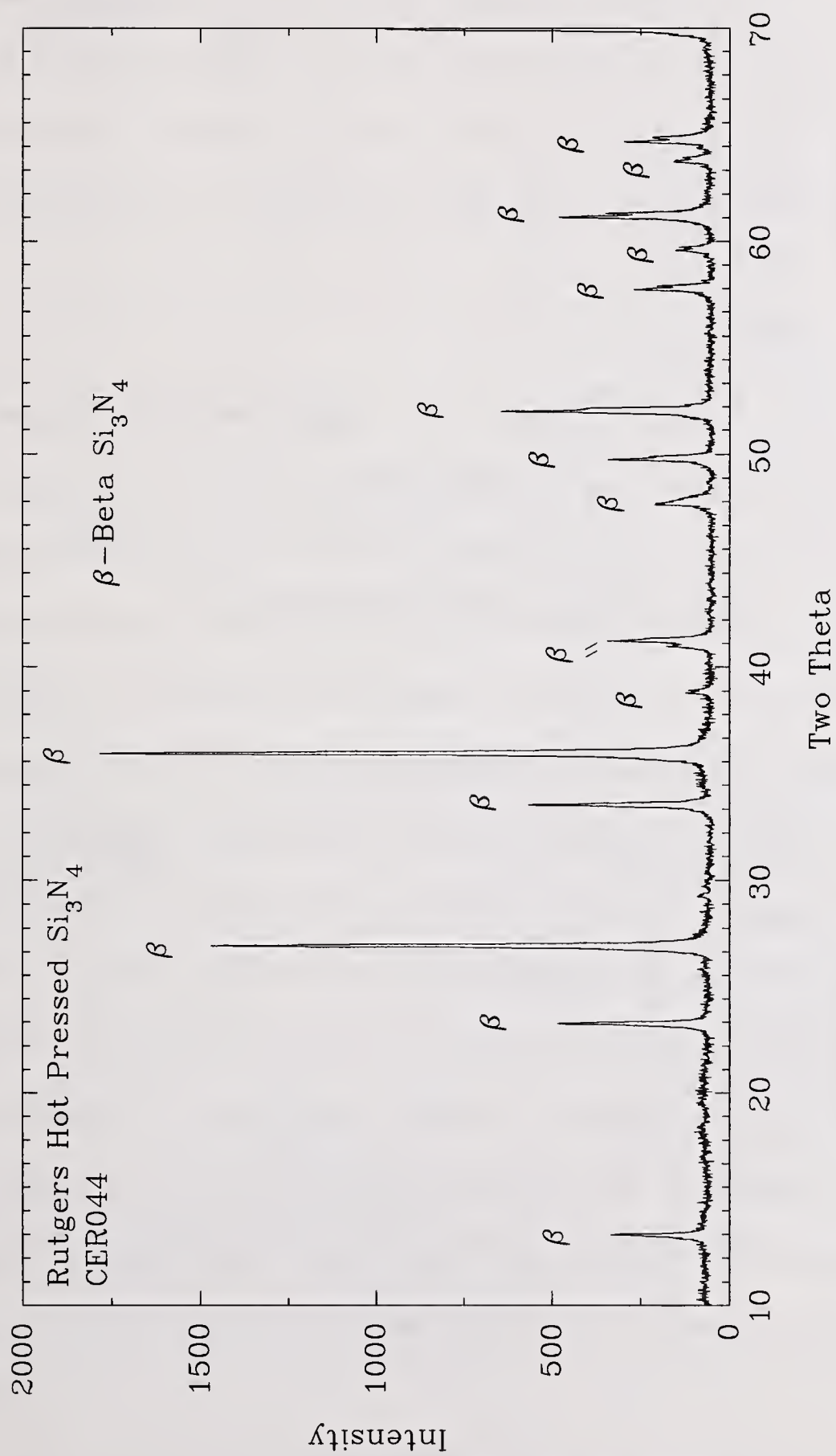


Figure 3.3 X-Ray Diffraction Pattern for Rutgers Hot Pressed Si_3N_4

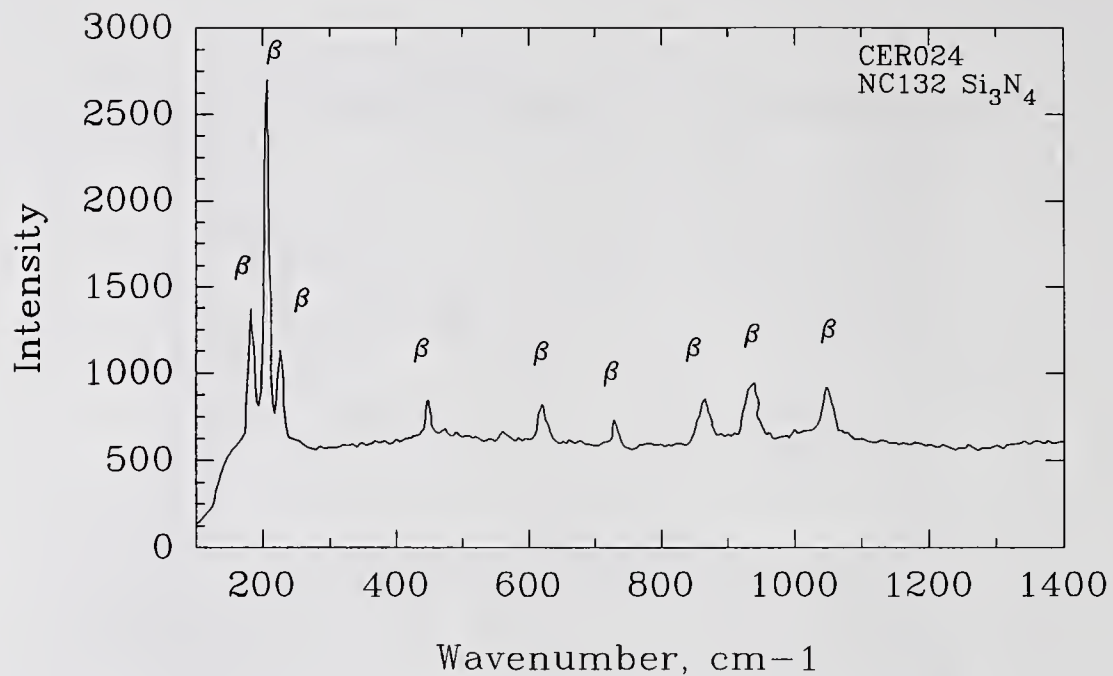


Figure 3.4 Raman Spectrum for NC132 Hot Pressed Si_3N_4

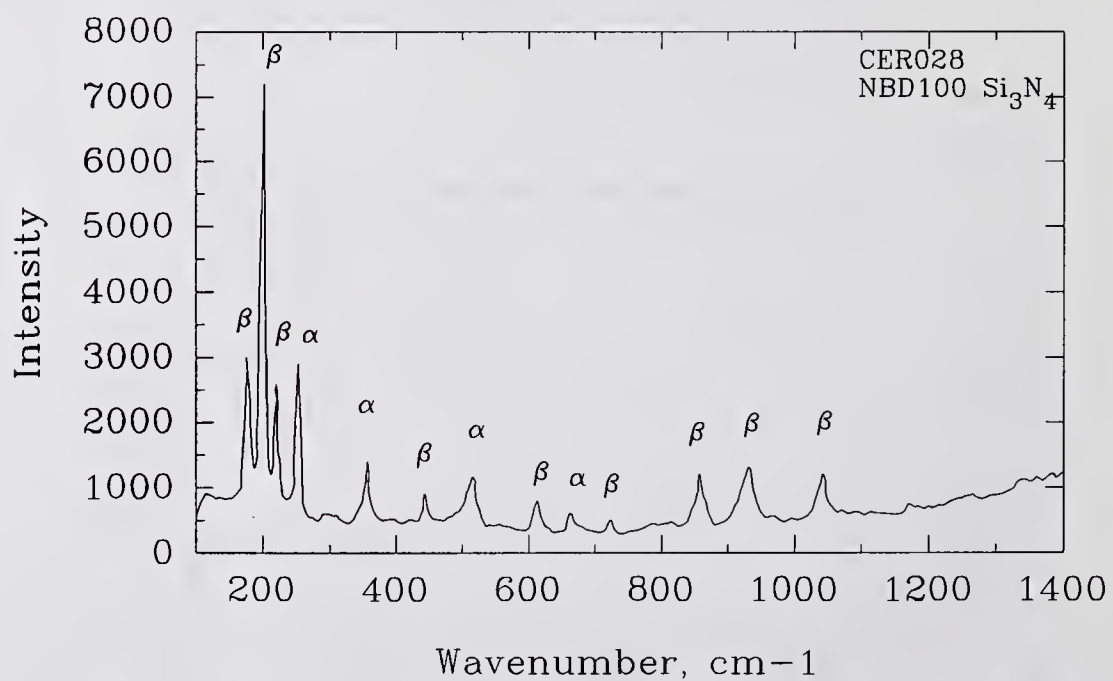


Figure 3.5 Raman Spectrum for NBD100 HIP'd Si_3N_4

observations were consistent with the XRD data.

The samples of Si_3N_4 had a tendency to fluoresce. This made the analysis more difficult, since fluorescence results in an increase in the broad background signal (noise). The fluorescence may be associated with silicon oxide on the surface of Si_3N_4 . This was an early indication that silicon oxide might play an important role in the surface chemistry of Si_3N_4 .

3.1.5. Ceramography and Fractography

The microstructure of the two commercial Si_3N_4 samples used in this study were examined using routine fractographic and ceramographic techniques. Fractography consisted of cutting part way through a sample of the Si_3N_4 , then using a wedge to cause a tensile crack which fractures the specimen into two pieces. Examination of the fracture surface revealed the grain structure since much of the fracture occurred along the weaker grain boundaries of the material. Ceramography consisted of grinding and polishing a flat cross-section of the material and etching it with molten KOH to dissolve away the grain boundaries at the surface. Observation in the SEM revealed the grain size and morphology of the cross-section. KOH is also corrosive to the grain itself, therefore this technique tends to distort the grain edge morphology a bit. In this work, the KOH was heated in a nickel crucible to 400°C and the Si_3N_4 sample was immersed for about 45 seconds. After etching, the sample was treated with concentrated aqua-regia (4 parts HNO_3 :1 part HCl) for 30 seconds to remove Ni hydroxide precipitates that sometimes formed on the surface (from corrosion of the Ni crucible).

The hot pressed Si_3N_4 (CER024) fracture surface (Figure 3.6) exhibited a mixture of broken and whole grains at a variety of orientations. Most of the grains appear to be less than one micron in width and vary in length up to about two or three microns. These elongated grains are consistent with the structure associated with $\beta\text{-Si}_3\text{N}_4$. Some small ($0.1\mu\text{m} - 0.5\mu\text{m}$) equiaxial particles are observed that may be fragment artifacts of the fracture process. The etched cross section of the same material (Figure 3.7) reveals more clearly the elongated grain nature of the sample. The equiaxial-looking grains may actually be sectioned elongated grains that were originally projecting out of the surface. This would be consistent with the x-ray diffraction and Raman data that indicated that the hot pressed sample was pure beta (crystalline) phase Si_3N_4 .

The HIP'd Si_3N_4 (CER028) fracture surface (Figure 3.8) appears similar to the previous sample; however, the dimensions of the fracture planes on each grain appears to be slightly smaller. The etched cross-section (Figure 3.9) reveals some elongated ($\beta\text{-Si}_3\text{N}_4$) grains, but there are fewer than in the hot pressed sample, and they are smaller in size. The abundance of small ($0.1\mu\text{m}-0.5\mu\text{m}$) equiaxial grains is probably partly due to the presence of $\alpha\text{-Si}_3\text{N}_4$ grains in this material (as detected using x-ray diffraction and Raman spectroscopy).

The combination of evidence on these two commercial Si_3N_4 's suggests that these two materials experienced a different temperature and/or time history during their sintering. Both materials started with the same $\alpha\text{-Si}_3\text{N}_4$ powder and sintering aids. The hot-pressed material was subjected to high temperature during pressing that resulted in complete conversion of the $\alpha\text{-Si}_3\text{N}_4$ to $\beta\text{-Si}_3\text{N}_4$ and relatively large grains (growth of larger grains occurs at the expense of smaller grains during sintering). The HIP'd material was probably subjected to higher

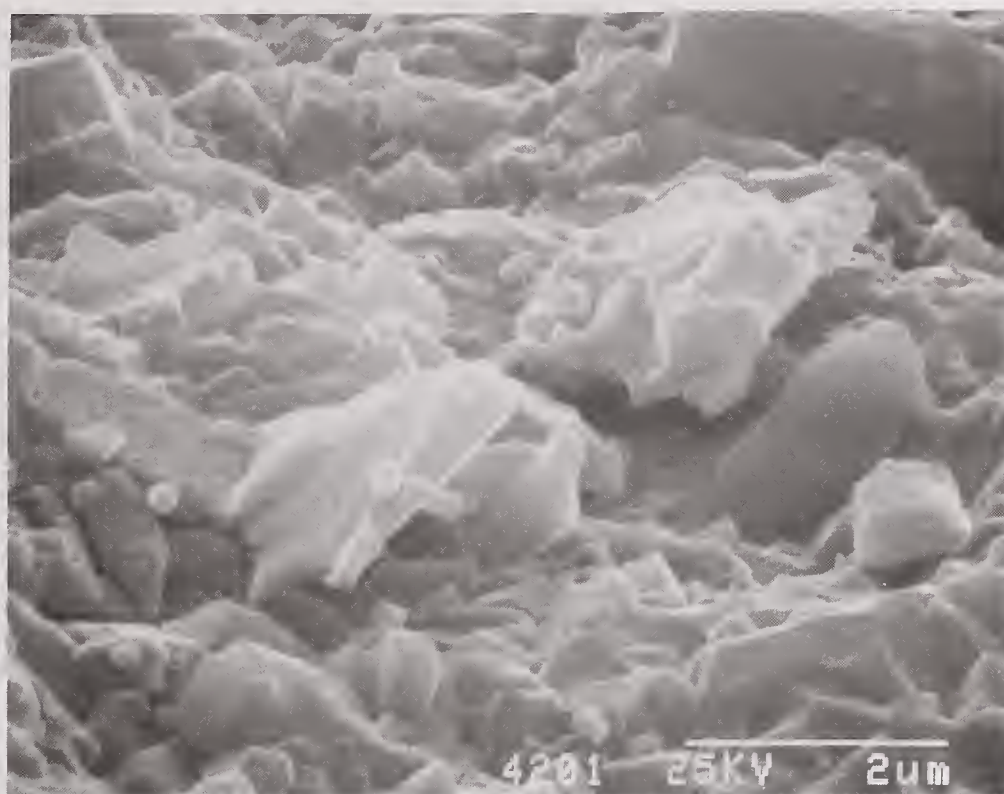


Figure 3.6 SEM Photomicrograph of NC132 Hot Pressed Si₃N₄ Fracture Surface

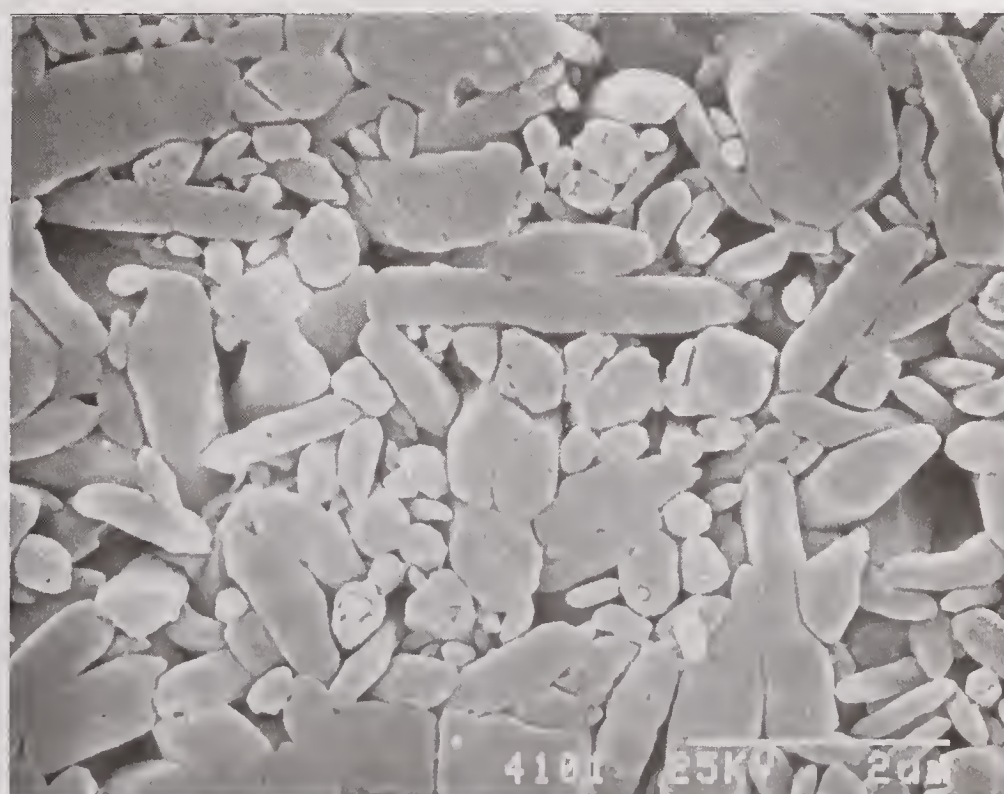


Figure 3.7 SEM Photomicrograph of NC132 Hot Pressed Si₃N₄ Polished/Etched Surface

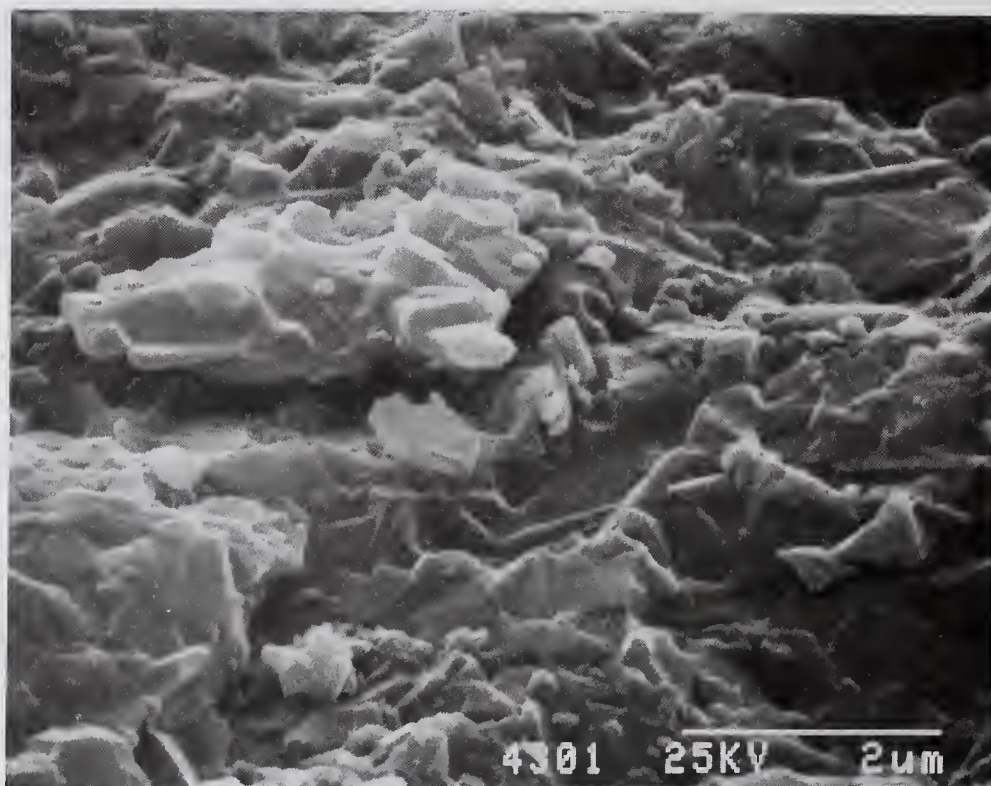


Figure 3.8 SEM Photomicrograph of NBD100 HIP'd Si₃N₄ Fracture Surface

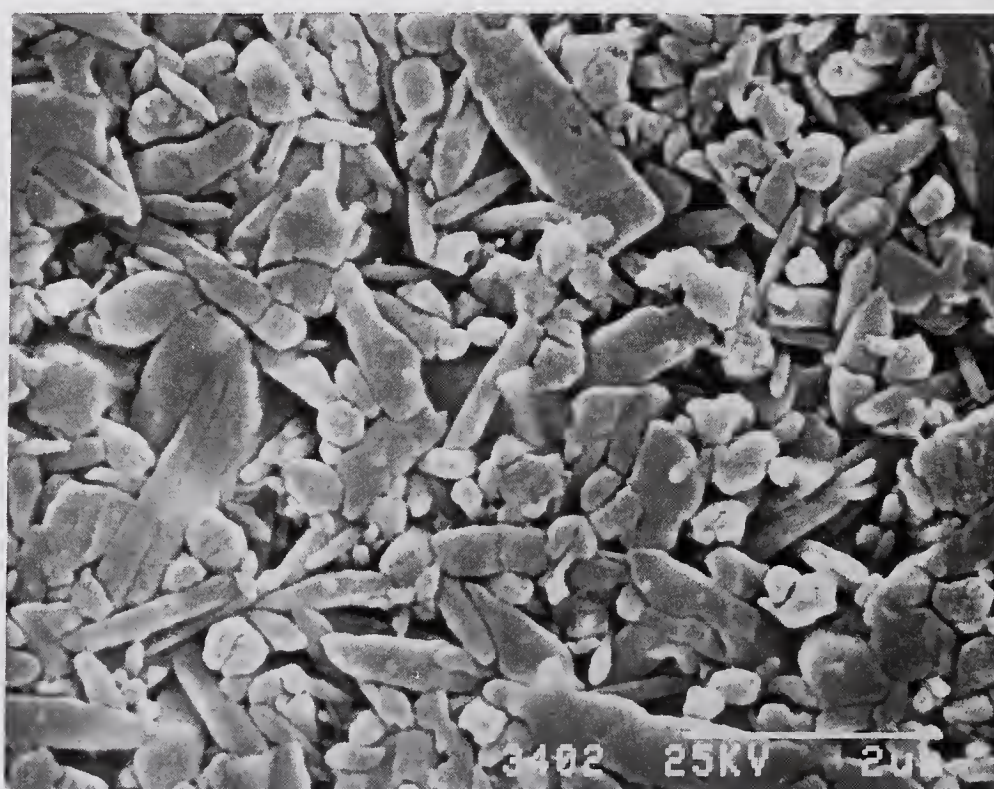


Figure 3.9 SEM Photomicrograph of NBD100 HIP'd Si₃N₄ Polished/Etched Surface

pressure and lower temperatures or shorter sintering times. This resulted in incomplete conversion from α to β and less grain growth. This difference in microstructure may affect macroscopic properties relevant to the tribological behavior of these materials.

3.1.6. ESCA and Auger Analysis

Two surface analytical techniques were employed to determine the composition and structure of the surface of the Si_3N_4 samples. Electron Spectroscopy for Chemical Analysis (ESCA, also known as X-ray Photoelectron Spectroscopy or XPS) was used to determine the near surface composition and structure. Auger analysis was used to determine the composition as a function of depth into the surface. Both analysis were performed at the University of Dayton Research Institute and the data were interpreted by Dr. Pu-sen Wang of the ceramics division at NIST.

ESCA analysis was performed on the polished surface of Si_3N_4 flats. The depth of analysis was estimated at 10 nm (100 Å). The analysis results from NC132 and NBD100 were identical, therefore only one data set is presented. The survey scan for the NC132 sample is shown in Figure 3.10. The main constituents observed are silicon, oxygen and nitrogen. The carbon signal is of a characteristic impurity strength and can be considered as insignificant. The O 1s scan (Figure 3.11) indicates a strong oxygen signal usually associated with SiO_2 . The Si 2p peaks were not used because the Si-O and Si-N peaks differ by only 0.7 eV and overlap too much as demonstrated by Wang.²⁵⁸ The Si KLL scan, however, (Figure 3.12) indicates two types of bonding with silicon, one associated with the Si-N bond in Si_3N_4 , and another associated with the Si-O bond in silicon oxides. The

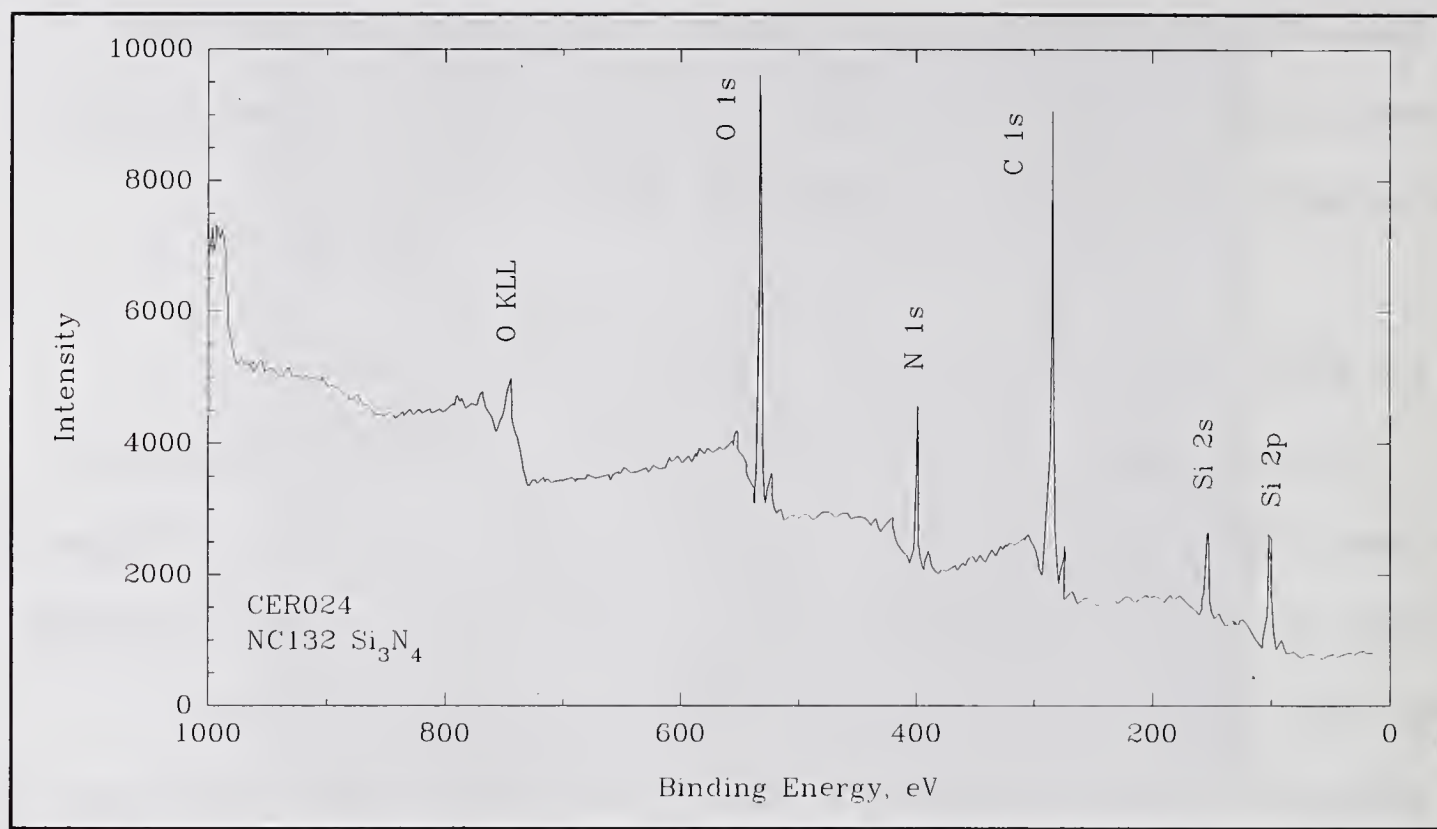


Figure 3.10 ESCA Survey Scan of Si_3N_4 Surface

nitrogen 1s scan (Figure 3.13) consisted mainly of a large peak at 397.3 eV, a peak associated with Si_3N_4 . There is also a small peak appearing as a shoulder to the larger peak that is may due to $\text{Si}_2\text{N}_2\text{O}$. The suggested compounds represented by the data are therefore Si_3N_4 , SiO_2 , and possibly $\text{Si}_2\text{N}_2\text{O}$. Sputtering the surface (removal of the outer layers) resulted in a decrease in the O signal, and an increase in both silicon and nitrogen. This indicates that

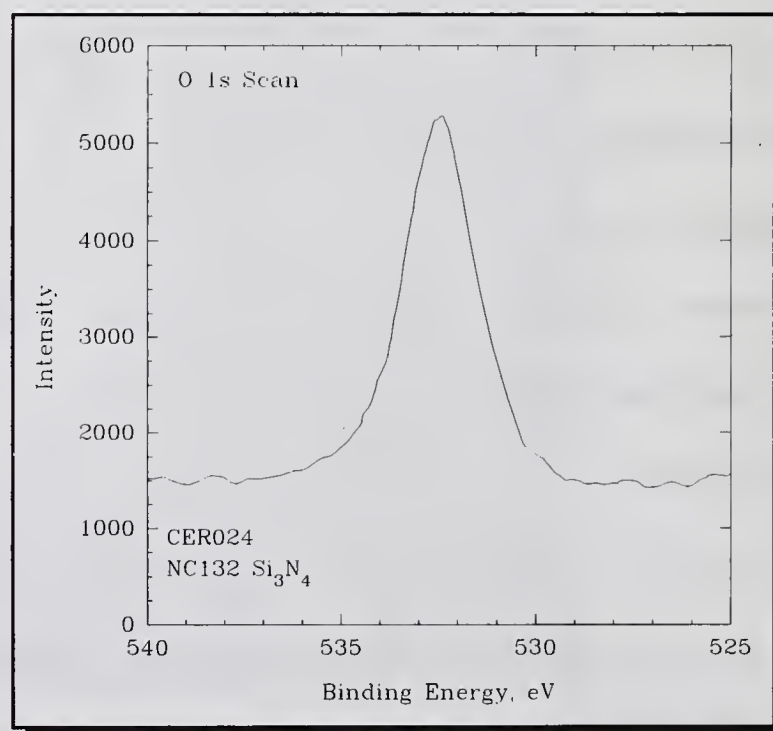


Figure 3.11 ESCA O 1s Scan for Si_3N_4 Surface

the oxygen is concentrated at the surface.

Auger depth profiling was performed to understand the variation in composition with depth into the surface. The sampling depth for any single scan of the surface was on the order of 10 nm (100 Å). The results are shown in Figure 3.14. The Auger data confirm a higher concentration for oxygen on the surface (12%) versus the bulk (3%).

The 3% bulk figure is in good agreement with the commercial data on bulk Si_3N_4 . There is a carbon contaminant on the surface which is quickly sputtered off, but since carbon is also an artifact of the analysis technique interpretation of the carbon concentration should be strictly qualitative. One of the most striking features in the depth profile is the crossover of Si and N with depth. Silicon is in higher relative abundance on the surface, but lower relative

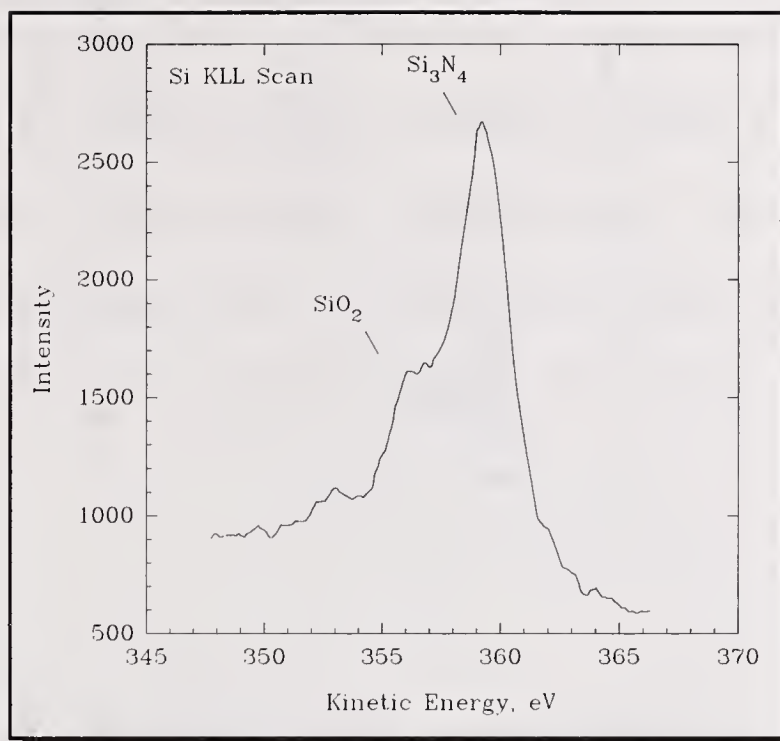


Figure 3.12 ESCA Si KLL Scan for Si_3N_4 Surface

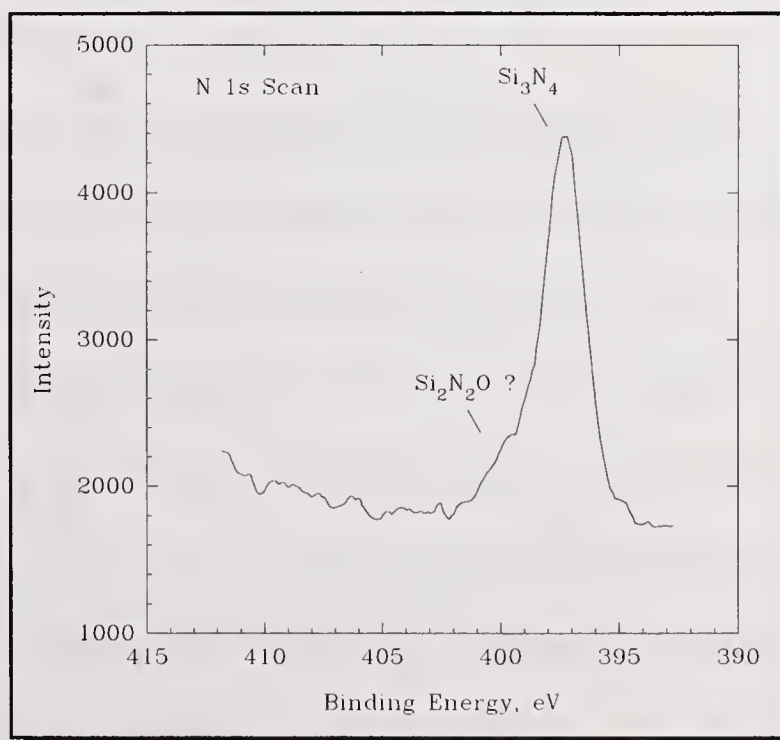
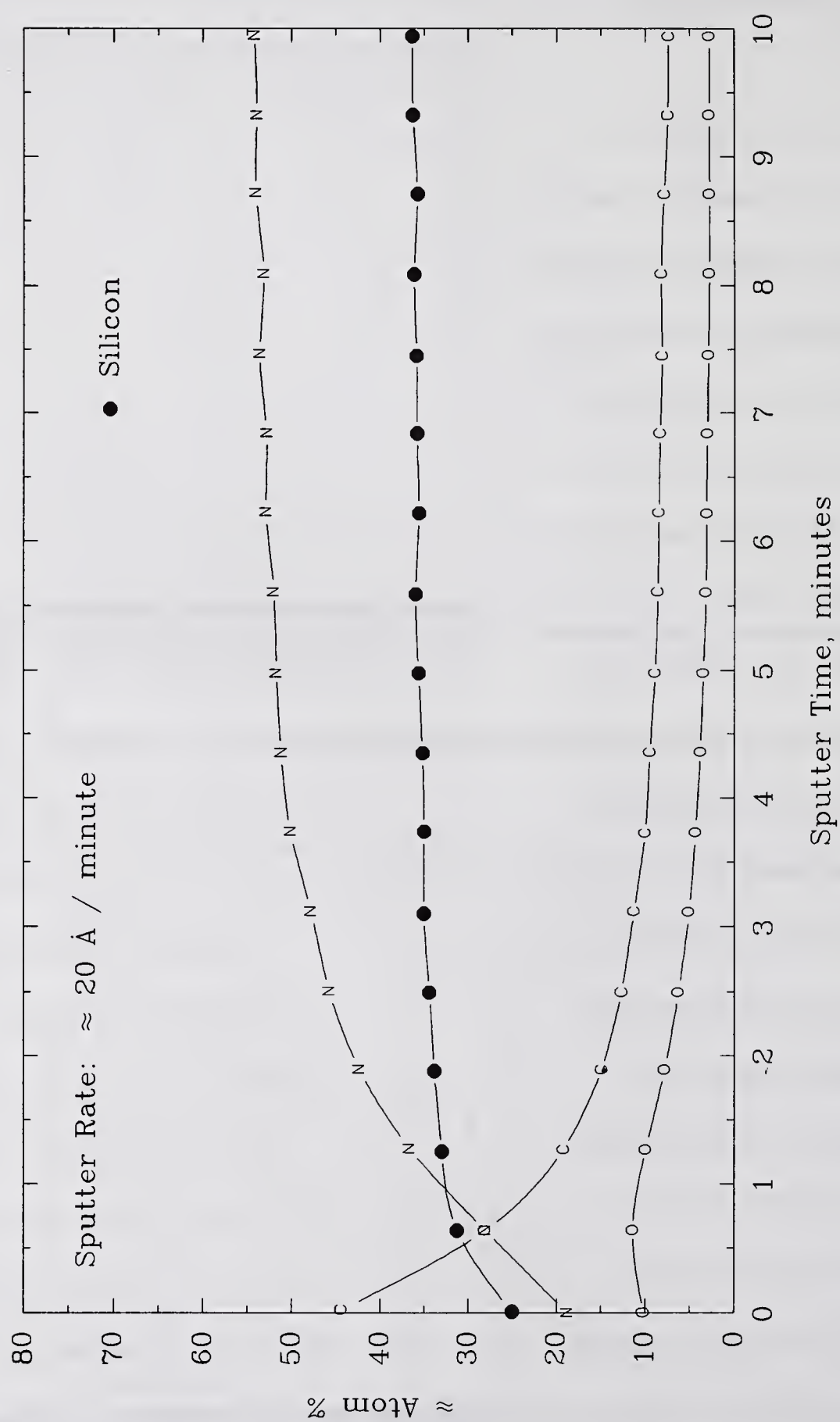


Figure 3.13 ESCA N 1s Scan for Si_3N_4 Surface

Figure 3.14 Auger Depth Profile for Si_3N_4 Surface

abundance deeper into the sample. According to the stoichiometry of Si_3N_4 , silicon should always be in lower relative abundance than nitrogen. There must be another species present in which the ratio of Si:N is greater than 1 (i.e. a silicon containing compound with little or no Nitrogen). $\text{Si}_2\text{N}_2\text{O}$ does not have the required ratio (but they are certainly closer). SiO_2 essentially has no nitrogens, and hence could explain the data. It would therefore appear that there is a SiO_2 rich layer on the surface of Si_3N_4 . The depth of this layer is estimated to be on the order of 6 nm (60 Å).

3.1.7. A Surface Model for Si_3N_4

Other researchers have looked at the surface of Si_3N_4 to find oxygen containing species. Raider²⁰⁴ used ESCA to find an oxynitride surface layer on Si_3N_4 thin films. Goto¹⁰⁰ found similar results on amorphous Si_3N_4 -C composite thin films using both ESCA and Auger. Rahaman²⁰³ used ESCA to look at the surface of powders, discovering an amorphous oxygen-rich surface layer 3-5 nm thick.

The analytical evidence is very clear in suggesting that the surface of Si_3N_4 is very rich in oxygen. The ratios of Si:O:N as a function of depth suggest that we may be looking at a high surface concentration of SiO_2 , with a decreasing concentration gradient into the surface such as depicted in Figure 3.15. The surface depicted in Figure 3.15 also suggests that there may be an intermediate silicon oxynitride layer. The bulk oxygen concentration of 3% suggests that there will still be oxygen containing species in the bulk, but they will be in minor concentration, and probably concentrated as glassy phases (grain boundaries) between Si_3N_4 crystallites along with other sintering aid metals (Mg, Al) and impurities.

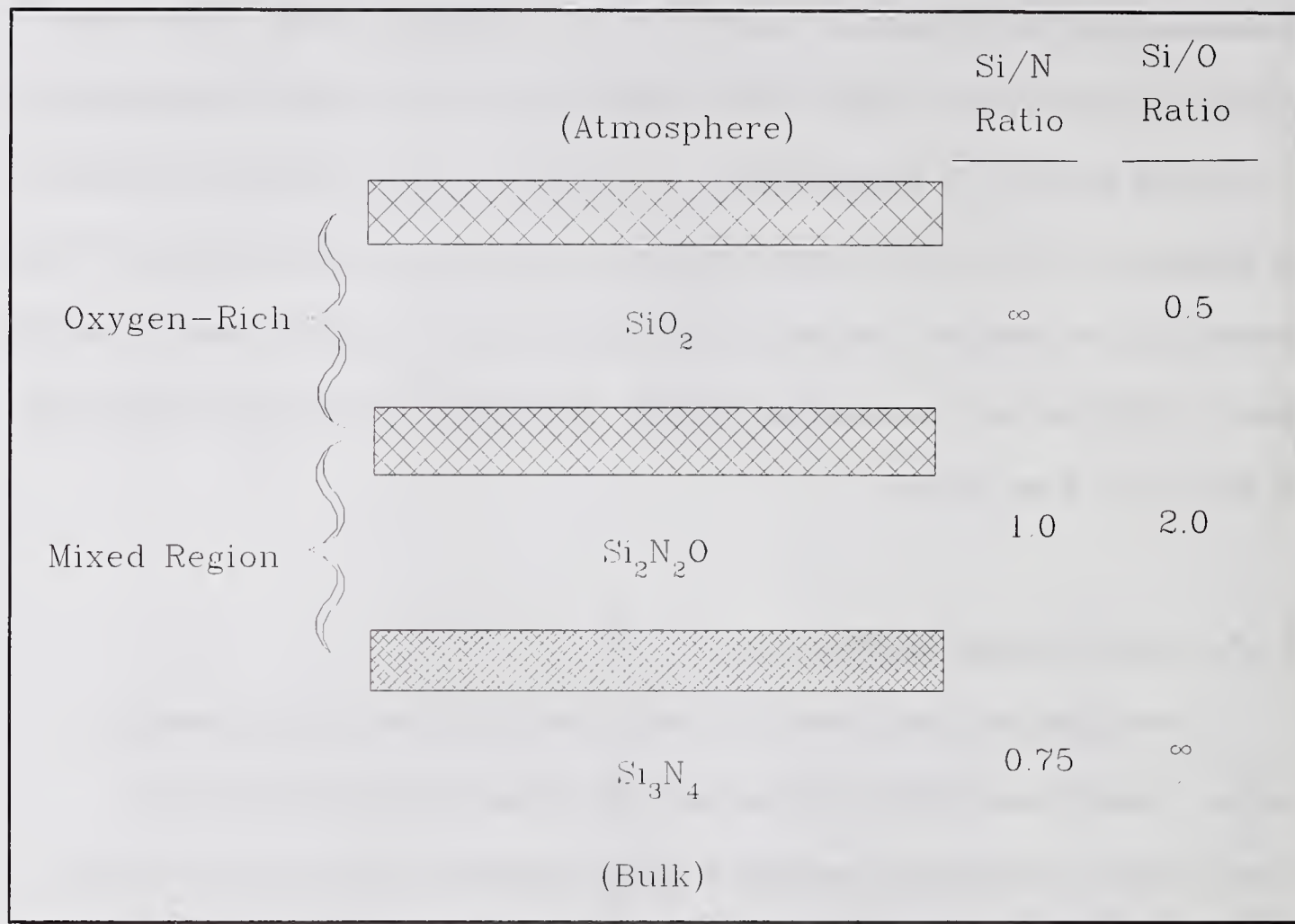


Figure 3.15 Surface Model for Silicon Nitride

Since we are primarily concerned with chemical reactions on the surface of Si_3N_4 , the chemical structure of the outer layer is important. If it is indeed a stable oxide of silicon, much like the stable "native" oxide layer that forms on silicon, it will have the chemical properties of the stable oxide. Fortunately, the surface chemistry of silica is well understood. In fact, it is a very well characterized material because silica and its related compounds (i.e. silicon wafers etc.) are so widely used. It can be found in a wide variety of applications from optics to semiconductors.

The basic structure of silica consists of silicon and oxygen in a ratio of one silicon for every two oxygens. Silicon has a tetrahedral bond structure with four bonds per atom.

Oxygen forms two bonds per atom. The bulk structure can vary from amorphous to crystalline (Figure 3.16). Among the crystalline forms, there are several primary phases such as quartz, tridymite, and cristobalite, however there are many other phases that have been described such as keatite, coesite, and stishovite, to name a few.

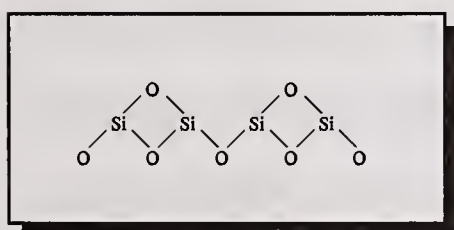
However, the chemical surface structure of both amorphous and crystalline silica is similar. They are considered to consist of three basic components:

- 1) silicon oxides
- 2) silicon hydroxides
- 3) adsorbed water

Silicon oxides are the highest temperature surface form found on

silica. The basic structure is depicted in the small figure below. Each silicon is bonded to

four different oxygen atoms, and each oxygen atom is bonded to two silicon atoms. Please note that some of the subsurface oxygen atoms bonded to the silicon atoms have been omitted for clarity of presentation.



In the presence of water, the silica surface is easily hydroxylated to give a silicon hydroxide surface structure.

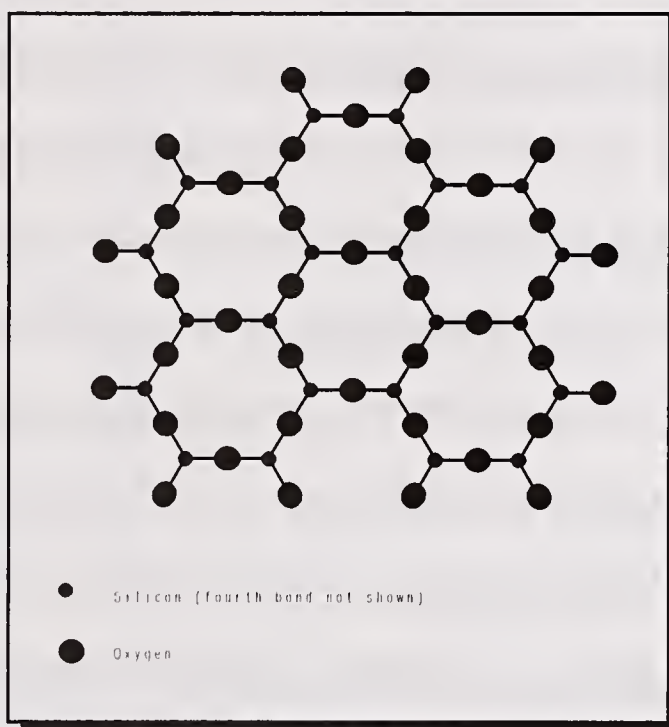
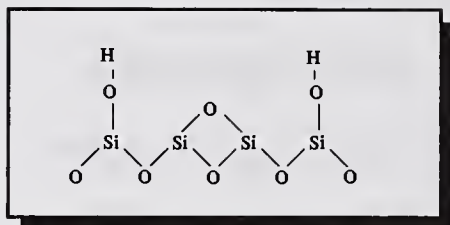


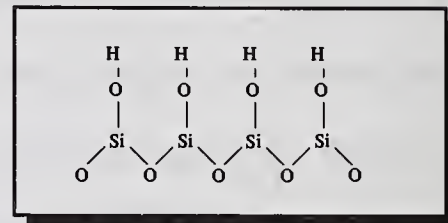
Figure 3.16 Structure of Crystalline Silica



A silicon hydroxide is also termed a silanol - as in a silicon alcohol. The structure to the left depicts the partial hydroxylation of the silica surface. When enough water is present, the surface of silica

can become fully hydroxylated as shown to the right.

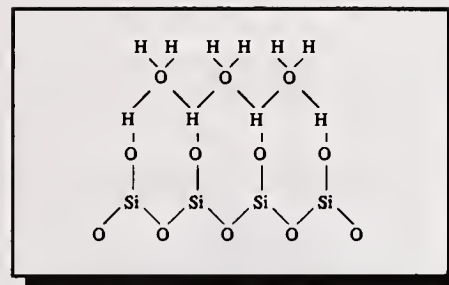
There is usually one surface hydroxide per surface silicon, but mixtures of surface oxide and hydroxide are possible. There



has been some debate about the existence of silicon surface atoms with two hydroxides (geminal hydroxides) however this postulated structure is generally discounted¹³⁸. It should be noted however, that free (non-surface) chemical structures containing two, three, and even four hydroxides are found. The special case of four hydroxides per silicon is called "silicic acid monomer." It is termed a "monomer" because of the tendency of the Si-OH groups from different molecules to combine into longer chains (polymers), gels, and particles. Since the surface of silica is easily hydroxylated, the tendency of silicon hydroxides to "condense" may explain some of the high adhesion tendencies of glasses⁴¹.

In the case of a mixed surface which contains both silicon oxide and silicon hydroxide, the relative location of the hydroxides makes a difference in the adsorption and reaction mechanisms for the surface. The term "vicinal" hydroxides describes hydroxides that are nearest neighbors. A silicon hydroxide without any other nearby hydroxide is termed an "isolated" hydroxide. Silicon hydroxides are also known as silanol groups. These different silanol groups (isolated versus vicinal) have different chemical reactivities.

Silanol groups can hydrogen bond with water molecules. A fully hydroxylated silica surface will easily adsorb water as depicted to the right. In fact, high surface area hydroxylated silica (silica gel) is used as a water adsorbent to remove water from



the atmosphere of closed containers with water sensitive contents.

The exact form of surface silica described above is a function of thermodynamic favorability, which is governed mainly by temperature. The relationship between temperature and the surface forms of silica are illustrated in Figure 3.17. At low temperature, adsorbed water on silanol groups are found. As the temperature is raised above the boiling point of water (373°K or 100°C), water desorbs, and the surface is fully hydroxylated silica. As the temperature is raised, vicinal surface silanol groups condense to give a silicon oxide surface with bridging oxygens. This structure is also termed a siloxane. Water is a byproduct of the condensation of vicinal silanol groups and leaves as a gas. This occurs from 100°C (373°K) to 200°C (473°K). Some of the hydroxyl groups are stranded as isolated silanols and remain stable to temperatures up to 400°C (673°K). Above this temperature, diffusion of silanol groups becomes possible, with the result that the isolated silanol groups find and condense with other isolated silanol groups, and the surface becomes a complete oxide.

The two basic forms of silica described above (siloxane and silicon hydroxide or silanol) constitute two of the main hypothesized reactants on the surface of Si_3N_4 . Many of the analytical procedures used to study the boundary lubrication of Si_3N_4 were developed

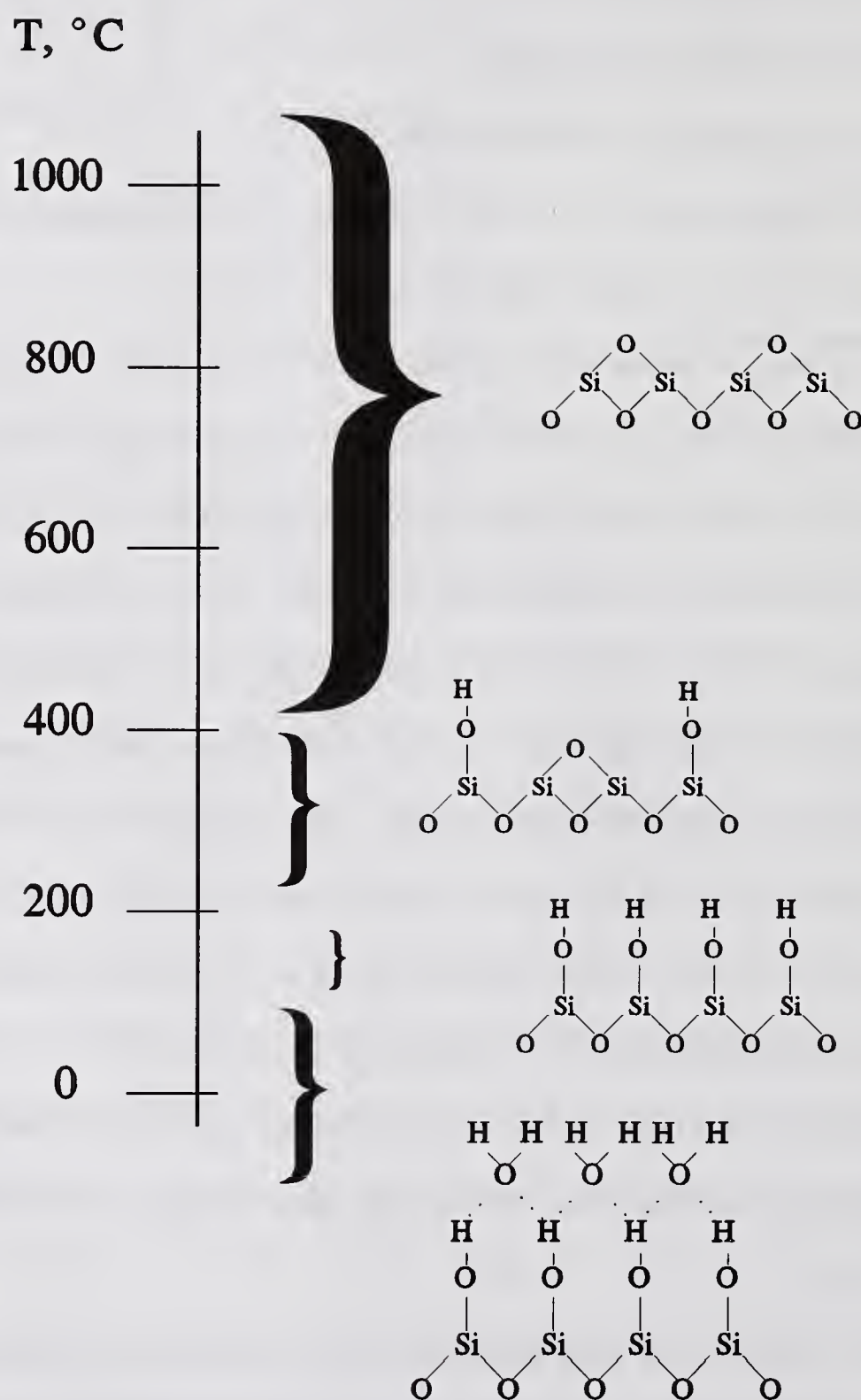


Figure 3.17 Different States of Silica as a Function of Temperature

with this surface model in mind.

3.2. Si_3N_4 Powders

Si_3N_4 powders were used to study the reactions between selected chemistries and Si_3N_4 surfaces in an observable and controlled way. One of the biggest problems in studying surface reactivity is the limitation on the quantity of reaction product available, which is usually a function of the surface area available for reaction. Because of this, most of the powders used had high surface areas. Another concern with studying the reactivity of Si_3N_4 in this way was the possible interference by minor impurities in the samples. As a result, only very high purity powders were used.

The Si_3N_4 powder used for studying surface reactivity was a commercially available powder manufactured by the Hermann C. Stark Company, and known as LC 12-N. The chemical composition of this powder is given in Table 3.4.

This powder has extremely low concentrations of iron (and other metal) impurities. The only contaminant found in any appreciable quantity is oxygen, which is found on the surface of all Si_3N_4 materials in much the same way as silicon has a "native" oxide layer. This powder is composed of 0.44 μm sized particles of 96.2% $\alpha\text{-Si}_3\text{N}_4$. The surface area of this powder is 18.3 m^2/g . This surface area is substantially higher than the surface areas

Table 3.4
Chemical Composition of
Stark LC 12-N Si_3N_4

Trace Element	%
N	38.71
O	1.58
C	0.15
Al	0.04
Ca	0.006
Fe	0.006

Source: Manufacturers Data

for other Si_3N_4 powders ($\approx 3 \text{ m}^2/\text{g}$) and is the principal reason that this powder was selected for chemical reactivity studies.

The powder reactivity study was intended to investigate the surface reactivity of Si_3N_4 . There are also potential surface reactivities due to sintering aids and contaminants that may play a role in the monolithic finished material that are not accounted for with the use of these high purity powders. The investigation of such effects is beyond the scope of this study.

3.3. Model Chemical Compounds

Model chemical compounds were obtained in as pure a form as possible and tested as received. The purity varied from compound to compound; however, most compounds were better than 98% pure. A few lubricant additives were supplied in diluent oils. In this study, only the global effects are observed. The purification and identification of specific active ingredients in some cases is beyond the scope of this study.

The compounds were selected based on bond energies for silicon compounds, silicon chemistry, and additive literature. In general, mixtures of compounds were avoided because of the possibility of synergistic or antagonistic interactions. No attempt was made to correct for inequalities in absolute concentration of compounds (due to its concentration in the commercial product) because the focus of this study was to detect gross effects.

The base oil used in this study was a $2.7 \times 10^{-5} \text{ m}^2/\text{s}$ (27 Cst) (@ 37.7°C or 100°F) paraffinic oil purified by percolating it through 200 mesh activated alumina. This resulted in a purified paraffin oil (PPO) free of polar impurities that might affect the wear results.

Chapter 4

EXPERIMENTAL APPARATUS AND OPERATING CONDITIONS

4.1. Dynamic Tests

The criteria used to evaluate the boundary lubrication effectiveness of various chemistries are friction and wear characteristics of the chemical compounds. Two different devices were used to measure the friction and wear properties of the different Si_3N_4 /lubricant combinations. The majority of the testing was performed using a ball-on-three-flat (BTF) modification of a four-ball (FB) wear tester. Special tests were also conducted on a pin-on-disc (POD) tester, and a new experimental two-ball collision tester. Consistency of results was ensured by developing and using specific procedures for the preparation and cleaning of specimens, operational procedures, and measurement of friction and wear.

4.1.1. Wear Tester

Most of the initial screening wear tests were conducted using a BTF tester. This equipment, manufactured by the Roxana Machine Works is an adaptation of the standard "Shell/GE/Brown" four-ball wear tester and allows for friction and wear testing of material/lubricant combinations in the boundary lubrication regime. A schematic of the general apparatus is shown in Figure 4.1, and demonstrates the salient features of this device including:

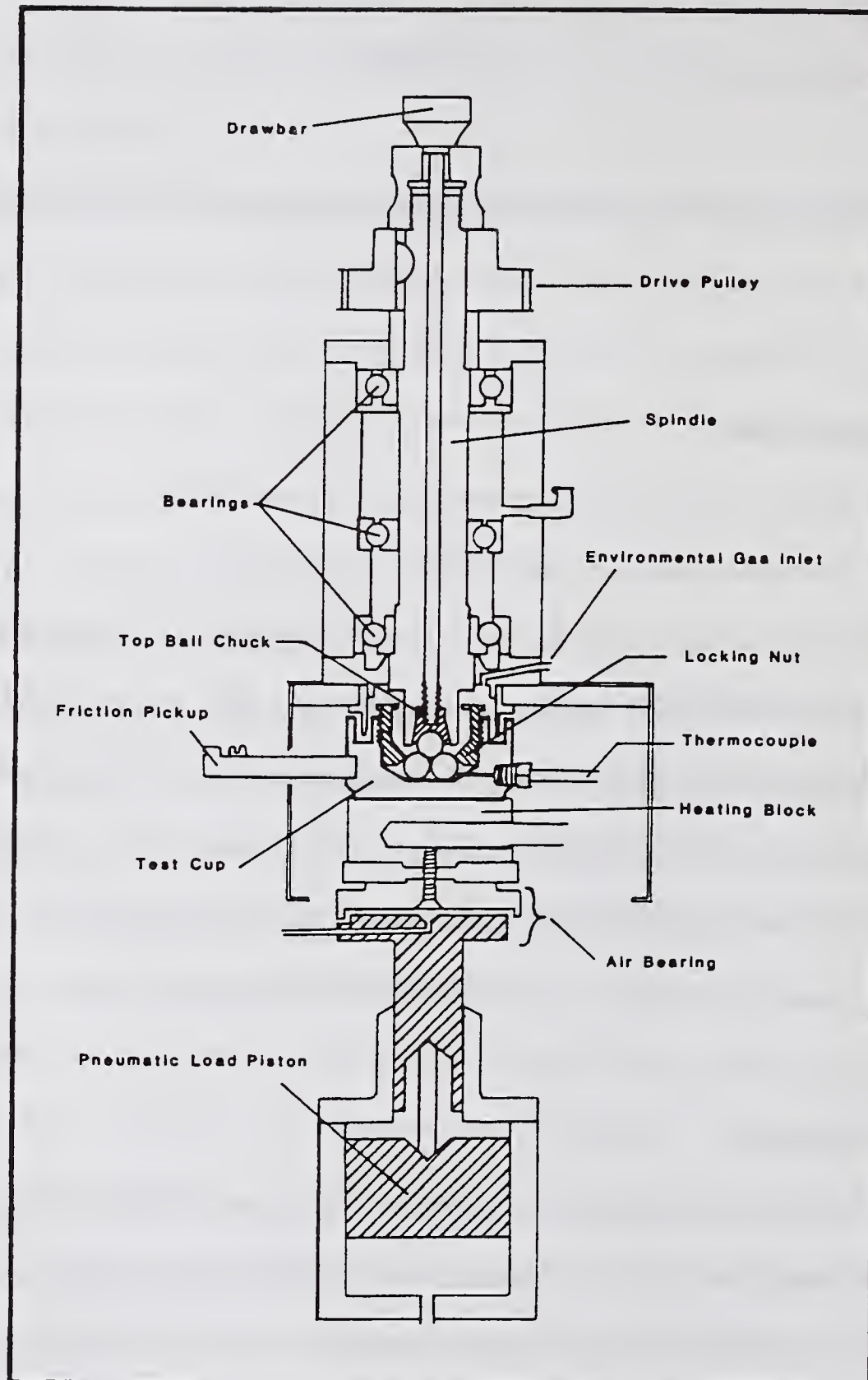


Figure 4.1 NIST-Modified Four-Ball Apparatus Design

- Pneumatic loading for infinitely adjustable loads
- Air bearing for more accurate friction measurement
- Heater block for controlled temperatures
- Test cups for either FB or BTF configuration
- Gas inlet for atmosphere control
- Drive spindle connected to variable speed motor

The geometry of the four-ball and ball-on-three-flat are similar and consist of a tetrahedral arrangement (see Figure 4.2) in which a ball is nested on top of a set of three specimens (either spheres or flats, locked in place). A load is applied axially, and the upper specimen rotates to provide sliding at the three contact points. The main difference between the two wear test configurations is that the FB contact is convex on convex while the BTF is convex on flat. This has some influence on the test severity at the beginning of the test. Hertzian elastic contact analysis on the two contact geometries showed that the contact pressures for the FB arrangement are 59% higher than the BTF for the same applied load (see appendices A and B). The BTF configuration has several advantages including less lubricant required (1.5 ml vs 10 ml), easier to optically measure the wear scars because the surface is flat, and post-test handling and analysis is much easier because the wear scar is centered on the flat and the flat is easy to mount on any flat surface. Both configurations use 12.7 mm (0.5 inch) diameter (minimum grade 25) balls, but the FB test requires four of them, while the BTF test only needs one. The BTF test additionally requires 6.35 mm (0.25 inch) diameter,

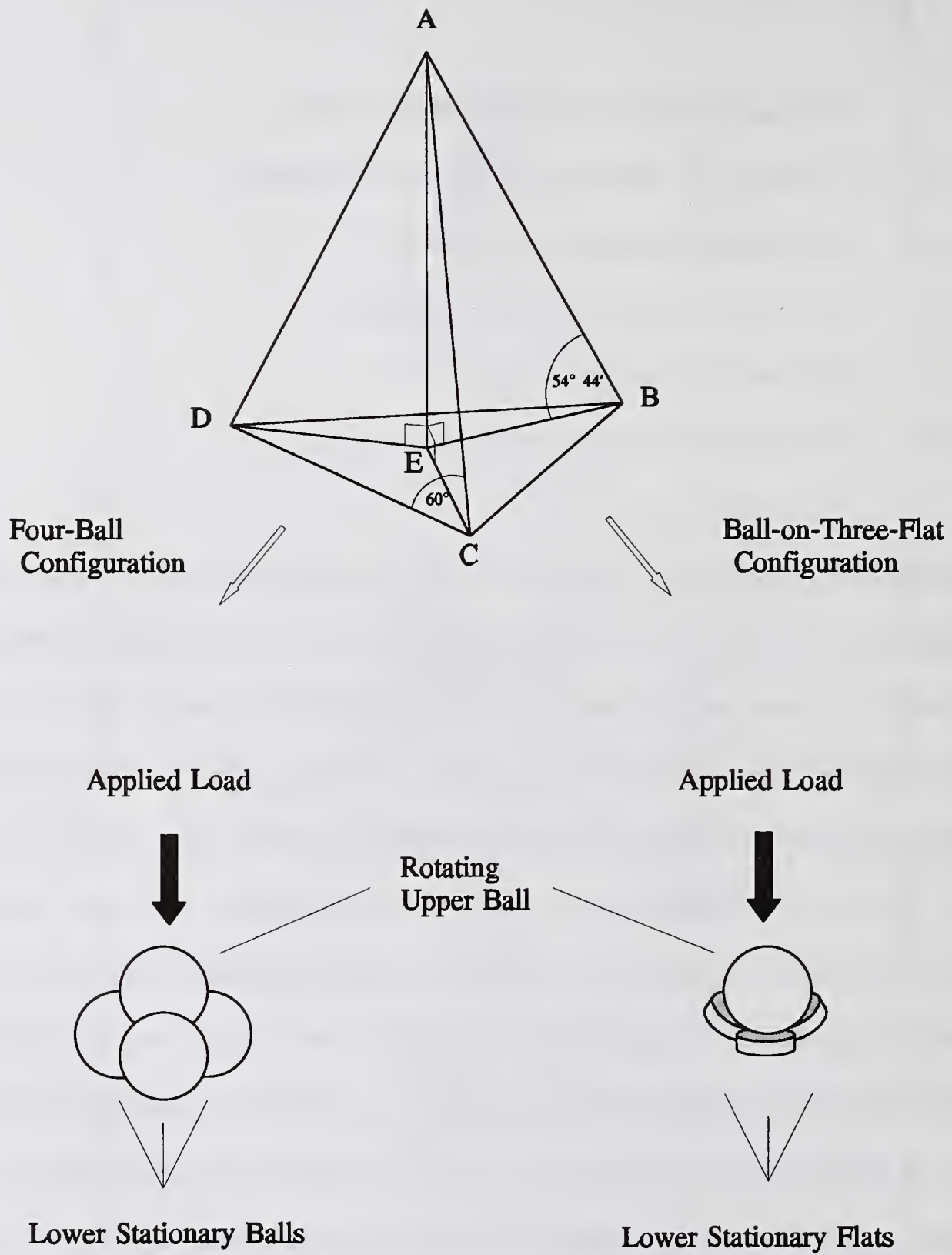


Figure 4.2 Four-Ball and Ball-on-Three-Flat Contact Geometries

1.59 mm (1/16 inch) thick flats which are polished on one side. A second type of wear tester known as the pin-on-disc (POD) wear tester was used for some of the wear tests on low iron impurity Si_3N_4 from Rutgers University. It was used due to the difficulty in fabricating bearing quality balls from experimental materials. The contact geometry for this tester is shown in Figure 4.3 and consists of a hemispherically tipped pin riding on a rotating flat disc. The contact geometry for this apparatus is similar to BTF in that it is convex on flat; however, in the case of the POD there is only a single point contact instead of three point contacts. The radius of the point of contact with respect to the center of rotation of the lower specimen is adjustable which allows for several wear tracks per flat disc. In addition, since the pin is inclined, it can be rotated between

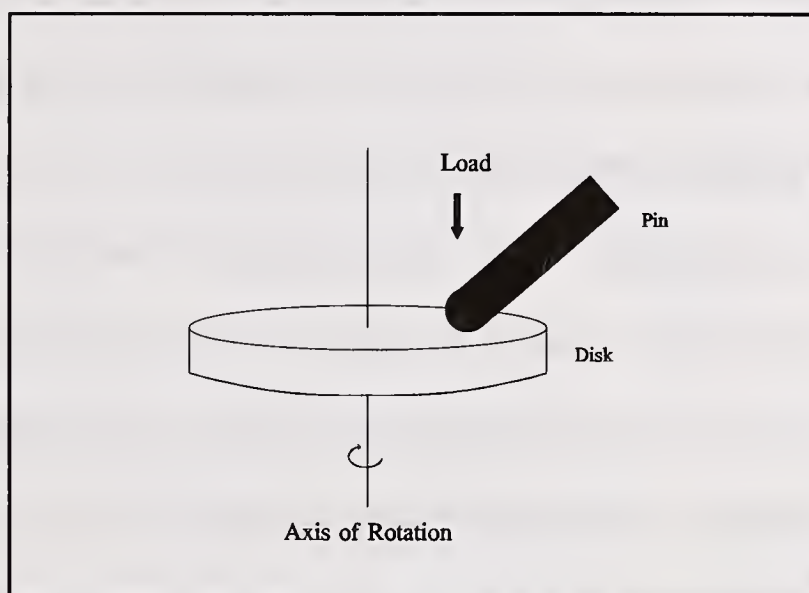


Figure 4.3 Pin-On-Disk Test

tests to allow for several tests per specimen. The ability to get several tests from a single set of specimens is very desirable since we are limited in our ability to generate large numbers of specimens. The POD apparatus was chosen for several reasons.

- i) The test geometry of the contact is exactly the same as the BTF.
- ii) With a slight modification of the loading the POD can give the same load and speed as the BTF conditions used.
- iii) The specimens can be fabricated from experimental materials.
- iv) Several tests can be conducted using a single set of samples avoiding potential differences from variable materials batches.

The POD tester can accommodate a range of pin (and optionally, ball) sizes, and a range of flat discs up to approximately 60 mm (2¼ inch) diameter. The tests described in this study used pins of 6.35 mm (0.25 inch) diameter, \approx 19 mm (0.75 inch) long, with hemispherical 6.35 mm (0.25 inch) tips. The flats were 6.35 mm (0.25 inch) thick and 50.8 mm (2 inch) diameter. Grinding and polishing steps were similar to that used for the BTF flats and resulted in mirror finishes on the specimens. Since the curvature of the pin in POD tests is greater than that of the similar geometry BTF test, a specific normal load will result in much higher Hertzian contact stresses at the beginning of the test. The derivation of the contact stresses as a function of load for the POD apparatus is supplied in appendix C along with calculated contact diameters and pressures.

The second wear test configuration used, the 2-ball collision tester, is a new experimental apparatus designed and developed by Ying and Hsu²⁶⁷ to study films on wearing surfaces. This device uses two 3.2 mm (1/8 inch) diameter balls to simulate single and multiple contacts between surface projections (such as asperities). Using this device it is possible to study the fundamental properties of films reacted onto surfaces. The speed, load and materials can all be varied to obtain data under a variety of conditions. All 2-ball collision tests were conducted with the help of Tsi-Neng Ying.

4.1.2. Specimen Preparation

Some of the specimens used for testing were purchased commercially and used without further modification. Balls were obtained from Norton Company in both 12.7 mm (0.5 inch) diameter (for BTF tests) and 3.2 mm (1/8 inch) diameter (for 2-ball collision tests)

with a uniformity of 0.000127 mm (0.000005 inch or grade 5). The rest of the specimens required some kind of fabrication and surface finishing before they could be used in wear tests. Flats for the BTF test were fabricated from 6.35 mm (0.25 inch) diameter rod stocks. Flats were sliced from these rods, then surface ground and polished using a combination of diamond grinding, SiC grinding, and diamond polishing. The exact procedure developed for preparing Si_3N_4 flats from rod stock is provided in appendix D. The final diamond polishing resulted in a mirror finish. Three dimensional topographic analysis of the surface using an optical interference technique (Figure 4.4) showed that it had an RMS roughness of approximately 5 nm. Several microscopic "pits" can also be seen. This technique also revealed that the specimen preparation procedure actually produced a slight domed curvature on the "flats." The radius of curvature was over 3 m, therefore this effect was insignificant for hertzian contact stress calculation purposes.

Monolithic Si_3N_4 for the disks and pins for the POD tests were made at Rutgers University by Ajoy Zutshi²⁷⁰. The grinding and polishing steps used to finish these materials into usable specimens was similar to the procedure described in appendix D.

4.1.3. Operating Procedure

All of the wear test procedures consisted of the sequence of specimen cleaning, assembly, application of lubricant, then testing. Specimen pre-treatment is a critical part of any wear testing procedure and was performed just prior to testing. The cleaning procedure used a sequence of solvents: hexane, acetone, detergent in deionized water, and pure deionized water. Ultrasonic agitation was used during each step. The detailed cleaning

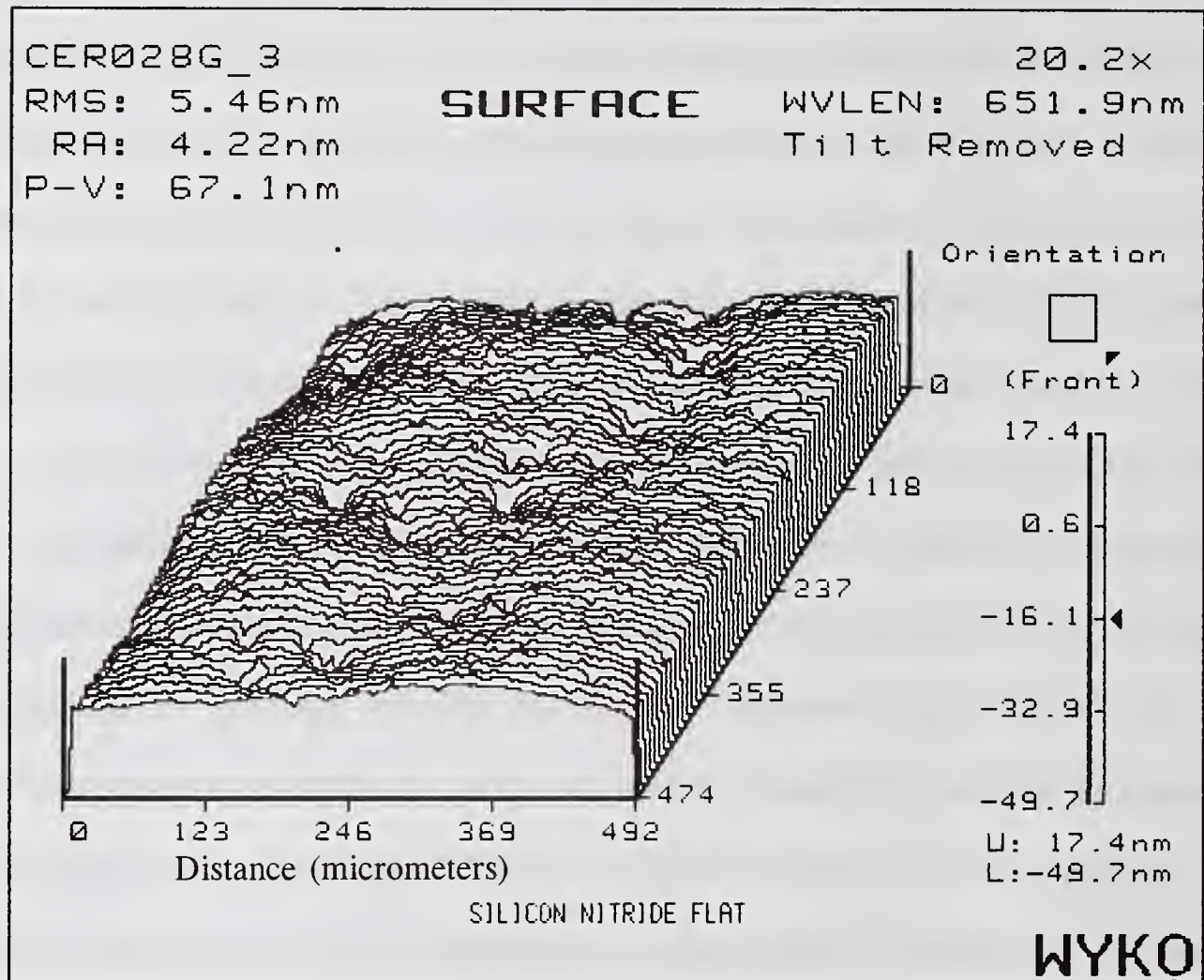


Figure 4.4 Three-Dimensional Surface Analysis of Polished Si_3N_4

procedure is provided in appendix E. The final step in the cleaning procedure was to dry the specimens under nitrogen gas. They were then immediately assembled into the testing apparatus for testing.

When running BTF tests, the following operating procedure was followed. The upper specimen was locked in place in the ball chuck and placed into the spindle assembly. The test cup assembly, with lubricant in place, was put onto the heater block. A load of 1-2 kg was slowly applied to gently bring specimens into contact. The spindle was then rotated by hand to ensure distribution of lubricant over the surface of the top ball and to check alignment and seating of the specimens. The friction force pickup chain was attached to the test cup and the friction and load were both balanced to register zero load and friction. The load was applied and the test began by starting the drive motor. At the end of the test, the drive motor was disengaged and the speed was allowed to decrease under full load until sliding stopped. The load was then removed and the post test analytical procedures were applied.

4.1.4. Friction and Wear Measurement

Friction was continuously measured during all of the tests. Wear scars were measured optically at the end of the test after the excess lubricant had been removed with hexane. The measurement was made on the specimen that was in constant contact during the test. In the case of the BTF tests, wear was measured on the flats. In the case of the POD test, the wear scar on the pin was measured. Wear scar measurement was accomplished using an Olympus stereozoom microscope at 144x magnification and a calibrated graduated eyepiece reticle. Measurements were taken to the nearest 0.004 mm. For all cases,

measurements were taken both parallel to and perpendicular to the direction of sliding. In the case of the BTF test, there were a total of six wear scar measurements that were averaged to give the final wear scar diameter measurement. The Hertzian diameter is the contact diameter formed between the ball and the flat wear specimens due to elastic deformation of the materials. It is theoretically possible for the material to have no appreciable wear, but have the Hertzian contact surface roughened slightly so that optically, a Hertzian diameter-sized wear scar can be seen. The Hertzian wear scar diameter therefore represents a theoretical minimum wear scar diameter for optical measurements. A better way to gauge the effectiveness of different chemistries therefore is to compare the wear scar diameters after subtracting the Hertzian wear scar diameter. Both wear scar diameter and diameter increase above the Hertzian contact diameter values are provided in this report.

Some researchers report wear as volume of material removed. Appendix F contains a derivation of equations that can be used to estimate wear volume from wear scar diameters for Four-Ball (FB), Ball-on-Three-Flat (BTF), and Pin-on-Disk (POD) tests. It has been found that these estimates lose their accuracy in cases of very high or very low wear, therefore they should be used with caution. High wear often results in wear of the rotating ball, changing its curvature. This can be detected by noting the ellipticity of the wear scar diameter. A perfectly circular wear scar diameter denotes little change in curvature of the upper ball. A wear scar in which the diameter in the direction of sliding is smaller than the diameter perpendicular to the direction of sliding denotes significant wear of the upper rotating specimen. The accuracy of the calculations suffers at low wear as the diameter approaches the Hertzian contact diameter because of the roughened surface argument

mentioned above. Independent wear volume measurements performed using optical interferometry confirm that the calculation equation in appendix F can overestimate the wear volume by at least an order of magnitude. Because of the potential inaccuracy in using calculated wear volumes, data in this study are reported as wear scar diameter, and diameter increase above the Hertzian contact diameter. Load capacity plots use the customary log/log plot of wear scar diameter versus load.

4.1.5. Selection of Wear Test Conditions

A rotational speed of 600 rpm in the BTF test was used to produce moderate (0.23 ms^{-1}) sliding speeds. At this speed there was a large database of wear test results from Penn State, NIST, and other literature sources.

The seven wear tests shown in Figure 4.5 constitute a load capacity plot (wear vs. load) for purified paraffin oil lubricated silicon nitride. According to these results, low wear is observed for loads up to 30 kg. In this load range, pressures in the wear scar at the end of these tests are very high: about 1.2 to 1.4 GPa (175 to 200 kpsia) indicating that paraffin oil by itself was capable of lubricating silicon nitride under this condition. The corresponding friction traces for these tests (Figure 4.6) are smooth. At 40 kg, a wear transition region can be identified. At this load, the friction coefficient starts out low (0.099) but at the three minute mark, friction rises and reaches 0.131, indicating a possible change in wear mechanism. After the three minute mark, the friction increases and becomes quite erratic. This region of the load capacity plot is termed the incipient wear transition region. At 60 and 80 kg loads, transition to high friction is more immediate and higher wear is found

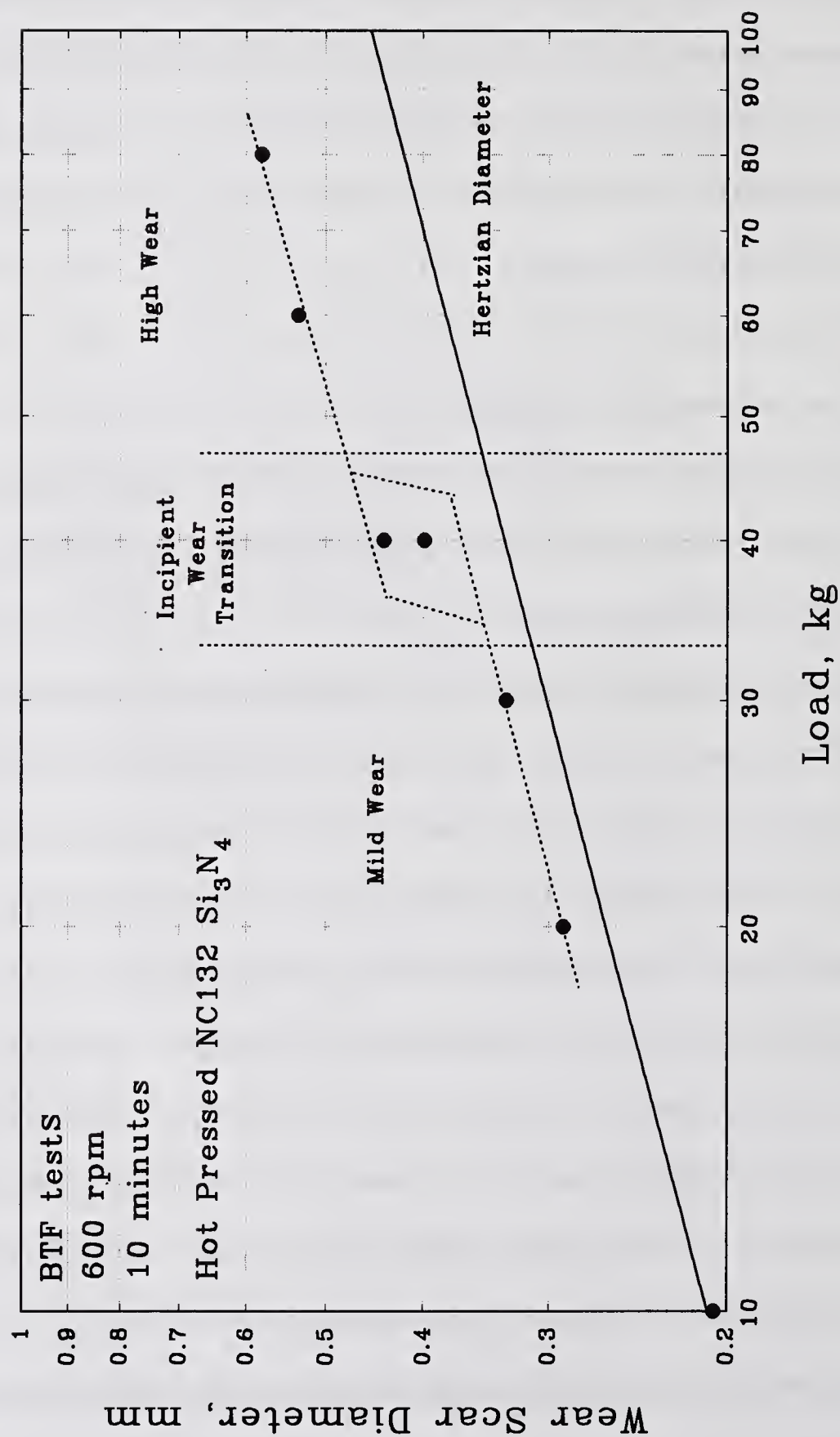


Figure 4.5 Load Capacity Plot for PPO Lubricated Si_3N_4

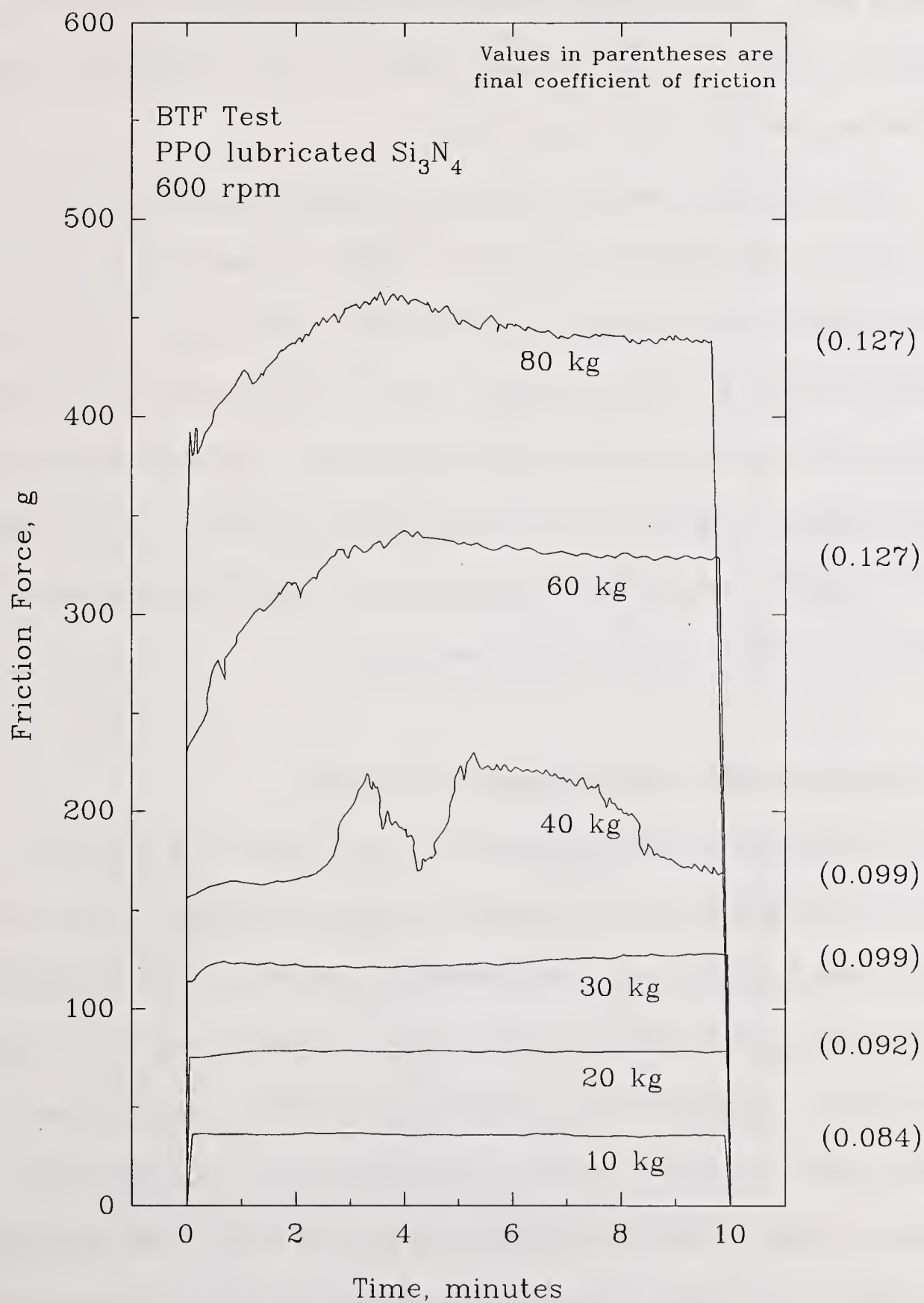


Figure 4.6 Friction Traces for PPO Lubricated Si_3N_4 at Several Loads

at the end of the test. Based on these results, a load of 60 kg was selected for the survey of chemistries study. This is admittedly a severe condition (initial mean Hertzian contact pressures are as high as 2.1 GPa (300 kpsia)). However, it offers the potential to show significant wear reduction due to chemical effects.

A wear-in study was conducted (Figure 4.7) to ensure that adequate times were selected to avoid wear-in repeatability problems. Figure 4.7 presents both wear scar diameter, and mean contact pressure as a function of time. According to this data, the first ten minutes of the test is a period of relatively high wear in which the wear scar diameter increases rapidly above that of the Hertzian contact diameter. As a result, the mean pressure is rapidly changing during this time. After thirty minutes, the rate of wear scar diameter increase is diminished and relatively steady pressures are observed. Based on these results, a duration of 30 minutes was selected for the wear testing.

4.1.6 Test Repeatability and Measurement Uncertainties

The uncertainties presented throughout this study are based on ± 1 standard deviation. Several BTF tests were conducted at the selected conditions of 60 kg, 600 rpm (0.23 ms^{-1}), and 30 minutes to check the repeatability of the wear test with PPO lubricant. The test summary given in Table 4.1 represents not only the original tests used to establish that the tests were repeatable, but also several tests conducted over a period of years as a "calibration check" on equipment and specimen performance, and operating procedures. These tests were run on batches of Si_3N_4 flats produced from different rods, and prepared at different times. Note however, the single CER designation for these flats indicates that they

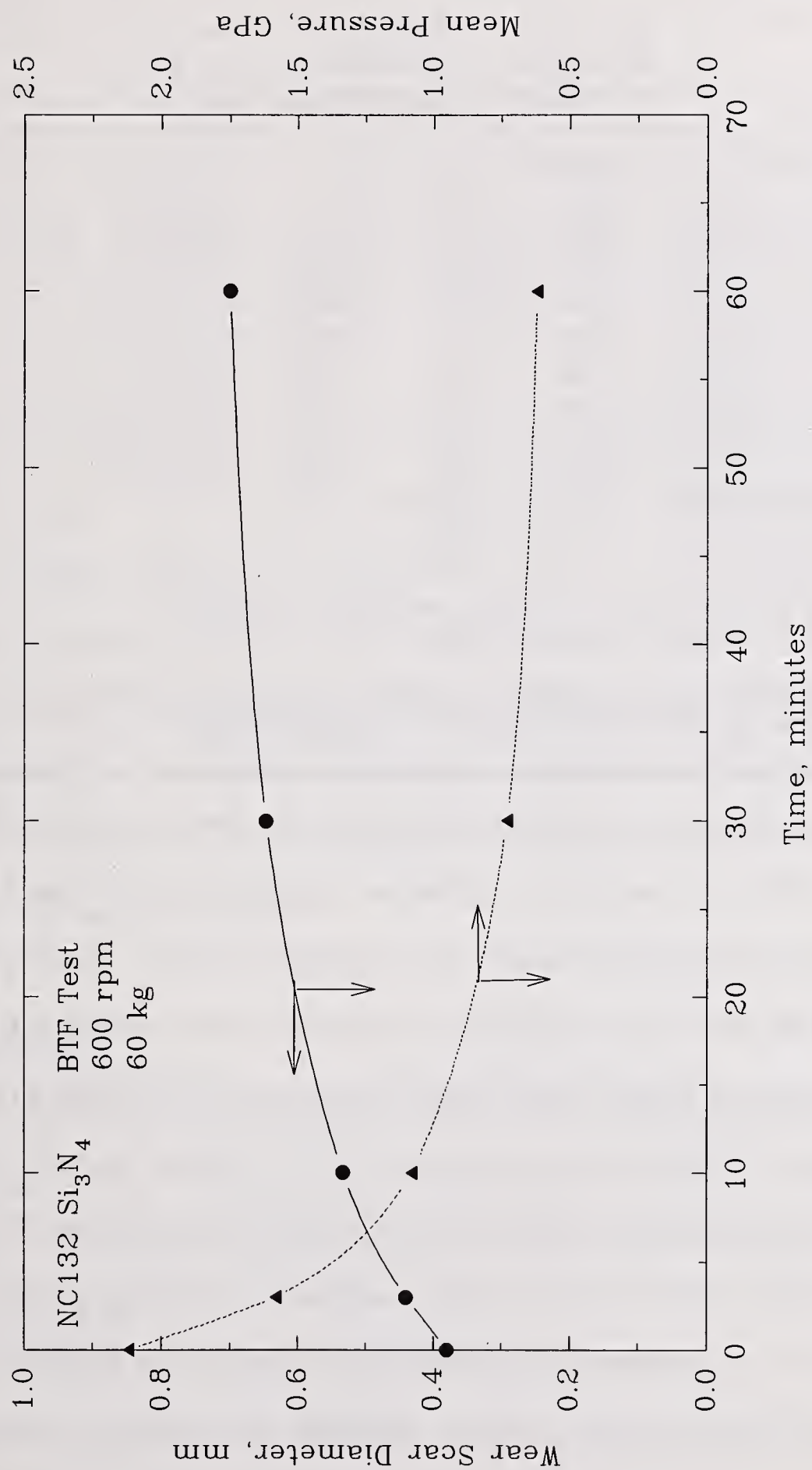


Figure 4.7 Wear-in Data for PPO Lubricated Si_3N_4

Table 4.1
Repeatability Data on PPO-Lubricated Si₃N₄
CER024 Batch of NC132 Flats

	WSD	WSD	COF ²	Run	Flat
	(mm)	Incr ¹ (mm)		#	Polishing Batch
	0.642	0.262	0.123	2813R	CER024 A
	0.650	0.270	0.115	2817R	CER024 A
	0.647	0.267	0.111	2821R	CER024 B
	0.648	0.268	0.120	2835R	CER024 C
	0.649	0.269	0.117	2858R	CER024 D
	0.640	0.260	0.101	2904R	CER024 D
	<u>0.652</u>	<u>0.272</u>	<u>0.105</u>	2922R	CER024 E
AVERAGE	0.647	0.267	0.113		
Std Deviation	0.004	0.004	0.008		

1 Wear Scar Diameter Increase above Hertian contact diameter (0.380 mm)
2 Steady state value measured at the end of the test

First five BTF Tests conducted on CER019 Si₃N₄ ball (NC132) at 600 rpm, 60 kg, 30 minutes, 1.5 ml PPO, 21°C. Last two tests used CER037 ball (still NC132) under same conditions.

all come from the same manufacturers processing batch. The high repeatability of these results is therefore a testament to a combination of high repeatability of specimen preparation, cleaning procedure and wear test operating procedure. The wear scar diameter obtained at the end of the test was 0.647 ± 0.004 mm. This is an increase of 0.267 mm above the expected Hertzian contact diameter for Si₃N₄ under the conditions of the wear test. The friction coefficient at the end of the test was 0.113 ± 0.008 . Note that during the course of this investigation CER037 balls were used instead of the original CER019. The wear test results indicate that these two processing batches of balls gave similar friction and wear data. One might argue that the CER037 balls seem to give a slightly lower friction coefficient at the end of the test; however, statistically, this is difficult to support.

These average results were used as a reference point to gauge the relative chemical effect of the 1 % compounds in PPO. Compounds that gave significantly lower wear scar diameters (< 0.55 mm) than the PPO case were considered to have demonstrated antiwear capability with Si_3N_4 . Compounds that gave significantly higher wear scar diameters (> 0.7 mm) than the PPO case were considered to have demonstrated prowear capability with Si_3N_4 .

In the course of this study, different batches of Si_3N_4 were used which appeared to have minor differences in friction and wear behavior with PPO. The PPO test data for these materials are provided in appendix H for completeness. The minor variations in performance were not significant enough to affect the antiwear/prowear criteria described above. The average of all 16 tests on PPO using three different batches of Si_3N_4 were used as comparison data in the tabulated and graphical data analysis as detailed in appendix H. The average wear scar diameter was 0.645 ± 0.018 mm. The average coefficient of friction at the end of the test was 0.117 ± 0.010 .

4.2. Static Tests

Static thermal tests were conducted to study the chemical reactions of interest without the complications of wear. Critical parameters such as temperature, duration, and concentration of reactants (including surface area) can be controlled to a degree not possible with a dynamic system.

4.2.1. Batch Reactor

Batch reactions were conducted between Si_3N_4 powders and Octanol using 1.5 ml polypropylene centrifuge tubes for a microcentrifuge. This had the advantage of allowing for immediate separation of the powder and liquid reactants. In addition, subsequent solvent rinses were carried out in these tubes, thus combining both product purification (solvent extraction) and separation (centrifugation) in a single container and eliminating transfer steps that might have resulted in contamination and loss of product. The 1.5 ml tubes contain snap caps that keep the samples intact during the reactions. The reactions were carried out in a constant temperature oil bath. Since the tubes tended to be buoyant in these baths, a buoyancy compensation device (1/4 inch nut) was attached to (screwed onto) the bottom of each tube. The tubes could then be placed onto a rack within the oil bath to allow for several tests to be conducted at the same time. This made it easier to conduct a series of tests and analyses as a function of time.

4.2.2. Procedures

Samples of Powder and octanol were placed into the reaction tube and mixed thoroughly using a spatula. The cap was snapped into place, a weight attached to the tube, and the reactor was placed into the constant temperature bath for a specified time. Careful temperature regulation ensured that the temperature in the bath did not deviate from the setpoint by more than 0.5°C at any time during the reaction. At the end of the specified time, the reactor was removed from the bath and the exterior was rinsed with hexane to remove the oil. The reactor was then centrifuged at 16 000 g for 10 seconds. Centrifugation

caused the powder to pack down to the bottom of the tube. The supernatant fluid was then poured off. Spectral grade hexane was added to the tube and mixed gently with a spatula to form a slurry. The slurry was then centrifuged to separate the liquid and powder and the supernatant fluid poured off. The hexane rinse was then repeated three more times. The solvent was then switched to a mixture of spectral grade acetone/water (9/1) and the mixing-centrifugation step was performed two more times. A final mixing and centrifugation with pure spectral grade acetone results in a powder sample that is free of octanol reactant. The powder was then removed with a spatula and dried on a watch glass to remove residual acetone solvent (≈ 10 minutes). This dried powder was analyzed using thermogravimetric analysis (TGA) within 2 hours. The entire purification/separation process can be performed in 30 minutes.

When conducting kinetic experiments, the duration of the reaction must be precisely known if quantitative results are to be obtained. Since the reactors start at room temperature, and are heated up by immersing them in a bath, there is a time lag between when the reactor is placed in the bath and when the reactants actually come to the proper temperature. There is a similar lag when the reactor is removed from the bath. This must be corrected for to get meaningful reaction duration information, especially for short reaction times. A reactor was fitted with a thermocouple in its center, and placed in the bath to see how long it took the reactor to heat up. The results, shown in Figure 4.8A, indicate that the reactor has reached within 10°C of the setpoint temperature in a bit more than a minute. On cooling, it takes 30 seconds for the reactor temperature to drop by more than 10°C (Figure 4.8B). The data suggest that the measured reaction times should be reduced by about 1

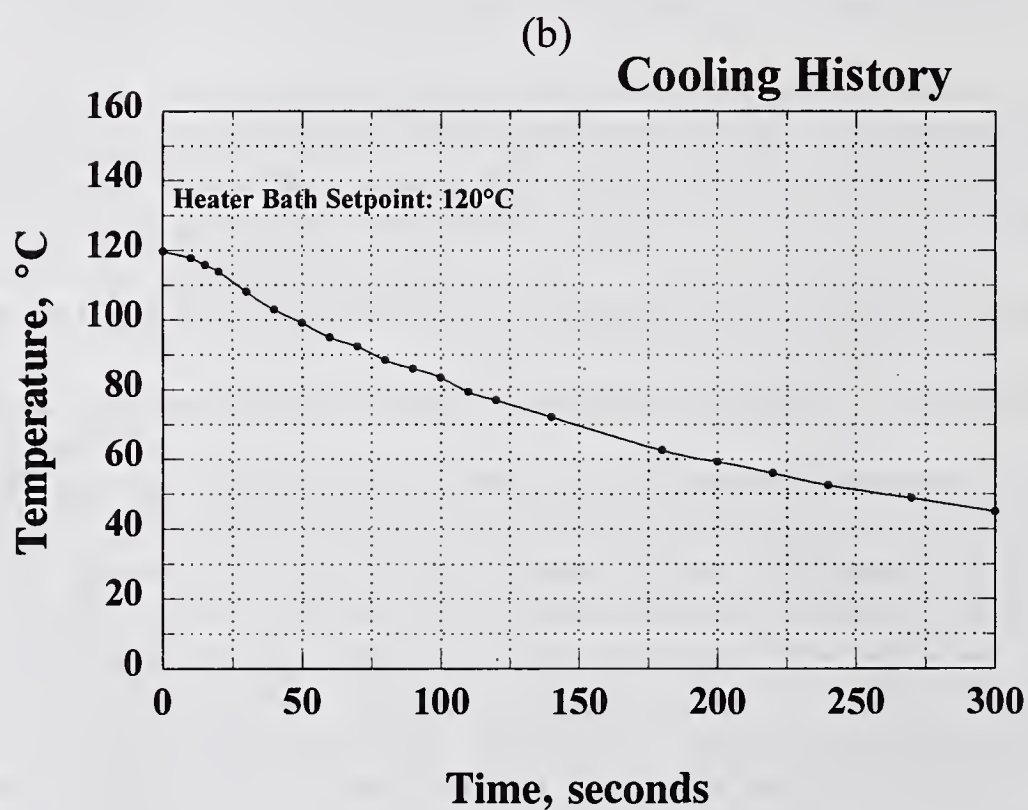
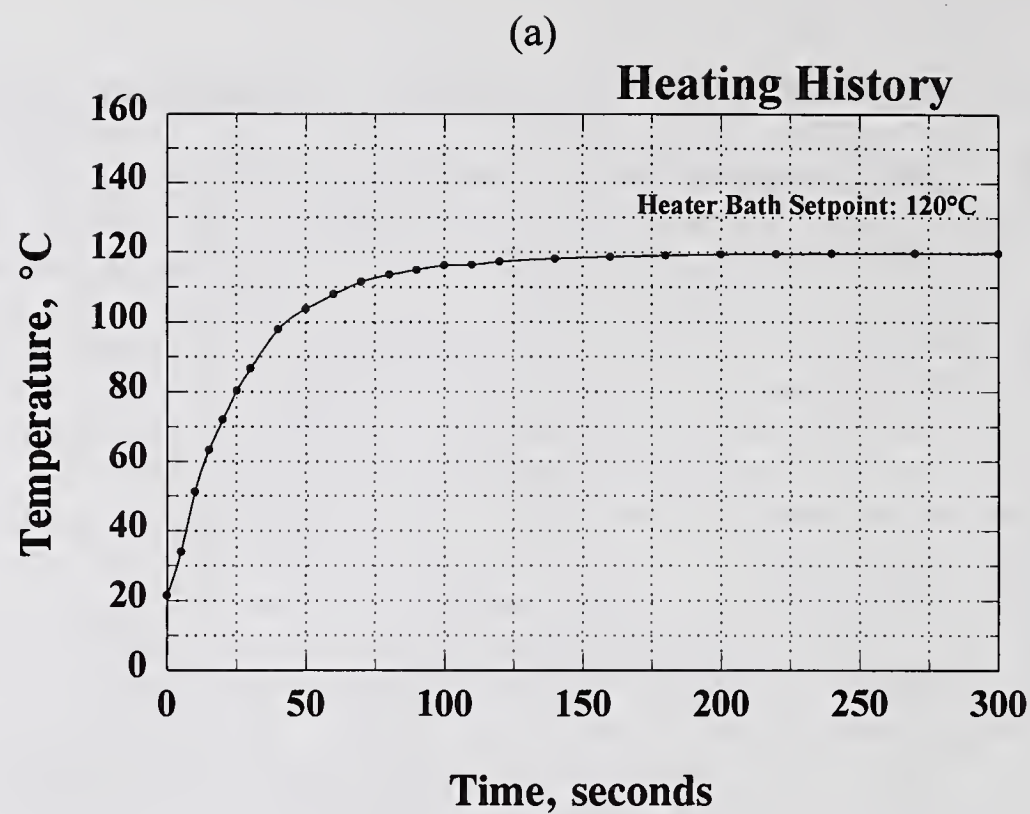


Figure 4.8 Micro-Reactor Thermal History: a) Heating, b) Cooling

minute to accommodate the thermal lag.

Chapter 5

BASELINE WEAR STUDY

5.1. Paraffin Oil Lubrication

All wear test results on various chemistries will be compared to the base case where only purified paraffinic oil (PPO) is present. This section describes the friction and wear characteristics of Si_3N_4 under PPO lubricated condition.

A typical worn surface and friction trace for a PPO lubricated Si_3N_4 test is shown in Figure 5.1. Friction is seen to rise to about 0.13 at the beginning of the test, and settle down to a level of 0.12 toward the end of the test. The optical micrograph shows the wear scar at the end of the test. The direction of sliding in this photograph (and all other photographs in this study) is from left to right. The wear scar at the end of the test is symmetric (≈ 0.65 mm), and smooth within the scar. The small striated discolorations within the wear scar suggest a micro-abrasion process by asperities or wear debris. The discolorations are brownish and are reminiscent of the oxidized organic compounds often observed in the metal systems. There are significant amounts of deposit surrounding the wear scar, in a pattern that indicates the flow field for the lubricant during the wear test. The deposit seen around the scar seem to be a mixture of solid materials including a plastic-looking accumulation both at the entrance and in the twin wakes at the exit of the wear scar. The interference fringes seen at the center of the exit and near the sides of the wear scar

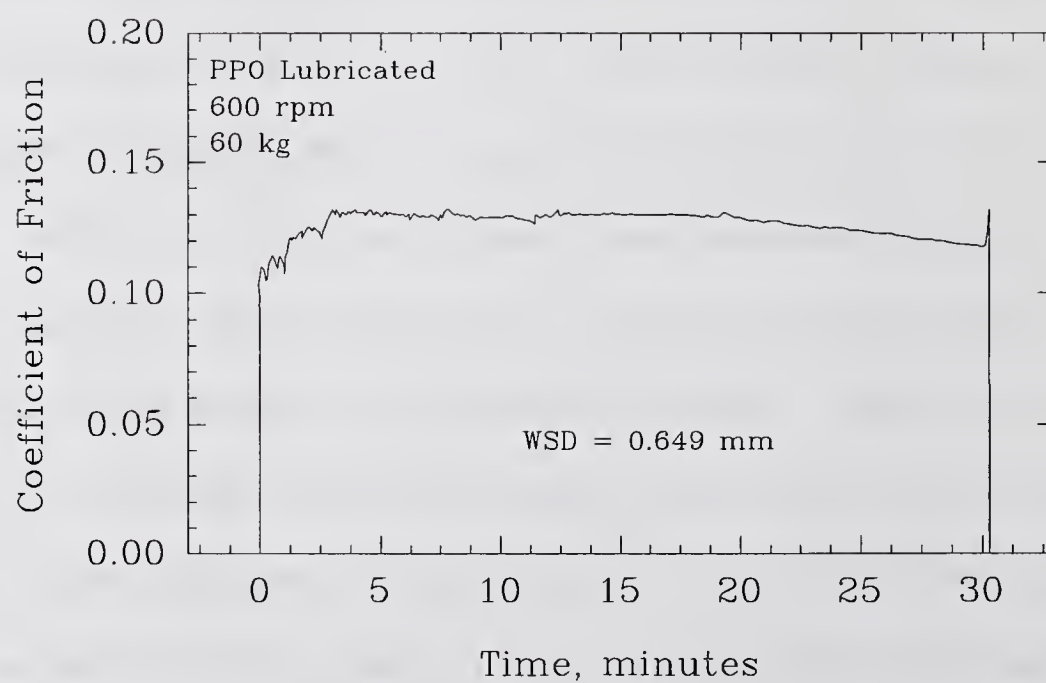


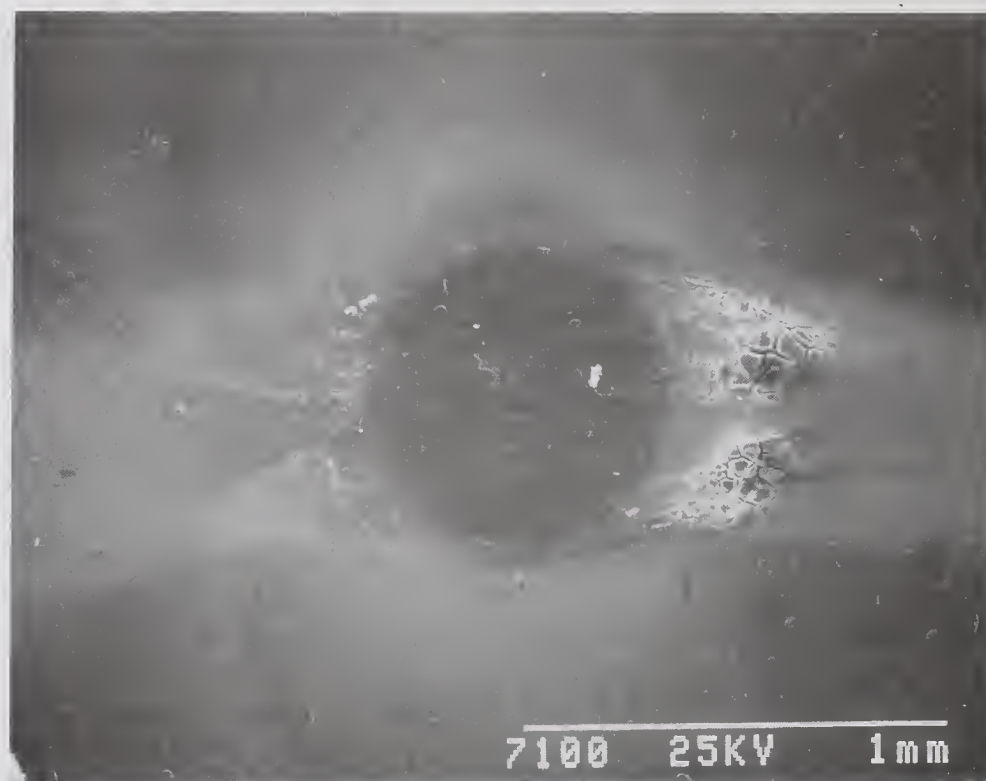
Figure 5.1 PPO Lubricated BTF Test at 60 kg: a) Optical Photomicrograph, b) Friction Trace

suggest that they are thin films and the rainbow-like color pattern observed suggests a variation in film thickness. The films seen here are soft and can easily be removed by scratching. They are not easily soluble in hexane, but can be removed with stronger organic solvents such as acetone and tetrahydrofuran (THF). FTIR analysis of the films confirmed the presence of organic constituents.

SEM photomicrographs of the worn surface on the flats reveal more details. The flow field in the low magnification SEM photograph (Figure 5.2A) is quite pronounced, even though the interference fringes are no longer visible. The size and extent of the accumulations are also more apparent. High magnification inside the wear scar (Figure 5.2B) shows the surface to be quite smooth with what appears to be a combination of compacted product and small, loosely attached, debris particles. The middle of the exit region outside the wear scar contains many particle clusters (Figure 5.3A). The clusters are large and appear fragile. EDX analysis of the clusters revealed the presence of silicon, oxygen, and carbon. The thick deposits that form the twin wakes (Figure 5.3B) have the appearance of a dried mud bed. It would appear that these thick deposits were composed of some kind of solid-like material mixed with a liquid. The vacuum of the SEM appears to have removed the liquid and resulted in the dried mud appearance of the deposit.

PPO lubricated wear tests seem to generate large amounts of reaction product deposits near the wear scar. Since there are only very minute amounts of "reactive" metals in the Si_3N_4 , this would suggest that very high temperatures are generated within the contact during a test. An estimate of the temperature in the contact junction, performed using Archards method¹¹ (Appendix I) suggested temperatures in the region of $\approx 250^\circ\text{C}$ for PPO lubricated

(a)



(b)

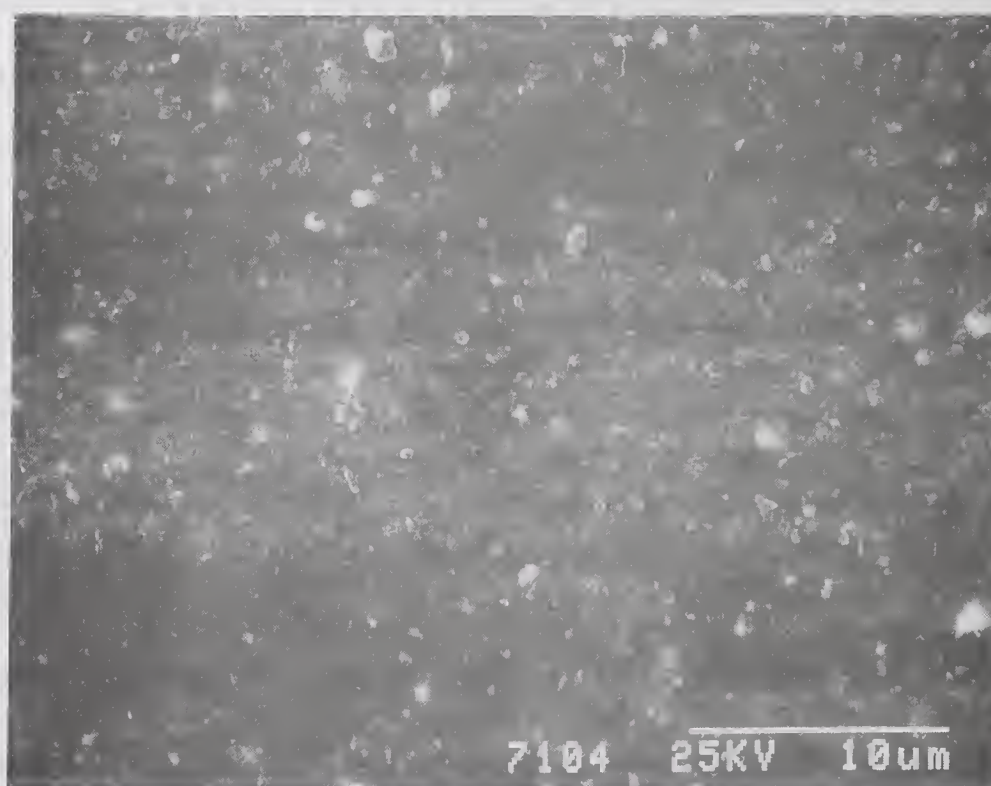
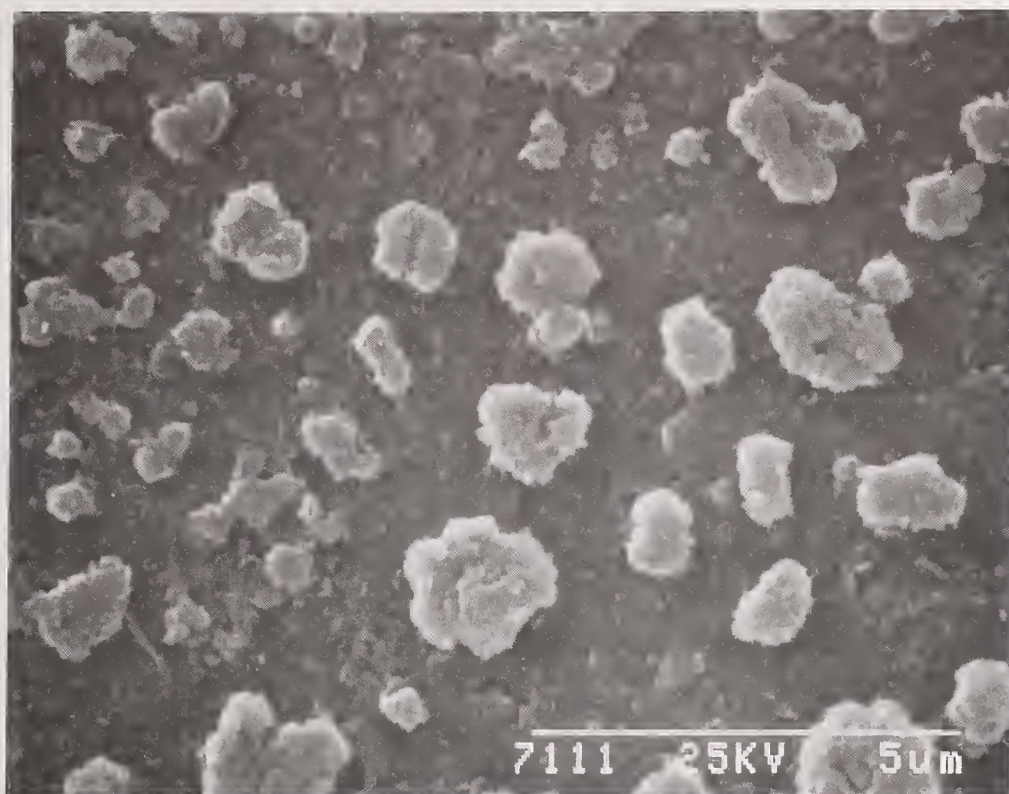


Figure 5.2 SEM Photomicrographs of PPO Lubricated Si_3N_4 Wear Scar: a) Low Magnification, b) High Magnification (within Scar)

(a)

79



(b)

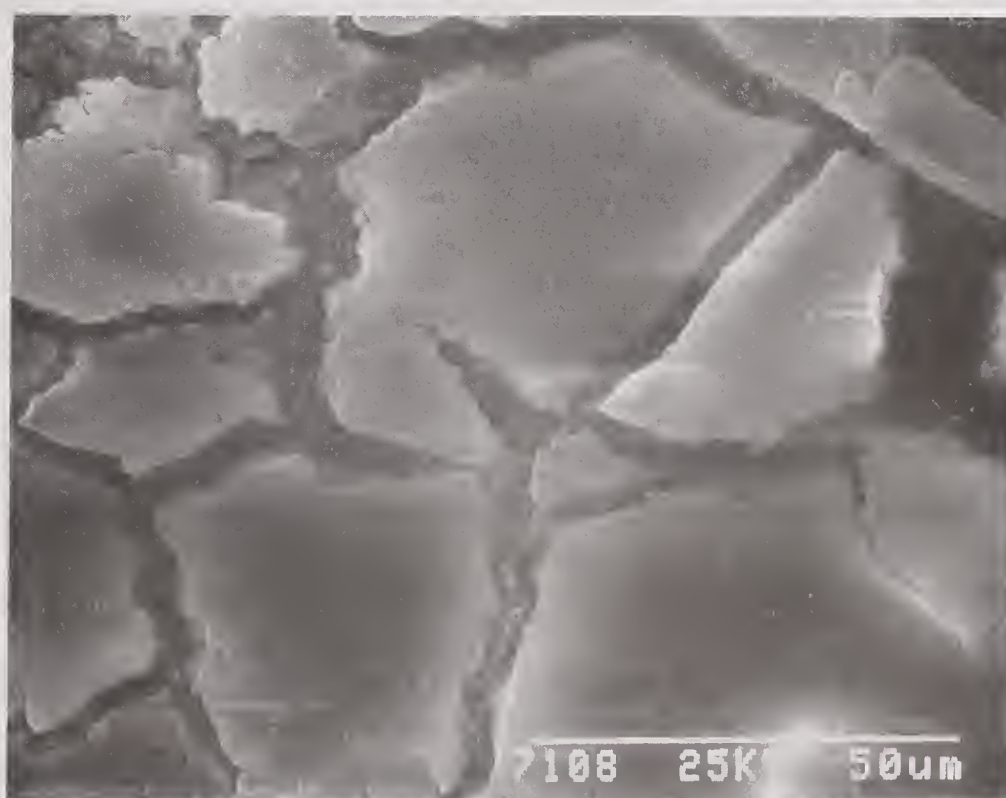


Figure 5.3 High Magnification SEM Photomicrographs of Exit Region Outside Wear Scar of PPO Lubricated Si_3N_4 Wear Test

tests. This temperature is sufficient to oxidize significant amounts of paraffin oil in 30 minutes.

Auger analysis was applied to wear test samples from PPO lubricated tests to try to determine the nature of the surface after a test. The samples had been rinsed with hexane to remove excess lubricant.

Four regions on a worn flat were examined (Table 5.1). Two spots were located inside the wear scar, a third spot was located just outside the wear scar, and a fourth was

Table 5.1
Auger Analysis of Worn Surface of PPO-Lubricated Si_3N_4
(Values are Atomic %)

Sample Location	C	O	Si	N
Inside Scar, Spot #1	70	17	9	2
Inside Scar, Spot #2	72	16	9	2
Outside Scar, Nearby	77	11	8	2
Outside Scar, Far Away	68	12	12	6
Unused Si_3N_4 specimen	45	11	25	19

located outside the wear scar far away from the scar. The results, presented in Table 5.1, also contains auger analysis data from an unused specimen for reference. According to the data, the surface of the entire flat is covered with a carbonaceous material. The data also suggests that oxygen is more concentrated inside the wear scar than outside; however, it is not clear whether it is associated with the carbon (as oxidized PPO), or silicon (as oxidized

Si_3N_4), or both. Since N is from Si_3N_4 and O can be associated with either Si or C, one can get an estimate of the relative amount of Si_3N_4 vs SiO_2 by comparing the N-Si ratio. The data suggests that at least some of the silicon inside the wear scar is associated with oxygen.

Auger depth profiling of the region within the wear scar (Figure 5.4) reveals some important details about the worn surface. The outermost layer is very rich in carbon and about 20 Å thick. This is most likely some kind of organic layer. After the carbon containing layer, an oxide layer is seen to a depth of perhaps 100 Å. Since the oxygen signal does not correspond with the carbon, it is probably associated with silicon. Silicon oxide is suggested. This is reinforced by the reduced nitrogen concentration observed with this region. Deeper into the surface, the characteristic bulk Si_3N_4 elemental intensities are observed. A comparison of these Auger depth profiles with the unused specimen (Figure 3.14) reinforces the interpretation of an outer organic layer followed by a silicon oxide sublayer. The fact that much more oxygen ends up in the surface of the wear scar coupled with the abundance of carbon suggests that both of these constituents are important in the wear and lubrication of Si_3N_4 .

Gel permeation chromatography (GPC) confirmed that a wide range of high molecular weight products were produced from PPO lubricated wear tests on Si_3N_4 . Gel permeation chromatography-graphite furnace atomic absorption (GPC-GFAA) analysis failed to detect any appreciable amounts of silicon-containing reaction products, suggesting a lack of reactivity with the Si_3N_4 surface.

The smooth wear scars and lack of fracture and cracking (severe wear) artifacts within the wear scar suggests that PPO is a reasonable base lubricant for Si_3N_4 . A load

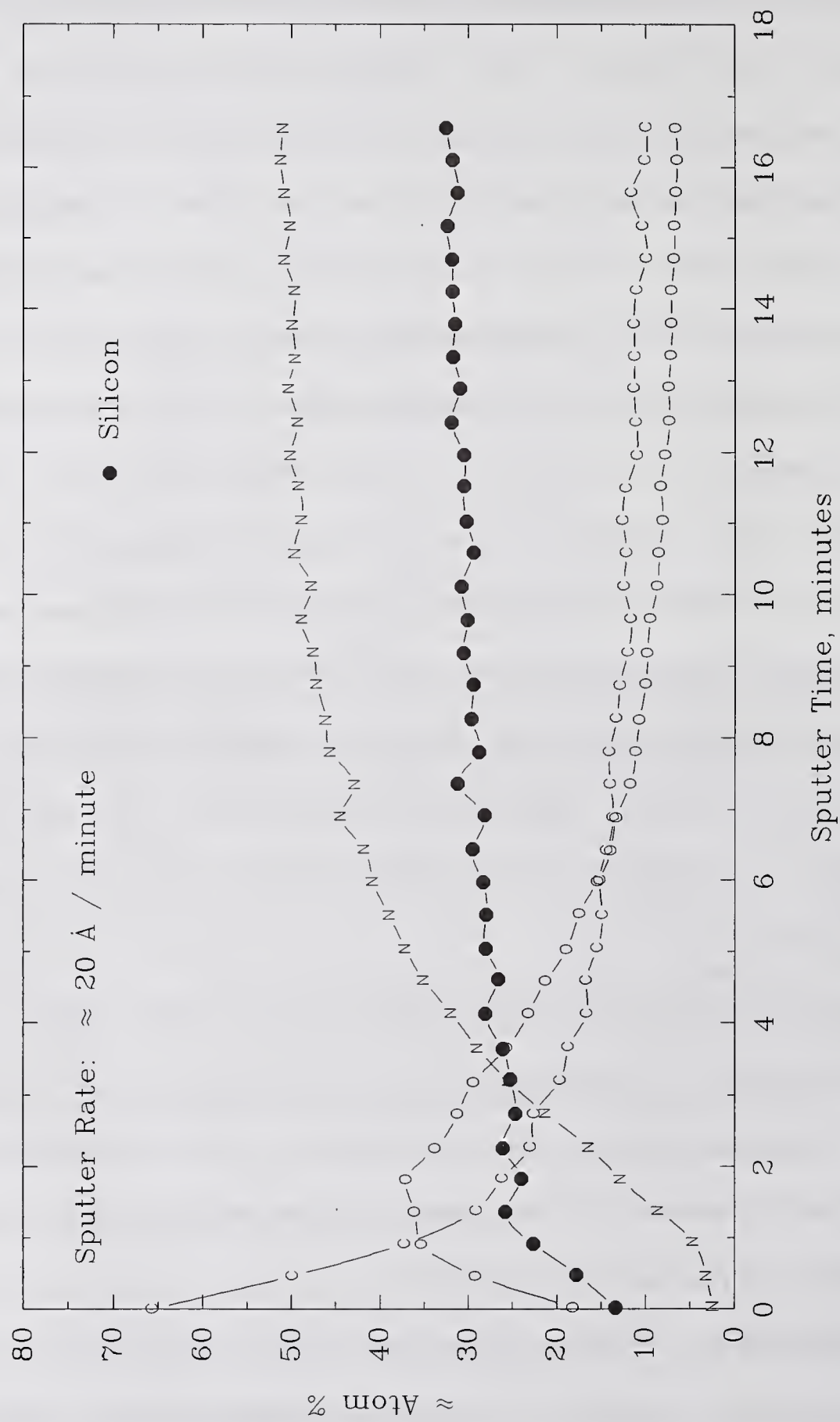







Figure 5.4 Auger Depth Profile of Region within Wear Scar for PPO Lubricated Si_3N_4 Wear Test at 60 kg

capacity study was conducted to understand the performance of PPO lubricated Si_3N_4 under different severities.

5.2. PPO Load Capacity Study

Thirty minute PPO lubricated BTF wear tests were conducted at a variety of loads to construct the load capacity plot shown in Figure 5.5. The behavior of the different tests can be categorized into five different regions based on wear and friction behavior. The information associated with each of the five wear regions are summarized in Table 5.2.

Table 5.2
Characteristic Features of the Five Wear Regions
for PPO-Lubricated Si_3N_4

Parameter	Wear Regime				
	I	II	III	IV	V
Friction Trace					
Friction Description	Low, Level	Transition / Recovery	High, ↓	Low, ↑	Seizure / Low, Level
Wear Scar Appearance	Smooth, Indistinct Edges	Smooth, Clear Edges	Smooth, Clear Edges	Grooved	Fractured, grooved, roughened
Lubrication	Good	Poor	Poor	Poor	Very Poor
Overall "Category"	PPO Lubricated	Incipient Transition, Recovery	Immediate Transition	Immediate Recovery Accelerated Wear w/time	Fracture

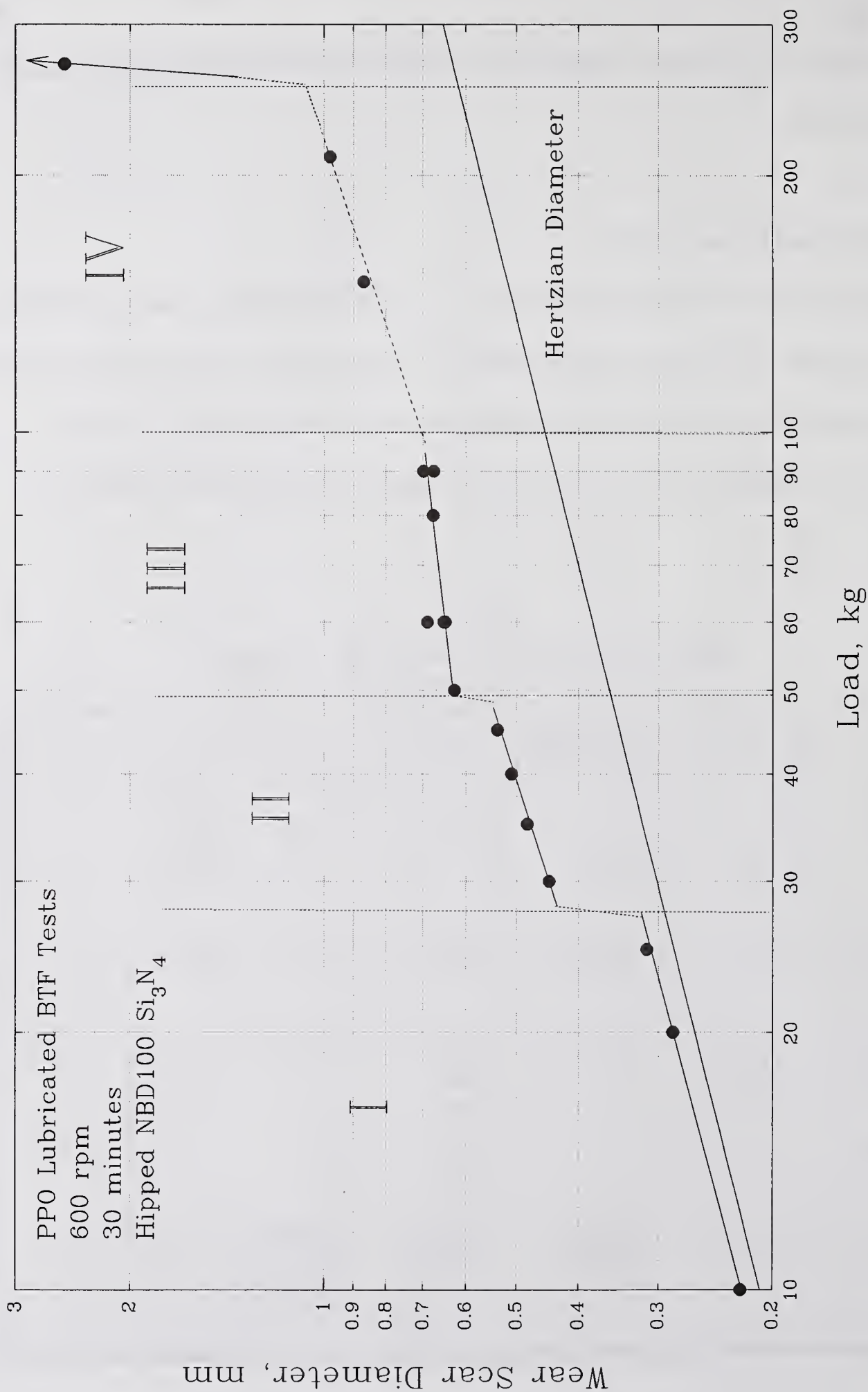


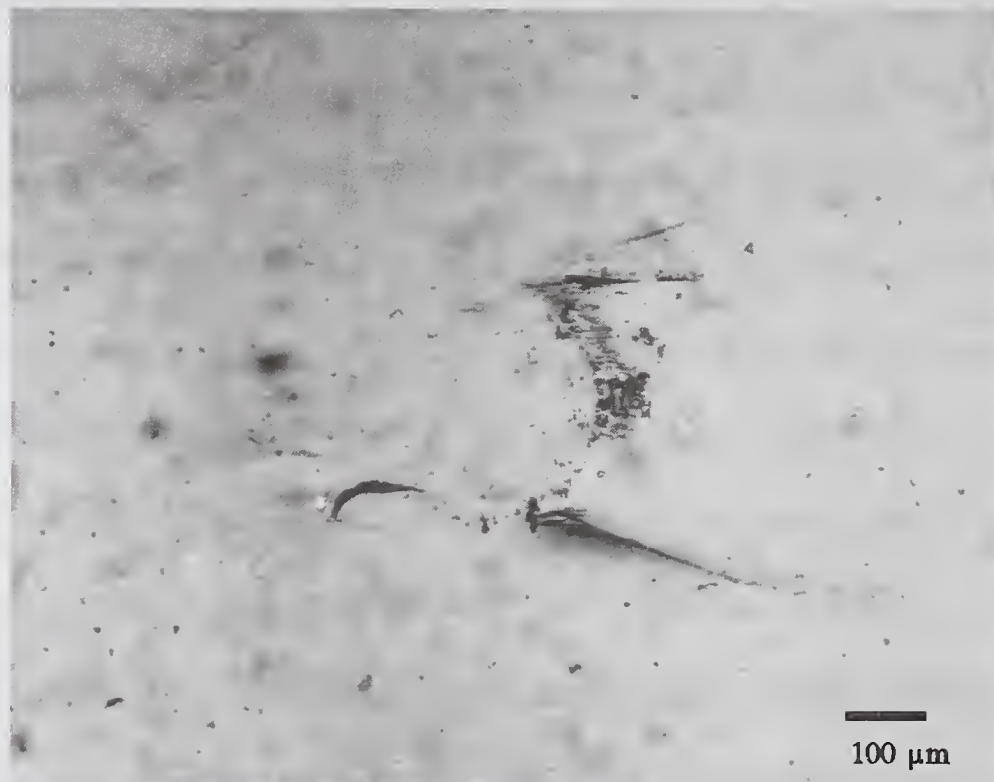
Figure 5.5 Load Capacity Plot for PPO Lubricated Si_3N_4 Detailing Different Wear Regimes

A typical friction trace and wear scar photomicrograph for PPO lubricated Si_3N_4 tests within region I are shown in Figure 5.6. The friction trace is level and relatively smooth. The coefficient of friction for these tests are low and steady at ≈ 0.09 throughout the tests. The wear scars are quite small and their edges are a bit hard to define. Small amounts of deposit are evident at the exit of the wear scar. The highest load within this region (25 kg) begins to show some evidence of additional deposit surrounding the wear scar, suggesting that significant chemical reactions were taking place in and near the wear scar. The wear scar diameter measurements for region I are very close to the Hertzian elastic contact diameter. Calculated initial Hertzian mean pressures for the 25 kg load are 1.58 GPa (229,000 psi). Overall, this region is classified as well lubricated.

Region II also parallels the Hertzian contact diameter line in Figure 5.5; however, it is displaced away from the line significantly, and a wear transition can be seen from region I to region II. Friction traces for tests (Figure 5.7) in this region typically have either spikes or humps in the trace signifying some kind of wear transition / recovery behavior. The friction spikes may be single wear events such as grain pullout within the wear scar. Coefficient of friction at the end of the test is still near 0.09. The wear scars are still smooth and circular, and the edges are more distinct. Significant amounts of reaction product can be seen in and around the wear scar. This region is classified as an incipient transition region, and indicates an unstable lubrication condition between good and poor lubrication.

Region III differs from region II by another apparent wear transition (Figure 5.5). The line joining the data in this region does not appear to parallel the Hertzian contact diameter line as well as the other data. The answer for the wear transition from region II to

(a)



(b)

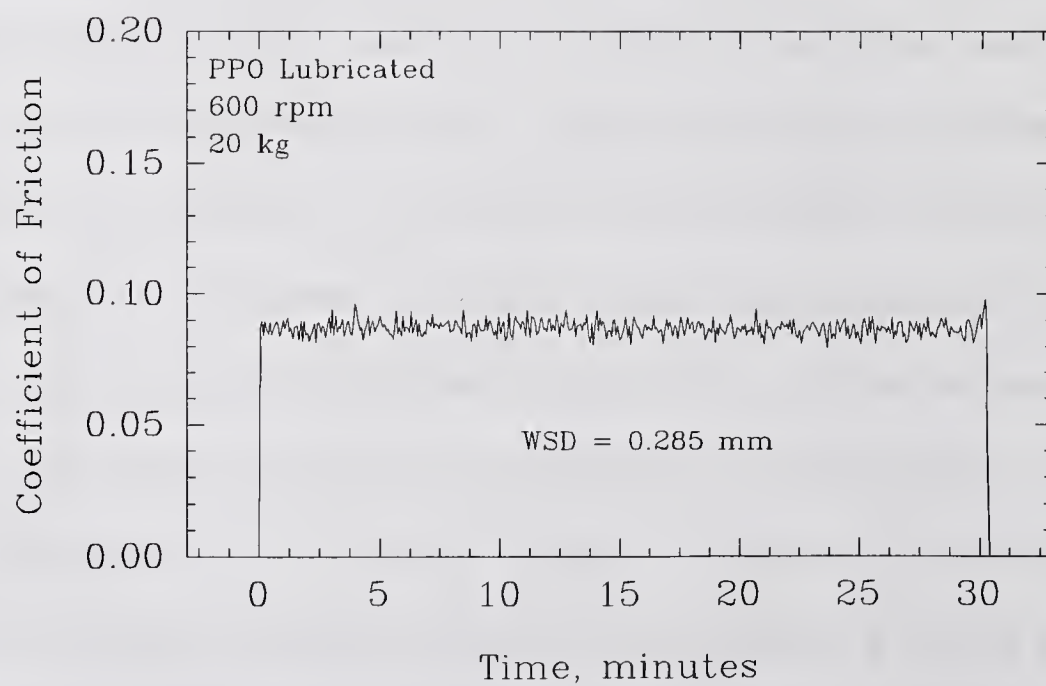


Figure 5.6 PPO Lubricated Si_3N_4 BTF Test at 20 kg: a) Optical Photomicrograph, b) Friction Trace

(a)



(b)

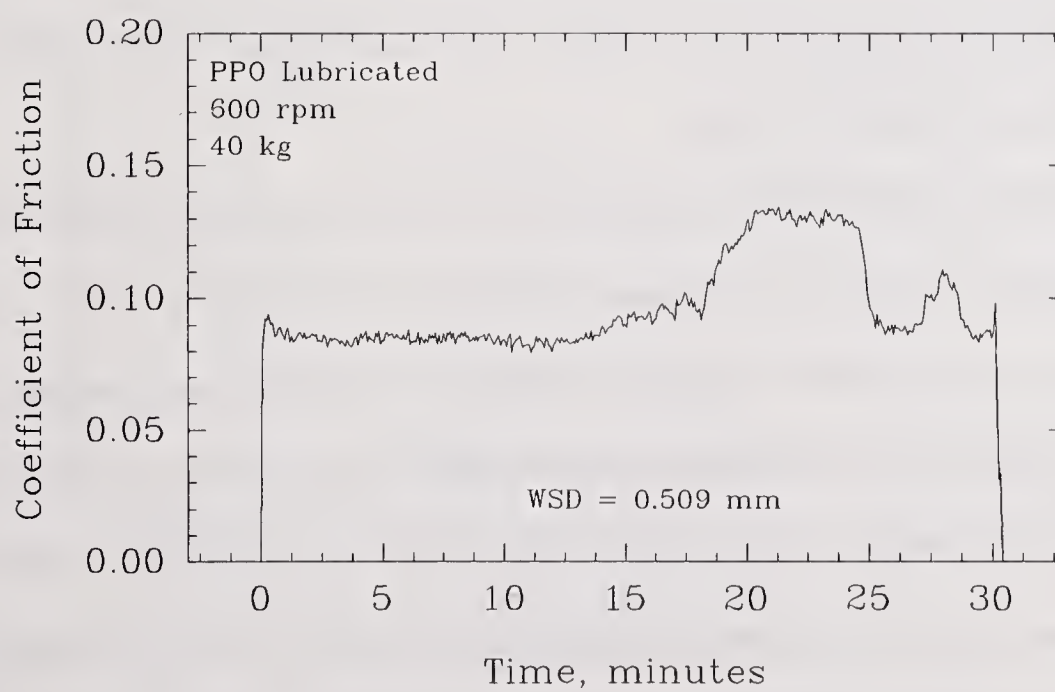


Figure 5.7 PPO Lubricated Si_3N_4 BTF Test at 40 kg: a) Optical Photomicrograph, b) Friction Trace

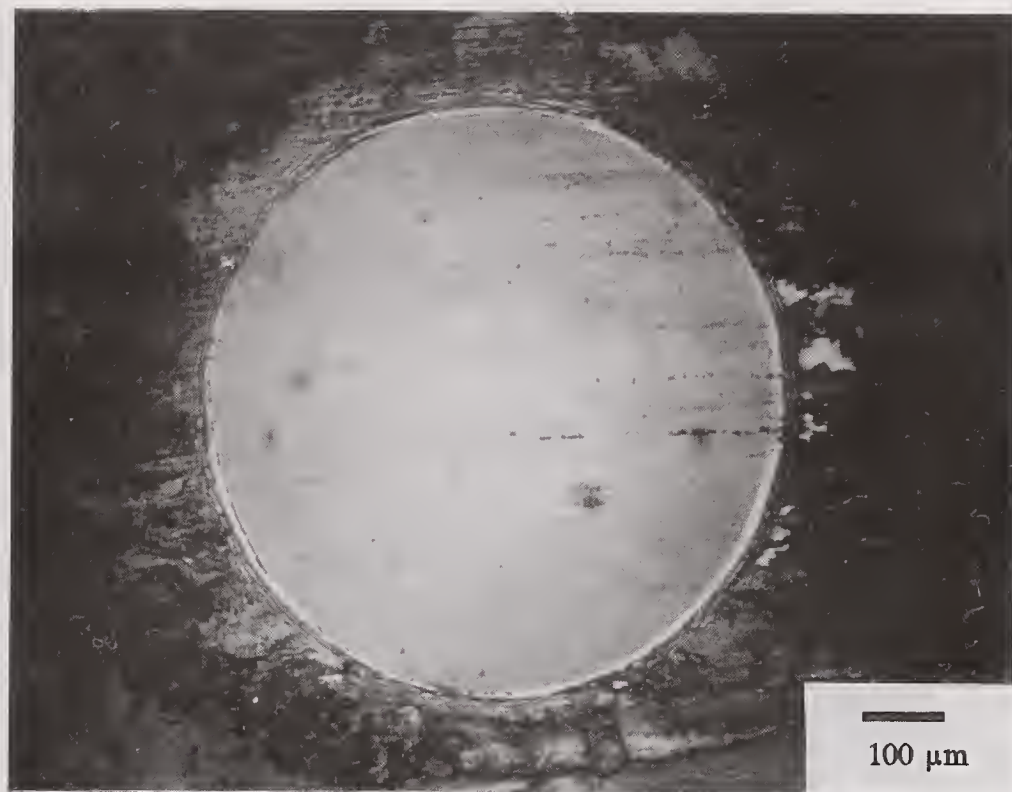
region III seems to lie in the friction behavior. Region II friction traces indicated transition / recovery behavior. Region III friction traces exhibit immediate transition to high friction, and friction remains at high levels throughout the test, with only a slight decrease with time (Figure 5.8). Coefficient of friction at the end of the test are approximately 0.12 to 0.13. Wear scars are large, smooth, and circular. A lot of deposit is seen around the wear scars. This region is classified as immediate transition (to high wear) and represents a relatively poor lubrication condition.

Region IV is also a poor lubrication condition. It is distinguished by the initial friction spike then low friction coefficient (0.06 to 0.07), and subsequent increase in friction with time to ≈ 0.11 (Figure 5.9). Wear scar diameters are very large (note the 2x scale change of Figure 5.9A from the preceding optical photomicrographs) and again seem to parallel the Hertian line of Figure 5.5. The wear scars themselves are severely grooved, yet very polished. Very large amounts of deposit are seen around the wear scar. This suggests that reactivity may be so high that some form of chemical polishing is taking place in the wear scar, leading to a large wear scar.

Region V is a very high wear region characterized by an immediate high friction "seizure" followed by a low steady coefficient of friction of 0.06 (Figure 5.10). Stresses were so severe that the specimens completely fractured. The cracks seen emanating from the wear scar go completely through the specimen; therefore this test result may have been influenced by the specimen geometry (thickness of the flat). The recesses that held the flats kept the fractured specimens in place throughout the test; however there was probably some re-alignment of the specimens after fracture that altered the contact stress distribution.

(a)

89



(b)

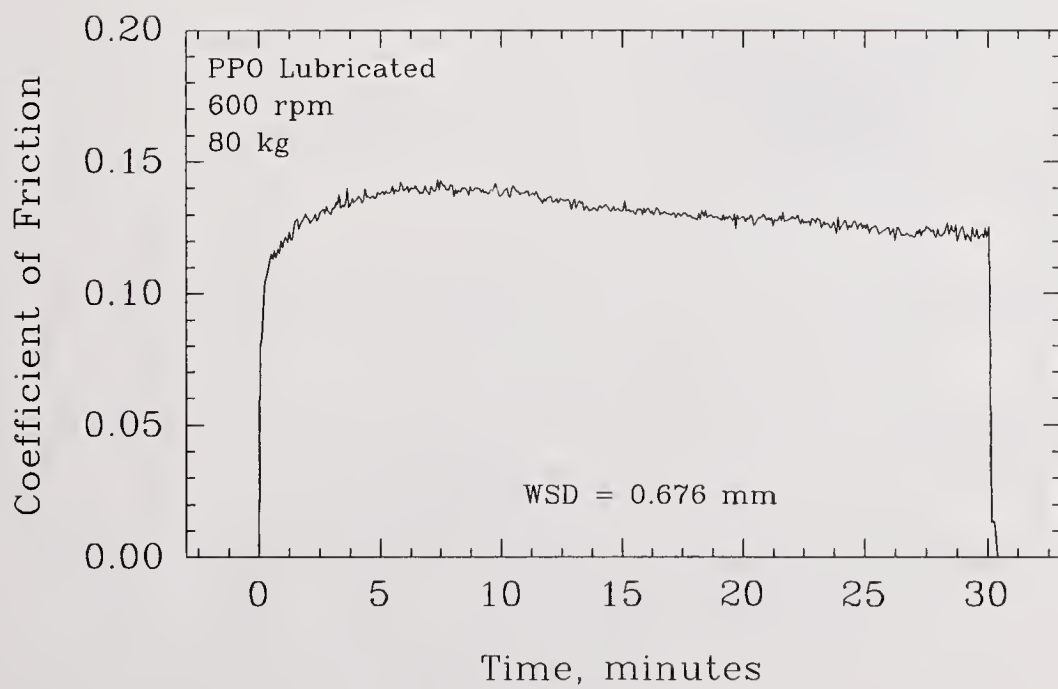
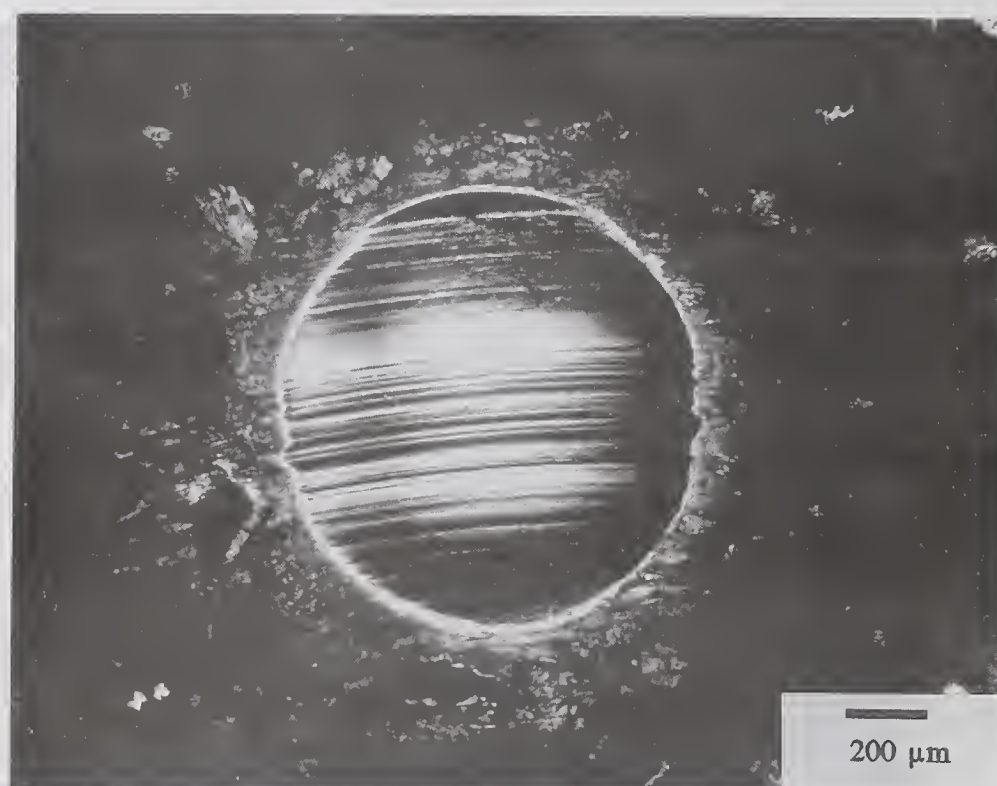


Figure 5.8 PPO Lubricated Si_3N_4 BTF Test at 80 kg: a) Optical Photomicrograph, b) Friction Trace

(a)



(b)

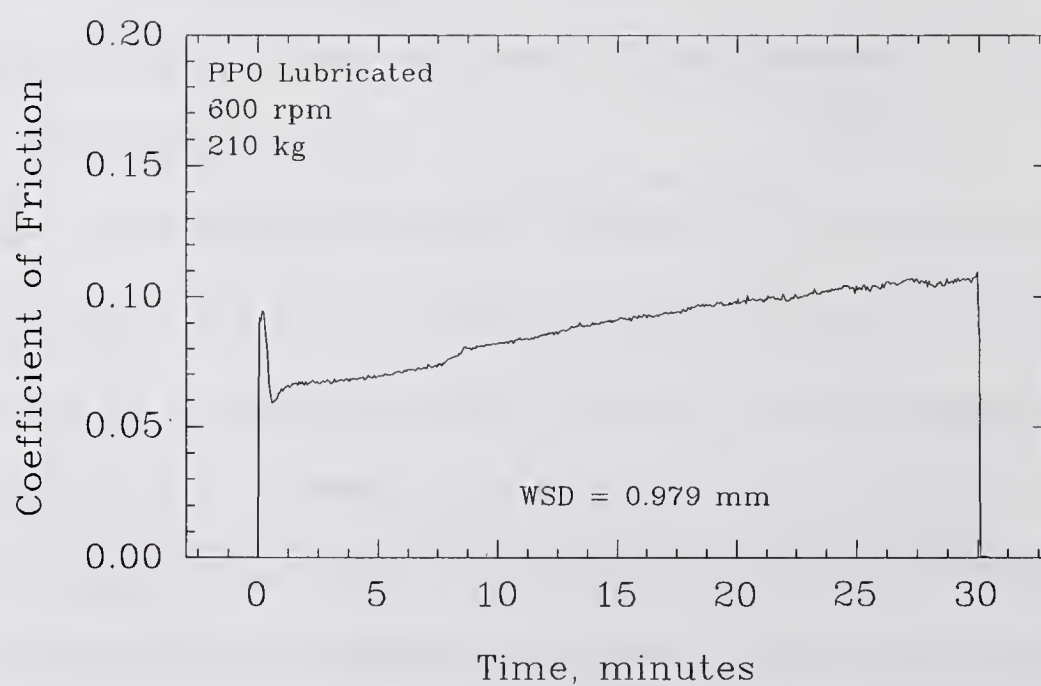


Figure 5.9 PPO Lubricated Si_3N_4 BTF Test at 210 kg: a) Optical Photomicrograph, b) Friction Trace

(a)



(b)

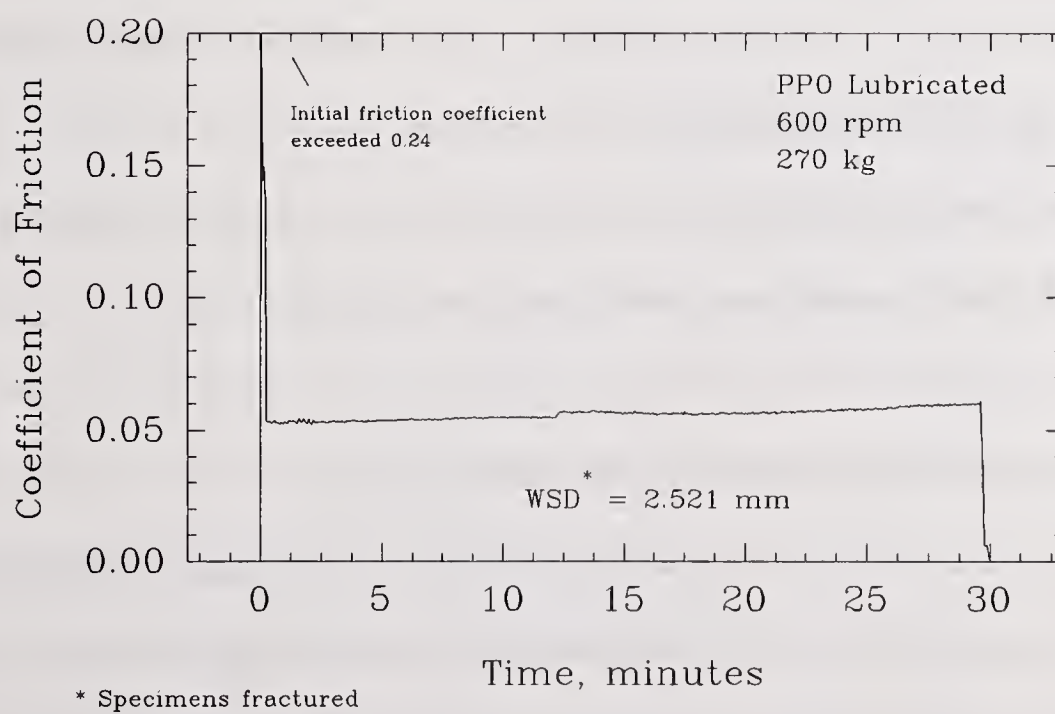


Figure 5.10 PPO Lubricated Si_3N_4 BTf Test at 270 kg: a) Optical Photomicrograph, b) Friction Trace

Severe grooving is also seen in this test. It is not clear to what degree the fracture of the specimen contributed to the high wear seen for this test.

The load capacity plot for PPO provides a reference in which one can understand the relative severity of the 60 kg tests (region III) and why it was chosen for the evaluation of lubricant chemistries. Region I is too mild since PPO appears to be a good lubricant in this region. There is little room for improvement in wear. Region II is an unstable region in which the time of transition to high wear cannot be predicted reliably. This unpredictability makes this region undesirable for evaluation of lubrication chemistries. Region III represents a severity in which poor lubrication is immediately encountered at the beginning of the test and seems to continue throughout the test as evidenced by the continued high friction. This region would provide a stable poor lubrication condition in which lubrication chemistries could be evaluated. Region IV appears to have an initial high friction spike, followed by a quick recovery to low friction. The expected unpredictability of this transition / recovery behavior would make this a less than desirable region in which to initially evaluate lubricant chemistries. Region V is not desirable for the same reasons.

For these reasons, region III (specifically, 60 kg) was selected for initially evaluating the effect of different chemistries on the lubrication of Si_3N_4 .

5.3. Speculated PPO Lubrication Mechanism for Si_3N_4

The combination of wear test results, observations, and analyses suggests that PPO has a definite, but limited, ability to lubricate Si_3N_4 . The abundance of HMW organic reaction products indicates that PPO oxidizes and polymerizes under the elevated

temperatures of the contact junction. This "friction polymer" should have a role in increasing the local viscosity and forming a protective film on the surfaces of the wear scar in a manner similar to that seen for metal lubricated systems. The lack of catalytic metals in the case of Si_3N_4 may be partially compensated by the elevated temperatures due to lower thermal diffusivity of the ceramic. In metal-lubricated systems, however, the metal is also associated with metalo-organic HMW polymer⁹², suggesting good adhesion between the polymer and the metal surface. The lack of Si-containing metalo-organic compounds indicates that PPO may not react directly with the Si_3N_4 surface to any measurable degree. This suggests a poor adhesion potential between a PPO film and the Si_3N_4 surface. This poor adhesion potential infers that PPO and HMW products from PPO may be easily squeezed out of the wear contact and explains why PPO cannot sustain high loads as observed in the load capacity tests.

5.4. Effect of Iron Impurities

One important concern with ceramics is the role of metal impurities. Chen⁵⁵ has shown that small amounts of metal impurities such as iron can influence lubrication significantly. The Si_3N_4 used in this study was known to contain ~ 2000 ppm of iron, probably concentrated in the grain boundaries; therefore analyses were conducted to determine whether we were merely observing effects from these iron impurities. Reaction products from PPO and octanol lubricated wear tests were analyzed using GPC-GFAA set to detect Fe. No iron-containing reaction products were found. Given the part-per-billion

sensitivity of the technique it is unlikely that iron impurities are dominating the reactions observed in these wear tests.

Pin-on-Disk (POD) tests were conducted using neat PPO and Rutgers Si_3N_4 with an iron impurity content below 10 ppm to see if the low load lubrication of Si_3N_4 by PPO was related to the iron impurity. The POD test was used because it was not feasible to make ball specimens from this experimental material. The results, given in Figure 5.11, show that the low iron Si_3N_4 can be lubricated by PPO at low loads (20 N), but not at higher loads (45 N). The transition region near 25-30 N is estimated from the BTF data and show that the data from the two tests are consistent with one another, even though the POD data is very limited.

All of this evidence suggests that iron chemistry is not dominating the reactivity in the Si_3N_4 lubricated contact.

5.5. Friction Trace Types Observed in this Study

Wear tests were conducted at the selected conditions using purified paraffin oil blended with 1 % (wt) of each chemical compound. The performance of the chemical compounds in this study was characterized by three parameters : i) Wear scar diameter, ii) Coefficient of friction at the end of the test, and iii) Friction trace type. The first two of these are self explanatory, however the third needs to be illustrated.

Four types of friction traces were observed in the course of this study and classified as types I, II, III, and IV (Figure 5.12). The first type (type I), is exhibited by purified paraffin oil without any additive. This friction behavior indicates a relatively poor lubrication condition. At the beginning of the test, friction immediately rises to a high level

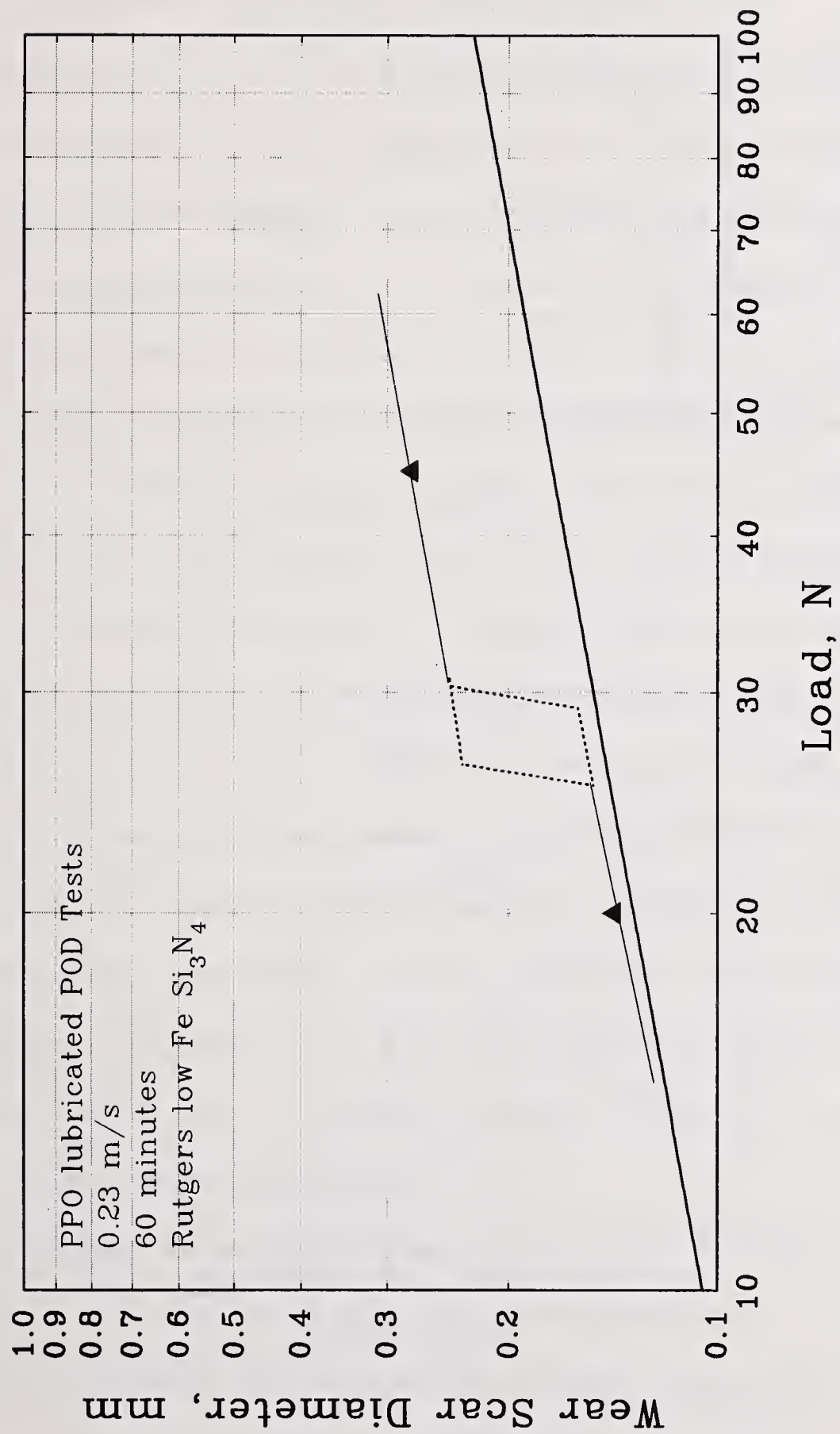
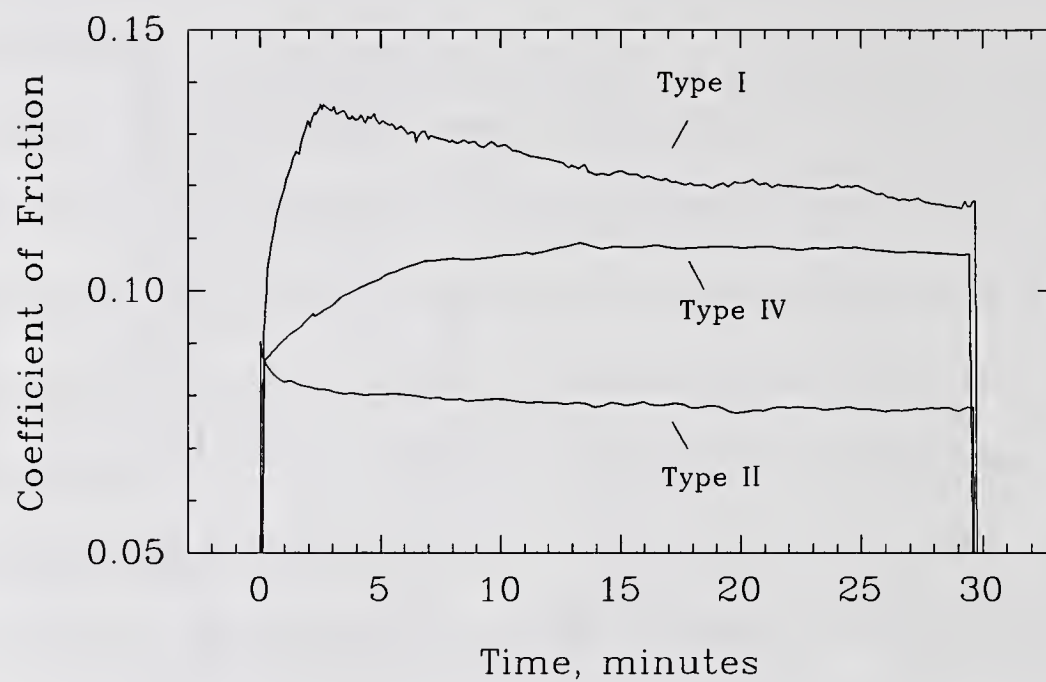


Figure 5.11 POD Test Results for Rutgers Low Fe Si_3N_4 Lubricated by PPO

(a)



(b)

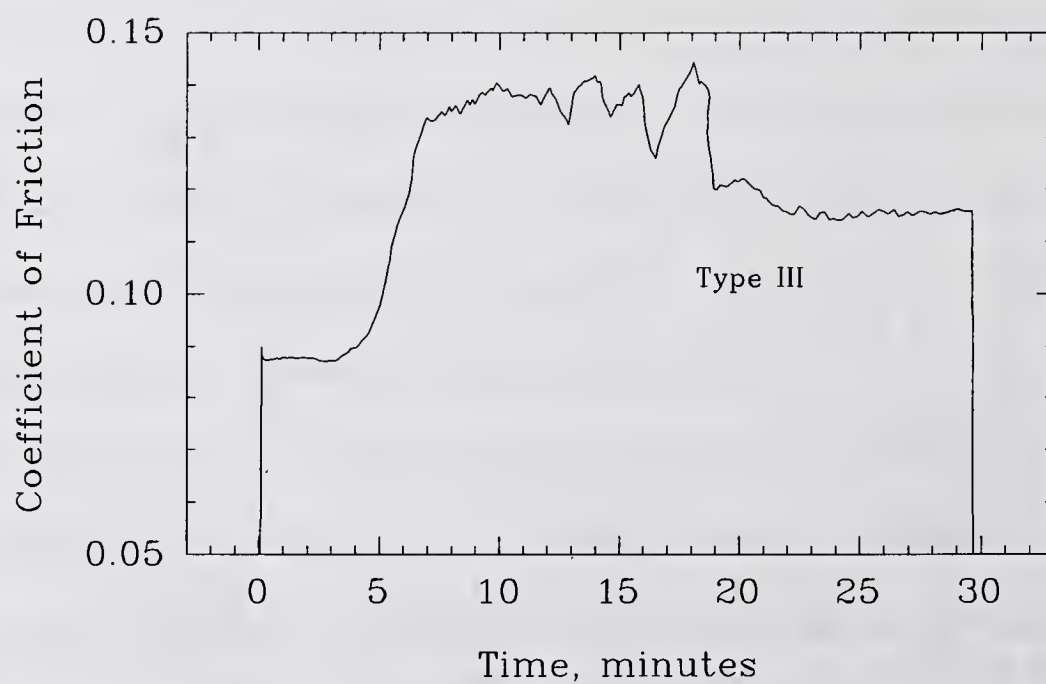


Figure 5.12 Different Friction Trace Types Encountered: a) Types I, II, and IV, b) Type III

(typically 0.13) and either remains high or gradually lowers during the test. The friction trace itself is usually fairly rough and can contain friction spikes.

Some chemical compounds exhibit a different kind of friction trace. For example, polypropylene glycol (triol) produces an immediate decrease in friction to a steady value. This is termed type II friction behavior. This type of behavior is usually characteristic of good lubrication. In general, the friction trace for type II behavior is smooth. However, small smooth friction "bumps" can sometimes be observed.

A third type of friction behavior (type III) is exemplified by polypropylene glycol (diol - 400 MW). Initially, friction is low, but at some point in the test, a transition to higher friction occurs. Final coefficient of friction values can be low or high depending on the complexity and severity of the transitions. This type of friction may be thought of as a sequential composite of types II and I. Initially, good lubrication exists (type II friction); then, at some point in the test, lubrication breaks down and a transition to high wear occurs (type I friction). This type of behavior indicates a potentially good lubricant which has exceeded its capability. This may be due to temperature or concentration considerations, which means that under lower severities or at higher concentrations the lubricant may function adequately. Alternatively, this type of behavior could be due to a time dependant wear transition similar to fatigue. In both cases, however, the indication is that the chemistry is initially providing good lubrication.

A fourth type of friction behavior (type IV) is exemplified by Mg salicylate. Friction starts out low (≈ 0.088), then slowly climbs to a steady, moderate value (≈ 0.108) as the test progresses. This friction type is associated with low wear. It is speculated that the

difference in the friction behavior for the two low wear friction types (II and IV) reflects a fundamental difference in the nature of the lubricating film.

These friction type classifications provide the second-level of evaluation for identifying potential boundary lubrication chemistries for Si_3N_4 . The first level (wear) is straightforward. Low wear is successful lubrication, and high wear is poor lubrication. Yet, within the high wear results are several possible reasons for failure: i) the chemistry doesn't work (Type I), ii) the chemistry works initially, but later fails (for a variety of reasons) (Type III). In general, the friction type interpretation is:

- Good lubrication: Type II, or Type IV
- Possible (temporary) lubrication: Type III
- Poor Lubrication: Type I

The use of friction types is especially valuable for interpreting results among chemistries within a single class of compounds.

Chapter 6

SURVEY OF OXYGEN-CONTAINING CHEMISTRIES

Oxygen-containing chemical compounds were evaluated for lubrication effectiveness with Si_3N_4 . The compounds included alcohols, acids, esters, and epoxides and were soluble in the base paraffinic oil used in the study. One of the reasons for selecting these oxygen-containing compounds is the high bonding energy between silicon and oxygen (higher than most of other bonds including Si-N). This suggests that compounds that contained oxygen have a high potential for forming a stable bond with Si_3N_4 .

Wear tests were conducted at concentrations of 1% in PPO. Standard wear test conditions of 0.23 m/s (600 rpm), 60 kg load, and 30 minutes were used. Some compounds were also tested in neat form under the same test conditions.

6.1. Wear Tests Results for 1% Oxygenates in PPO

The wear tests results of oxygen-containing compounds is mixed; some compounds reduce wear and some increases wear, as illustrated in Figure 6.1. The numerical data are also summarized in Table 6.1. Graphically, there are two groups of compounds: one set of seven compounds gave reduced friction and wear, and a second set of compounds that gave little benefit or even higher wear than PPO.

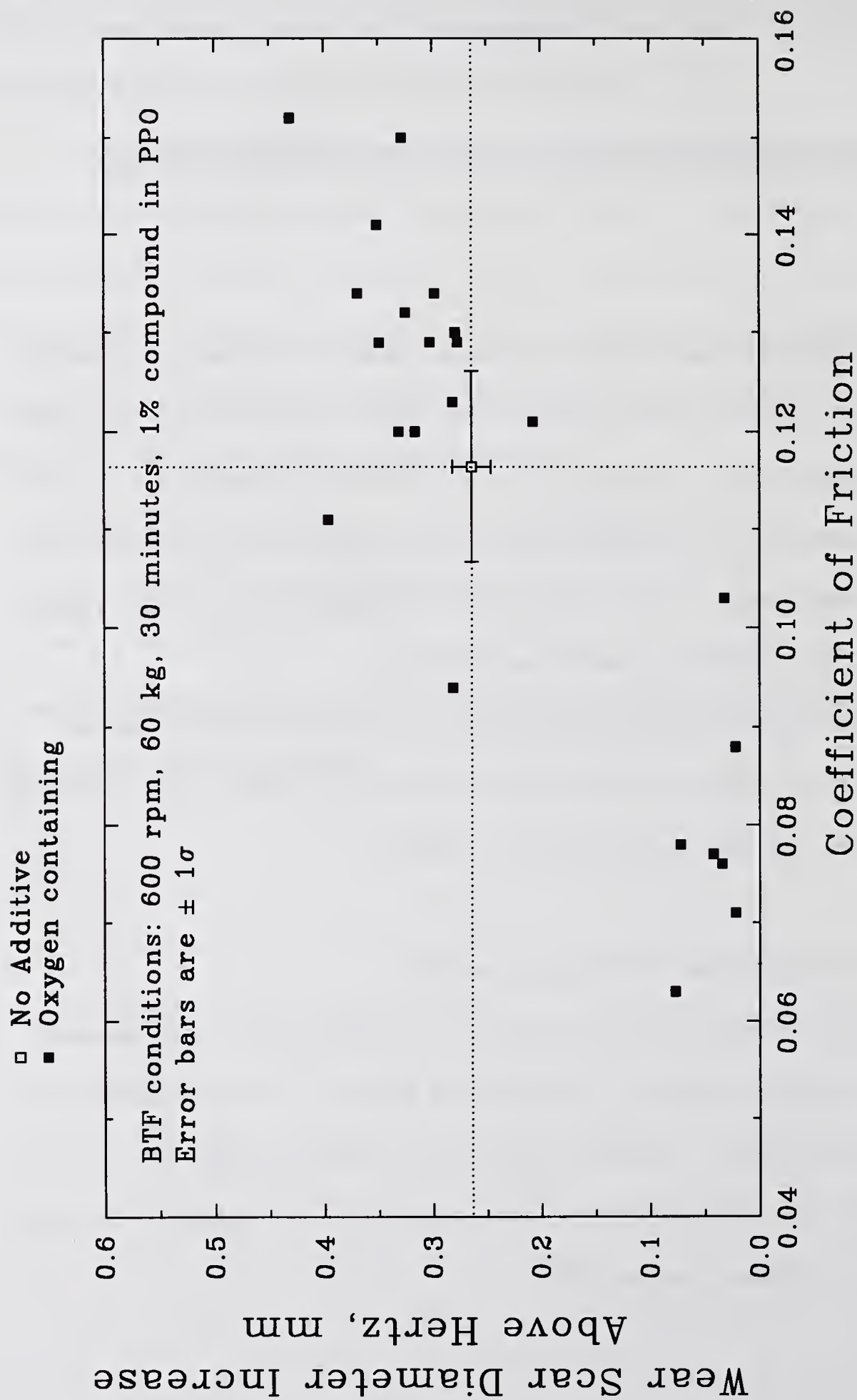


Figure 6.1 Summary Friction and Wear Data for Si_3N_4 BTF Tests on 1% Oxygen-Containing Compounds in PPO

Table 6.1
Friction and Wear Data on Selected Oxygen-Containing Model Compounds

Chemical Compound ¹ NONE (average of 16 tests)	WSD (mm) 0.645	Dia increase above Hz, mm 0.265	COF ²	Frict. Type ³ I	Wear Scar Appearance smooth	Film in Scar ? no	Lubrication Classification Poor
3-n-Pentadecyl Phenol	0.402	0.022	0.071	II	roughened	yes - plastic	Good
Mannich Product	0.402	0.022	0.088	II	smooth	yes - spotty	Good
Magnesium Salicylate (Ca overbased)	0.412	0.032	0.103	IV	smooth	yes	Good
Oleic Acid	0.414	0.034	0.076	II	smooth	yes - plastic	Good
Polypropylene Glycol (diol) [1000 MW]	0.422	0.042	0.077	II	smooth	yes - plastic	Good
Polypropylene Glycol (triol) [600 MW]	0.452	0.072	0.078	II	smooth	yes - plastic	Good
Polyethylene Glycol (diol) [400 MW]	0.457	0.077	0.063	II	smooth	yes - plastic	Good
Polydimethylsiloxane [350 cSt]	0.587	0.207	0.121	I	smooth	no	Poor
Epoxidized polybutene (E16) [028]	0.657	0.277	0.129	I	smooth	no	Poor
Polypropylene Glycol (diol) [400 MW]	0.659	0.279	0.130	III (22)	smooth	no	Temporary
Polyalkylene Glycol Der. (WS) [460 SUS]	0.661	0.281	0.094	I	smooth	no	Poor
2,6-di-tertiarybutyl-p-cresol	0.661	0.281	0.123	I	smooth	no	Poor
Bis (2-ethylhexyl) Phthalate [038]	0.678	0.298	0.134	III (2)	smooth	no	Temporary
Epoxidized polybutene (E6) [028]	0.682	0.302	0.129	I	smooth	no	Poor
Ethyl Stearate	0.696	0.316	0.120	III (3)	smooth	no	Temporary
1-Octanol	0.705	0.325	0.132	III (1)	grooved	no	Temporary
Diacid [560 MW]	0.708	0.328	0.150	III (2)	grooved	no	Temporary
High Erucic Acid Rapeseed Oil	0.711	0.331	0.120	III (1)	smooth	no	Temporary
Bis (2-ethylhexyl) Sebacate [038]	0.729	0.349	0.129	III (2)	smooth	no	Temporary
Polyalkylene Glycol Der. (WS) [260 SUS]	0.731	0.351	0.141	III (18)	smooth	no	Temporary
Polyol Ester	0.749	0.369	0.134	I	smooth	no	Poor
Fatty and Synthetic Esters	0.776	0.396	0.111	III (1)	smooth	no	Temporary
Polyalkylene Glycol Der. (WD) [285 SUS]	0.811	0.431	0.152	I	roughened	no	Poor

¹ 1 wt % in purified paraffin oil

² Measured at the end of the test

³ Number in parenthesis indicates time to friction transition in minutes.

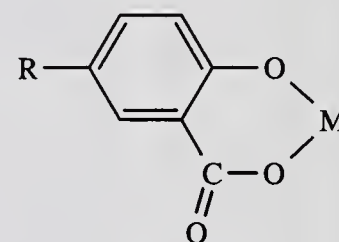
All Tests conducted on CER024 NC132 Hot pressed Si₃N₄ (unless otherwise noted-eg. [028])
Conditions of BTF tests: 600 rpm, 60 kg, 30 minutes, 1% additive in PPO, 21°C.

Within each of the two groups, there are different chemical compound types, and varying degree of effectiveness. The results will be discussed by chemical compound class, starting with the effective ones.

Compounds found to reduce wear at 1% by weight in PPO included a metal salicylate, oleic acid, and several alcohols including glycols. All of the antiwear oxygen-containing compounds also exhibited low friction, type II or IV friction type, and observable film-like features inside the wear scar. The appearance of the film varied from compound to compound. In most cases, the surfaces of the wear scars were smooth.

Salicylates are normally used as detergents in metal systems. They are not antiwear agents for metals, but for Si_3N_4 , the salicylate used exhibits significant antiwear activity at 1% in PPO. According to Figure 6.2, this compound exhibited type IV friction behavior (initial slight increase in friction at the beginning of the test).

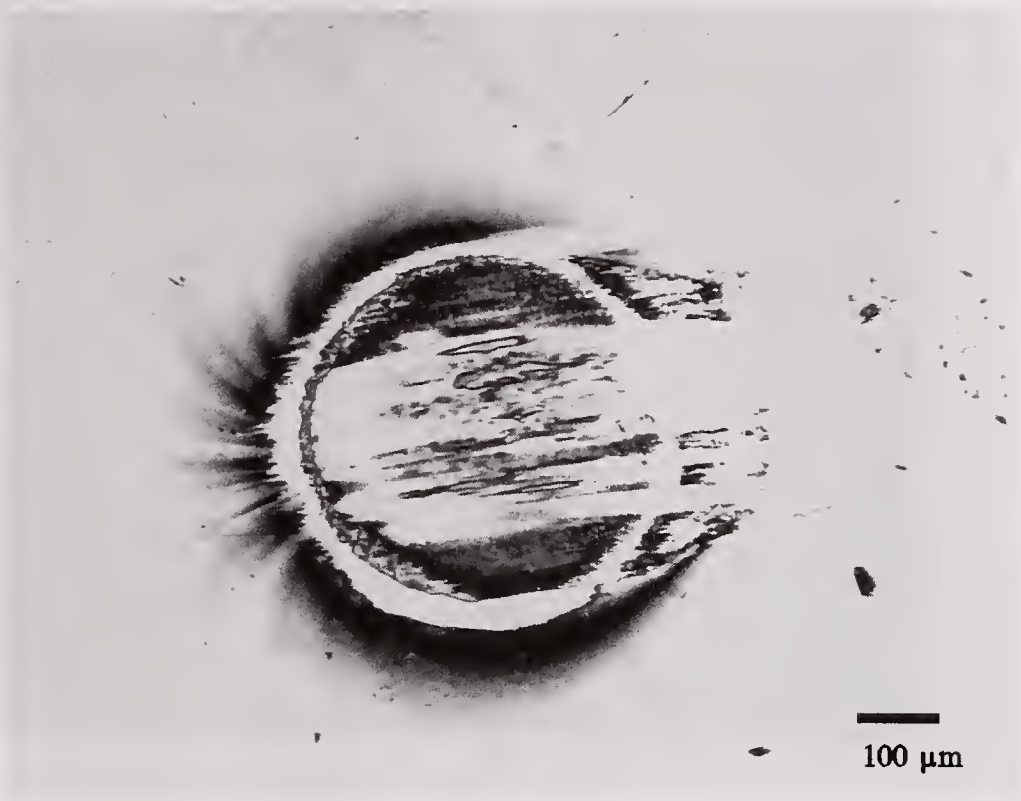
A solid-looking film was visible optically, and very little deposit could be seen surrounding the wear scar. SEM analysis confirmed the solid-looking nature of this coherent film (Figure 6.3A). The salicylate used was a magnesium salicylate, and



Salicylate

contained the usual calcium carbonate overbasing (Total Base Number: 346). The EDX analysis of the wear scar (Figure 6.4) indicated that the protective film within the wear scar contained Mg but no Ca (Ca would show up at 3.7 keV). This suggests that the active antiwear functional group is the salicylate itself, and the overbasing calcium carbonate was not incorporated into the protective film. The iron (Fe) and tungsten (W) seen in the EDX analysis are impurities in the original Si_3N_4 material. The concentrations observed are the

(a)



(b)

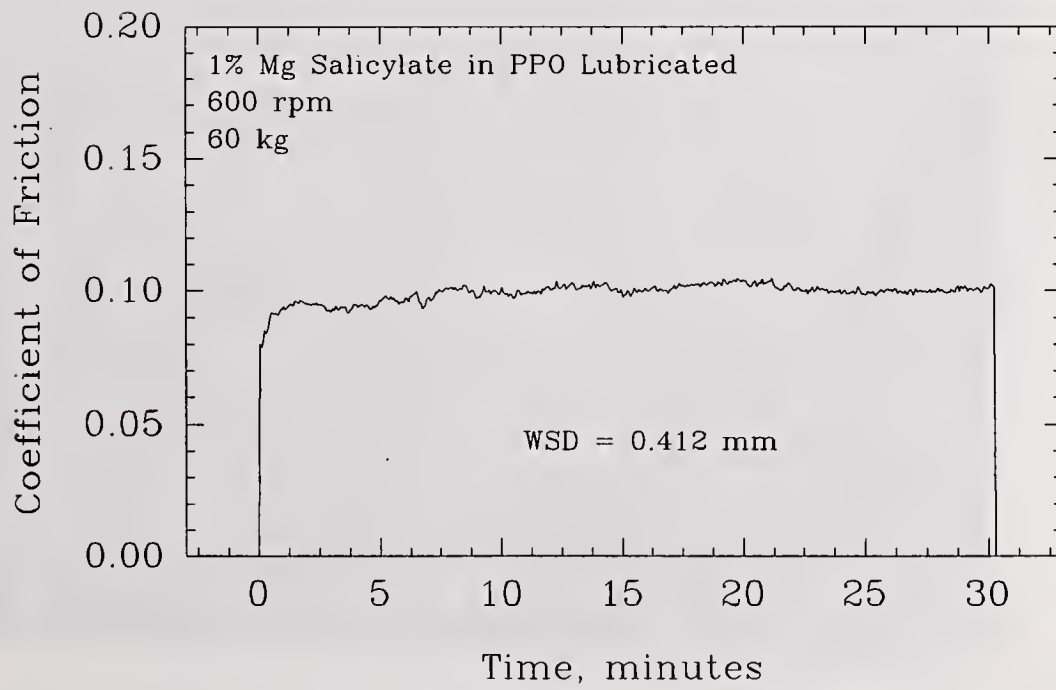


Figure 6.2 1% Mg Salicylate in PPO Lubricated Si_3N_4 BTF Test at 60 kg: a) Optical Photomicrograph, b) Friction Trace

(a)



(b)

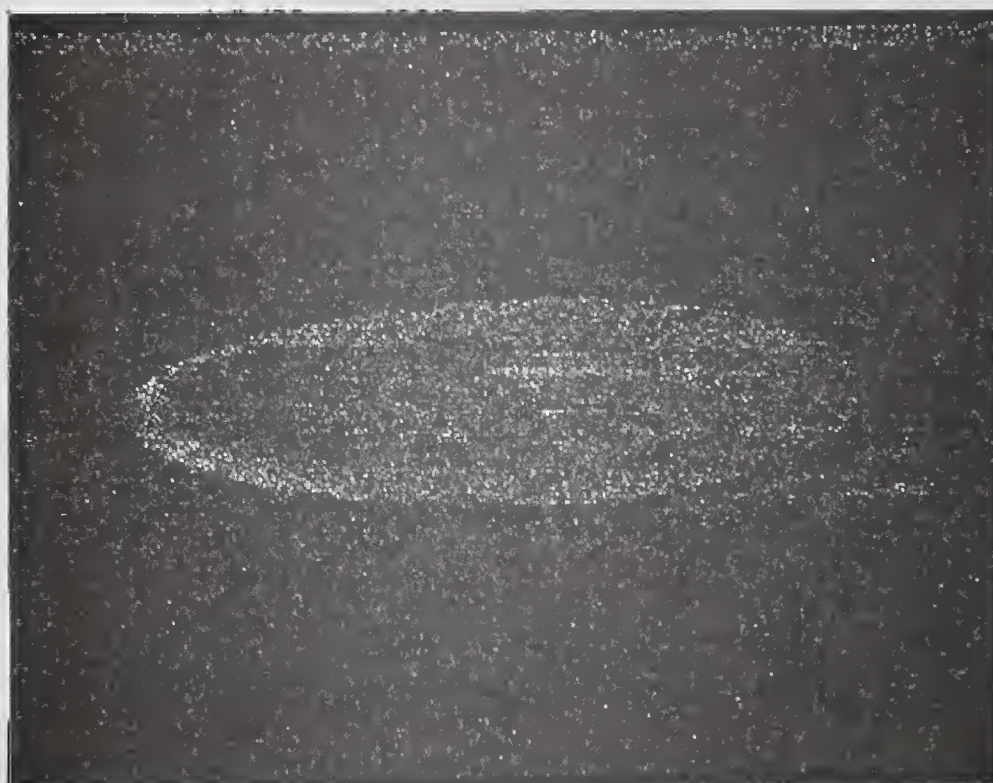


Figure 6.3 SEM Photomicrographs for 1% Mg Salicylate in PPO Lubricated Si_3N_4 BTF Test at 60 kg: a) Secondary Electron Image, b) EDX Image (Mg)

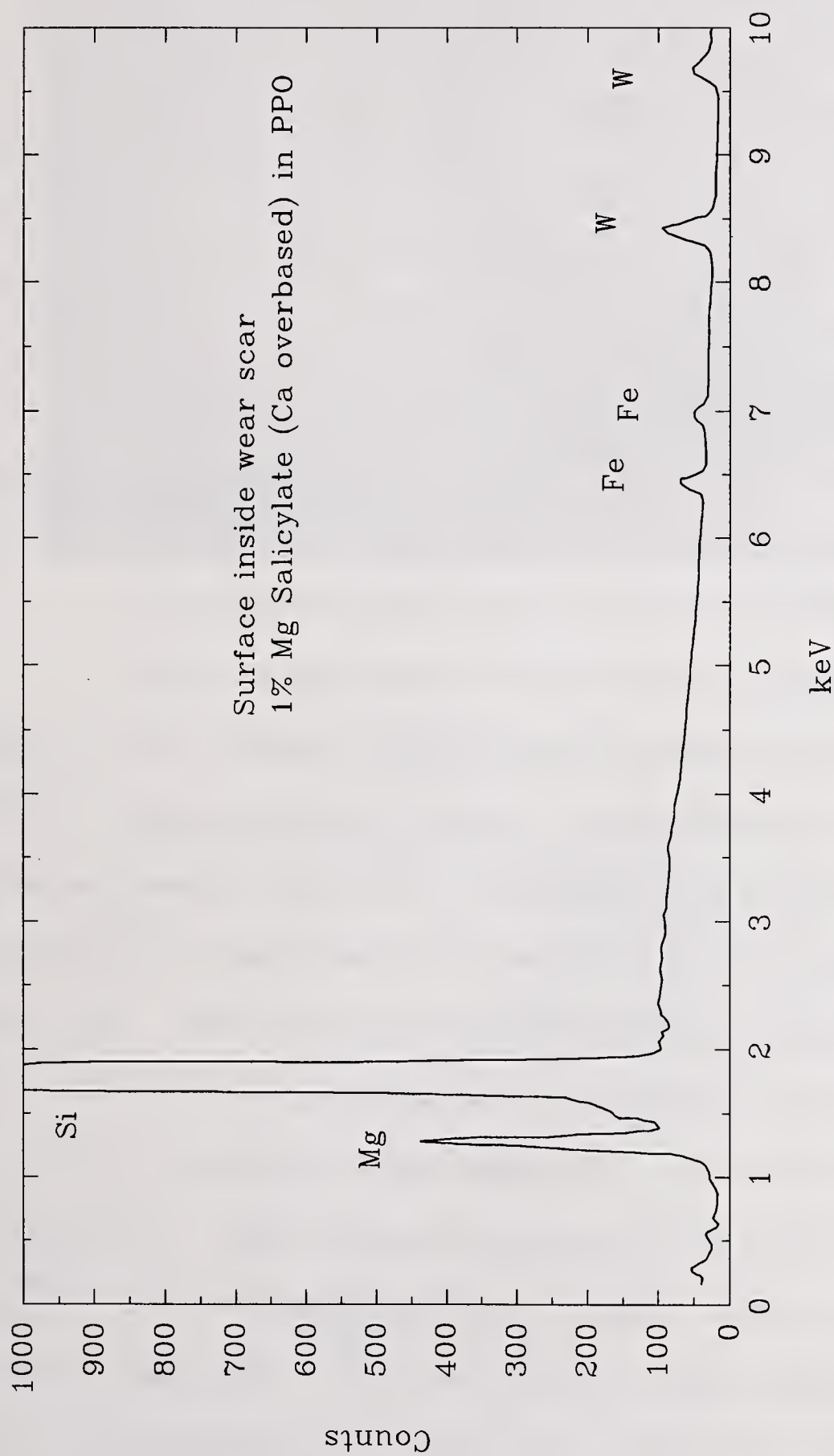
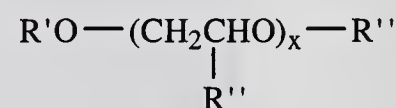
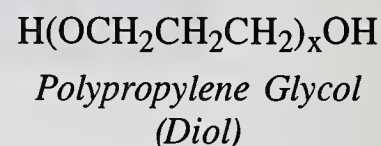
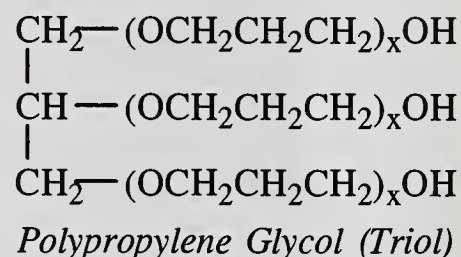


Figure 6.4 EDX Spectrum for Surface inside Wear Scar for 1% Mg Salicylate (Ca Overbased) in PPO Lubricated Si_3N_4 BTF Test at 60 kg

same as in the parent material. A Mg x-ray elemental mapping of the surface inside the wear scar at the same orientation and magnification as Figure 6.3A confirms that the distribution of Mg in the wear scar is associated with the film (Figure 6.3B).

Several glycols were tested, and within the glycol family, there are some trends. Polypropylene glycol (triol) [600MW] (Figure 6.5) had a wear scar and friction trace fairly typical of the effective glycol compounds. The film observed inside the wear scar had the appearance of a solid-like plastically deformed material. Similar film shapes were obtained with polypropylene glycol (diol) [1000 MW], and polyethylene glycol [400 MW]. Polypropylene glycol (diol) [400 MW] started with a low friction just like the 1000 MW version and the 600 MW triol, however, twenty-two minutes into the test, a transition to high friction took place (Figure 6.6). As a result, wear at the end of the test was the same as the pure paraffin oil. The wear scar surface is smooth and similar to the PPO case; however there are two small grooves running across the scar.

The polyalkylene glycol derivatives were not successful at 1% in PPO. This may be due to the different chemical nature of the derivatives. The R group substitutions will yield no more than one hydroxyl group per molecule (the water soluble derivatives). In the case of the water insoluble ones, the substitutions result in only ether linkages ($R'' = \text{alkyl group}$). These derivatives are

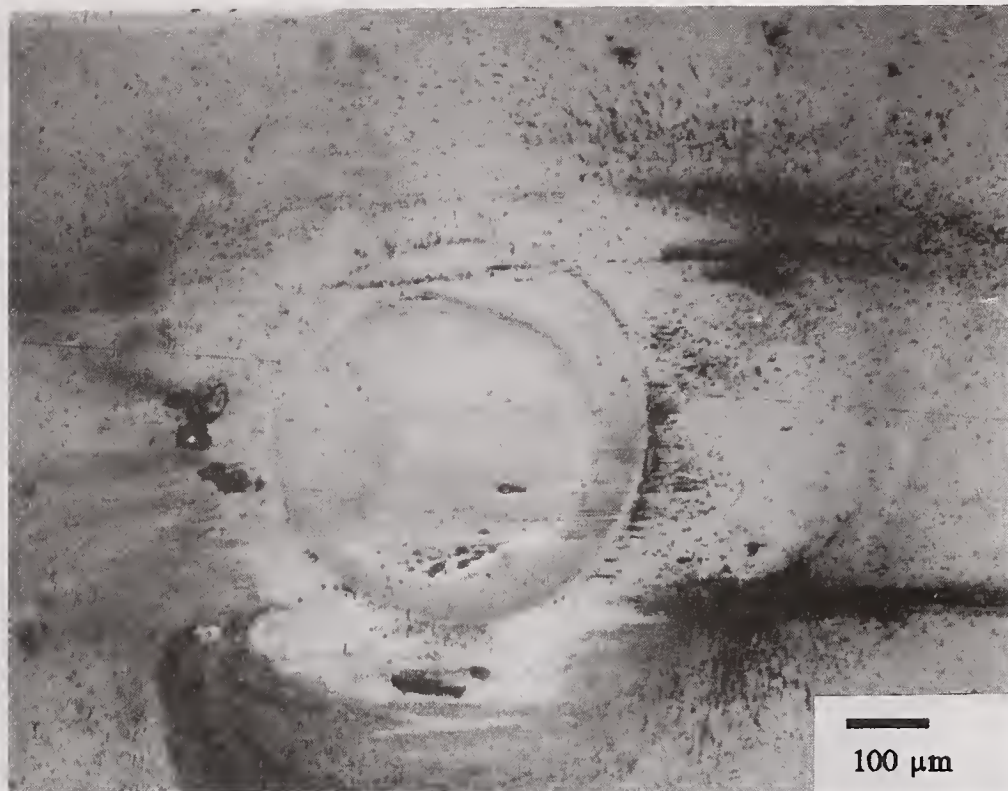


$\text{R}' = \text{Alkyl group}$

$\text{R}'' = \text{Alkyl group or H}$

Polyalkylene Glycol Derivatives

(a)



(b)

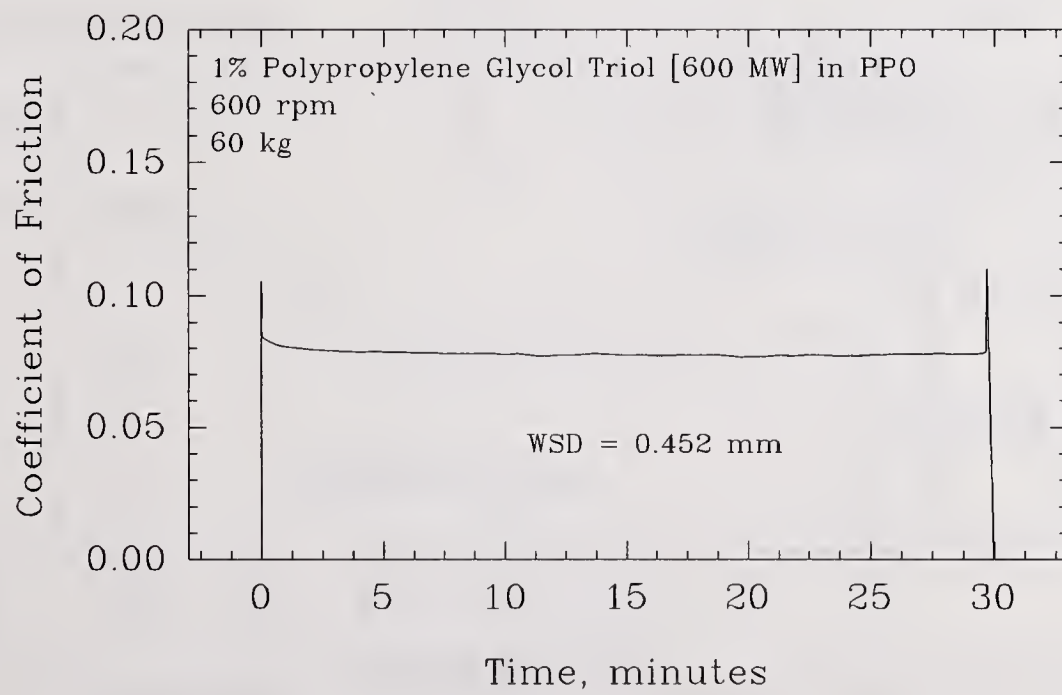
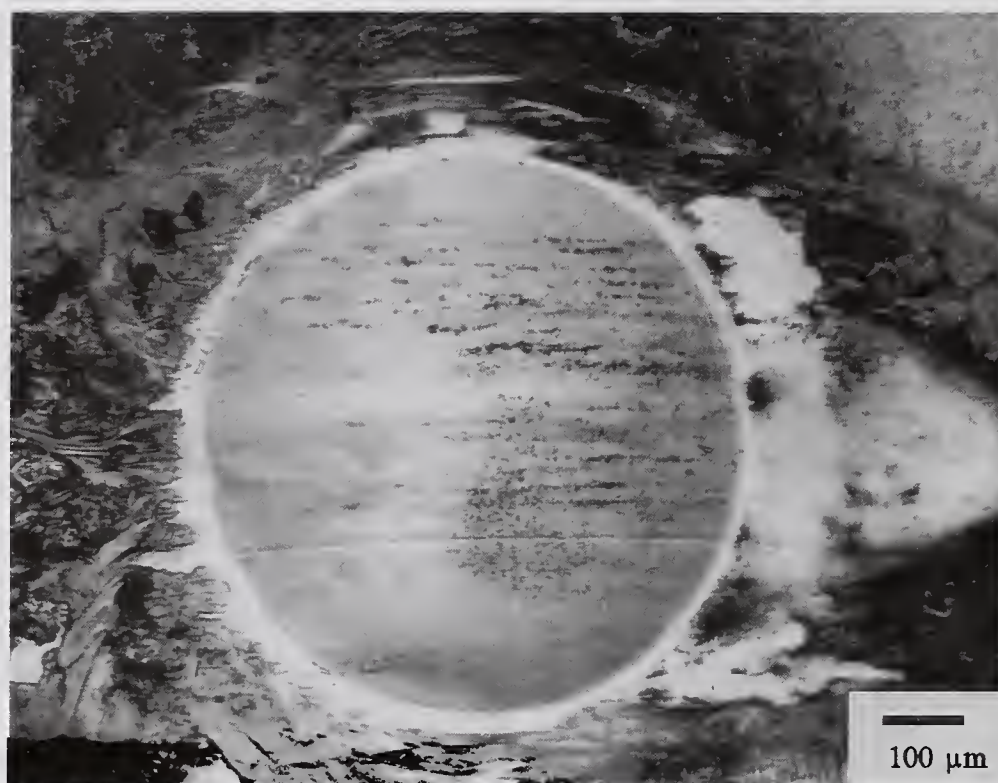


Figure 6.5 1% Polypropylene Glycol Triol [600 MW] in PPO Lubricated Si_3N_4 BTf Test at 60 kg: a) Optical Photomicrograph, b) Friction Trace

(a)



(b)

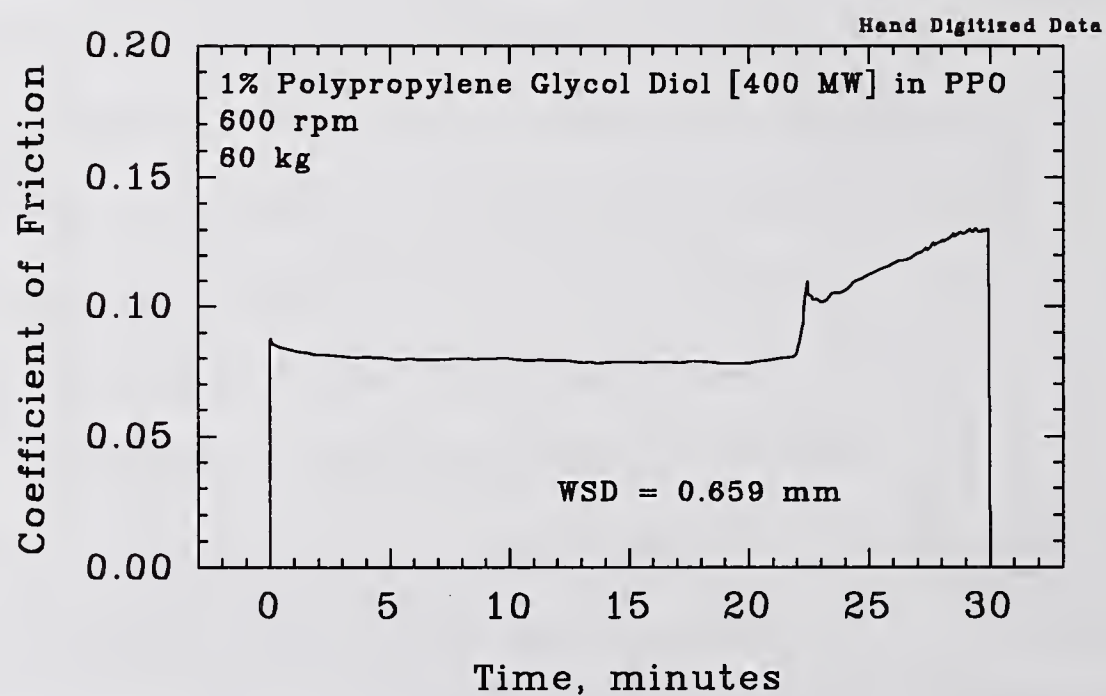
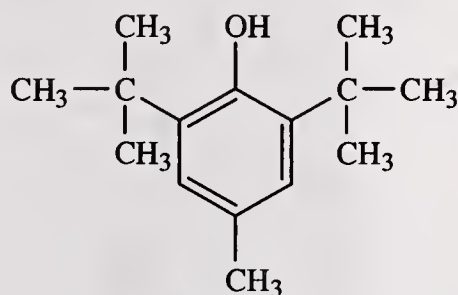


Figure 6.6 1% Polypropylene Glycol Diol [400 MW] in PPO Lubricated Si_3N_4 BTF Test at 60 kg: a) Optical Photomicrograph, b) Friction Trace

therefore only HMW monoalcohols or ethers.

Some other mono-alcohols were not effective at 1% in PPO. Octanol blended into PPO at 1% gave low friction for only about one minute before a transition to high friction occurred.

A typical hindered phenol antioxidant (2,6 di-*t*-butyl-*p*-cresol) did not affect the wear significantly.



Di-t-butyl p-cresol

The Mannich reaction product is an ashless

dispersant that contains both an aromatic OH and an amine group. It has a polyamine chain structure similar to a succinamide. The Mannich reaction product normally does not have any antiwear function in metal systems

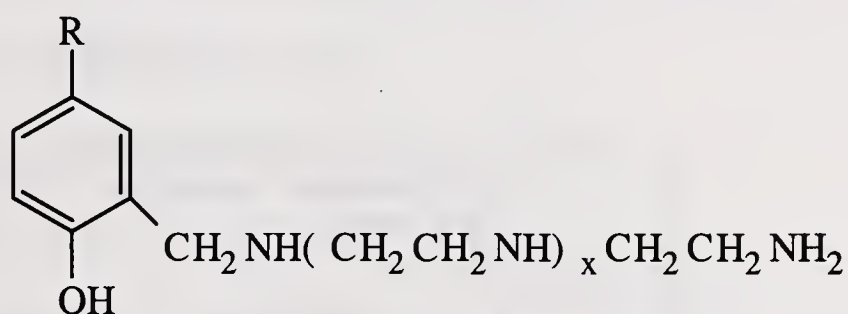
but gave low wear and friction and

type II friction behavior with

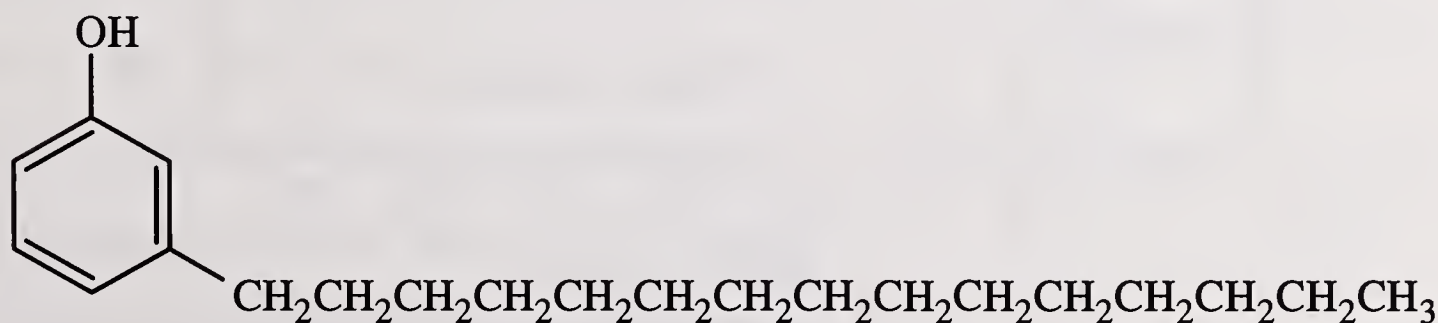
silicon nitride (Figure 6.7). The

wear scar surface at the end of the

test had a patchy surface film.



Mannich Product



3-n-pentadecyl Phenol

(a)



(b)

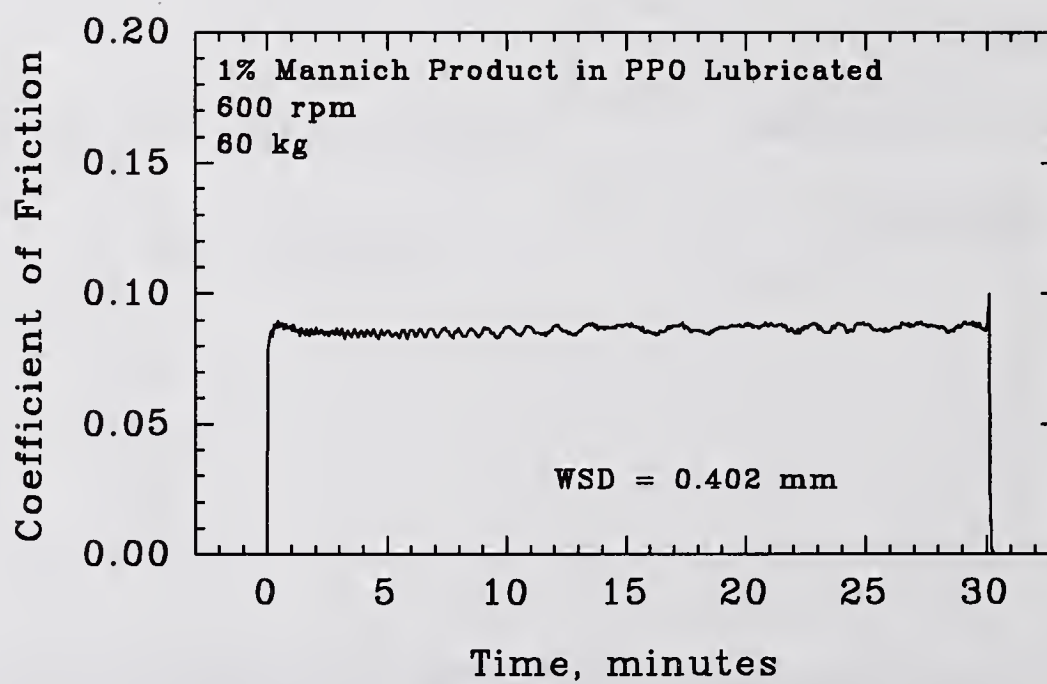
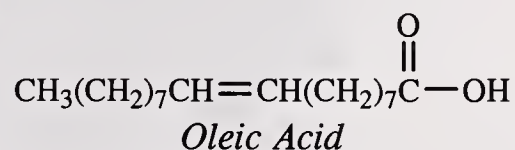


Figure 6.7 1% Mannich Product in PPO Lubricated Si_3N_4 BTf Test at 60 kg: a) Optical Photomicrograph, b) Friction Trace

Another phenol, 3-n-pentadecyl phenol, gave very low wear and friction when blended into PPO at 1%. The wear scar diameter is very close to the Hertzian wear scar diameter. The wear scar has a somewhat roughened surface (Figure 6.8) and the friction coefficient is low and steady throughout the test. These results may suggest that the phenol (aromatic hydroxyl) group is active and may lubricate Si_3N_4 if it is not sterically hindered (as in the case of the 2,6-ditertiarybutyl-p-cresol).

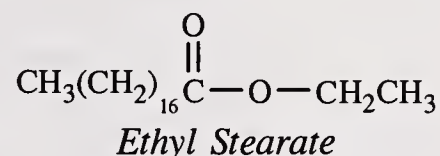
Oleic acid was found to be effective at 1% in PPO. Other higher MW acids such as the diacid, and the high euricic acid rapeseed oil, were not effective at this concentration; although they did exhibit type III friction.



This suggests that they may be effective at lower test severity or higher concentration.

Esters do not seem to be effective under the conditions of this test. The monoester (ethyl stearate) had low friction for the first 3 minutes of the test, but then friction increased (type III friction behavior).

The friction trace (Figure 6.9) is fairly typical for the esters used in this study. The wear scar appearance at the end of the



test was similar to PPO; however, wear was slightly

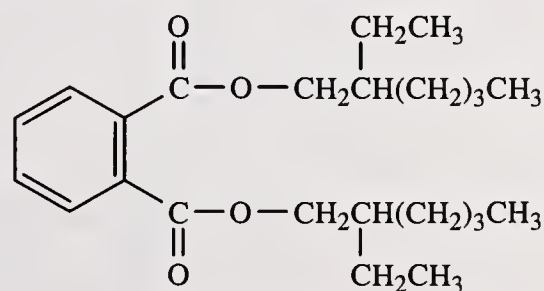
higher. The aryl di-ester [bis (2-ethylhexyl) phthalate]

also exhibit a lower friction for the first 2 minutes of

the test; however, the wear scar diameter and wear

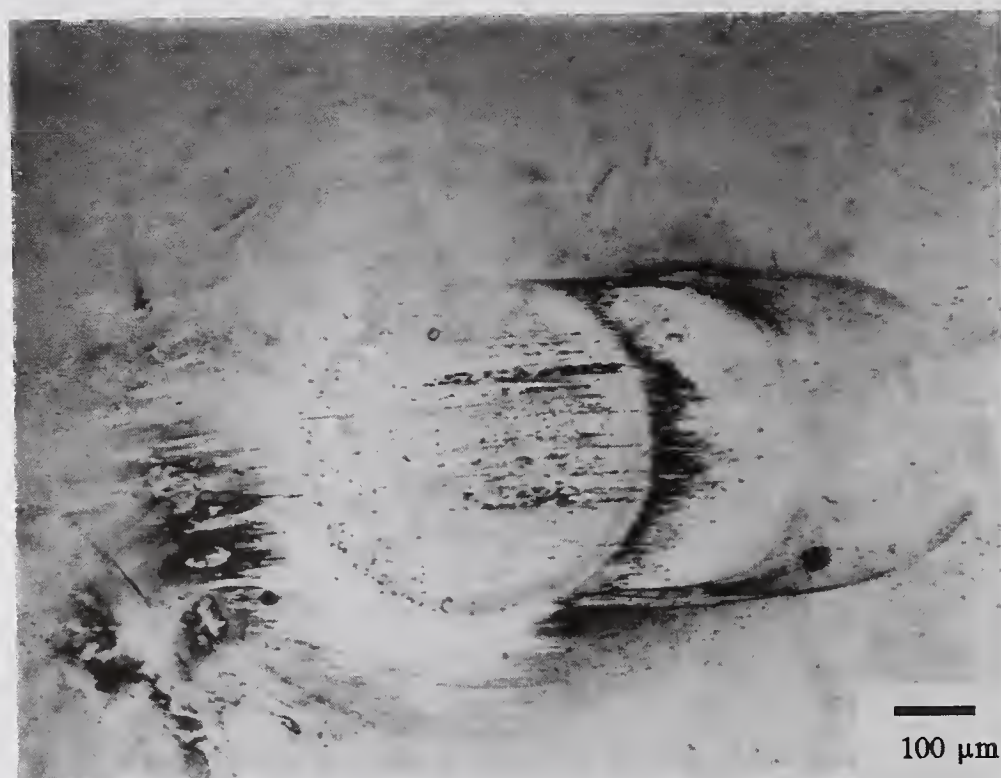
scar appearance were very similar to PPO. The alkyl

version of this ester [bis (2-ethylhexyl) sebacate] had



Bis (2-ethylhexyl) Phthalate

(a)



(b)

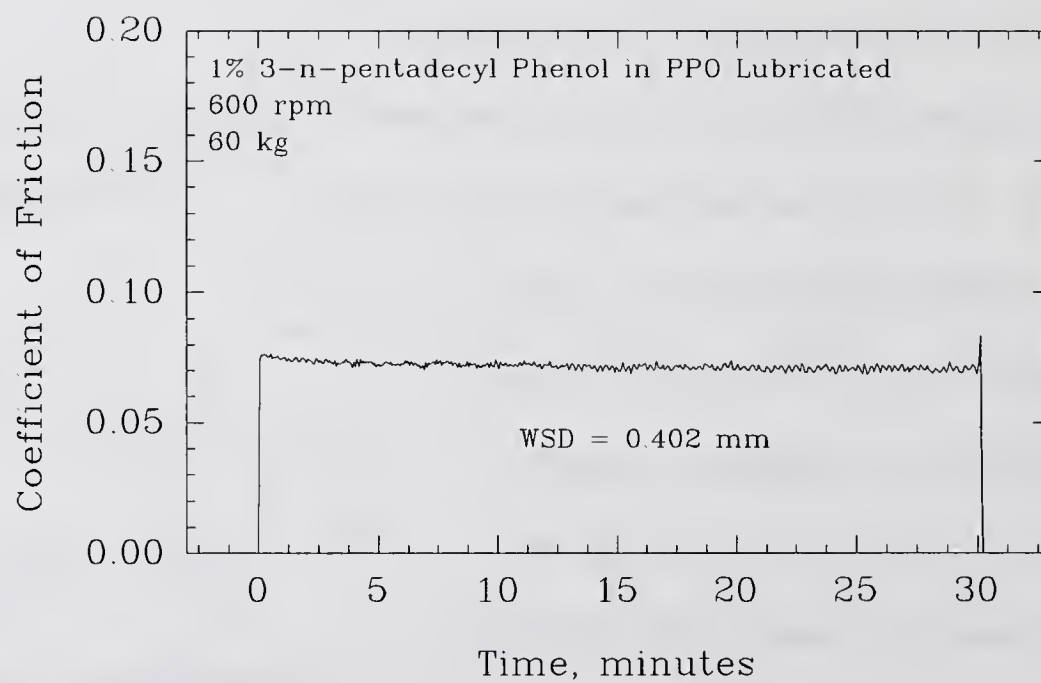


Figure 6.8 1% 3-n-Pentadecyl Phenol in PPO Lubricated Si_3N_4 BTf Test at 60 kg: a) Optical Photomicrograph, b) Friction Trace

(a)

113



(b)

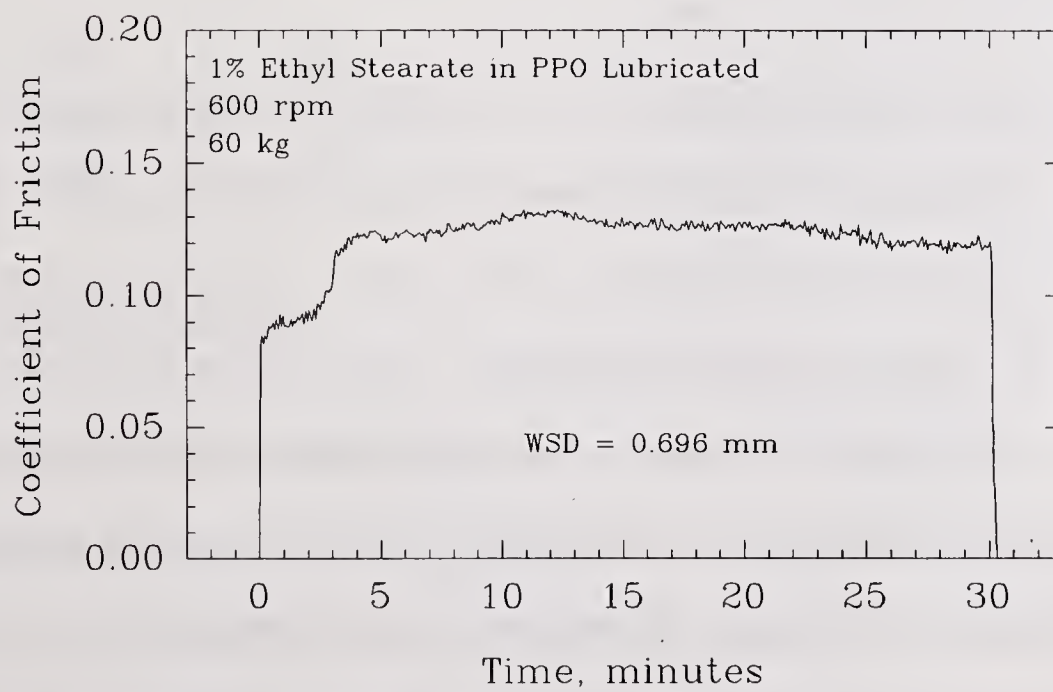
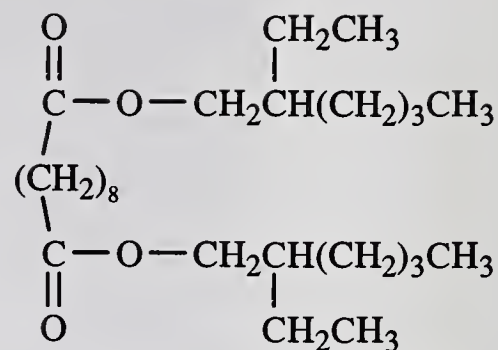


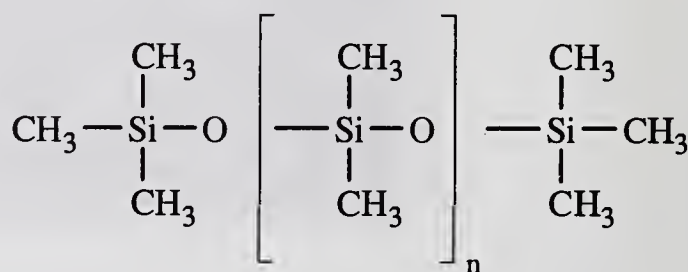
Figure 6.9 1% Ethyl Stearate in PPO Lubricated Si_3N_4 BTFT Test at 60 kg: a) Optical Photomicrograph, b) Friction Trace

lower friction for only the first 2 minutes. The wear scar diameter was significantly higher than that of PPO. The polyol ester had no measurable low friction region during the test and the wear scar at the end of the test was similar in appearance to PPO.



Bis (2-ethylhexyl) Sebacate

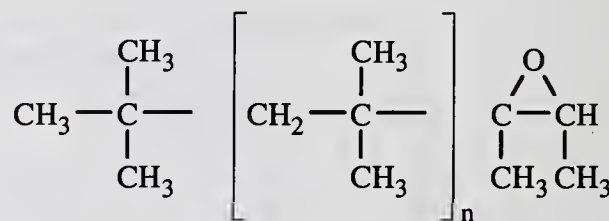
Polydimethylsiloxane did not seem to have much of an effect on the friction and wear of Si_3N_4 at a concentration of 1% in PPO. The wear scar diameter was only slightly smaller than PPO. The friction type and level was similar to PPO.



Polydimethylsiloxane

The polymeric epoxides (epoxidized polybutenes) did not have any appreciable performance differences from neat PPO.

These results indicate that structure, number, and molecular weight of the functional groups are important. Oxygen-containing compounds can interact with the silicon nitride



epoxidized polybutene

surface, but the combination of chemical structure and molecular weight determines whether or not the interaction is beneficial. Hydroxyl groups seem to be especially important. The number and location of OH groups with respect to each other is probably also a factor. If these alcohols interact with the surface to form silicate esters as hypothesized by Tsunai²⁴⁰,

then it would make sense that a compound with two (or more) OH groups such as glycols might be more tenaciously bound to the surface.

In order to study the chemistry of these oxygen-containing compounds, several tests were conducted on neat compounds. When it became apparent that the alcohol functional group was able to lubricate Si_3N_4 , the study was broadened to include several different types of alcohol functional groupings and chain lengths.

6.2. Wear Test Results for Neat Compounds

A summary of the BTF wear test results of neat oxygen-containing compounds is shown in Table 6.2. Polyphenyl ether, bis (2-ethylhexyl) sebacate (ester), and polydimethylsiloxane could not lubricate as effectively as PPO. Polydimethylsiloxane actually had such poor lubrication that the test was terminated after seventeen seconds due to excessive friction ($\mu > 0.6$). In this short time, the wear scar diameter had grown to almost 2 mm.

Many neat alcohols and acids lubricated Si_3N_4 better than PPO under the test conditions. The high molecular weight diacid had the lowest wear of any of the compounds tested. The wear scar (Figure 6.10A) is visible mainly because of a residue present inside and in the exit region of the wear scar. This residue is slightly soluble in hexane, since further treatment of the flat with hexane could completely remove the residue. There is very little reaction product visible surrounding the wear scar, in contrast to that seen in the PPO case. Part of the reason for this may be due to the lower frictional heating observed. The friction trace is smooth, and the coefficient of friction remained near 0.06 throughout the

Table 6.2
Summary of Neat Oxygen-Containing Compound BTF Wear Test Data

<u>Compound</u>	<u>WSD</u> <u>(mm)</u>	<u>WSD</u> <u>Incr¹</u> <u>(mm)</u>	<u>Final</u> <u>COF</u>
PPO ²	0.645	0.265	0.117
Diacid [560 MW]	0.391	0.011	0.063
Oleic Acid	0.407	0.027	0.049
Oleil Alcohol	0.429	0.049	0.049
Polyalkylene Glycol Deriv. (WS) [260 SUS]	0.463	0.083	0.065
Polyalkylene Glycol Deriv. (WI) [285 SUS]	0.480	0.100	0.083
Polyalkylene Glycol Deriv. (WS) [460 SUS]	0.484	0.104	0.058
C ₁₈ OH (75°C)	0.495	0.115	0.046
Polyethylene Glycol (Diol) [400 MW]	0.522	0.142	0.055
Epoxidized Polybutene (E6)	0.524	0.144	0.099
Polypropylene Glycol (Diol) [1000 MW]	0.546	0.166	0.099
Glycerol	0.547	0.167	0.051
Polypropylene Glycol (Triol) [600 MW]	0.552	0.172	0.100
Polypropylene Glycol (Diol) [400 MW]	0.602	0.222	0.103
Polyphenyl Ether	0.733	0.353	0.095
Bis (2-ethylhexyl) Sebacate	0.919	0.539	0.148
Polydimethylsiloxane [350 cSt] ³	1.9 ³	1.5 ³	0.45 ³

1 Wear Scar Diameter Increase above the Hertzian Contact diameter (0.380 mm)
2 Average of 16 tests
3 Test terminated at 17 seconds due to excessive friction coefficient (>0.6). Friction coefficient was the steady-state value prior to test termination.

WS = Water Soluble
WI = Water Insoluble

test (Figure 6.10B). The dimer acid used was quite viscous, having a dynamic viscosity of 8 Pa•s (8,000 cP) at 25°C; therefore, elastohydrodynamic lubrication may be contributing to the low friction observed.



(b)

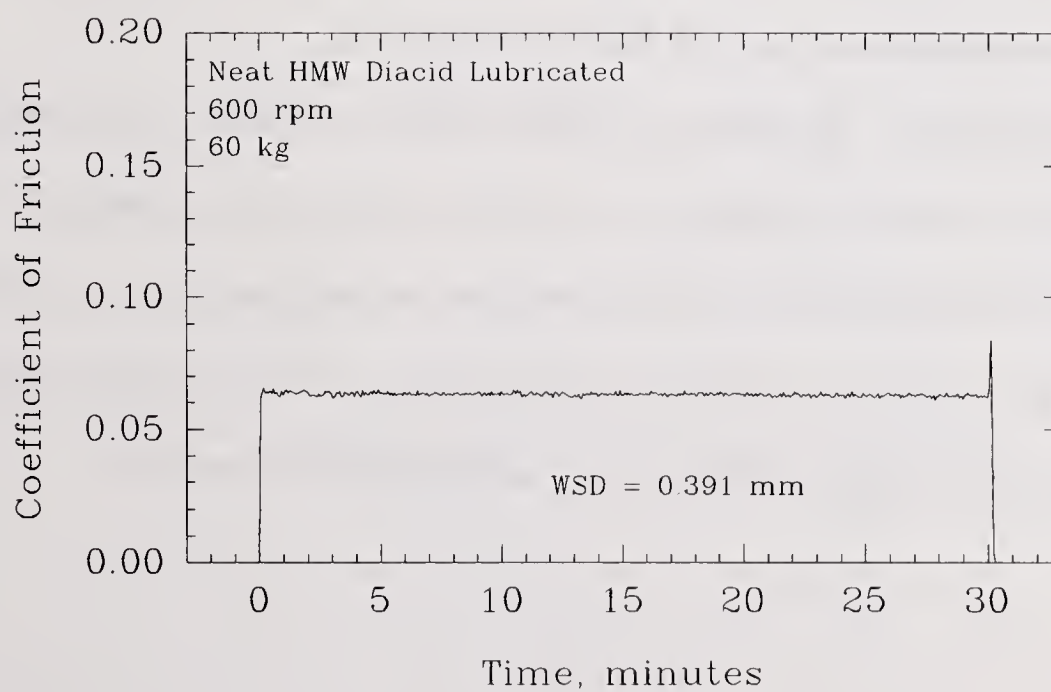
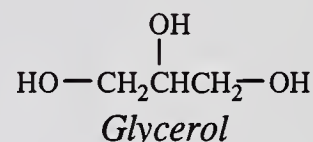


Figure 6.10 Neat HMW Diacid Lubricated Si_3N_4 BTf Test at 60 kg: a) Optical Photomicrograph, b) Friction Trace

Oleic acid produced the next lowest lowest wear and one of the lowest friction coefficients of any of the compounds tested. The wear scar (Figure 6.11A) contained some kind of deformed region that looked like it might be some kind of solid-like film. This feature seemed to cover all of the wear scar except the trailing edge of the scar. Very little reaction product was observed outside the wear scar. The friction trace (Figure 6.11B) is low and steady at a coefficient of friction of ≈ 0.05 .

Oleil alcohol had similar friction and only slightly higher wear than oleic acid. Octadecanol ($C_{18}OH$) was a solid at room temperature; therefore, it was tested at $75^{\circ}C$. Even at this higher temperature, this long chain alcohol managed to produce very low friction and wear.

The viscous polyalcohol glycerol, with three carbons and three OH groups, had slightly higher wear, but low friction. The other compounds tested were a variety of higher molecular weight alcohols with different number and



locations of OH groups. They also had different polymer backbones which affected other properties such as solubility (in water and organics), viscosity, and melting point. All of the glycols had lower wear than PPO, whether they were polyalkylene (PA) glycol derivatives, polyethylene (PE) glycols, or polypropylene (PP) glycols. Within a single structural type such as polypropylene glycol (Diol), longer chain length gives lower wear.

(a)

119



(b)

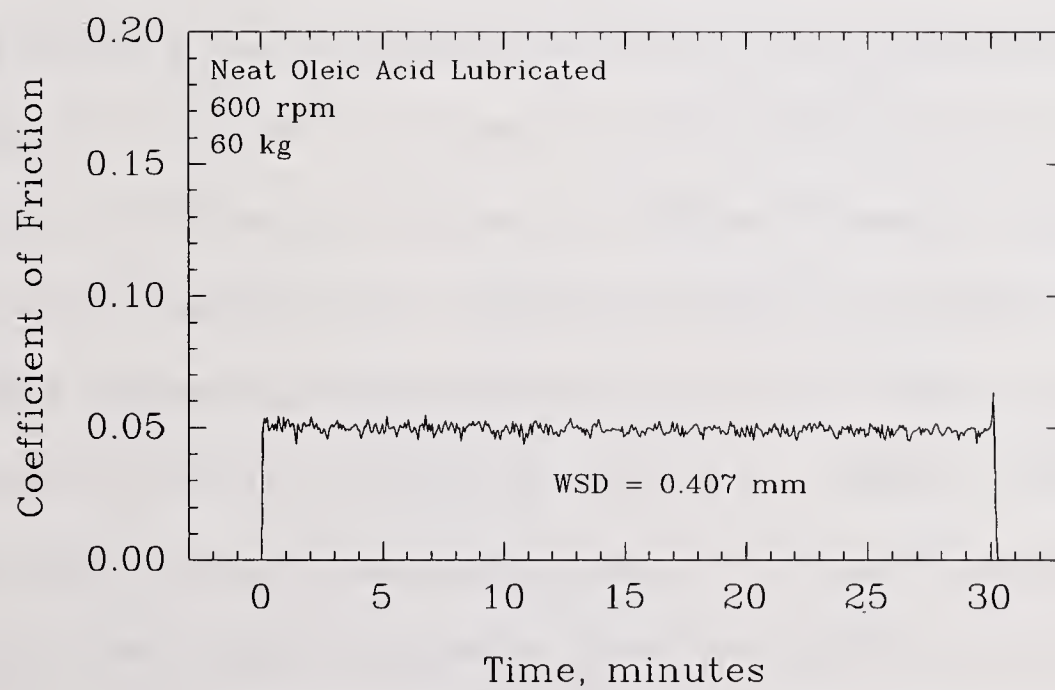


Figure 6.11 Neat Oleic Acid Lubricated Si_3N_4 BTF Test at 60 kg: a) Optical Photomicrograph, b) Friction Trace

6.3 Wear Tests on C₈ Compounds

A series of tests were also conducted on several oxygen-containing eight carbon (C₈) compounds in order to systematically see the effects of functional groups on lubrication of Si₃N₄ within a single chain length. This would reduce some of the chain length effects observed previously and allow a direct comparison of chemical structural effects. Eight carbon compounds were chosen because model compound were available in sufficient purity, and the proper "window" of melting point/boiling point existed.

According to the data in Table 6.3, the primary alcohol (1-octanol) is the only one that can lubricate under the standard wear test conditions. Figure 6.12 indicates that the friction was very low throughout the test, with a coefficient of friction of 0.049. This is very low considering that we are using an eight carbon alcohol with a room temperature absolute viscosity of less than 0.01 Pa•s (10 cP) and suggests that distinct chemical reactions may take place in the Si₃N₄ contact in the presence of alcohols. The wear scar was very circular. A wedge-shaped feature can be seen within the wear scar in the leading edge portion. No deposit is visible surrounding the wear scar. Some of the other compounds did lubricate for a few minutes before there was a transition to higher friction, suggesting that under milder conditions, they might work adequately. The compound 2-octanol sustained low friction ($\mu=0.06$) for a bit longer than 6 minutes before experiencing a friction transition (Figure 6.13A). The steady-state coefficient of friction was 0.12 at the end of the test. Octanoic acid had a lower friction coefficient of approximately 0.05 for about a minute before rising to 0.175 for the rest of the test (Figure 6.13B). Octyl aldehyde and octyl ketone had immediate high friction levels and large wear scars.

Table 6.3
Summary of Neat C₈ Series Oxygen-Containing Compound BTF Wear Test Data

<u>Compound</u>	<u>WSD</u> <u>WSD</u> <u>(mm)</u>	<u>Final</u> <u>Incr</u> ¹ <u>(mm)</u>	<u>COF</u>	<u>Frict.</u> <u>Type</u> ²
PPO*	0.645	0.265	0.117	I
1-Octanol	0.557	0.177	0.049	II
3-Octanone	0.970	0.590	0.175	I
Octanoic Acid	1.068	0.688	0.187	III (1)
2-Octanol	1.076	0.696	0.126	III (6)
Octyl Aldehyde	1.250	0.870	0.141	I

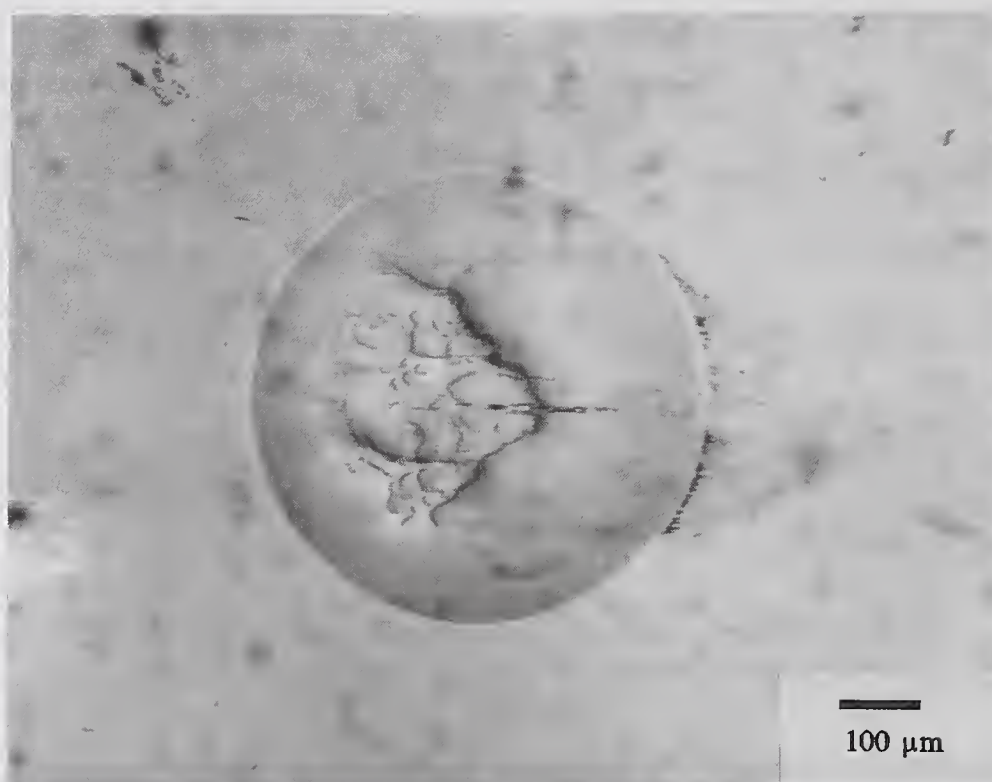
1 Wear Scar Diameter Increase above the Hertzian Contact diameter (0.380 mm)

2 Number in parenthesis indicates time to friction transition in minutes.

* Average of 16 tests

According to these BTF wear test results, alcohols possess a unique lubricating ability with Si₃N₄. Testing was expanded to measure effects of chain length, and water on lubrication by these compounds. Various surface analyses and wear product analyses were performed to determine whether these compounds were actually chemically reacting with the Si₃N₄ surface.

(a)



(b)

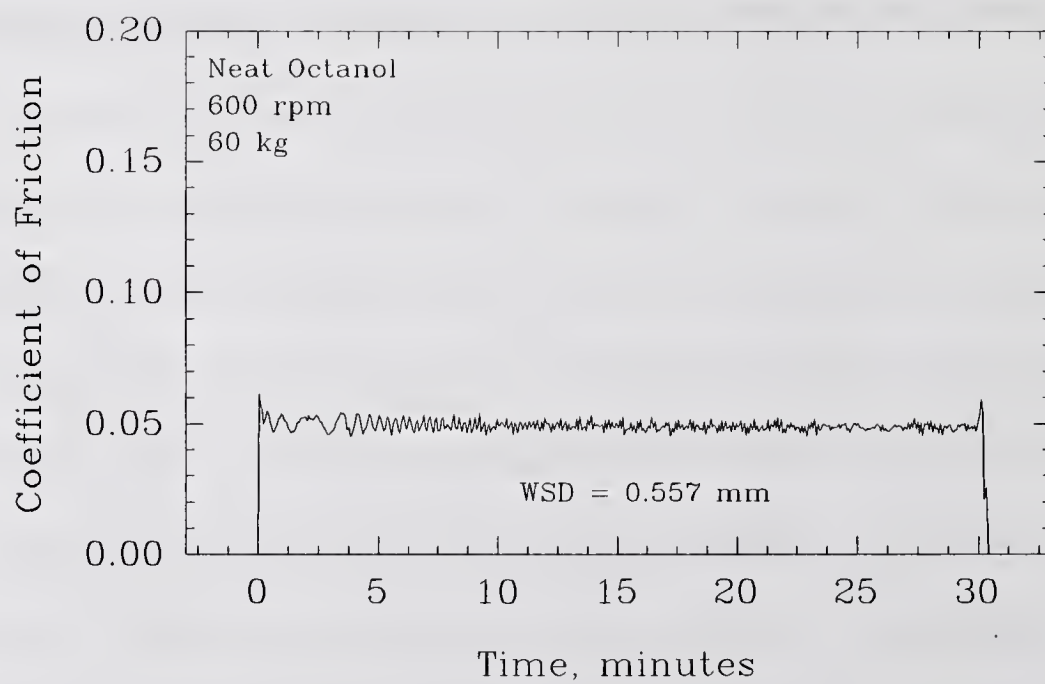
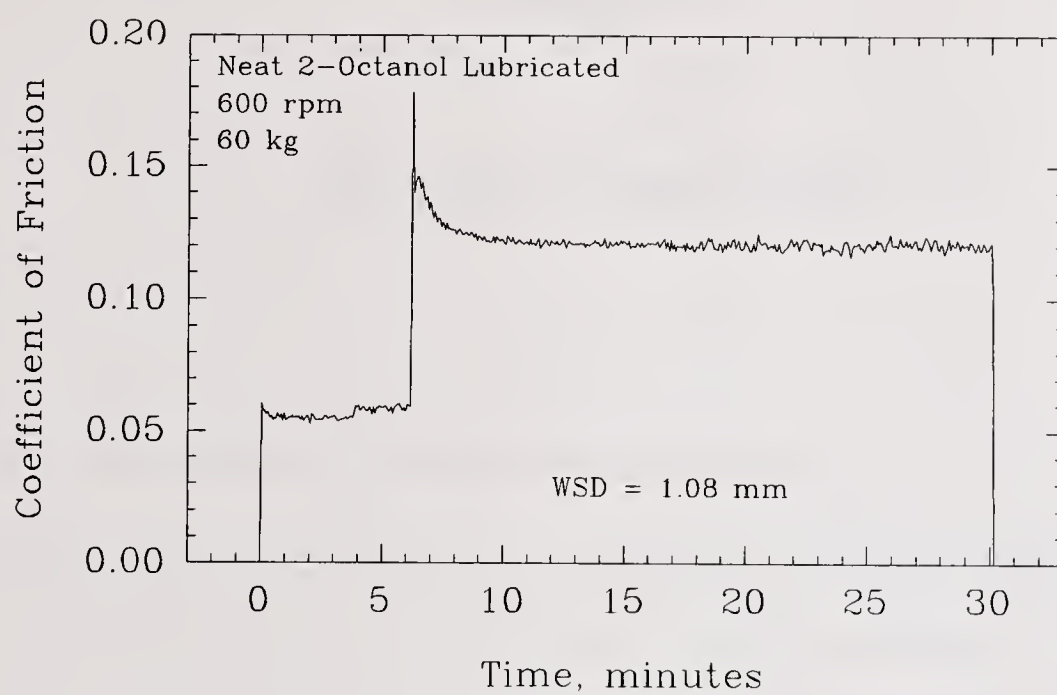


Figure 6.12 Neat Octanol Lubricated Si_3N_4 BTF Test at 60 kg: a) Optical Photomicrograph, b) Friction Trace

(a)

123



(b)

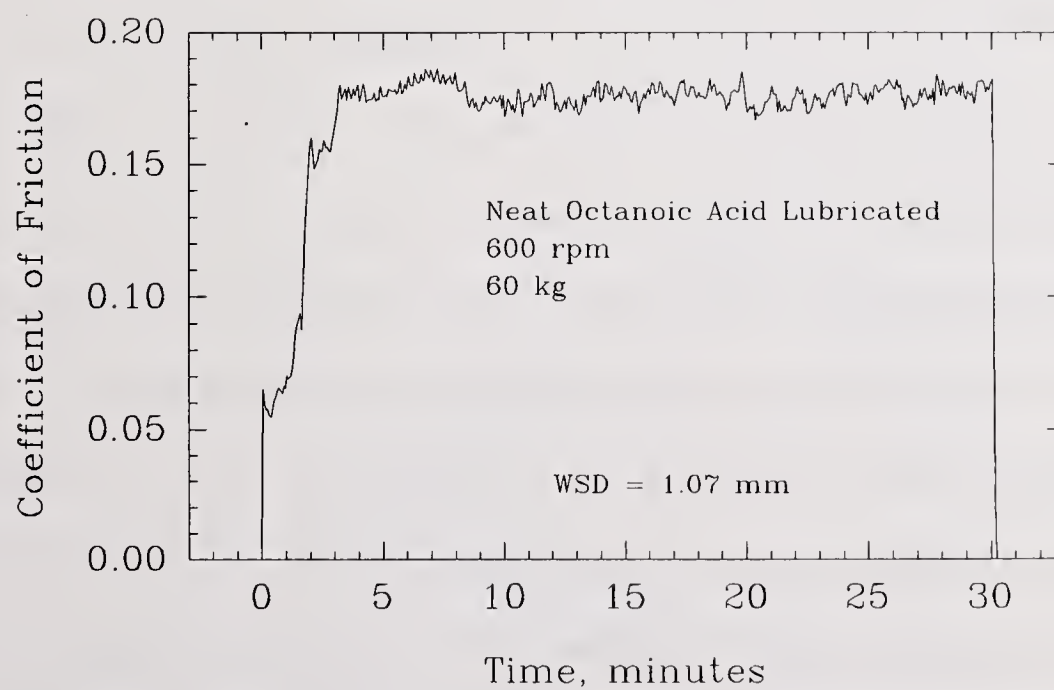


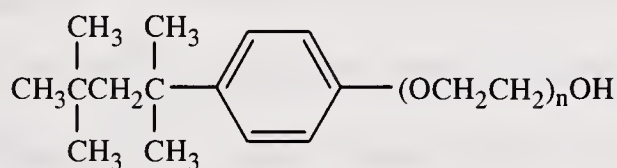
Figure 6.13 Neat C_8 Compound Lubricated Si_3N_4 BTF Test Friction Traces: a) 2-Octanol, b) Octanoic Acid

Chapter 7

ALCOHOL LUBRICATION

7.1. Effect of Alcohol Chain Length on Wear and Friction

When it became apparent that alcohol functional groups were successful in lubricating Si_3N_4 , series of alcohols were tested to see the effect of chain length within a single structural type. The first alcohols selected were a series of octylaryl polyether based alcohols. They were selected because they had long chain lengths, and were liquids at room temperature. They were also available in a variety of molecular weights, controlled by the number (n) of ethoxy "mer" units in the polyether chain. In these tests, compounds of $n=1$, 5, and 9 were used.



Octylaryl Polyether-Based Alcohols

The data in Table 7.1 shows that within an alcohol series, longer chains provide better lubrication because both friction and wear are seen to decrease slightly as chain length increases. This may be attributed to the fact that longer chain may form thicker films which lubricate better. A wear scar from the $n=9$ octylaryl polyether alcohol lubricated wear test is shown in Figure 7.1A. The scar is small and has many small scratches running in the direction of sliding at the trailing half of the wear scar. The clear definition of the edge of the wear scar at the trailing edge and the poor definition of the scar at the leading edge

suggests that more wear may be occurring at the trailing half of the scar. The friction is low and steady throughout the test (Figure 7.1B), characteristic for these well-lubricated tests.

In a second series of tests, three linear primary alcohols were tested to determine the effects of chain length on friction and wear. The alcohols were comprised of

hexanol, octanol, and decanol. The data are summarized in Table 7.2. Decanol (Figure 7.2) had a slightly smaller wear scar diameter than octanol, and a similar low coefficient of friction. The wedge-shaped film-like feature in the wear scar is well defined. Hexanol (Figure 7.3) has the highest wear, but the coefficient of friction remains low. The wedge-shaped accumulation inside the wear scar is thin and barely recognizable. The level and the characteristics of the friction suggest that the same basic lubrication mechanism is responsible for these three linear primary alcohols. The fact that the wedge-

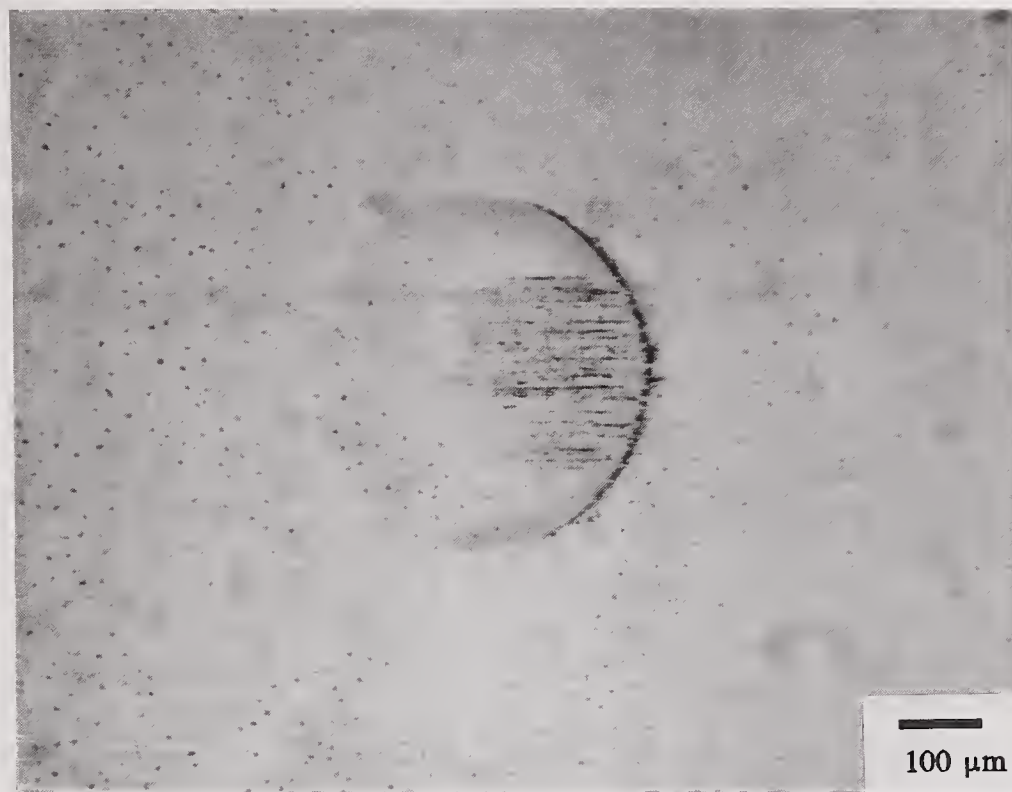
Table 7.1
Summary of Neat Octylaryl Polyether-Based Alcohol
BTF Wear Test Data

<u>Compound</u>	WSD		Final
	<u>WSD</u> <u>(mm)</u>	<u>Incr¹</u> <u>(mm)</u>	
PPO*	0.645	0.265	0.117
n=9	0.420	0.040	0.067
n=5	0.465	0.085	0.073
n=1	0.528	0.148	0.081
1 Wear Scar Diameter Increase above the Hertzian Contact diameter (0.380 mm)			
* Average of 16 tests			
n Refers to the number of ethoxy "mer" units comprising the ether side chain.			

Table 7.2
BTF Wear Test Results on
Primary Linear Alcohols

<u>Alcohol</u>	WSD		Final
	<u>WSD</u> <u>(mm)</u>	<u>Incr¹</u> <u>(mm)</u>	
Decanol	0.503	0.123	0.045
Octanol	0.557	0.177	0.049
Hexanol	0.633	0.253	0.051
1 Wear Scar Diameter Increase above the Hertzian diameter (0.38 mm)			

(a)



(b)

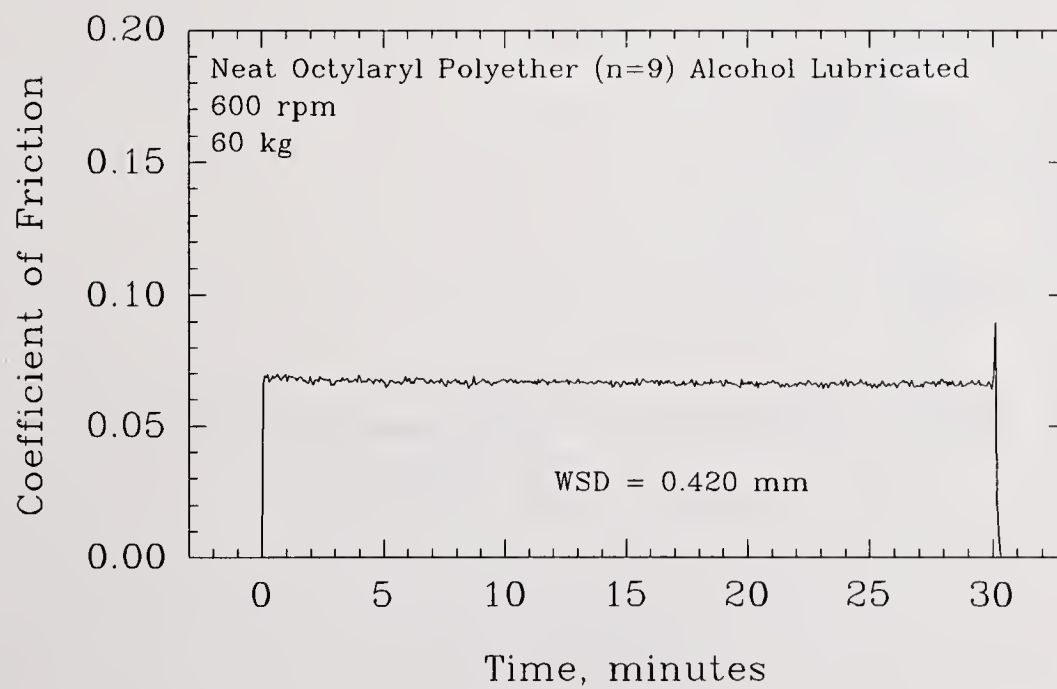
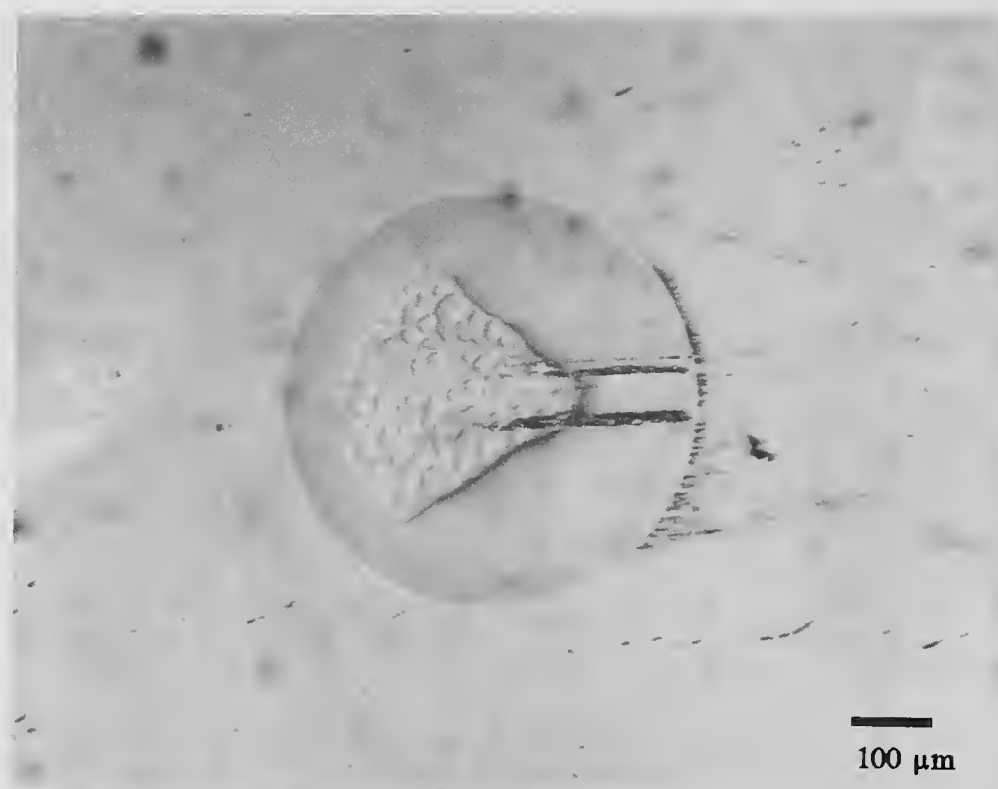


Figure 7.1 Neat Octylaryl Polyether Alcohol Lubricated Si_3N_4 BTF Test at 60 kg:
a) Optical Photomicrograph, b) Friction Trace

(a)



(b)

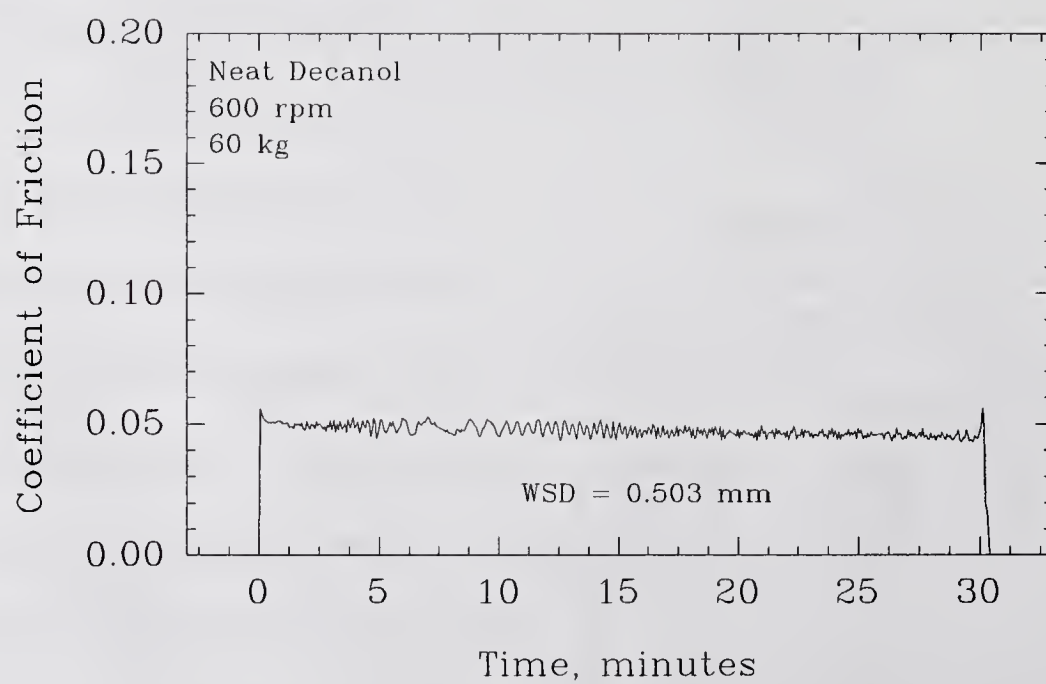
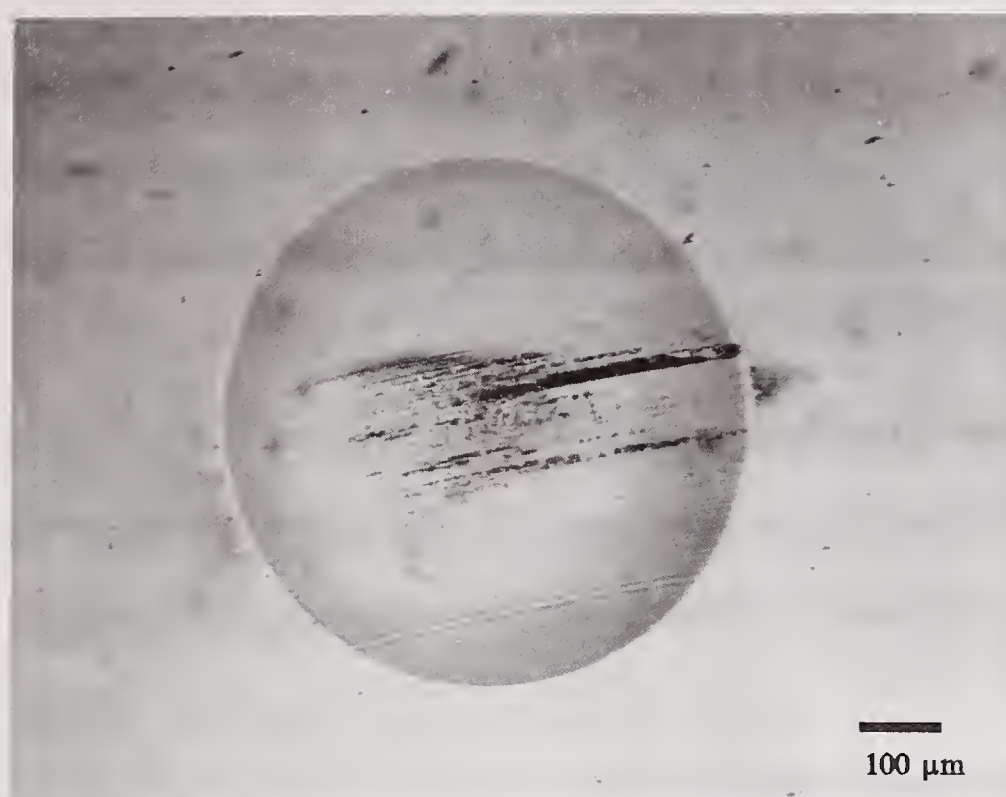


Figure 7.2 Neat Decanol Lubricated Si_3N_4 BTF Test at 60 kg: a) Optical Photomicrograph, b) Friction Trace

(a)



(b)

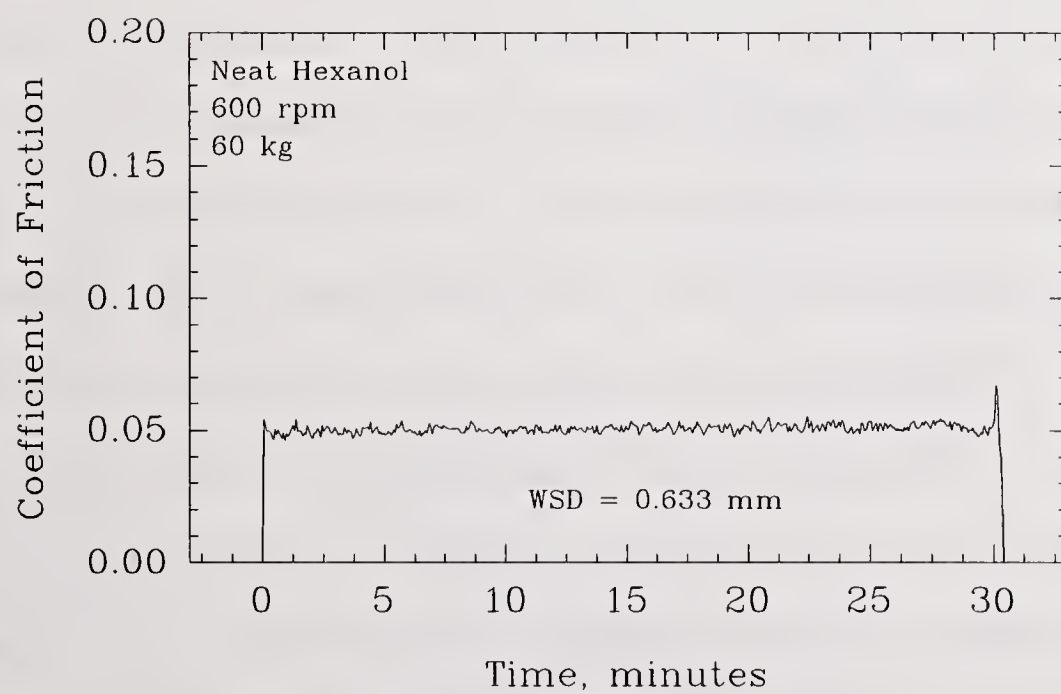


Figure 7.3 Neat Hexanol Lubricated Si_3N_4 BTF Test at 60 kg: a) Optical Photomicrograph, b) Friction Trace

shaped accumulation gets smaller and thinner in appearance as chain length decreases and wear and friction increase suggests that this feature is associated with good lubrication.

The same three linear primary alcohols were tested at different loads to compare the load-wear relationship for these compounds (Figure 7.4). All three compounds roughly parallel the Hertzian contact diameter line. In general, hexanol has the highest wear at all loads. In addition, there is an increase in wear at 90 kg that defines the load capacity of this compound under the BTF test conditions. The other alcohols exhibit behavior consistent with the previous observation that longer chain lengths provide better lubrication.

7.2. Wedge-Shaped Feature Analysis

Previously, it had been suggested that the wedge-shaped feature observed in many of the alcohol-lubricated Si_3N_4 wear tests is associated with good lubrication. The series of tests at different loads for the linear primary alcohols supports this hypothesis. The data for hexanol will serve as an example. At 20 kg load (Figure 7.5) friction is very smooth and low coefficient of friction of 0.047 is observed at the end of the test. The wear scar, while being fairly small, is very well shaped and distinct. The wedge-shaped feature is clearly seen near the entrance region of the scar. At 40 kg load (Figure 7.6) the wedge-shaped feature is still visible inside the scar, but it has not grown in proportion to the wear scar diameter increase. At 60 kg load (Figure 7.3 already shown) the friction behavior is similar, but the accumulation seems to be disappearing. At 80 kg load, there was a distinct "grating" sound at the end of the test as the speed dropped to zero under load. This is reflected in the wear scar (Figure 7.7), which has a large rough region where the accumulation used to be.

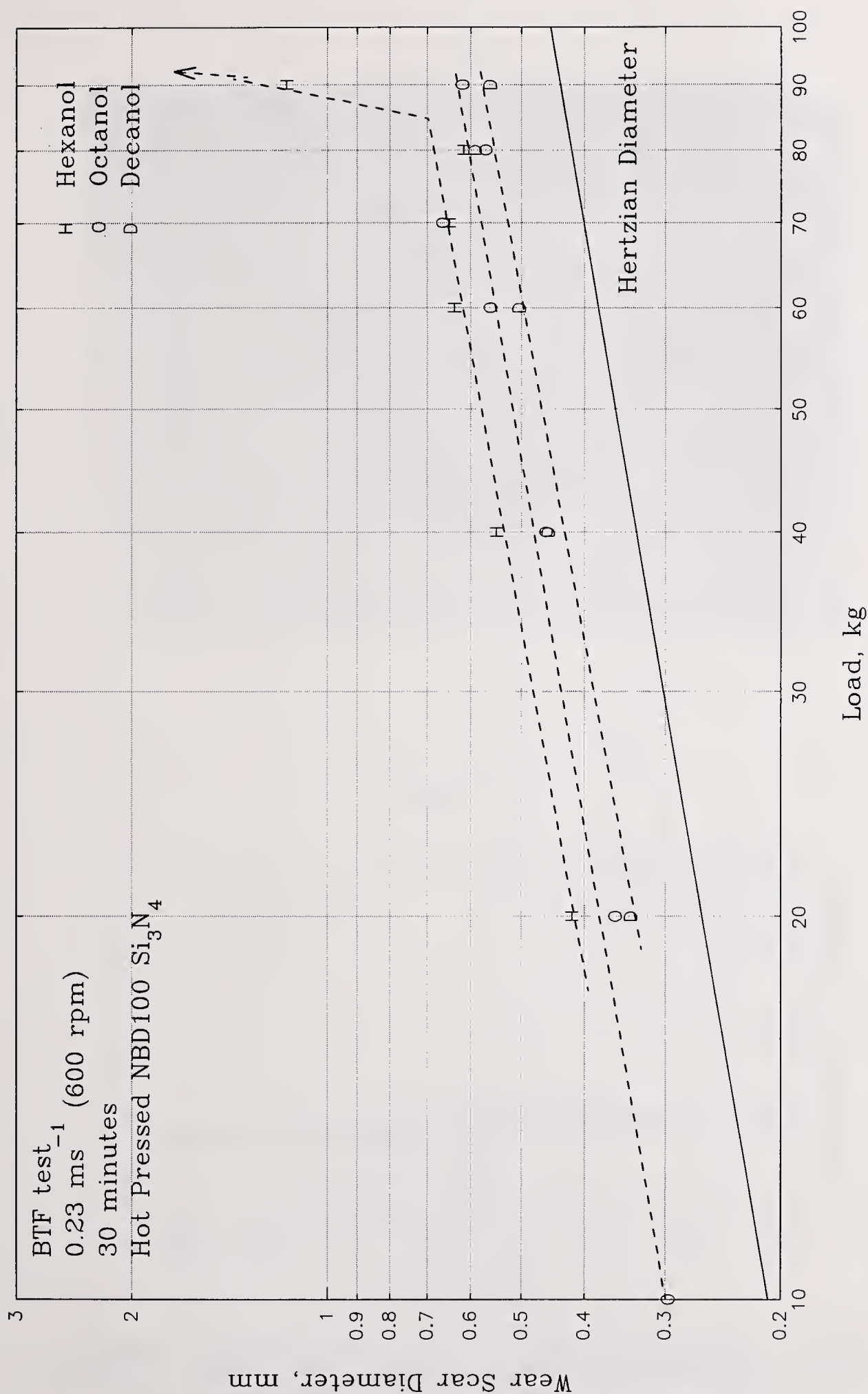
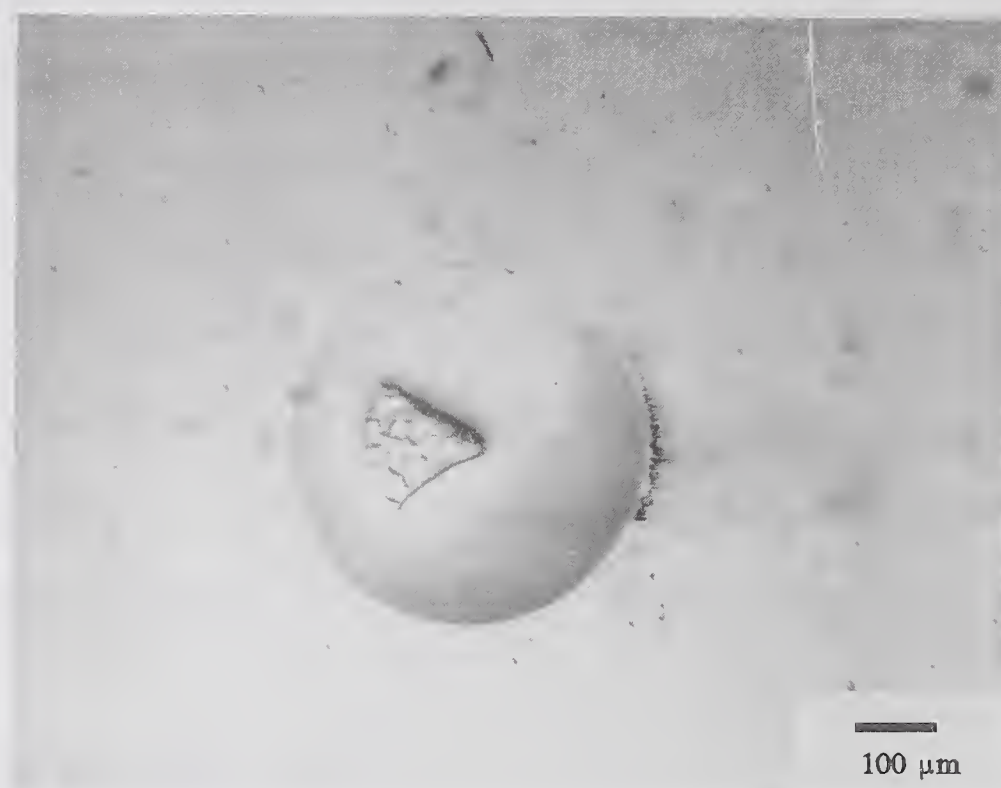


Figure 7.4 Load Capacity Plots for Neat Linear Alcohols (C_6 , C_8 , C_{10})

(a)



(b)

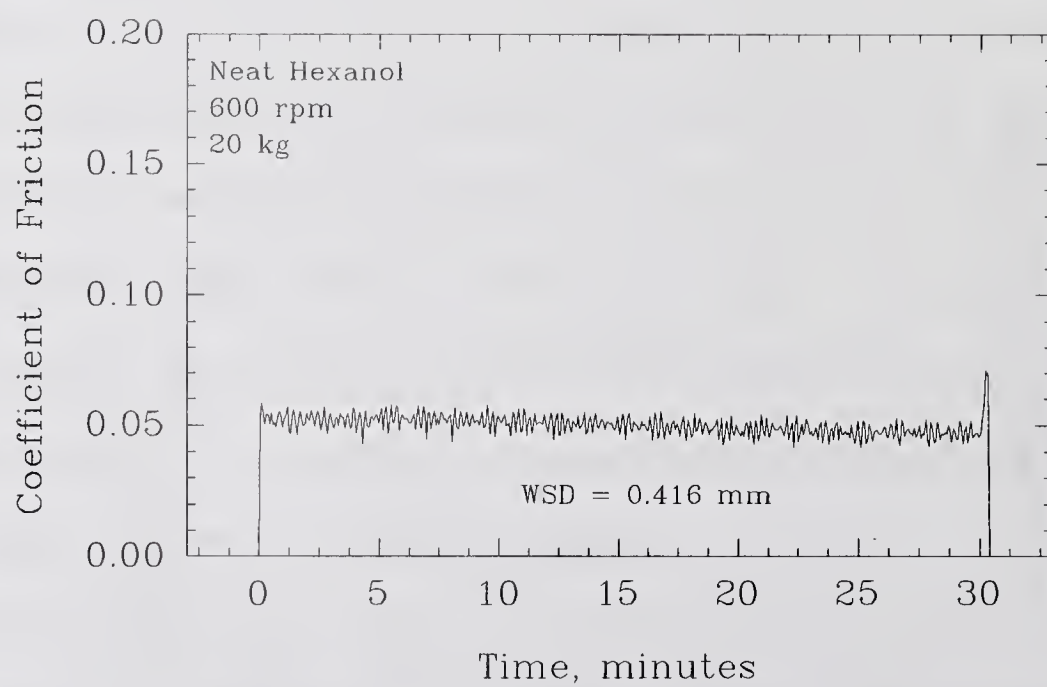


Figure 7.5 Neat Hexanol Lubricated Si_3N_4 BTF Test at 20 kg: a) Optical Photomicrograph, b) Friction Trace

(a)



(b)

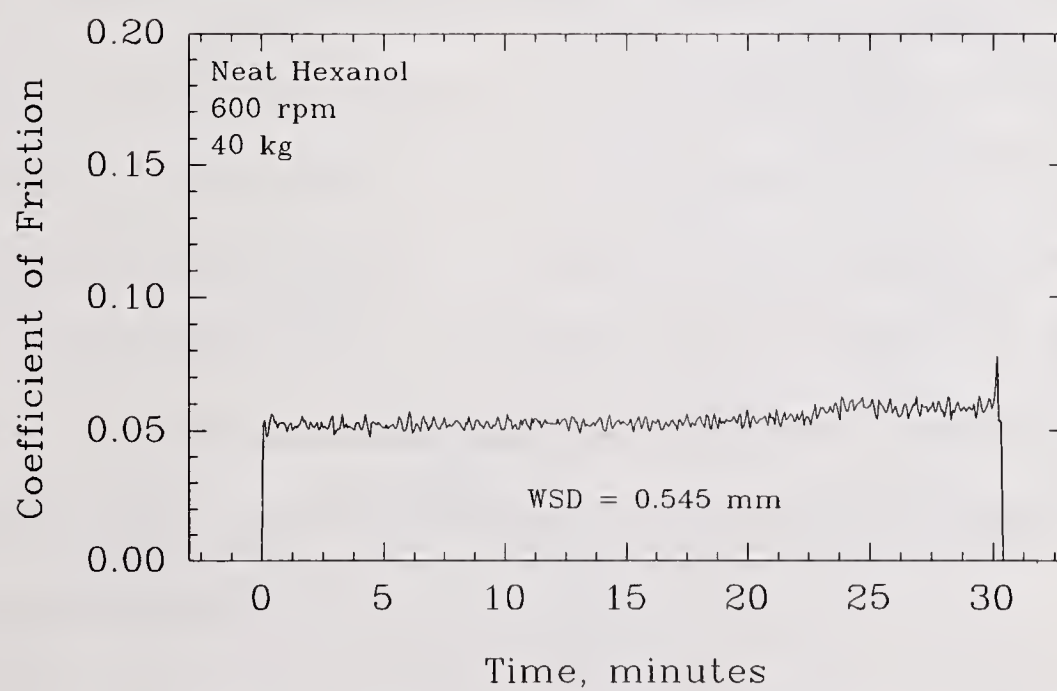
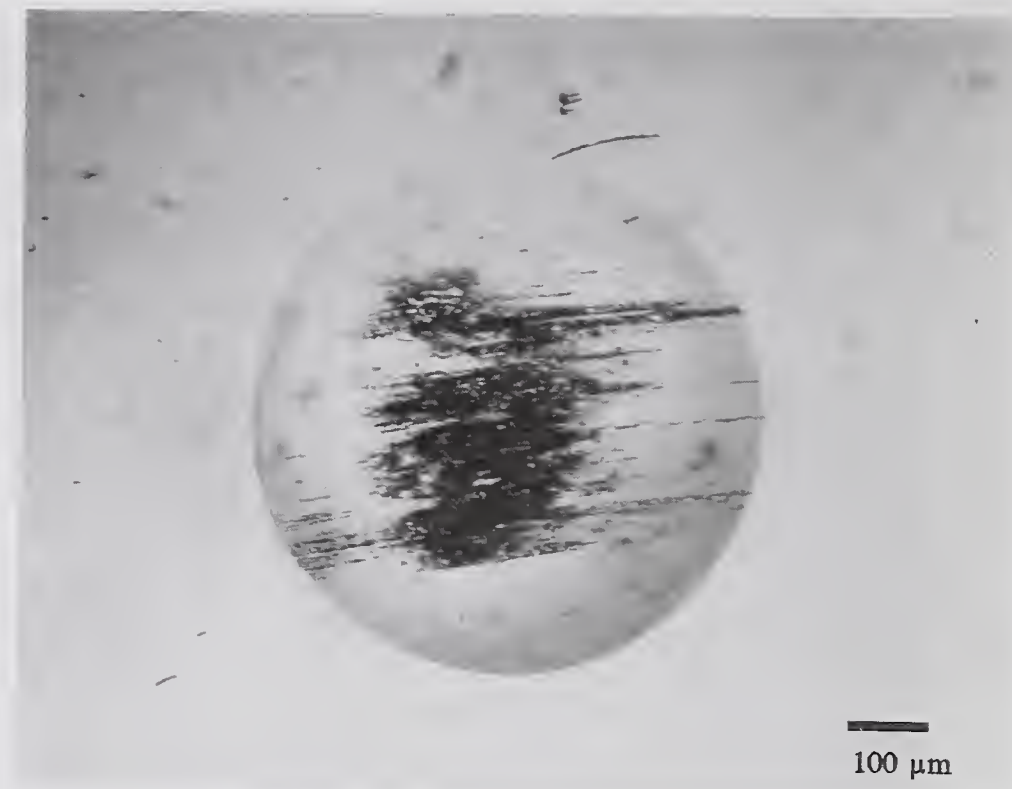


Figure 7.6 Neat Hexanol Lubricated Si_3N_4 BTFT Test at 40 kg: a) Optical Photomicrograph, b) Friction Trace

(a)



(b)

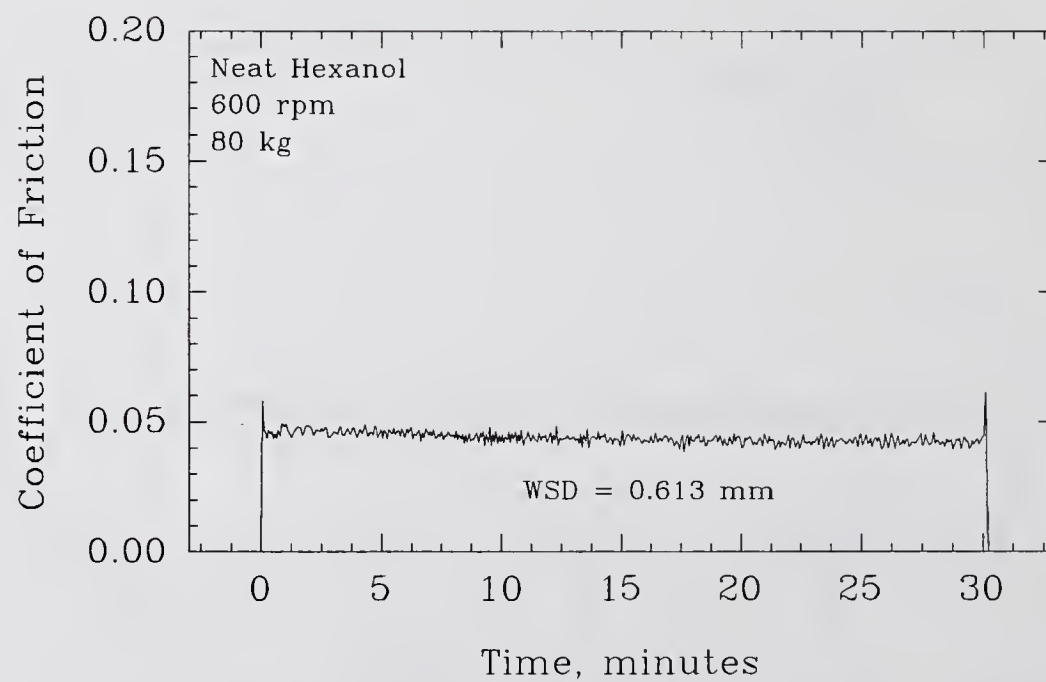


Figure 7.7 Neat Hexanol Lubricated Si_3N_4 BTFT Test at 80 kg: a) Optical Photomicrograph, b) Friction Trace

Apparently, as the speed dropped in the final second of deceleration, the surfaces were no longer lubricated and the surface was worn by a combination of fracture and abrasion. This apparent loss of lubrication indicates that hexanol at 80 kg is near a transition to higher wear. This is supported by the observation of very high wear at 90 kg load for hexanol. The wear scar at the end of the 90 kg test (Figure 7.8 - note change in scale for the wear scar) is large, and very smooth, with no evidence of any wedge-shaped feature. The decrease in lubrication effectiveness is associated with disappearance of the wedge-shaped feature within the wear scar.

Disappearance of the wedge-shaped feature can also be associated with appearance of fracture wear mechanisms within the Si_3N_4 contact. This is shown in Figure 7.9 which compares SEM micrographs from two decanol-lubricated Si_3N_4 BTF tests. Both of these photomicrographs were taken at the same tilt angle (75°) and similar magnification, oriented with the direction of sliding from left to right. The upper photomicrograph shows the wedge-shaped feature present under good lubrication at 60 kg load. At 80 kg load, a grating sound was heard during the final deceleration of the specimens at the end of the test and the friction coefficient jumped to greater than 0.5. The wear scar at the end of the test is shown in the lower photomicrograph of figure 7.9. Evidence of tensile cracks and severe fracture are seen at the leading edge indicating that lubrication failure resulted in catastrophic failure of the ceramic. The observation that these failures occurred during the deceleration phase of the test suggests an EHD component of lubrication may be present, since EHD lubrication is known to be speed dependant.

(a)



(b)

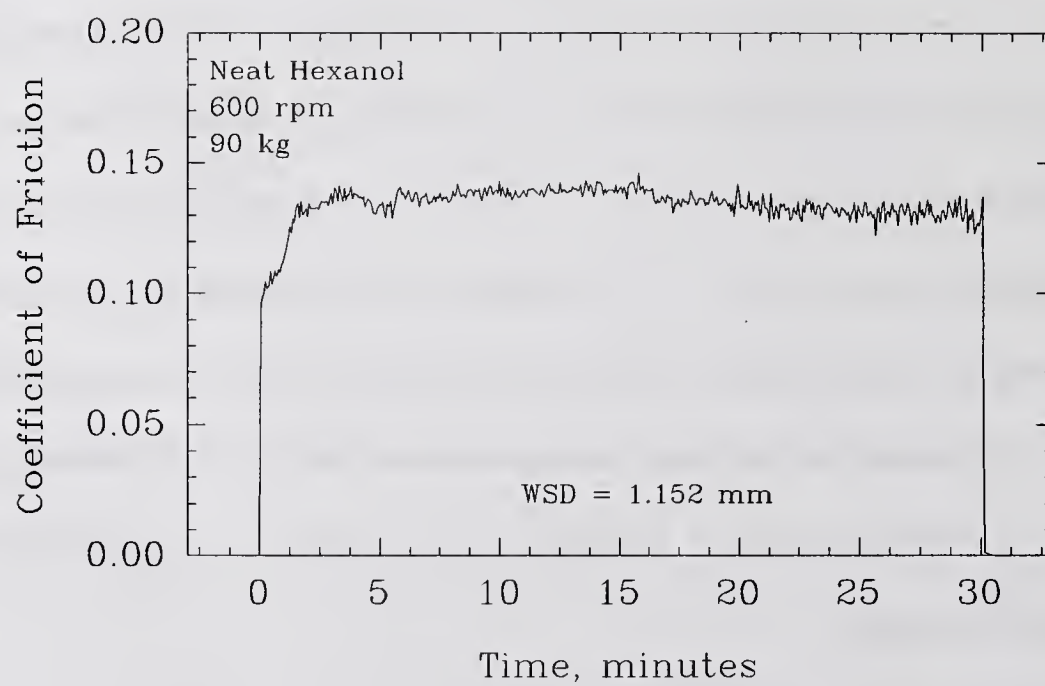


Figure 7.8 Neat Hexanol Lubricated Si₃N₄ BTFT Test at 90 kg: a) Optical Photomicrograph, b) Friction Trace

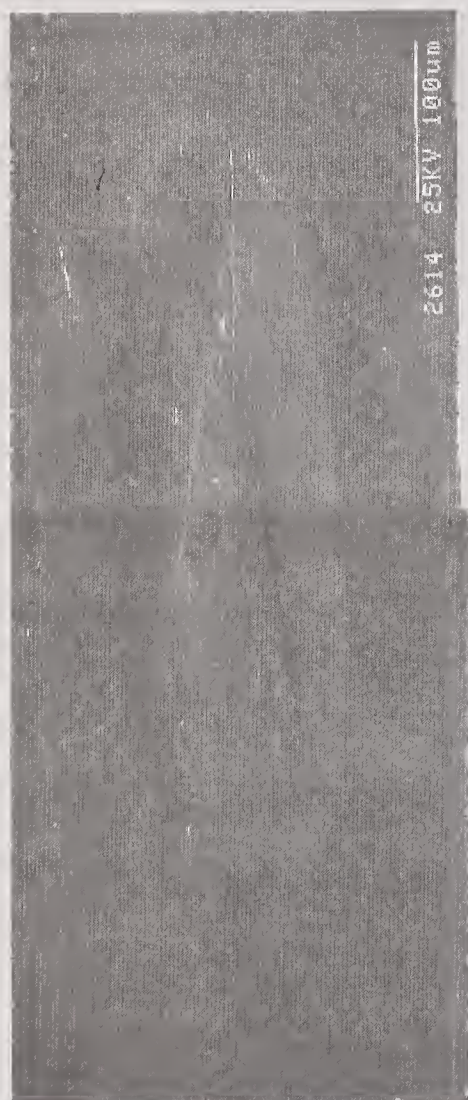
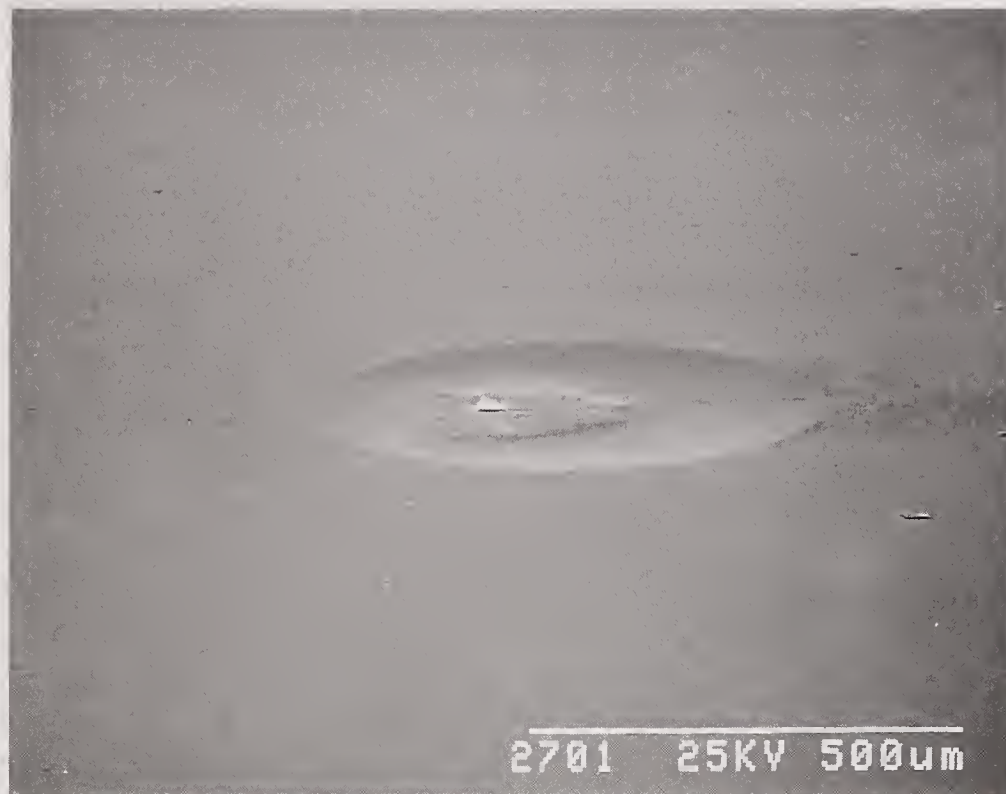


Figure 7.9 SEM Photomicrographs of Neat Decanol Lubricated Si_3N_4 BTF Tests: a) 60 kg Load, b) 80 kg Load

More detailed analyses of the wedge-shaped feature were performed using flats from an octanol-lubricated BTF test. Optically, the wedge-shaped feature (see Figure 6.12) appears to be an accumulation of material inside the wear scar projecting from the surface like a plastic film undergoing deformation. There is very little deposit outside the wear scar. SEM photomicrographs of this wear scar (Figure 7.10) show the wear scar to be very smooth except for the feature region. Surface profilometry was used to confirm that the film was actually protruding from the bottom of the wear scar. The surface profile (Figure 7.11) shows that the film appears to be $\approx 2 \mu\text{m}$ thick, relative to a wear scar that is only $\approx 4 \mu\text{m}$ deep. A more three-dimensional view of the wear scar can be obtained by using optical interferometry to look at the wear scar depth variation throughout the scar. Figures 7.12A and B compare the normal optical view of the wear scar to the interferometric view of the exact same wear scar. Because of different optical characteristics of the two instruments used, the photographs are (vertically) mirror images of one another. The photographs confirm that the wear scar is deeper in the horseshoe-shaped region toward the trailing half of the wear scar. Since each fringe represents $0.27 \mu\text{m}$ vertical displacement, the wear scar is $3.5 \mu\text{m}$ deep at its deepest point, with the wedge projecting out of the surface approximately $2 \mu\text{m}$. Initially, it was thought that the wedge shaped feature seen at the end of the test was an artifact of the test termination - as the speed decreased under load, film thicknesses decreased until a pressure wedge strong enough to scrape the reaction product from the upper wear track was formed. This reaction product then compacted to form what we see at the end of the test. To address this issue a wear test was conducted in which the specimens were shock unloaded prior to stopping the test. The feature was still present in

(a)

139



(b)



Figure 7.10 SEM Photomicrographs of Neat 1-Octanol Lubricated Si_3N_4 BTF Test (Direction of Sliding is from Left to Right)

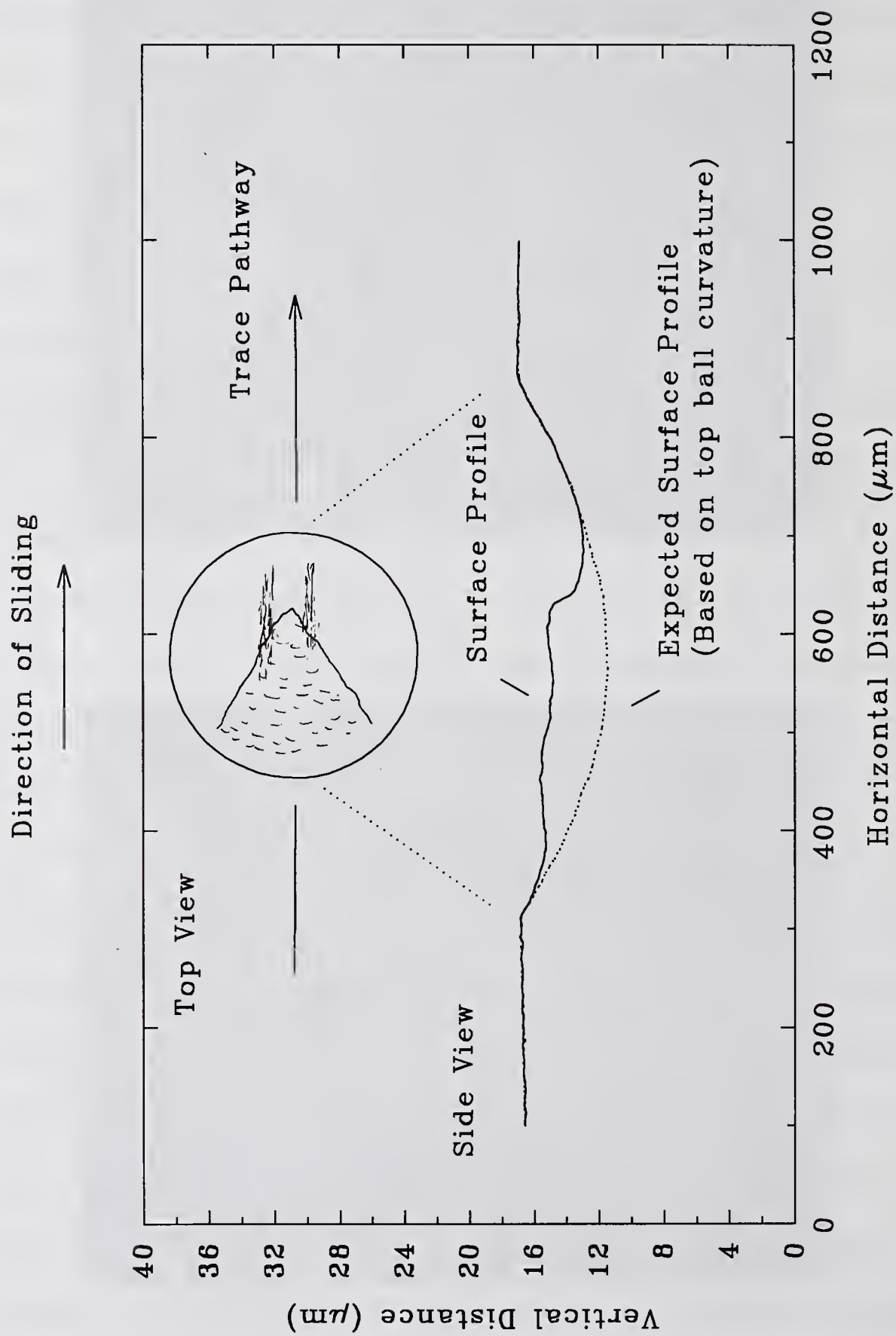


Figure 7.11 Surface Profile of Wear Scar from Neat 1-Octanol Lubricated Si_3N_4 BTF Test (Compared to Expected Surface Profile)

(a)

141



(b)



Figure 7.12 Wear Scar from Neat 1-Octanol Lubricated Si_3N_4 BTF Test: a) Optical Photomicrograph, b) Interferometric Photomicrograph

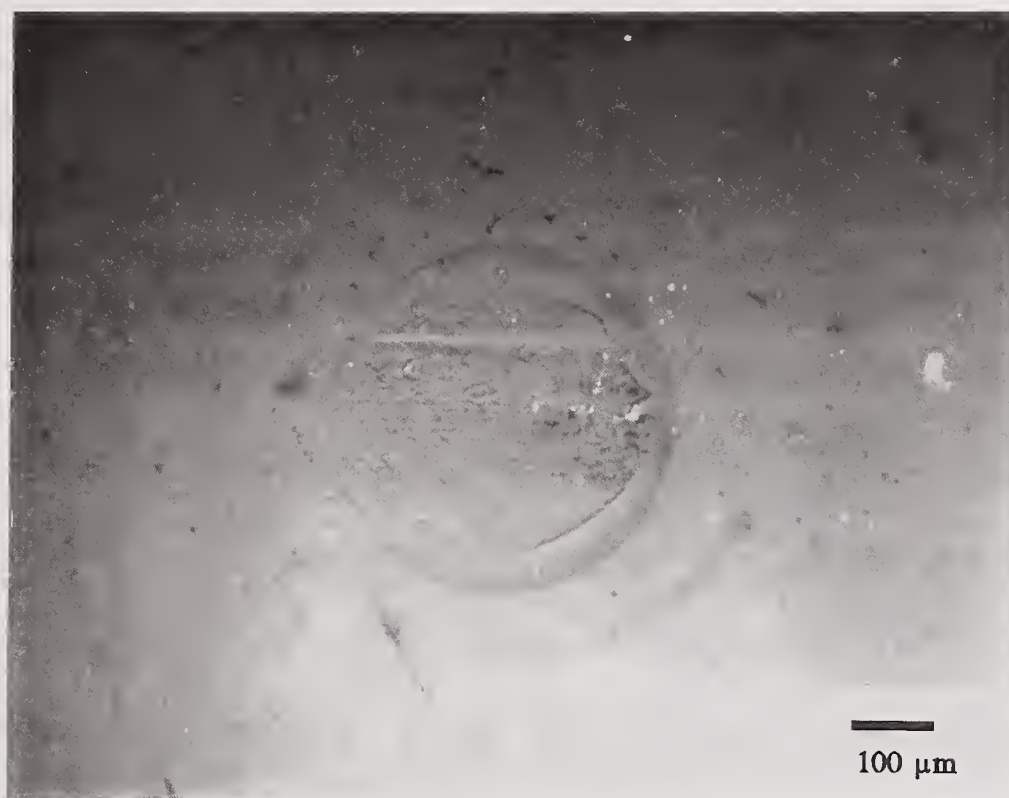
the same shape and quantity as before; therefore, the feature is not considered to be an artifact of the test termination.

A series of tests was conducted as a function of time in order to see how the feature changed during the test. In all of these tests the load was quickly decreased at the end of the test before the speed had dropped. Optical micrographs of the wear scars from wear tests of 18 seconds and 180 seconds are shown in Figures 7.13A and B respectively. According to these figures, the feature is present from the very beginning of the test. It should be noted that the wear scar diameter increases as a function of time, while the feature area decreases. The feature also changes shape from circular to wedge shaped, and it moves from covering almost all of the scar to covering the entrance region more than the other regions.

Attempts were made to dissolve this wedge-shaped feature using organic and inorganic solvents. It would not be removed by organic solvents such as hexane, acetone, ethanol, THF, or pyridine (both cold and hot). Acids such HCL, HNO₃, and even HF were ineffective at both low and high concentrations. Weak and strong alkalais were also ineffective. Heating the sample 600°C in 1.4 MPa of pure oxygen for 60 minutes had no effect, therefore it was not merely a compacted form of carbon. A diamond scribe was used to scratch the surface of the wedge-shaped film. The film was very hard and difficult to scratch. It could not be chipped out and detached from the wear scar, but could be scratched about as easily as the surrounding Si₃N₄ surface itself. All of these observations lead to the conclusion that the wedge is inorganic, hard, and very adherent to the Si₃N₄ surface.

(a)

143



(b)

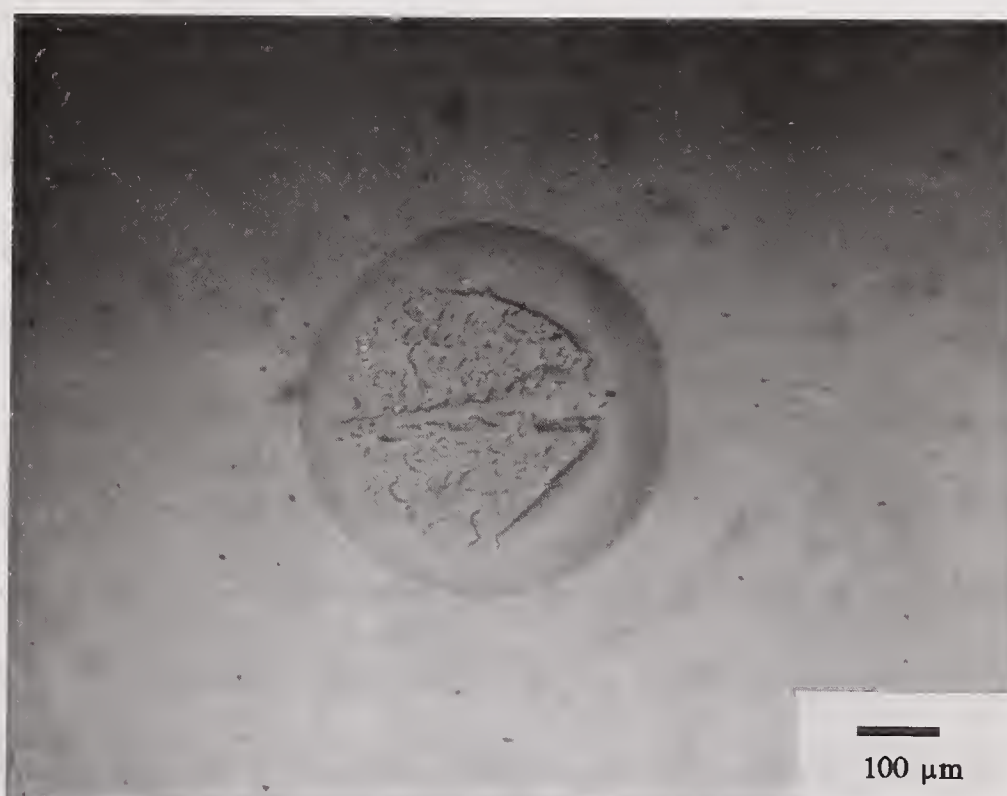


Figure 7.13 Optical Photomicrographs of Neat 1-Octanol Lubricated Si_3N_4 BTF Tests: a) 18 Second Duration, b) 180 Second Duration

Auger depth profiling analysis of the wedge-shaped region within the wear scar, determined that the feature had the same composition with depth as the Si_3N_4 surrounding the wear scar. This data is provided in appendix J. This means that the wedge-shaped feature within the wear scar is unworn Si_3N_4 material. This lends a new interpretation to the surface profile originally shown in Figure 7.11. The surface profile actually represents the surface of unworn Si_3N_4 . Figure 7.14 shows the same surface profile in relation to the original surface of the flat. The highest amount of wear occurs at the back (trailing edge) of the wear scar. These results also reinforce that caution must be used in calculating wear volumes from wear scar diameters in cases where good lubrication may be protecting the surface. In these cases, octanol has preferentially protected the leading half of the wear scar, resulting in a wear pattern that does not correspond to the curvature of the upper (ball) specimen.

Taking a more three-dimensional look, the wear scar for oleil alcohol lubricated Si_3N_4 (Figure 7.15A) has a horseshoe-shaped region at the back of the wear scar that represents the region of highest wear. This shape is reminiscent of the horseshoe-shaped region in an interferometry image of EHD lubricated point contacts (Figure 7.15B). In EHD lubrication, the horseshoe-shaped region represents the region of the highest pressure, minimum film thickness, and highest temperature.²⁶⁵ This suggests that in the case of alcohol-lubricated Si_3N_4 chemical reactions take place preferentially in the high temperature region of the wear scar causing corrosive wear. Hence the horse-shoe shape formation. The reaction products enable the existence of a EHD operating condition either through local viscosity increase or through thick surface film formation. This explanation is supported in part by the low

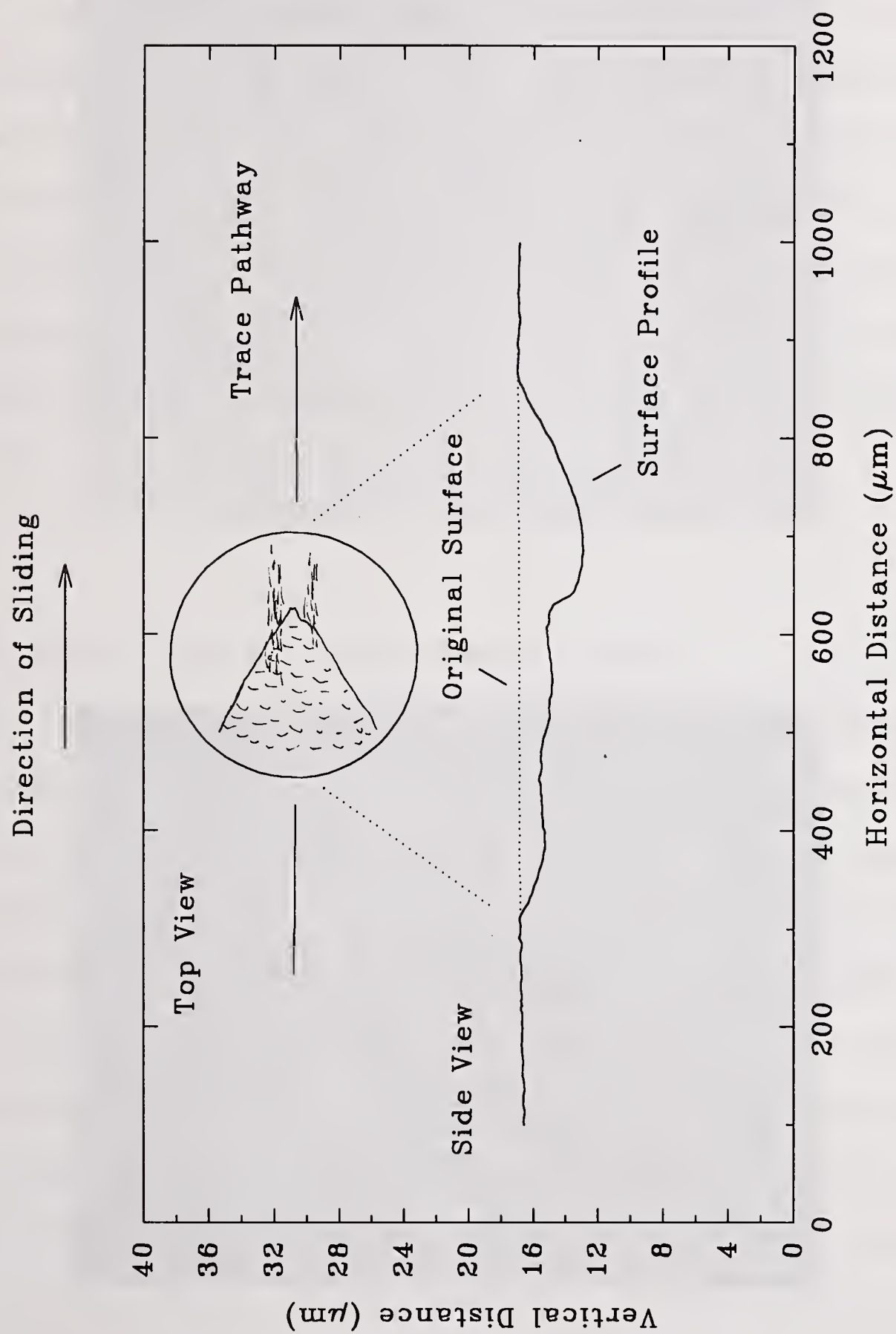


Figure 7.14 Surface Profile of Wear Scar from Neat 1-Octanol Lubricated Si_3N_4 BTF Test (Compared to Original Surface)

(a)



(b)

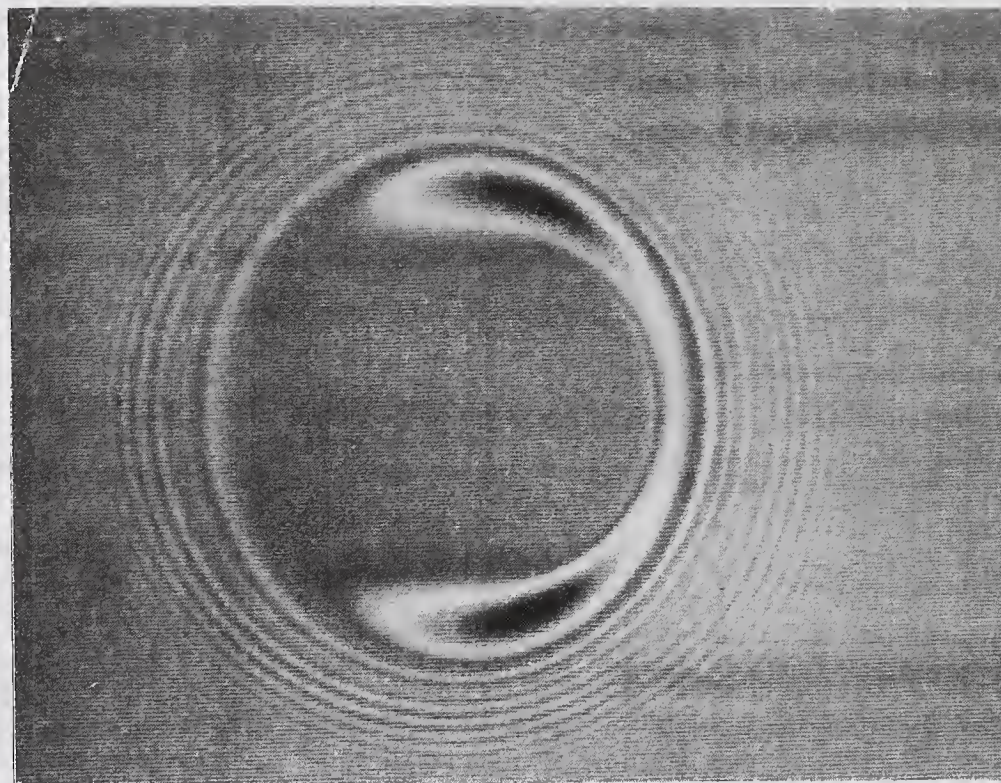


Figure 7.15 Comparison of Wear Contact Morphologies: a) Neat Oleil Alcohol Lubricated Si_3N_4 Wear Scar, b) General EHL Contact Interferometry

friction coefficients ($\mu=0.05$) observed for these compounds.

An estimate of the minimum film thickness for an octanol (EHD) lubricated Si_3N_4 point contact was calculated using Hamrock and Dowson's¹⁰⁹ equation (Appendix K). The minimum film thickness was found to be about 4 nm for the octanol lubricated case. This is a very thin film and suggests that either very smooth surfaces must be involved, or a much higher effective viscosity of the fluid must be operating. Both of these explanations can be attributable to tribochemical reactions which can polish the surface making it smoother or the reaction can form high molecular weight polymers increasing the effective viscosity in the contact.

7.3. Effect of Water on Lubrication of Si_3N_4 by Alcohols

Some researchers have speculated that it is the water in the alcohols that are responsible for the chain-length effects. Water has been demonstrated to have a significant effect on the lubrication of Si_3N_4 . Sugita²³⁰ and others^{237, 241, 120} have shown wear results in which there is a chemical removal of the silicon nitride surface through reaction with water. Freiman⁸⁵ indicated that water can enhance crack propagation in ceramic materials. Both of these mechanisms may explain enhanced wear rates in the presence of water. Smaller chain length alcohol compounds have a higher polarity and higher ability to pick up atmospheric water; therefore, the higher wear associated with smaller chain length alcohols could be merely due to a higher concentration of (reactive) water. Indeed Tsunai^{241*} has shown that

1% water in methanol doubled the wear rate over that of neat methanol. Experiments were therefore conducted to determine whether water was affecting wear in this study.

The neat octanol used in this study contained a nominal 100 ppm water. A test was conducted using octanol with 1% water added. As shown in Table 7.3, addition of 1% water to octanol gave friction and

wear results identical to the neat octanol case. A similar experiment conducted with a polyalkylene glycol derivative (460 SUS water soluble) also showed no change in friction or wear with the addition of

Table 7.3
Effect of Water on Lubrication
of Si_3N_4 by Octanol

[water] in <u>Alcohol</u>	WSD (mm)	WSD Incr ¹ (mm)	Final COF _____
100 ppm	0.557	0.177	0.049
10,000 ppm	0.560	0.180	0.055

1 Wear Scar Diameter Increase above the Hertzian diameter (0.38 mm)

1% water. These results suggest that the water effect is not dominant in these tests and most of the lubrication effect is due to some unique reactivity between alcohols and the Si_3N_4 surface. A series of alcohol-lubricated Si_3N_4 micro sample tests was conducted, and the reaction products were analyzed to elucidate this unique reactivity.

7.4. Alcohol Lubricated Micro Sample Wear Tests on Si_3N_4

Micro sample wear tests conducted for this study were run under the standard BTF test conditions, except 6 μl of lubricant were used instead of the usual 1.5 ml. The benefit of this test is that the lubricant, while circulating, is restricted to a volume of 6 μl . As a result, the reaction products are not diluted in a larger circulating bulk lubricant reservoir.

This increase in reaction product concentration enhances the ability to detect the products. The micro sample test can also have a higher test severity due to reduced cooling effects (smaller lubricant reservoir), and less chance of oxygen depletion (thin film). Micro sample tests conducted using octanol, decanol, and an octylaryl polyether were compared to results from normal (1.5 ml) tests to ensure that this increase in test severity did not fundamentally change the lubrication mechanisms observed. This comparison (Table 7.4) indicate that the two tests are substantially equivalent. Specimens and reaction products from the micro sample tests were analyzed to try to isolate specific products and determine what reactions might be occurring.

Table 7.4
Comparison of 1.5 ml and 6 μ l BTF Wear Tests Results on
Primary Alcohols

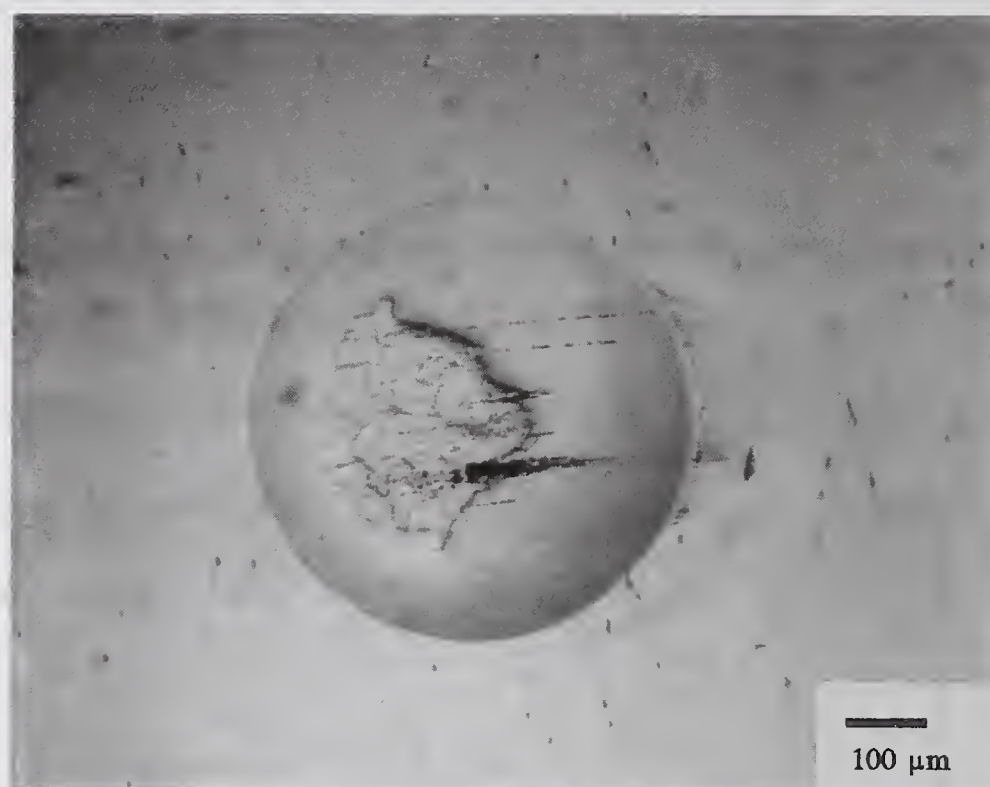
<u>Alcohol</u>	<u>1.5 ml BTF Test</u>			<u>6-μl BTF Test</u>		
	WSD		Final	WSD		Final
	WSD	Incr ¹	COF	WSD	Incr ¹	COF
	(mm)	(mm)	_____	(mm)	(mm)	_____
Octanol	0.557	0.177	0.049	0.544	0.164	0.052
Decanol	0.503	0.123	0.045	0.502	0.122	0.046
Octylaryl polyether (n=1)	0.528	0.148	0.081	0.599	0.219	0.085

1 Wear Scar Diameter Increase above the Hertzian diameter (0.38 mm)

7.5. Analysis of Worn Si₃N₄ Specimens

The typical boundary lubricating ability of alcohols with Si₃N₄ is illustrated in Figure 7.16 for a 6 μ l octanol-lubricated BTF test. The wear scar is smooth and circular, with a wedge-shaped feature similar to that seen in the 1.5 ml BTF case. The friction coefficient is smooth and low throughout the test. In this micro-sample test, for the FTIR and Auger

(a)



(b)

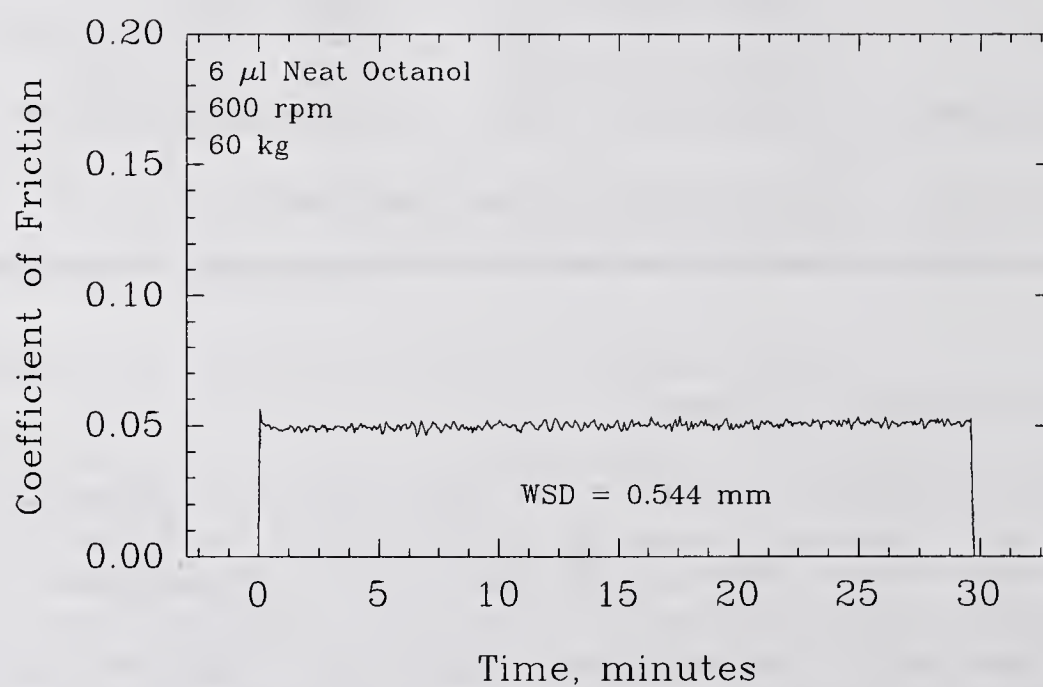


Figure 7.16 6 μl Neat Octanol Lubricated Si₃N₄ BTF Test at 60 kg: a) Optical Photomicrograph, b) Friction Trace

analysis, residual lubricant was allowed to evaporate from the surface under argon after the wear scars were measured. In the case of octanol, this only took a few hours. The resulting concentration of reaction products show up as residue in and around the wear scar (Figure 7.17). The interference fringes observed at higher magnification in some regions indicate some kind of non-volatile liquid. Since octanol itself is volatile, some kind of reaction product must have been formed that is less volatile.

Auger analysis of the worn flats after evaporating the excess octanol revealed a carbon-containing material covered the entire surface. This material was present in a layer 260 Å thick in the wear scar and 500 Å outside the wear scar. The observation of high carbon concentration suggests that the reaction product formed is probably organic in nature. The data are provided in Appendix J.

7.5.1. FTIR Analysis of Octanol Lubrication Reaction Products

FTIR analysis of the of the film left on the surface of the wear scar after the excess lubricant (octanol) had evaporated was conducted using FTIR (Figure 7.18). C-H stretches are evident, indicating organic compounds are present. Octanol is the only source of organic material in this test, therefore the reaction product observed must come from some kind of reaction with the octanol that retains (at least some) C-H groups from octanol. The strong, broad OH peak normally see for octanol is missing. This functional group is either missing or has been modified, suggesting octanol has reacted with something, resulting in the loss of the OH functional group. A strong relatively broad peak at 1050 cm^{-1} is indicative of Si-O-Si. Si-O-C will also show up in this region, so it is difficult to distinguish the two

(a)



(b)

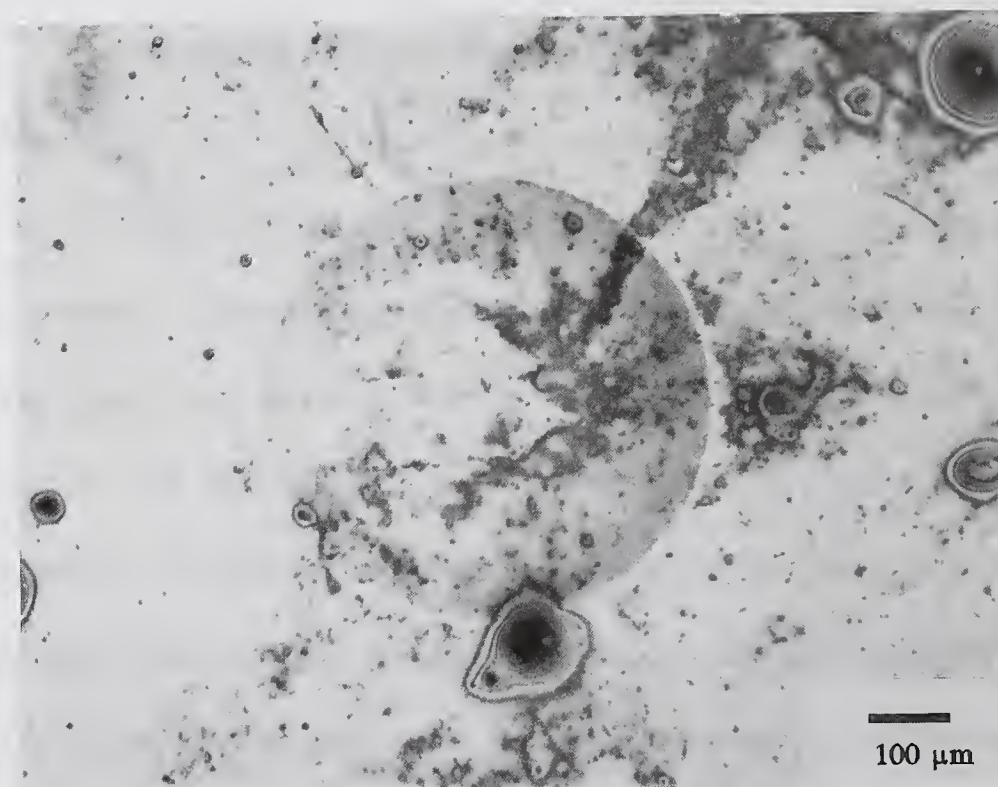


Figure 7.17 Optical Photomicrographs of 6 μ l Neat Octanol Lubricated Si_3N_4 BTF Test at 60 kg: a) Low Magnification, b) High Magnification

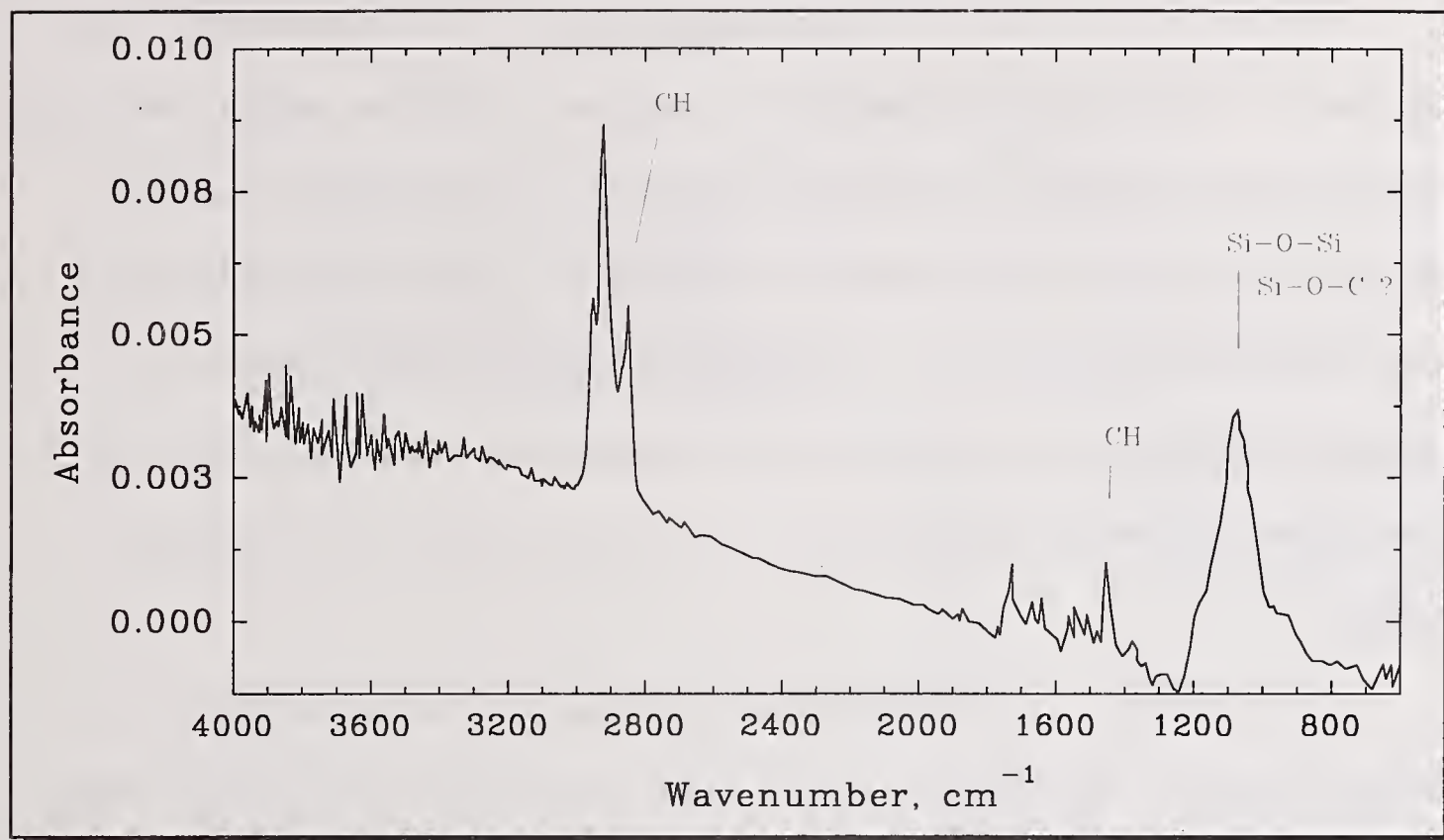


Figure 7.18 FTIR Spectrum of Film in Wear Scar for Octanol-Lubricated Si_3N_4

structures, especially if the Si-O-Si peak is pronounced. The data indicate that the reaction product is at least partially organic in nature and is formed from octanol.

7.5.2. Evidence for Organo-Silicon Reaction Product Formation as Demonstrated by GPC-GFAA

For the detection of silicon-based organometallic polymers, Gel Permeation Chromatography-Graphite Furnace Atomic Absorption (GPC-GFAA) analysis was performed without allowing the excess octanol lubricant to evaporate. Immediately after the 6- μl wear test, the top ball with the chuck was removed and soaked in one ml of tetrahydrofuran (THF) for two minutes. The solution was then filtered through a 0.02 μm filter, and 100 μl of the filtrate was injected into the GPC-GFAA for analysis.

The chromatogram from the octanol lubricated wear test is shown in Figure 7.19. A large peak in the GFAA chromatogram indicates the presence of silicon, associated with high molecular weight compounds in the range of 300 to 3000. The UV detector trace shows relatively small amount of reaction products as indicated by a broad peak coinciding with the MW range of the GFAA trace. A second, sharper peak at 250 MW indicates UV absorbing compounds at about the same molecular weight as the parent octanol (RI trace). Since octanol itself does not absorb in the UV, the UV peaks must be due to reaction products.

Decanol (Figure 7.20) has chromatograms very similar to octanol but slightly different in intensity. The alkylaryl polyether alcohol wear product was also similar (Figure 7.21), but molecular weights were shifted to higher values, reflecting the higher MW of this compound compared to octanol and decanol. The GFAA chromatogram indicates significant amounts of HMW silicon-containing material from 400 MW to 30 000 MW with a maximum near 3000 MW. The RI detector observed only the base lubricant at 400 MW. The UV chromatogram has a strong signal because the polyether alcohol contains an aromatic ring in its structure. Aromatic rings absorb in the UV.

The GPC-GFAA data demonstrate that HMW silicon-containing compounds are formed in wear tests lubricated by alcohols. This is the first direct evidence that alcohols are chemically reacting with silicon nitride surfaces during rubbing. Static reactions were carried out using Si_3N_4 powders to observe this phenomenon under more controlled conditions.

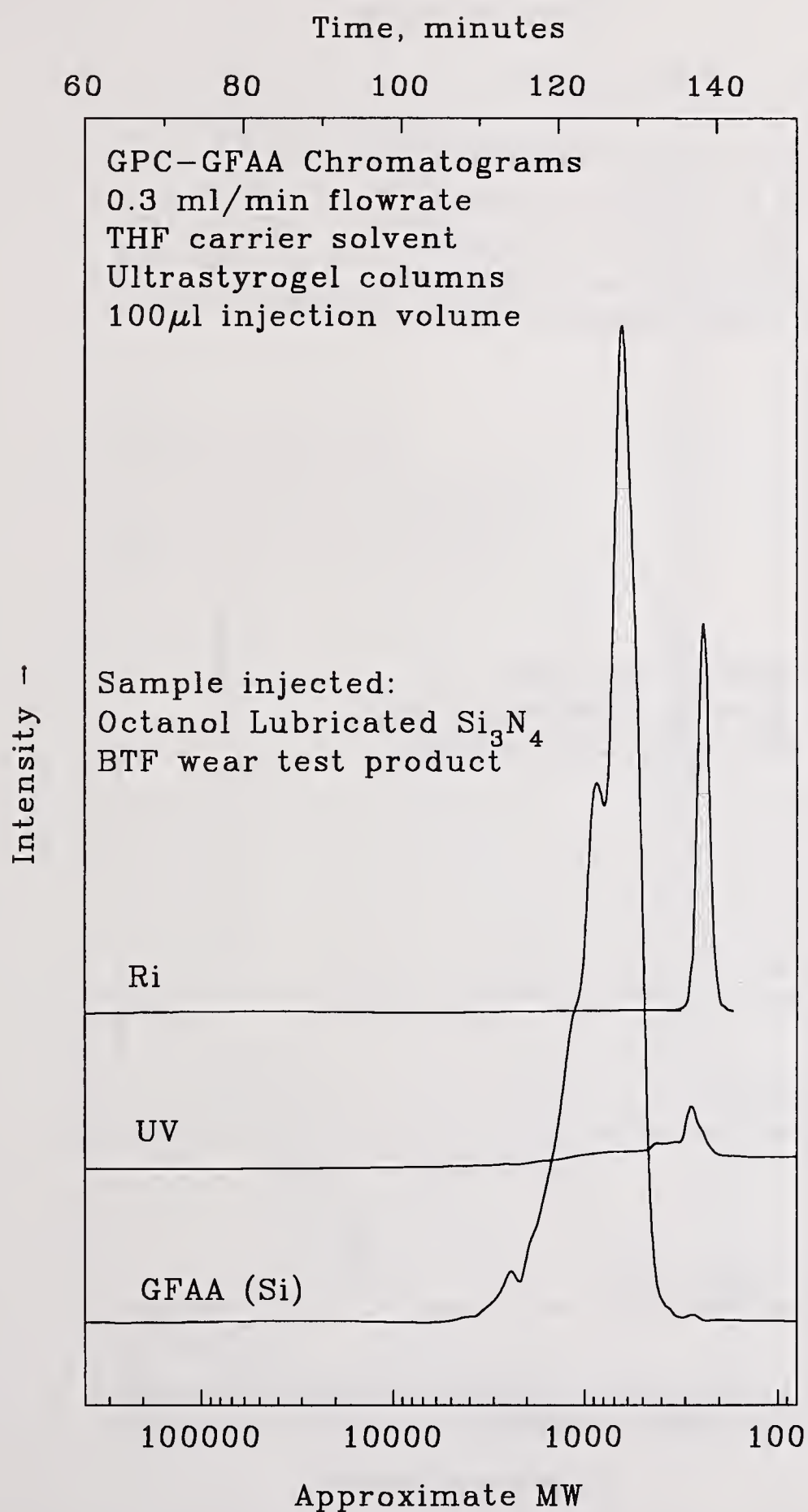


Figure 7.19 GPC-GFAA Analysis of Reaction Product from 6 μ l Neat Octanol Lubricated Si_3N_4 BTF Test

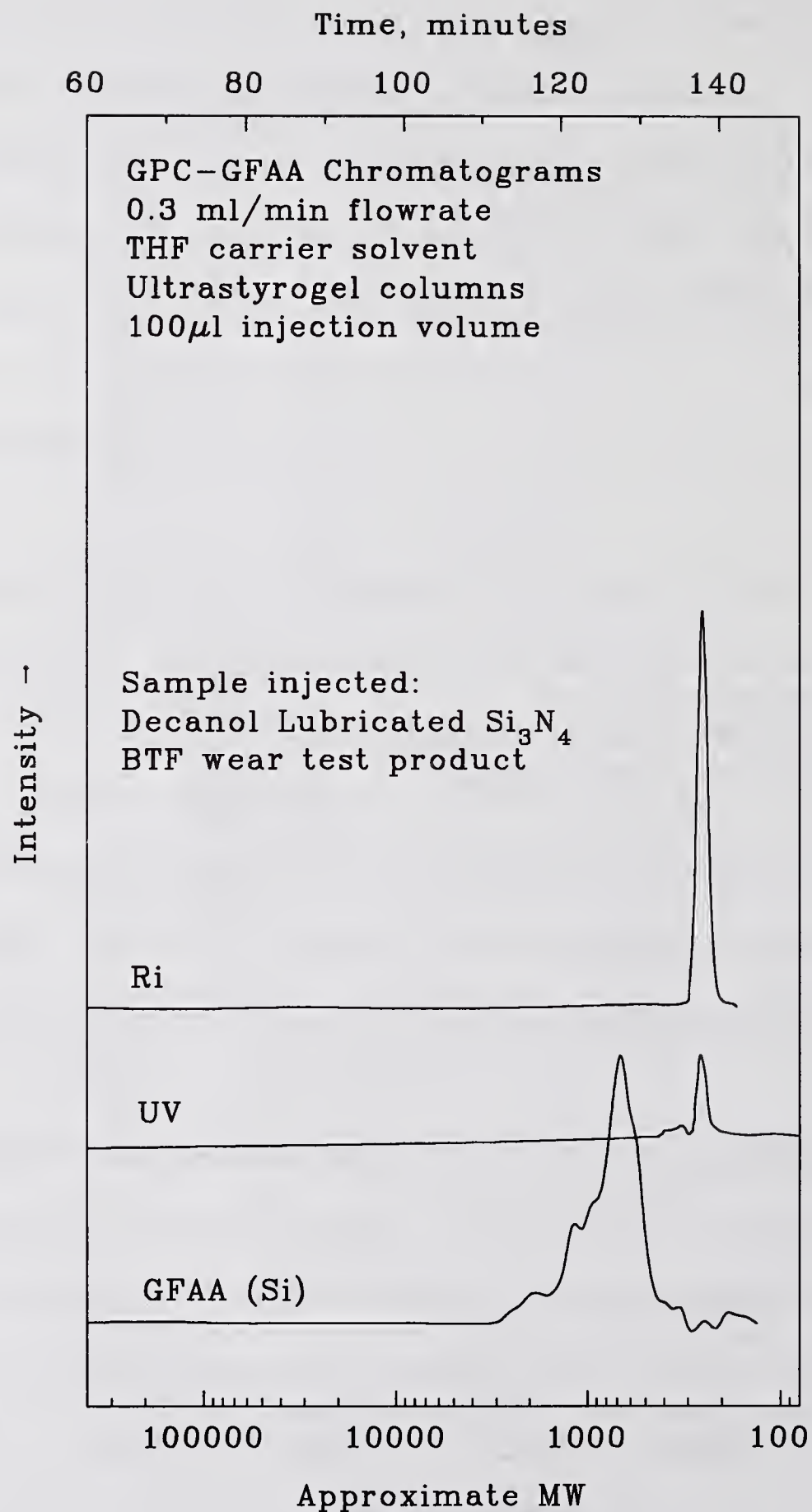


Figure 7.20 GPC-GFAA Analysis of Reaction Product from 6 μ l Neat Decanol Lubricated Si_3N_4 BTF Test

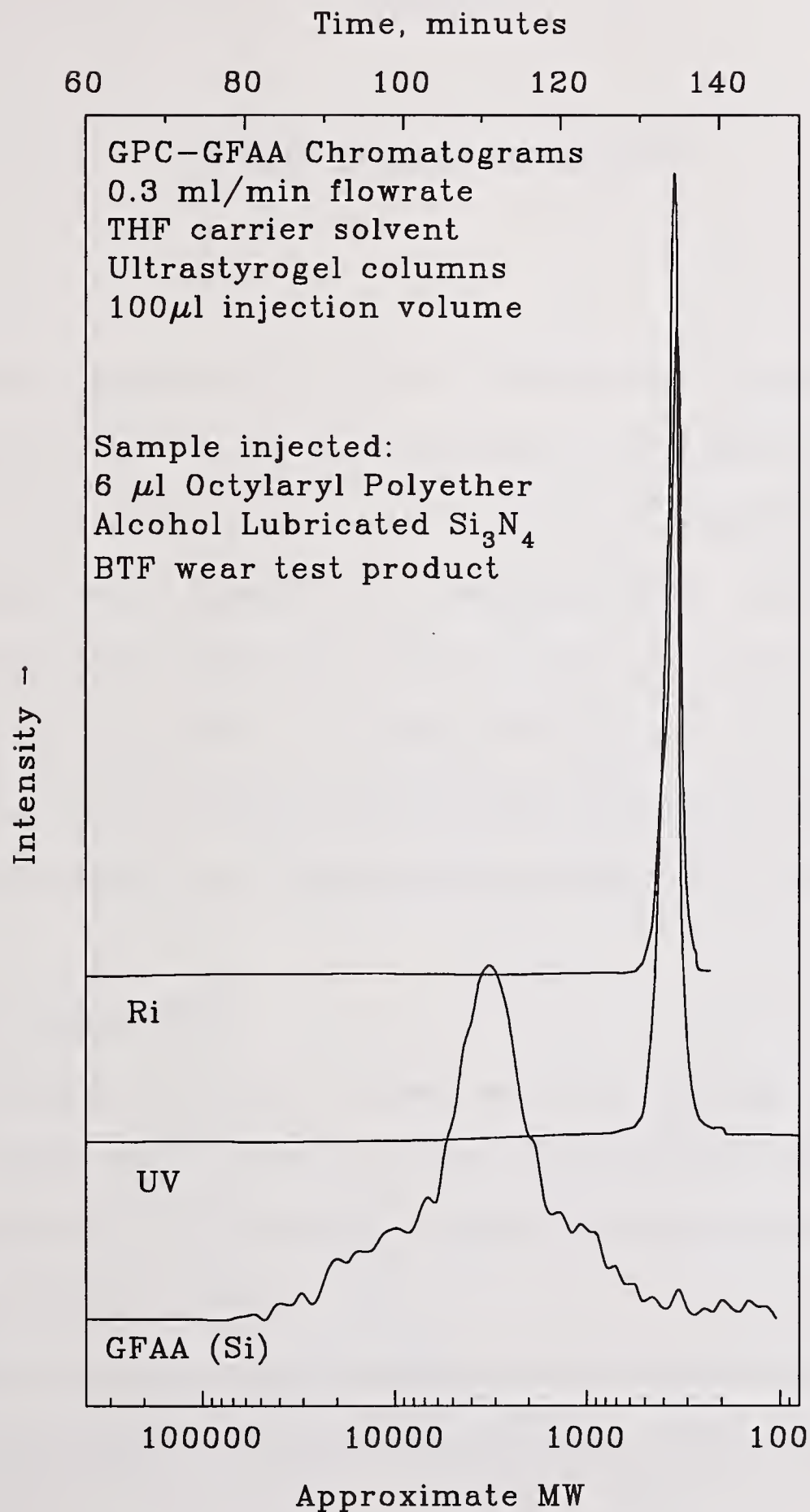


Figure 7.21 GPC-GFAA Analysis of Reaction Product from 6 μ l neat Octylaryl Polyether Alcohol Lubricated Si_3N_4 BTF Test

Chapter 8

STATIC REACTION STUDY

It has been demonstrated that some kind of surface reactions are taking place between Si_3N_4 and alcohols under boundary lubrication conditions. Static reaction experiments were conducted using Si_3N_4 powder and octanol in an attempt to isolate the first stage of these surface reaction. Initial batch reactions were conducted near 100°C . Measurement of the organic reaction product on the surface of the Si_3N_4 powders after reaction was performed by Thermogravimetric Analysis (TGA). As mentioned previously, the surface of Si_3N_4 is oxidized. The discussion of surface chemistry offered in this section is therefore based on the chemistry of silicon oxide and hydroxides present on oxidized silicon nitride surfaces.

8.1. TGA Analysis Method

TGA analysis of the powders from batch reactions involved taking a small (≈ 40 mg) sample of the dried powders, placing it in a gold pan, and recording the weight of the sample as it was heated under oxygen atmosphere. Temperature ramping was controlled at $10^\circ\text{C}/\text{minute}$ from 50°C to 700°C .

TGA is an extremely sensitive technique that does not discriminate among the different potential sources of weight loss, therefore care must be taken to calibrate against

weight loss artifacts such as bouyancy effects and residual solvent effects. These effects were carefully measured and accounted for.

TGA analysis of the raw Si_3N_4 powder under oxygen atmosphere is given in Figure 8.1 as % weight as a function of temperature. The lower trace represents the powder "as received." The upper trace is a repeat TGA run of the same powder. The apparent weight gain in the second (repeat) heating is due to bouyancy effects in the TGA furnace that were not compensated for. In the case of the procedure used, this bouyancy effect accounts for approximately 0.06% weight gain over the course of the analysis. The difference between the two traces actually represents the weight loss due to heating. The overall weight loss from the raw Si_3N_4 is minor (0.10%) and occurs over a very wide temperature range. Solvent extraction-centrifugation experiments on raw powders demonstrated that the procedure did not introduce any artifacts into the TGA weight loss analysis.

Octanol was selected for the static reaction study because it had demonstrated lubricating ability with Si_3N_4 . Figure 8.2 is the TGA trace for pure octanol. Note that the scale is 0-100% weight loss, and that the octanol has a maximum rate of weight loss at $\approx 100^\circ\text{C}$. This is far lower than the boiling point for pure octanol (196°C) because there is a constant flow of gas around the sample pan that removes any gases generated from the liquid. The temperature merely has to get high enough to generate sufficient vapor pressure in the sample to provide suitable material removal rates.

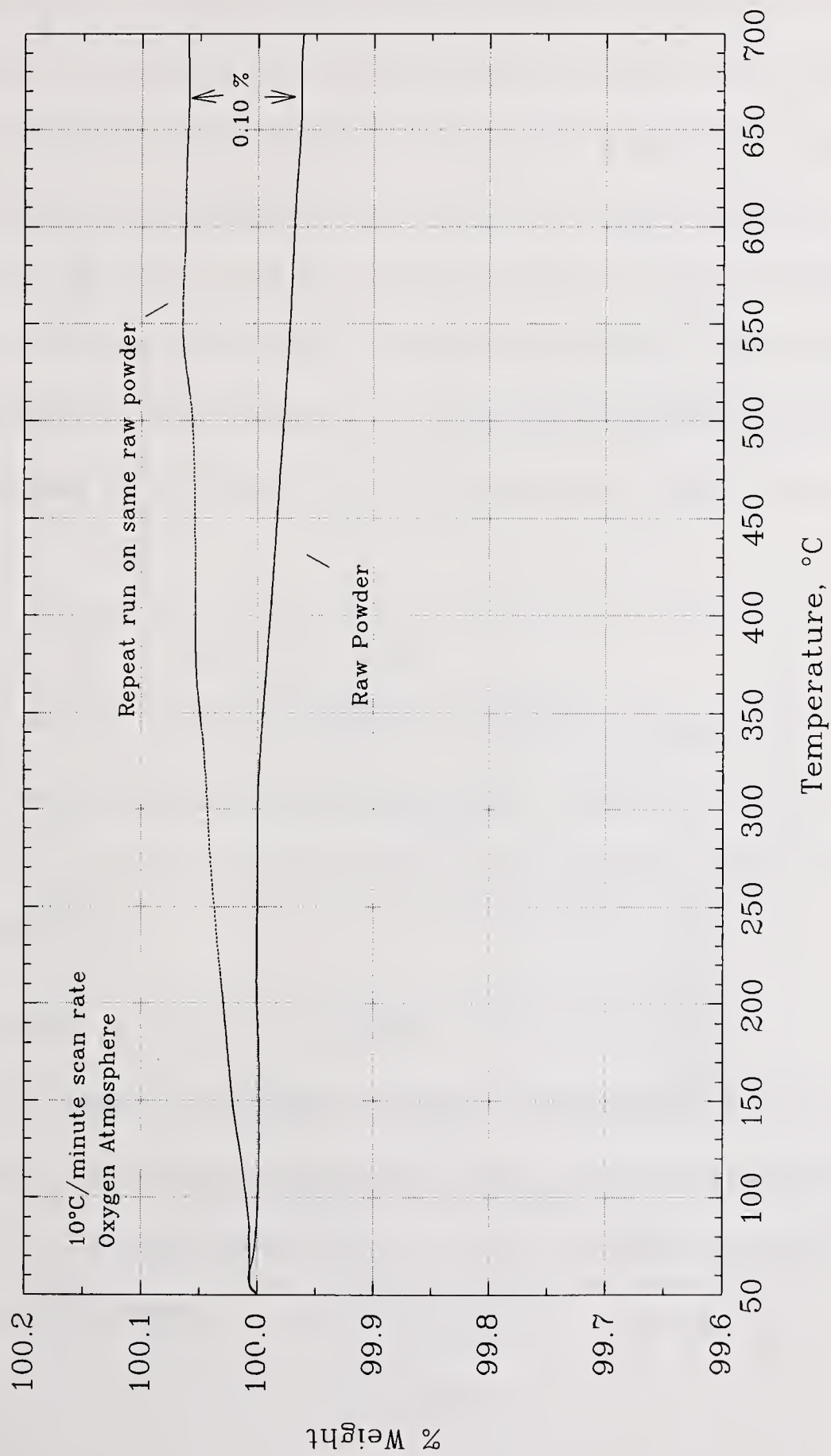


Figure 8.1 TGA Analysis of Si_3N_4 Powder

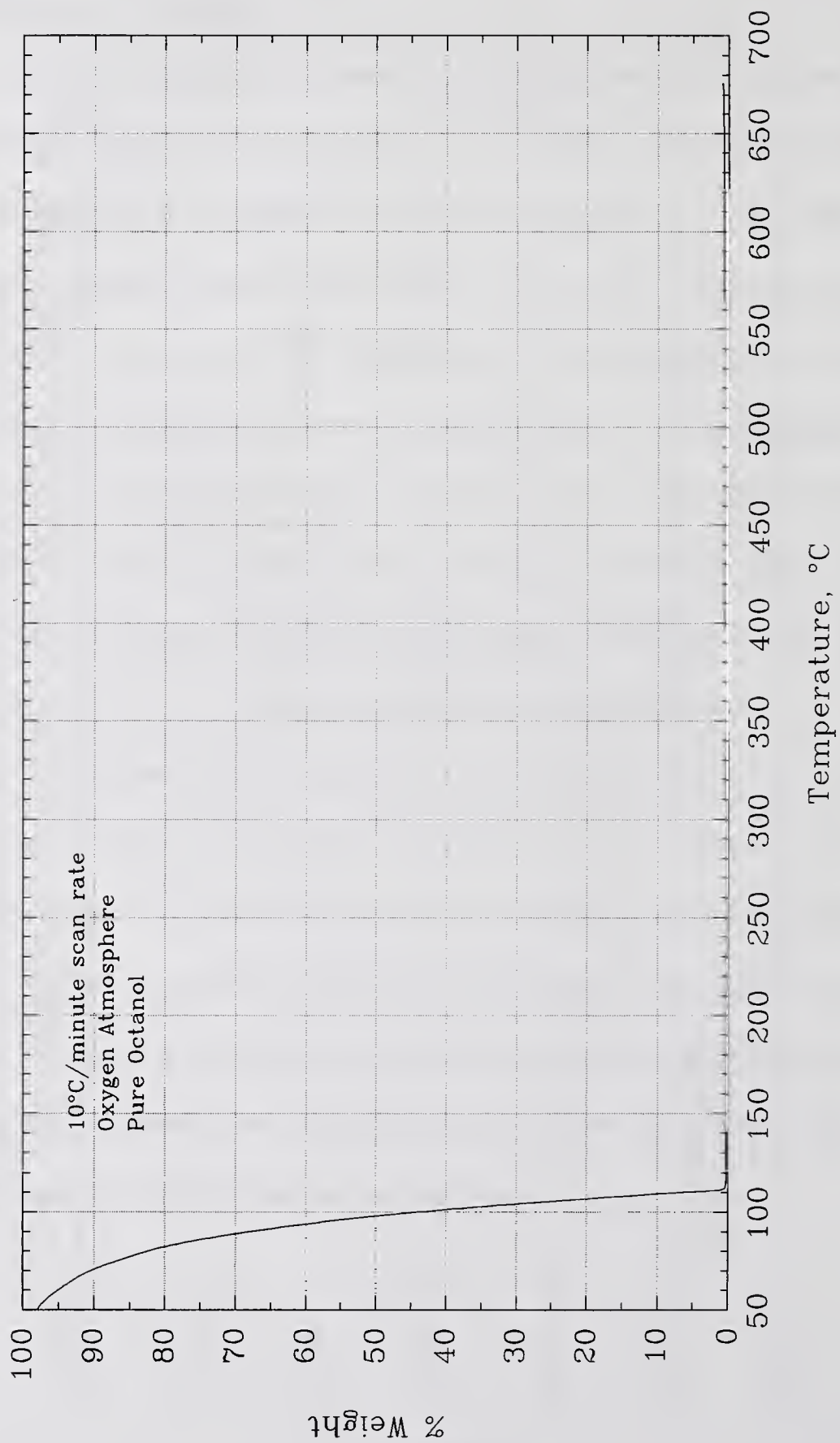
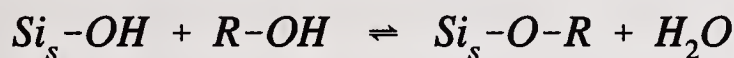


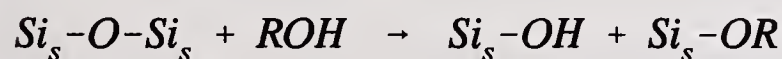
Figure 8.2 TGA Analysis of Neat Octanol

8.2 Surface Reactions of Alcohols with Si₃N₄ Powder

A sample of Si₃N₄ powder was mixed with octanol and heated to 100°C for 48 hours. The excess octanol was removed using the solvent extraction procedure already mentioned. An example of a typical TGA weight loss curve for the reaction product between Si₃N₄ powder and octanol is shown in Figure 8.3. The weight loss is very distinct, with a maximum rate of weight loss at $\approx 270^\circ\text{C}$. This temperature is too high to be merely adsorbed octanol, and suggests some kind of reaction product has formed on the surface. Given the oxidized nature of the Si₃N₄ surface, it was thought that the product might be a surface reaction bonded silicon alkoxide, formed from reaction with surface hydroxyl groups as in:



These reactions have been observed with silica^{138, 37} and have been speculated to occur with Si₃N₄^{240, 120}; however, no direct evidence has been provided. Brinker³⁷ also indicates that reactions can take place between alcohols and siloxane functional groups to form alkoxides and silanols (alcoholysis).



If these are indeed the reactions taking place on Si₃N₄, it explains how alcohols can react with Si₃N₄ to form a bonded surface layer that might help in boundary lubrication. FTIR, DSC, GPC-GFAA and TGA/Mass Spectrometry were used to understand the chemical nature of the surface reaction products.

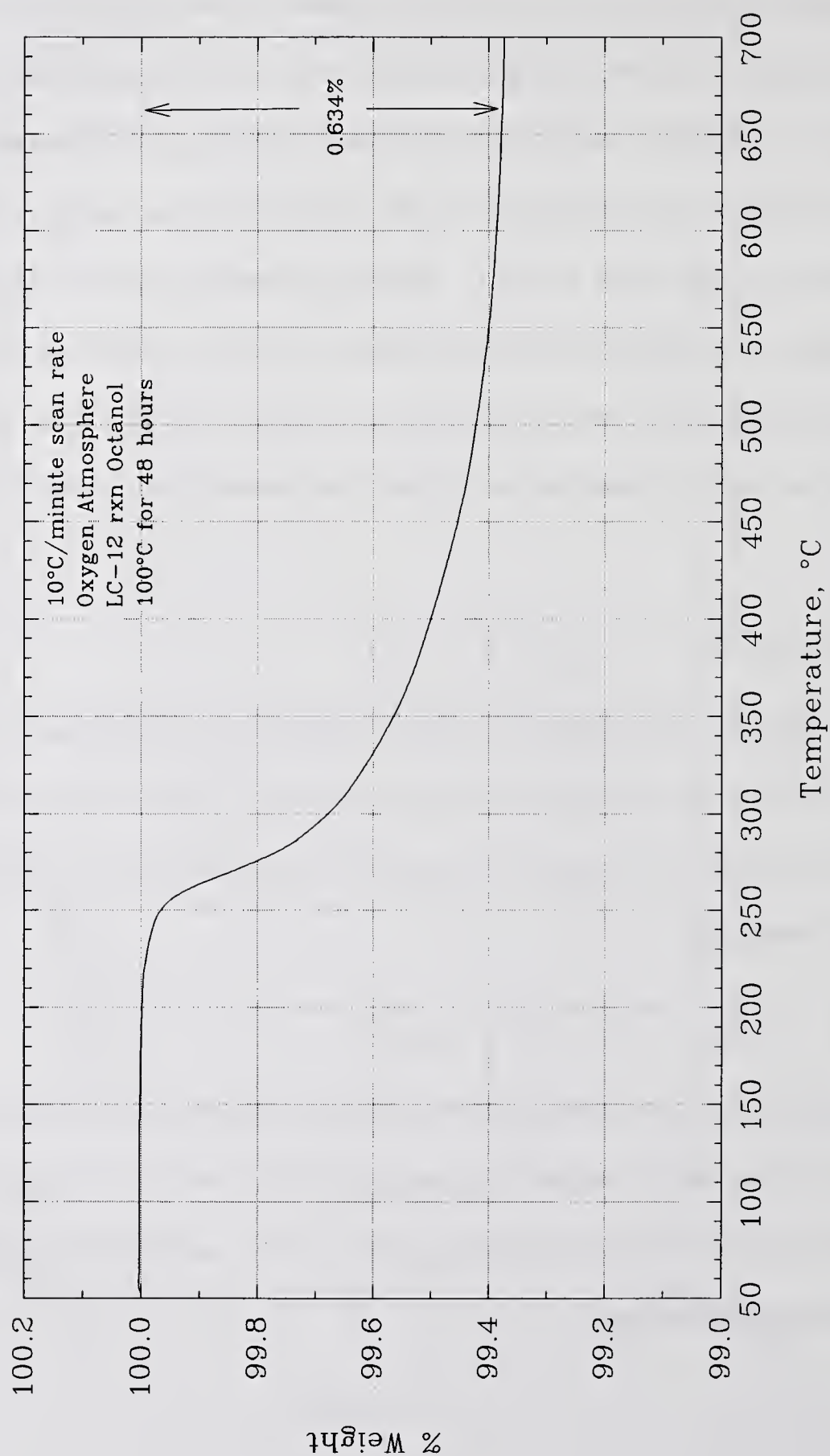


Figure 8.3 TGA Analysis of Si_3N_4 Powder Reacted with Octanol at 100°C for 48 Hours Immediately After Solvent Extraction

8.3. Evidence of the Chemical Structure of Alcohol-Si₃N₄ Powder Reaction Products

FTIR was used to analyze the surface of the Si₃N₄ powders after reaction and subsequent solvent extraction. Figure 8.4 compares the spectrum of the reacted powder to a powder that has been exposed to octanol (at room temperature) and has undergone the same solvent extraction procedure. The reacted powder contains three peaks at 2855, 2924, and 2955 cm⁻¹ that are not present in the "exposed" sample. These three peaks are associated with C-H stretch frequencies and indicate the presence of an organic compound on the Si₃N₄ surface containing C-H bonds. The presence of reaction bonded octanol is consistent with this observation.

DSC analysis of a sample of Si₃N₄ powder (Figure 8.5) under oxygen indicates a strong exothermic peak with a maximum at 250°C consistent with the oxidation of a surface organic compound such as reaction bonded octanol (Si alkoxide).

Another TGA analysis was performed on one of the reacted Si₃N₄ powders in which the evolved gases from the system were monitored using a mass spectrometer. The mass peaks associated with H₂O and CO₂ (Figure 8.6) go through a maxima at approximately 300°C, demonstrating that the species on the surface of Si₃N₄ reacts with oxygen to form H₂O and CO₂, i.e., it is a carbon and hydrogen containing organic compound. Again, this is consistent with the hypothesized silicon alkoxide surface bonded species.

GPC-GFAA analysis of the supernatant fluid left after reacting the octanol with the Si₃N₄ powder was analyzed using GPC-GFAA to try to detect dissolved silicon-containing compounds. None could be found, therefore it was concluded that the pathway from surface alkoxide to soluble silicon-containing compound is not purely thermal in nature. Iler¹³⁸

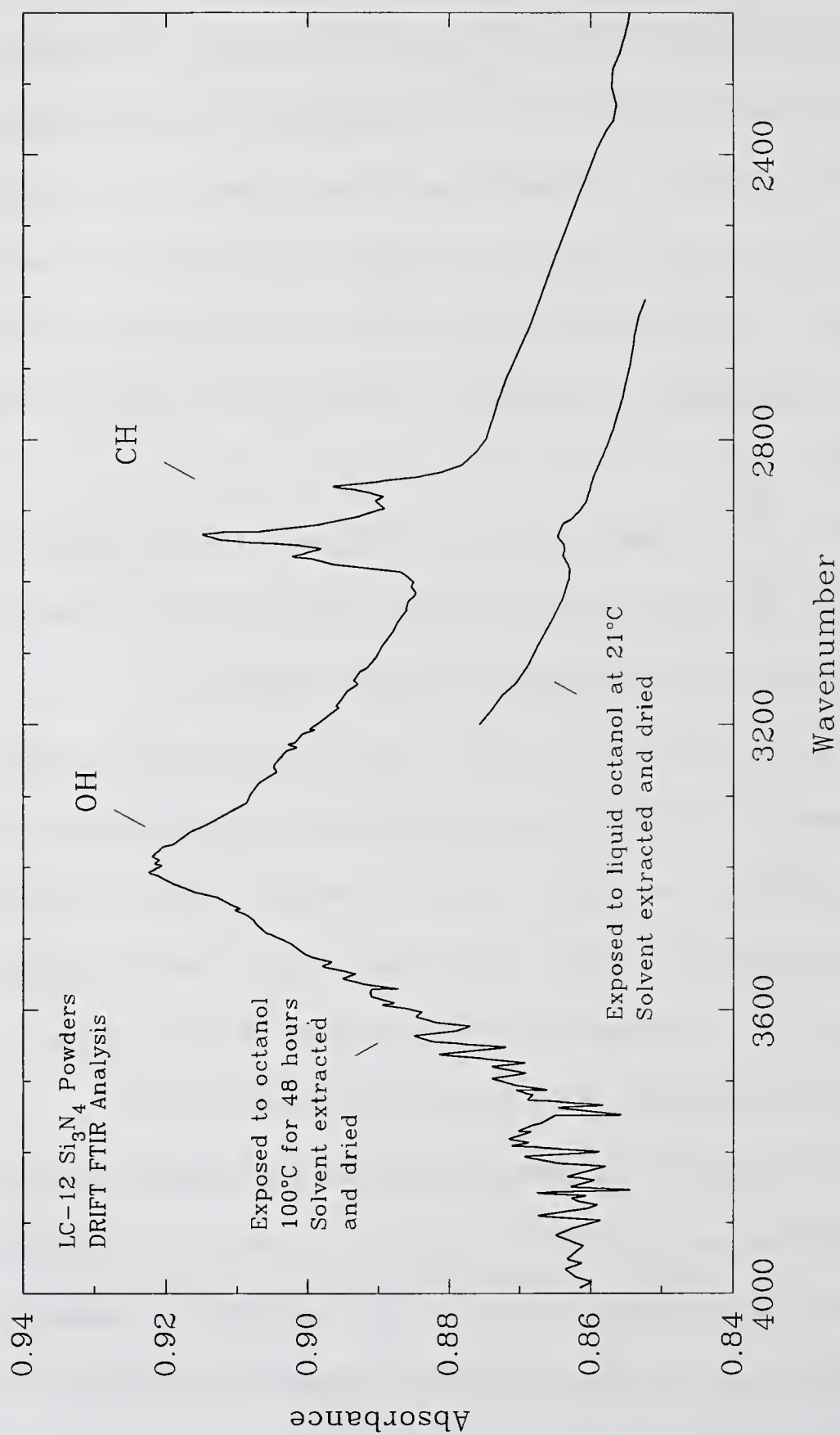


Figure 8.4 FTIR Spectrum of Si_3N_4 Powder Reacted with Octanol at 100°C for 48 Hours

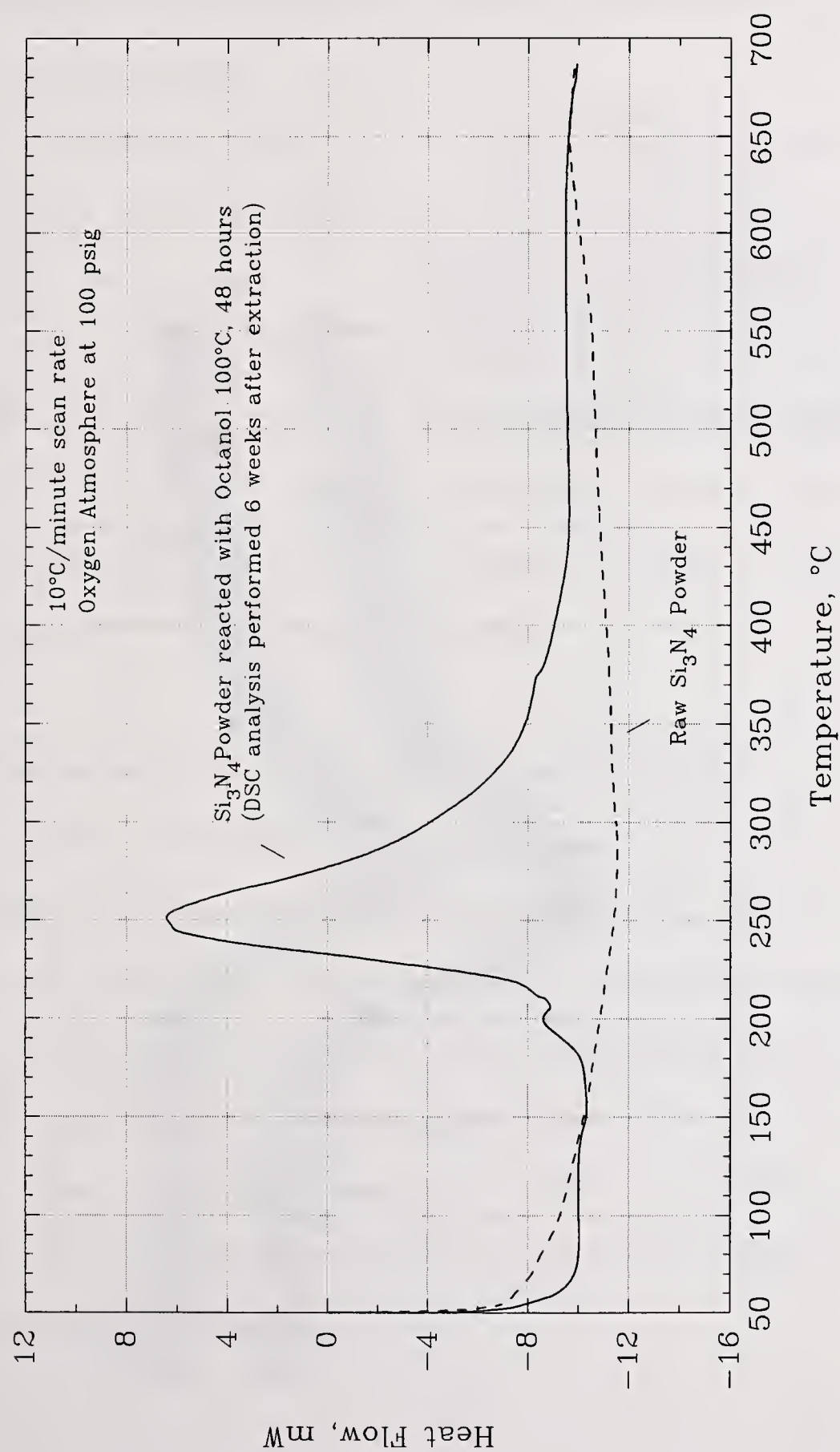


Figure 8.5 PDSC Analysis of Si₃N₄ Powder Reacted with Octanol at 100°C for 48 Hours

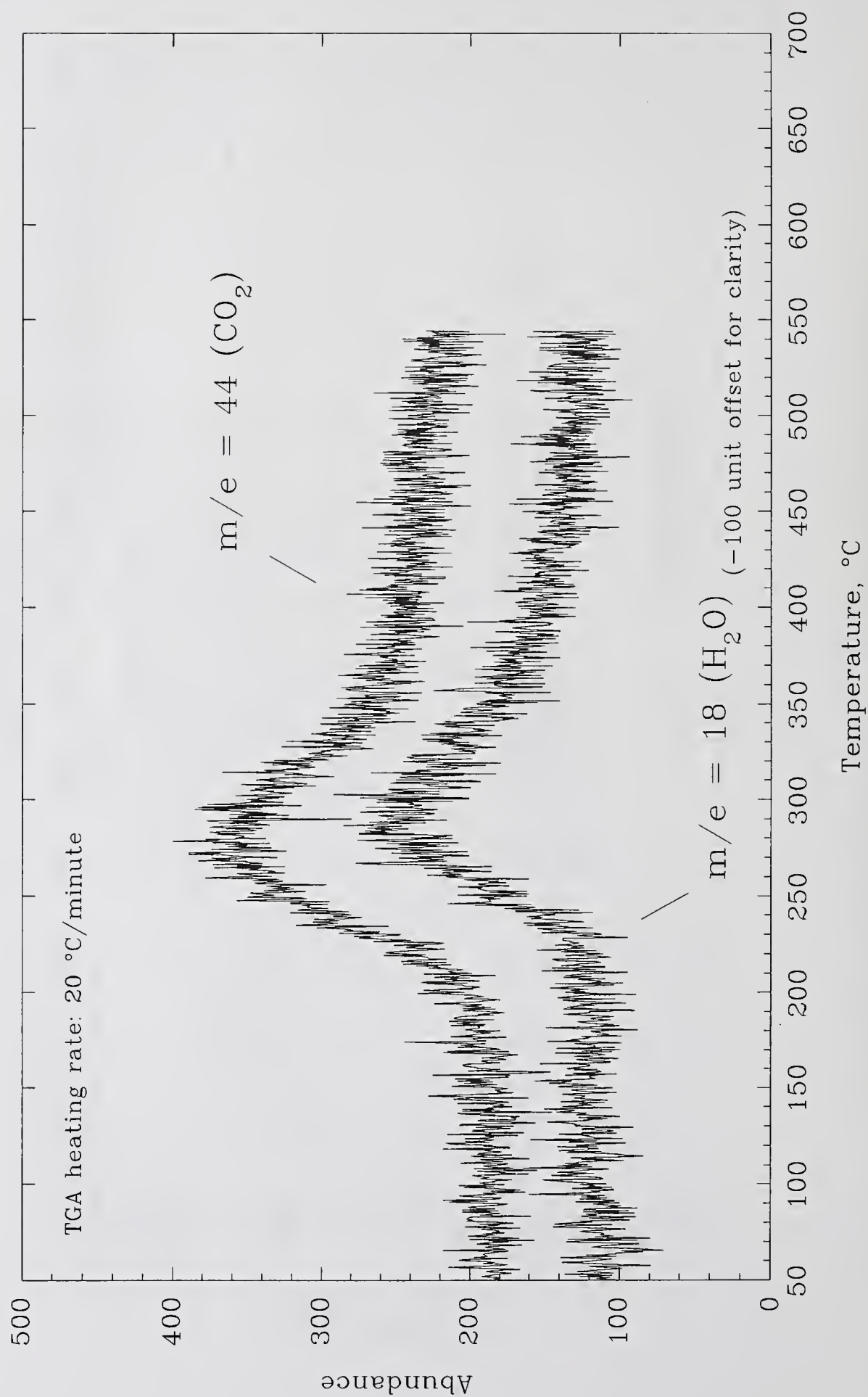


Figure 8.6 CO₂ and H₂O Mass Spectral Analysis of TGA Gases from Si₃N₄ Powder Reacted with Octanol at 100°C for 48 Hours

describes the solubility of silica gel in three alcohols at 500°C as shown in Table 8.1. Given the trend of solubility, it is not surprising that C₈ alcohols would not form any detectable octanol soluble silicon compounds.

Apparently there is some special factor introduced by rubbing (tribochemistry) that makes it possible to produce these compounds. This may be either dangling bonds, or perhaps some element of bond

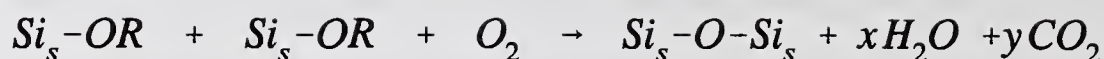
Table 8.1
Solubility of Silica in Alcohols
(Source: Iler¹³⁸ p. 62)

<u>Alcohol</u>	<u>Solubility (ppm)</u>
CH ₃ OH	1890
C ₂ H ₅ OH	164
n-C ₃ H ₇ OH	8

strain introduced through the surface shear stress that influences reactivity. Indeed there is some evidence in the literature⁶⁹ that grinding of silicates in the presence of alcohol resulted in chemical reactions between the alcohol and the surface.

8.4. Discussion on the Nature of the Alcohol-Si₃N₄ Surface Reaction

The analytical evidence suggests that the reaction product from the batch reaction of octanol with Si₃N₄ powders is a surface bonded silicon alkoxide. The weight loss shown in Figure 8.3; therefore represents the oxidative decomposition of the organic surface alkoxide Si-O-C₈H₁₇. The weight loss seems to be level at 700°C indicating that all of the organic material has been removed from the surface by this temperature. This is very convenient because it means that the weight loss between 200°C and 700 °C can be used to estimate the number of moles of octanol bonded to the surface assuming the decomposition follows a pathway similar to that seen on silica²¹²:



If the TGA analysis is carried out under argon instead of oxygen, the weight loss curve is different in shape (not as sharp a drop), but it reaches the same final end point at 700°C. This is because the oxidative decomposition pathway for the surface bonded organic compound is faster than the thermal decomposition one. All of the experimental data used to quantify the reaction product on the surface of Si₃N₄ was generated using an oxygen atmosphere.

In the course of this study it was found that some TGA curves exhibited two weight losses as exemplified in Figure 8.7. The initial weight loss at $\approx 150^\circ\text{C}$ is at too high a temperature to be due to either water, or residual liquid octanol, therefore it was suspected that it represented octanol that was adsorbed on the surface of the Si₃N₄ (probably through hydrogen bonding). The hypothesized structures associated with each weight loss are superimposed on Figure 8.7. This additional initial weight loss was observed if : i) the residual octanol reactant was not adequately extracted from the reacted powder, or ii) the extracted (and dried) reaction product powder was not immediately analyzed.

Improperly extracted powders had the extra initial weight loss shown in Figure 8.7, but they also suffered from poor repeatability in quantifying the weight loss due to silicon alkoxide (the higher temperature weight loss). It became apparent that the presence of adsorbed octanol on Si₃N₄ somehow contributed to an increase in the amount of reacted octanol (silicon alkoxide). An experiment was conducted in which a dish of powder was suspended above a beaker of octanol in a sealed container. The octanol was allowed to saturate the chamber and adsorb onto the Si₃N₄ powder. TGA analysis of the resulting

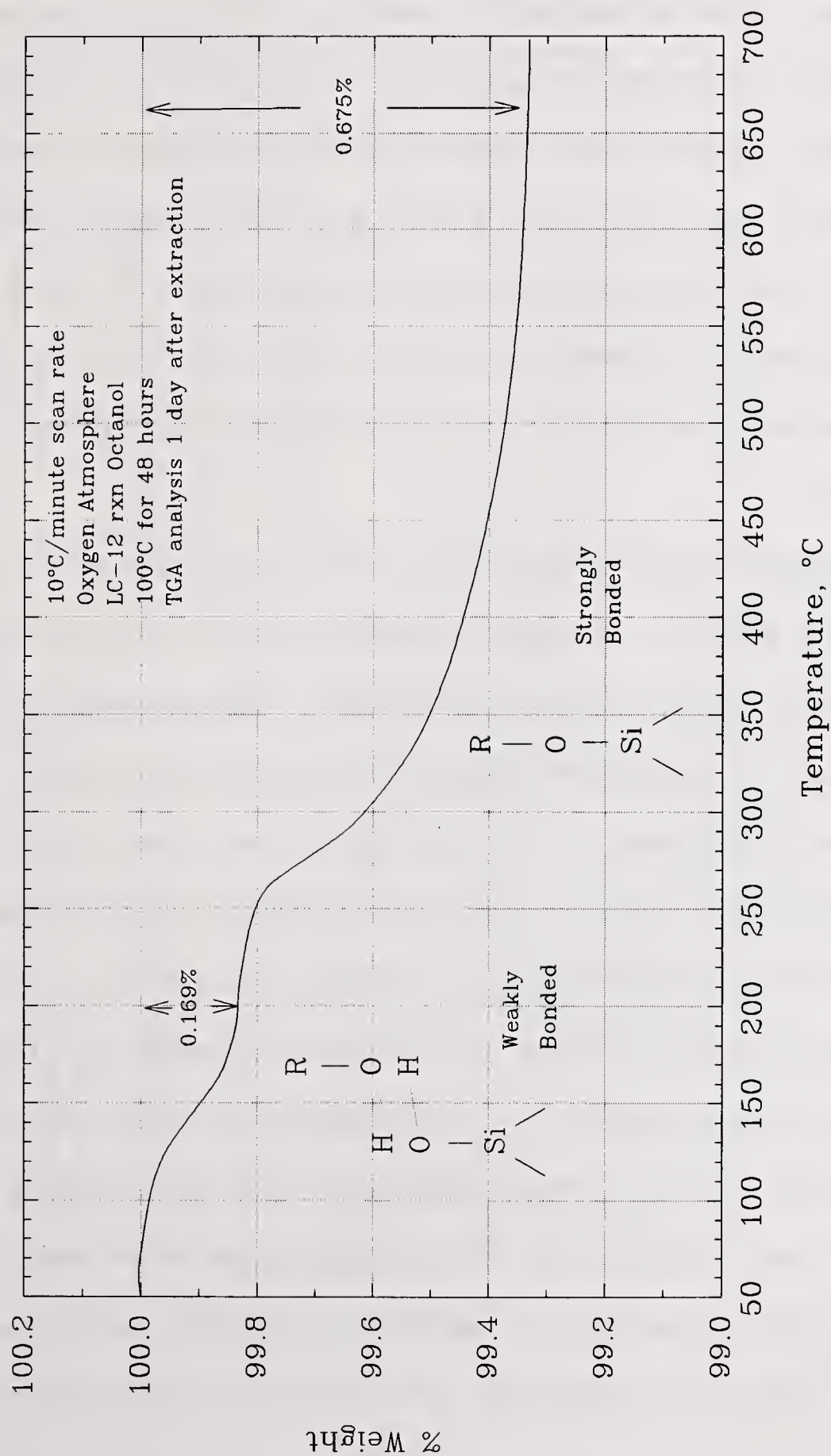
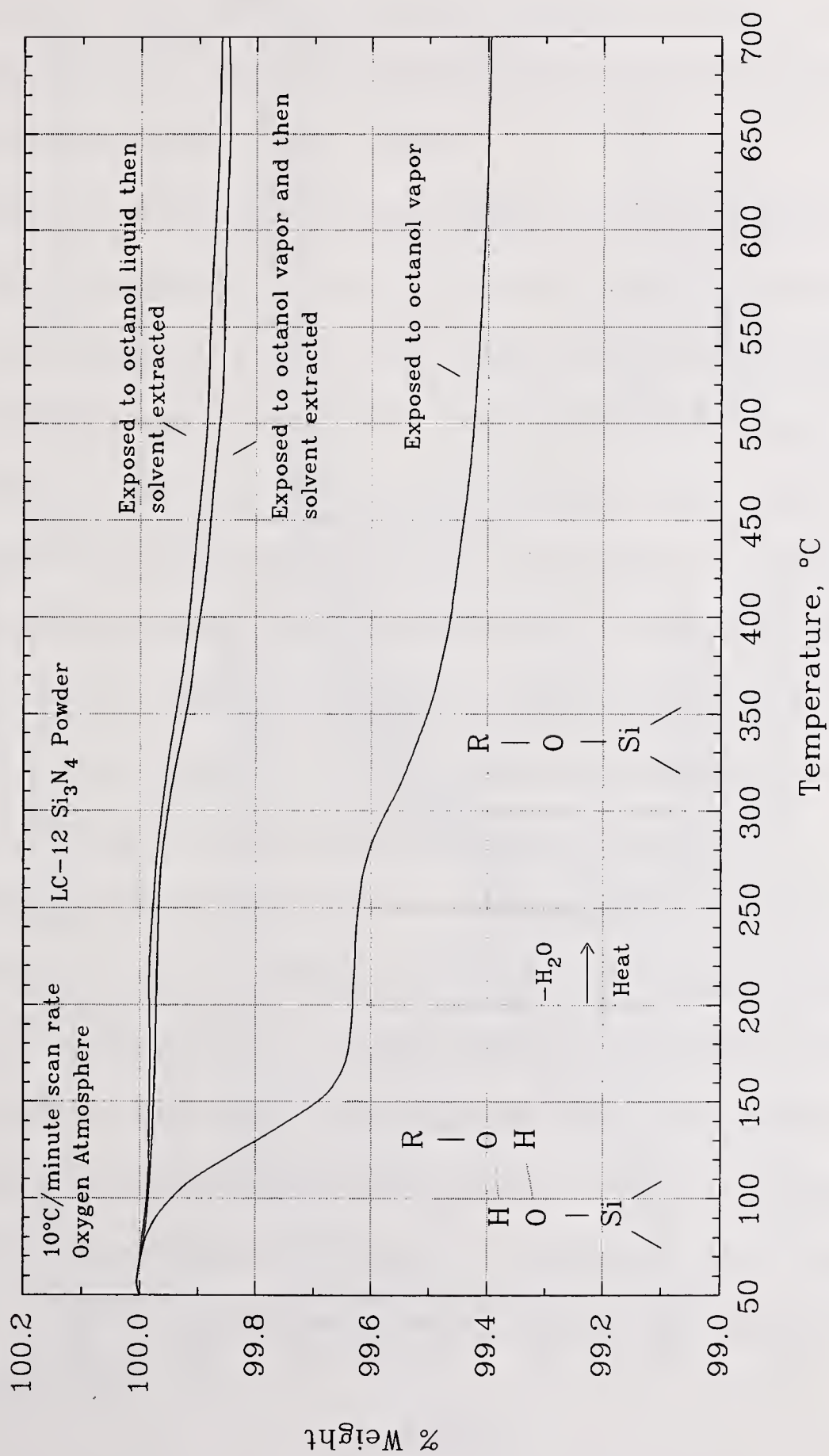


Figure 8.7 TGA Analysis of the Same Powder 1 Day After Solvent Extraction

powder (no solvent extraction) indicated both adsorbed and bonded were present (Figure 8.8 - lower trace). When the vapor exposed powder was solvent extracted, the weight loss curve changed back to the baseline case (upper trace). Apparently, the heat supplied to the sample during heating (and prior to loss of the adsorbed octanol) is sufficient to promote reaction and formation of the surface alkoxide as shown in the reaction sequence superimposed on Figure 8.8. These results indicated that it was very important to accurately quantify the results to remove any adsorbed octanol prior to TGA analysis. The ability to measure the adsorbed octanol weight loss was used to optimize the extraction procedure to eliminate this problem.

The second observation that powders, on sitting, can develop the initial weight loss is exemplified in Figure 8.9. The uppermost weight loss curve is for the reaction product powder analyzed immediately after solvent extraction. The single peak is due only to bonded octanol. The other curves represent TGA analyses on the exact same powder, but the analyses were performed 1, 4, 11, and 35 days after the solvent extraction. The growth of the initial weight loss with time indicates that the quantity of adsorbed octanol on the surface of the Si_3N_4 increases with time. The overall weight loss increases with time, but at a much smaller rate than the growth in the adsorbed octanol weight loss. The data suggest that bonded octanol is transformed to adsorbed octanol on the surface, probably due to the presence of water vapor. The overall weight gain can more than accommodate the water necessary to carry out this reaction. This information means that the reaction to form surface alkoxides of octanol on the surface of Si_3N_4 is reversible, and apparently the reverse reaction is favored at room temperature. The observation that this reversible reaction seems

Figure 8.8 TGA Analysis of Si_3N_4 Powder Exposed to Octanol Vapor

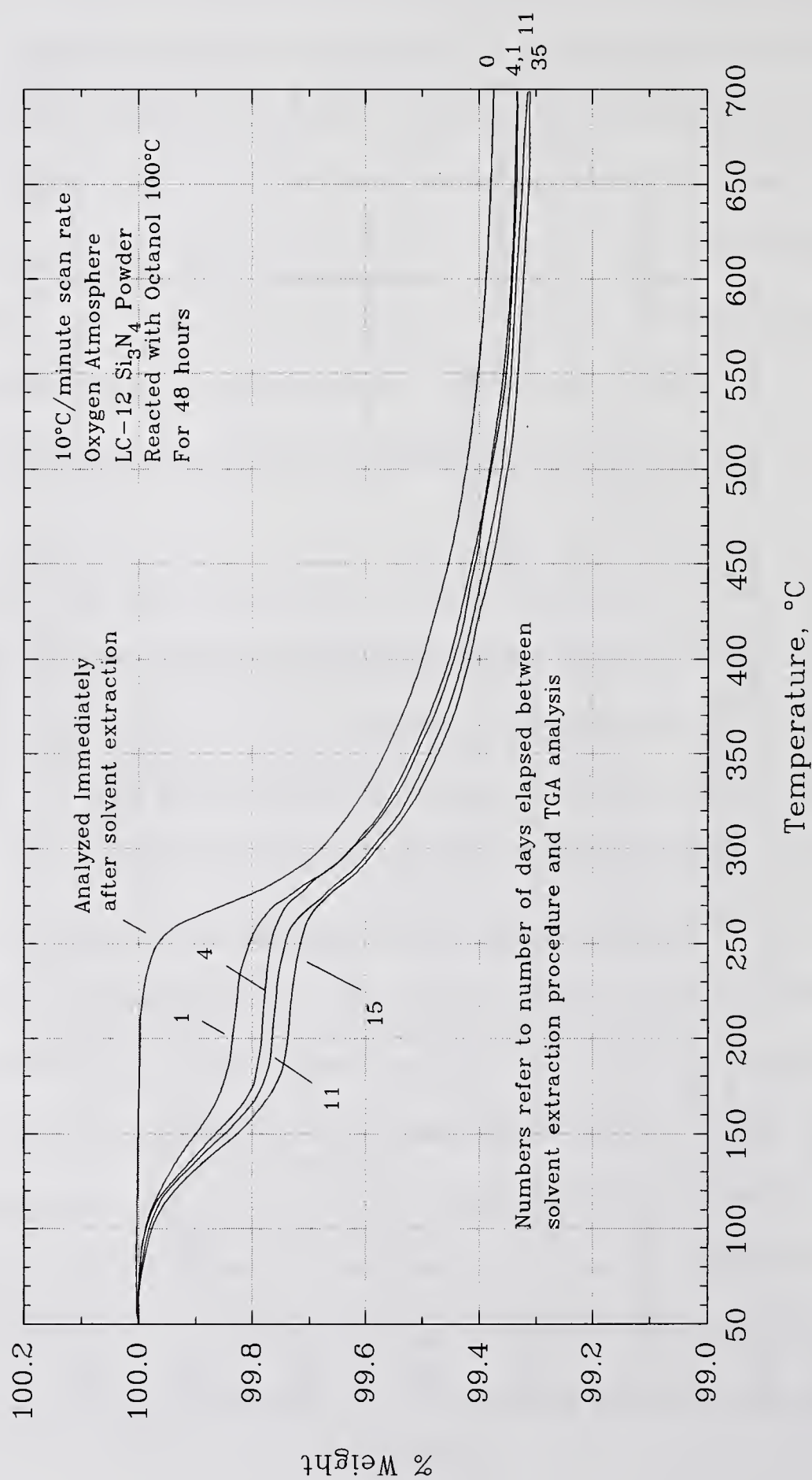


Figure 8.9 TGA Analysis of Si_3N_4 Powder Reacted with Octanol at 100°C for 48 Hours as a Function of Time Since Solvent Extraction

to reach an equilibrium at finite values of bonded octanol seems to indicate that there may be more than one type of surface site on Si_3N_4 , one that can easily revert back to the adsorbed octanol, and one that cannot. The data also underscores the importance of analyzing the reacted powders immediately after solvent extraction.

TGA analysis of Si_3N_4 powders reacted for different times at 100°C (Figure 8.10) indicated that the reaction qualitatively exhibited expected kinetic behavior of increased coverage with time, approaching a limiting value. Attempts to fit the data to a simple pseudo first order kinetic expression (as used by Rossi²¹² on silica) were not successful. This suggests that while silica and silicon nitride may have qualitatively similar silicon oxide surfaces, they appear to have different kinetic behavior. One explanation, suggested by the observation of partial reversibility seen with the Si_3N_4 powder, is that there may be multiple sites on the Si_3N_4 that have different kinetic behavior, resulting in non pseudo first order (lumped) kinetics. This is supported by Brinkers³⁷ contention that alcohols can react with both silanol (esterification) and siloxane (alcoholysis) groups in silica.

Qualitatively, the results obtained on Si_3N_4 are quite similar with the results obtained by the other researchers on silica. Additional static reactions were carried out between octanol and Si_3N_4 at higher temperatures. At 200°C and 245°C similar bonded surface products were observed. An estimate of flash temperatures in the octanol lubricated Si_3N_4 contact, performed using Archard's¹¹ method (see appendix I), indicated temperatures of only 120°C . This temperature is comfortably bracketed by the temperatures of the "static" reactions (100°C to 245°C) and reinforces the notion that these reactions may be taking place in the contact junction.

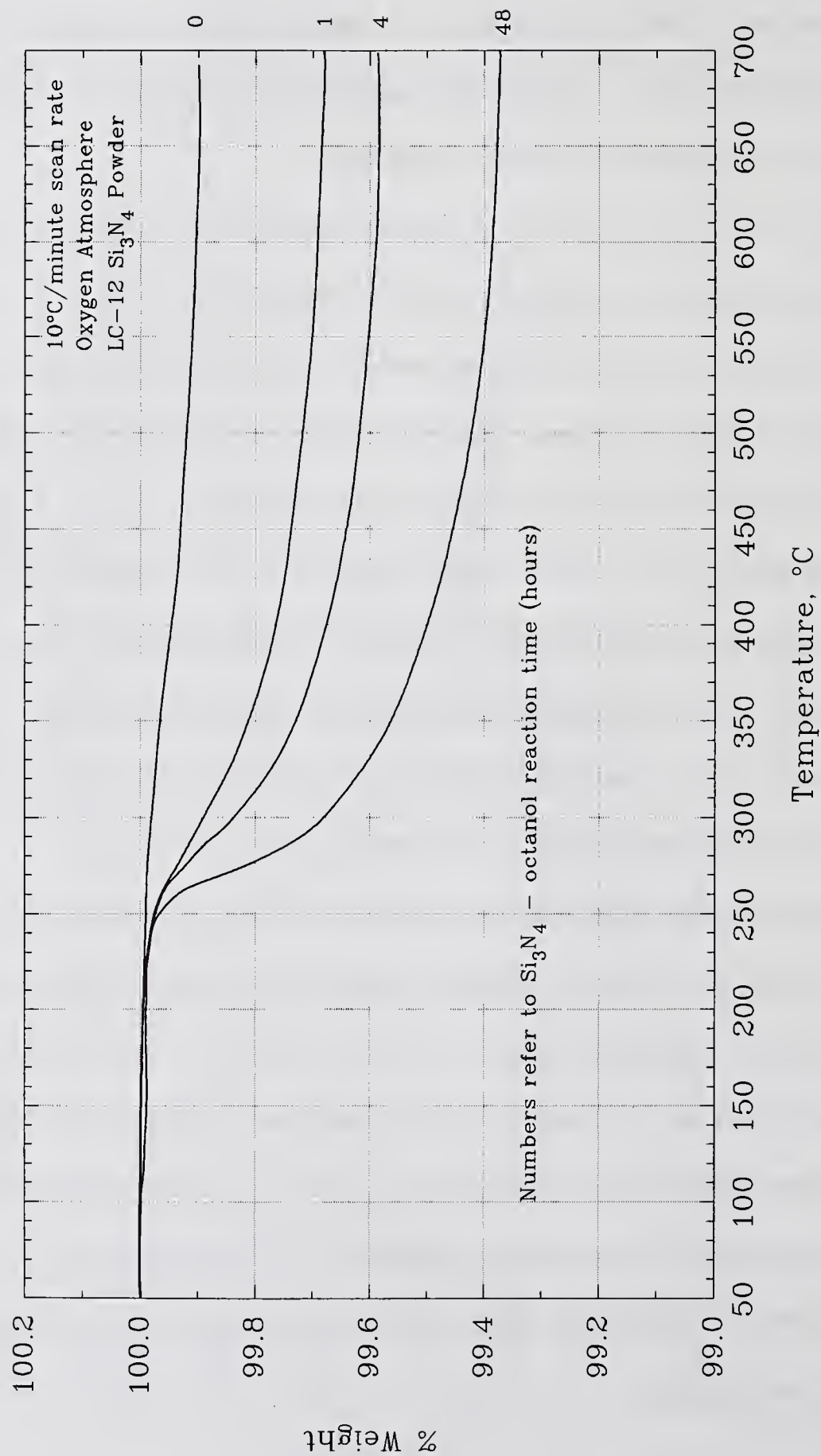


Figure 8.10 TGA Analysis of Si_3N_4 Powder Reacted with Octanol at 100°C for 1, 4, and 48 Hours

Chapter 9

MECHANISTIC MODEL FOR ALCOHOL LUBRICATION

Analysis of the reaction products from an alcohol-lubricated wear test indicated that direct chemical reactions were occurring that incorporate silicon from the Si_3N_4 surface. Static reactions have demonstrated that alcohols can adsorb and react with the surface of Si_3N_4 to form a surface bonded phase that appears to be a silicon alkoxide. Secondary Ion Mass Spectrometry (SIMS) analysis was then performed on the wear test reaction product to clarify the chemical structure of these products.

9.1. SIMS Analysis of the 6 μl BTF Reaction Products

In order to try to determine the structure of the reaction products from these wear tests, "Static" Secondary Ion Mass Spectrometry (SIMS) was employed. This is a high vacuum microanalysis technique that used heavy ions (in this case gallium) to bombard the surface of the sample. This process causes material to be energetically kicked off the surface so that they can be subsequently analyzed with a time of flight mass spectrometer. The term "static" applied to this technique describes the fact that bombardment is very gentle and does not result in appreciable damage to the surface such as would be apparent in the more severe "dynamic" SIMS in which the surface is actually sputtered away during the analysis. The static SIMS technique allows very high molecular weight organic compounds to be removed

from the surface relatively intact. It also has the capability to focus down to very small regions (≈ 100 nm) which allows for good spacial resolution among features if necessary.

SIMS analysis of the residue from the 6 μ l BTF test resulted in the mass spectrum seen in Figure 9.1, which was taken while focussed on a region of the flat away from the wear scar. This region had several condensed residue "islands" that were formed when the excess octanol lubricant was allowed to evaporate. Immediately apparent are several peaks at mass/charge (m/e) ratios of 15, 29, 43, 57, and 71. These peaks represent the hydrocarbon compounds CH_3^+ , C_2H_5^+ , C_3H_7^+ , C_4H_9^+ , and $\text{C}_5\text{H}_{11}^+$ respectively. They are indicative of the fragmentation seen for a linear hydrocarbon, and only differ from one another by m/e 14 (CH_2). The smaller, lower m/e peaks near each of these peaks represent fragments of the parent ion that have been stripped of additional pairs of hydrogens (hence they differ by 2 mass units). There are also less intense peaks that differ by only one hydrogen (1 mass unit). Additional peaks present that overlap some of the hydrocarbon peaks are silicon ($m/e = 28$), and gallium ($m/e = 69$), which is an artifact of the ion bombardment. The fragmentation pattern seen in this spectrum indicates a linear hydrocarbon of at least C_5 . This makes sense since we started with C_8 in the original octanol lubricant. Since we allowed the octanol to evaporate from the surface, the data suggests that there are C_8 linear ligands attached to some kind of parent molecule which is non-volatile.

Careful analysis of the higher m/e region above 100 indicated the presence of several peaks at m/e 157, 285, 415, 543, and 718. These peaks are very close to what would be expected for several silicon alkoxides of the series shown in Table 9.1. It is not apparent why the observed peaks at 285 and 543 are off by one unit from the calculated peak.

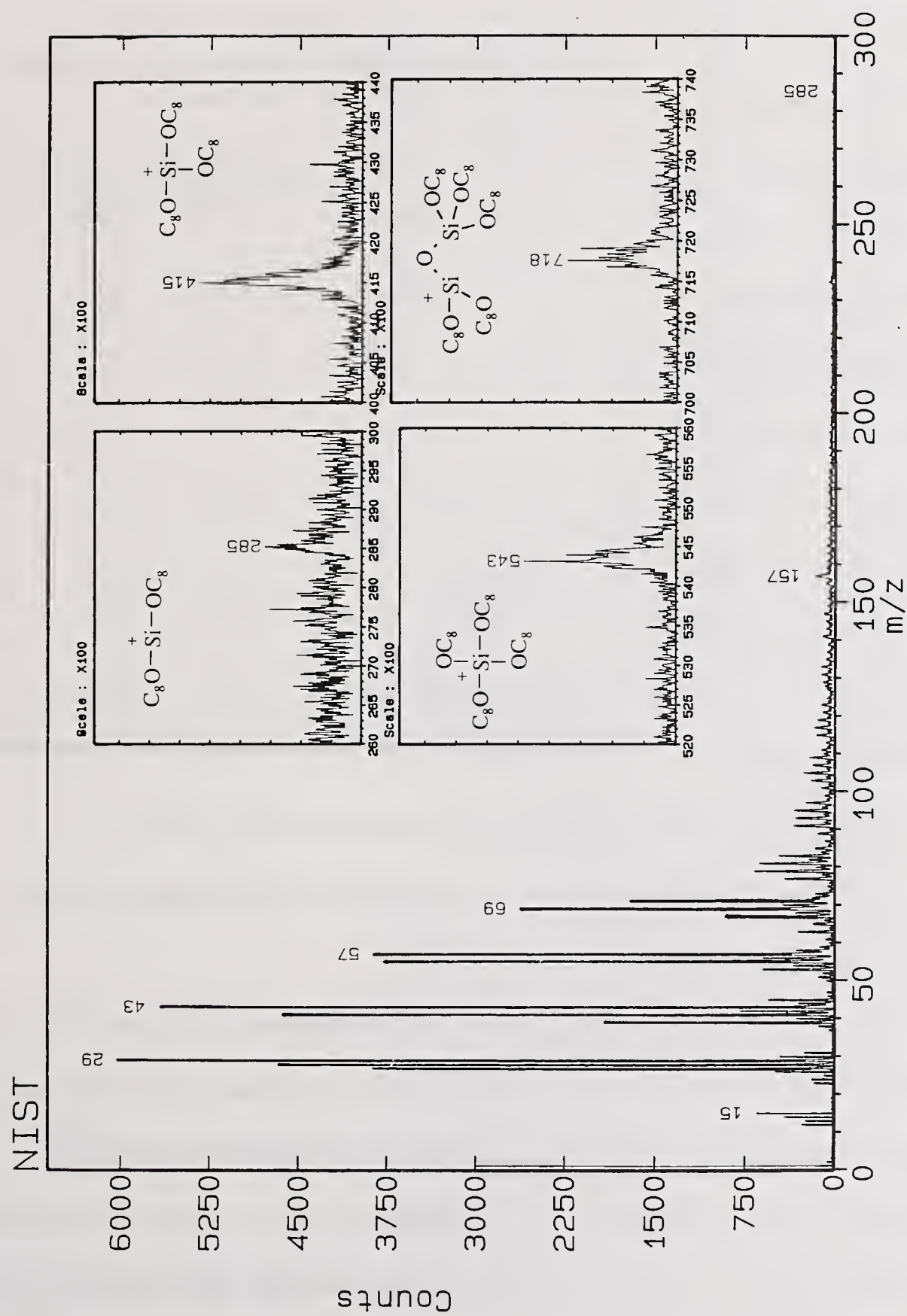


Figure 9.1 SIMS Analysis of Residue from 6 μ l Neat Octanol Lubricated Si_3N_4 BTF Test

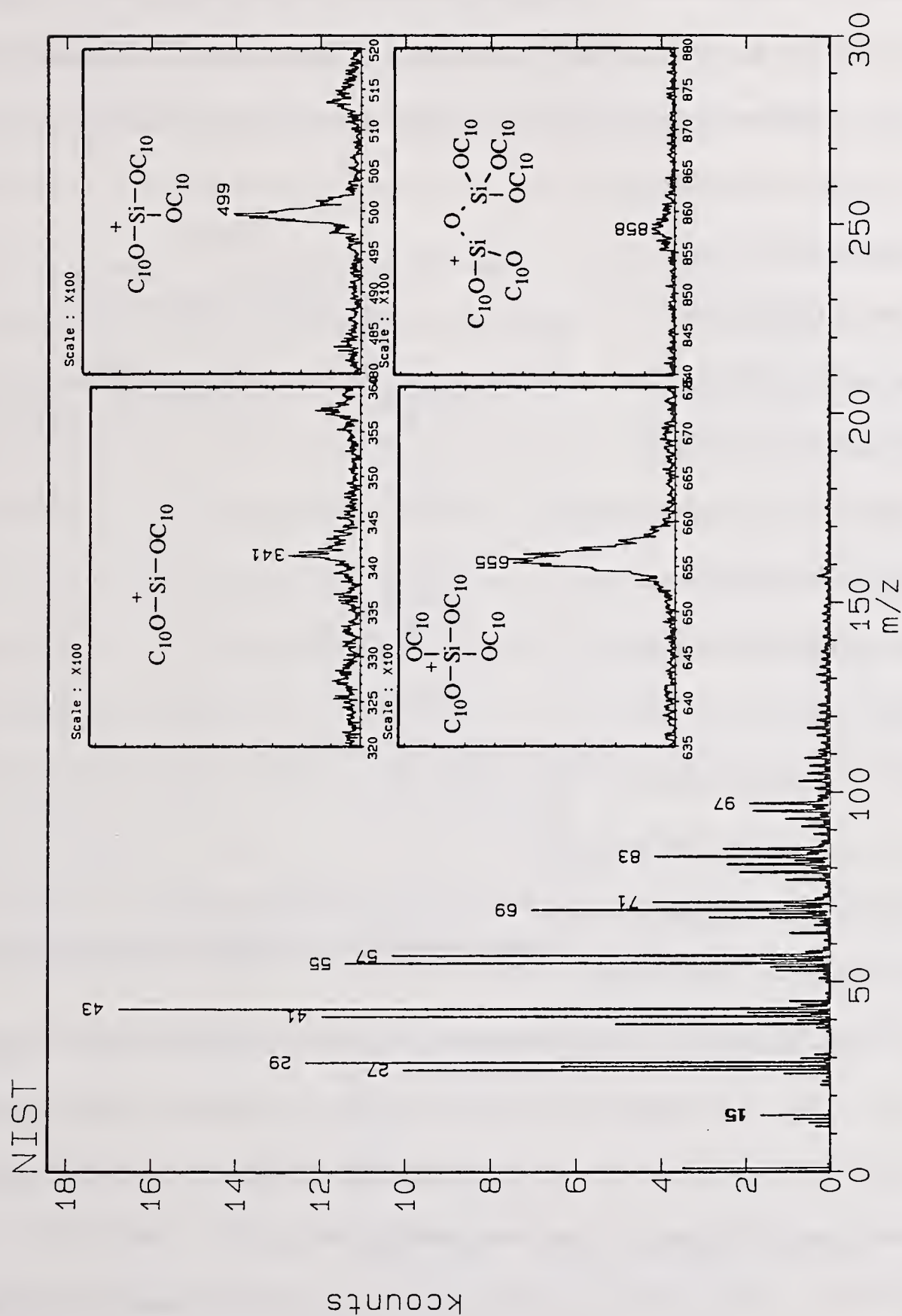
Several attempts were made to calculate m/e ratios for compounds that might be expected from oxidation / polymerization of pure octanol, however these products were not consistent with the observations. It should be noted that the tetra-alkoxy compound (@ m/e 543) and the disiloxane compound (@ m/e 718) are both present in the reaction product since fragmentation in the mass

Table 9.1
SIMS Mass Spectral Data for Octanol Lubricated
Si₃N₄ Wear Test Product

<u>Compound</u>	<u>m/e</u>	
	<u>Calculated</u>	<u>Observed</u>
+ Si-O-C ₈	157	157
+ Si-(O-C ₈) ₂	286	285
+ Si-(O-C ₈) ₃	415	415
+ Si-(O-C ₈) ₄	544	543
+ (C ₈ -O) ₂ -Si-O-Si-(O-C ₈) ₃	718	718

spectrum does not occur through breakdown of the siloxane skeleton as noted by Polivanov¹⁹⁸. The lower alkoxides may be due (at least partially) to fragmentation of the parent tetra-alkoxide.

Repeating the SIMS analysis on a flat from decanol lubricated Si₃N₄ resulted in the mass spectrum shown in Figure 9.2. This spectrum contains the same hydrocarbon fragment series seen in the octanol case; however it is apparent that the decanol lubricated case extends to higher m/e ratio compounds. This is consistent with the fact that decanol has two more carbons than octanol and would be expected to generate higher m/e fragments because of the larger parent compound.

Figure 9.2 SIMS Analysis of Residue from 6 μl Neat Decanol Lubricated Si_3N_4 BTF Test

The m/e peaks seen for the mass range above 100 are at m/e 157, 341, 499, 655, and 858. These m/e ratios are consistent with the assignments shown in Table 9.2. The peak at 341 is consistent with the dialkoxide, similar to the one seen with octanol, but displaced to higher m/e to reflect

the C₁₀ ligands instead of C₈. The peaks at 499 and 655 can be

assigned to the tri and tetra-

alkoxide respectively. The 858 peak is quite weak, but is consistent

with the Si-O-Si linked alkoxide indicated. Again, all of these peaks

are displaced to higher m/e values

that reflect the larger organic ligand expected (C₁₀ versus C₈). The peak

for the monoalkoxide expected at

185 was not detected. The fact that

there was a peak detected at 157 (same peak m/e as for octanol) indicates that the original assignment of 157 for the monoalkoxide of Si with octanol was incorrect. The 157 peak is probably a product not related to any organic ligand since it is present in both the octanol and decanol lubricated Si₃N₄ cases. The source of this peak has not been identified.

GPC-GFAA analysis of the reaction products from octanol-lubricated Si₃N₄ indicated HMW silicon-containing organic compounds were formed. SIMS analysis identified

Table 9.2
SIMS Mass Spectral Data for Decanol Lubricated
Si₃N₄ Wear Test Product

<u>Compound</u>	<u>m/e</u>	
	<u>Calculated</u>	<u>Observed</u>
+ Si-O-C ₁₀	185	None
+ Si-(O-C ₁₀) ₂	342	341
+ Si-(O-C ₁₀) ₃	499	499
+ Si-(O-C ₁₀) ₄	656	655
+ (C ₁₀ -O) ₂ -Si-O-Si-(O-C ₁₀) ₃	858	858

compounds in the reaction product consistent with silicon alkoxide structures. This is further reinforced by the static test data which suggests that alcohols can adsorb and bond with the Si_3N_4 surface to form silicon alkoxides. One question that remains is which reaction product can lubricate? This question was addressed using two-ball collision tests.

9.2. Evaluation of Lubrication Effectiveness Using the Two-Ball Collision Test

The Two-Ball collision apparatus was designed and built at NIST to study single and multiple contacts in a controlled and repeatable manner. It is described in detail in the introductory paper by Ying and Hsu²⁶⁷. The basic geometry consists of two spheres that move past one another (Figure 9.3). The force of the contact is dictated by the overlap (h) and the mechanical and elastic response of the apparatus and specimen materials. A triaxial force transducer, mounted in a

plates supporting one of the balls allows measurement of normal and friction forces throughout the test. Initially, it was used to study surface and subsurface deformation due to contact in metals and ceramics, but for the purposes of this study, it was applied to measuring the ability of films to lubricate.

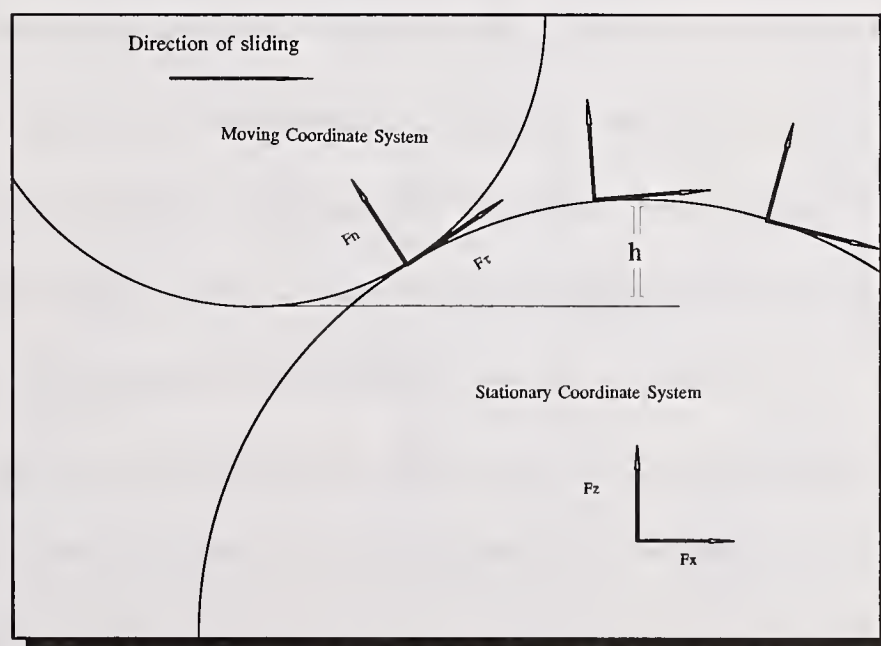
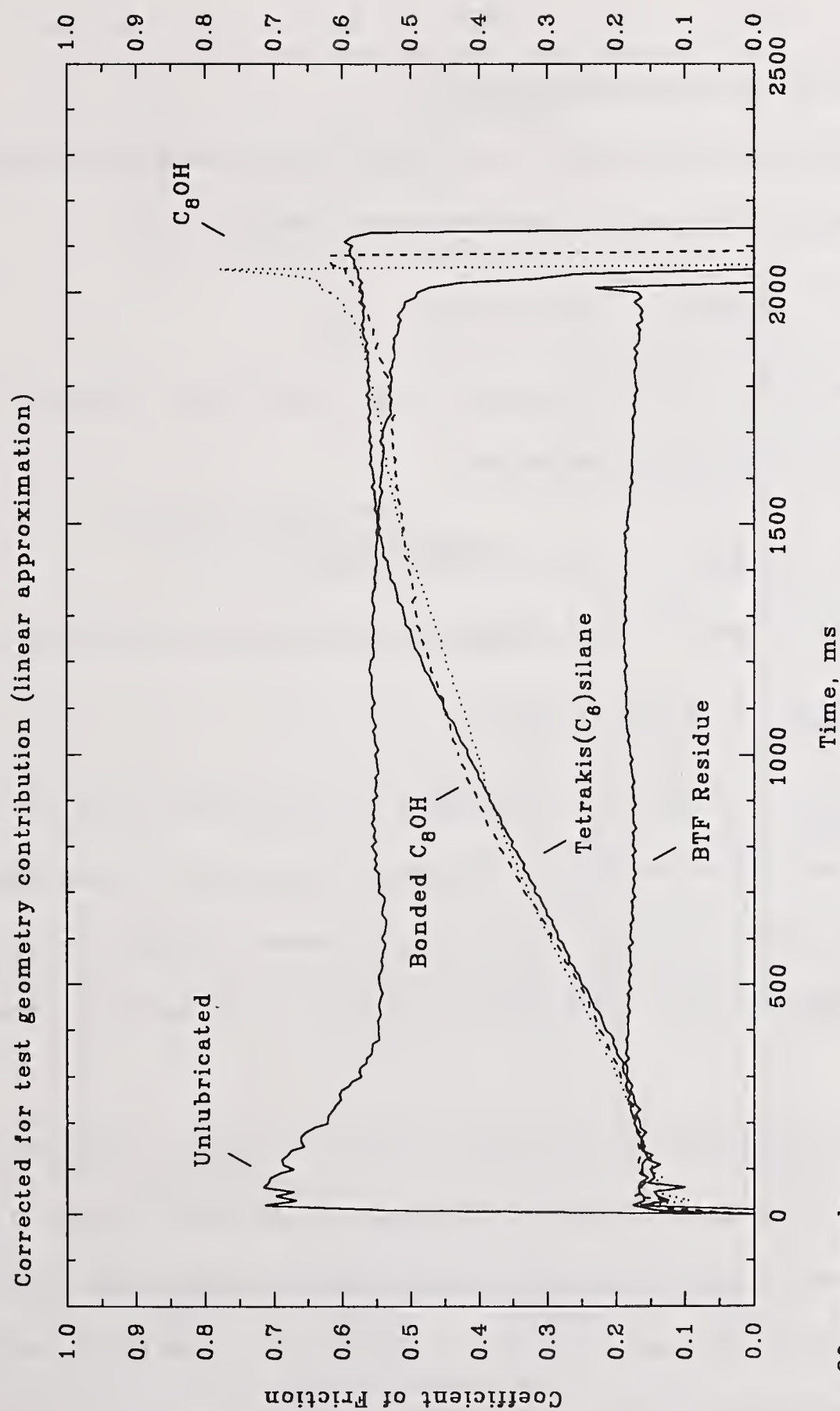


Figure 9.3 Two-Ball Collision Test Geometry

A series of tests conducted using NC132 hot pressed Si_3N_4 indicated the ability of different films to lubricate (Figure 9.4). Unlubricated Si_3N_4 starts and ends with a high coefficient of 0.5 to 0.7, which is consistent with values obtained in the literature. Octanol gave low friction only during the beginning of the test. This may indicate some initial lubricating ability, but the film lacks the tenacity or "film strength" to maintain low friction. Since reaction with the surface to form the bonded octanol may be important, a second test was conducted using balls that had been heated to 150°C for 30 minutes, immersed in octanol. This test was also run with liquid octanol present. It did not lubricate effectively throughout the test. A fourth test was conducted using a C_6 tetra-alkoxide model compound that, also, did not lubricate.

A test was conducted using the residue from a six microliter BTF test (after the excess octanol had evaporated). The material was transferred by direct contact between one of the flats from a BTF test with one of the balls from the Two-Ball test. Low friction was observed throughout this test. This result indicates that there is some ingredient present in the residue that is capable of lubricating throughout this test that has not been duplicated by the chemistries used (octanol, bonded octanol, and C_6 silicon tetra-alkoxide).

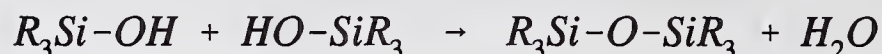
GPC-GFAA analysis of the residue from the BTF test indicated that high molecular weight silicon containing organic compounds were present. Approximate molecular weights of over 1000 were observed. SIMS analysis confirms the high molecular weight nature of the residue and even indicates silicon alkoxides. The highest molecular weight species detected with SIMS were thought to be silicon "polyalkoxide" with a siloxane (Si-O-Si) backbone. A series of experiments were designed to determine if these "polyalkoxides"

Figure 9.4 Two-Ball Collision Test Results for Unlubricated and Lubricated Si_3N_4

could be generated by heating silicon tetra-alkoxide.

9.3 Tetra-Alkoxide Heating Experiments

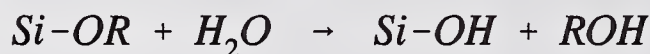
According to several sources^{37, 138} silica can polymerize through condensation reactions involving silanol groups (water condensation reaction).



Polymerization reactions can also take place between a silanol and an alkoxide group in a process Brinker³⁷ terms alcohol condensation.



Given the ability to hydrolyze silicon alkoxides (reverse reaction of esterification):



it may be possible for for trace water (atmospheric etc.) to hydrolyze silicon tetra-alkoxide and form a silanol, which can then react with another tetra-alkoxide to form a silicon alkoxide with a siloxane backbone. In this way, high molecular weight silicon alkoxide "polymers" might be formed. Batch reactions were carried out to verify this reaction pathway.

Silicon tetra-alkoxide (C₆) was heated to $\approx 200^\circ\text{C}$ for 5 hours. At the end of this time, the fluid had thickened noticeably and contained a second, thicker, semi-solid phase. Figure 9.5 shows the GPC-GFAA analysis for the original C₆ tetra-alkoxide model compound. A single large peak is observed at ≈ 600 MW in both the GFAA and RI traces. Analysis of the liquid phase from the tetra-alkoxide sample that was heated for 5 hours at

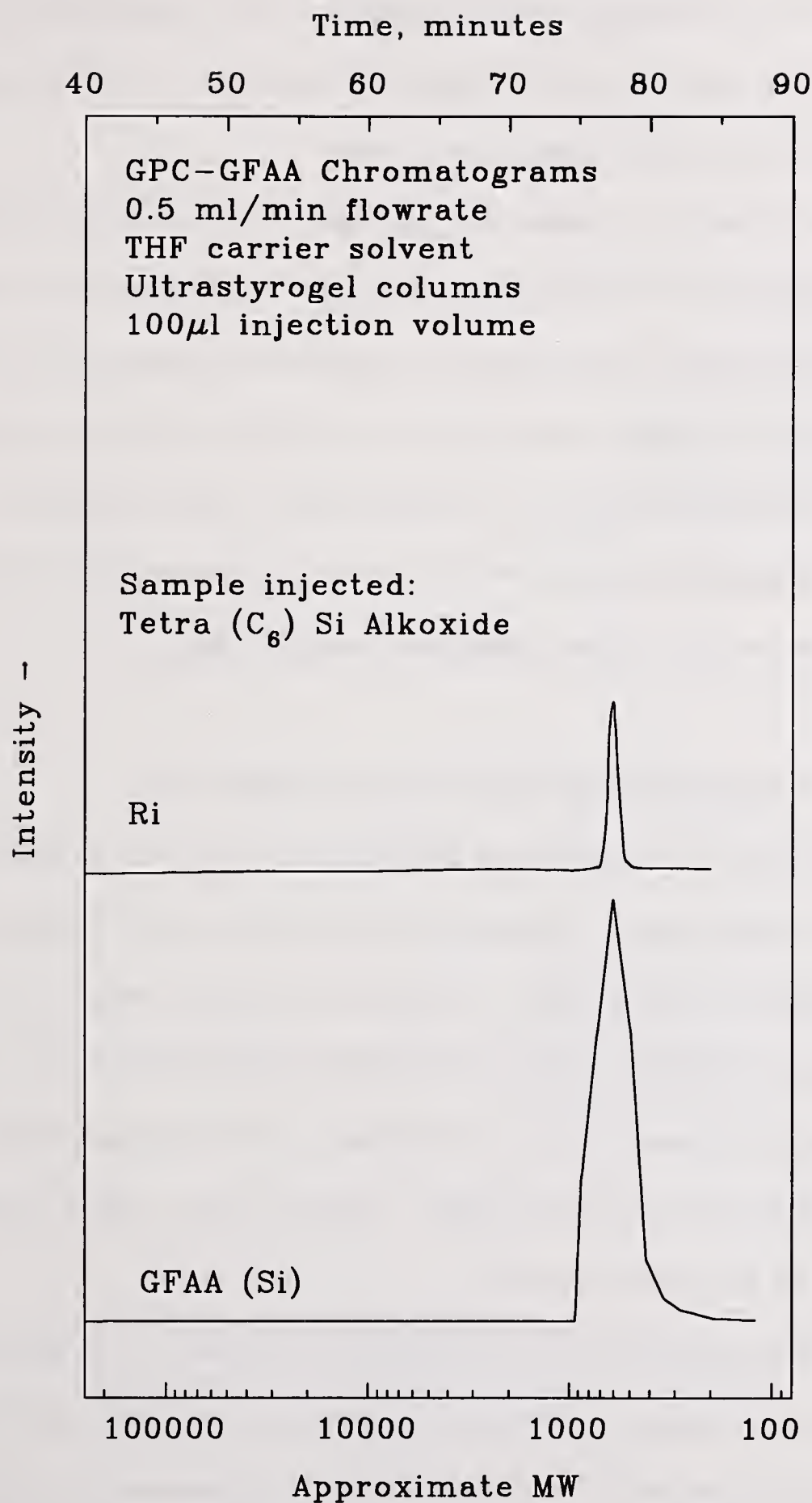


Figure 9.5 GPC-GFAA Analysis of Neat Tetra(C₆) Si Alkoxide

200°C resulted in the chromatogram shown in Figure 9.6. This chromatogram indicates that the HMW silicon-containing reaction products have been formed. The GFAA peak maxima coincides with the HMW bump on the RI trace.

A two-ball collision test conducted using the liquid phase from the heated tetraalkoxide sample (Figure 9.7) failed to give low friction by the end of the test. A similar test conducted using the semi-solid higher molecular weight reaction product gave low friction throughout the test. This suggests that the residue from the BTF test that can give low friction in the two-ball collision test is a very high molecular weight polysiloxane-polyalkoxide. It is suggested however, that other, lower molecular weight compounds, may also lubricate under the higher sliding speeds found in the BTF test.

9.4 Proposed Mechanism for Alcohol and Acid Lubricated Si_3N_4

The combination of performance and analytical data coupled with information available in the literature suggests a sequence of reactions that can be developed into a lubrication mechanism for silicon nitride. The first detail is that the surface of silicon nitride is easily oxidized and hydrolyzed to form silicon oxides and hydroxides. This surface can react with alcohols in the series of "static" and "dynamic" reactions proposed below. Static reactions are inducible purely by thermal means. Dynamic reactions require an element of rubbing in order for the reaction to proceed.

First, alcohol groups adsorb onto and react with the surface of Si_3N_4 to provide a bonded, tenacious surface layer. Evidence of this reaction has been observed using static reactions on Si_3N_4 powders and TGA. Further reactions in the presence of the temperatures

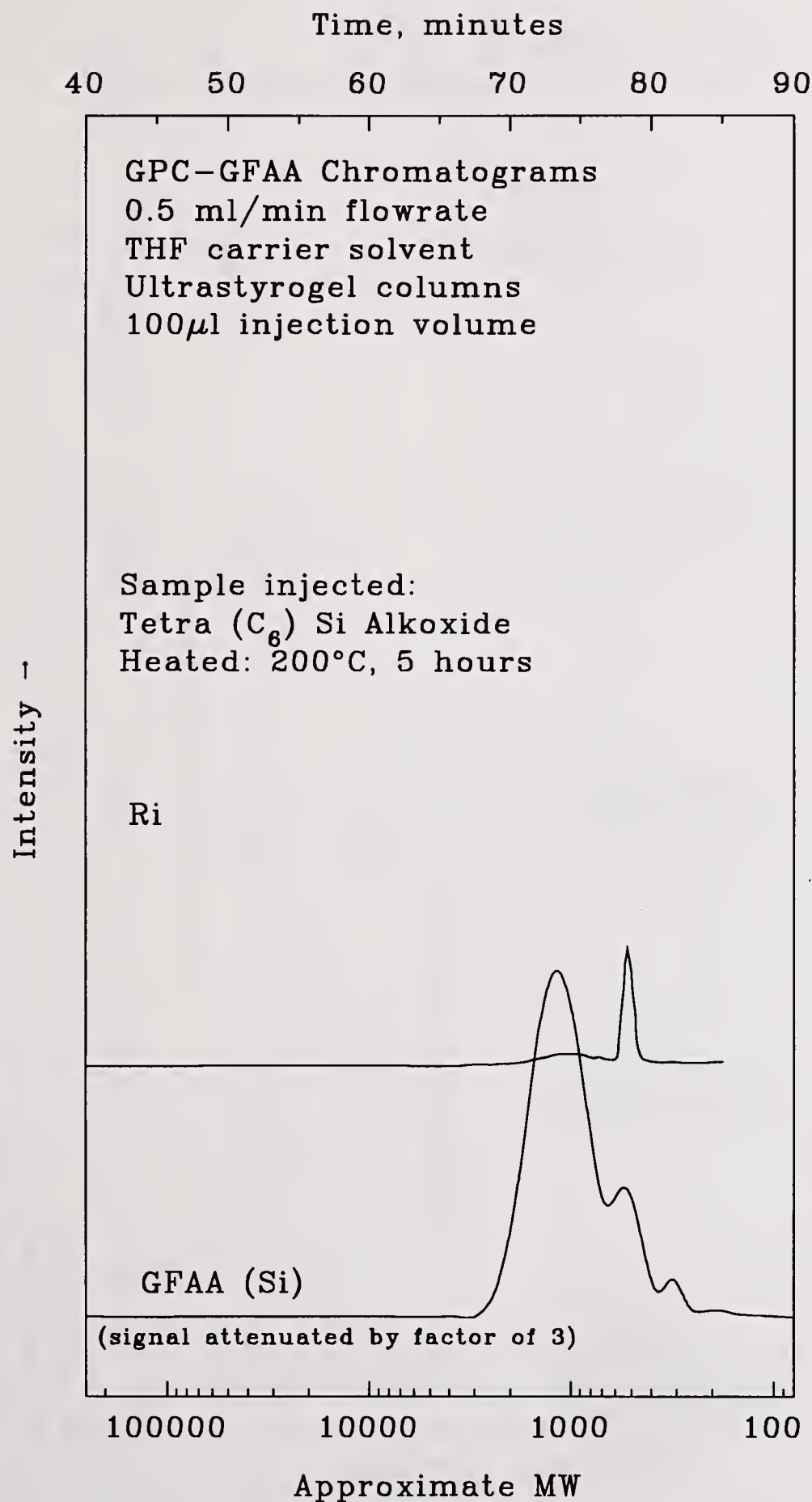


Figure 9.6 GPC-GFAA Analysis of Neat Tetra(C₆) Si Alkoxide Heated at 200°C for 5 Hours

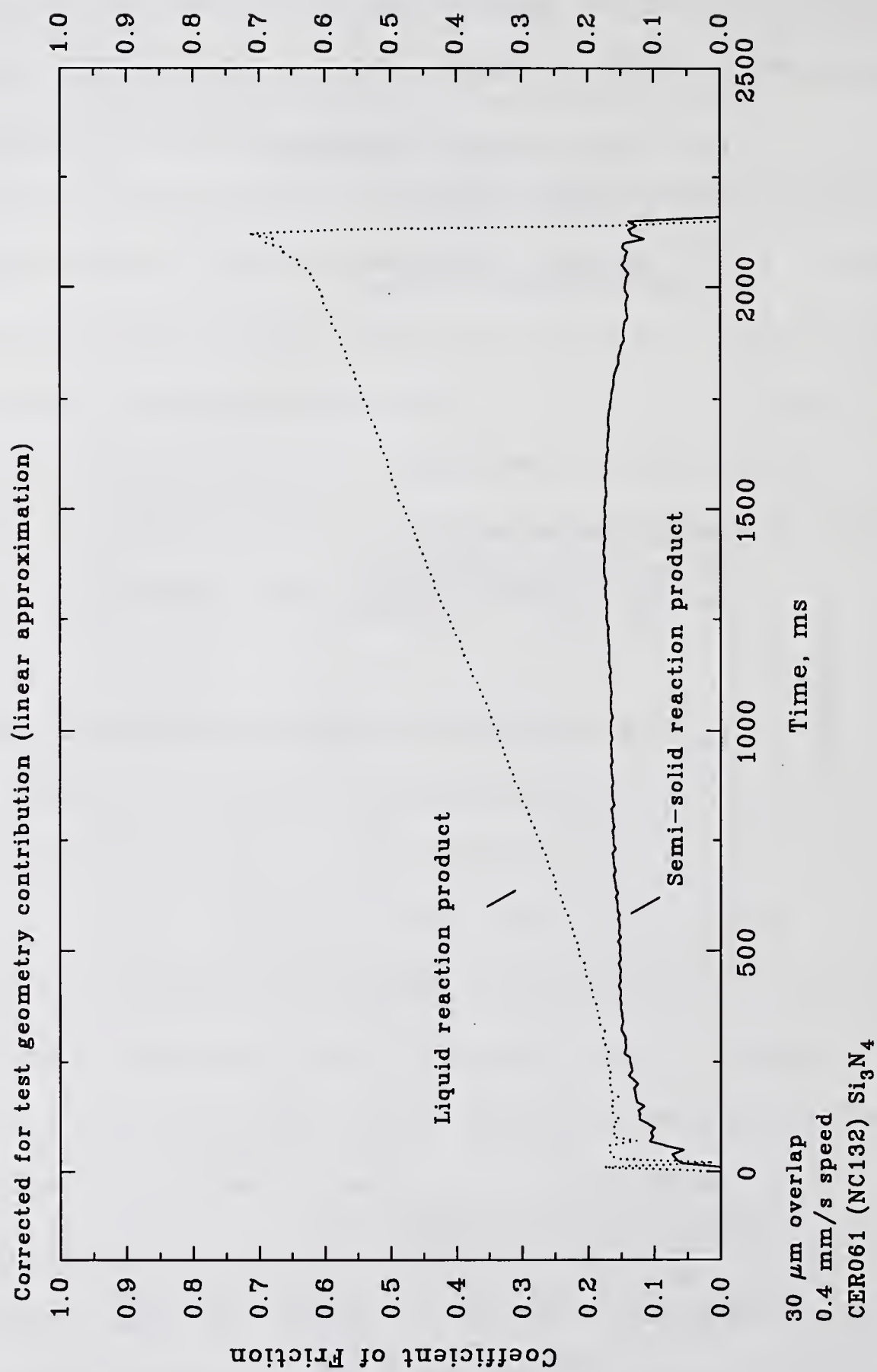
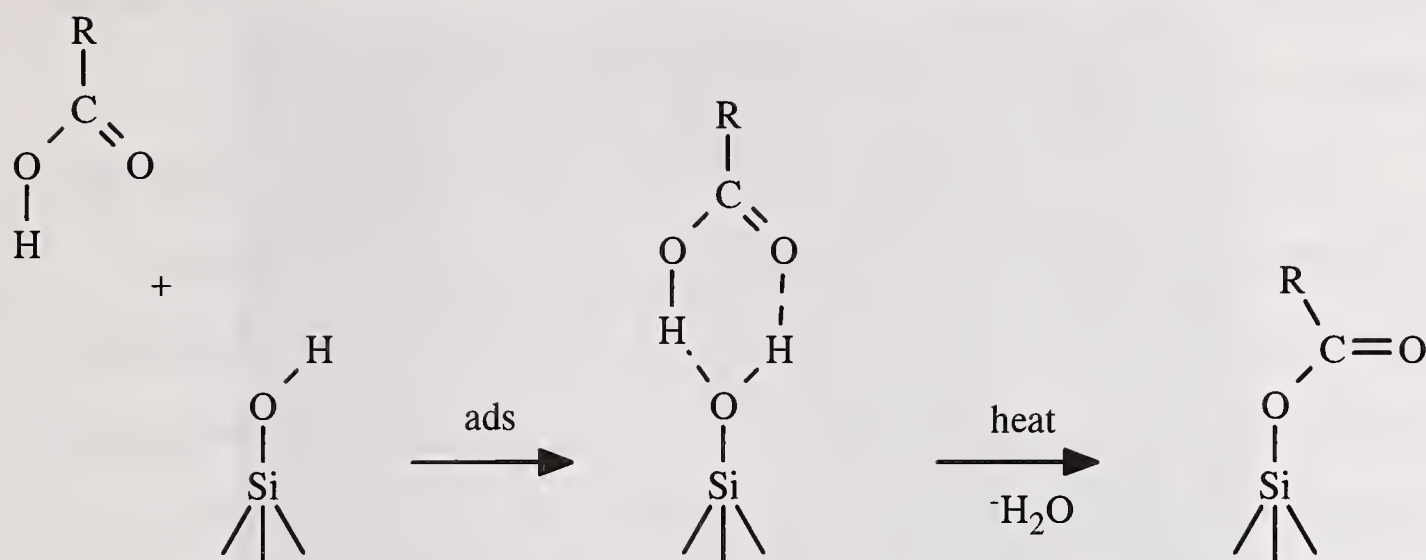


Figure 9.7 Two-Ball Collision Test Results for Heated Neat Tetra(C_6) Si Alkoxide Reaction Product

Reaction	Category	Detection Method
	Surface Alkoxylation [Static Reaction]	TGA
	"Free Alkoxylation" [Dynamic Reaction]	SIMS GPC-GFAA
	"Polymerization" [Static Reaction]	SIMS GPC-GFAA
	"Polymerization" [Static Reaction]	GPC-GFAA
	"Particulate Formation" [Static Reaction] (Ostwald ripening mechanism)	GPC-GFAA

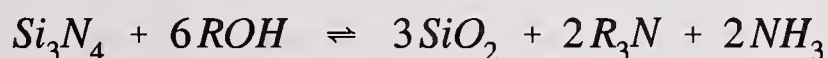
and shear stresses of the contact result in the formation of free (non-surface or "free") silicon alkoxides (detected using SIMS). These alkoxides can react with each other (and the surface) through condensation reactions to form HMW polyalkoxides with siloxane backbones, and thicker surface films. These products were detected in a wear test using SIMS and GPC-GFAA. A static simulation of this reaction was confirmed to produce HMW silicon-containing organic compounds with demonstrated (2-Ball collision test) lubricating ability. It is also possible that this reaction sequence can take place on the surface of small wear particles that may be generated in wear tests. This would produce organic coatings on the particles and reduce possible particle aggregation and growth in the contact. These coated particles may have a gel-thickening or grease-forming type effect within the contact. The formation of high molecular weight silicon-containing organic compounds has two implications with respect to lubrication observed with these compounds. First, reaction and removal of silicon from the surface of Si_3N_4 may take place on the tips of asperities, reducing stress concentrations. The smooth regions observed in the high temperature zones of the wear scar may be indications of this chemical polishing mechanism. Second, the formation of higher molecular weight, higher viscosity, products will result in thicker EHD films in the contact. This is consistent with the low friction coefficients observed in these tests.

Marshall¹⁷³ studied the adsorption of oleic and linoleic acid on silica. He found that when heated, the adsorbed acid reacted with the surface to form a bonded species. The combination of spectroscopic information coupled with the observation of water loss during the reaction prompted them to propose the surface reaction shown below. This is analogous



to the reaction that occurs with alcohols and explains why the acid functional groups also lubricate Si_3N_4 . This reaction was also cited by Hair¹⁰⁷ who indicated that the reaction needed the presence of other ions on the silica surface.

It should be mentioned that the proposed mechanism for alcohol (and acid) lubricated Si_3N_4 has several possible variations that depend on the actual nature of the surface during rubbing. It has been mentioned that dangling bonds may play a role in the reaction sequence. It is also possible that reactions may take place with the (unoxidized) subsurface of Si_3N_4 if the oxide surface layer is removed faster than it can be produced. In this case, direct reaction may be possible as hypothesized by Hattori¹¹¹:



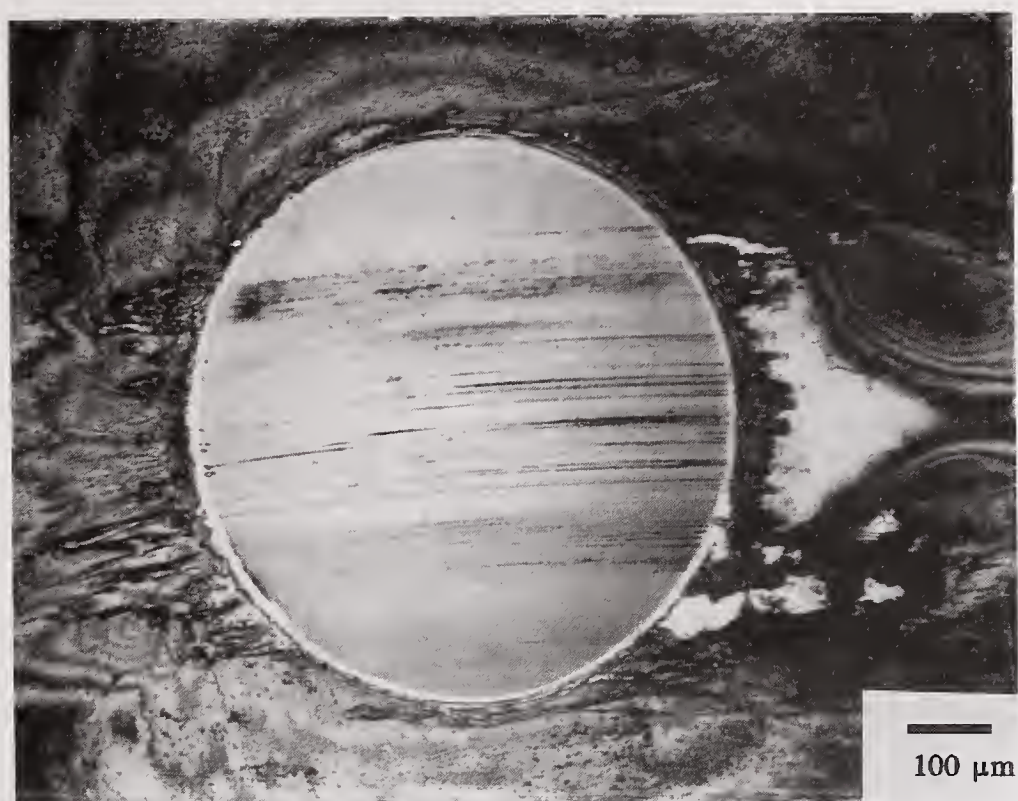
In both Hattori's static case, and (dynamic) grinding experiments by Tsunai^{240*}, "amines and ammonia" were detected by ion chromatography. This reaction does not account for the observation that silicon is associated with the high molecular weight reaction products, but perhaps Si-O-R and $\text{Si}_x\text{-N-R}_{3-x}$ species can be formed from subsequent reactions. Indeed

Tsunai admitted that some nitrogen compounds different from R_3N were detected but their structure was unknown.

It was surprising that no appreciable silicon-containing compounds were detected for PPO lubricated Si_3N_4 , since frictional heating should have produced acid and alcohol oxidation products²⁵ that can react with the Si_3N_4 surface as per the proposed mechanism. The observation of HMW products indicated that some oxidation was indeed taking place, but perhaps not in sufficient quantity. A 6 μ l BTF test was conducted using PPO in an attempt to provide a more oxidatively severe condition and produce more oxidation products. The wear scar diameter at the end of this test was 0.638 mm (0.258 mm greater than the Hertzian contact diameter), with a final coefficient of friction of 0.113. The wear scar (Figure 9.8A) is similar in appearance and size to the 1.5 ml lubricated case. Significant amounts of reaction product were observed surrounding the wear scar. The friction trace (Figure 9.8B) has an unusual dip to lower friction near end of the test. After the test was terminated, it was allowed to cool to room temperature (under load). When the ball pot was lowered, it was discovered that so much sludge-like oxidized products (a grease?) were produced that the flats stuck to the ball. The viscous deposit may explain the dip in friction at the end of the test.

GPC-GFAA analysis of the wear test product (Figure 9.9) confirmed the abundance of HMW reaction product, both with RI and UV detectors. In the case of this 6 μ l test, small amounts of silicon-containing reaction products were indeed detected, with higher amounts at very high molecular weights. Apparently, when sufficient oxidation products are formed, reactions can take place with the Si_3N_4 surface, resulting in detectable amounts of

(a)



(b)

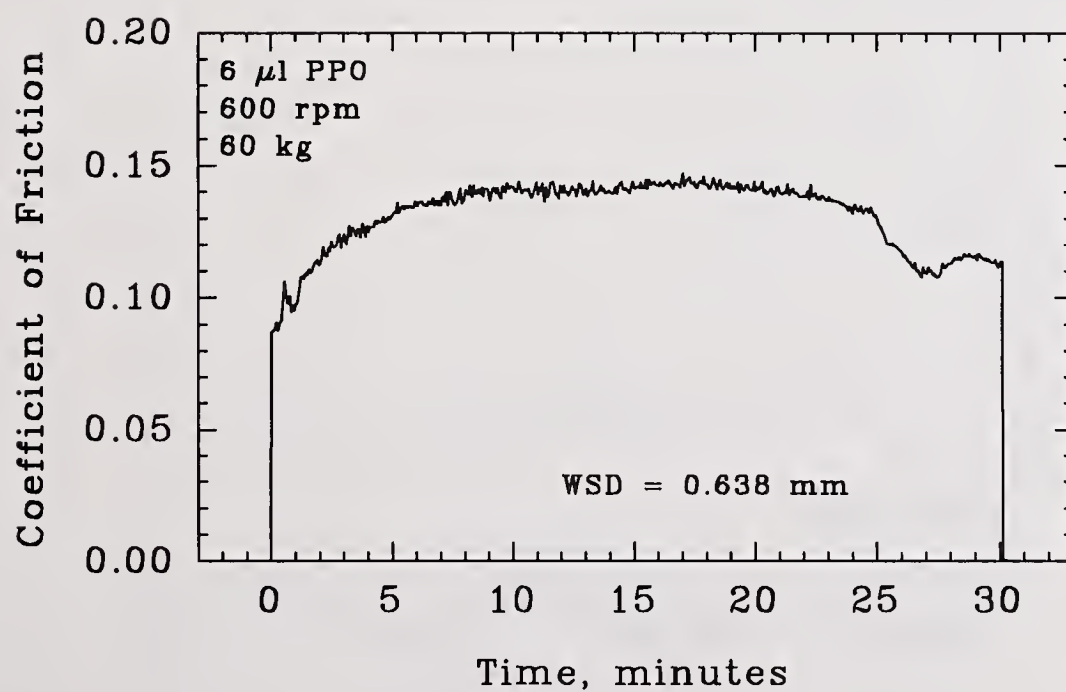


Figure 9.8 Neat 6 μl PPO Lubricated Si_3N_4 BTF Test at 60 kg: a) Optical Photomicrograph, b) Friction Trace

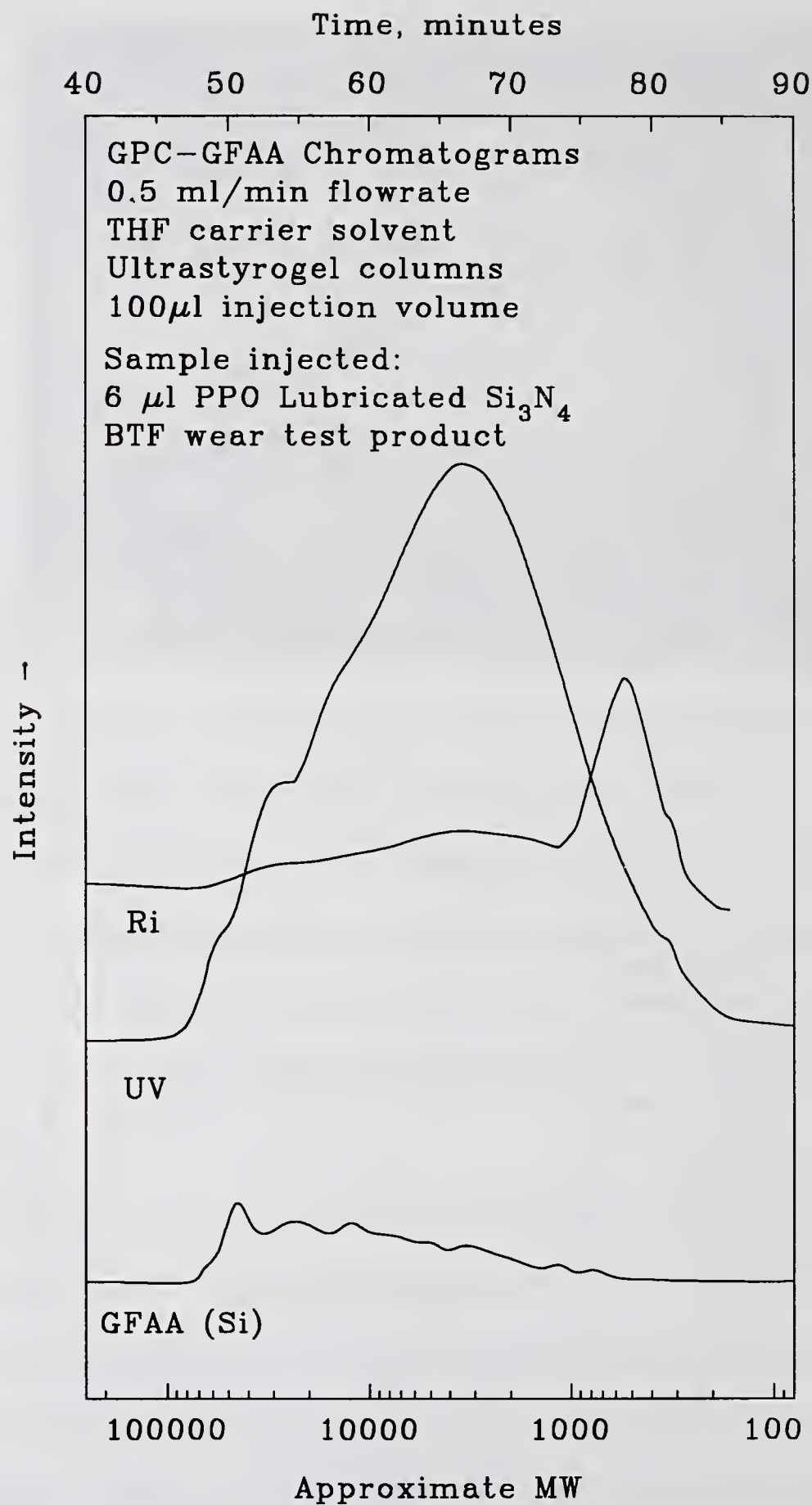


Figure 9.9 GPC-GFAA Analysis of Reaction Product from 6 μ l PPO Lubricated Si_3N_4 BTF Test

silicon-containing organic products. Blaine and Savage²⁵ found that carboxylic acids and alcohols are the most abundant products of oxidation of a paraffin. Since it has been demonstrated that alcohols can lubricate Si_3N_4 by reacting with the surface to form silicon-containing organic products, it is reasonable to suggest that the in-situ formation of alcohols (and acids) in the wearing Si_3N_4 may contribute to the boundary lubricating ability of paraffin oil at low loads. This implies that it may be possible to modify the reactivity of paraffin oil and improve the boundary lubricating ability of paraffin oil to higher loads. Indeed, addition of 1000 ppm soluble iron naphthenate to PPO decreases the wear scar diameter from 0.645 mm down to 0.583 mm. This agrees with Chen's⁵⁵ observation of better lubrication of Si_3N_4 in the presence of metal salts which he attributed to higher production of friction polymer caused by the catalytic effect of the metal. In light of the results of this study, it is suggested that there may also be a contribution from increased in-situ formation of alcohols and acids.

Chapter 10

SURVEY OF PHOSPHORUS CHEMISTRIES

The phosphorous-containing compounds used were all commercially available with long chain alkyl or aryl groups attached to make them soluble in oils. Three of the phosphates were dialkyldithiophosphates (DP) and contained sulfur as well as metals (Zn and Sb). Some of the other compounds also contained other heteroatoms such as chlorine, nitrogen, or boron.

10.1. 1% Phosphorus Compounds in PPO

The data from all of the 1% phosphorus compounds in PPO are summarized in Table 10.1 and presented graphically in Figure 10.1. The first striking aspect of the data is that all of the phosphorous-containing model compounds very effectively reduced both wear and friction. It did not seem to matter whether they were phosphates, thiophosphates, phosphites, or phosphonates. The best performer produced a wear scar of only 0.024 mm above the Hertz diameter, which is a tremendous drop from the 0.267 mm for the paraffin oil itself. The other striking aspects of the data are that all of the phosphates had type II friction traces, and produced some form of film in the wear scar. In most cases, the film was easily visible optically, but a few could only be observed using SEM.

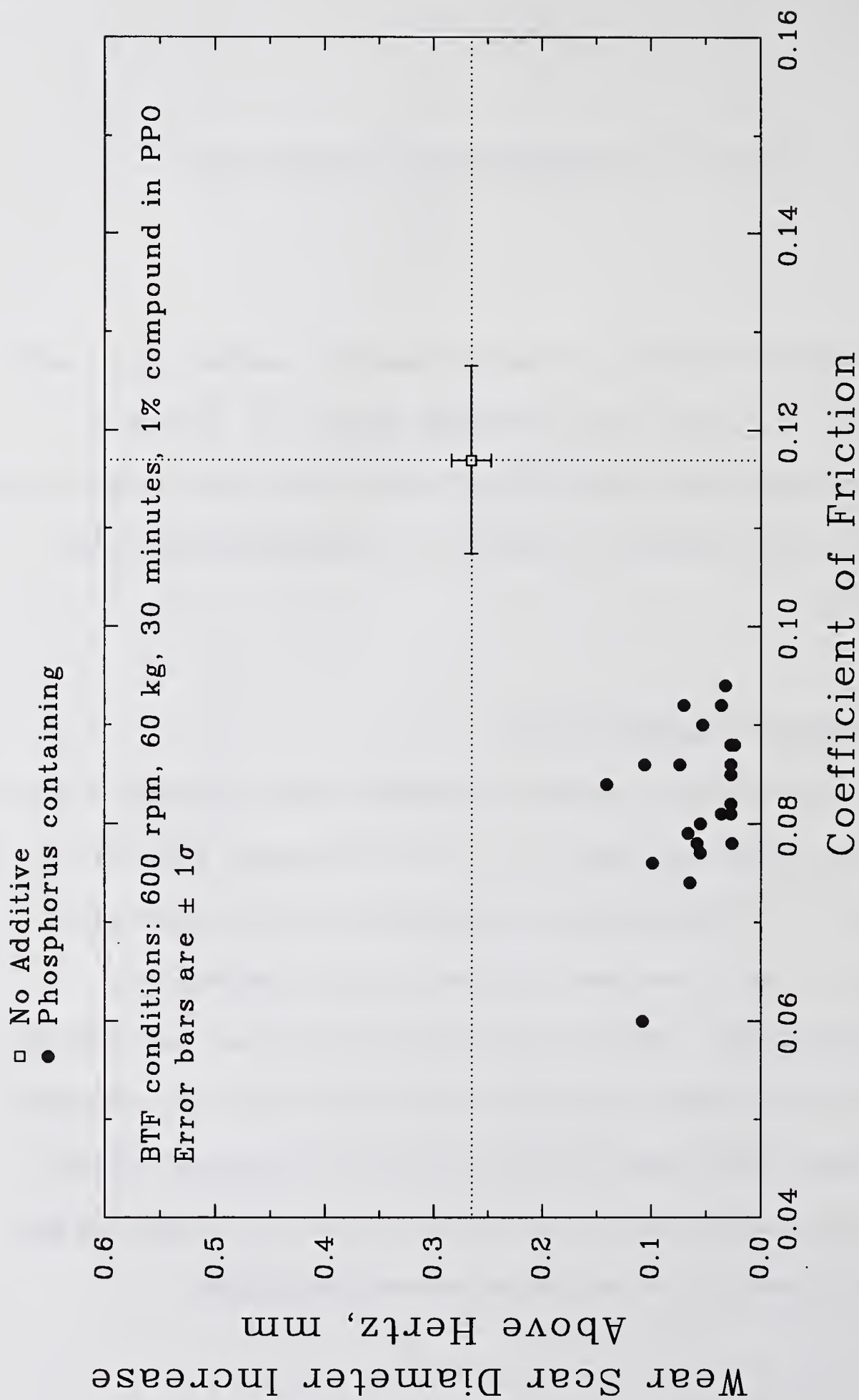


Figure 10.1 Summary Friction and Wear Data for Si_3N_4 BTF Tests on 1% Phosphorus-Containing Compounds in PPO

Table 10.1
Friction and Wear Data on Selected Phosphorus-Containing Model Compounds

Chemical Compound ¹	WSD (mm)	Dia increase above Hz, mm	COF ²	Frict. Type	Wear Scar Appearance	Film in Scar ?
NONE (average of 16 tests)	0.645	0.265	0.117	I	smooth	no
Isodecyl ZDP (#1)	0.404	0.024	0.088	II	smooth	yes - fluid
Tris (2-ethylhexyl) Phosphate [038]	0.406	0.026	0.078	II	smooth	no (optical)
2-Ethylhexyl ZDP (#1)	0.407	0.027	0.081	II	smooth	yes - fluid
2-Ethylhexyl ZDP (#2) [028]	0.407	0.027	0.088	II	smooth	yes - fluid
Butylated Triphenylphosphate	0.407	0.027	0.086	II	smooth	no (optical)
Diocetylphenyl Phosphonate	0.407	0.027	0.085	II	smooth	yes - plastic
Zinc Diaryldithiophosphate (#1) [038]	0.407	0.027	0.082	II	smooth	yes - fluid
Triphenyl Phosphorothionate [038]	0.407	0.027	0.081	II	smooth	yes - spotty
Isodecyl ZDP (#2) [028]	0.412	0.032	0.094	II	smooth	yes-fluid
Zinc Diaryldithiophosphate (#2) [028]	0.416	0.036	0.092	II	smooth	yes - fluid
Tricresyl Phosphate	0.416	0.036	0.081	II	smooth	yes - plastic
Triphenyl Phosphate	0.433	0.053	0.090	II	smooth	yes - plastic
SbDP	0.435	0.055	0.077	II	blotchy	yes - plastic
Tributyl Phosphate	0.435	0.055	0.080	II	smooth	yes - plastic
Trimethylsilylpolylphosphate	0.438	0.058	0.078	II	smooth	yes - plastic
Triphenyl Phosphite	0.444	0.064	0.074	II	smooth	no (optical)
Diphenylchlorophosphate [038]	0.446	0.066	0.079	II	smooth	yes - plastic
Triethyl Phosphate	0.450	0.070	0.092	II	smooth	yes - spotty
Tri-n-butyl Phosphite	0.454	0.074	0.086	II	smooth	yes - plastic
Acid Phosphate	0.479	0.099	0.076	II	roughened	yes - plastic
P,B,N containing Polymeric Additive	0.486	0.106	0.086	II	smooth	yes - spotty
Oxymolybdenum DP (sulfurized)	0.488	0.108	0.060	II	smooth	yes - plastic
Aromatic Amine-Phosphate	0.521	0.141	0.084	II	blotchy	yes - plastic

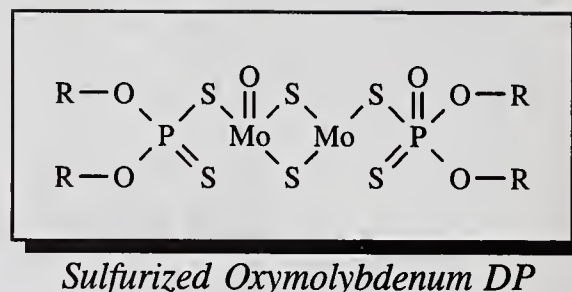
antiwear

¹ 1 wt % in purified paraffin oil

² Measured at the end of the test

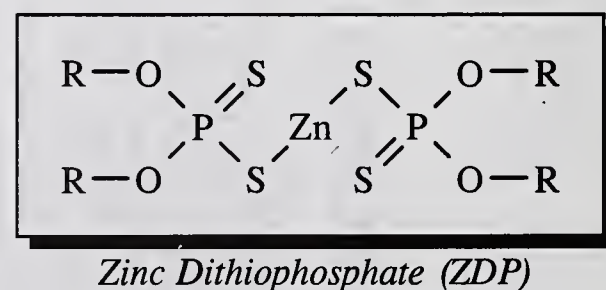
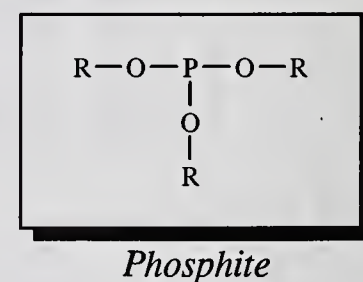
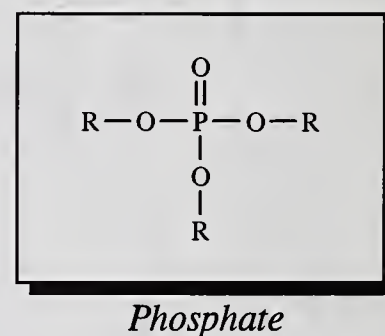
All Tests conducted on CER024 NC132 Hot pressed Si₃N₄ (unless otherwise noted) at 600 rpm, 60 kg, 30 minutes, 1% additive in PPO, 21°C.

The first data point that catches ones eye in Figure 10.1 is the very low friction case for sulfurized oxymolybdenum dithiophosphate (Figure 10.2). This compound contains both Mo and S and appears to have the same characteristic low friction of



the other Mo-S compounds discussed later in the sulfur chemistry chapter. The Mo-S dithiophosphate compound seems to have acquired the best attributes of both types of chemistries: the low friction of the Mo-S chemistry and the low wear of the P chemistry.

The phosphates which contained zinc produced optically visible, thick, fluid-like films within the wear scar. A typical wear scar and friction trace for these compounds is shown in Figure 10.3. The friction trace is smooth and level throughout the test, with a coefficient of friction near 0.08. The wear scar is small and circular, with a fluid-like film covering most of the contact region. SEM analysis of the wear scar surface revealed that the film actually covered the entire wear scar and the optically visible film was thicker regions of film. The thick-film region within the wear scar (Figure 10.4A) had a pock-marked appearance reminiscent of swiss cheese. It is apparent that some kind of gas-entrainment has occurred within the film, possibly a by-product gas



from decomposition of the ZDP (a sulfur smell is often noted during wear tests of ZDP on

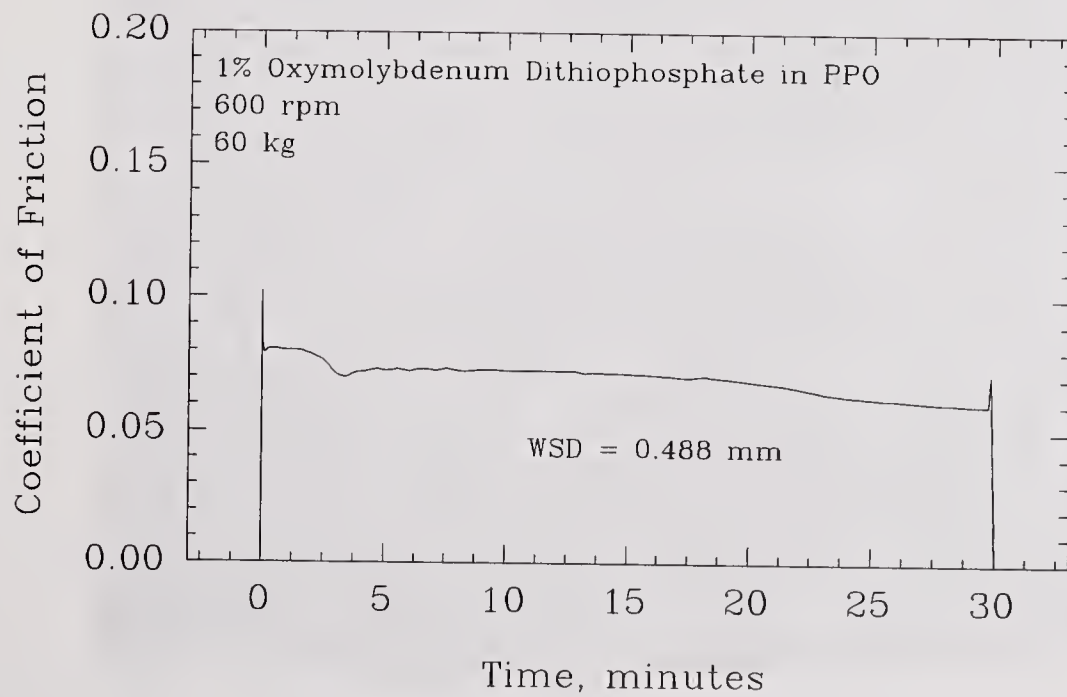
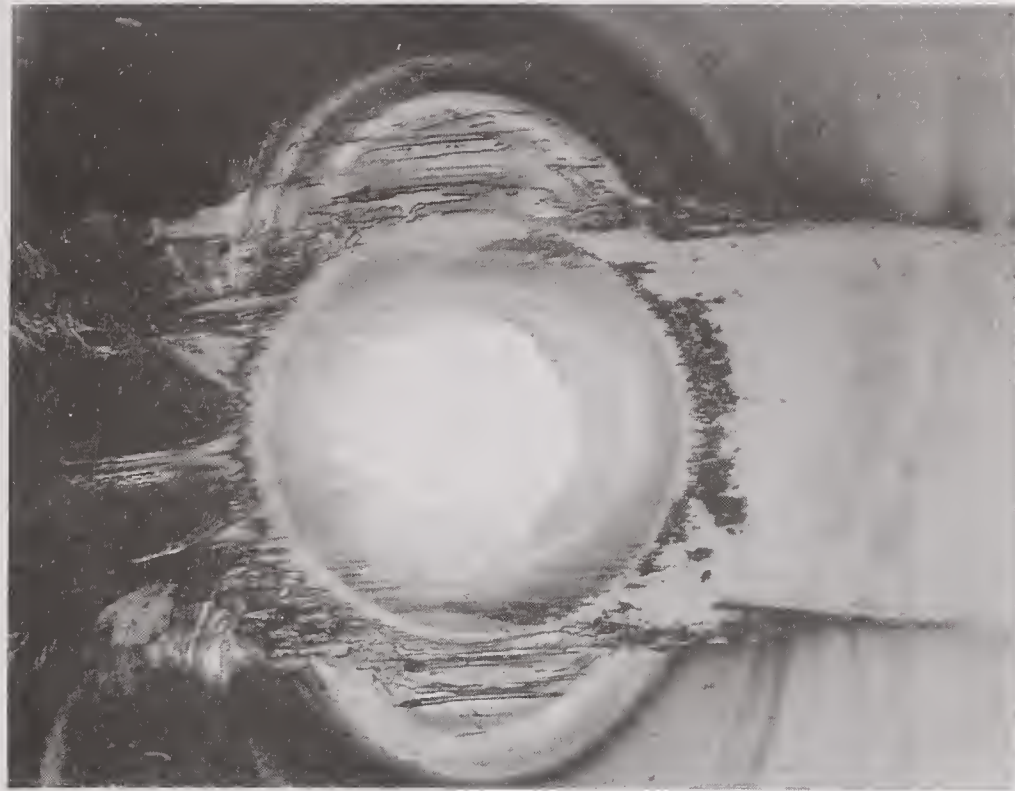


Figure 10.2 1% Oxymolybdenum Dithiophosphate in PPO Lubricated Si_3N_4 BTF Test at 60 kg: a) Optical Photomicrograph, b) Friction Trace

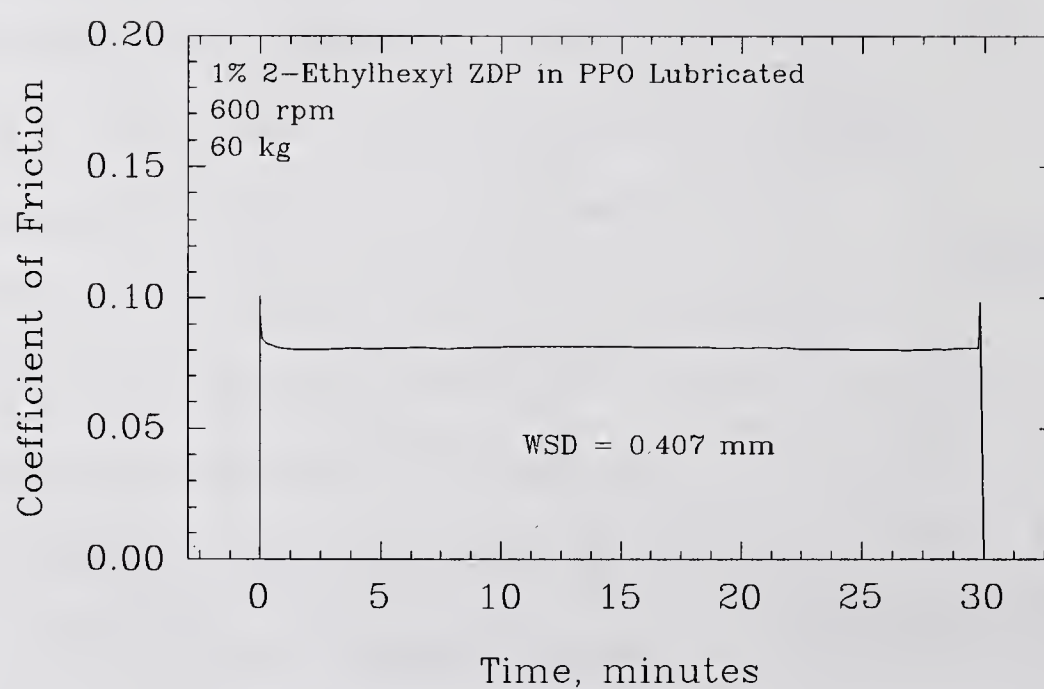


Figure 10.3 1% 2-Ethylhexyl ZDP in PPO Lubricated Si_3N_4 BTf Test at 60 kg: a) Optical Photomicrograph, b) Friction Trace

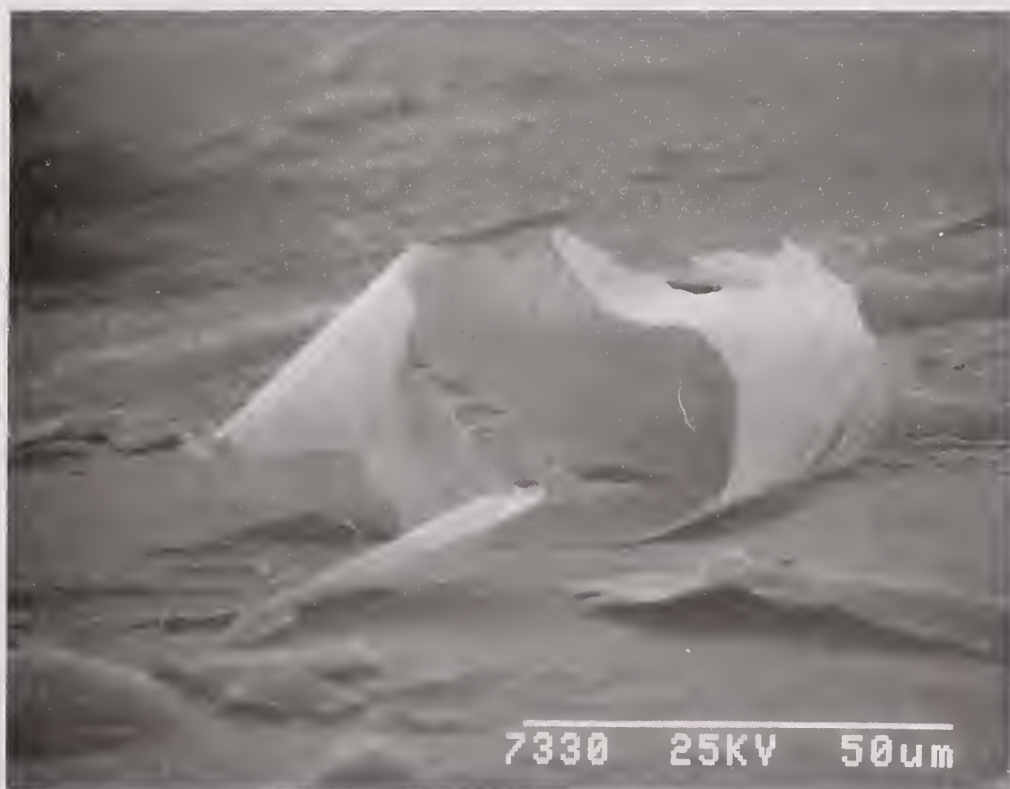
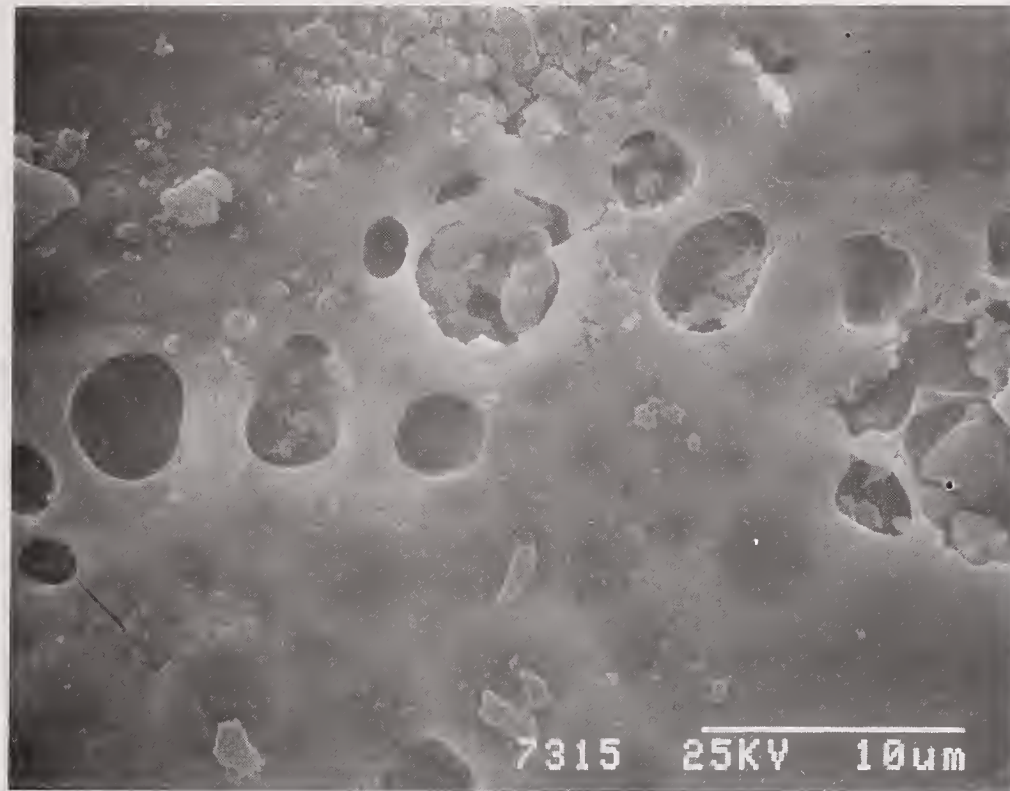
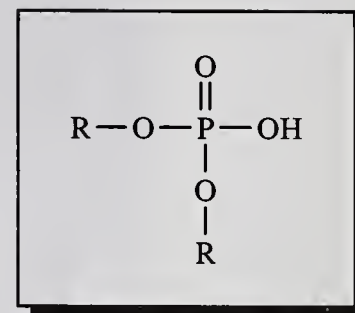
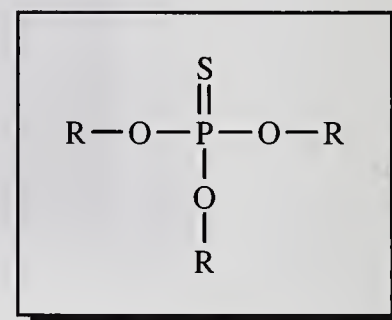
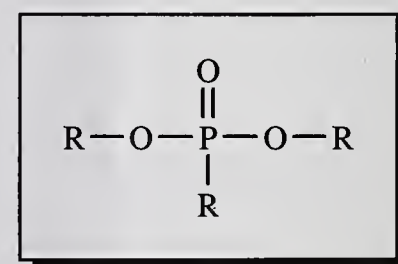


Figure 10.4 SEM Photomicrographs of Reaction Product Film from 1% 2-Ethylhexyl ZDP in PPO Lubricated Si_3N_4 BTF Test at 60 kg: a) Film inside Wear Scar, b) Flake Outside Entrance

Si₃N₄). The lower half of the picture shows several subsurface bubbles in which one can see through the film to the bubble underneath. This reveals that the film is very homogeneous in nature. Higher magnification failed to reveal any distinguishable wear debris in the film.. The nature of this fluid-like film is further evident by the flake observed in the entrance region (Figure 10.4B). The film is so pliant that it can wrap over on itself. Closer inspection of this flake revealed that it was only 0.1 μm thick. EDX analysis revealed the presence of Si, P, and Zn, with small amounts of sulfur and carbon. A soft film such as this would be a protective barrier for the harder, more brittle silicon nitride surface and suggests that a possible mechanism of wear reduction in this system is through the interposition of a friction reducing, stress reducing, soft film.

*Acid Phosphate**Phosphorothionate*

The other phosphorus compounds produced films with a different, more plastic nature. These films were often not clearly visible under an optical microscope, and required a scanning electron microscope (SEM) in order to be seen. In addition, significant amounts of the film were observed outside the wear

*Phosphonate*

scar for many of these cases. A BTF wear test on Si₃N₄ using 1% tricresylphosphate (TCP) produces a very small wear scar of only 0.42 mm. The film within the wear scar is fairly indistinct, with some grooving apparent optically (Figure 10.5A). The friction trace is very smooth and flat (Figure 10.5B). A large amount of reaction product/debris is visible

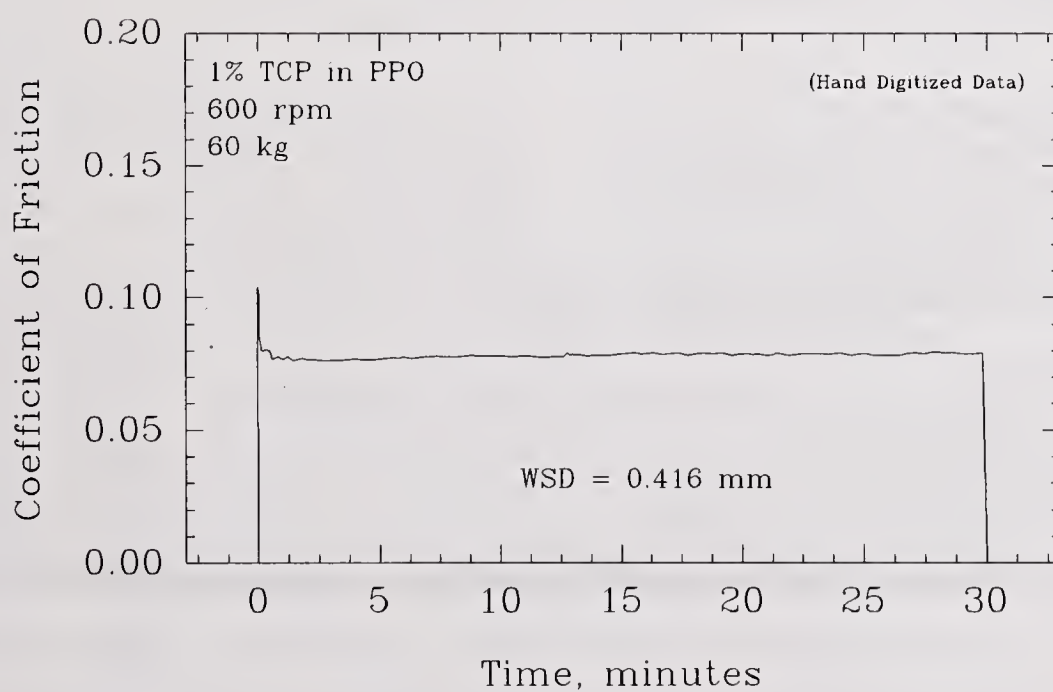


Figure 10.5 1% TCP in PPO Lubricated Si_3N_4 BTFT Test at 60 kg: a) Optical Photomicrograph, b) Friction Trace

surrounding the wear scar, and is concentrated mainly at the entrance - perhaps evidence that it is scraped from the rotating ball during the test. The acid phosphate wear scar surface appeared to be rougher than the other surfaces and may reflect more of a corrosive action from this compound. This would be consistent in a model in which the acid phosphate was responsible for the antiwear action as has been hypothesized for iron systems¹⁵⁵.

BTF tests conducted at 200°C (Table 10.2) indicate that some compounds still work while others do not. The metal-containing phosphorus compounds continued to work. The non metal-containing compounds did not.

Table 10.2
Summary of 200°C BTF Data on 1% Phosphorus-Containing Compounds in PPO

<u>Chemical Compound</u> ¹	WSD		
	WSD (mm)	Incr ² (mm)	COF ³ —
None [024]	0.916	0.536	0.130
None [038]	0.839	0.459	0.119
None [038]	0.772	0.392	0.125
2-Ethylhexyl ZDP [024]	0.421	0.041	0.075
Oxymolybdenum DP (sulfurized) [038]	0.441	0.061	0.044
Triphenyl Phosphorothionate [028]	0.831	0.451	0.144
Tricresyl Phosphate [024]	0.928	0.548	0.151
Butylated Triphenyl Phosphate [024]	0.969	0.589	0.156

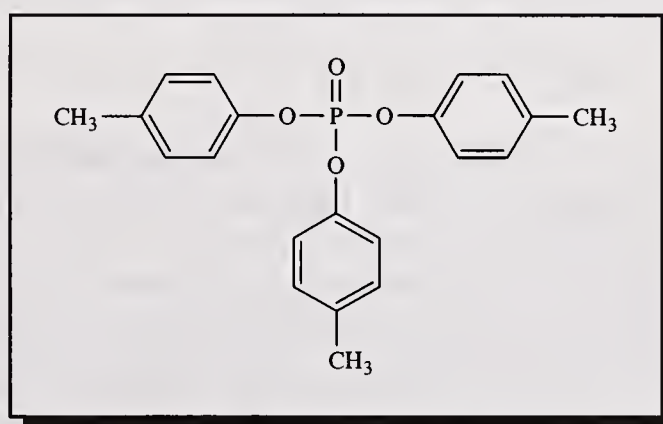
1 1 wt % in PPO
2 Wear Scar Diameter Increase above the Hertzian contact diameter (0.38 mm)
3 Measured at the end of the test

Numbers in [] refer to Si₃N₄ batch used for flats

A series of small studies were conducted on selected phosphorus containing compounds to try to unravel the mystery of how they work. The reasoning behind these studies are outlined below and the results are described in the following sections.

A series of pure compound tests were conducted to see the effectiveness and chemistry of the compound could be sustained at higher concentrations, or without PPO. SEM observation coupled with EDX analysis of the surfaces and films helped provide insight into the role of phosphorus in the lubrication of silicon nitride.

In order to study phosphate chemistry more closely, TCP was selected as a representative of a non metal containing phosphate for more detailed reaction product analysis. Metals were intentionally excluded because they are known to react with TCP and it was desirable to know if TCP had any intrinsic reactivity with Si_3N_4 itself. TCP also had the advantage of having aromatic rings which would absorb UV light and allow detection of low concentrations. Surface analysis was performed on wear test samples run using 1% TCP in PPO.



Tricresylphosphate

A load capacity plot of 1% TCP in PPO established the load limit for

Si_3N_4 lubrication of this compound in the BTF test. A series of tests were conducted using various concentrations of TCP in PPO to see the limits of effectiveness of this compound. The finding that very low concentrations of TCP were effective suggested that adsorption was an important consideration in the lubrication mechanism of this compound. A series of

adsorption experiments were then designed and performed to see if this phenomenon could be observed for these materials. Finally, a series of experiments were performed to see if the antiwear effects we were observing were due merely to the presence of Fe impurities in the Si_3N_4 , since phosphates are known to work with iron based materials, possibly through the formation of iron phosphates. Finally a reaction was conducted to study the reaction between the surface of Si_3N_4 and phosphates.

10.2. Pure Compound BTF Tests

Several phosphorus containing compounds were tested neat in order to see if they were capable of lubricating Si_3N_4 in the absence of PPO. The results, summarized in Table 10.3, indicate that some of the compounds do not work without PPO.

Table 10.3
Summary of Pure Phosphorus-Containing Compound BTF Wear Test Data

<u>Compound</u>	<u>WSD</u> <u>(mm)</u>	<u>WSD</u> <u>Incr¹</u> <u>(mm)</u>	<u>Final</u> <u>COF</u>
PPO ²	0.645	0.265	0.117
Zn diaryl DP	0.398	0.018	0.086
2-Ethylhexyl ZDP (100%)	0.426	0.046	0.089
Tris-(2-ethylhexyl) P.	0.697	0.317	0.086
TBP	0.752	0.372	0.095
TCP	1.470	1.090	0.122

1 Wear Scar Diameter Increase above the Hertzian Contact Diameter (0.380 mm)
2 Average of 16 tests

The two metal (Zn) containing phosphates give low wear, and form visible films inside the contact. In the case of the aryl ZDP (Figure 10.6), the film inside the wear scar was somewhat spotty, while the film deposited outside the wear scar was very fluid and continuous. The alkyl ZDP (Figure 10.7) had a more continuous film inside the wear scar, but much less deposit visible outside the scar. The aryl ZDP was a commercial product and contained some diluent mineral oil. The alkyl ZDP (2-ethylhexyl) was a special research sample that contained no diluent oil. The phosphates without metals gave higher wear than PPO. Pure Tributyl phosphate for example (Figure 10.8), gave a very large wear scar with grooves visible inside the scar. The deposit outside the wear scar seemed to contain particulate debris. Pure TCP was such a poor lubricant that there was an initial friction spike at the beginning of the test that exceeded $\mu=0.5$. The wear scar at the end of the test contained many pits suggesting intergranular fracture and grain pullout may have occurred during the test. Perhaps these compounds are too reactive at these concentrations. The other observation of the data is that the longer alkyl chains seem to be more effective. This may be related to a polymerization mechanism for HMW product formation. The TCP only contains CH_3 groups on each aromatic ring of the phosphate R group, and gives the highest wear. The TBP gives intermediate wear, and contains slightly longer butyl groups. The lowest wear (of the non metal containing phosphates) comes from the longest 2-ethylhexyl R groups of this phosphate. Friction follows a similar trend. If the formation of beneficial HMW products is through polymerization of these alkyl groups (and not P-O-P condensation) as postulated by Cho and Klaus^{57a}, then the trend of the results makes sense.

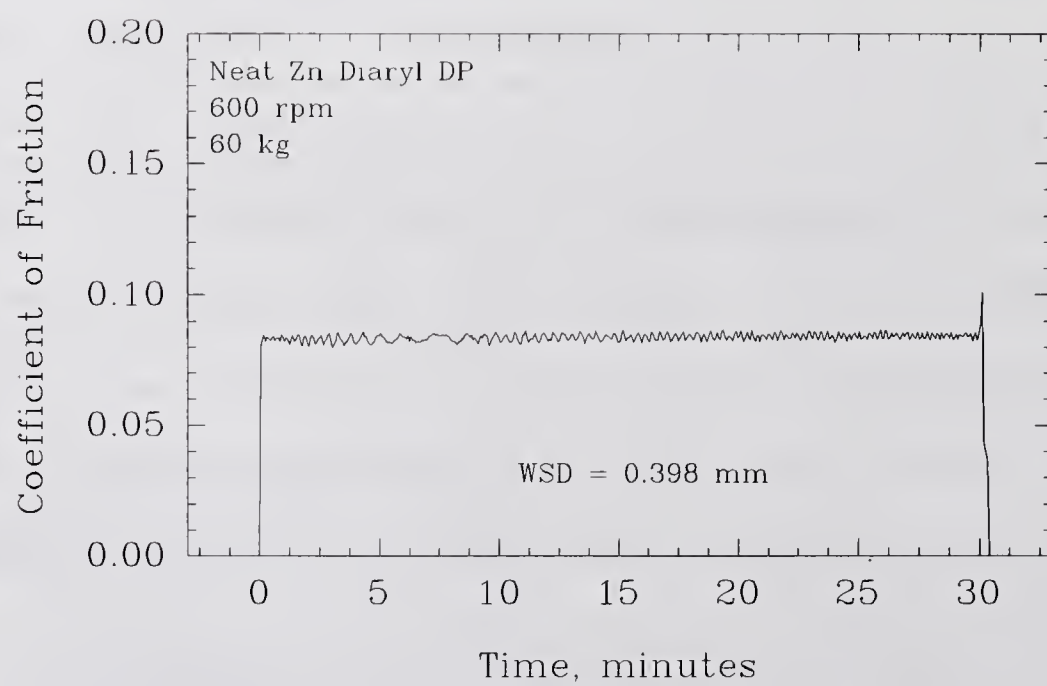
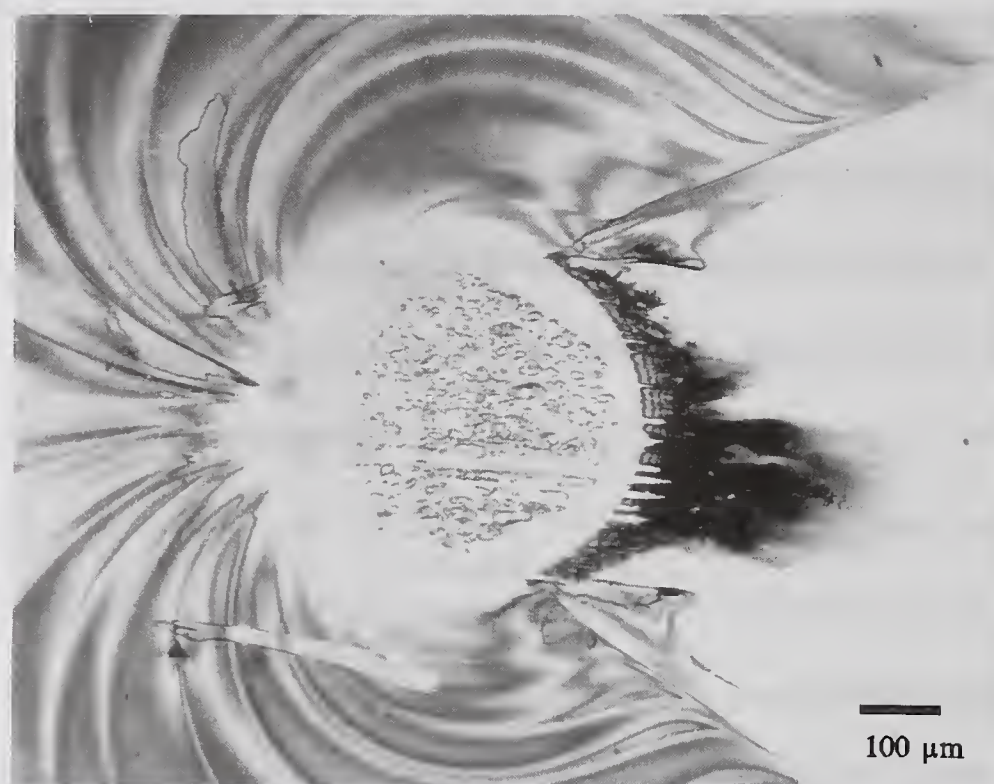


Figure 10.6 Neat Zn Diaryl DP Lubricated Si_3N_4 BTF Test at 60 kg: a) Optical Photomicrograph, b) Friction Trace

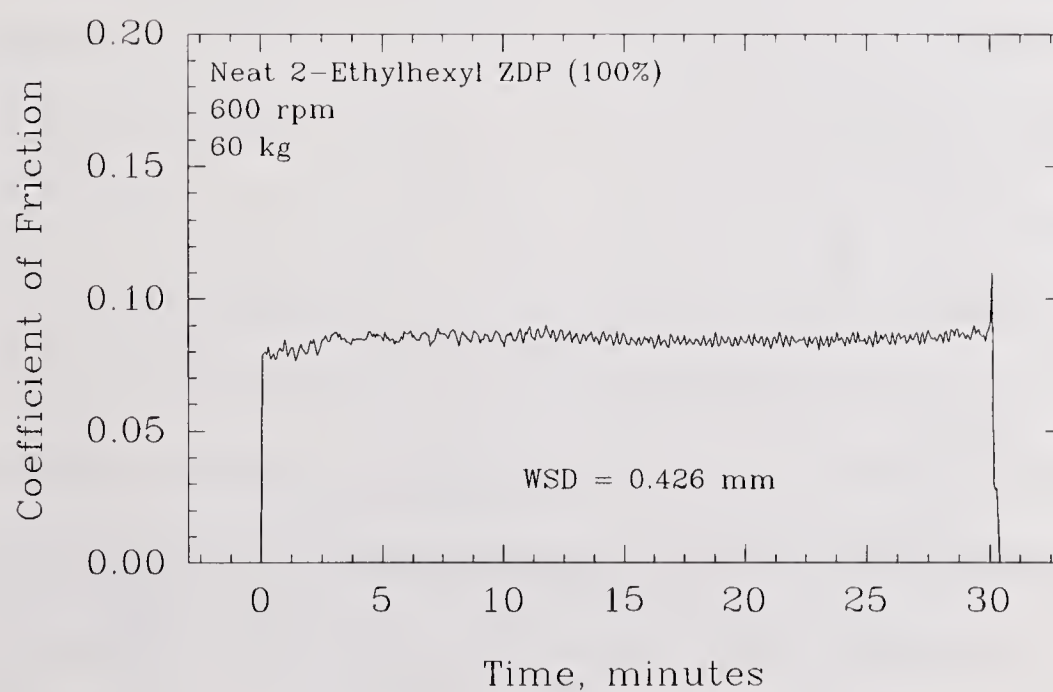


Figure 10.7 Neat 2-Ethylhexyl ZDP Lubricated Si_3N_4 BTFT Test at 60 kg: a) Optical Photomicrograph, b) Friction Trace

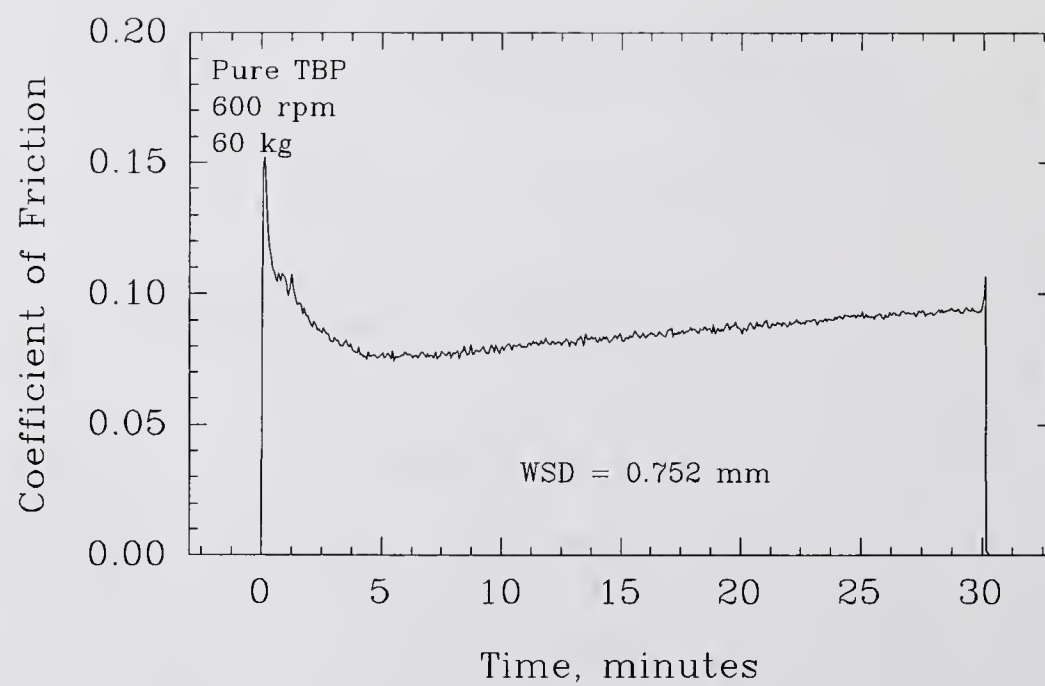
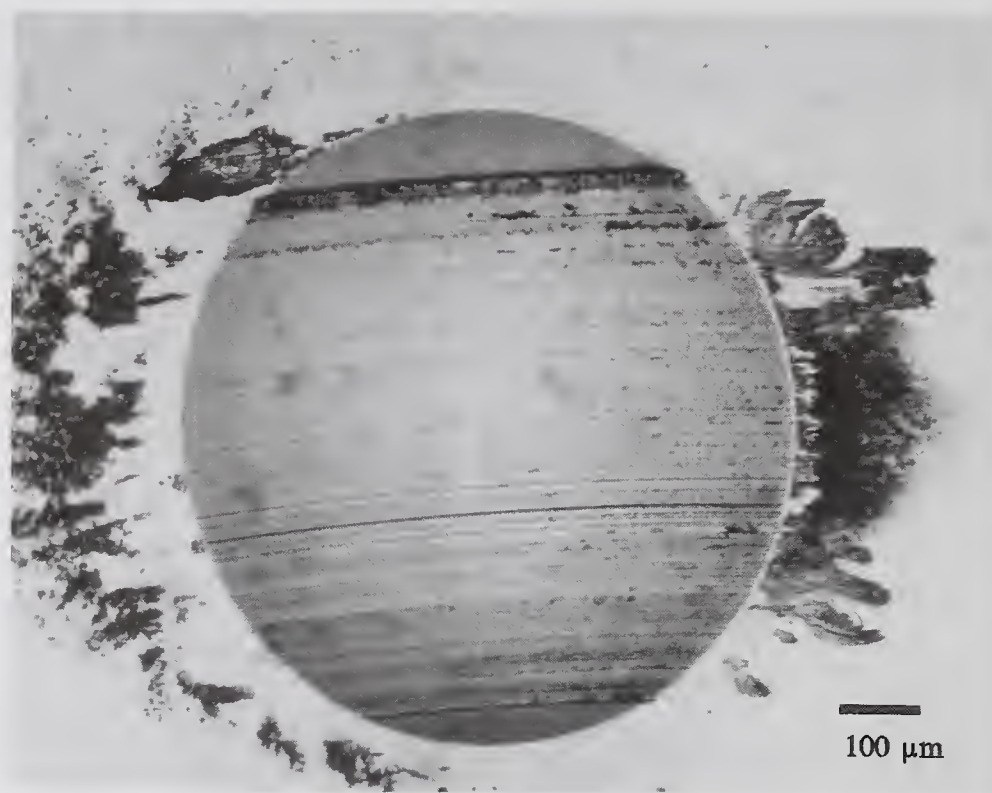


Figure 10.8 Neat TBP Lubricated Si_3N_4 BTFT Test at 60 kg: a) Optical Photomicrograph, b) Friction Trace

10.3. EDX Analysis of Wear Products

EDX analyses were performed on the wear scars of several phosphorus compound lubricated tests in an attempt to isolate the Si_3N_4 lubrication mechanism of these compounds. Both pure compound and 1% compound in PPO wear products were examined.

SEM had indicated that the inside of the wear scar for the Pure TCP lubricated Si_3N_4 had many "flakes" in addition to the pits mentioned earlier. These flakes (Figure 10.9) appeared to be a semi-solid extruded reaction product, pressed out onto the surface of the wear scar. EDX analysis of the flake showed it to be composed mainly of silicon, phosphorus and carbon (Figure 10.10). A stream of hexane was used to rinse the wear scar and physically remove wear product from the contact region. This solution was then filtered using a teflon filter, and the resulting trapped debris analyzed using SEM/EDX. In addition to a large amount of semi-solid reaction product containing silicon, phosphorus, and carbon (similar to the flake seen in the wear scar), several distinct particles were observed. EDX analysis of these particles (Figure 10.11) indicated only small amounts of phosphorus, but higher than normal concentrations of Mg, Al, and Fe. These are impurities in the Si_3N_4 that are expected to concentrate in grain boundaries. Their observation in this instance suggests that we are looking at a particle that has been plucked out of the Si_3N_4 matrix along its grain boundary. This is consistent with the idea that pure TCP is causing high wear through grain pullout and intergranular fracture. It is still not clear whether this is due to a chemically enhanced fracture mechanism, a preferential chemical corrosion of the grain boundary, or merely the inability of the pure TCP reaction product to protect the surface and modify the contact stress distribution.

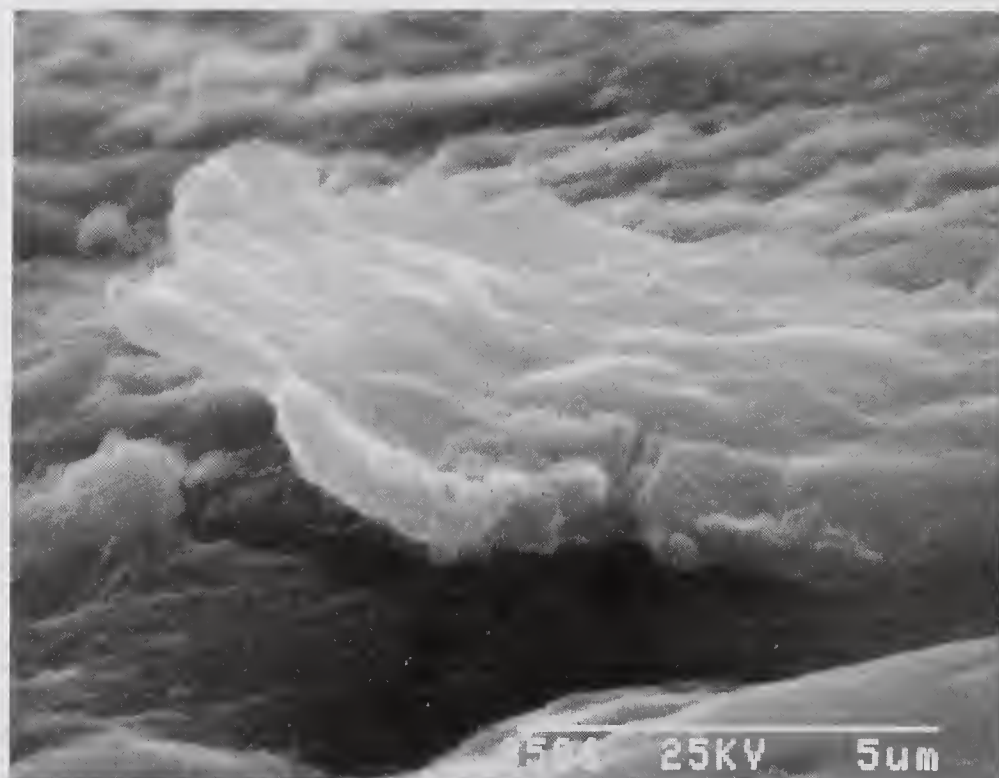


Figure 10.9 SEM Photomicrographs of Regions within Wear Scar for Neat TCP Lubricated Si_3N_4 BTF Test at 60 kg

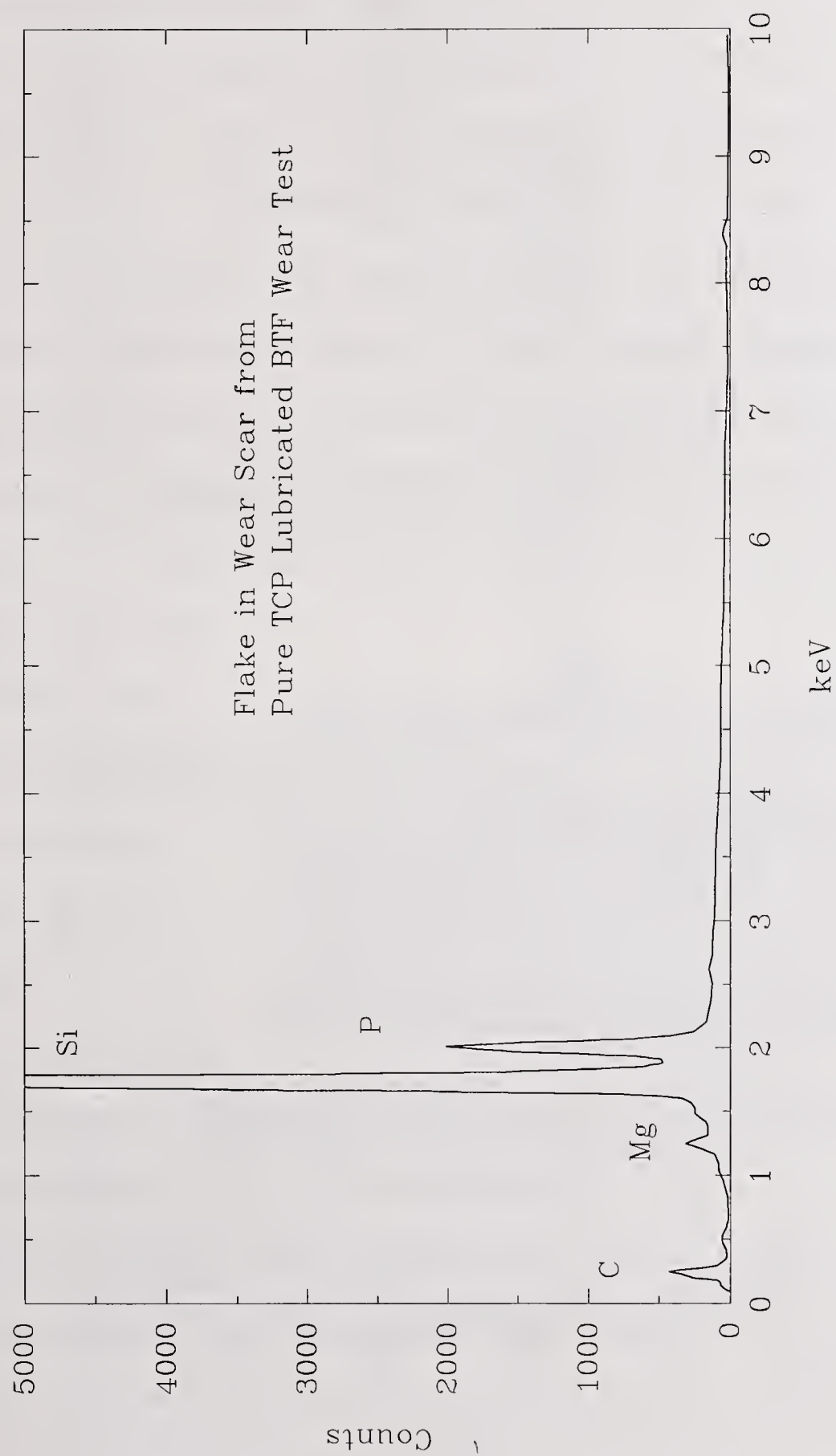


Figure 10.10 EDX Analysis of Flake within Wear Scar for Neat TCP Lubricated Si_3N_4 BTF Test at 60 kg

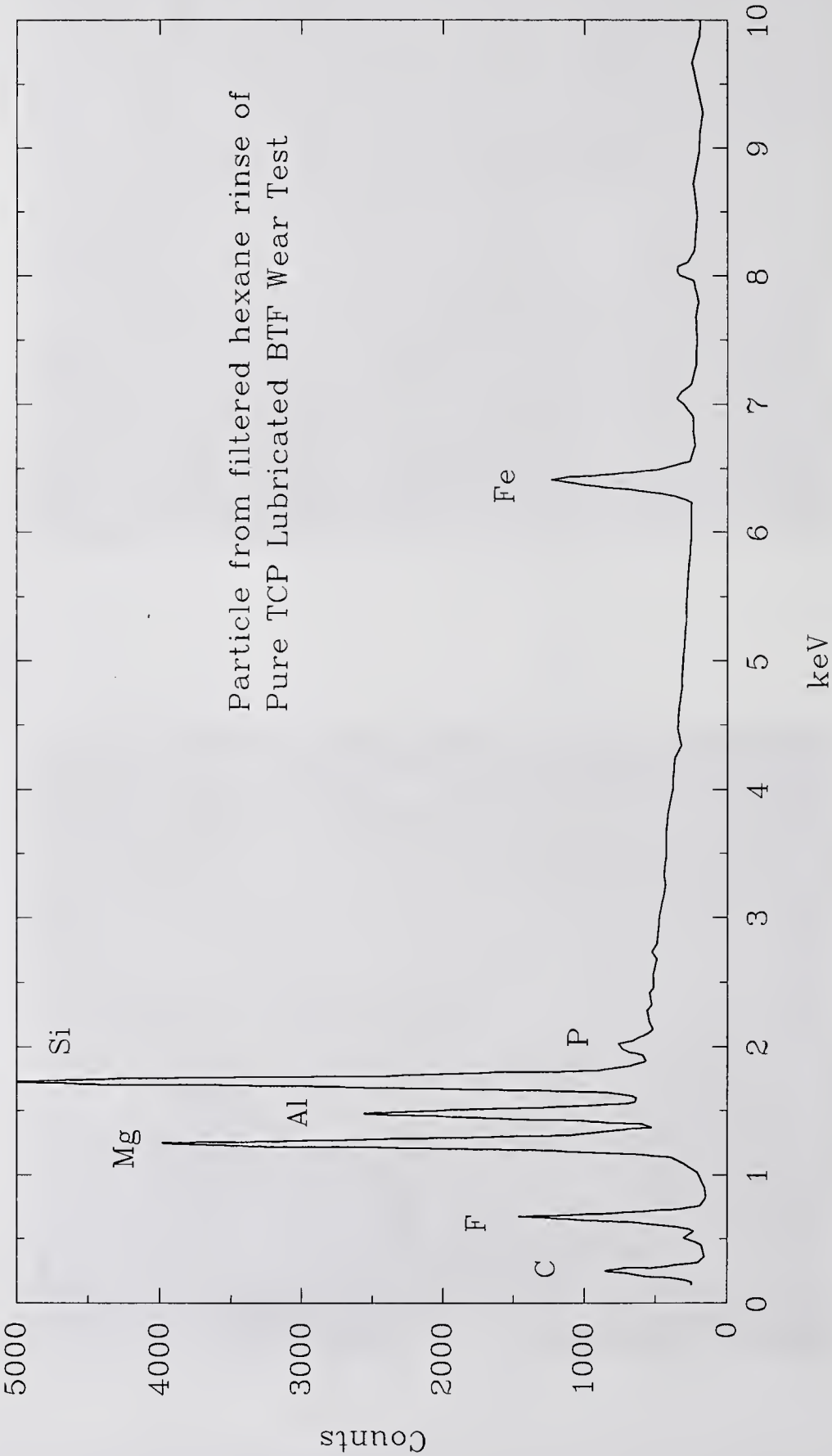


Figure 10.11 EDX Analysis of Wear Particles (on Teflon Filter) from Neat TCP Lubricated Si_3N_4 BTF Test at 60 kg

BTF tests conducted using 1% metal thiophosphates (ZDP etc.) in PPO tended to give very small wear scars and fluid-like films within the wear scar. In addition, deposit regions outside the wear scar were an accumulation of reaction products that were pliant and flake-like. EDX analysis of the exit flake region of a ZDP (isodecyl) wear product (Figure 10.12) indicated the presence of Si, P, and Zn with lesser amounts of sulfur and carbon. It is not surprising that the carbon signal is so low because the sensitivity of the technique to carbon and oxygen (and other light elements $< \text{Na}$) is low. What is surprising is that sulfur is so low. Originally the ZDP contains a ratio of Zn/P/S of 1/2/4 (Table 10.4). The wear product in the Si_3N_4 case is mostly zinc and phosphorus, maintaining the same ratio as in the original compound.. The concentration of sulfur has decreased by two orders of magnitude. The lack of sulfur suggests that

the ZDP has undergone some kind of reaction or decomposition

in which sulfur is eliminated from the contact. Rounds^{212a} conducted similar analyses on steels; however, he still found

Table 10.4
EDX Analysis Data on ZDP Reaction Product Films

<u>Source of Data</u>	<u>Relative Atomic Amounts</u>		
	<u>Zn</u>	<u>P</u>	<u>S</u>
Initial Compound	1	2	4
Rounds (steel)	1	2.1	0.7
Gates (Si_3N_4)	1	2.0	0.06

appreciable amounts of sulfur in the product. This suggests that some of the reactions in the Si_3N_4 case may be different than those of the iron (steel) case.

An SEM photomicrograph of the wear scar from a BTF wear test using 1% TCP in PPO is shown in Figure 10.13A and indicates clearly the shape and extent of the entrance and exit deposits. The same wear scar at 75° tilt in the SEM (Figure 10.13B) indicates that

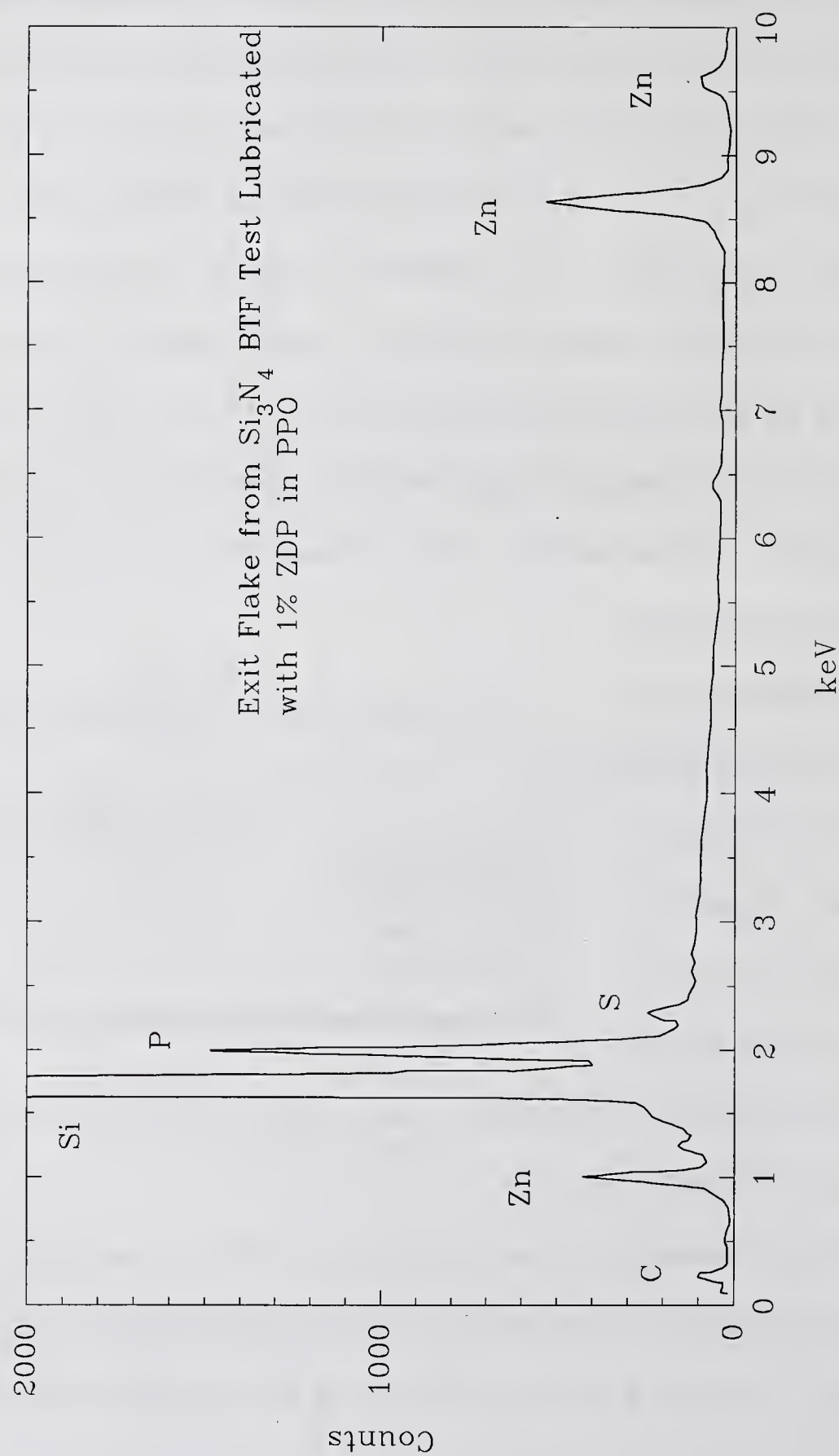


Figure 10.12 EDX Analysis of Flake outside Wear Scar for 1% Isodecyl ZDP in PPO Lubricated Si_3N_4 BTF Test at 60 kg



Figure 10.13 SEM Photomicrographs of Wear Scar from 1% TCP in PPO Lubricated Si_3N_4 BTF Test at 60 kg: a) Zero Tilt Angle, b) 75° Tilt Angle

the deposit is quite thick ($\approx 10\ \mu\text{m}$ in some locations). The nature of this deposit is suggested by SEM photographs (Figure 10.14A) in which the electron beam was focussed onto a small spot on the surface of the deposit. The upper photograph shows a bubble that has grown out of the surface because the electron beam has decomposed the deposit and produced subsurface gasses which inflate the bubble. The second picture, taken later, shows the bubble has popped and is slowly collapsing. A second bubble is forming behind and to the left of the original bubble because the electron spot was moved to this position. These photographs show that the deposit is actually quite pliant. EDX analysis on the entrance deposit (Figure 10.15) showed it to be composed mainly of silicon and phosphorus, with oxygen and carbon also present. It is difficult to be quantitative about the relative amounts of oxygen and carbon because the detector is not as sensitive to these elements as it is to others (Na and above). Also, some carbon is from the carbon coating that had to be applied make the sample electrically conductive. Based on experience with EDX, it was concluded that the sample does contain significant amounts of carbon and oxygen. Silicon and phosphorus are easier to quantify. Based on the integration of the peaks from each element (and various equipment and excitation efficiency parameters) the silicon and phosphorus are present at about the same concentration. It is difficult to say anything about the relative amounts of silicon versus oxygen or carbon. It can be stated; however, that phosphorus is present at a much higher concentration than 1 % of the surface film (the original concentration in PPO). This demonstrates that phosphorus must be concentrating in the deposit, suggesting an adsorption/reaction mechanism involving phosphorus, preferential to any reactions involving the PPO.

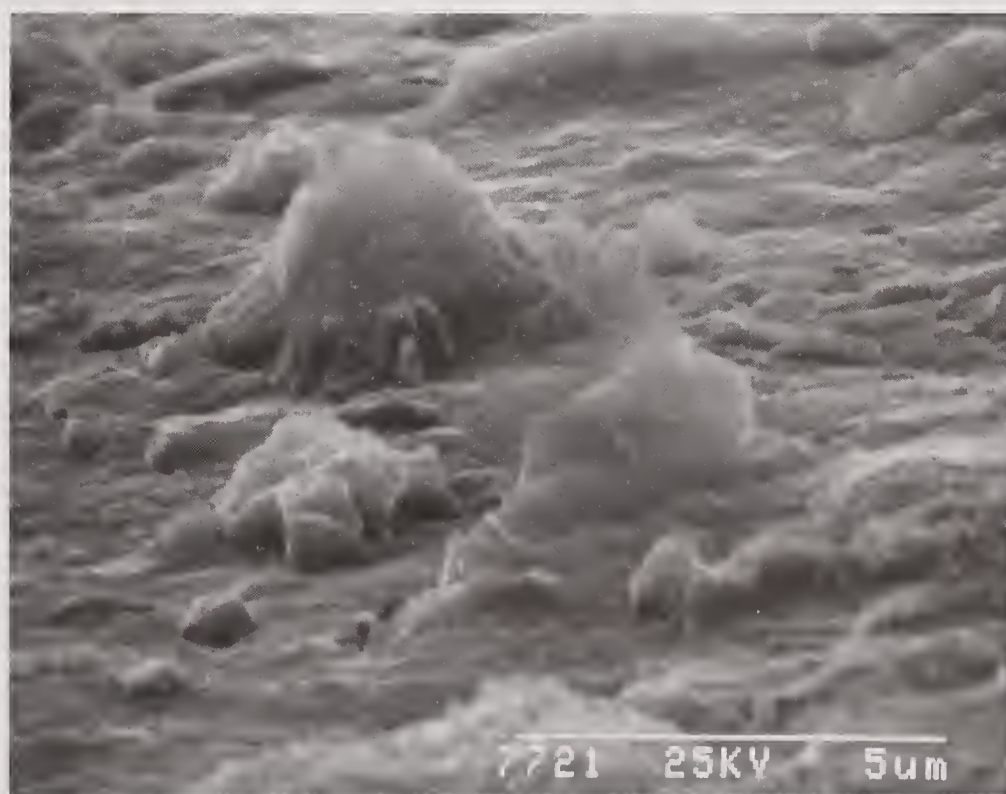


Figure 10.14 SEM Photomicrograph of Entrance Deposit for 1% TCP in PPO Lubricated Si_3N_4 BTF Test at 60 kg: a) Bubble Formed from Electron Beam Spot Damage, b) Same Region after Bubble has Popped

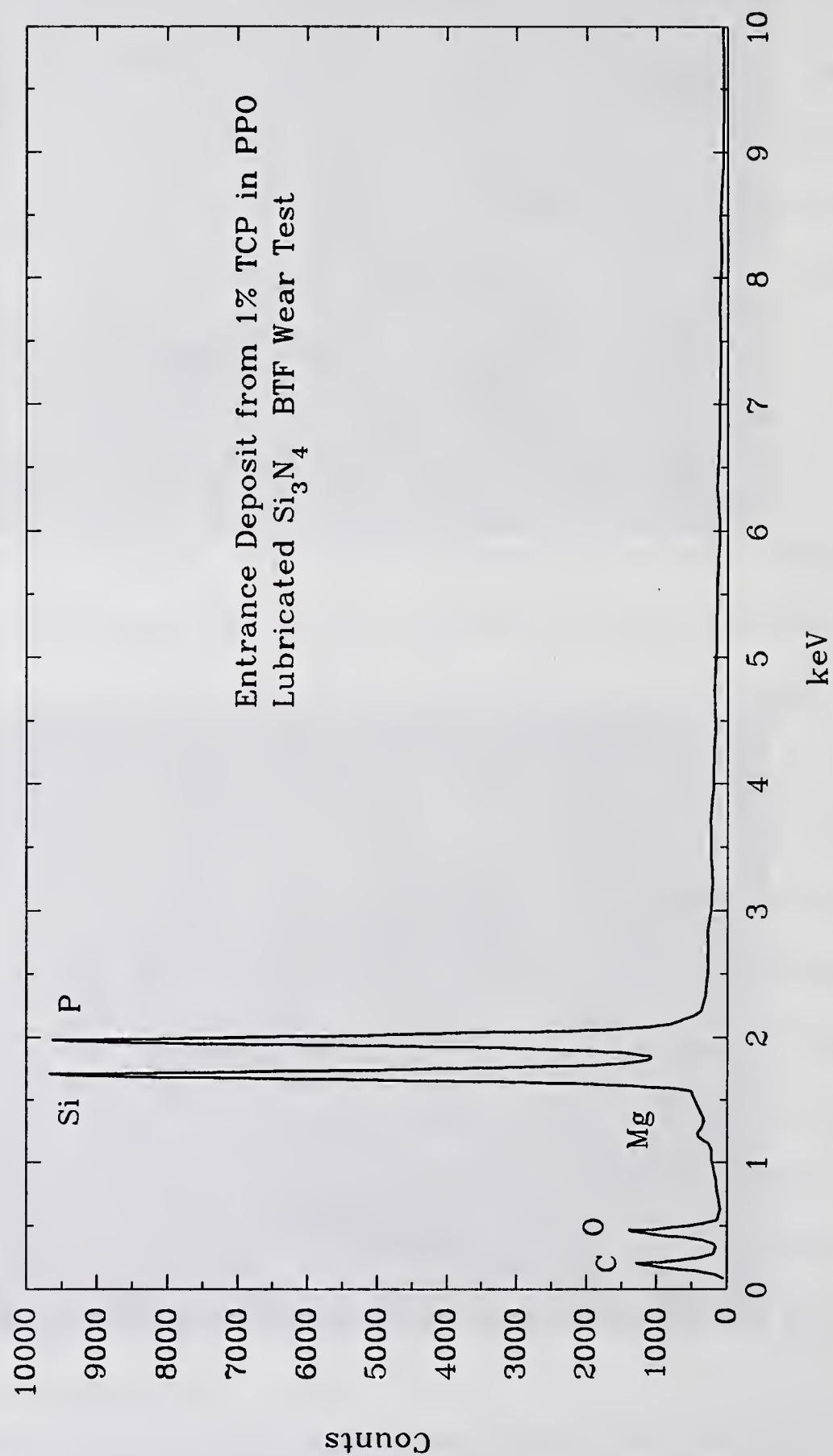


Figure 10.15 EDX Analysis of Entrance Deposit from 1 % TCP in PPO Lubricated Si_3N_4 BTF Test at 60 kg

Iron is not detected in any appreciable quantity in this reaction product. Fe-Phosphorus reactions are known to lubricate in iron based systems. In order to make sure iron chemistry is not affecting lubrication, the EDX was checked for sensitivity to iron phosphate. Figure 10.16 is the EDX spectrum for pure FePO_4 model compound. Comparison of this spectrum to Figure 10.15 clearly shows that no iron phosphate is found in the 1% TCP lubricated Si_3N_4 wear test. The very low signal for oxygen in the FePO_4 model compound also demonstrates the difficulty in detecting this light element, since we know that four times as many oxygen atoms are present than either Fe or P.

10.4. Auger Analysis of Wear Products

Auger analyses were performed on two wear test flats from wear tests conducted using 1% TCP and 1% 2-ethylhexyl ZDP in PPO. Each flat was examined in two locations inside the wear scar, and one or two locations outside the wear scar.

In the case of 1% ZDP in PPO, the spots inside the wear scar were similar in elemental composition (Table 10.5). The ratio of Zn/P/S/O is 1/1/0/2.6 which is quite different from the 1/2/4/4 in the original ZDP. The lack of sulfur in the reaction products is consistent with the same observation with EDX, and indicates a chemical reaction has taken place in which sulfur is essentially eliminated. Auger analysis indicated a ratio of Zn:P of 1:1, whereas the EDX analysis had indicated a stronger presence of phosphorus (1:2). The difference may be due in part to the difference in sampling depth for the two techniques: 10 nm for Auger, and 1000 nm for EDX. Some of the oxygen signal probably comes from silicon oxides and oxidized hydrocarbons that are present. Outside the wear scar, one sees

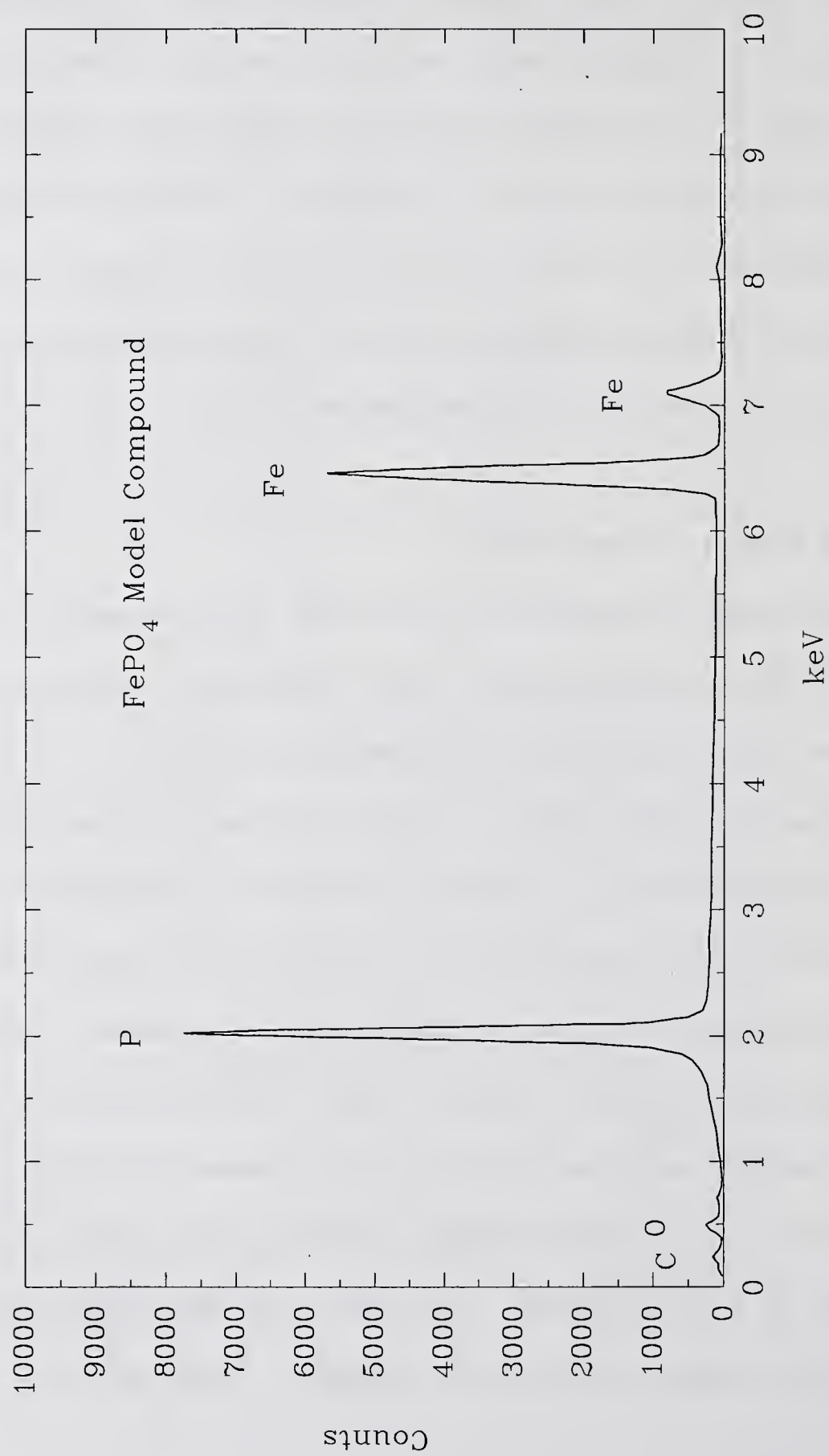
Figure 10.16 EDX of FePO_4 Model Compound

Table 10.5
Auger Analysis Results on 1% ZDP in PPO Lubricated Si_3N_4
(Results are in atomic %)

Sample Location	Zn	P	S	O	C	Si	N
Inside Scar, Spot #1	15	13	0.6	39	26	4	3
Inside Scar, Spot #2	17	12	0.6	40	24	4	3
Outside Scar, Nearby	8	3	0.9	22	51	4	6
Outside Scar, Far Away	2	<1	0.6	12	67	10	7

less phosphorus (and zinc) containing compounds and more carbon containing compounds. Finally, away from the wear scar, we see mostly carbonaceous material, similar to what we see in the pure PPO case.

Auger depth profiling of the region within the wear scar (Figure 10.17) reveals that the outermost layer is a thin carbon rich coating 10 Å deep. This could very well be only an adsorbed hydrocarbon layer that was not removed with the hexane solvent used to prepare the specimens for analysis. Beyond the outer hydrocarbon layer is an O,P,Zn rich layer about 100 Å thick. Perhaps this is some kind of inorganic ZnPO_4 layer. The ratios of atomic concentrations are not far from these values.

In the case of 1% TCP in PPO (Table 10.6), only a small amount of phosphorus was seen inside the wear scar. Most of the signal seems to be due to carbon containing compounds. Auger depth profiling (Figure 10.18) confirms the strong presence of carbon containing material to a depth of approximately 100 Å. This outer layer also appears to be

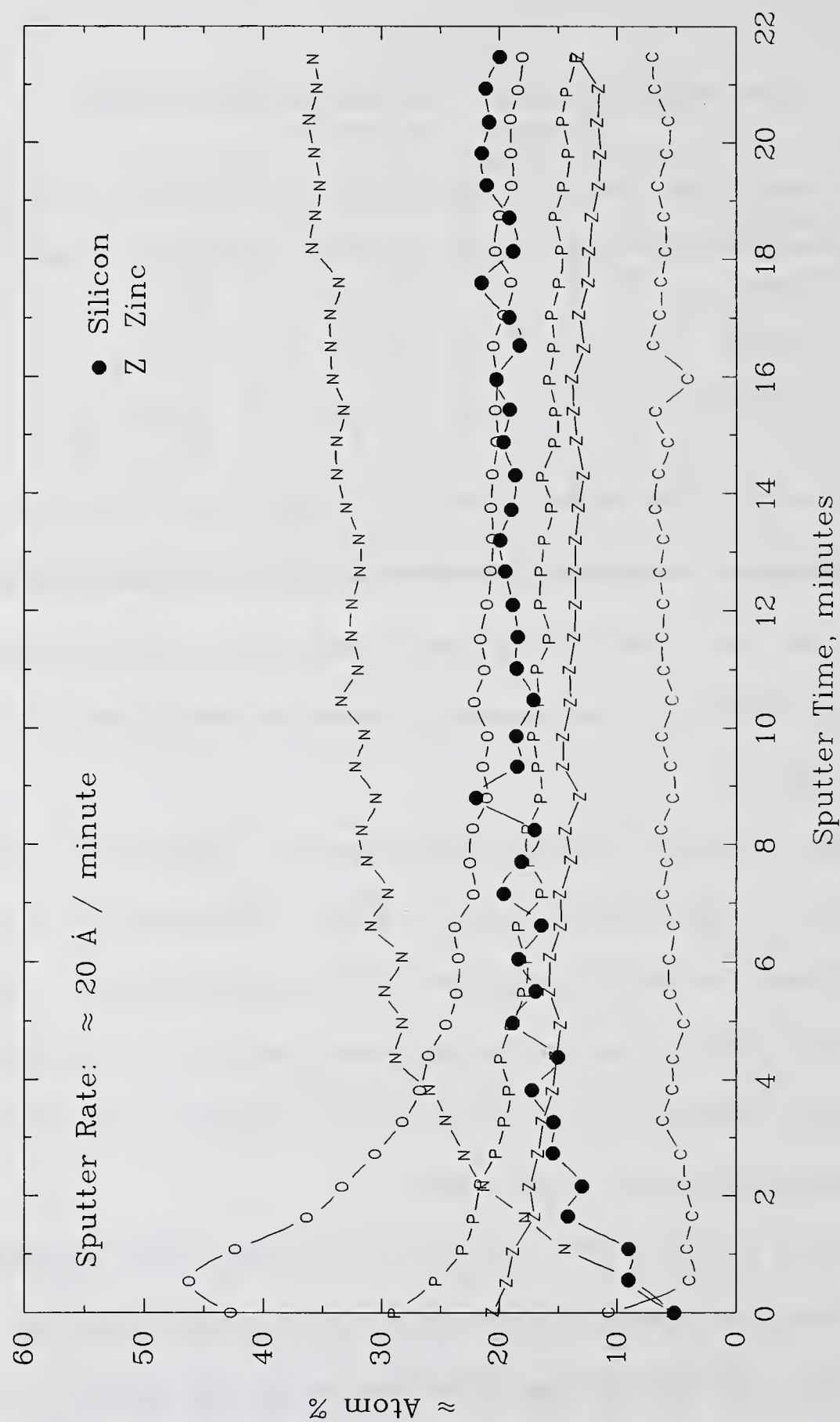


Figure 10.17 Auger Depth Profile for Region Within Wear Scar of 1% ZDP in PPO Lubricated Si_3N_4 BTF Test at 60 kg

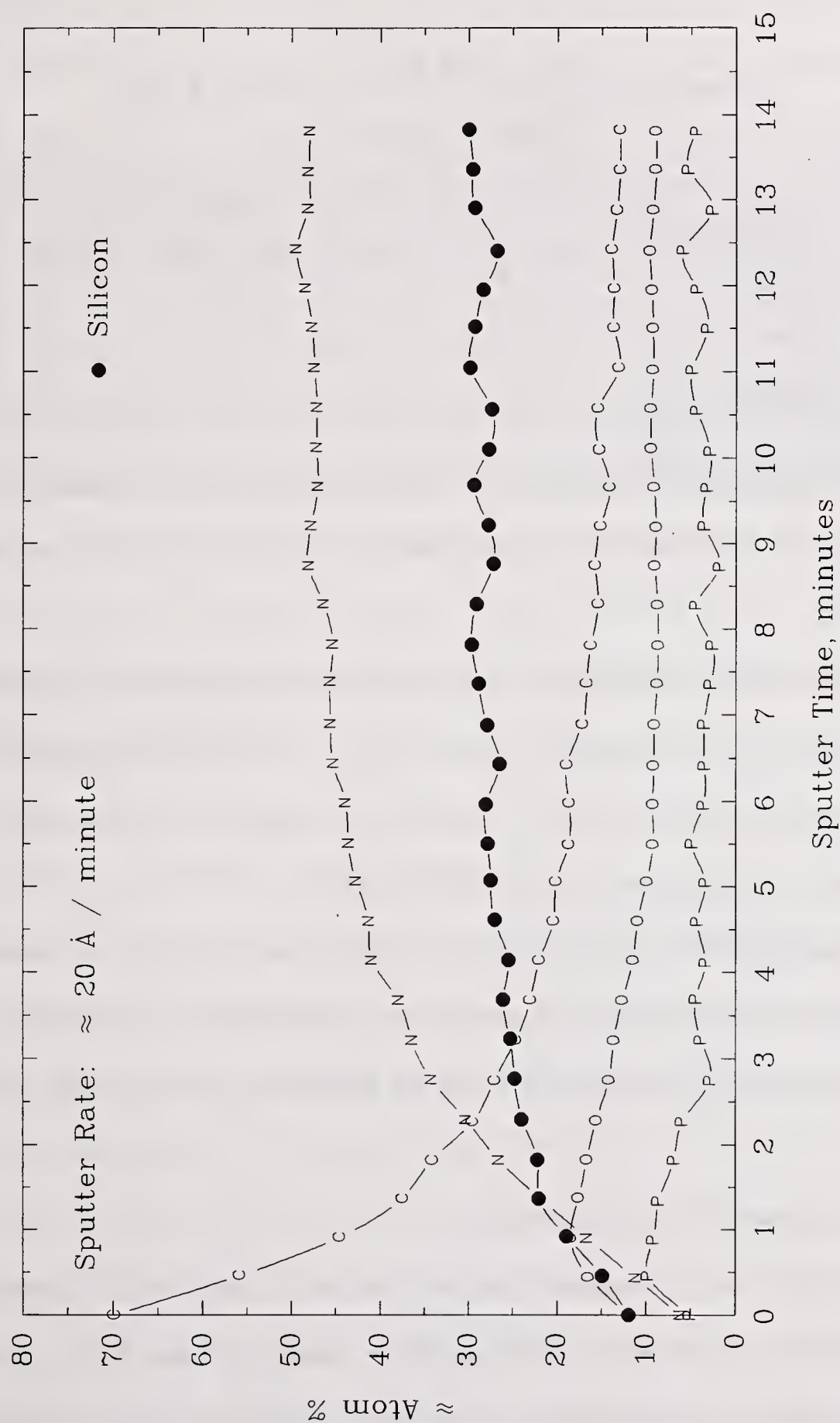


Figure 10.18 Auger Depth Profile for Region Within Wear Scar of 1% TCP in PPO Lubricated Si_3N_4 BTF Test at 60 kg

Table 10.6
Auger Analysis Results on 1% TCP Lubricated Si_3N_4
(Values are Atomic %)

Sample Location	P	O	C	Si	N
Inside Scar, Spot #1	2	10	68	11	7
Inside Scar, Spot #2	2	10	68	10	8
Outside Scar, Far Away	< 1	10	69	11	8

slightly oxygen and phosphorus rich, although the penetration of phosphorus does not seem to exceed 50 Å.

The Auger analysis results indicate surface phosphorus concentrations inside the wear scars far in excess of their concentration in the original lubricant. This information, coupled with the observation in the case of ZDP, that sulfur is eliminated from the product suggests complex reactions are taking place in the wearing contact.

Unfortunately, EDX and Auger only tells us that elements like silicon, phosphorus, oxygen and carbon are present; they do not give us any information about bonding. To get information about bonding, we must use a chemical structure analytical tool like FTIR.

10.5. FTIR Analysis of TCP Wear Product

FTIR analyses were performed on the reaction product from a 1% TCP in PPO lubricated BTF test. In order to get any chemical structural information from such a small amount of material, a procedure was developed in which the deposit was carefully scraped

from the surface of the Si_3N_4 flat with a scalpel blade, and transferred to a KBr pellet. The dark color of the deposit allowed for location of the transferred spot of deposit on the larger area of the KBr pellet. The sample could then be analyzed in transmission mode to try to determine the chemical structure of the constituents of the deposit.

The spectrum of the residue from a 1% TCP in PPO lubricated test (Figure 10.19) contains very little information to suggest much of an organic reaction product. The few peaks that are seen are consistent with silicate particles and some hydroxide (perhaps from acid and alcohol groups). It is not clear from this data exactly how phosphorus may be incorporated. The spectrum is markedly different from the spectrum of TCP, indicating that the high concentration of phosphorus observed in Auger and EDX analyses are not merely concentration of TCP, but a new phosphorus-containing material. Complex reactions must have taken place in the contact.

10.6. Load Capacity Plot for 1% TCP in PPO

In order to get an idea of the effective load range for 1% TCP in PPO a series of tests were conducted at different loads. The results of this series of tests are shown in Figures 10.20 (friction traces) and 10.21 (plot of wear scar diameters versus load). A wear test at 20 kg produced very low wear and friction. The friction trace is very smooth and steady, and the friction coefficient at the end of the test is 0.084. The wear scar diameter is slightly greater than the Hertz diameter at this load and is similar in size to the pure PPO performance. At 60 and 70 kg load, the friction traces are still smooth and level, and wear scar diameters are still only slightly higher than the Hertzian contact diameter. Coefficient

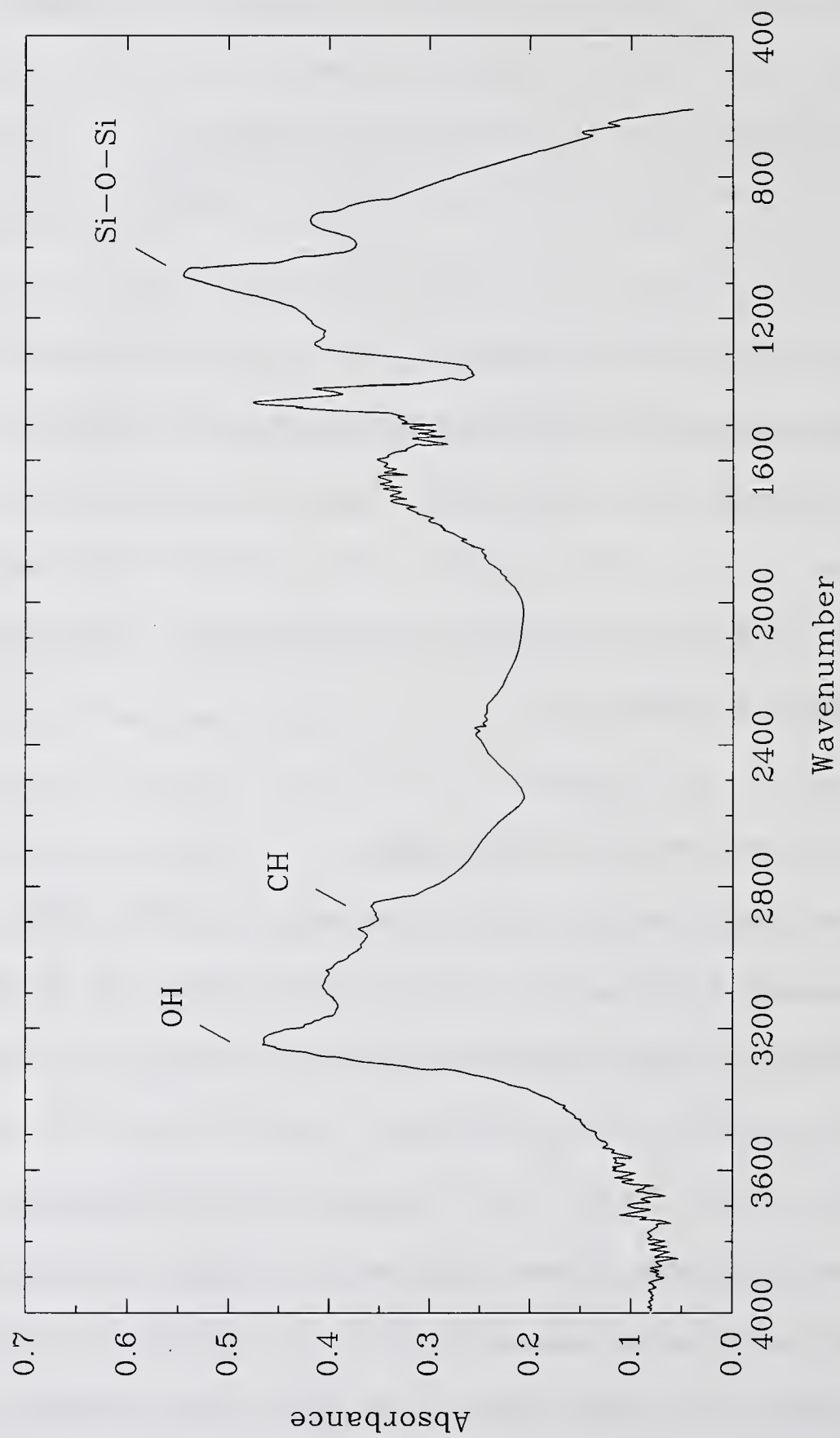


Figure 10.19 FTIR Analysis of Reaction Product from 1% TCP in PPO Lubricated Si_3N_4 BTF Test at 60 kg

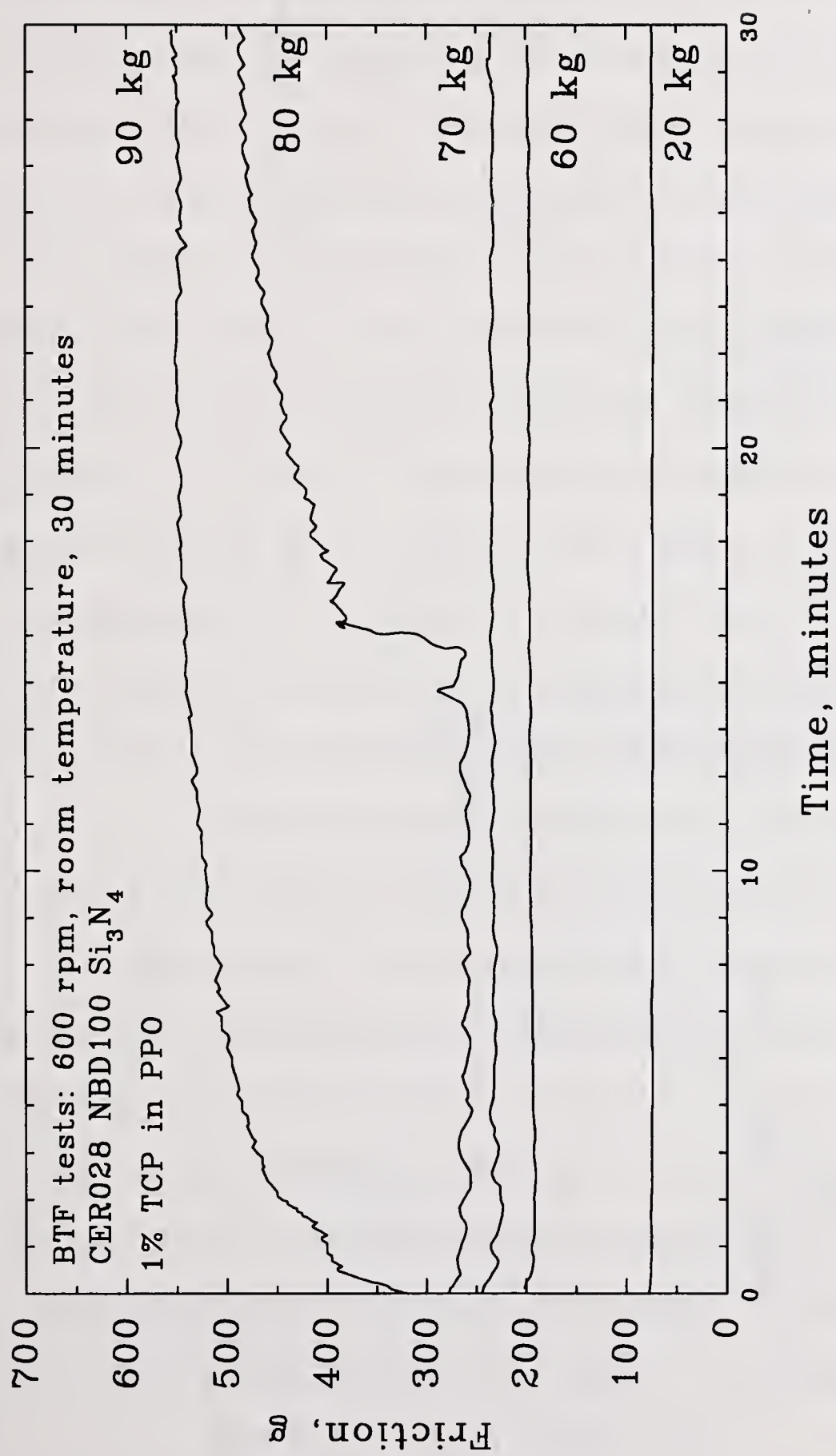


Figure 10.20 Friction Traces for 1% TCP in PPO Lubricated Si_3N_4 BTF Tests

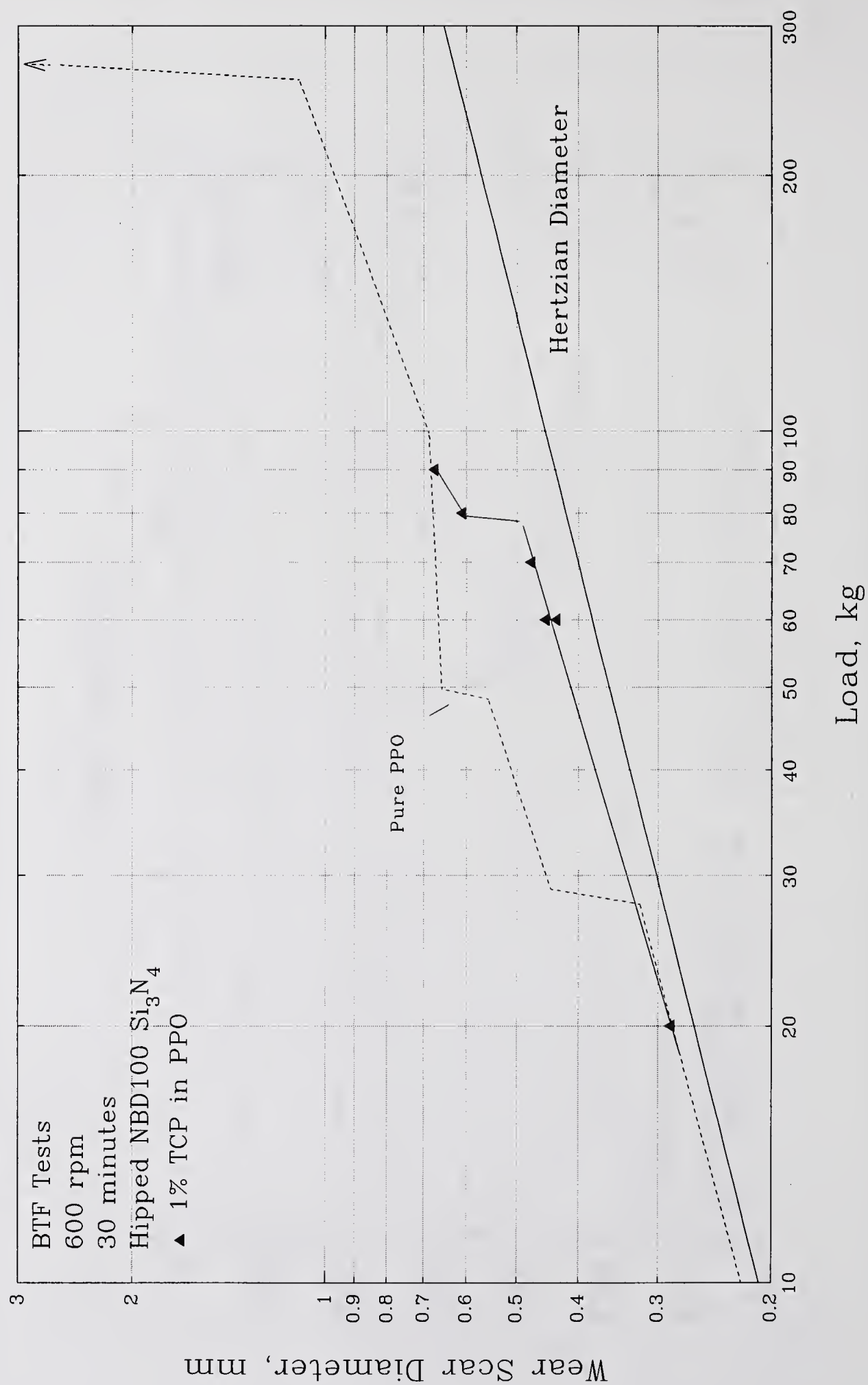


Figure 10.21 Load Capacity Plot for 1% TCP in PPO Lubricated Si_3N_4 BTF Tests (Compared to Pure PPO Data)

of friction at the end of the test is 0.077-0.078. This is in contrast to the pure PPO behavior in which friction and wear had increased at loads of 30 kg and above. At 80 kg load, friction starts out low and steady; however, midway through the test there is a transition to higher friction (and presumably higher wear). This transition signals a change in the wear mechanism that results in a larger wear rates, and higher final coefficient of friction (0.142). A wear test at 90 kg produces an almost immediate increase to a high level of friction. The shape of the friction trace is similar to that seen for pure PPO lubricated tests at this load. Wear at the end of the test is about as high as the pure PPO case. The severity of the test is apparently so high that 1% TCP in PPO is no longer effective, and the lubricant behaves as if it were merely PPO. Since the 1% TCP in PPO test at 200°C indicated that TCP was no longer effective at this temperature, one might hypothesize that the failure of TCP at 90 kg is related to the higher temperatures generated in the wear contact at this higher load.

In order to get a better idea of the temperature limit of TCP lubricated Si_3N_4 a test was conducted in which the temperature was increased gradually during the test. Figure 10.22 shows the friction trace for this test in which the bulk lubricant temperature has been superimposed. According to this figure, the friction increase which signals the wear transition occurs near 175°C bulk oil temperature. FTIR analysis of the lubricant after the higher temperature tests revealed that the TCP was still present. A special wear test was also conducted using a sequence of temperatures. First, the test was started at 200°C. Friction was high signalling failure of the TCP to lubricate adequately. The test was then allowed to cool down to room temperature, and the test was continued. Friction for this second phase of the test was low indicating TCP was now effective. This information

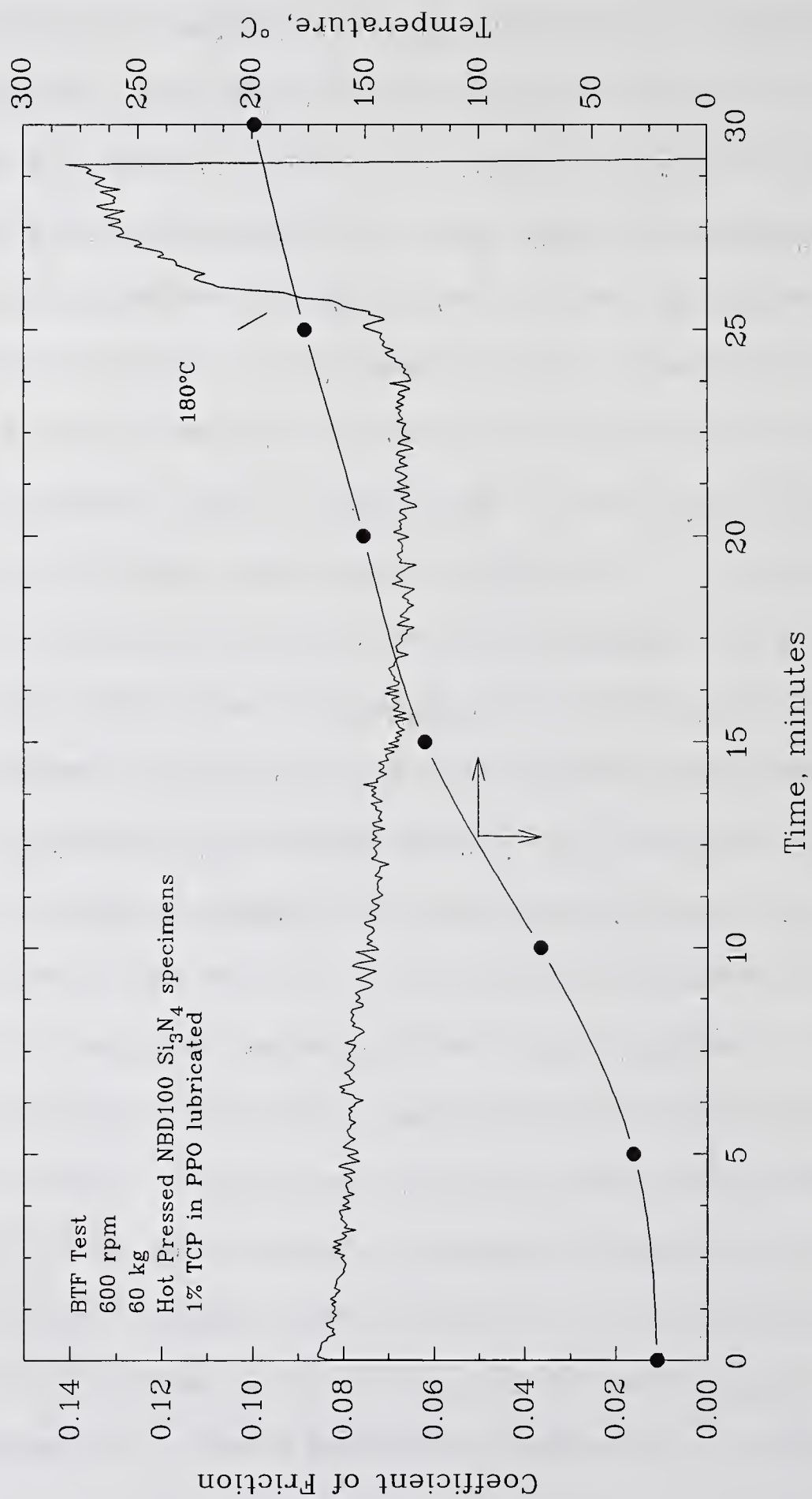


Figure 10.22 Friction as a Function of Test Temperature for 1% TCP in PPO Lubricated Si_3N_4
BTf Test at 60 kg

indicates that the change in wear mechanism promoted by increasing temperature is reversible. Of course the critical temperature that causes the wear mechanism transition is the actual temperature inside the contact and not the bulk lubricant temperature.

Two additional tests were conducted at 200°C to determine whether this wear transition for TCP lubricated Si_3N_4 is concentration dependant. This was because there may be several reasons why 1% TCP fails as a function of temperature. The first possibility is that at higher temperatures the reactivity is so high that the additive gets depleted before it goes all of the way through the scar. If this were true, then a higher concentration of TCP in PPO should lubricate. A second possibility is that the higher temperatures cause 1% TCP to be too aggressive and it corrodes the surface. If this were true, then lower concentrations of TCP in PPO might be effective at higher temperatures. In order to address these two possibilities, 200°C BTF wear tests were conducted on Si_3N_4 using 0.1% TCP in PPO, and 5.0% TCP in PPO. Wear tests conducted with these two other concentrations of TCP produced high friction and wear indicating that neither of these two proposed reasons for the temperature dependance of TCP were correct.

Another test was performed at 200°C using 1% TCP in PPO and 0.1% Fe naphthenate to see if the presence of Fe would allow TCP to work at this temperature. The addition of Fe failed to allow TCP to work at 200°C.

From the above data it was concluded that the failure of TCP to lubricate Si_3N_4 at higher temperatures is not due to a kinetic barrier (i.e., insufficient or excessive reaction rate), but to a change in the chemical mechanism of lubrication. This could be due to a lack

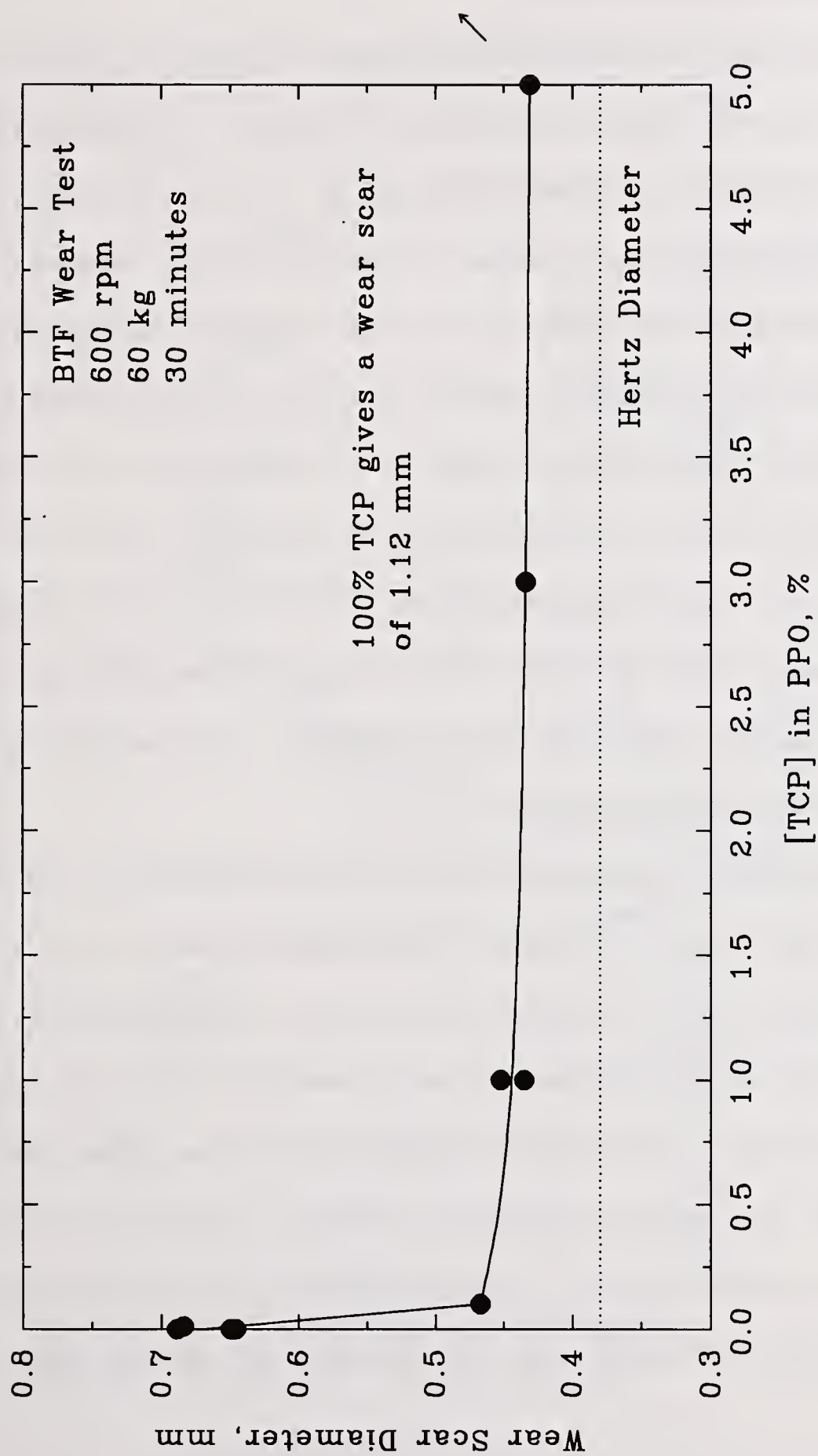
of adequate adsorption of TCP on the surface at this temperature, or a change in the actual chemical surface reaction that results in lubrication.

10.7. Effect of [TCP] on Wear of Si_3N_4

Another variable that determines the effectiveness of a compound in boundary lubrication is its concentration. The initial screening study used 1% compounds in PPO because the 0.5-2.0% range is a common concentration for many antiwear additives. In order to understand the effectiveness of TCP at other concentrations, a series of tests were conducted using as little as 0.01% to as much as 100%. The results of these tests are presented in Figure 10.23. According to the data, 0.01% TCP is not effective, however 0.1% is effective. Too high a concentration (such as 100%), is also not effective. In fact, the pure TCP gave a much higher wear scar diameter than pure PPO. This may be due to too high a chemical corrosivity as suggested in the theory of optimum reactivity¹²⁷.

According to this theory, too little antiwear additive causes higher than optimal (lowest) wear because of insufficient production of beneficial reaction products. Essentially, the film is physically removed at a faster rate than it is formed. Too much antiwear additive causes higher than optimal wear because there is too much reaction with the surface and the dominant wear mechanism begins to shift toward a corrosive wear mechanism.

Alternatively, wear for the pure TCP case may be due to poor viscous lubrication contribution because of the low pressure-viscosity coefficient for TCP. It is also possible that the reaction product of both TCP and PPO may be necessary for adequate lubrication.

Figure 10.23 Wear Versus TCP Concentration for Si_3N_4

10.8. Powder Adsorption Studies

In the course of investigating why phosphates in general, and TCP in particular, can lubricate Si_3N_4 , several literature references were found that provided important clues. Klaus and Bieber¹⁵⁵ studied the mechanism of TCP with Fe. In using silica gel thin layer chromatography (TLC) plates to separate TCP into its constituent components, they demonstrated that TCP had an affinity for the silica gel surface. Sinitsyn et al.^{224a} studied TCP in greases and found that the concentration of TCP in the oil decreased significantly when a silica was used as a thickening agent. It was thought that these two observations were related and suggest that phosphates can adsorb onto silica. In some cases, the adsorption may be strong enough to reduce the concentration of "active" phosphate to affect wear performance. Since the surface of Si_3N_4 is oxidized silicon, it may be very similar in chemistry to the silica used in these studies. Therefore, a study was conducted to see whether TCP could adsorb on Si_3N_4 .

Approximately 1.5 ml of a solution of 1% TCP in hexadecane was passed through 300 mg of Stark H2 Si_3N_4 . IR spectra were taken before and after the elution, and are compared in Figure 10.24. According to this data, there are absorption bands at 970 cm^{-1} , 1145 cm^{-1} , and 1245 cm^{-1} (and others) that are characteristic of TCP. It is apparent that percolation through Si_3N_4 has reduced the intensity of these characteristic bands approximately 35%. GC-MS confirmed this reduction in concentration of TCP due to percolation through Si_3N_4 powder. A second experiment was performed using silica gel instead of Si_3N_4 powder (surface area: $300\text{ m}^2/\text{g}$ versus $3\text{ m}^2/\text{g}$ for Si_3N_4 powder used). The

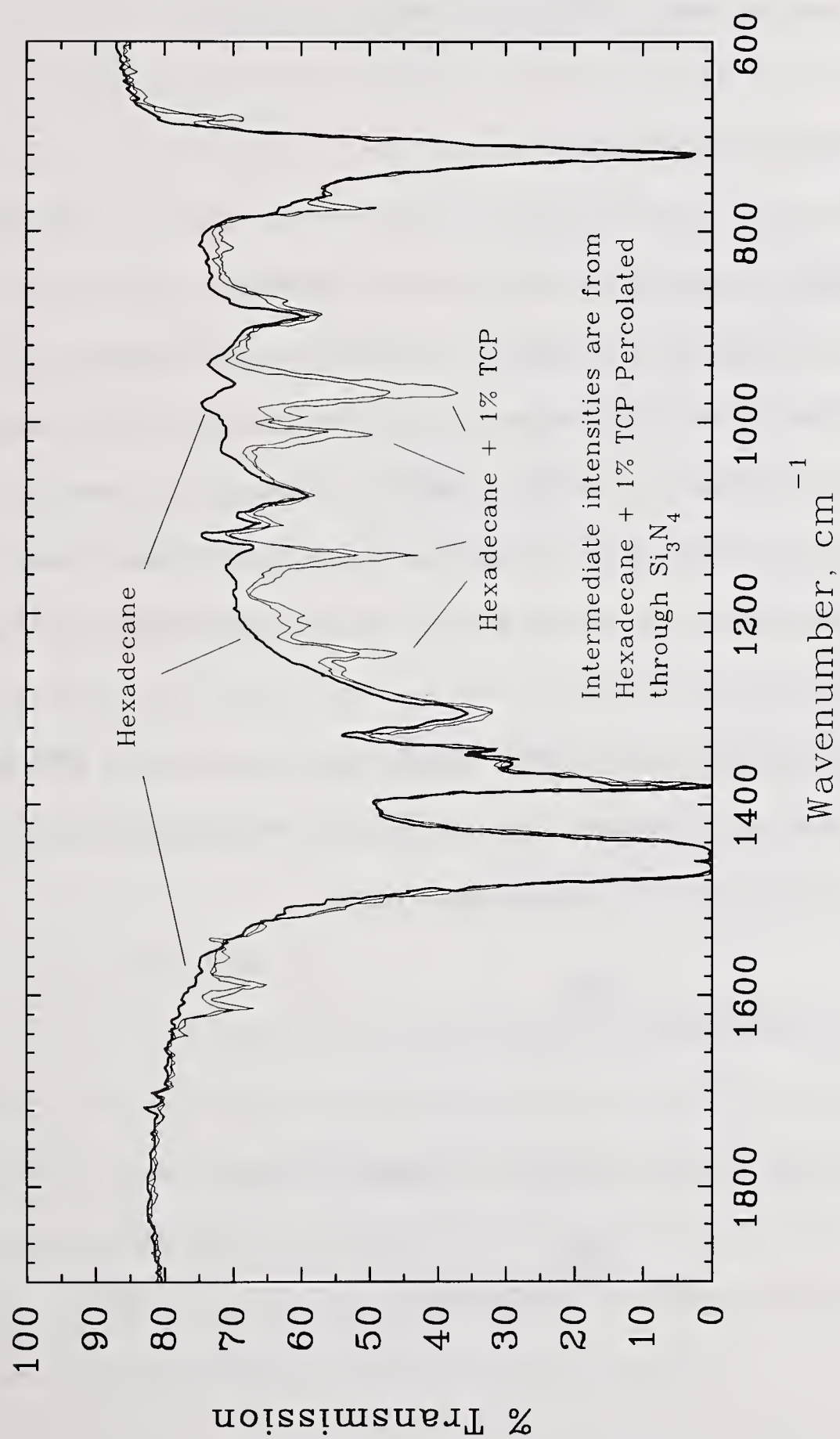


Figure 10.24 FTIR Spectra for TCP Adsorption on Si_3N_4 Powder Experiment

silica gel removed all of the TCP from the hexadecane. Clearly, there is some kind of chemical interaction between TCP and the oxidized Si_3N_4 surface.

10.9. Effect of Iron Impurities

One critical question that must be addressed is the possible role of iron in lubrication of Si_3N_4 . Many researchers have studied the antiwear behavior of TCP on iron surfaces. Godfrey^{98a} contended that iron phosphate was formed in the wearing contact as a reaction between acid impurities in TCP and the iron in his steel specimens. This concept is supported by data from Klaus et al.¹⁵⁵ and Bieber et al.^{24a} during the same time period (1965-1968). Later work by Klaus et al.^{157a} indicated crystalline FePO_4 wear debris for steel on silicon nitride wear tests lubricated with TCP. Clearly, iron is an important constituent in these studies.

Jeng's PHD thesis (May 1987)^{143a} indicates that the deposition of TCP reaction product from the vapor phase was "catalyzed" by iron. He determined that the deposition on stainless steel followed the first order kinetic equation:

$$\text{Rate} = 3.06 \times 10^{13} e^{-\frac{37100}{RT}} C$$

On a "non-catalytic" (Quartz) substrate the equation becomes:

$$\text{Rate} = 2.34 \times 10^{15} e^{-\frac{55200}{RT}} C$$

Unfortunately, Jeng does not make a distinction between the material formed in the two reactions. In the case of the steel surface, Jeng suggests that the deposit consists of a mixture of iron phosphate and organic polyphosphate. If the same reactions can apply to the ball-on-three-flat tests, then one must be aware that iron may play a significant role in catalyzing reactions.

A BTF wear test conducted using 1% TCP + 0.1% Fe naphthenate in PPO was conducted to see if additions of iron would affect the test results. The wear scar was only slightly smaller and the friction level was similar to the case of the 1% TCP in PPO. The most obvious difference was the texture of the film in the wear scar. The test conducted using the Fe naphthenate had a film that was much more fluid in nature (Figure 10.25). EDX analysis of the film revealed a ratio of Fe:P of approximately 1:7, indicating that even with Fe present the film is not purely FePO_4 . A wear test conducted using just 0.1% Fe naphthenate in PPO resulted in a wear scar of 0.583 mm and final coefficient of friction of 0.105; therefore the Fe naphthenate by itself is not a great lubricant.

10.10. Pin-On-Disc Wear Tests

Since iron can play an important role in lubrication in iron based systems, and concentrations of as little as 200 ppm may influence the chemistry of TCP, attempts were made to conduct wear tests using low iron materials. Initially, tests were run using fused silica, based on the concept that the surface of Si_3N_4 is chemically similar to silica. Fused silica is readily available in very high purity with trace iron content below 2.5 ppm. Pin-on-disc tests were selected because pins were easier to fabricate than balls.

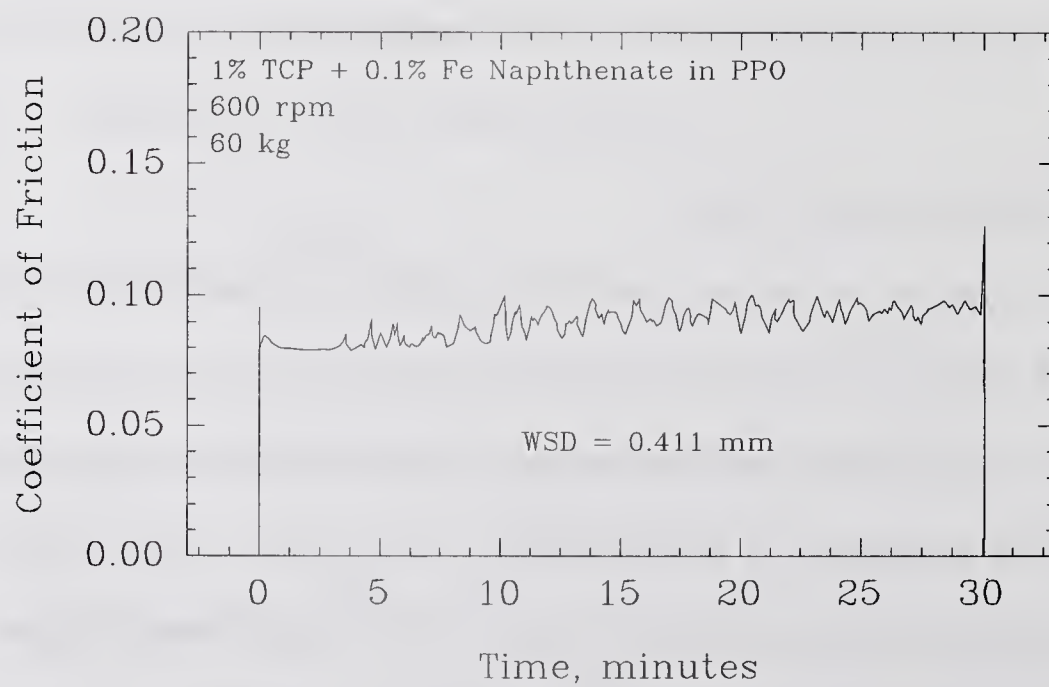
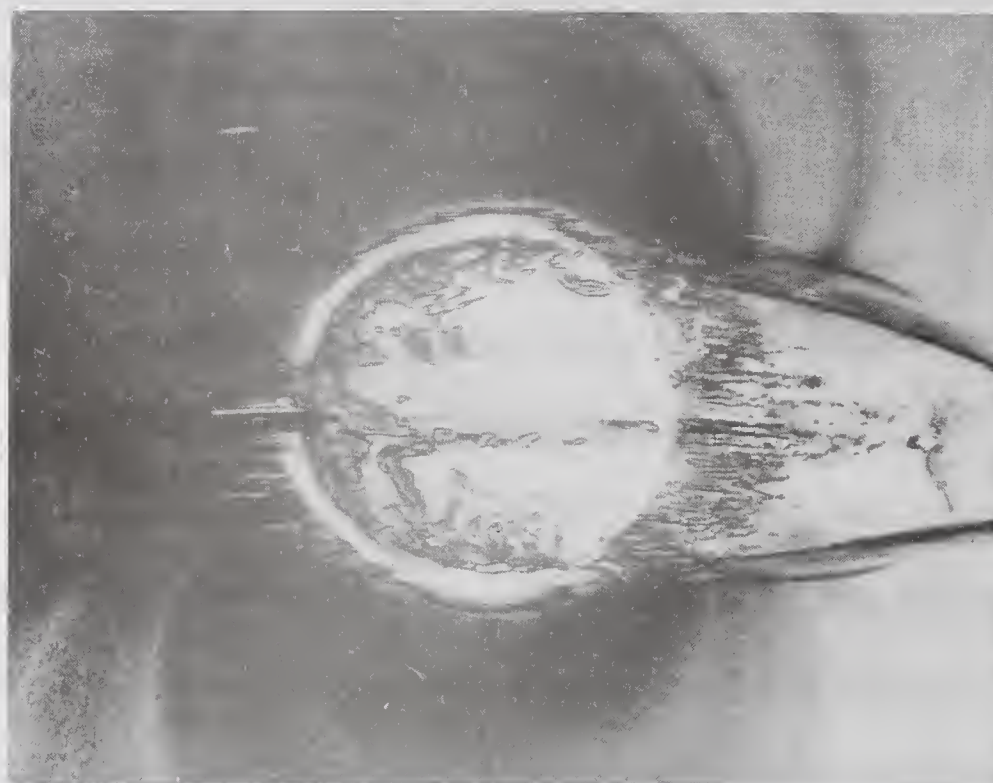


Figure 10.25 1% TCP + 0.1% Fe Naphthenate in PPO Lubricated Si_3N_4 BTF Test at 60 kg:
a) Optical Photomicrograph, b) Friction Trace

Optically smooth disks of 31.75 mm diameter (1.25 in) were used as the lower specimens. Upper specimens were made from 6.35 mm (0.25 in) diameter rods approximately 17 mm (0.7 in) long. A hemispherical tip was fashioned using a series of diamond and silicon carbide grinding and diamond polishing.

POD tests were conducted using a 45° pin holder. Since the contact point on the hemisphere is midway between the tip and the equator, the pin may be rotated between tests and several tests can be conducted on a single pin. Four tests were conducted per pin. Four tests were conducted on each disk by varying the radius of rotation of the contact point between runs.

Specimens were cleaned using the standard cleaning procedure (hexane, acetone, Micro, DI water, N₂ dry) just prior to testing. Specimens were locked in place, and vertical uniformity of the rotating disk was checked just prior to testing using a dial gauge. A vertical uniformity of better than 125 μm (0.005 in) could be obtained with careful adjustment. Wear scars on the pin were measured after each test, and friction was continuously monitored during a test. Tests were run at 10 cm/s, 20 N, 60 min, ambient T and humidity, and 50 μl lubricant.

A paraffin oil lubricated test gave a relatively smooth and level friction trace (Figure 10.26B). The wear scar observed after the test was relatively small and well defined with a rough surface (Figure 10.26A). Several dark lines can be seen emanating radially from the scar. These are radial cracks and are visible due to the transparent nature of the fused silica. Closer magnification using SEM (Figure 10.27) indicates that these cracks are also visible on the surface. The direction of sliding in these photographs are indicated by the arrows. The

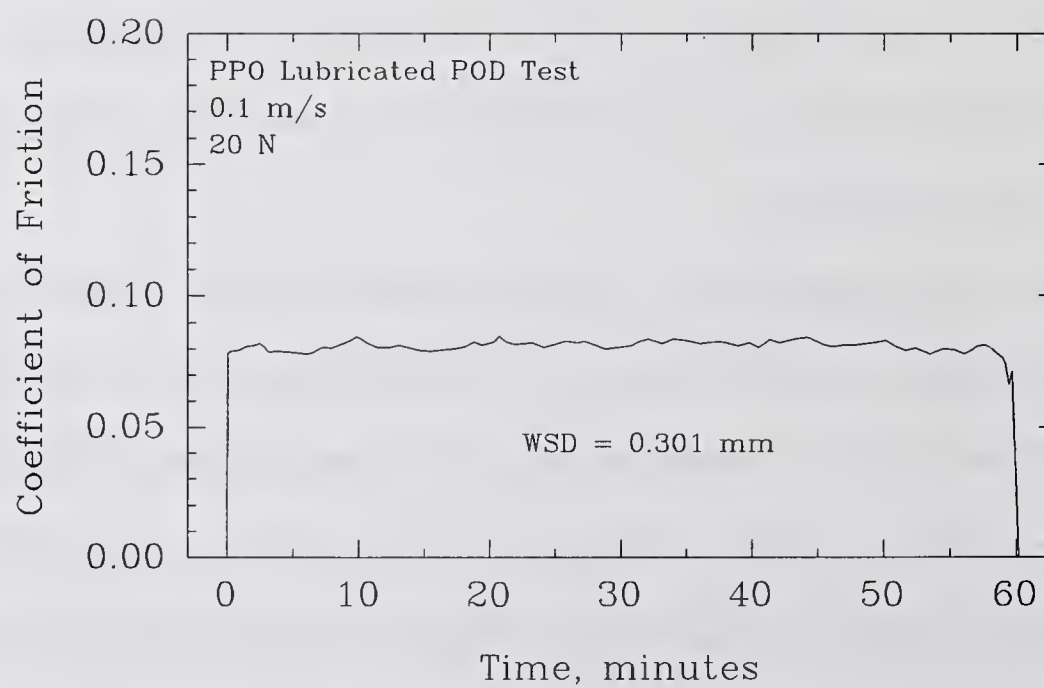
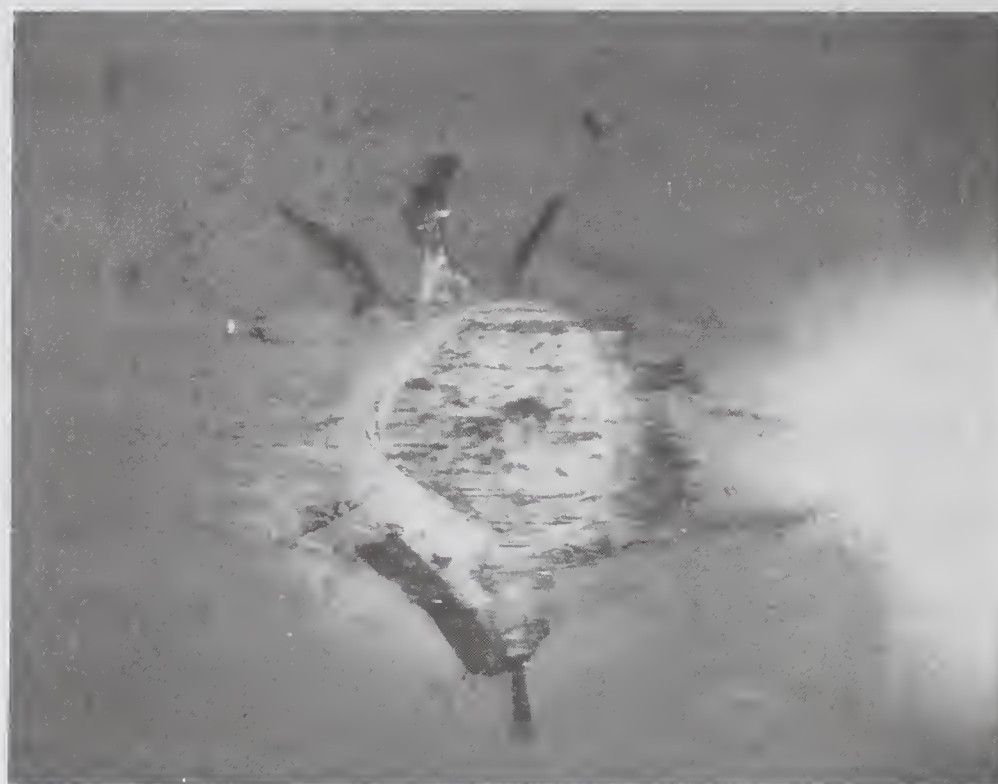


Figure 10.26 PPO Lubricated POD Test on Fused Silica: a) Optical Photomicrograph, b) Friction Trace

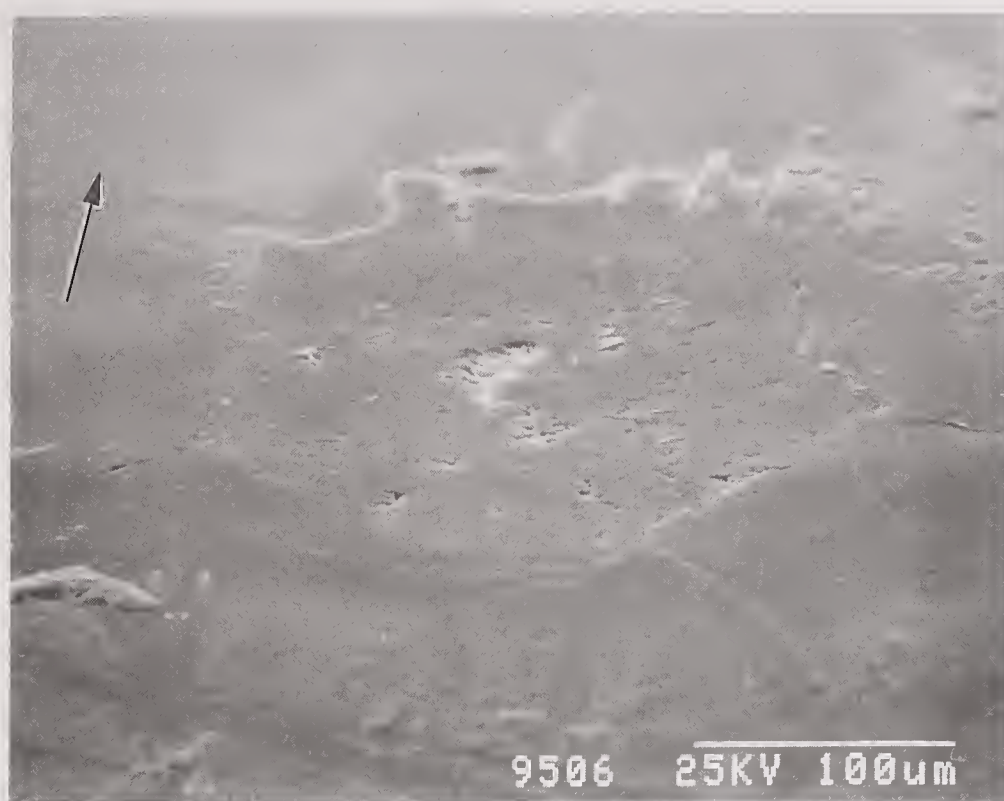


Figure 10.27 SEM Photomicrograph of Wear Scar on Pin from PPO Lubricated POD Test on Fused Silica: a) Wear Scar, b) Higher Magnification of Radial and Tensile Cracks outside Wear Scar

surface of the wear scar is pitted and a small, severely fractured region can be seen. The large, curved crack just outside and parallel to the wear scar near the entrance is a tensile crack. The large dark feature outside the wear scar in the lower left portion of Figure 10.26A is not visible on the surface of the SEM photographs (Figures 10.27), suggesting that it represents a subsurface lateral crack. These characteristic cracks are described in detail by many researchers^{163a}. The observation of these modes of cracking and fracture suggest that this material is undergoing a very different wear mechanism than that observed for Si_3N_4 and may not be suitable as a chemically similar wear analog of the Si_3N_4 surface.

A wear test conducted using 1% TCP in PPO and 1% TCP + 0.1% Fe naphthenate in PPO gave considerably higher wear than PPO by itself (Table 10.7). Radial cracking was much reduced; however the

fracture region within the wear scar was more pronounced for

these two tests (Figures 10.28).

The TCP lubricated test (Figure 10.28A) had significantly higher levels of deposit surrounding the wear scar than the PPO case.

This deposit was rich in

phosphorus. The TCP + Fe

naphthenate lubricated test (Figure 10.28B) had even more deposit. These deposits were rich in both phosphorus and iron. The elemental composition of the deposits is similar to that

Table 10.7
Wear Test Results for POD Tests on Fused Silica

<u>Lubricant</u>	<u>WSD</u> <u>(mm)</u>	<u>Final</u> <u>COF¹</u>
PPO	0.277	0.073
PPO	0.301	0.078
PPO + 1% TCP	0.435	0.091
PPO + 1% TCP + 0.1% Fe N. ²	0.476	0.110

Pin-on-disk Tester, 0.1 ms⁻¹, 20 N, 60 minutes, 50 μl lubricant, 21°C, 50% Relative Humidity

¹ measured at the end of the test

² Ferric Naphthenate

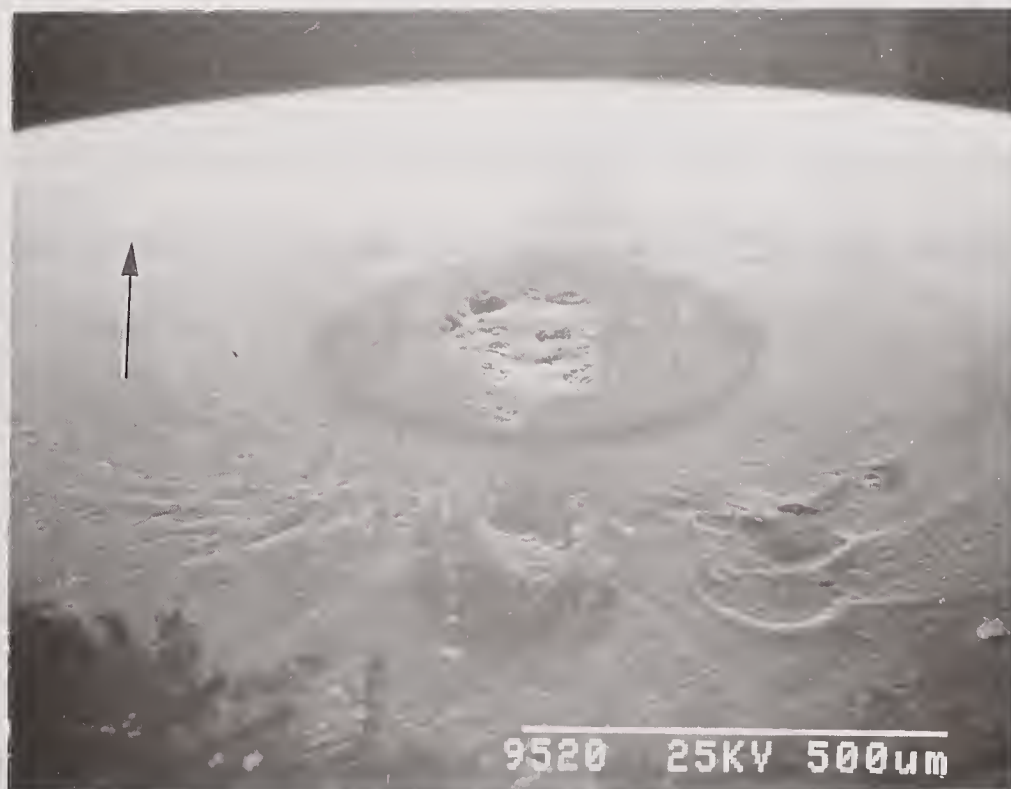


Figure 10.28 SEM Photomicrographs of Pin Wear Scars from POD Tests on Fused Silica: a) 1% TCP in PPO, b) 1% TCP + 0.1% Fe Naphthenate in PPO

observed for the Si_3N_4 BTF tests; however, the wear results are not. The higher wear observed for the TCP lubricated cases, coupled with the observation of severe fracture within the wear scar suggests that TCP (and Fe naphthenate) may be enhancing the fracture process. This type of behavior has been demonstrated by Freiman⁸⁵ in his study of fracture of glasses. The lack of comparable wear mechanism between Si_3N_4 and fused silica indicates that fused silica is not suitable as a model for studying the low iron lubrication of Si_3N_4 under boundary lubrication conditions.

Low iron impurity Si_3N_4 produced at Rutgers University was used to fabricate pins (0.25 in dia.) and disks (1.5 in diameter) for Pin-on-Disk (POD) wear tests. A 0.125 in radius, diamond polished hemisphere was produced on one end of the pin. A 0.25 in thick, 2 in diameter disk was ground and polished using the standard procedure, and resulted in a mirror finish on one surface. Wear tests were conducted using the CSEM POD apparatus.

Initially conditions of 23 cm/s (same as BTF) and 20 N for 60 minutes were used, but the wear scar obtained was only 0.142 mm using PPO without any additive. This is only 0.01 mm greater than the Hertzian contact diameter for these materials and conditions. This is too mild to allow the additive any opportunity to show improvement. Therefore, conditions were made more severe. The second PPO lubricated test was conducted at 45 N load and the same speed as before. The wear scar diameter at the end of the test was 0.279 mm (0.106 mm greater than the Hertzian contact diameter of 0.173 mm). A wear test conducted under the same speed and load using 1% TCP in PPO produced a wear scar of only 0.195 mm (only 0.022 mm greater than the Hertzian contact diameter). The results are summarized in Figure 10.29. The dotted line in this figure represents the transition from

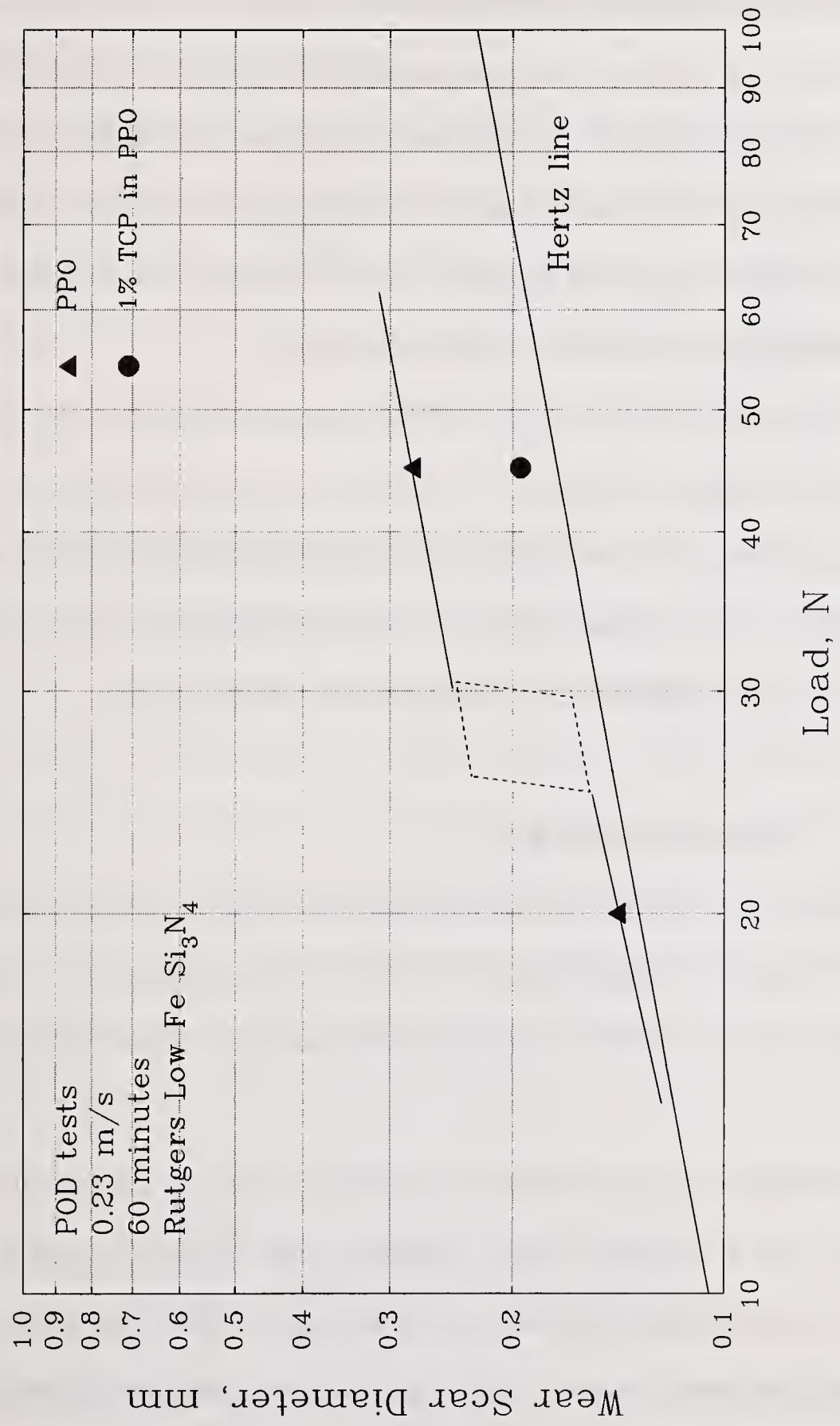


Figure 10.29 Load Capacity Plot for 1% TCP in PPO Lubricated Si_3N_4 (Low Iron Impurity) POD Test

low to high wear that is expected somewhere between 20 N and 45 N load for PPO. The BTF test showed a transition for PPO at between 100 and 120 N (25-30 kg applied load). The difference in transition is due to the smaller curvature for the POD test (0.25 in diameter versus 0.5 in diameter for the BTF). When one calculates the hertzian contact pressures for the BTF test at the PPO transition, one finds mean pressures of 1.58 to 1.68 GPa (229 to 243 kpsi). This corresponds to an applied load of 25 to 30 N in the POD test. Therefore, the transition has been tentatively drawn in at this load.

The data shows that 1% TCP in PPO is capable of lubricating Si_3N_4 in the absence of iron under the conditions of this test. It is still anticipated that iron may help promote additional reactivity and enhance lubrication in ceramic materials, as was shown using 0.1% Fe naphthenate. This suggests that it may be possible to add small amounts of iron to ceramics to ensure adequate reactivity at certain operating conditions.

10.11. Powder Reaction Study

Bogatyrev^{29a} found that di- and triethyl phosphites could react with the surface of silica to produce bonded organo-phosphorus films. These reactions were possible at temperatures as low as 200°C. He also notes that the Si-O-P bond is thermally stable up to 1000°C.

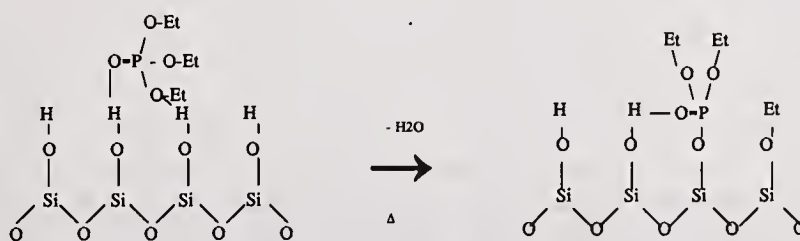
Batch reactions were conducted using high surface area Si_3N_4 powders and pure phosphates to try to determine whether phosphates could directly react with the Si_3N_4 surface. A mixture of Si_3N_4 powder and trioctylphosphate (TOP) was heated to 150-175°C for 1 hour. On cooling, the excess TOP was solvent extracted using hexane. The resulting

powder was dried, and analyzed using thermogravimetric analysis (TGA). The TGA weight loss curve (Figure 10.30) indicates a 1.1% weight loss due to burnoff of a surface product that had remained after the solvent extraction.

A similar experiment was conducted using TCP with the modification that a hexane/toluene (9/1) mixture had to be used to extract the residual TCP. The resulting weight loss curve of the dried powder (Figure 10.31) exhibited a 1.3% weight loss. These results are consistent with the hypothesis that these phosphates can react directly with the surface of Si_3N_4 .

10.12. Proposed Reaction Mechanism Between Si_3N_4 and Phosphates

The data suggest that phosphates can react with the Si_3N_4 to form a lubricious surface compound. The first phase of the mechanism is thought to be adsorption of the phosphate onto the Si_3N_4 surface. Since the surface of Si_3N_4 is actually a partially hydroxylated silica, hydrogen bonding may exist between the oxygen of the phosphate and the hydrogen of the Si-OH. Upon heating, one of the alkyl groups may be removed, resulting in a bonded surface phosphate and possibly a surface alkoxide. This mechanism was proposed by Iler¹³⁸ to explain the interaction between trialkyl phosphates and polysilicic acid as shown below.



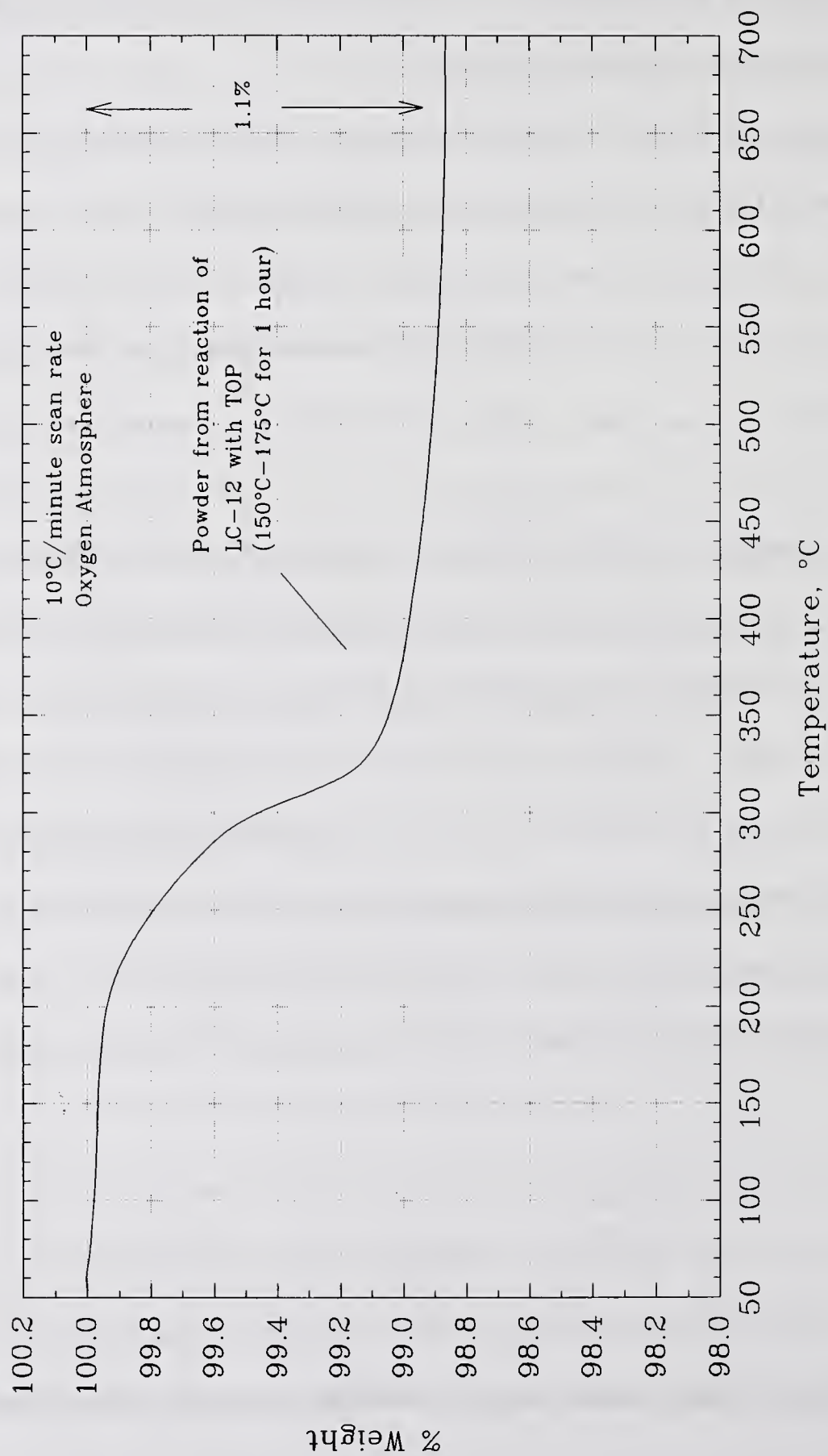


Figure 10.30 TGA Analysis of Reaction Product on Surface of Si_3N_4 Powder After Reaction with TOP

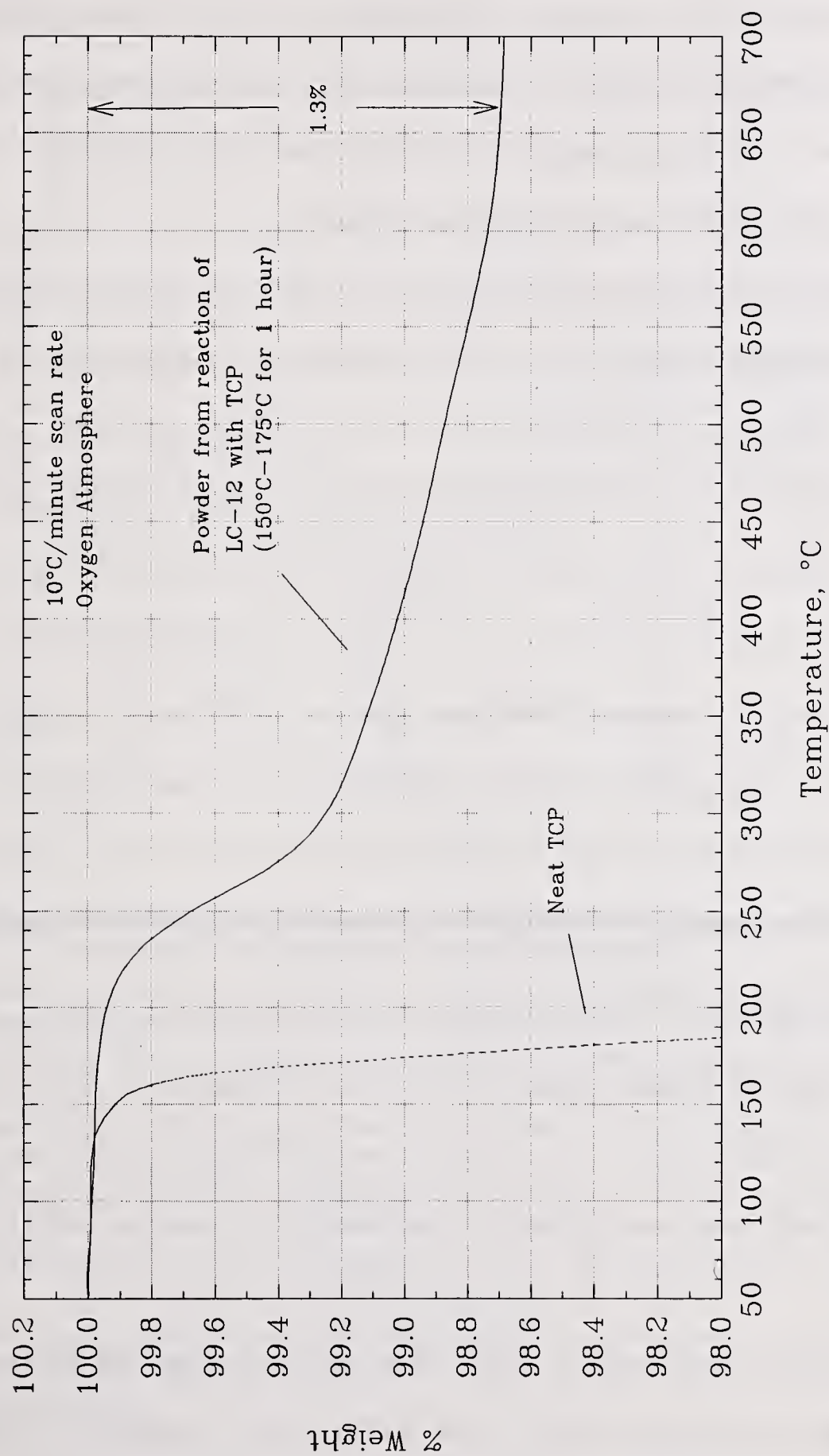
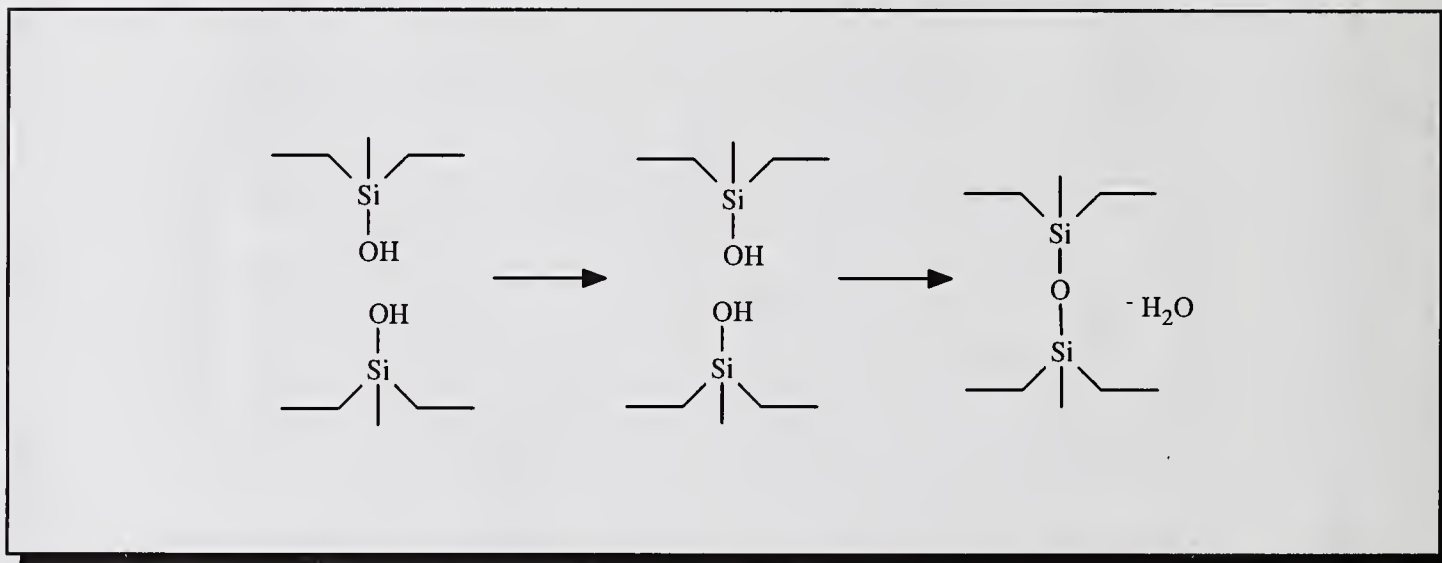


Figure 10.31 TGA Analysis of Reaction Product on Surface of Si_3N_4 Powder After Reaction with TCP

The reaction is described in a bit more detail in Iler's patent¹³³ which indicates ways of attaching organic groups to silicic acid for the purpose of separation and purification. An additional feature of the phosphate ligand on the silicic acid mentioned in the patent, is that it reduced the rate of the polymerization reaction that tends to form condensed silica structures. This may offer a clue as to why phosphates lubricate.

When two asperities approach each other and they contain surface Si-OH, the pressure and heat of the contact may cause a condensation reaction, resulting in several Si-O-Si bonds



Condensation Reaction Model for Si₃N₄ Asperities

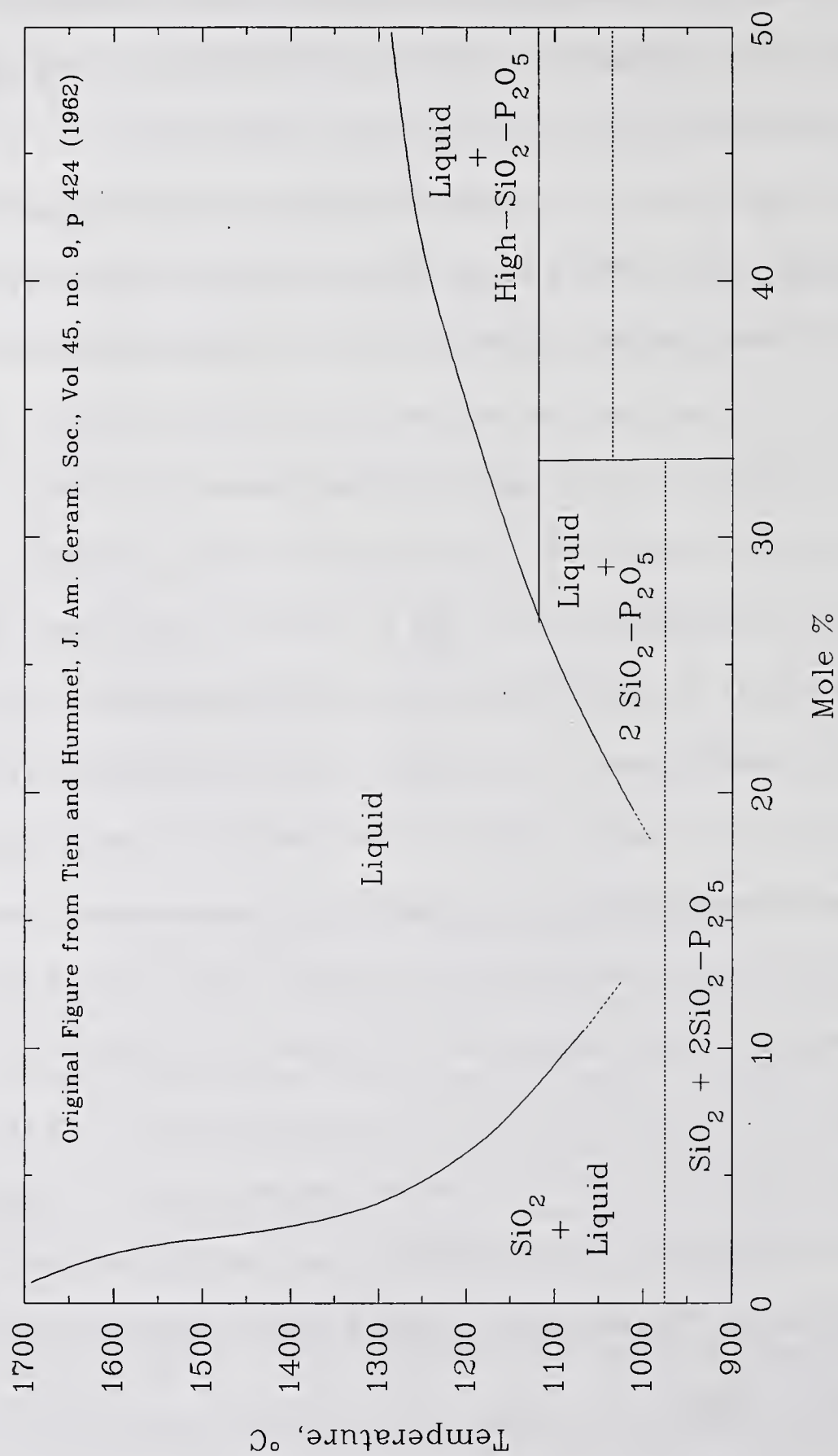
between the asperities. These strong bonds will lock the asperities together and cause high friction. When the tensile and shear forces become high enough, the asperity will break off resulting in a wear particle. This would be a very high wear process. A surface bonded phosphate might keep these condensation reactions from occurring and result in lower friction and wear.

A British patent issued in 1954^{194a} offers additional insight into what reactions may be occurring between phosphate esters and the Si₃N₄ surface. In this patent, "mixed condensates

of polymeric polyanhydric structure" are formed in reacting trimethyl phosphate and several silicon alkoxy compounds. Since silicon alkoxides can be formed on Si_3N_4 in the presence of alcohols (PPO oxidation products), this reaction may be occurring in wearing contacts. This also explains why some PPO may be necessary for lower wear rates.

At some point, however, temperatures could become so great that organic phosphate films can no longer lubricate. Some thermal decomposition of the surface organic phosphate might occur. If this happens, it is hypothesized that the remaining phosphorus oxide might form an inorganic silicophosphate glass with the surface silica as demonstrated by Eldridge^{173a}. Silicophosphate glasses can form eutectic mixtures with a lower melting point than silica as shown in Figure 10.32^{235a}. According to this figure, pure silica has a melting point of over 1700°C , while addition of as little as 15 mole % P_2O_5 can reduce the melting point to below 1000°C . In addition to lower melting point, phosphosilicate glasses also possess different physical properties than pure silica. This lower melting glass would be a protective soft layer on the surface of Si_3N_4 that would reduce point stresses at asperity contacts and reduce wear.

GPC-GFAA analysis was performed on the reaction product from a 6 μl BTF wear test to see whether any silicon-containing reaction products could be detected. The wear scar diameter (Figure 10.33) is slightly larger than that obtained from the 1.55 ml case. A large groove runs through the center of this (and also the other two) wear scar. Significant amounts of reaction product are seen surrounding the scar, with little evidence of any fluid-like film inside the scar. The friction trace is smooth and level throughout the test after an initial, brief wear-in stage.

Figure 10.32 Phase Diagram for SiO_2 - P_2O_5 System

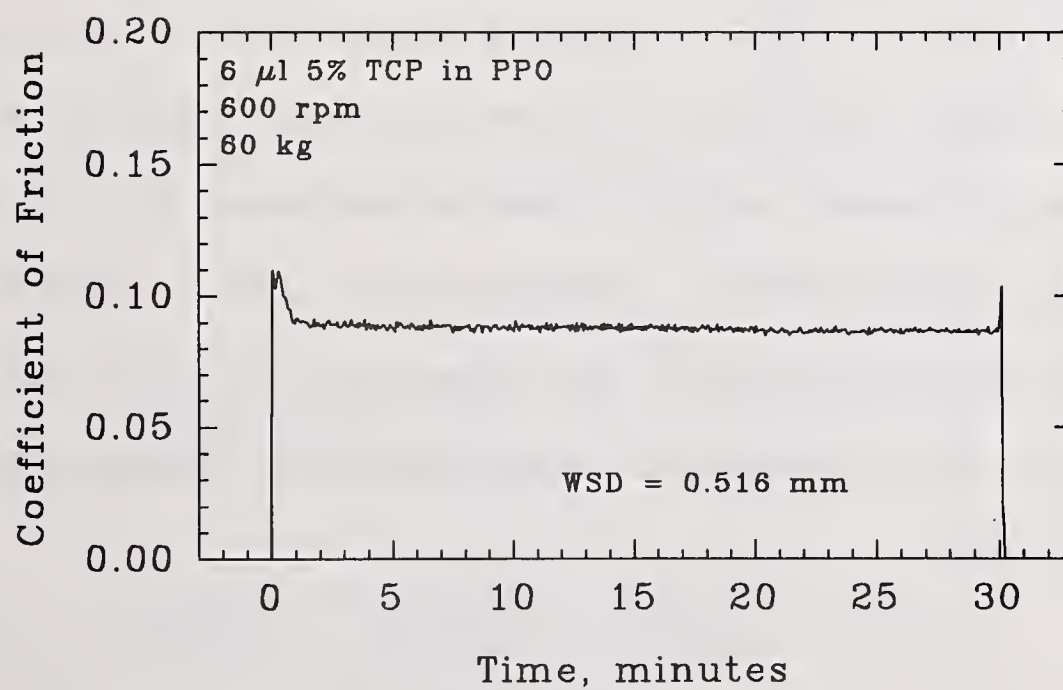
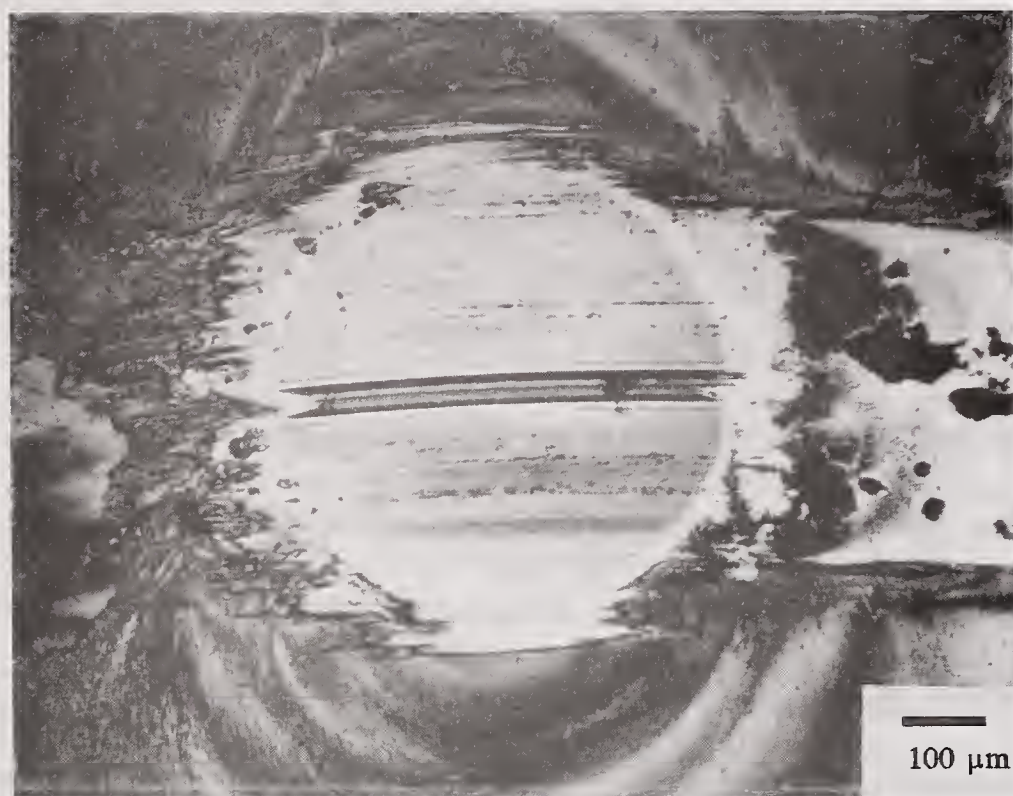


Figure 10.33 6 μl 5% TCP in PPO Lubricated Si₃N₄ BTFT Test at 60 kg: a) Optical Photomicrograph, b) Friction Trace

The GPC-GFAA analysis (Figure 10.34) indicates little besides the original PPO (higher MW peak) and TCP (lower MW peak) in the RI trace, and TCP in the UV trace. No silicon-containing species were detected. One problem noted during the analysis was that the reaction product film observed around the wear scar was not very soluble in the THF used for the extraction and GPC-GFAA analysis. A second extraction was performed using THF and ultrasonic agitation to loosen and dissolve the reaction product. This second extraction was successful in dissolving the product visible in the optical micrograph. GPC-GFAA analysis of the extracted material (Figure 10.35) indicated a single peak of material similar in MW to the original MW range of TCP (both RI and UV). A small shoulder is seen on the HMW side of this peak in UV, probably indicating a higher MW reaction product involving TCP. Again, no silicon-containing species were found.

The results indicate a fundamental difference in reaction product film for the PPO, and TCP in PPO, lubricated cases. In the case of PPO, significant amounts of THF soluble HMW reaction products are formed. If oxidation is enhanced (6 μ l test), silicon-containing species can be detected. In the case of TCP in PPO, reaction products are still formed, although at lower temperatures, due to the reduced frictional heating. However, these products are not as soluble in THF (i.e., different chemical structure), and they seem to be more associated with TCP than the PPO. This suggests more of an organic polyphosphate type of film than the organic-polymeric and organo-silicon types of films suggested in the PPO lubricated cases.

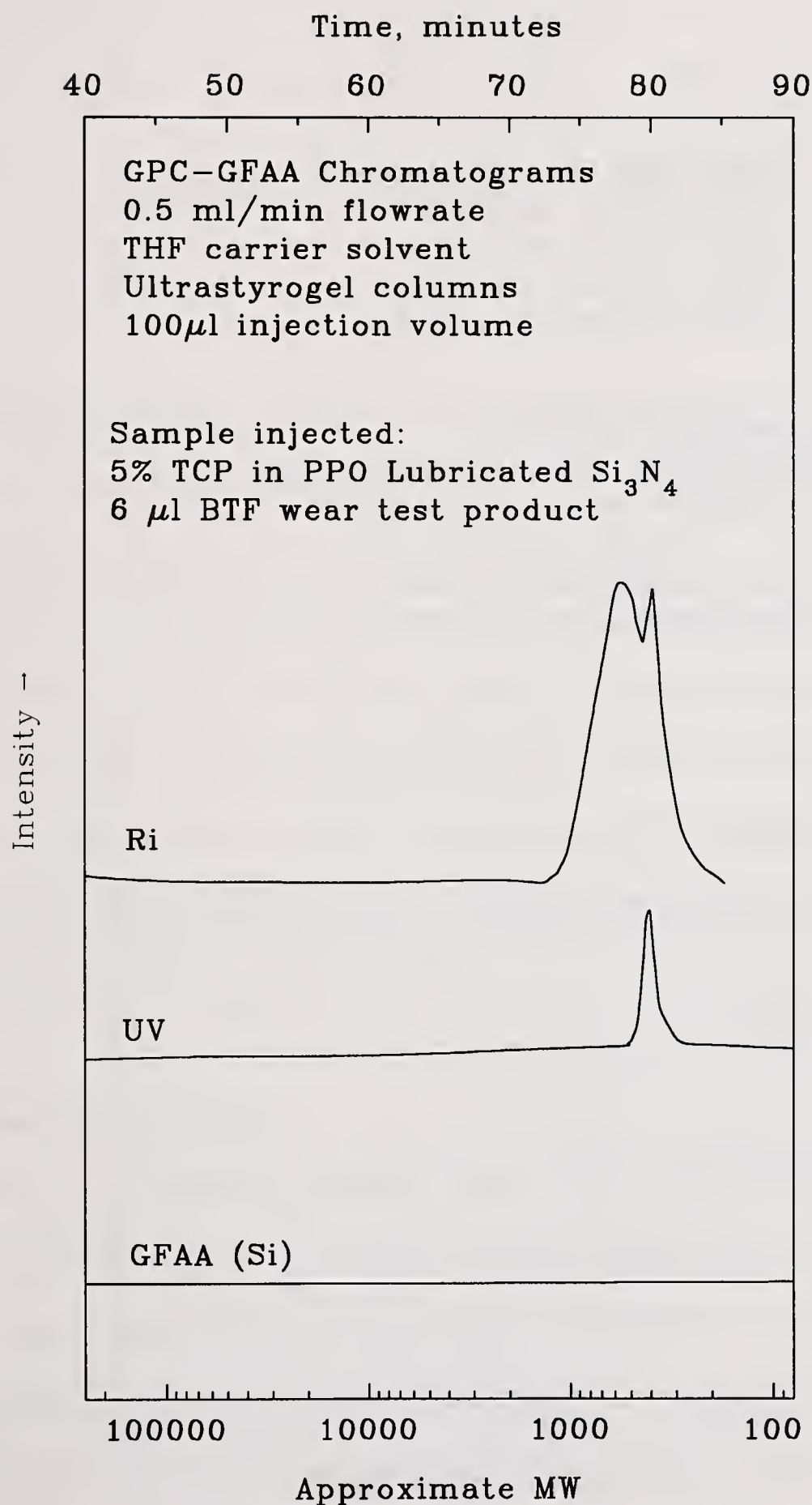


Figure 10.34 GPC-GFAA Analysis of Reaction Product from 5% TCP in PPO Lubricated Si₃N₄ BTF Test at 60 kg

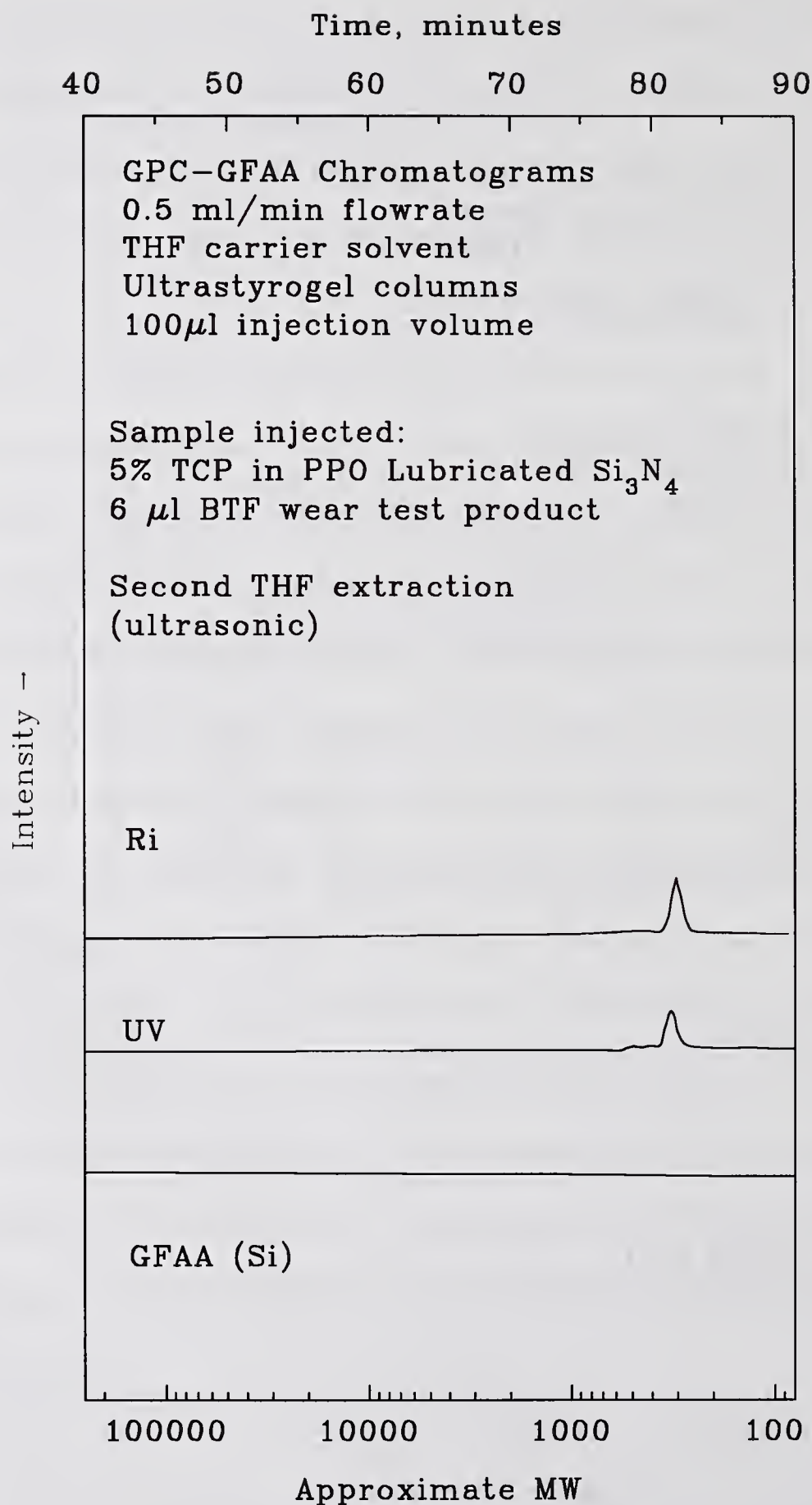


Figure 10.35 GPC-GFAA of Second Extraction (with Ultrasonic) of Same Reaction Product

Chapter 11

SURVEY OF HALOGEN CHEMISTRIES

BTF wear test data on the chlorine-containing compounds at 1% in PPO are summarized in Table 11.1 and presented graphically in Figure 11.1. Fluorinated compounds were not soluble in PPO and had to be tested neat (section 11.3).

None of the chlorine-containing compounds gave significantly lower wear and/or friction than PPO when used at 1% by weight in PPO. Two general types of chlorine-containing compounds were tested. One type were the chlorinated compounds, which included fatty acid and ester compounds. The second type were the chlorosilanes, which contained chlorine attached to a silicon atom at one end of the molecule. Both types had distinctive behavior different than the pure PPO.

11.1. Chlorinated Compounds

The four high wear data points seen in Figure 11.1 are chlorinated compounds. The wear scars were very large and very smooth, exemplified by chlorinated paraffin (Figure 11.2A). This combination of large wear scar and very smooth finish suggests some kind of chemical reaction and polishing action by the additives. The chlorinated paraffin oil produced a friction trace with a similar appearance (type I) and final friction level (0.118) as the purified paraffin oil base fluid, however, wear had increased substantially. The

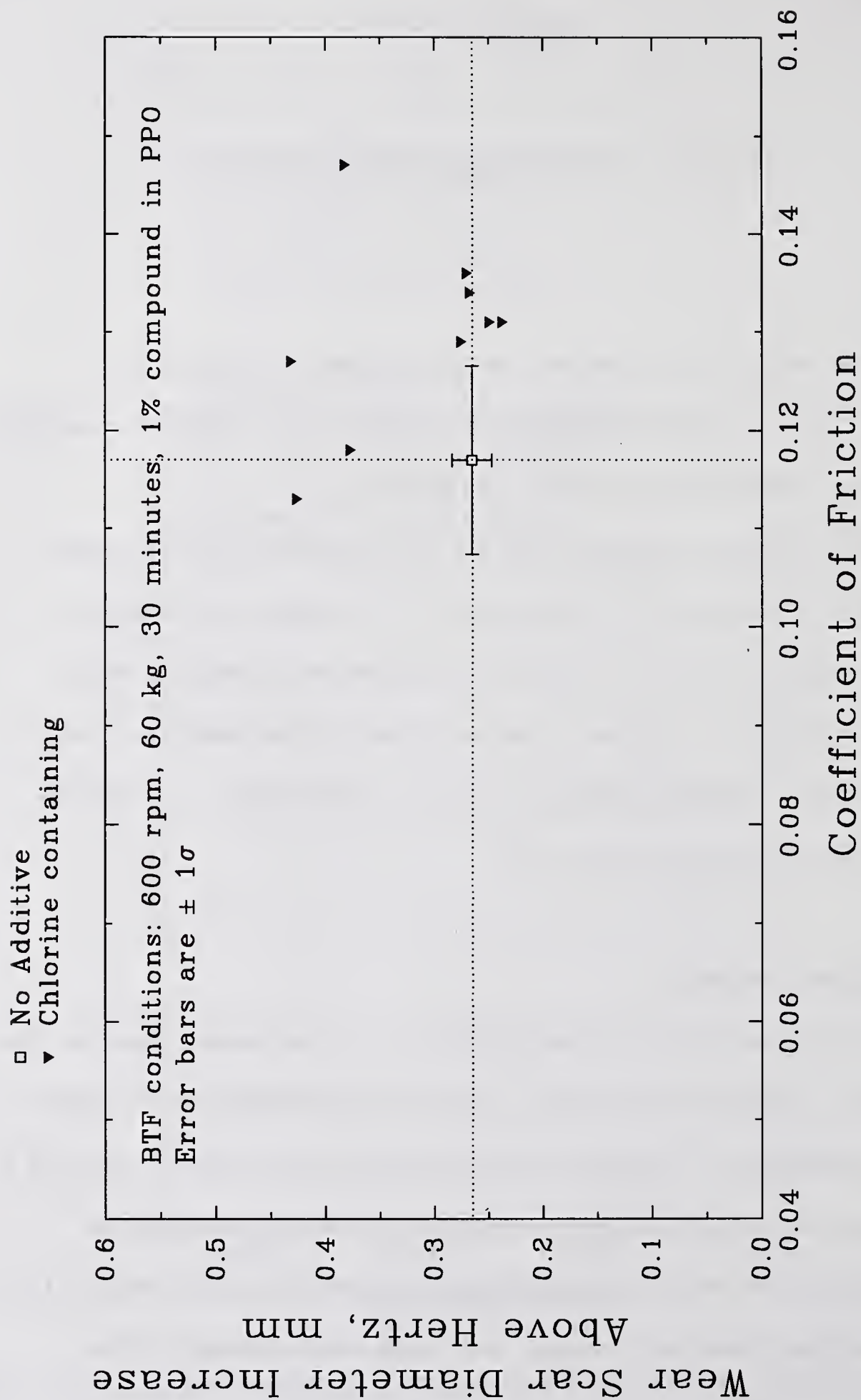


Figure 11.1 Summary Friction and Wear Data for Si_3N_4 BTF Tests on 1% Chlorine-Containing Compounds in PPO

Table 11.1
Friction and Wear Data on Selected Chlorine-Containing Model Compounds

Chemical Compound ¹ NONE (average of 16 tests)	WSD (mm) 0.645	Dia increase above Hz, mm 0.265	COF ²	Frict. Type I	Wear Scar Appearance smooth	Film in Scar? no
(BPE)dimethylchlorosilane [028]	0.617	0.237	0.131	III (2)	smooth	no
Dimethyl-n-octadecylchlorosilane [028]	0.629	0.249	0.131	III (2)	smooth	no
Methyl-n-octadecyldichlorosilane [028]	0.647	0.267	0.134	III (1)	smooth	no
n-Octadecyltrichlorosilane [028]	0.650	0.270	0.136	III (1)	smooth	no
n-Triacontyltrichlorosilane [028]	0.655	0.275	0.129	III (1)	smooth	no
Chlorinated Paraffin	0.757	0.377	0.118	I	smooth	no
Chloro-sulfurized Lard Oil	0.762	0.382	0.147	III (1)	sl. grooved	no
Chlorinated Fatty Acid (FA)	0.806	0.426	0.113	III (4)	sl. grooved	no
Chlorinated FA Ester	0.811	0.431	0.127	III (1)	smooth	no

¹ 1 wt % in purified paraffin oil

² Measured at the end of the test

All Tests conducted on CER024 NC132 Hot pressed Si₃N₄ (unless otherwise noted) at 600 rpm, 60 kg, 30 minutes, 1% additive in PPO, 21°C.

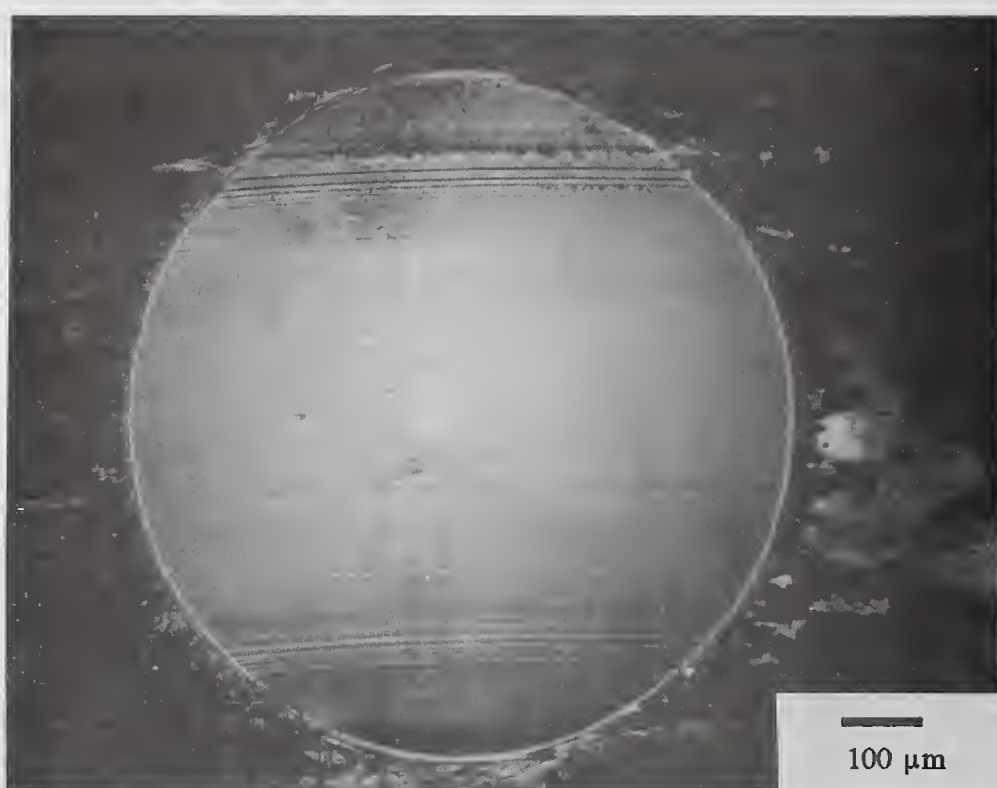


Figure 11.2 Optical Photomicrographs 1% Chlorine-Containing Compounds in PPO Lubricated Si_3N_4 BTF Tests at 60 kg: a) Chlorinated Paraffin, b) Chlorinated Fatty Acid

chlorinated fatty acid (Figure 11.2B) also exhibited a small degree of grooving within the wear scar. This type of artifact is usually associated with a corrosive type of wear mechanism and can lead to surface conformity in the wearing contact^{257a}. Chlorinated fatty acid and the other two chlorinated compounds gave type III friction behavior, but in all cases the transition to high friction occurred during the first five minutes of the wear test. No films were visible inside the wear scar for any of the chlorine-containing compounds. The apparent corrosion of the silicon nitride surface by chlorine-containing compounds agrees well with literature findings that some chlorine compounds can chemically corrode silicon nitride¹⁶⁴.

A wear test conducted at 200°C using 1% chlorinated paraffin oil in PPO had similar wear and friction to the pure PPO case. The wear scar diameter was only slightly higher at 0.923 mm. The friction type was type I.

BTF tests conducted on neat chlorinated paraffins (Table 11.2) gave low wear and friction. In both cases, no films could be observed within the wear scar.

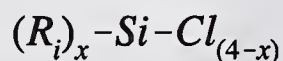
Table 11.2
BTF Test Results on Neat Chlorine-Containing Compounds

<u>Chemical Compound</u>	<u>WSD</u> <u>(mm)</u>	<u>Dia Increase</u> <u>above Hz, mm</u>	<u>COF</u>
None	0.647	0.267	0.113
Chlorinated Paraffin [389 cSt]	0.402	0.024	0.079
Chlorinated Paraffin [121 cSt]	0.402	0.024	0.076

It is not obvious why 1 % chlorinated paraffin would have a corrosive effect with Si_3N_4 , yet neat chlorinated paraffin would lubricate, but there are some possible explanations. The behavior of the interfacial reaction product film will be dictated in part by its environment. This environment includes the surface and the bulk fluid. The properties of the fluid, such as surface wetting and solubility (of the film in the fluid) may therefore influence the lubricating ability of the film. It is also possible that there is an impurity in the chlorinated paraffin that is responsible for the low wear. In the neat fluid, it is at a high enough concentration to be effective. At the lower dilution in PPO it may fall below its effective concentration range.

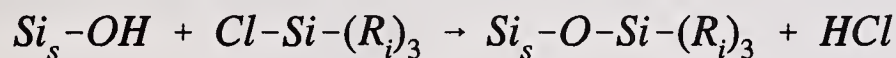
11.2. Chlorosilanes

The chlorosilanes used in this study were silicon containing compounds with organic groups to give them solubility in PPO, and chlorine functionalities attached to the silicon to allow them to react with and bond to the Si_3N_4 surface. The general structure of the chlorosilanes used is:



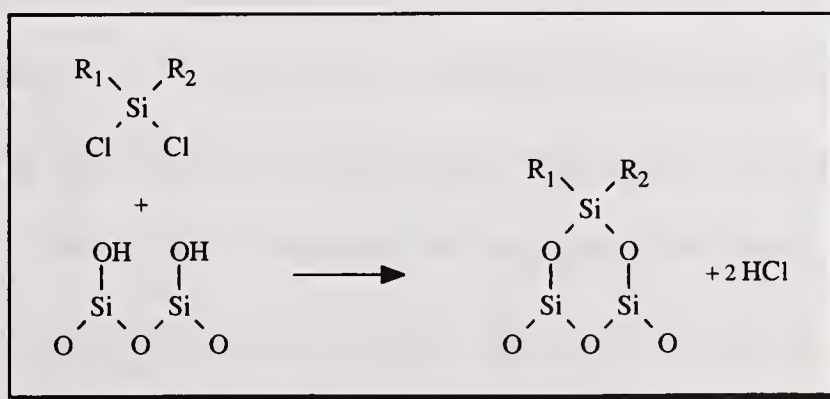
Where the i represents different organic functional groups. In most cases, R_1 is a long chain hydrocarbon (C_{18} for example), and R_2 and R_3 are usually methyl groups. If three R groups are present, then only one chlorine compound can be present on the silicon (e.g., dimethyl-n-octadecylchlorosilane). If only two R groups are present, two chlorine groups can be present (e.g., methyl-n-octadecyldichlorosilane). If only one R groups are present, three chlorine groups can be present (e.g., n-octadecyltrichlorosilane).

Originally, these compounds were selected for wear testing because they are known to react with silica surfaces²⁴⁵. In fact, these compounds are used commercially to modify the surface chemistry of silica for chromatographic applications. The reaction is considered to proceed through the silicon hydroxide on the surface of silica:



Where the subscript s indicates that the silicon atom is on a surface and contains bonds to other atoms. The result is an organophilic modification of the silica surface instead of the hydrophylic one originally present. It was thought that if this reaction could take place in the contact junction, a protective organophilic layer could be formed "in-situ" to lubricate the surface. This was the reason that the chlorosilanes were used in this study.

One variable in studying this class of compounds is the effect of number of chlorines on the reactions. It is thought that if two chlorine groups are present, they can cause two bonds to be formed with silica. It is generally considered that this does not occur with the same silicon atom (i.e., geminal hydroxyl groups), but instead with neighboring silicon atoms (i.e., vicinal hydroxyl groups) such as:



Possible Dichlorosilane Reaction Mechanism

It might also be possible that they could form a bridge between silicon atoms on two different particles thus bonding the particles together. Another thought was that this mechanism might be beneficial in bonding two slightly separated sides of a crack in silica together, possibly arresting propagation of the crack. Since it was not known beforehand which reaction would be most beneficial, several different chlorosilanes were used. Initially, they were all used at 1% in PPO.

Dimethyl-n-octadecylchlorosilane (Figure 11.3) seemed to provide lubrication for the first 2 minutes of the test, then a transition to high friction occurred that looked like the friction for pure PPO. The final wear scar diameter was not much smaller than that of pure PPO. Methyl-n-octadecyldichlorosilane (Figure 11.4) and n-octadecyltrichlorosilane (Figure 11.5) provided lubrication for only the first minute of the test. Another monochlorosilane was used to see if the long chain organic group made a difference in lubrication performance. The compound (p-t-butylphenethyl)dimethylchlorosilane succeeded in protecting the Si_3N_4 surface for only 2 minutes (Figure 11.6).

There are several reasons why these compounds might only work for a few moments before failing. First, they might be so reactive that they are depleted in this time. Second, they might only work in a limited temperature range, and when the surface of the Si_3N_4 gets too hot, they fail. Third, they may fail because we wear and/or react through the oxide layer necessary for this reaction. Finally, PPO may produce (oxidation and degradation) reaction products that compete with the chlorosilanes for the critical surface sites.

SEM analysis was performed on the wear scar from a wear test conducted using 1% dimethyl-n-octadecylchlorosilane in PPO. The wear scar (Figure 11.7A) is very smooth,

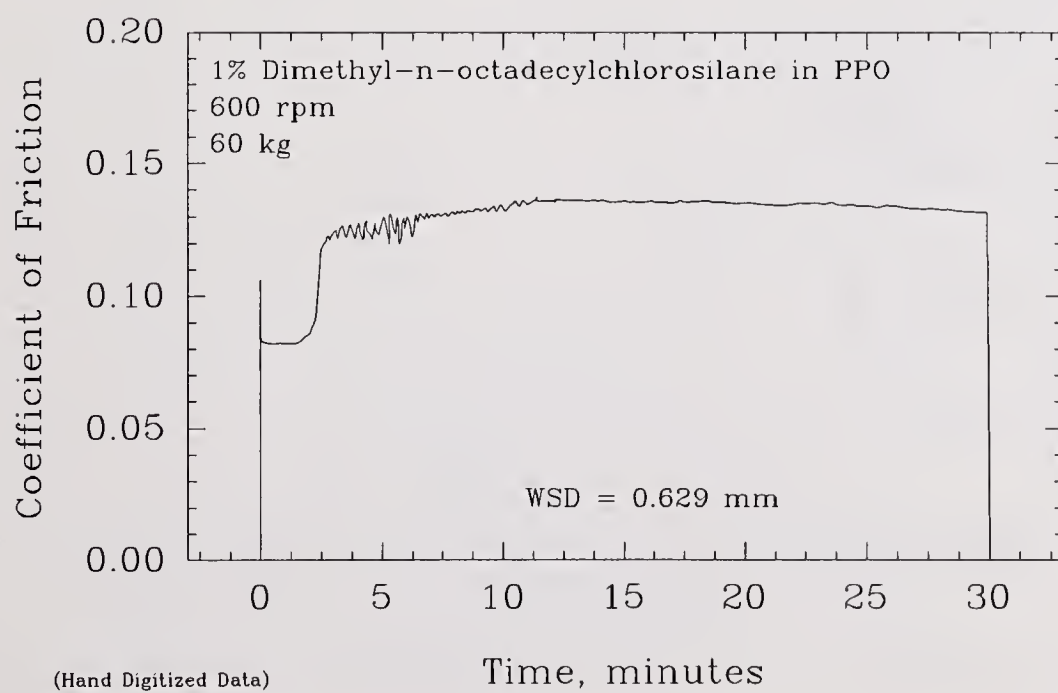


Figure 11.3 1% Dimethy-n-Octadecylchlorosilane in PPO Lubricated Si_3N_4 BTf Test at 60 kg: a) Optical Photomicrograph, b) Friction Trace

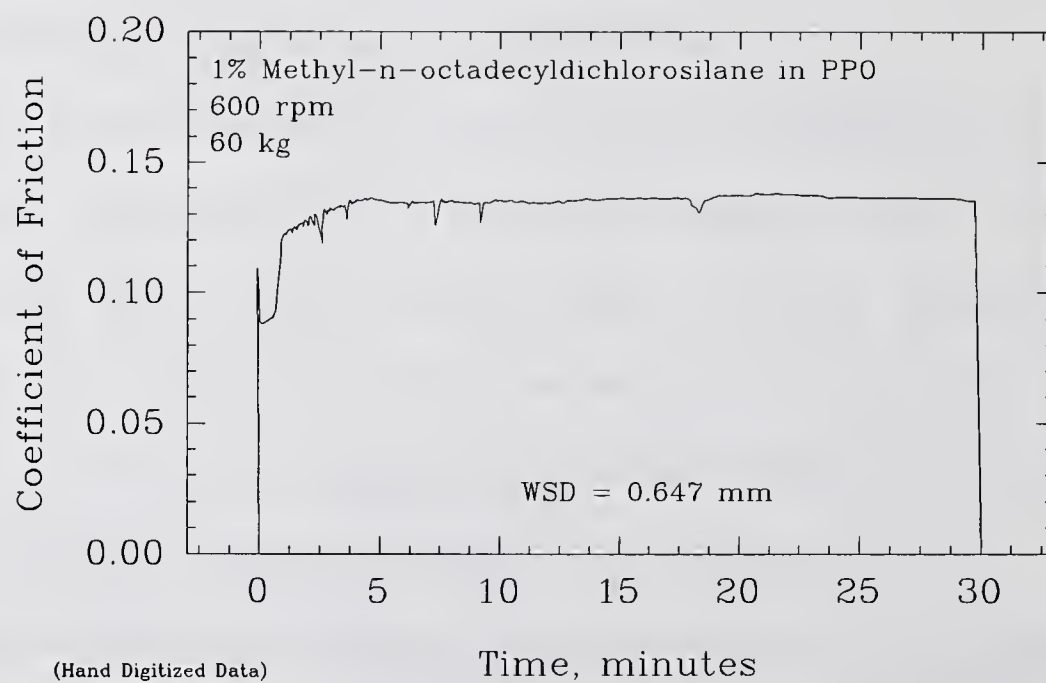
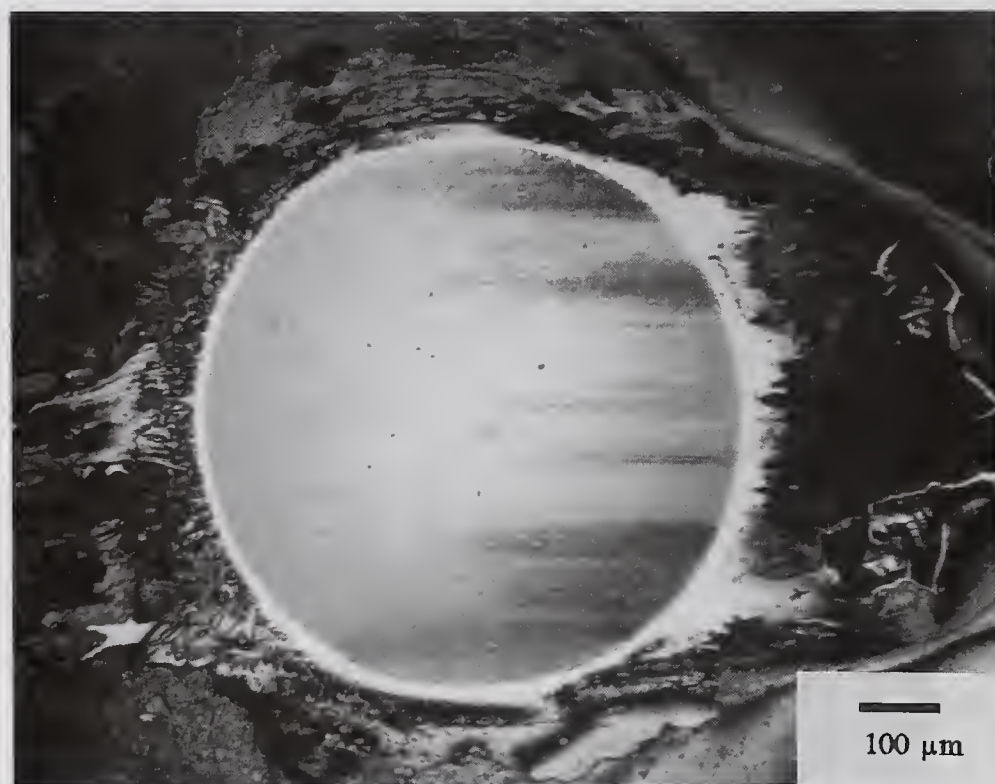


Figure 11.4 1% Methyl-n-Octadecyldichlorosilane in PPO Lubricated Si_3N_4 BTFT Test at 60 kg: a) Optical Photomicrograph, b) Friction Trace

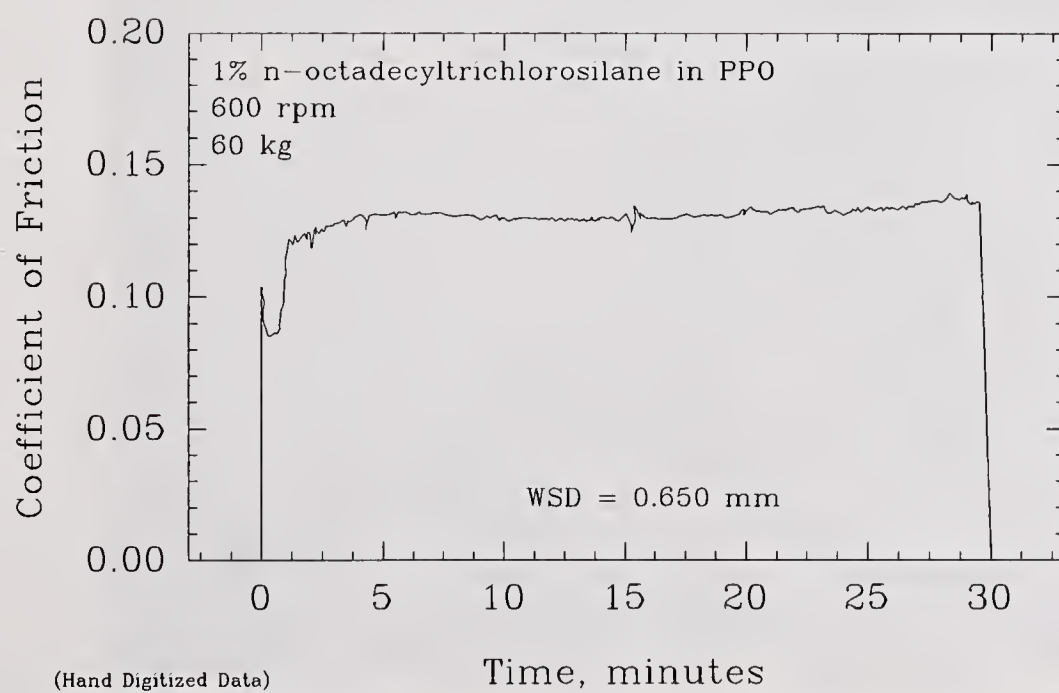
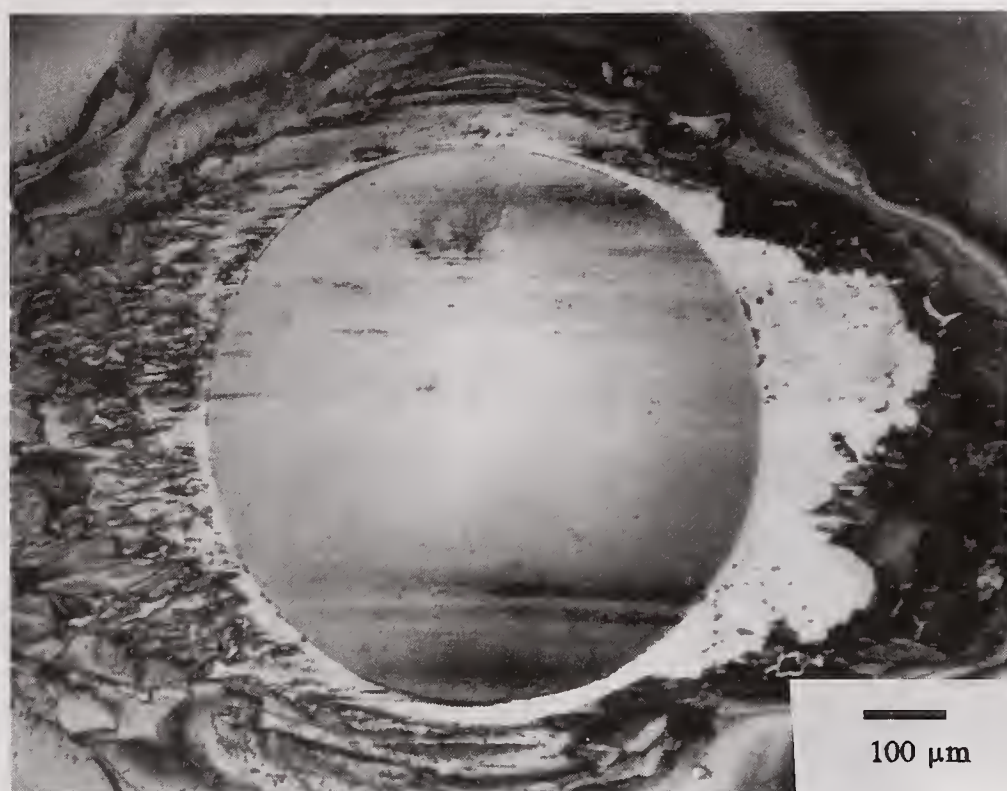


Figure 11.5 1% n-Octadecyltrichlorosilane in PPO Lubricated Si_3N_4 BTF Test at 60 kg: a) Optical Photomicrograph, b) Friction Trace

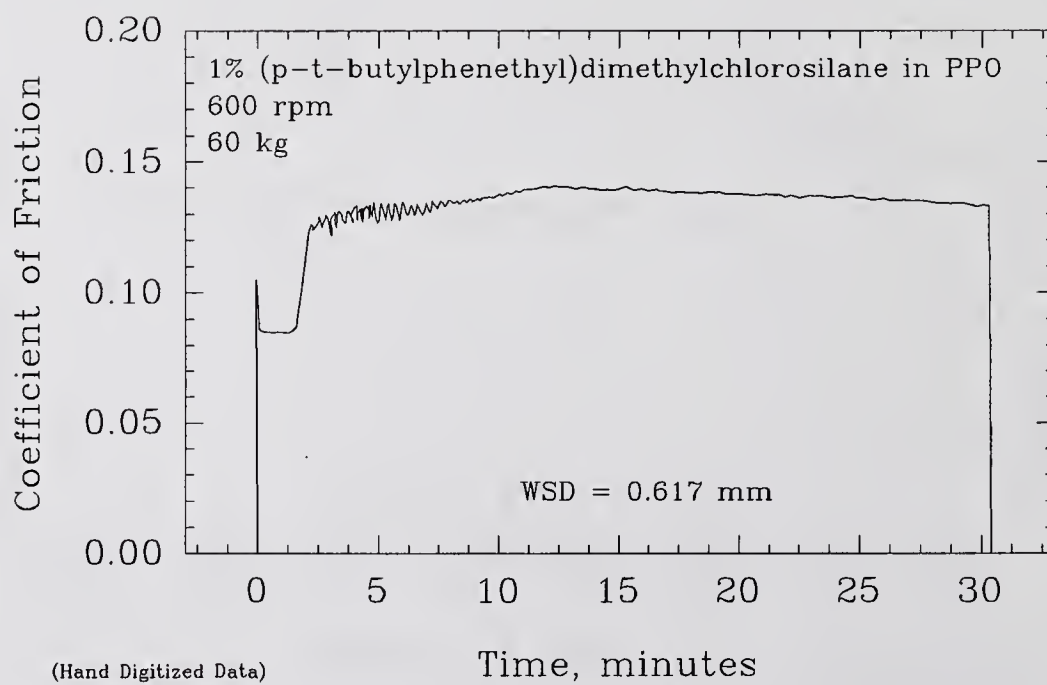
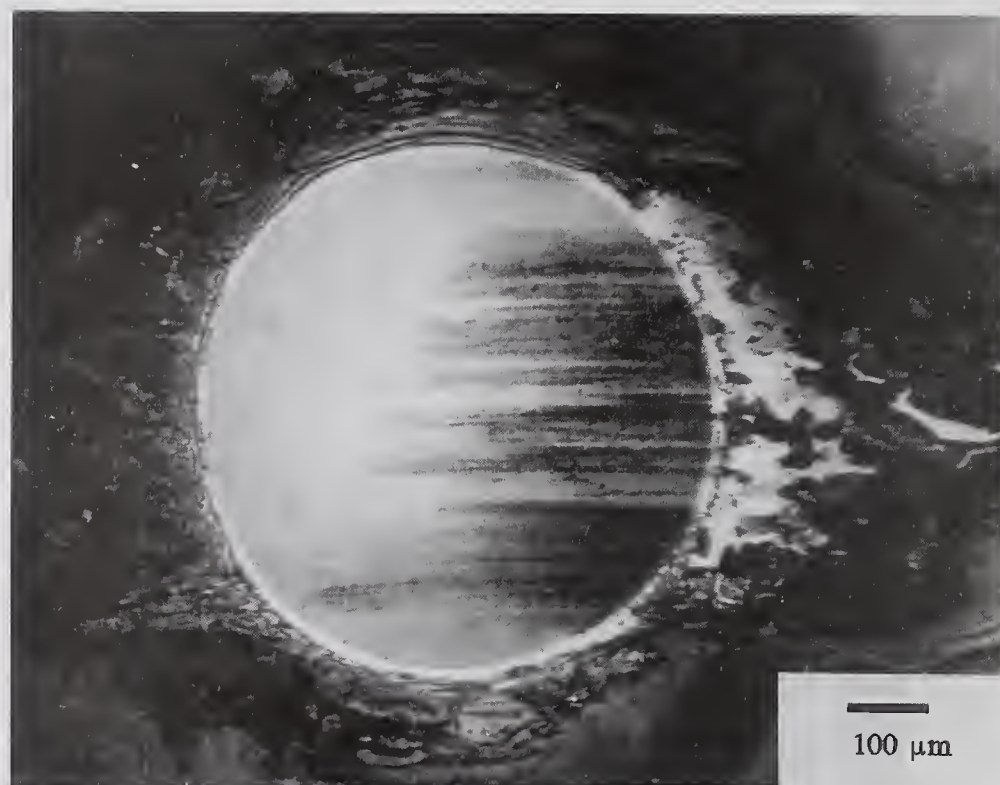


Figure 11.6 1% (p-t-butylphenethyl)dimethylchlorosilane in PPO Lubricated Si_3N_4 BTF Test at 60 kg: a) Optical Photomicrograph, b) Friction Trace

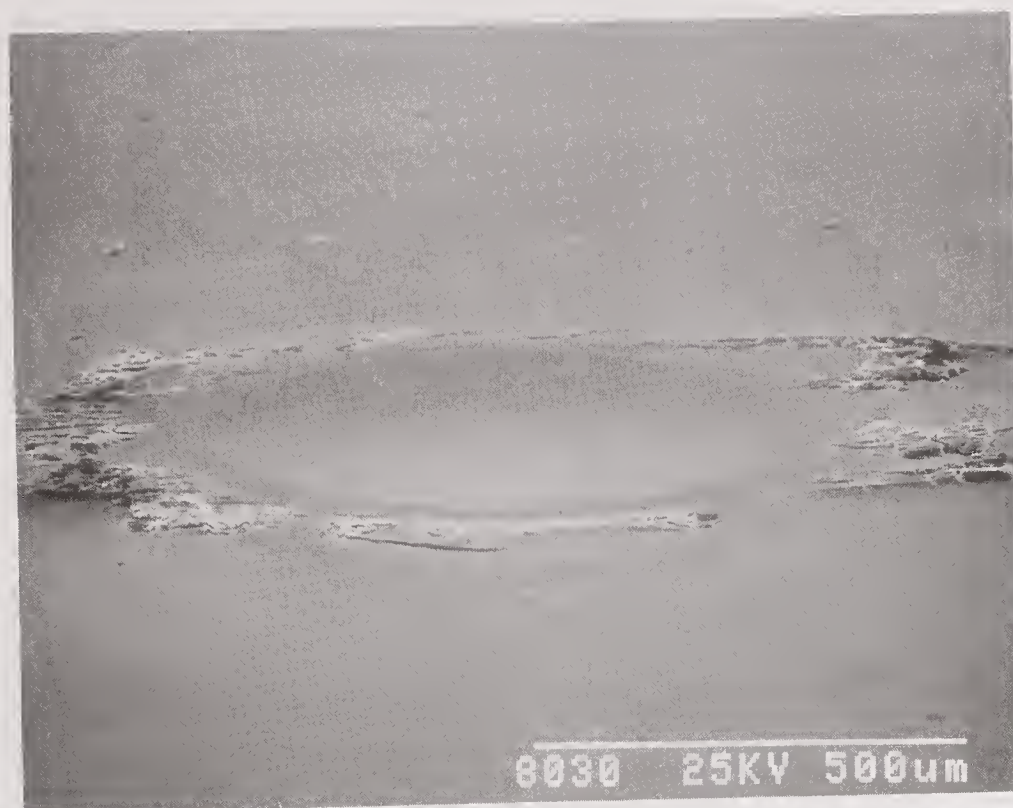


Figure 11.7 75° Tilt SEM Photomicrographs of Flat from 1% Dimethy-n-Octadecylchlorosilane in PPO Lubricated Si_3N_4 BTF Test at 60 kg: a) Wear Scar, b) Entrance Region

with deposits surrounding the worn surface. Most of the accumulation is in front of (Figure 11.7B), and behind (Figure 11.8), the wear scar. The exit debris consists of the usual twin wakes seen in many tests, but it also contains small "islands" of product in the center of the wake (Figure 11.8). These "islands" are quite unusual in shape (Figure 11.9) and seem to reflect an oil insoluble reaction product that has condensed out as it cooled on leaving the wear scar. EDX analysis of these products indicated they contained a higher concentration of chlorine.

Octadecyltrichlorosilane was also tested neat to see if it would lubricate in the absence of PPO (Figure 11.10). Initially, friction was low ($\mu=0.060$); however, in the course of the test, several large spikes were seen. This information, coupled with the observation of pits in the wear scar, indicate possible grain pullout during the test. This may indicate that the compound is too reactive and attacks the grain boundaries during the test. The oval shape of the wear scar indicates that substantial wear has occurred on the top ball.

11.3. Fluorine-Containing Compounds

The bond strength data indicates that Si-F bonds are stronger than Si-Cl bonds. This suggests that if the chlorine-containing compounds are not reactive enough, fluorinated compounds might be more successful. BTF wear tests were conducted on several neat fluorine containing compounds to investigate this possibility. Results of these tests are summarized in Table 11.3

All of the fluids tested had type II friction traces, but in these cases, the friction levels were relatively high. Wear scars were grooved or roughened, and none of the fluids gave

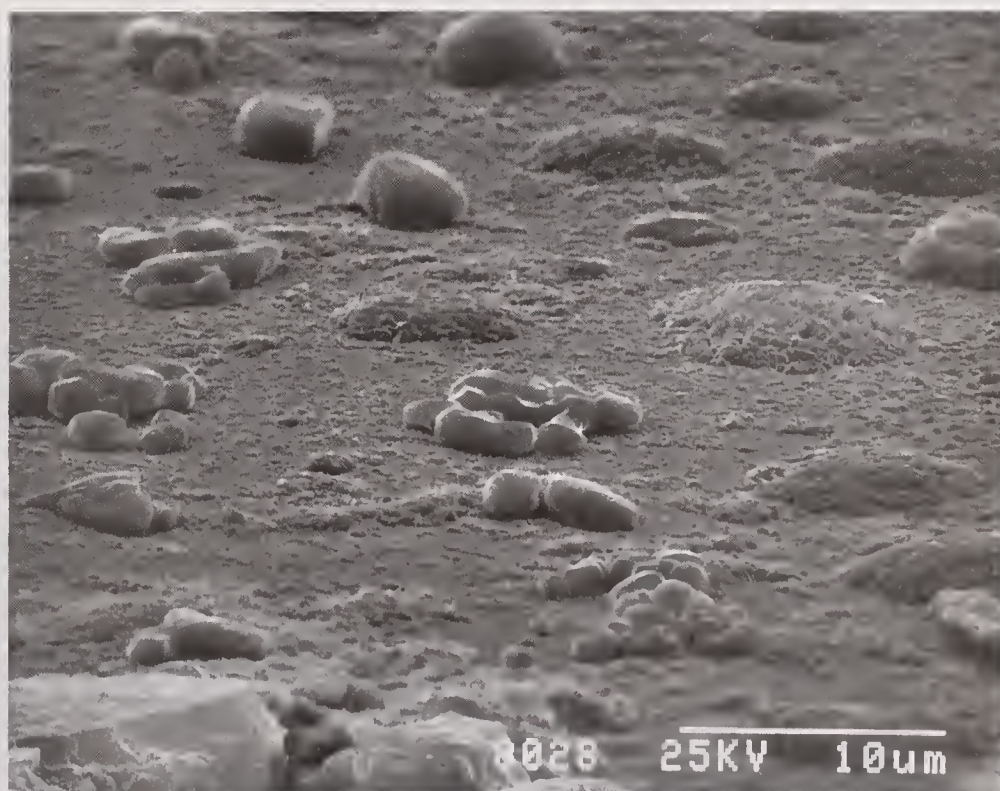
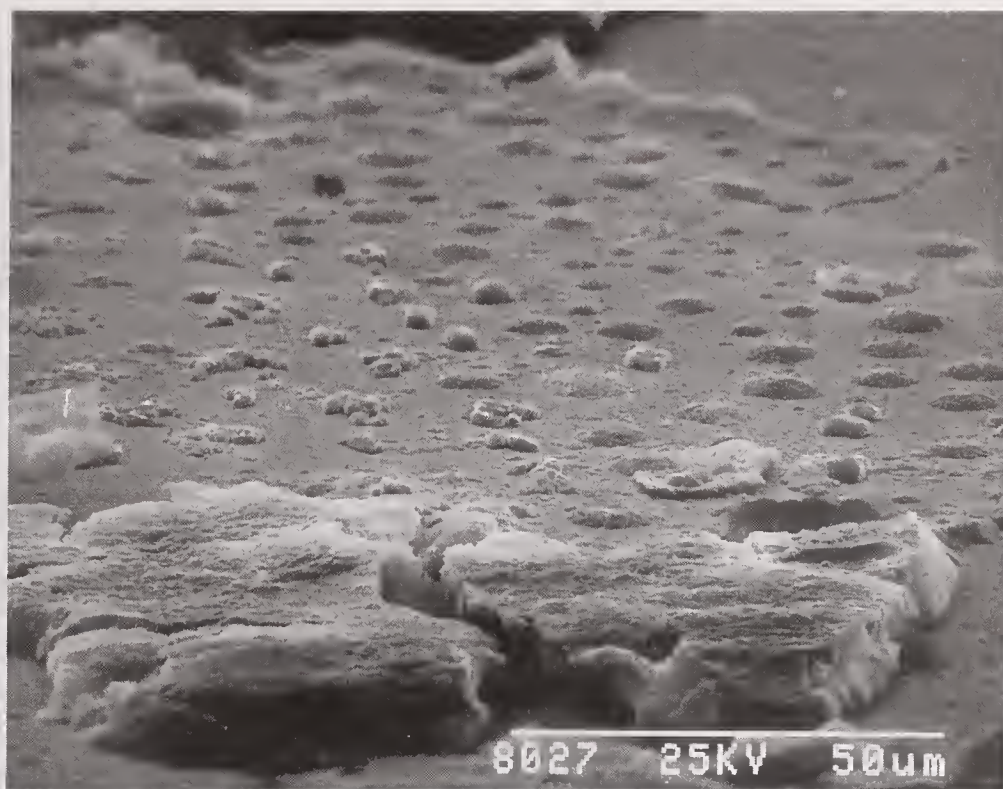


Figure 11.8 75° Tilt SEM Photomicrographs of Flat from 1% Dimethy-n-Octadecylchlorosilane in PPO Lubricated Si_3N_4 BTF Test at 60 kg: a) Exit Region, b) Exit Region (Higher Magnification)



Figure 11.9 0° Tilt SEM Photomicrographs of Flat from 1 % Dimethy-n-Octadecylchlorosilane in PPO Lubricated Si_3N_4 BTF Test at 60 kg: a) Exit Region, b) Exit Region (Higher Magnification)

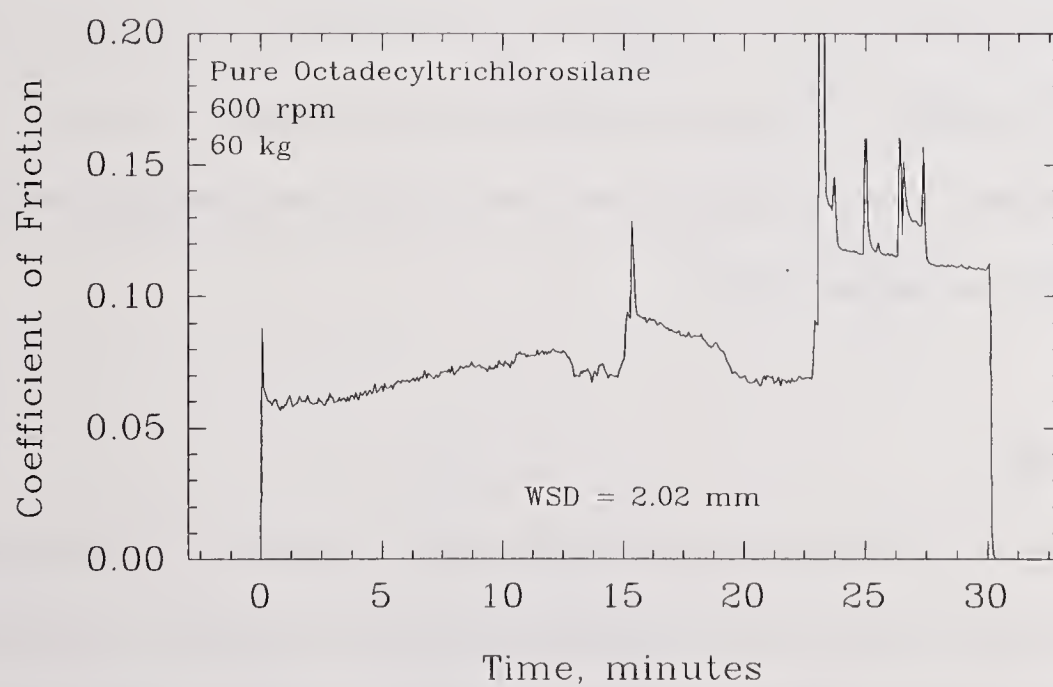
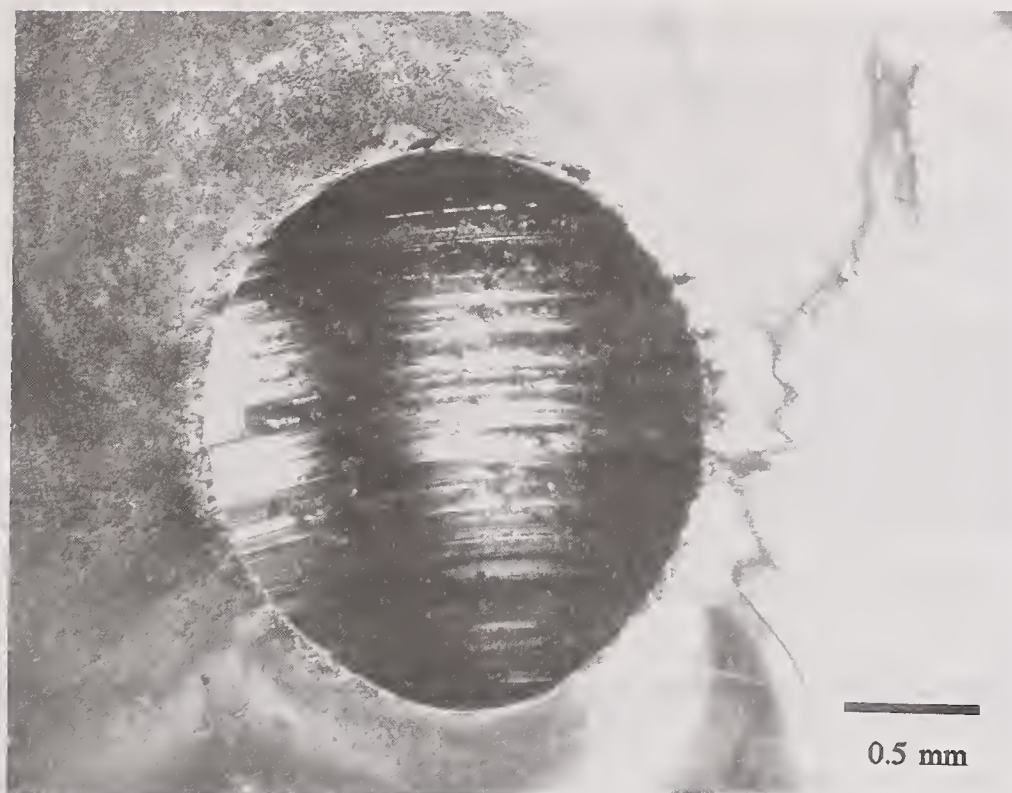


Figure 11.10 Neat n-Octadecyltrichlorosilane Lubricated Si_3N_4 BTFT Test at 60 kg: a) Optical Photomicrograph, b) Friction Trace

Table 11.3
BTF Test Results on Neat Fluorine-Containing Compounds

<u>Chemical Compound</u>	<u>WSD (mm)</u>	<u>Dia increase above Hz, mm</u>	<u>COF¹</u>
NONE [028] (average of 5 tests)	0.662	0.282	0.127
Perfluoropolyether [85 cSt]	0.509	0.128	0.105
Perfluoropolyether [18 cSt]	0.582	0.202	0.116
Polymethyltrifluoropropylsiloxane	0.634	0.254	0.088
Perfluoropolyethermonoacid	0.670	0.290	0.107
Polychlorotrifluoroethylene [27 cSt]	0.700	0.320	0.107
Perfluoropolyethermonoalcohol	0.800	0.420	0.101

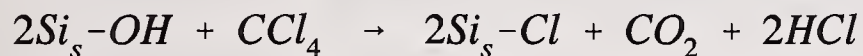
All tests conducted on CER028 NBD100 HIP'd Si₃N₄ at 600 rpm, 60 kg, 30 minutes, 1.5 ml neat fluid, 21°C

very low wear. The two perfluoropolyethers were identical except for chain length; therefore, there seems to be a slight viscosity effect in these tests. No films could be observed inside the wear scar; however, some reaction product deposits could be seen outside the wear scars. The chlorotrifluoroethylene polymer fluid contained both chlorine and fluorine molecules, but it too had high wear and grooving of the wear scar suggestive of corrosion of the surface. Fluorinated monoacids and monoalcohols were tested to see if they might work because normal (hydrogen based) monoalcohols and monoacids were successful. The fluorinated ones did not work.

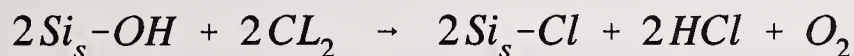
11.4. Summary

As a class, halogenated compounds were not very successful in lubricating Si₃N₄. The only exceptions were the very viscous neat chlorinated compounds. In the case of 1% chlorinated compound in PPO, many of the compounds give accelerated wear. This may be

due to reaction of the chlorine with the silica surface of Si_3N_4 . For example, Iler¹³⁸ and Hair¹⁰⁷ noted the reaction between silica and carbon tetrachloride.



This reaction was noted to occur at temperatures above 350°C (the decomposition temperature of CCl_4). Hair also proposed that Cl_2 dehydroxylates the silica surface according to the following reaction.



This is thought to actually be a two step reaction consisting of an initial (rate limiting) decomposition of Cl_2 to form Cl radical. These types of homolytic decomposition reactions to form chlorine radicals are probably rare for the particular chlorinated compounds tested, but no literature evidence was found to suggest alternative reactions that might take place.

Chapter 12

SURVEY OF SULFUR CHEMISTRIES

The sulfur-containing compounds gave a wide range of response depending on the specific compound used. Individual data is summarized in Table 12.1, and presented graphically in Figure 12.1.

The data shown in Figure 12.1 seems to naturally cluster into three distinct groups. Each of these groups will be discussed in more detail. One cluster, near the PPO friction and wear data represents compounds that have little beneficial affect on friction or wear. For the sake of discussion, these are termed sulfur-containing compounds. A second cluster of two compounds represent compounds that contain both molybdenum and sulfur and exhibit very low friction but moderate to high levels of wear (like PPO). These are termed Mo-S containing compounds. The third cluster represents sulfur containing compounds that are classified as detergent type compounds. These compounds are normally put into lubricant formulations to reduce deposit formation on surfaces and neutralize acids that may be generated through lubricant oxidation. They are all able to lubricate Si_3N_4 at concentration of 1% in PPO under the conditions of these tests.

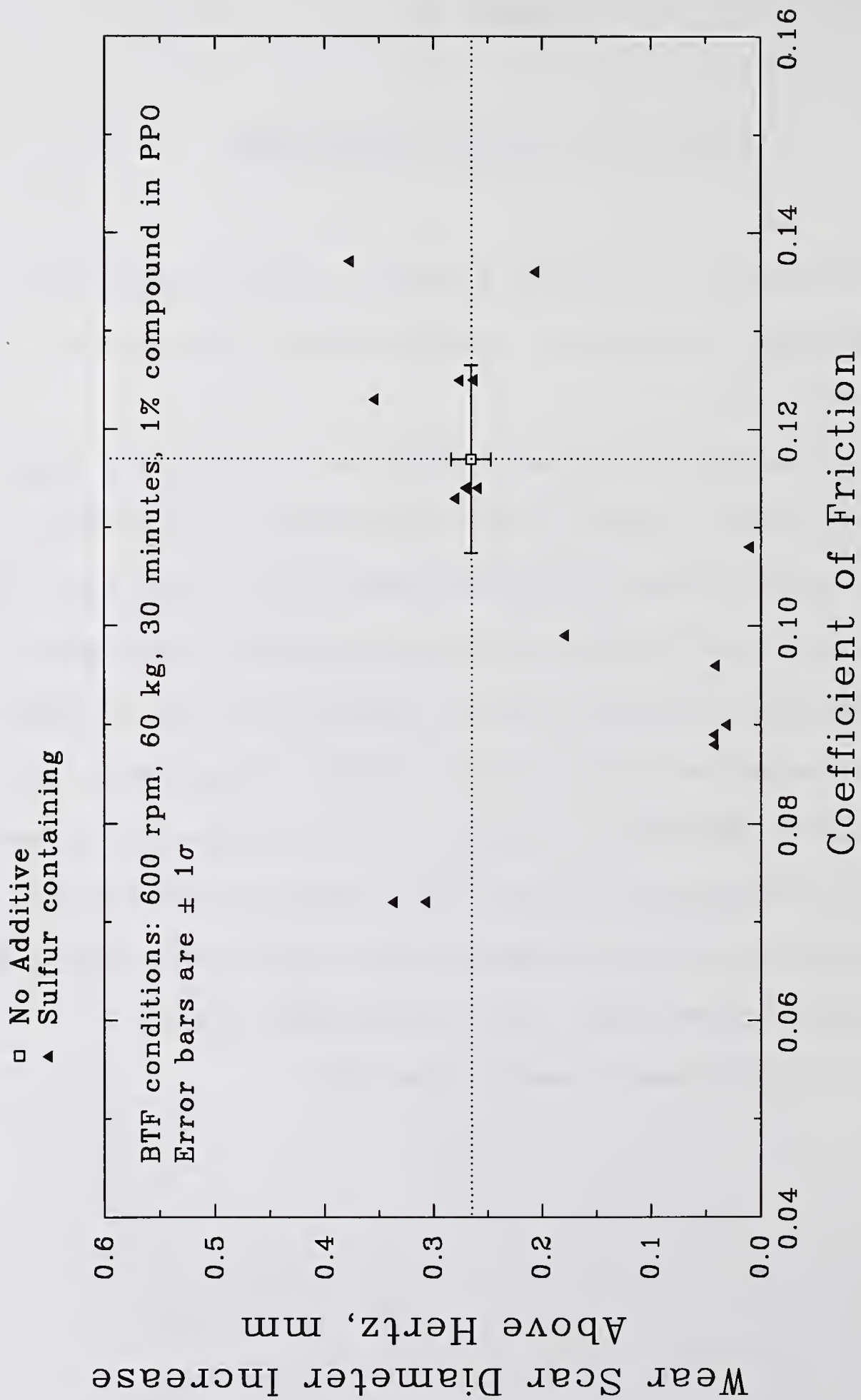


Figure 12.1 Summary Friction and Wear Data for Si_3N_4 BTF Tests on 1% Sulfur-Containing Compounds in PPO

Table 12.1
Friction and Wear Data on Selected Sulfur-Containing Model Compounds

Chemical Compound ¹ NONE (average of 16 tests)	WSD (mm) 0.645	Dia increase above Hz, mm 0.265	COF ²	Frict. Type ³ I	Wear Scar Appearance smooth	Film in Scar? no
Magnesium Sulfonate (overbased)	0.391	0.011	0.108	IV	smooth	yes
Magnesium Sulfonate (overbased) [028]	0.412	0.032	0.090	IV	smooth	yes
Calcium Phenate (overbased)	0.422	0.042	0.096	II	smooth	yes
Calcium Sulfonate (low base)	0.423	0.043	0.089	II	smooth	yes
Zinc Dinonylnaphthalene Sulfonate blend	0.423	0.043	0.088	II	grooved	yes - uneven
Octadecyl Disulfide	0.560	0.180	0.099	I ⁴	blotchy	yes
Benzyl Disulfide	0.587	0.207	0.136	I ⁴	smooth	streaked
Antimony dialkylidithiocarbamate	0.640	0.260	0.114	I	smooth	no
Octadecyl Sulfide	0.644	0.264	0.125	I	smooth	no
Sulfurized Hydrocarbon	0.651	0.271	0.114	I	smooth	no
Methylene bis(dibutylidithiocarbamate)	0.657	0.277	0.125	I	smooth	no
Jojoba Oil	0.661	0.281	0.113	I	smooth	no
Organo Molybdenum Dithiocarbamate	0.688	0.308	0.072	II	blotchy	yes - plastic
Sulfur-Molybdenum Compound	0.718	0.338	0.072	II	blotchy	yes - plastic
Lead Dialkylidithiocarbamate [028]	0.724	0.344	0.165	I	smooth	no
Sperm Whale Oil	0.735	0.355	0.123	III (2)	smooth	no
Sulfurized Fatty Oil	0.758	0.378	0.137	III (2)	smooth	no

¹ 1 wt % in purified paraffin oil

² Measured at the end of the test

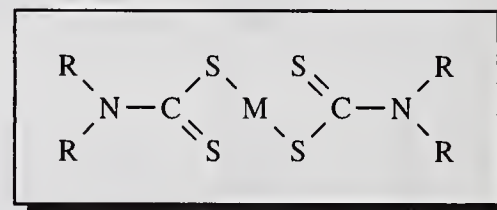
³ The number in parenthesis refers to the time until transition in minutes.

⁴ Spikes observed in friction trace

All Tests conducted on CER024 NC132 Hot pressed Si₃N₄ (unless otherwise noted) at 600 rpm, 60 kg, 30 minutes, 1% additive in PPO, 21°C.

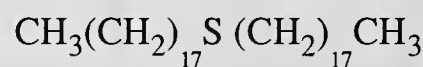
12.1. Sulfur Containing Compounds

Five compounds fall within the PPO repeatability envelope and in all respects behave like pure PPO without any additive. These include two dithiocarbamates which are commonly used as antioxidant/EP agents in iron-based metal systems. Other compounds include sulfurized hydrocarbon, octadecyl sulfide, and johoba oil (a natural sulfur containing oil extracted from the jojoba plant and intended as a replacement for sperm whale



Dithiocarbamate

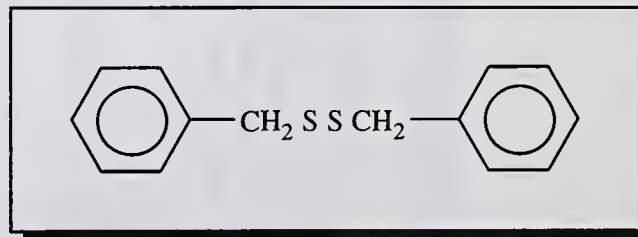
oil). All five of these compounds exhibit type I friction behavior (just like pure PPO), and no visible films in the wear scars. In the same region, with slightly higher wear, we find two compounds with type III friction behavior and higher wear than pure PPO: sperm whale oil, and sulfurized fatty oil. These compounds seem to lubricate initially, but they have a transition to



Octadecyl Sulfide

higher friction during the test. In the case of the sulfurized fatty oil and sperm whale oil, this takes less than two minutes. No films are visible in the wear scars after the test.

Two compounds with slightly smaller wear scar diameters than PPO include two disulfides. Benzyl disulfide (or dibenzyl disulfide) provides a small amount of antiwear effect, although the final coefficient of friction was quite high by the end of the test. The friction trace



Benzyl Disulfide

(Figure 12.2B) contains several spikes at the beginning of the test that may be evidence of partial lubrication. By the end of the test, these spikes are gone. The wear scar (Figure 12.2A) has a streaky partial film on both sides of the central region. The film does not cover the central region. The other disulfide (octadecyl disulfide) has a slightly better antiwear performance. The friction trace

(Figure 12.3B) contains many of the same spikes seen in the benzyl disulfide case, but the alkyl disulfide maintains these spikes

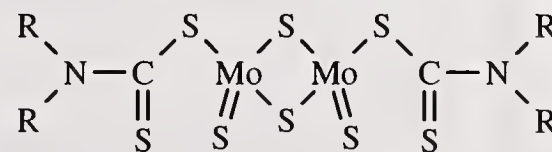


Octadecyl Disulfide

throughout the test. The film in the wear scar (Figure 12.3A) is also more coherent, and covers the entire wear scar. The film has more of a spotty or blotchy appearance than the aromatic disulfide.

12.2. Mo-S Containing Compounds

The second class of sulfur compounds is distinguished by the very low friction coefficient, but moderately high levels of wear and type II friction behavior. These are the only two examples of type II friction behavior giving moderate levels of wear, slightly higher than PPO itself. Both of these compounds are organic molybdenum-sulfur compounds. The interior of the wear scar for these tests (Figure 12.4) contains a somewhat blotchy surface that could be some kind of solid



Organomolybdenum Dithiocarbamate

film. EDX analysis confirmed the presence of molybdenum. The overlap of Mo and S

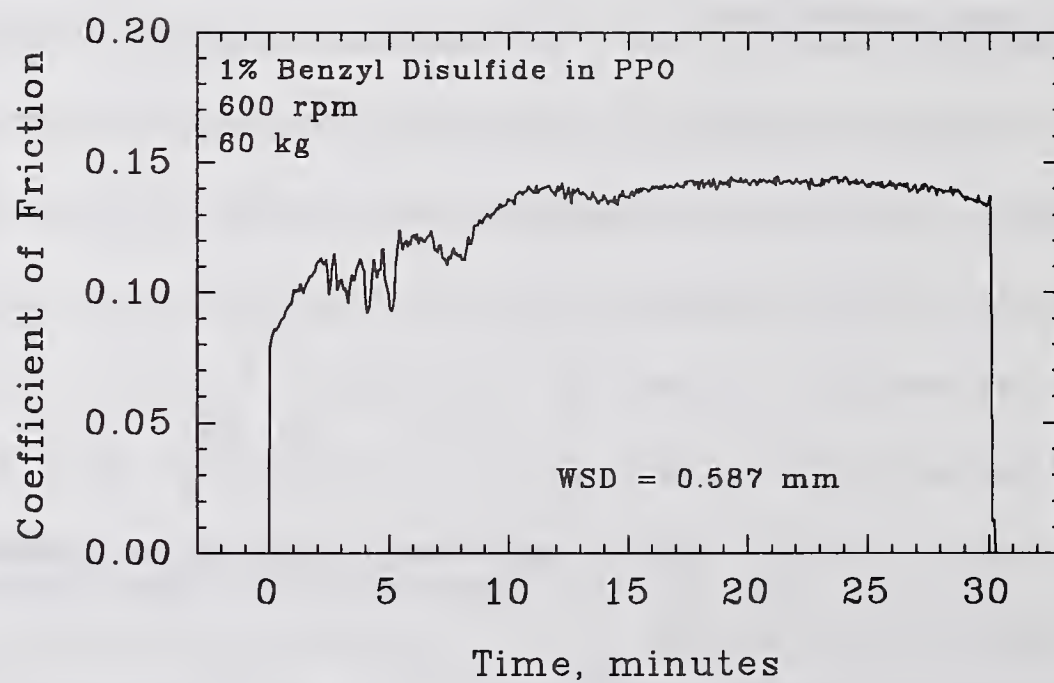
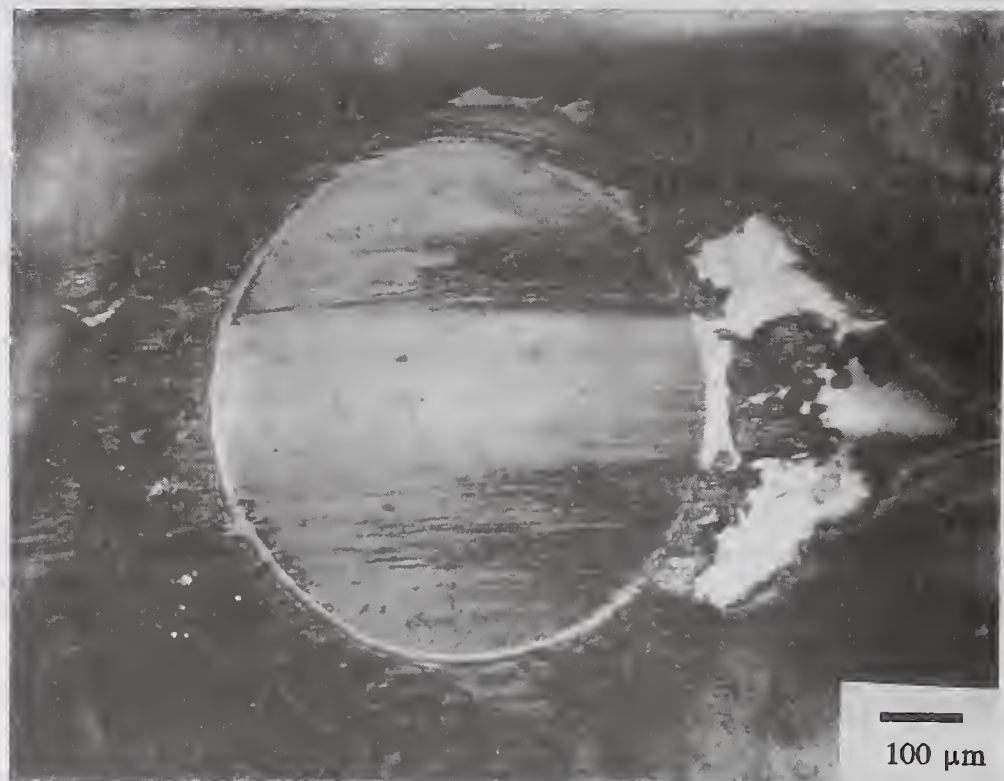


Figure 12.2 1% Benzyl Disulfide in PPO Lubricated Si_3N_4 BTF Test at 60 kg: a) Optical Photomicrograph, b) Friction Trace

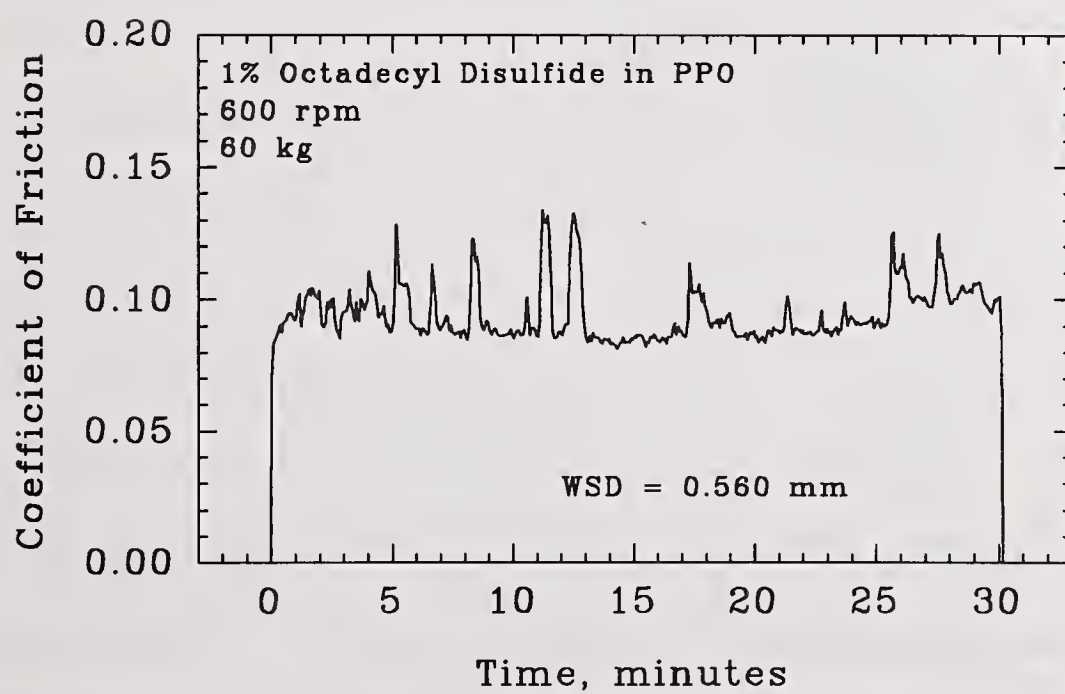
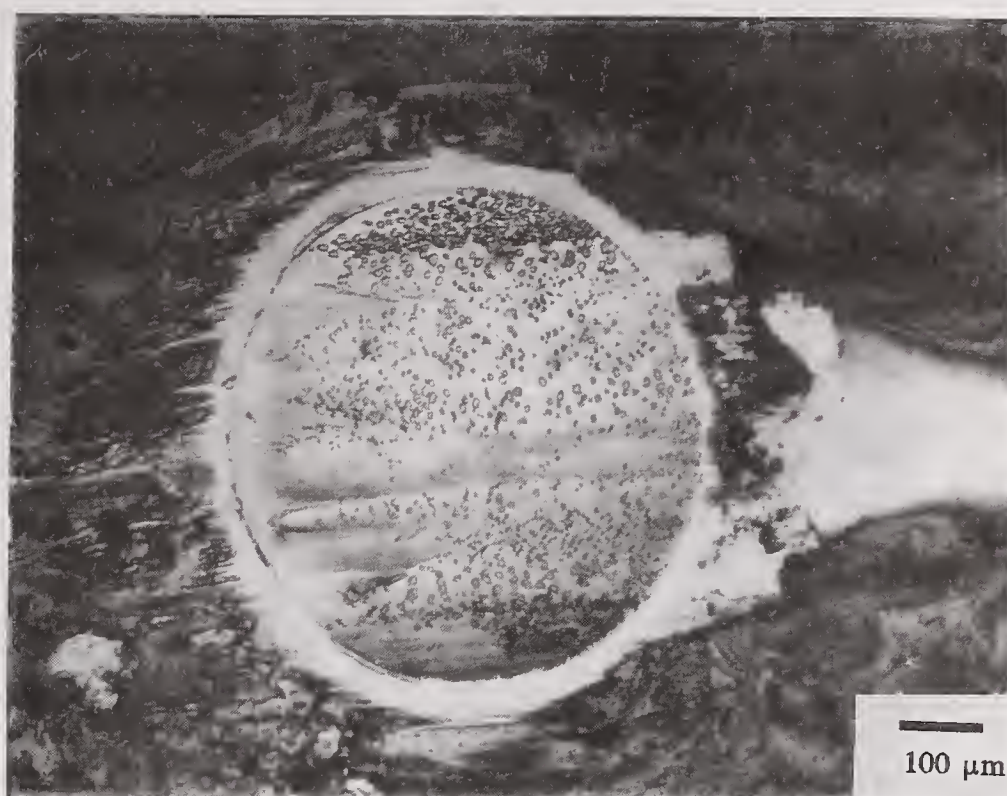


Figure 12.3 1% Octadecyl Disulfide in PPO Lubricated Si₃N₄ BTF Test at 60 kg: a) Optical Photomicrograph, b) Friction Trace

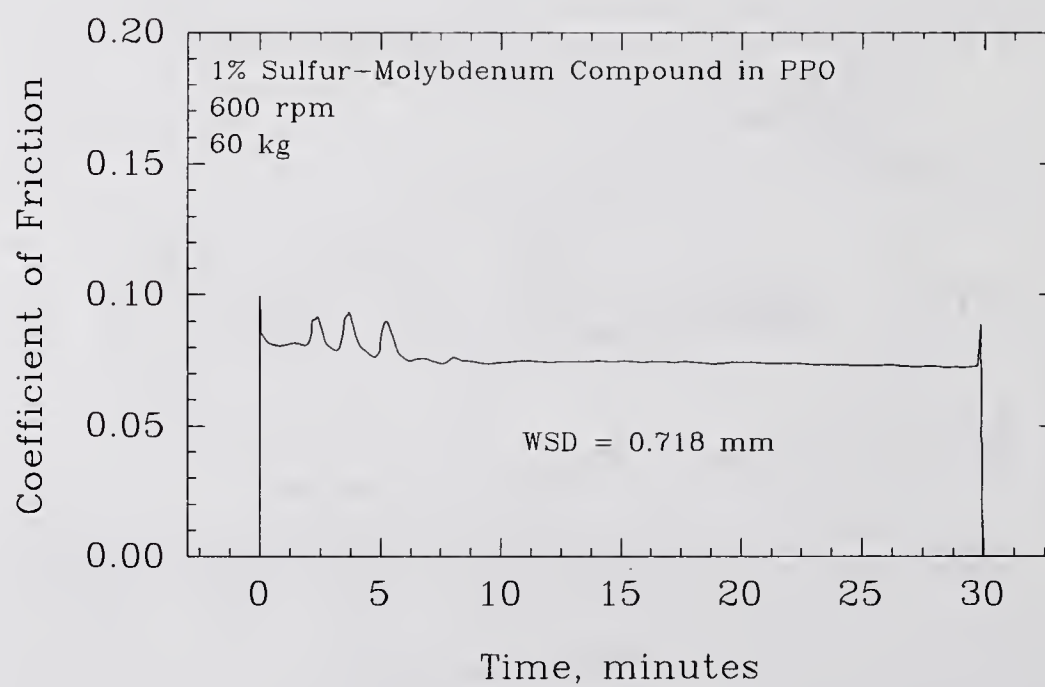


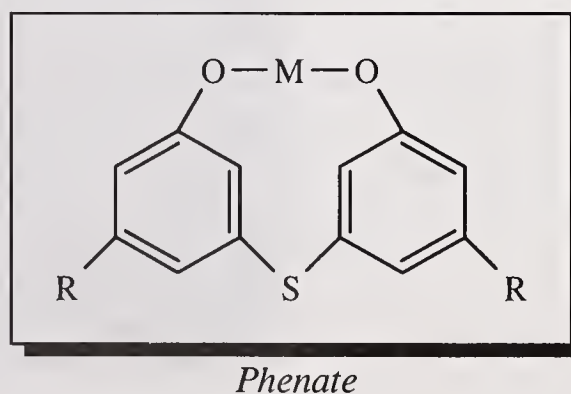
Figure 12.4 1% Sulfur-Molybdenum Compound in PPO Lubricated Si₃N₄ BTFT Test at 60 kg:
a) Optical Photomicrograph, b) Friction Trace

peaks did not allow definitive confirmation of the presence of S, however the ratio of intensity of the Mo peak at 17.48 keV to the Mo/S peak at 2.31 keV suggested the presence of sulfur. It is thought that the organic Molybdenum/sulfur compounds may be decomposing in the high temperatures of the contact to provide MoS₂ solid lubricating films with low friction. Raman spectroscopy was attempted to try to detect MoS₂; however no identifiable signal could be found due to the strong fluorescence of the silica surface layer.

12.3. Sulfur Containing Detergent Type Compounds

The third class of sulfur compounds (S containing detergent compounds) is distinguished by low wear and somewhat lower friction than pure PPO and includes both sulfonates and phenates. They exhibit either type II or type IV friction behavior, and films within the wear scar. All of the sulfur containing detergents contain metals (Ca, Mg, or Zn) incorporated through oxygen linkages. In the case of the overbased detergents, calcium or magnesium carbonates and hydroxides have also been incorporated into the micellar^{239a} structure of the compound to neutralize acidic reaction products of lubricant degradation.

Calcium phenate exhibits low wear and type II friction behavior. Friction is smooth and low throughout the test. According to an optical photograph (Figure 12.5A) calcium phenate has a somewhat streaky organic-looking film, and has some deposit surrounding the wear scar that outlines the lubricant flow field. An SEM photomicrograph



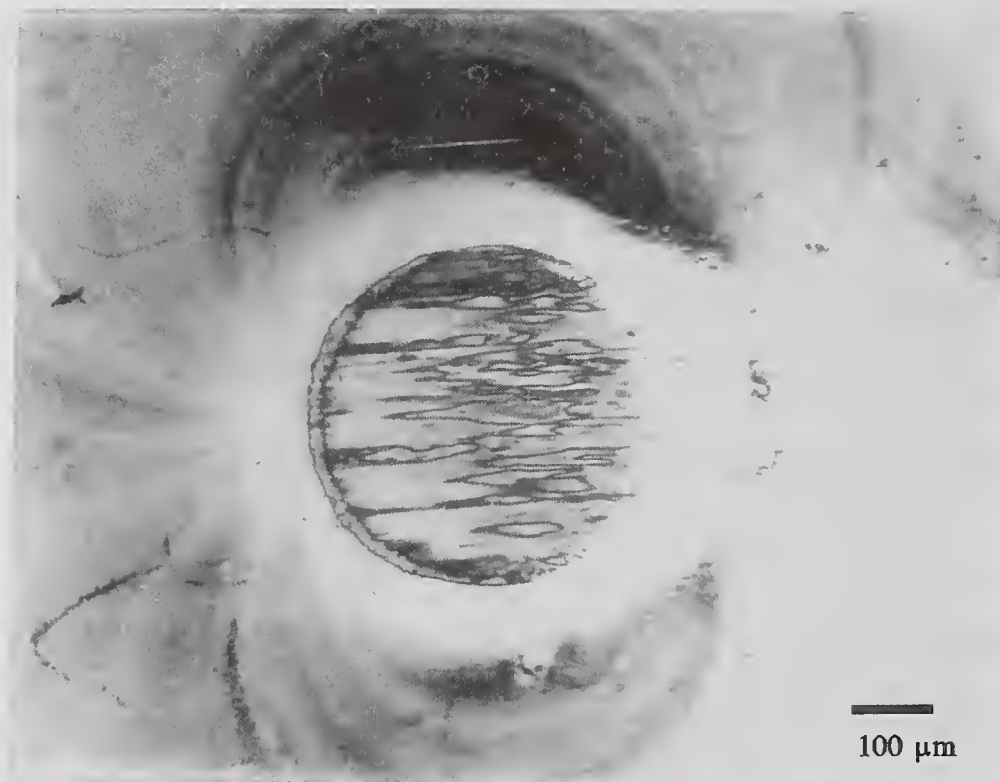


Figure 12.5 1% Calcium Phenate in PPO Lubricated Si_3N_4 BTF Test at 60 kg: a) Optical Photomicrograph, b) SEM Photomicrograph at 75° Tilt

(Figure 12.5B) indicates the film is actually very continuous, and amorphous-looking. EDX analysis of the wear scar film (Figure 12.6) indicates a buildup of Ca in the film. Sulfur does not seem to be present in any appreciable quantity. The Ca metal can come from the overbasing component and/or the phenate molecule. The lack of sulfur suggests that if the phenate molecule is involved, some kind of decomposition has taken place within the contact junction resulting in deposition of the Ca (probably as an oxide).

The optical micrograph of the (overbased)

Mg sulfonate lubricated test (Figure 12.7) shows a more solid-looking film, and contains little deposit around the scar. The friction behavior is type IV.

This friction behavior exhibits an initial, gradual,

increase in friction to steady state ($\mu=0.108$

in this case). The wear scar is only 0.391

mm, 0.011 mm above the Hertzian contact

diameter. Optically, there appears to be a

coherent, thick coherent film covering the

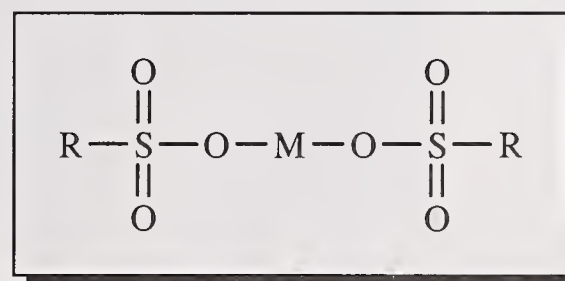
surface of the wear scar. Outside the wear

scar, there is very little evidence of any deposit usually associated with wear tests conducted

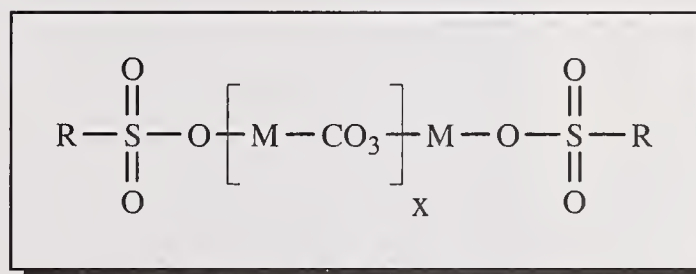
in the presence of PPO. This is not surprising since sulfonates are used in oil formulations

as detergents. The lack of deposit is a testament to the detergent capability of these

compounds in addition to the antiwear capability with Si_3N_4 .



Sulfonate



Overbased Sulfonate

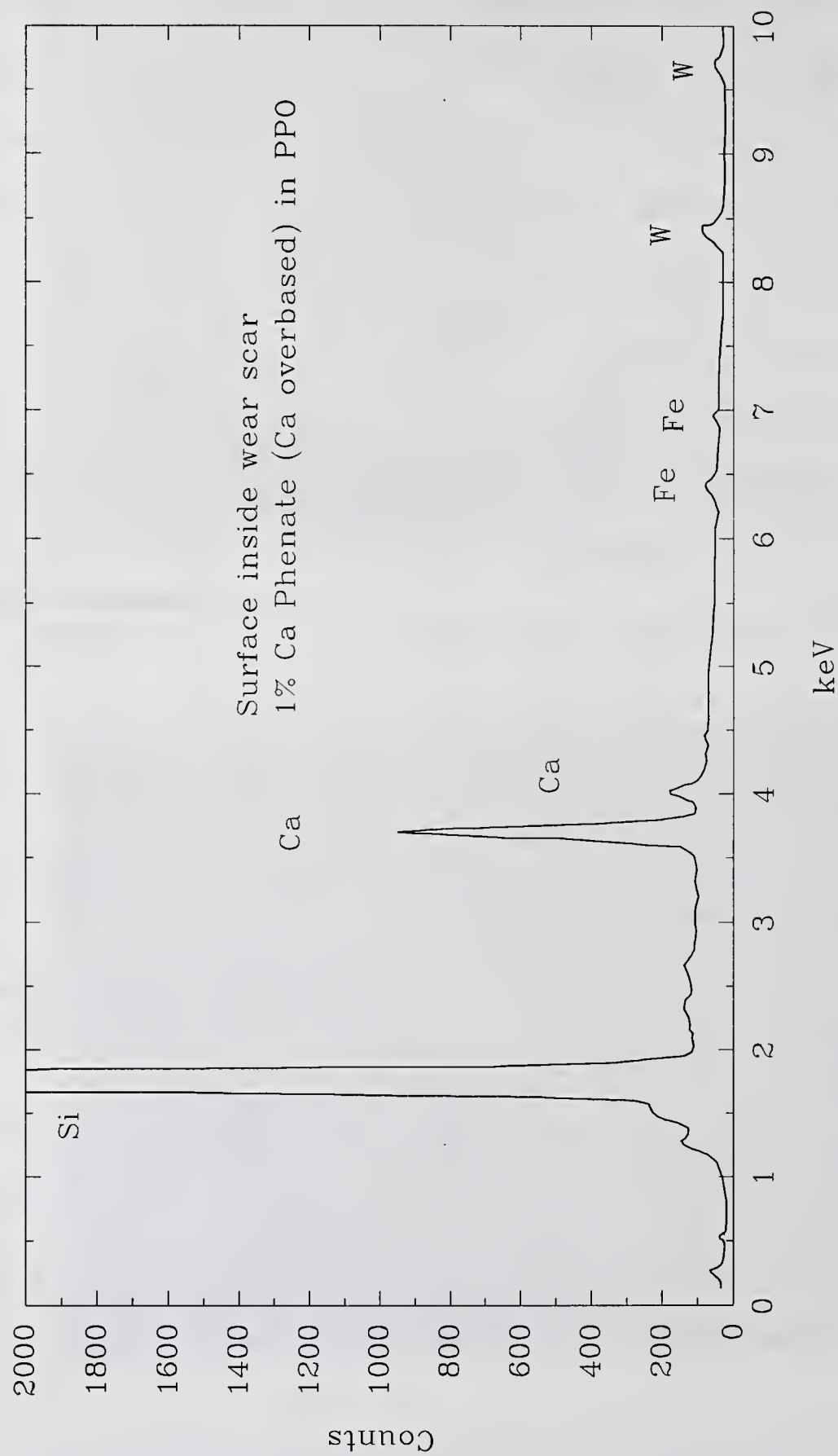


Figure 12.6 EDX Analysis of Film Inside Wear Scar for 1% Ca Phenate in PPO Lubricated Si_3N_4 BTF Test

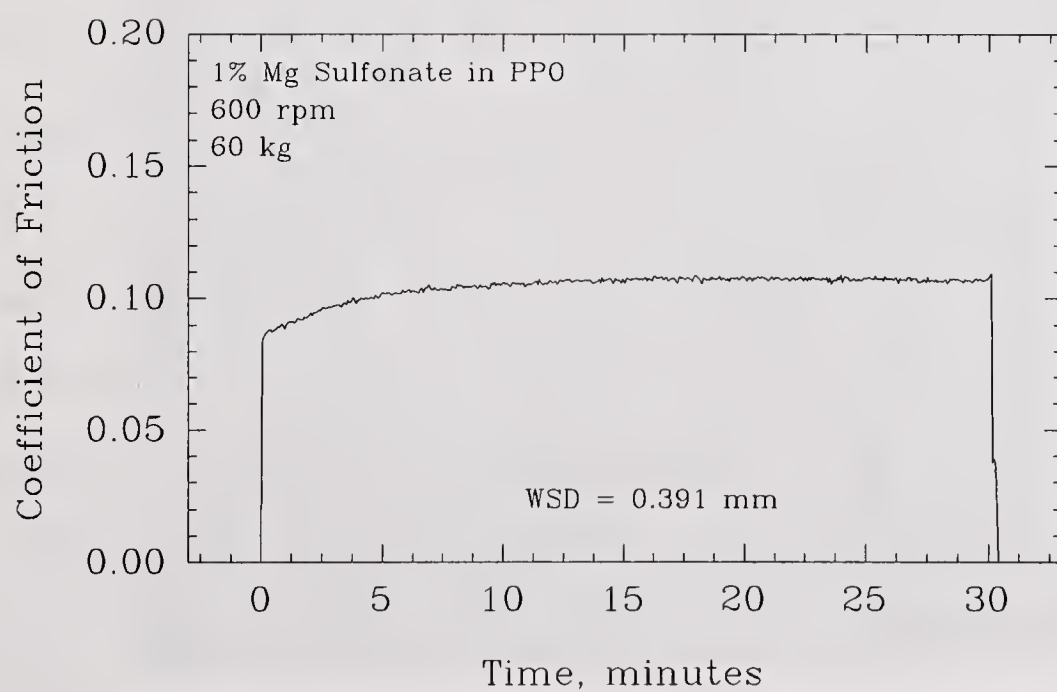
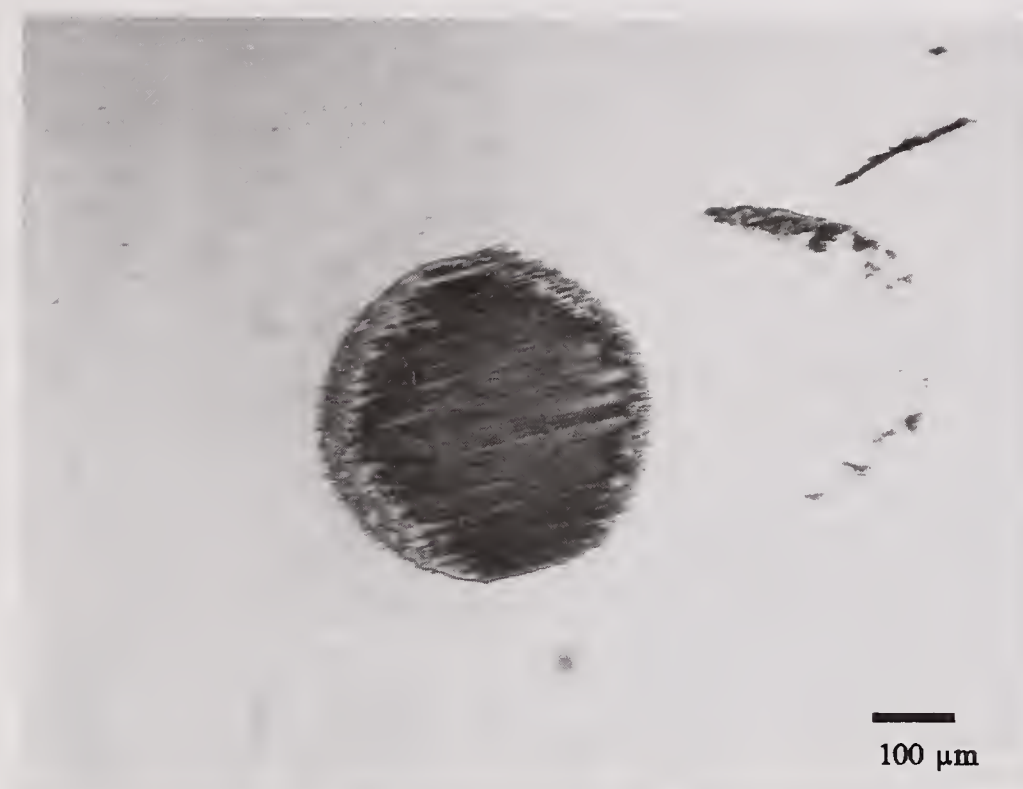


Figure 12.7 1% Mg Sulfonate in PPO Lubricated Si_3N_4 BTFT Test at 60 kg: a) Optical Photomicrograph, b) Friction Trace

SEM photomicrographs taken at higher magnification reveal something of the nature of the surface film. The photomicrographs were taken at 75° tilt and oriented so that the direction of sliding is from left to right as you look at the picture. The film in the wear scar (Figure 12.8A) has an obvious orientation in the direction of sliding that is consistent from the leading edge of the wear scar to the trailing edge. The film is similar in appearance to the phenate film. A magnification of the center of the wear scar (Figure 12.8B) shows the film to be fairly uniform with occasional "pits" interrupting the film. The film appears very solid in nature. Very fine debris seems to be incorporated into the film, throughout the wear scar.

The entrance region to the wear scar (Figure 12.9A), shows the film to have laid down as solid "fingers" on top of the surface of the flat. Similar artifacts at the exit (Figure 12.8B) suggests that the film is a reaction product that at one time had liquid-like properties. EDX analysis of the region inside the wear scar indicated the presence of magnesium, oxygen, nitrogen, and sulfur in addition to silicon and the usual metal impurities found in the parent Si_3N_4 (Figure 12.10). Magnesium has become concentrated in the wear scar during the test in a similar way to what was observed for Ca in the Ca phenate test. Analysis of the low base Ca sulfonate gave similar results. This suggests that the metal (Ca in this case) can become concentrated in the contact junction film due to the decomposition of the original sulfonate molecule (i.e., overbasing is not necessary). This indicates a different antiwear mechanism than the compacted overbasing mechanism suggested by Hoornaert^{125a} or Georges⁹⁷ (for steels).

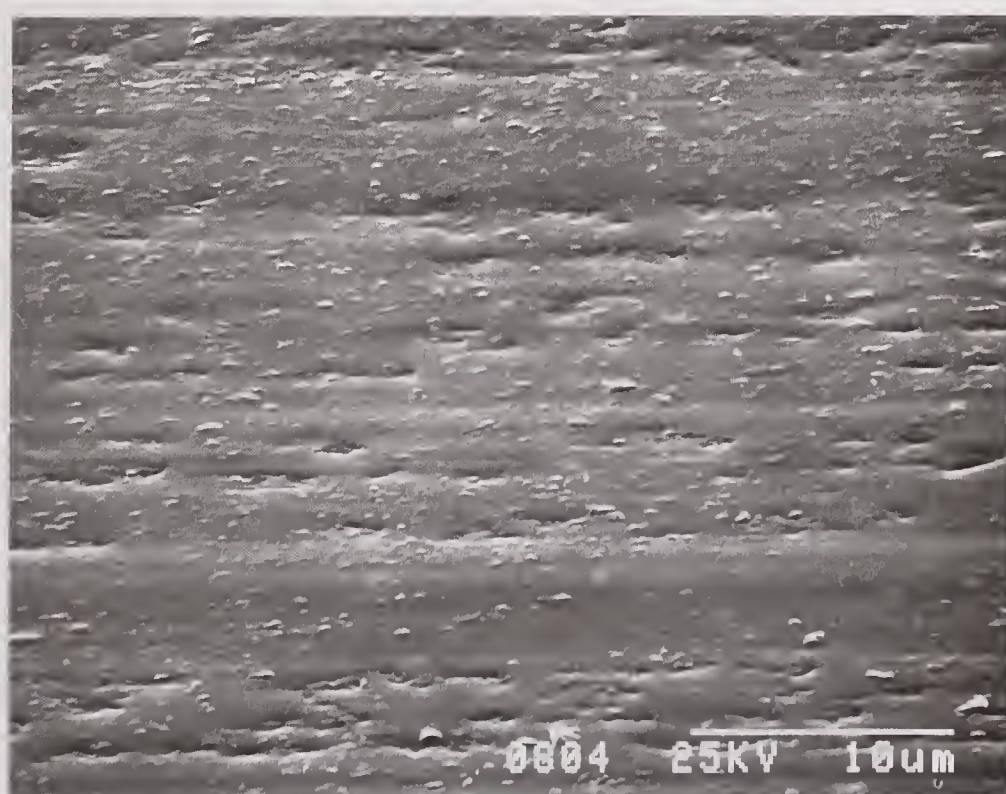


Figure 12.8 SEM Photomicrographs of 1% Mg Sulfonate in PPO Lubricated Si_3N_4 BTF Test at 60 kg: a) Wear Scar, b) Film Within Wear Scar

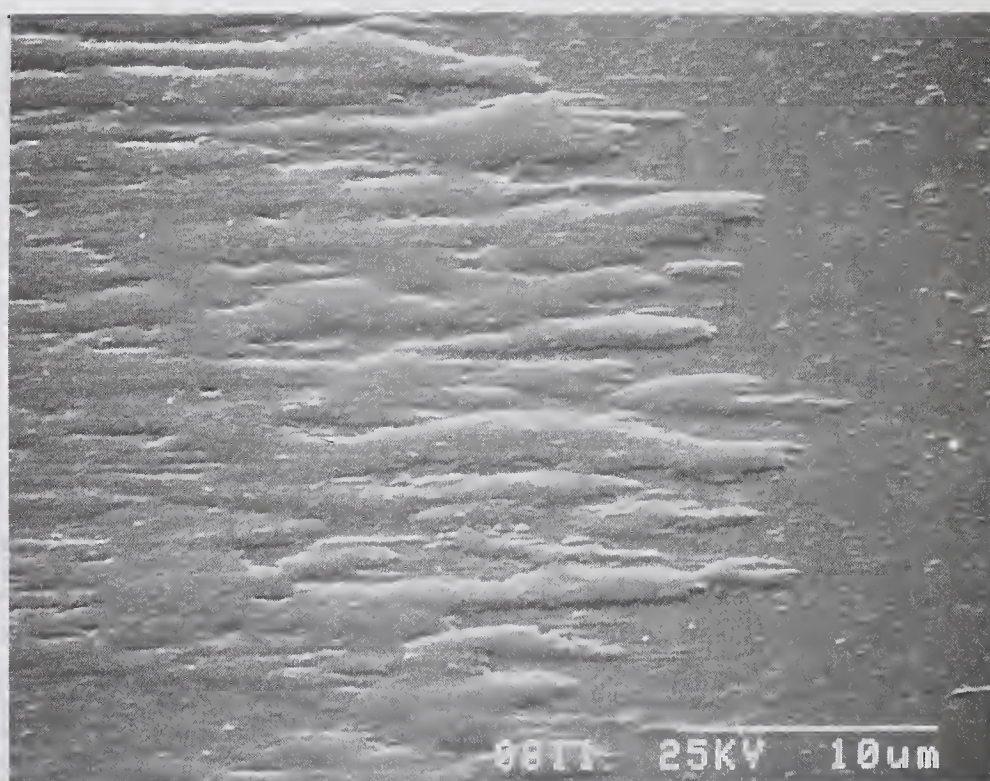
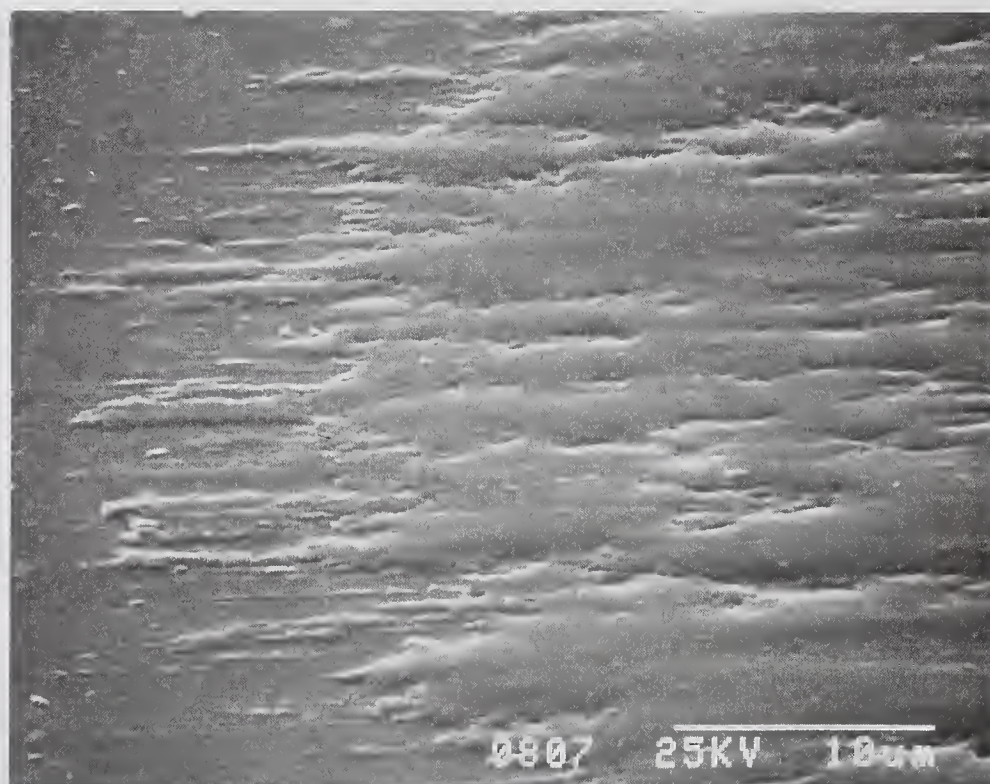


Figure 12.9 SEM Photomicrographs of 1% Mg Sulfonate in PPO Lubricated Si₃N₄ BTFT Test at 60 kg: a) Entrance Region, b) Exit Region

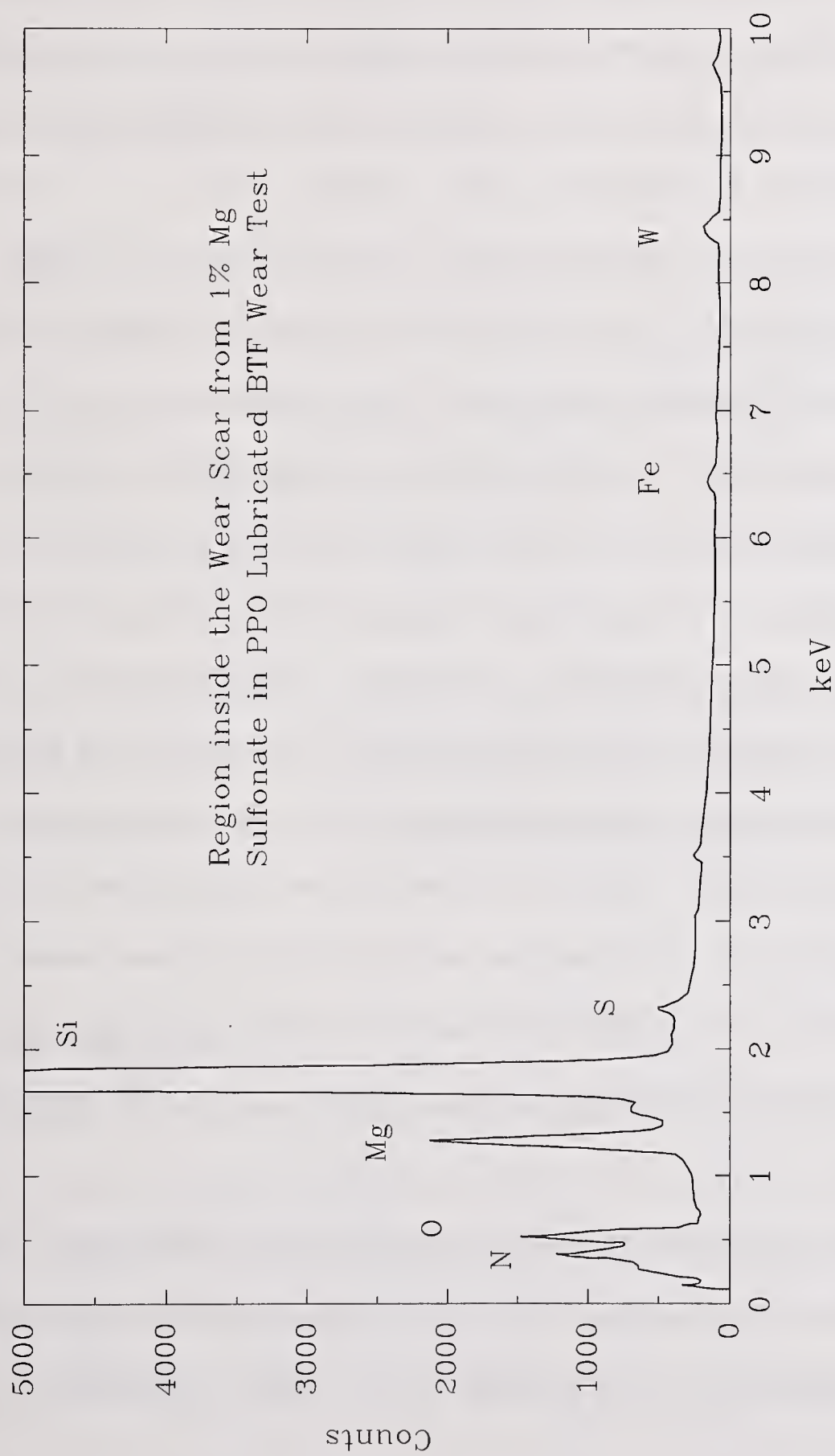


Figure 12.10 EDX Analysis of Film Inside Wear Scar from 1% Mg Sulfonate in PPO Lubricated Si_3N_4 BTF Test at 60 kg

The observation that the concentration of metals has increased so dramatically while the sulfur concentration is relatively low suggests that the detergent type compounds might be providing a delivery mechanism for metals into the wear scar. It is not clear how these metals help in lubricating Si_3N_4 ; however there are indications that the presence of metals on silica modifies the ion exchange and adsorptive properties of the surface¹³⁸. Perhaps they modify the chemical interaction between Si_3N_4 and PPO and its reaction products. Chen⁵⁵ found that certain metals (Fe, Co, Ni) had a catalytic effect on deposition of TMPTH. Magnesium was not tested and calcium was not found to be effective; however it may be possible that these metals may catalyze beneficial reactions with PPO to lubricate Si_3N_4 .

Another possibility is that the metals react with the silica surface layer to form Ca or Mg silicate glasses. According to phase diagram information, eutectics can be formed that are mixtures of silicon oxides, and Ca or Mg oxides. These eutectics melt at much lower temperatures (1200-1400°C) than pure silica (1700°C). In addition, these glasses may possess different physical and mechanical properties. The films certainly appear to have a more liquid-like behavior. This may alter asperity stress distributions and reduce wear.

Mg sulfonate was also tested neat, resulting in friction and wear behavior indistinguishable from the results obtained using 1% in PPO. Additional tests were also conducted on the 1% Mg sulfonate in PPO over a range of loads to see the extent of its capabilities.

The exact mechanism of lubrication of Si_3N_4 by these detergent type (S containing) compounds is not entirely clear, however the following sequence of events is postulated. First, the detergents adsorb onto the surface of Si_3N_4 . Once on the surface, they can be

carried into the contact during sliding. Under the high local temperatures of the contact, the adsorbed sulfonate molecules may decompose to give metal oxides which can react with (and perhaps mechanically mix with) the silica surface layer of Si_3N_4 . The combination of mechanical and chemical properties of this new surface film then allows lower wear.

12.3.1. Load Capacity Plot for 1% Mg Sulfonate in PPO

BTF wear tests were conducted using 1% Mg sulfonate in PPO at a variety of loads, constituting a load capacity plot. The resulting plot (Figure 12.11) indicates that this compound is very effective at lubricating Si_3N_4 , even at high loads. The wear scar diameter actually follows the Hertzian contact diameter quite closely all the way to just above 200 kg load. Even at 270 kg load, the wear scar diameter is only 0.8 mm. This translates to a mean pressure in the contact junction of over 2.0 GPa (300 000 psi) at the end of the test. At the beginning of the 270 kg test, the high elastic modulus of Si_3N_4 generates Hertzian mean pressures of 3.5 GPa (500 000 psi) and maximum Hertzian pressures of 5.2 GPa (750 000 psi).

12.4. BTF Wear Tests at 200°C

It was expected that Mg sulfonate would work at higher bulk lubricant temperatures, since it had such a high load capacity. BTF tests conducted at 200°C (Figure 12.12) confirmed this. Wear increased slightly above the room temperature case and the friction level was relatively high in the initial stages of the test. The nature of the surface film had also changed visibly according to Figure 12.12A. There was still no evidence of any deposit

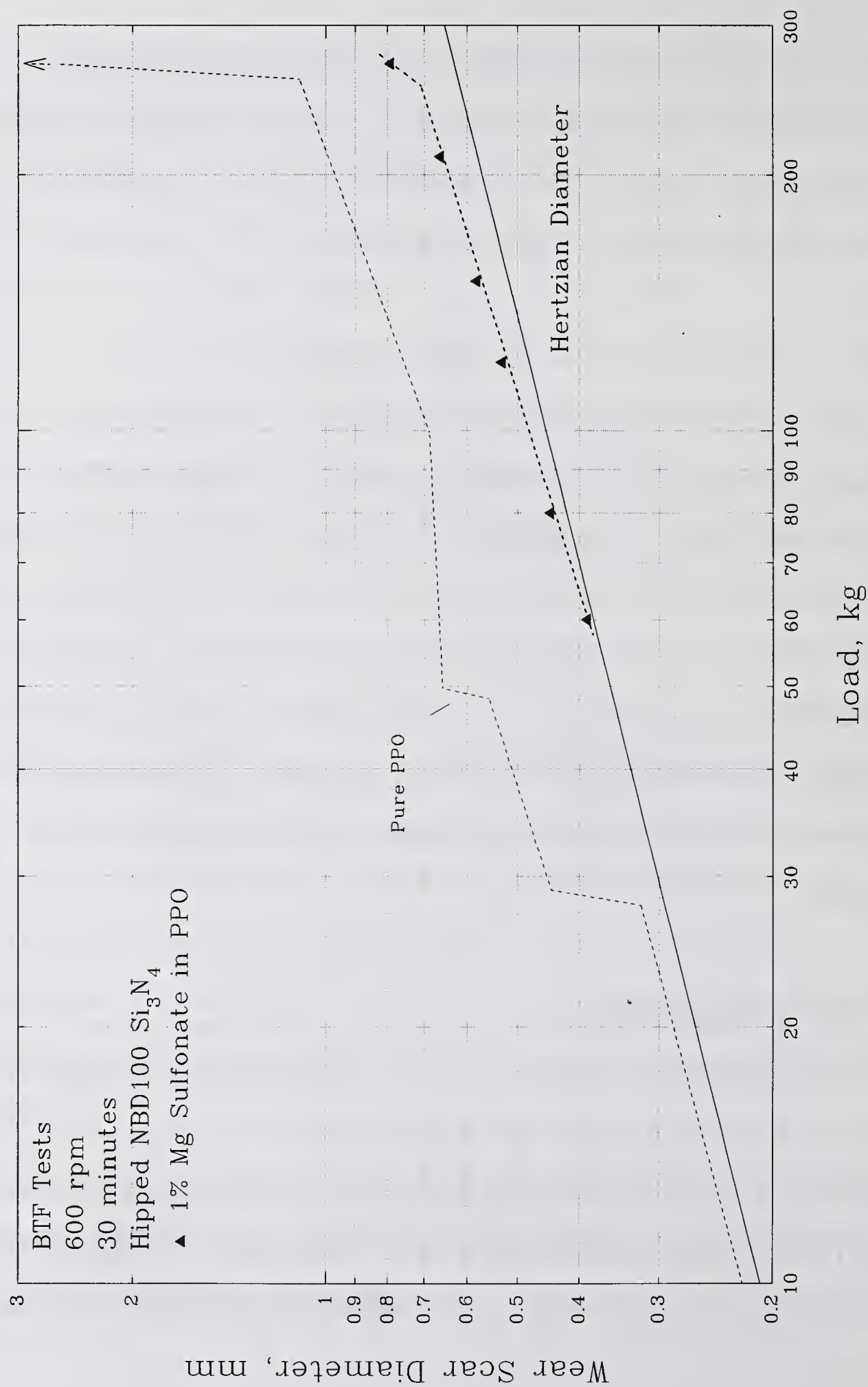


Figure 12.11 Load Capacity Plot for 1% Mg Sulfonate in PPO Lubricated Si_3N_4 BTF Tests (Compared to PPO)

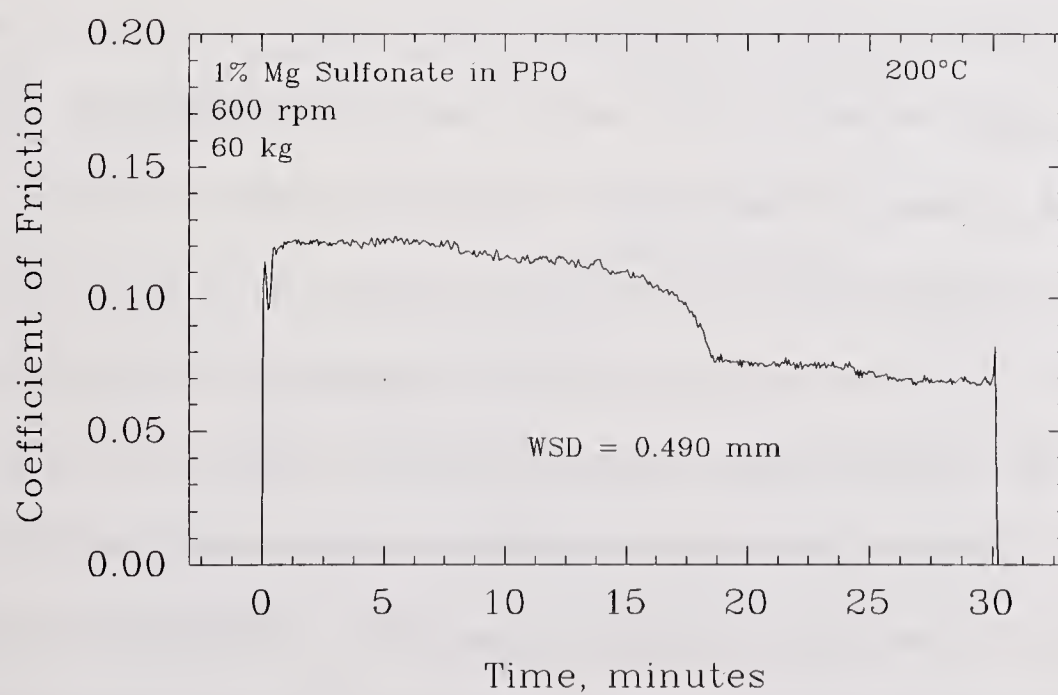
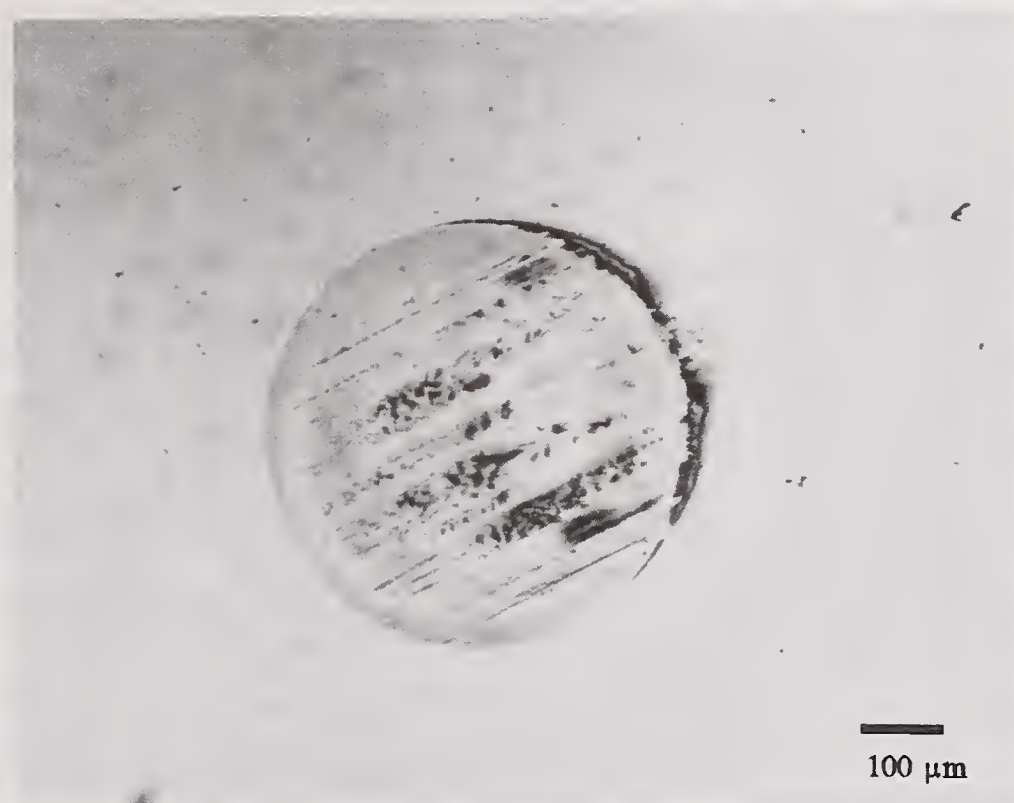


Figure 12.12 1% Mg Sulfonate in PPO Lubricated Si_3N_4 BTF Test at 200°C: a) Optical Photomicrograph, b) Friction Trace

around the wear scar. As a point of reference, PPO by itself had an increase in wear scar diameter to 0.8-0.9 mm for the same temperature.

A 200°C BTF wear test conducted using 1% sulfurized hydrocarbon in PPO (Figure 12.13) also gave lower wear than PPO, but higher than the sulfonate. In this case; however, there was a tremendous amount of reaction product deposit surrounding the wear scar. The friction coefficient is very low initially, and rises substantially about halfway through the test. If this higher friction is associated with a higher wear rate, it would suggest that the sulfurized hydrocarbon was very effective initially, but perhaps became depleted during the course of the test. The wear scar diameter at 200°C is actually lower than the same test conducted at room temperature. This suggests that higher temperatures are necessary to promote the reactions necessary to lubricate Si_3N_4 with sulfurized hydrocarbons.

12.5. Summary and Discussion

Room temperature BTF tests on Si_3N_4 conducted using sulfur containing compounds gave different results depending on the chemical structures of the compounds. In general, compounds that contained only sulfur did not work under the conditions selected. Compounds that contained both sulfur metals were successful. In the case of Mo-S compounds, friction was low, but wear was high. It is thought that decomposition of the Mo-S containing compounds in the contact junction may be forming MoS_2 in-situ.

In the case of the metal-S containing detergent type compounds, low friction and wear were achieved. The data suggests a mechanism that includes adsorption and decomposition of the compound inside the wear scar to form surface films rich in the specific metals (Ca,

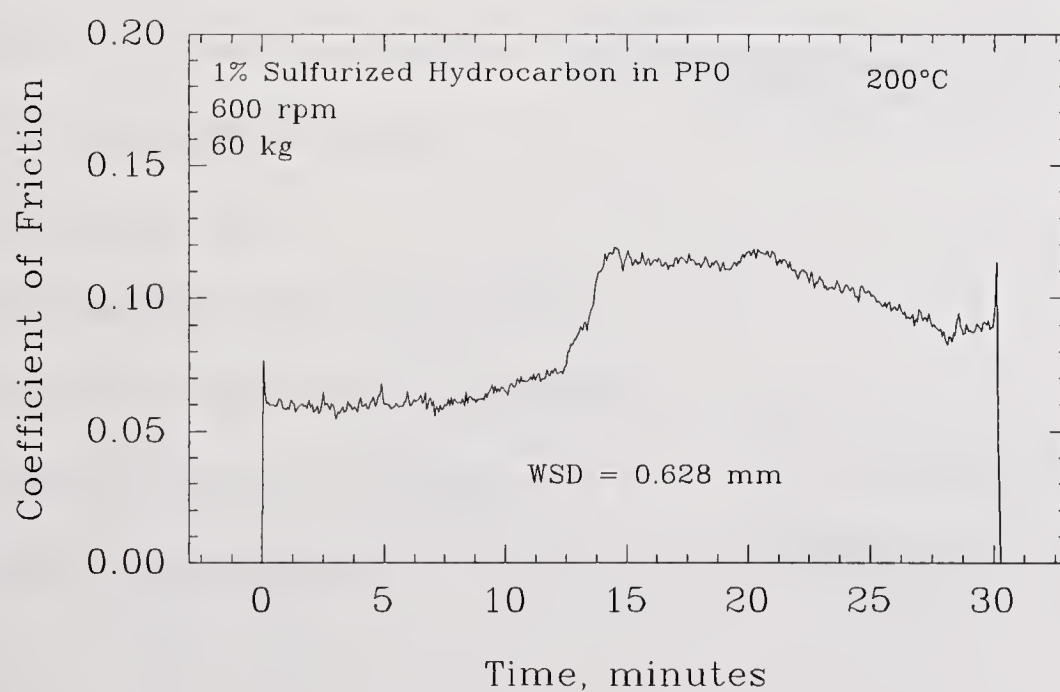


Figure 12.13 1% Sulfurized Hydrocarbon in PPO Lubricated Si_3N_4 BTFT Test at 200°C: a) Optical Photomicrograph, b) Friction Trace

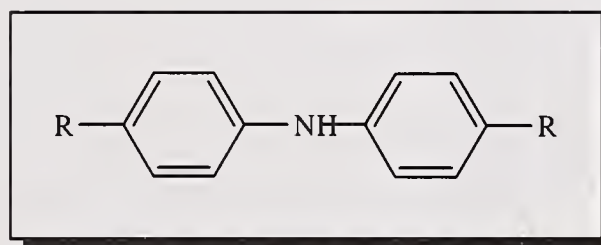
Mg, Zn). The exact role of this metal-rich film in the lubrication of Si_3N_4 by these compounds is uncertain. Sulfur was not found in these films in any appreciable quantity.

Chapter 13

SURVEY OF NITROGEN CHEMISTRIES

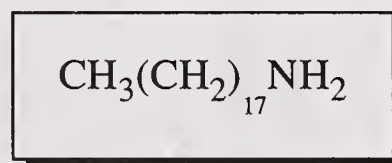
Several different nitrogen-containing compounds were tested at 1% in PPO. They were all high molecular weight compounds that have been used in lubricant formulations; however, they are regarded as antioxidants, corrosion inhibitors, and dispersants, not antiwear compounds. Amine compounds were specifically selected because they were known to adsorb onto the surface of silica¹³⁸. The results are summarized in Table 13.1 and presented graphically in Figure 13.1.

Diphenylamine is a typical amine type antioxidant. It had little or no effect on friction or wear. There were no characteristics in either the friction behavior or the wear scar appearance that could distinguish it from pure PPO.



Dialkyldiphenylamine

A long chain alkyl amine model compound (octadecyl amine) gave slightly higher wear than PPO. The friction trace and wear scar appearance were indistinguishable from the PPO case.



Octadecyl Amine

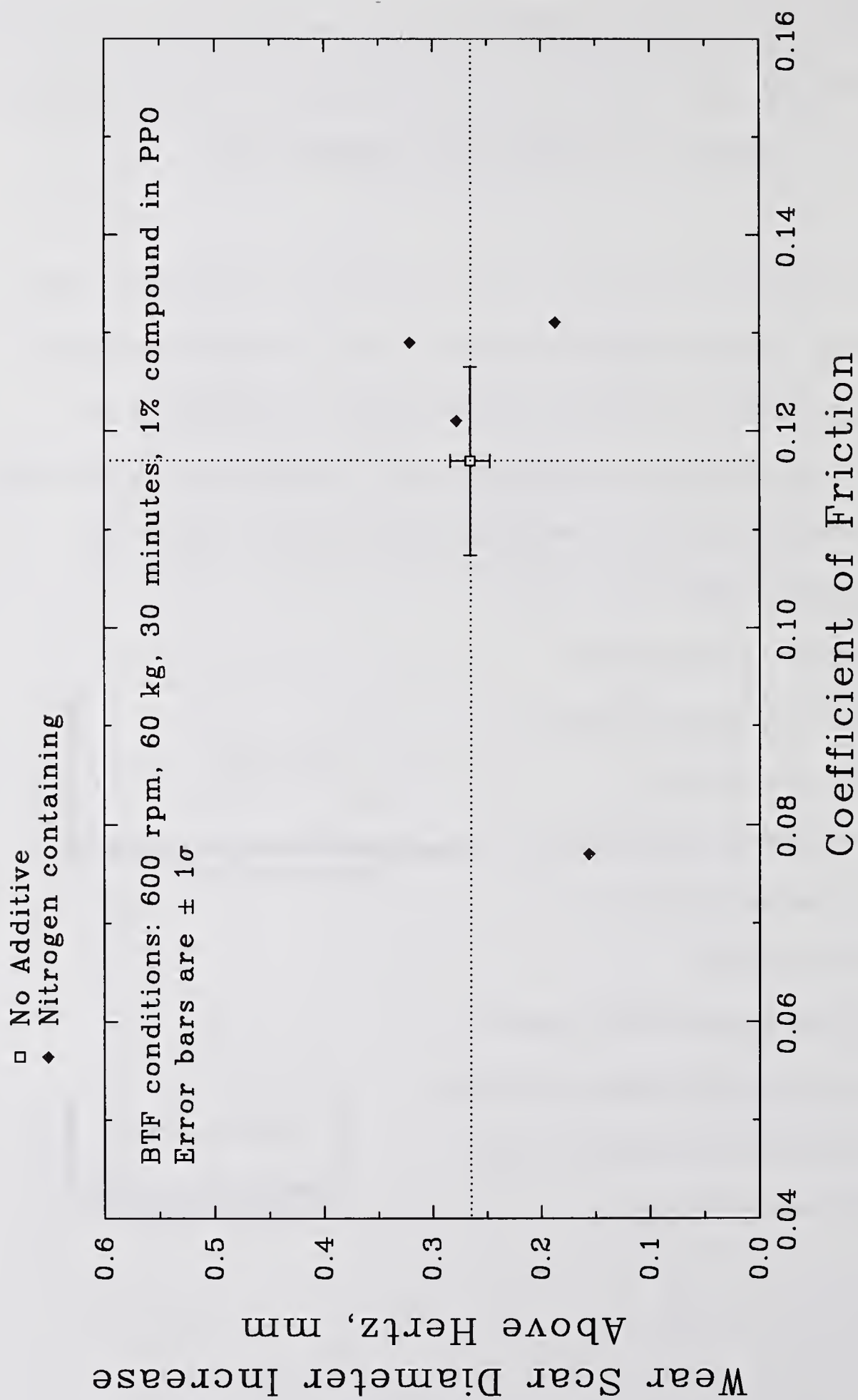


Figure 13.1 Summary Friction and Wear Data for Si_3N_4 BTF Tests on 1% Nitrogen-Containing Compounds in PPO

Table 13.1
Friction and Wear Data on Selected Nitrogen-Containing Model Compounds

Chemical Compound ¹ NONE (average of 16 tests)	WSD (mm) 0.645	Dia increase above Hz, mm 0.265	COF ²	Frict. Type I	Wear Scar Appearance smooth	Film in Scar ? no
High MW Substituted Imidazoline	0.536	0.156	0.077	II	smooth	no
Succinamide	0.567	0.187	0.131	III (20)	smooth	no
Dinonyldiphenylamine	0.658	0.278	0.121	I	smooth	no
Octadecyl Amine [028]	0.701	0.321	0.129	I	smooth	no

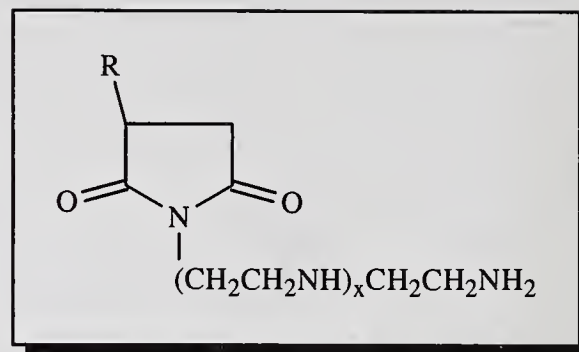
¹ 1 wt % in purified paraffin oil

² Measured at the end of the test

All Tests conducted on CER024 NC132 Hot pressed Si₃N₄ (unless otherwise noted) at 600 rpm, 60 kg, 30 minutes, 1% additive in PPO, 21°C.

13.1. Dispersant Type Compounds

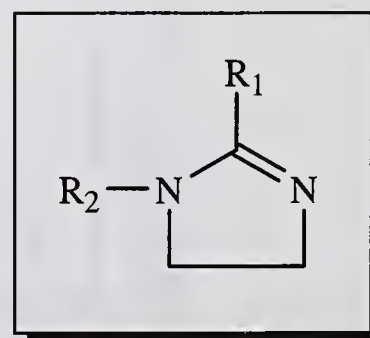
The succinamide (typical ashless dispersant) gave significantly lower wear but relatively high friction than PPO as shown in Figure 13.2. The high friction measured at the end of the test was due to the transition (Type III friction behavior) from low friction (≈ 0.09) to high friction (≈ 0.13) at the twenty minute mark of the test. The wear scar is quite smooth, with little deposit around it, and no visible film within the wear scar. The size of the wear scar would probably have been even smaller if there had not been a transition before the end of the test. The transition may have also erased any film that might have been present. The lack of deposit is probably a testament of the dispersency of the succinamide, and is reminiscent of the lack of deposit seen for the detergent type compounds discussed in the sulfur chemistry section.



Succinamide

13.2. Imidazoline

The substituted imidazoline reduced wear and friction (Figure 13.3); however, no visible film could be found in the wear scar even in the SEM. Significant amounts of smooth polymeric film were found outside the wear scar for this compound suggesting that high temperatures in the contact junction had promoted polymerization of the additive. The film may have been present inside the wear scar, but



Imidazoline

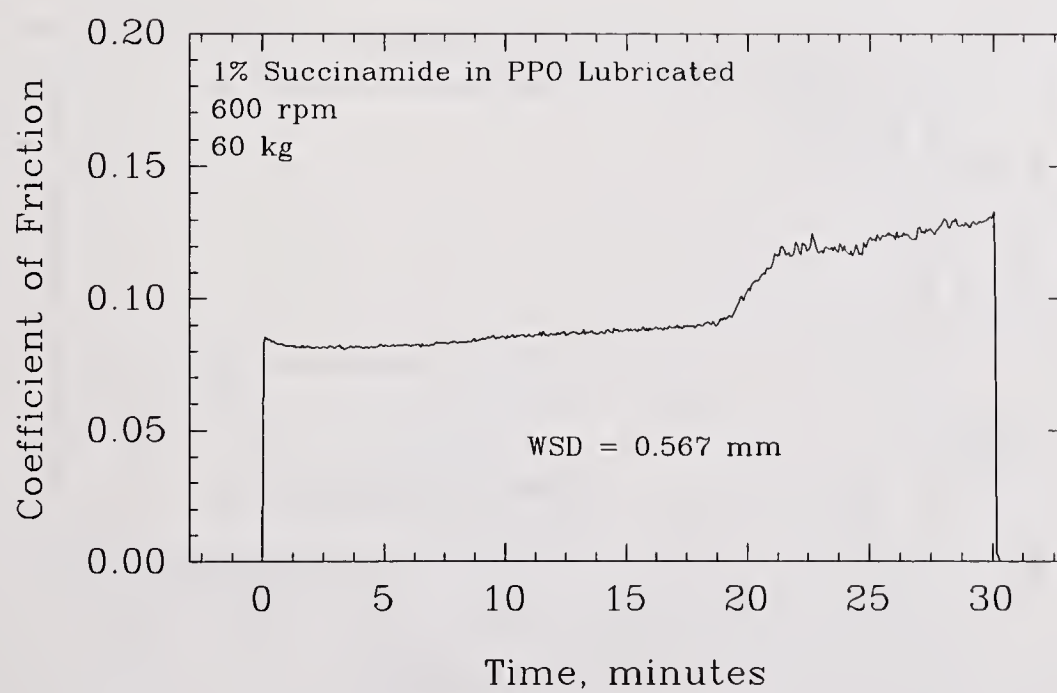
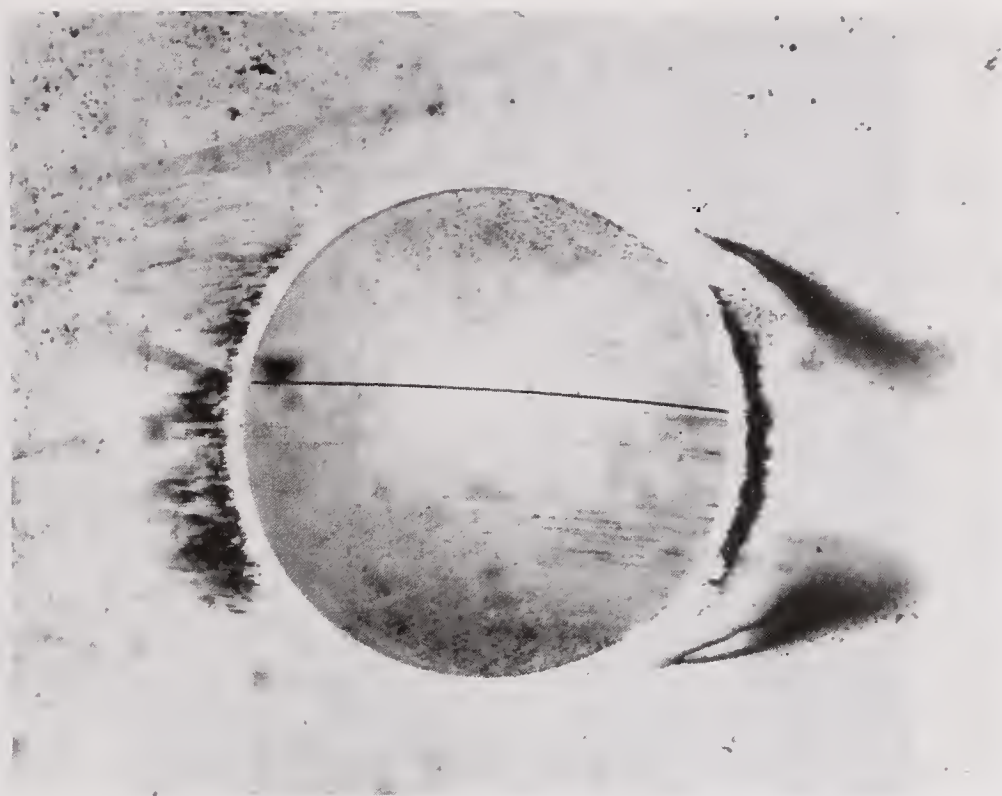


Figure 13.2 1% Succinimide in PPO Lubricated Si_3N_4 BTFT Test at 60 kg: a) Optical Photomicrograph, b) Friction Trace

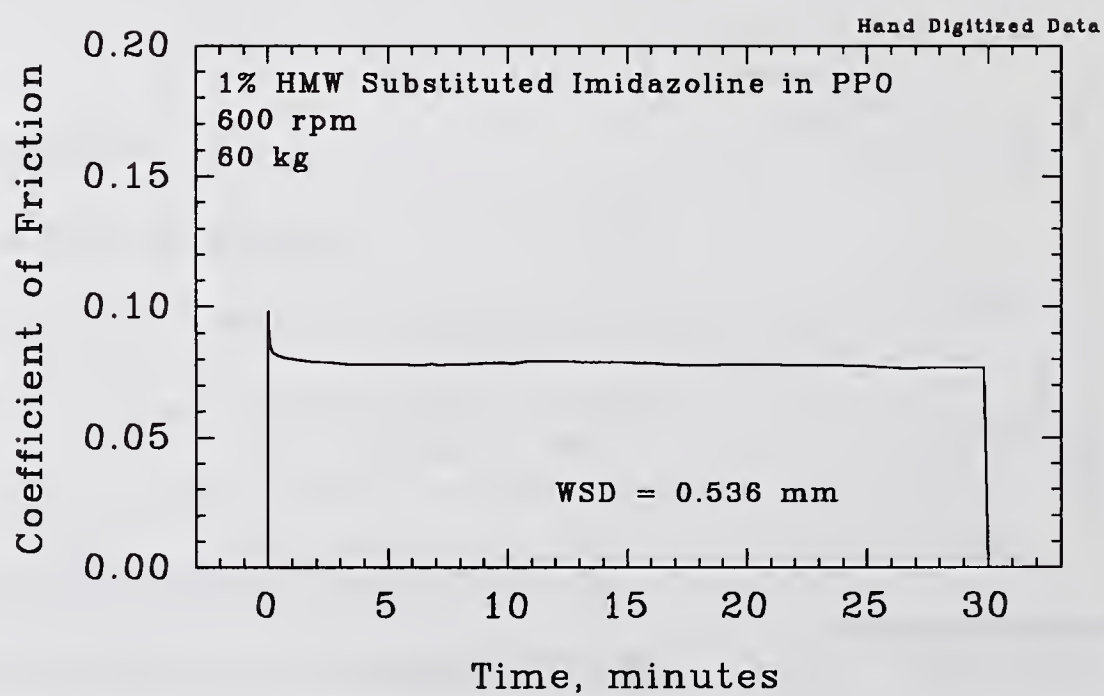
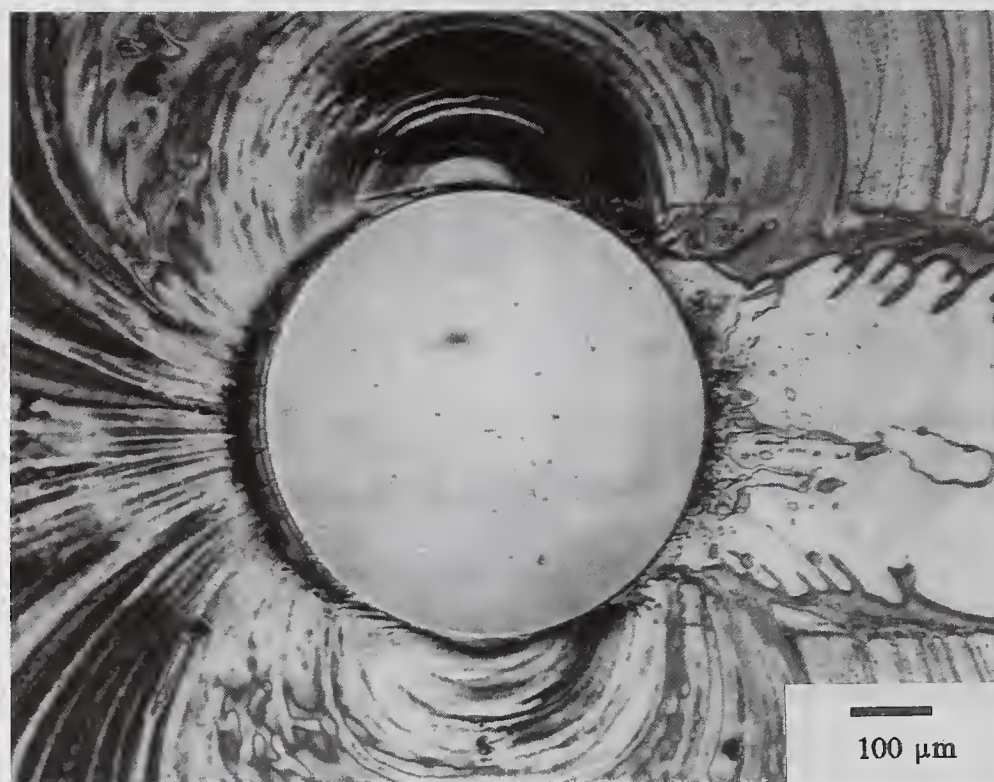


Figure 13.3 1% HMW Substituted Imidazoline in PPO Lubricated Si_3N_4 BTF Test at 60 kg:
a) Optical Photomicrograph, b) Friction Trace

perhaps too smooth to be detected.

Nilsen¹⁸⁸ studied the use of imidazolines as dispersants for Si_3N_4 powder in hexane solutions. He hypothesized that imidazolines reacted with water adsorbed on the surface of Si_3N_4 to form secondary amides. It is not apparent how this mechanism might explain the high molecular weight polymeric material found around the wear scar.

Chapter 14

SUMMARY AND CONCLUSIONS

This study has uncovered several important characteristics of the surface chemistry of Si_3N_4 related to the boundary lubrication of this material. Several classes of compounds have been discovered that have the capability of reducing friction and wear of Si_3N_4 under boundary lubrication conditions. Where possible, mechanisms have been postulated to help explain the type of reaction sequences responsible for lubrication. A specific chemical reaction mechanism is proposed to explain the boundary lubrication of Si_3N_4 by alcohols.

Oxides and hydroxides easily form on the surface of Si_3N_4 . Because it is on the surface, the oxide layer is very important to the surface chemistry and hence the boundary lubrication of Si_3N_4 . The Si_3N_4 surface chemistry observed in this study is consistent with silica chemistry, suggesting that the silica chemistry literature is a rich resource for relevant information. Many of the concepts for what might react and lubricate Si_3N_4 were developed based on the notion that the Si_3N_4 surface may behave similar to silicon oxide chemically.

Both adsorption and chemical reaction have been observed to occur on the surface of Si_3N_4 . Literature sources indicate that alcohols and acids can adsorb and react with silica surfaces. These observations, coupled to the knowledge that the surface of Si_3N_4 is silicon oxide, suggests that these compounds adsorb and react on Si_3N_4 in a similar manner.

The ball-on-three-flat (BTF) test can be an effective tool to study the boundary lubricating effectiveness of a wide variety of chemical compounds on ceramics. Both large bulk sample (1.5 ml) and micro sample (6 μ l) techniques have been developed and applied to Si_3N_4 lubricated by many different chemistries. Effective boundary lubrication was associated with low wear, low and stable friction, and the presence of films in and around the wear contact. Using this technique, it was determined that Si_3N_4 can be effectively lubricated at high loads (60 kg) by a variety of chemical compounds including the following compounds in paraffin oil at a concentration of 1% (wt): phosphorus-containing organic compounds, metal sulfonates, Ca phenate, Mg salicylate, a succinamide, a Mannich product, an imidazoline, and several acids and alcohols. Using neat compounds, Si_3N_4 was effectively lubricated by a wide variety of acids and alcohols including polyalcohols (glycols) and polyacids (diacid). Purified paraffin oil (PPO) by itself can be effective at lower loads (20 kg).

Alcohols react with the Si_3N_4 surface to produce surface alkoxides. Static kinetic experiments conducted at temperatures from 100°C to 245°C using Si_3N_4 powders showed that reactions can take place between the Si_3N_4 surface and alcohols to produce surface bonded silicon alkoxides.

Analysis of reaction products from dynamic (wear) tests have for the first time provided direct evidence of silicon containing organic species. Gel permeation chromatography (GPC) indicated HMW material in this product. Gel permeation chromatography-graphite furnace atomic absorption (GPC-GFAA) analysis confirmed the presence of silicon in the HMW reaction product, suggesting direct reaction between the

alcohol and the surface silicon of Si_3N_4 . SIMS analysis of the reaction product revealed that the wearing contact produced silicon containing alkoxides with up to four alkoxide groups per silicon atom. A compound was also found consisting of two silicon atoms bridged by an oxygen atom, with five alkoxy ligands. The HMW silicon-containing compounds observed by GPC-GFAA suggest that much larger polyalkoxy molecules are also formed.

Analysis of the shape of the wear scar for octanol lubricated Si_3N_4 wear tests indicate that elastohydrodynamic lubrication may be influencing the lubrication mechanism for this material/lubricant combination. This is supported by the low coefficient of friction obtained in this test and may be explained by a combination of chemical effects of surface reaction (corrosion) to reduce asperities and promote surface conformity, and HMW formation to provide viscous lubricating films. The lubricating ability of HMW silicon alkoxides was demonstrated using two-ball collision tests.

It is proposed that Si_3N_4 is lubricated by alcohols through a sequence of reactions. Adsorption and subsequent reaction of alcohol groups with surface silanol and siloxy groups of the oxidized Si_3N_4 surface results in the formation of surface bonded alkoxides. Further chemical reaction in the high shear stress environment of the wearing contact produce free silicon alkoxides, which dissolve in the alcohol. Subsequent condensation reactions in the high temperatures of the contact result in formation of higher molecular weight silicon-containing compounds (silicon alkoxides). These high molecular weight silicon alkoxides may have beneficial local boundary layer properties in the contact that enhance lubrication within the contact. Similar reactions are thought to occur with organic acid functional groups.

The observation that oxygenated compounds such as organic acids and alcohols can lubricate Si_3N_4 under boundary lubrication conditions offers significant advantages for ceramic engine technology. These compounds are non-ashing, commercially available, and more compatible with alcohol fuels that are being considered as more environmentally friendly alternatives to conventional fuels.

All phosphorus-containing compounds tested were found to be effective in boundary lubricating Si_3N_4 under the conditions selected for this study. Detailed analysis of the reaction products and study of the interaction between Si_3N_4 surfaces and model phosphorus-containing compounds suggest that the lubrication mechanism involves a complex sequence of organic and inorganic chemical interactions. Phosphorus compounds were found to adsorb onto the surface of Si_3N_4 . TGA analysis confirms a tenacious surface product that is thought to be a bonded phosphate film similar to films observed in reactions between silicic acid and trialkyl phosphates. It is also hypothesized that the success of phosphorus-containing compounds is due, in part, to the modification of the properties of the glassy surface phase to make it more pliant, especially at the elevated temperatures of the contact junction. Phosphorus is known to be a network (glass) former. It can combine with silica and result in glasses that have lower melting points and less brittle nature than silica itself. Thus a network forming compound such as phosphorus may lubricate by providing a softer, less brittle layer on the surface of Si_3N_4 .

It is hypothesized that the metal containing compounds (Mg sulfonate, Ca phenate, Mg salicylate etc.) are successful lubricants because i) they are surface active and readily adsorb onto the Si_3N_4 surface, and ii) the metals may modify the silica network, resulting in

lower melting points and viscous glassy phases. They may also modify the adsorptive properties of the surface silica and catalyze reactions.

In general, halogenated compounds were not successful in lubricating Si_3N_4 . In many cases, wear was increased substantially, suggesting a corrosion mechanism may be taking place with the Si_3N_4 surface. Chlorosilanes were found to lubricate for a short time before failing. Chlorine-containing reaction products with a distinctive morphology were observed surrounding the wear scar in tests lubricated by these compounds. Fluorinated acids and alcohols were tested neat, but were not as effective as their hydrocarbon-based analogs.

Sulfur-containing compounds offered mixed lubrication effectiveness with Si_3N_4 . Compounds containing molybdenum and sulfur gave low friction, but did not decrease wear. When phosphorus was also present, both low friction and low wear were obtained. It is thought that the friction reducing compound MoS_2 may be forming in the wearing contact. Detergent-type sulfur-containing compounds were successful in reducing wear; however, it is thought that this is due to the presence of metals (Mg, Ca, Zn) and oxygen (sulfonate, phenate) structures rather than the sulfur itself since sulfur was lacking in the reaction product films. Most compounds containing only sulfur were ineffective or actually increased wear. The exceptions were two disulfide compounds which appeared to be partially effective.

Effective lubrication was observed for succinamide and imidazoline nitrogen-containing compounds. In the case of imidazoline, polymeric reaction products were observed surrounding the wear scar.

CHAPTER 15

RECOMMENDATIONS FOR FUTURE WORK

In the course of this study, there were issues that could not be answered and should be addressed by additional research.

The issue of the role of dangling bonds in tribochemistry is largely a mystery. This area is especially important in ceramics where brittle fracture is such an important mechanism, since the propagating crack tip is a potential source of dangling bonds. Experiments conducted in this study have noted that "free" silicon-containing compounds (silicon alkoxides) are formed in wear tests. The reactions to form these compounds could not be duplicated with controlled "static" tests at temperatures up to 245°C. One possibility is that dangling bonds from wear provide the key mechanism to form these compounds. Several well controlled experiments are necessary to further investigate this area.

Lubrication mechanisms have been postulated for some classes of compounds; however these mechanisms need further investigation. For example, the mechanism of lubrication by phosphorus containing compounds needs some work to substantiate the glass forming hypothesis. The mechanism of lubrication by detergents (sulfonates, phenates, and salicylates) needs more clarification to determine the exact reaction sequence and the specific roles of the organic and metal constituents.

The results of this study has suggested that there may be an EHD lubrication influence with alcohol lubricated Si_3N_4 . Specifically, the morphology of the wear scar is very similar to interferometric photographs of EHD point contacts. In addition, the

coefficient of friction observed ($\mu=0.05$) is also significantly lower than usually observed in boundary lubrication ($\mu=0.10$). The possible EHD influence is even more surprising given the high severity of the wear tests in which it was observed. More adequate investigation of this system, including EHD modelling is required to verify this hypothesis.

REFERENCES

1. Adamson, A. W., Physical Chemistry of Surfaces, 5th Ed., John Wiley and Sons, New York (1990)
2. Adewoye, O. O., and Page, T. F., "Frictional Deformation and Fracture in Polycrystalline SiC and Si₃N₄," *Wear*, 70, pp 37-51 (1981)
3. Ajayi, O. O., and Ludema, K. C., "Surface Damage of Structural Ceramics: Implications for Wear Modeling," *Wear* 124, pp 237-257 (1988)
4. Ajayi, O. O., and Ludema, K. C., "Formation of Transfer Film During Ceramics/Ceramics Repeat Pass Sliding," *Wear of Materials* (1989)
5. Akazawa, M., Kato, K., and Umeya, K., "Wear Properties of Silicon Nitride in Rolling Contact," *Wear*, 110, pp 285-293 (1986)
6. Akazawa, M., "Wear Properties of Si₃N₄ in Rolling-Sliding Contact," *Wear* 124, pp 123-132 (1988)
7. Alexander, G. P. and Her, R. K., "Grease Thickened With Organosilyl-Coated Siliceous Material," Patent # 2,818,385, Dec 31 (1957)
8. Allen, T., and Patel, R. M., "Adsorption of Alcohols on Finely Divided Powders," *J. Appl. Chem.*, 20, pp 165-171 (1970)
9. Allen, T., and Patel, R. M., "The Adsorption of Long-Chain Fatty Acids on Finely Divided Solids Using a Flow Microcalorimeter," *Journal of Colloid and Interface Science*, 35, 4, pp 647-655 (1971)
10. Anderson, H., Kodas, T. T., and Smith, D. M., "Vapor-Phase Processing of Powders: Plasma Synthesis and Aerosol Decomposition," *Ceramic Bulletin*, 68, No. 5 (1989)
11. Archard, J. F., "The Temperature of Rubbing Surfaces," *Wear*, 2, pp 438-455 (1959)
12. Arkles, B., "Techniques for Silylation," Silicon Compounds Register and Review, Volume S-5, Petrarch Systems (1982)
13. Arkles, B., "Silane Coupling Agent Chemistry," Silicon Compounds Register and Review, Volume S-7, Petrarch Systems (1987)

14. Baik, Sunggi, "Liquid-Phase Bonding of Silicon Nitride Ceramics," J. Am. Ceram. Soc., 70, 5, pp C105-C107 (1987)
15. Bailey, R. R., and Wightman, J. P., "Interaction of Gaseous Hydrogen Chloride and Water with Oxide Surfaces," Journal of Colloid and Interface Science, 70, 1, pp 112-123, (1979)
16. Baraton, J. I., Marchand, R., and Quintard, P., "Comparative Infrared Study of Silicon and Germanium Nitrides," Journal of Molecular Structure, 143, pp 9-12 (1986)
17. Battelle Laboratories, Engineering Property Data on Selected Ceramics, Vol. 1, Nitrides, Metals and Ceramics Information Center, Battelle, Columbus (1976)
18. Bauer, V., and Stöber, W., "Chemisorption aus Alkohol-Wasser-Systemen an Amorphem Siliziumdioxid," Kolloid Zeitschrift, 160, 2, pp 142-146 (1958) [in German]
19. Beeck, O., Givens, J. W., and Smith, A. E., "On the Mechanism of Boundary Lubrication I. The Action of Long-Chain, Polar Compounds," Proc. Roy. Soc., A177, pp 90-102 (1940)
20. Beeck, O., Givens, J. W., and Williams, E. C., "On the Mechanism of Boundary Lubrication II. Wear Prevention by, Addition Agents," Proc. Roy. Soc., A177, pp 103-118 (1940)
21. Belyakova, M. D., and Kiselev, A.V., "Adsorption and Chemisorption of Methanol by Silica Gel with Different Degrees of Surface Hydration," Zh. Fiz. Khim., 33, 7, pp 1534-1543 (1959) [In Russian]
22. Benson, R. E., and Castle, J. E., "Reactions of Freshly Formed Surfaces of Silica," Journal of Physical Chemistry, 62, pp 840-843 (1958)
23. Bergstrom, L., and Pugh, R., "Interfacial Characterization of Silicon Nitride Powders," J. Am. Cer. Soc., 72, 1, pp 103-109 (1989)
24. Bhushan, B., and Gupta, B.K., Handbook of Tribology, McGraw-Hill, New York, 1991
- 24a. Bieber, H. E., Klaus, E. E., and Tewksbury, E. J., "A Study of Tricresyl Phosphate as an Additive for Boundary Lubrication," ASLE Trans. 11, 155-166 (1968)
25. Blaine, S., and Savage, P., "Reaction Pathways in Lubricant Degradation. 2. n-Hexadecane Autoxidation," Ind. Eng. Chem. Res., 30, 9, pp 2185-2191 (1991)

26. Blattenberger, J. W., "Hydrophobic Silica Base Lubricants Containing 1,3-Diols as Anti-Gelation Agents," Patent # 2,752,310, Jun 26 (1956)
27. Blomberg, A., Olsson, M., Bratthall, J., Engstrom, H., and Hogmark, S., "Sliding Wear Behaviour of Al_2O_3 , SiC and Sialon Face Seals," Proceedings of JITC, Nagoya, pp 1371-1376 (1990)
28. Boberski, C., Hamminger, R., Peuckert, M., Aldinger, F., Dillinger, R., Heinrich, J., and Huber, J., "High-Performance Silicon Nitride," Angew. Chem. Int. Ed. Adv. Mater., 28, 11, pp 1560-1569 (1989)
29. Boch, P., Platon, F., Kapelski, G., Godet, M., Berthier, Y., Trabelsi, R., Briggs, J., Arbabi, H., and Azema, O., "Tribology and Velocity Accommodation Mechanisms of Ceramics (SiC and Si_3N_4) as a Function of Temperature and Environment," Proceedings of JITC, Nagoya, pp 1395-1400 (1990)
- 29a. Bogatyrev, V.M., and Chuiko, A.A., "The Investigation of the Reaction of Di- and Triethyl Phosphites with the Dispersed Silica Surface by IR-Spectroscopic Method," Ukrainian Journal of Chemistry, Vol. 52, No 12, pp 1260-1263 (1986)
30. Bonnell, D. A., Tien, T. Y., and Ruhle, Manfred, "Controlled Crystallization of the Amorphous Phase in Silicon Nitride Ceramics," J. Am. Ceram. Soc., 70 (7) 460-65 (1987)
31. Booser, E. R., editor: "CRC Handbook of Lubrication (Theory and Practice of Tribology) Volume II, Theory and Design," CRC Press, Boca Raton, 1986
32. Bos, A., "The Temperature at the Wear Scars of the Four-Ball Apparatus," Wear, 31, 17-27 (1975)
33. Bowden, Dr. F. P., "Friction," Nature, 166, pp 330-334 (1950)
34. Bowen, H. K., "Advanced Ceramics," Scientific American, October, pp 169-176, (1986)
35. Braendle, R. O., Estersil-Thickened Lubricating Composition Modified With Hydrogen-Bonding Donor Compound, and Process of Making," Patent # 2,746,922, May 22 (1956)
36. Braza, J. F., Cheng, H. S., and Fine, M. E., "Silicon Nitride Wear Mechanisms: Rolling and Sliding Contact," Tribology Transactions, 32, 4, pp 439-446 (1989)

37. Brinker, C. J., Clark, D. E., and Ulrich, D. R., Better Ceramics Through Chemistry, North-Holland, New York (1984)
38. Brinker, C. J., Clark, D. E., and Ulrich, D. R., Better Ceramics Through Chemistry II, North Holland, New York (1986)
39. Brinker, C. J., and Scherer, G. W., Sol-Gel Science, Academic Press, New York (1990)
40. Brow, R. K., and Pantano, C. G., "Thermochemical Nitridation of Microporous Silica Films in Ammonia," J. Am. Ceram. Soc., 70, 1, pp 9-14 (1987)
41. Brown, Jr., E. D., "The Friction and Wear of Glass," STLE SP-23 Tribology of Ceramics Volume 1, pp 68-74 (1987)
42. Buckley, D. H., Friction, Wear, and Lubrication in Vacuum, NASA SP-277, Washington, DC (1971)
43. Buckley, D. H., "Friction and Wear of Ceramics," Ceramic Bulletin, 51, 12 (1972)
44. Buckley, D. H., Surface Effects in Adhesion, Friction, Wear, and Lubrication, Tribology Series #5, Elsevier, New York (1981)
45. Buckley, D. H. and Miyoshi, K., "Friction and Wear of Ceramics," Wear, 100, pp 333-353 (1984)
46. Buckley, D. H. and Miyoshi K., "Fundamental Tribological Properties of Ceramics," American Ceramic Society, ISSN 0196-6219, pp 919-939 (1985)
47. Bull, S. J., and Page, T. F., "The Friction and Wear of Ion-Implanted Ceramics: The Role of Adhesion," Nuclear Instruments and Methods in Physics Research B, 32, pp 91-95 (1988)
48. Burwell, R. L., "Modified Silica Gels as Adsorbents and Catalysts," Chemtech, June, pp 370-377 (1974)
49. Busca, G., Lorenzelli, V., Baraton, M. I., Quintard, P., and Marchand R., "FT-IR Characterization of Silicon Nitride Si_3N_4 and Silicon Oxynitride Si_2ON_2 Surfaces," Journal of Molecular Structure 143, pp 525-528 (1986)
50. Busca, G., Lorenzelli, V., and Porcile, G., "FT-IR Study of the Surface Properties of Silicon Nitride," Materials Chemistry and Physics, 14, pp 123-140 (1986)

51. Canby, T., "Reshaping Our Lives, Advanced Materials," National Geographic, December, pp 746-781 (1989)
52. Ceramic Source, American Ceramic Society, Vol. 1, p 341, (1985)
53. Chandrasekar, S. and Bhushan, Bharat, "Friction and Wear of Ceramics for Magnetic Recording Applications - Part I: A Review," Journal of Tribology, 112 (Jan 1990)
54. Charles River Associates Incorporated, "Technological and Economic Assessment of Advanced Ceramic Materials --, Vol 1: Summary and Conclusions," 19 Planning Report, NBS GCR 84-470-1, (1984)
55. Chen, C. I., "Utilization of Metals to Improve the Lubrication of Ceramic Load-Bearing Surfaces," MS Thesis in Chemical Engineering, The Pennsylvania State University (1990)
56. Chiang, J. N., Ghanayem, S. G., and Hess, D. W., "Low-Temperature Hydrolysis (Oxidation) of Plasma-Deposited Silicon Nitride Films," Chemistry of Materials, 1, pp 194-198 (1989)
57. Childs, T. H. C. and Parker, I. K., "The Fine Friction Cutting of Sialon and Silicon Nitride Ceramics," Proceedings of JITC, Nagoya, pp 373-378 (1990)
- 57a. Cho, L. and Klaus, E. E., "Oxidative Degradation of Phosphate Esters," ASLE Trans., 24, 1, 119-124 (1979)
58. Chuiko, A. A., Mashchenko, V. M., Tertykh, V. A., Finn, L. P., Khaber, N. V., and Manchenko, L. V., "Kinetics of the Chemisorption of n-Butanol Vapor by Silica Surface," Kolloida, Zh., 35, pp 89-94 (1973)
- 58a. Clark, D. B., Klaus, E. E., and Hsu, S. M., "The Role of Iron and Copper in the Oxidative Degradation of Lubricating Oils," Lubrication Engineering, 41, 5, pp 280-287 (1985)
59. Coon, D. N., Tallman, R. L., and Neilson, Jr., R. M., "Hot Isostatically Pressed Si_3N_4 - Si_3N_4 Joints Bonded with Oxynitride Glass," Advanced Ceramic Materials, 3, 2, pp 154-58 (1988)
60. Cotter, D. J., Koenigsberg, W. D., Pasto, A. E., and Bowen, L. J., "Improving the Reliability of High-Performance Ceramics Using Nondestructive Evaluation," Ceram. Eng. Sci. Proc., 9, pp 1503-1516 (1988)
61. Cranmer, D. C., "Friction and Wear Properties of Monolithic Silicon-Based Ceramics," Journal of Materials Science, 20, pp 2029-2037 (1985)

62. Cranmer, D. C., "Ceramic Tribology - Needs and Opportunities," *Tribology Transactions*, 31, 2, pp 164-173 (1987)
63. Cranmer, D. C., "Wear Surface Analysis of Silicon Nitride," *Lubrication Engineering*, 44, 12, pp 975-980 (1987)
64. Crosbie, G. M., Predmesky, R. L., Nicholson, J. M. and Stiles, E. D., "Prepilot Scale Synthesis of Silicon Nitride Under Pressure," *Ceramic Bulletin*, 68, No. 5 (1989)
65. Curthoys, G., Davydov, V. Ya, Kiselev, A. V., Kiselev, S. A., and Kuznetsov, B. V., "Hydrogen Bonding in Adsorption on Silica," *Journal of Colloid and Interface Science*, 48, 1, (1974)
66. Czernuszka, J. T. and Page, T. F., "Characterizing the Surface Contact Behaviour of Ceramics - Part 2 Chemo-Mechanical Effects," *Journal of Materials Science*, 22, pp 3917-3923 (1987)
67. Czichos, H., Becker, S., and Lexow, J., "Multilaboratory Tribotesting: Results from the Versailles Advanced Materials and Standards Programme on Wear Test Methods," *Wear*, 114, pp 109-130 (1987)
68. Dean, J. A., editor: "Lange's Handbook of Chemistry," 12th edition, McGraw-Hill, New York (1979)
69. Deuel, H., and Gentili, R., "Über das Mahlen von Quarzpulvern in Gegenwart Organischer Verbindungen," *Helvetica Chimica Acta*, 39, 6, pp 1586-1589 (1956) [in German]
70. Doremus, R. H., Glass Science, John Wiley and Sons, New York (1973)
71. Dufrane, K. F., "Wear Performance of Ceramics in Ring/Cylinder Applications," *Ceram. Eng. Sci. Proc.*, 9, pp 1409-1418 (1988)
72. Durham, B. G., Murtha, M. J., and Burnet, G., " Si_3N_4 by the Carbothermal Ammonolysis of Silica," *Advanced Ceramic Materials*, 3, 1, pp 45-48 (1988)
73. Ekelund, M., Forslund, B., Eriksson, G., and Johansson, T., "Si-C-O-N High-Pressure Equilibria and ΔG°_f for Si_2ON_2 ," *J. Am. Ceram. Soc.*, 71, 11, pp 956-60 (1988)
- 73a. Eldridge, J. M. and Balk, P., "Formation of Phosphosilicate Glass Films on Silicon Dioxide," *Transactions of the Metallurgical Society of AIME*, Vol. 242 (Mar 1968)

74. Engineering Science Data: Physical Data, Chemical Engineering, "Viscosity of Liquid Aliphatic Alcohols," Sub-Series Volume 5, April (1988)
75. Enomoto, Y., "Wearing Behavior of Silicon Nitride in Plane Contact," Proceedings of the Institute of Mechanical Engineers International Conference Tribology- Friction, Lubrication and Wear Fifty Years On, vol. 1, pp 173-178 (1987)
76. Erdemir, A., Fenske, G. R., Nichols, F. A., Erck, R. A., and Busch, D. E., "Self-Lubricating Boric Acid Films for Tribological Applications," Proceedings of JITC, Nagoya, pp 1797-1802 (1990)
77. Ermer, E. and Ptak, W. S., "Infrared Studies of Silicon Nitride," Journal of Molecular Structure 143, 5-8 (1986)
78. Fein, R. S., and Villforth, F. J. Jr., "Lubrication Fundamentals," Lubrication, 59, Oct-Dec, pp 77-88 (1973)
79. Fein, R. S., "Boundary Lubrication," pp 49-68, CRC Handbook of Lubrication Vol II Theory and Design, CRC Press, Boca Raton (1986)
80. Fein, R. S., "A Perspective on Boundary Lubrication," Ind. Eng. Chem. Fundam, 25, pp 518-524 (1986)
81. Fein, R. S., "Boundary Lubrication," Lubrication Engineering, 47, 12, pp 1005-1008 (1991)
82. Fischer, T. E. and Tomizawa, H., "Interaction of Tribochemistry and Microfracture in the Friction and Wear of Silicon Nitride," Wear, 105, pp 29-45 (1985)
83. Ford, J. F., "Lubricating Oil Additives - A Chemist's Eye View," Journal of the Institute of Petroleum, 54, 535, pp 198-210 (1968)
84. Fox, D. S. and Jacobson, N. S., "Molten-Salt Corrosion of Silicon Nitride: I, Sodium Carbonate," J. Am. Ceram. Soc., 71, 2, pp 128-38 (1988)
85. Freiman, S. W., "Effects of Chemical Environments on Slow Crack Growth in Glasses and Ceramics," Journal of Geophysical Research, 89, B6, pp 4072-4076 (1984)
86. Fronczak, E. T., "Silica-Thickened Grease Containing Alkylene Carbonate Dispersant," Patent # 2,939,840, Jun 7 (1960)
87. Fukuhara, M., "Effect of Nitrogen on the α/β Phase Conversion in Silicon Nitride," Communications of the American Ceramic Society, September (1985)

88. Furey, M. J. and Kajdas, C., "Models of Tribopolymerization as an Anti-Wear Mechanism," Proceedings of JITC, Nagoya, pp 1089-1094 (1990)
89. Furey, M. J. and Jayaram, S., "Advanced Techniques in Infrared Measurements of Surface Temperatures Produced by Friction," Proceedings of JITC, Nagoya, pp 1569-1574 (1990)
90. Garcia-Borras, T., "Lube Oil Additives," Chemtech, Dec, pp 752-755 (1986)
91. Gates, R. S., Yellets, J. P., Deckman, D. E., and Hsu, S. M., "Considerations in Ceramic Friction and Wear Measurements," ASTM STP 1010 Selection and Use of Wear Tests for Ceramics, C. S. Yust and R. G Bayer Eds., ASTM, Philadelphia, pp 1-23 (1985)
92. Gates, R. S., Jewett, K. L., and Hsu, S. M., "A Study on the Nature of Boundary Lubricating Film: Analytical Method Development," STLE Tribology Transactions, 32, 4, 423-430 (1989)
93. Gates, R. S., Hsu, S. M., and Klaus, E. E., "Tribochemical Mechanism of Alumina with Water," Trib Trans., 32, 3, pp 357-363 (1989)
94. Gates, R. S., and Hsu, S. M., "Effect of Selected Chemical Compounds on the Lubrication of Silicon Nitride," STLE Tribology Transactions, Vol 34, 3, pp 417-425 (1991)
95. Gecim, B., "Transient Hot Spot Temperatures at a Sliding Ceramic Contact Including Surface Coating Effects," Wear, 123, pp 59-76 (1988)
96. Gee, M. G., Matharu, C. S., Almond, E. A., and Eyre, T. S., "The Measurement of Sliding Friction and Wear of Ceramics at High Temperature," Wear of Materials, pp 387-397 (1989)
97. Georges, J-M, Loubet, J-L, Tonck, A., Mazuyer, D., and Hoornaert, P., "On the Mechanical Properties of Overbased Calcium Detergent Films," Proceedings of JITC, Nagoya, pp 517-522 (1990)
98. Glaeser, W., "Friction," Lubrication Engineering, Feb, pp 129-132 (1992)
- 98a. Godfrey, D, "The Lubrication Mechanism of Tricresyl Phosphate on Steel," ASLE Trans., Vol. 8, 1-11 (1965)
99. Goebel, M. T., "Method of Activating and Esterifying the Surface of Finely Divided Particles of Silica Having Surface Silanol Groups," Patent # 2,736,669, Feb 28 (1956)

100. Goto, T., Itoh, F., Suzuki, K., and Hirai, T., "ESCA Study of Amorphous CVD Si_3N_4 -C Composites," *J. Mat. Sci. Lett.*, 2, pp 805-807 (1983)
101. Gregory, O. J. and Richman, M. H., "Thermal Oxidation of Sputter-Coated Reaction-Bonded Silicon Nitride," *J. Am. Ceram. Soc.*, 67, 5, pp 335-340 (1984)
102. Groszek, A. J., "Role of Adsorption in Liquid Lubrication," NASA SP-318 Interdisciplinary Approach to Liquid Lubricant Technology, pp 477-525 (1973)
103. Gruss, W. W., "Ceramic Tools Improve Cutting Performance," *Ceramic Bulletin*, 67, 6 (1988)
104. Guglielmi, M., Scarinci, G., and Maliavsky, N., "Preparation and Properties of Silica and Silicate Gels by the Alkoxide, Colloidal and Amine-Silicate Methods," *Ceramics International*, 14, pp 153-161 (1988)
105. Gutkowski, Structures: Fundamental Theory, Van Nostrand Reinhold, New York (1990)
106. Habeeb, J. J., Blahey, A. G., and Rogers, W. N., "Wear and Lubrication of Ceramics," *IMEchE*, pp 554-564 (1987)
107. Hair, M. L., Infrared Spectroscopy in Surface Chemistry, Marcel Dekker, New York (1967)
108. Hampshire, S., Non-Oxide Technical and Engineering Ceramics, Elsevier, New York (1986)
109. Hamrock, B. J., and Dowson, D., "Isothermal Elastohydrodynamic Lubrication of Point Contacts Part III - Fully Flooded Results," *Journal of Lubrication Technology*, Apr. , pp 264-276 (1977)
110. Hart, A. M., Peters, B. C., Plonka, J. H., and Werst, Jr., W. H., "Advanced Ceramic Opportunities: A Review," *Chem. Eng. Progress*, April, pp 32-43 (1989)
111. Hattori, M., and Wagata, S., "Reactions of Silicon Nitrides and Alcohols," 56th Annual Meeting of the Chemical Society of Japan, Abstracts, Vol I, p 790, Tokyo, Apr. (1988) [In Japanese]
112. Hecht, N. L., McCullum, D. E., and Graves, G. A., "Investigation of Selected Silicon Nitride and Silicon Carbide Ceramics," *Ceram. Eng. Sci. Proc.*, 9, pp 1313-1332 (1988)

113. Heinrich, J., Backer, E., and Bohmer M., "Hot Isostatic Pressing of Si_3N_4 Powder Compacts and Reaction-Bonded Si_3N_4 ," J. Am. Ceram. Soc., 71, 1, pp C-28-C-31 (1988)
114. Helden, A. K. Van, Vroegop, P. H., and Jongh, J. J. M., "Dynamic Adsorption in Mixed Lubrication," Tribology Transactions, 32, 2, pp 239-245 (1989)
115. Henager, Jr., C. H. and Jones, R. H., "Environmental Effects on Slow Crack Growth in Silicon Nitride," Ceram. Eng. Sci. Proc., 9, pp 1525-1530 (1988)
116. Her, R. K., "Lubricating Composition Containing Surface-Esterified Siliceous Solid," Patent # 2,676,148, Apr 20 (1954)
117. Her, R. K., "Composition Containing Surface-Esterified Siliceous Solid and Silicone Oil," Patent # 2,705,700, Apr 5 (1955)
118. Hertz, W. H., "Ueber die Beruthrung fester elastischer Korper," Journal fur die Reine und angewandte Mathematik, pp, 156-171 (1882) [In German]
119. Hibi, Y. and Enomoto, Y., "Lubrication of Ceramics in Water with Silane Coupling Agents," Proceedings of JITC, Nagoya, pp 451-456 (1990)
120. Hibi, Y. and Enomoto, Y., "Friction and Wear of Silicon Nitride in Water, n-Alcohols, Water-Methanol, and Water-Glycol," Bulletin of Mechanical Engineering Laboratory No. 53, (1990)
121. Hira, F., Kuwano, N., and Ohno, N., "Static and Dynamic Conditions Concerning Glass Transition and Elastic-Plastic Transition of Lubricants," Proceedings of JITC, Nagoya, pp 1629-1634 (1990)
122. Hirao, K. and Tomozawa, M., "Microhardness of SiO_2 Glass in Various Environments," J. Am. Ceram. Soc., 70, 7, pp 497-502 (1987)
123. Hirosaki, N., Okada, A., and Matoba, K., "Sintering of Si_3N_4 with the Addition of Rare-Earth Oxides," Communications of the American Ceramic Society, Mar. , pp C144-C147 (1988)
124. Hokkirigawa, K., Kato, K., Kitsunai, H., and Mizumoto, M., "Microscopic Wear Mechanism of Alumina and Silicon Nitride Observed in the Fe-SEM-Tribosystem," Proceedings of JITC, Nagoya, pp 1413-1418 (1990)
125. Homeny, J., Nelson, G. G., and Paulik S. W., "Comparison of the Properties of Oxycarbide and Oxynitride Glasses," J. Am. Ceram. Soc., 70 (5) C114-C116 (1987)

- 125a. Hoornaert, P., Faure, D., Hallouis, M., and Martin, J. M., "Tribiochemistry of Overbased Sulfonate Detergents a TEM Study," Proceedings of JITC, Nagoya, pp 415-429 (1990)
126. Horn, R. G., Smith, D. T., and Haller, W., "Surface Forces and Viscosity of Water Measured Between Silica Sheets," Chemical Physics Letters, 162, 4, pp 404-408 (1989)
127. Hsu, S. M., "Boundary Lubrication of Materials," MRS Bulletin, October, pp 54-57 (1991)
128. Hsu, S. M., Pei, P., and Ku, C. S., "Mechanisms of Additive Effectiveness," Lub. Sci., 1, 2, pp 165-184 (1989)
129. Hsu, S. M., Klaus, E. E., and Cheng, H. S., "A Mechano-Chemical Descriptive Model for Wear Under Mixed Lubrication Conditions," Wear, 128, pp 307-323 (1988)
130. Hsu, S. M., Wang, Y. S., and Munro, R. G., "Quantitative Wear Maps as a Visualization of Wear Mechanism Transitions in Ceramic Materials," Reprint from Wear of Materials, Vol. 2, Book No. HO456B, pp 723-728 (1989)
131. Hyde, J. F., "Siloxane Elastomers Comprising a Modified Acid Polymer and Filler," Patent # 2,571,039, Oct. 9 (1951)
132. Iler, R. K., "Silicic Acid Compositions," Patent # 2,408,655, Oct 1 (1946)
133. Iler, R. K., "Method of Esterifying the Surface of a Silica Substrate Having a Reactive Silanol Surface and Product Thereof," Patent # 2,657,149, Oct 27 (1953)
134. Iler, R. K., "Lubricating Composition Containing Surface-Esterified Silaceous Solid," Patent # 2,676,148, Apr 20 (1954)
135. Iler, R. K., "Composition Containing Surface-Esterified Siliceous Solid and Silicon Oil," Patent # 2,705,700, Apr 5 (1955)
136. Iler, R. K., "Chemical Process and Product," Patent # 2,739,074, Mar 20 (1956)
137. Iler, R. K., "Product Comprising a Skin of Dense Hydrated Amorphous Silica Bound Upon a Core of Another Solid Material and Process of Making the Same," Patent # 2,885,366, May 5 (1959)
138. Iler, R. K., The Chemistry of Silica, John Wiley and Sons, New York (1979)

139. Ishigaki, H., Kawaguchi, I., Iwasa, M., and Tokbana, Y., "Friction and Wear of Hot Pressed Silicon Nitride and Other Ceramics," *Wear of Materials*, pp 13-21 (1985)
140. Jackson, A., "Elastohydrodynamic Lubrication (EHL)," *Lubrication Engineering*, 47, 10, pp 833-835 (1991)
141. Jacobson, N. S., "Kinetics and Mechanism of Corrosion of SiC by Molten Salts," *J. Am. Ceram. Soc.* 69, 1, pp 74-82 (1986)
142. Jacobson, N. S. and Fox, D. S., "Molten-Salt Corrosion of Silicon Nitride: II, Sodium Sulfate," *J. Am. Ceram. Soc.*, 71, 2, pp 139-48 (1988)
143. Jahanmir, S. and Fischer, T. E., "Friction and Wear of Silicon Nitride Lubricated by Humid Air, Water, Hexadecane and Hexadecane + 0.5 Percent Stearic Acid," *STLE Transactions*, 31, 1, pp 32-43 (1986)
- 143a. Jeng, G.S., "Interaction at High Temperatures of Phosphate Esters in the Vapor Phase with Metal Surfaces," PHD thesis, The Pennsylvania State University, May 1987
144. Jennings, H., "On the Influence of Iron on the Reaction Between Silicon and Nitrogen," *J. Mater. Res.*, 3, 5, pp 907-910 (1988)
145. Kanno, Y., Suzuki, K., and Yoshitaka, K., "NH₃ Formation Caused by the Presence of H₂O in the Wet Grinding of Silicon Nitride Powder," *Yogyo-Kyokai-shi*, 131, pp 386-387 (1983) [In Japanese]
146. Kato, K., "Tribology of Ceramics," *Wear*, 136, pp 117-133 (1990)
147. Kiehle, A. J., Heung, L. K., Gielisse, P. J., and Rockett, T. J., "Oxidation Behavior of Hot-Pressed Si₃N₄," *Journal of the American Ceramic Society*, 58, 1, pp 17-20 (1975)
148. Killman, E., and Eckart, R., "Kalorimetrische Untersuchungen zur Adsorption von Macromolekullen aus verdunnten Losungen," *Die Makromolekulare Chemie*, 144, pp 45-61 (1971) [In German]
149. Kimura Y., Okada, K., and Enomoto, Y., "Sliding Damage of Silicon Nitride in Plane Contact," *Wear of Materials*, pp 361-368 (1989)
150. Kingery, W. D., Bowen, H. K., and Uhlmann, D. R., Introduction to Ceramics, John Wiley and Sons, New York (1976)

151. Kingsbury, E. P., "Some Aspects of the Thermal Desorption of a boundary Lubricant," *Journal of Applied Physics*, 29, 6, pp 888-891 (1958)
152. Kirchner, Henry P., "Damage Penetration at Elongated Machining Grooves in Hot-Pressed Si_3N_4 ," *J. Am. Ceram. Soc.*, 67, 2, pp 127-132 (1984)
153. Kiselev, A. V., Korolev, A. Y., and Él'tekov, Y. A., "Adsorption on Estersils," *Colloid Journal of the USSR (Eng Trans)*, 25, pp 140-142 (1963)
154. Kistler, S., "Gel and Lubricant Made Therefrom," Patent # 2,260,625, Oct 28 (1941)
155. Klaus, E. E. and Bieber, H. E., "Effects of P^{32} Impurities on the Behavior of Tricresyl Phosphate-32 as an Antiwear Additive," *ASLE Trans.*, 8, pp 12-20 (1965)
156. Klaus, E. E., Duda, J. L., and Wu, W. T., "Lubricated Wear of Silicon Nitride," *Lubrication Engineering*, 47, 8, pp 679-684 (1991)
157. Klaus, E. E., Duda, J. L., and Chao, K. K., "A Study of Wear Chemistry Using a Micro Sample Four-Ball Wear Test," *Tribology Transactions*, 34, 3, pp 426-432 (1991)
- 157b. Klaus, E. E., Krishnamacher, V., Dang, H., "Evaluation of Basestock and Formulated Lubes Using the Penn State Microoxidation Test," *Proceedings of the conference on Measurements and Standards for Recycled Oil*, NBS Special Publication 584, pp 285-295 (1980)
- 157a. Klaus, E. E., Phillips, J., Lin, S. C., Wu, N. L., and Duda, J. L., "Structure of Films Formed During the Deposition of Lubrication Molecules on Iron and Silicon Carbide," *Tribology Transactions*, 33, 1, pp 25-32, (1990)
158. Kooi, E., The Surface Properties of Oxidized Silicon, Springer-Verlag, New York, (1967)
159. Kuzuba, T., Kijima, K., and Bando, Y., "Raman-Active Modes of Alpha Silicon Nitride," *J. Chem. Phys.* 69, 1, pp 40-42 (1978)
160. Lambert, R., and Singer, N., "An Isomer Effect on the Chemisorption of the Pentanols on Cab-O-Sil," *Journal of Colloid and Interface Science*, 45, 3, pp 440-448 (1973)
161. Lange, K. R., "Reactive Organic Molecules on Silica Surfaces," *Chemistry and Industry*, Sep. 6, pp 1273-1274 (1969)

162. Larsen, R. P. and Vyas, A. D., "The Outlook for Ceramics in Heat Engines, 1990-2010: Results of a Worldwide Delphi Survey," SAE Technical Paper Series 880514, pp 1-23 (1988)
163. Lauer, J. L. and Dwyer, S. R., "Lubrication of Ceramics by Surface-Generated Carbon From Gaseous Feed," Proceedings of JITC, Nagoya, pp 989-994 (1990)
- 163a. Lawn, B., and Wilshaw, R., "Indentation Fracture: Principles and Applications," Journal of Material Science, 10, pp 1049-1081 (1975)
164. Lay, L., "Corrosion Resistance of Technical Ceramics," National Physical Laboratory, London (1984)
165. Lee, L-H, Fundamentals of Adhesion, Plenum Press, New York (1991)
166. Levitz, P., Van Damme, H., and Keravis, D., "Fluorescence Decay Study of the Adsorption of Nonionic Surfactants at the Solid-Liquid Interface. 1. Structure of the Adsorption Layer on a Hydrophilic Solid," The Journal of Physical Chemistry, 88, 11, pp 2228-2235 (1984)
167. Levitz, P., and Van Damme, H., "Fluorescence Decay Study of the Adsorption of Nonionic Surfactants at the Solid-Liquid Interface. 2. Influence of Polar Chain Length," The Journal of Physical Chemistry, 90, 7, pp 1302-1310 (1986)
168. Levy, A. V. and Nee, N., "Unlubricated Sliding Wear of Ceramic Materials," Wear, 121, 363-380 (1988)
169. Ling, F. F., and Pan, C. H. T., Approaches to Modeling of Friction and Wear, Springer Verlag, New York (1988)
170. Longson, B., "Lubrication of High Temperature Ceramic Materials," Tribology International, 16, 4, pp 177-232 (1983)
171. Luongo, J. P., "Infrared Characterization of α - and β -Crystalline Silicon Nitride," J. Electrochem. Soc.: Solid-State Science and Technology, 130, 7, pp 1560-1562 (1983)
172. Marra, J. E. and Kreidler, E. R. (Ohio State), Jacobson, N. S., and Fox, D. S., (NASA), "Reactions of Silicon-Based Ceramics in Mixed Oxidation Chlorination Environments," Journal of the American Ceramic Society, 71, 12, pp 1067-1073 (1988)

173. Marshall, K. and Rochester, C. H., "Infrared Study of the Adsorption of Oleic and Linolenic Acids onto the Surface of Silica Immersed in Carbon Tetrachloride," J. Chem. Soc. Faraday Trans. 1, 71, pp 1754-1761 (1975)
174. Mecartney, M. L. and Sinclair, R., "Silicon Nitride Joining," J. Am. Ceram. Soc., 68, 9, pp 472-478 (1985)
175. Mieskowski, D. M. and Sanders, W. A., "Microstructure of Reaction-Bonded Silicon Nitride Consolidated by Isostatic Hot-Pressing," Communications of the American Ceramic Society, Aug., pp C217-218 (1985)
176. Mieskowski, D. M. and Sanders, W. A., "Oxidation of Silicon Nitride Sintered with Rare-Earth Oxide Additions," Communications of the American Ceramic Society, Jul., pp C160-C163 (1985)
177. Miyake, S., Takahashi, S., Watanabe, I., and Yoshihara, H., "Friction and Wear Behavior of Hard Carbon Films," ASLE Transactions, 30, 1, pp 121-127 (1987)
178. Mizutani, Y., Shimura, Y., Yahagi, Y., and Hotta, S., "Friction and Wear of Ceramics in Various Environments," Proceedings of JITC, Nagoya, pp 1461-1466 (1990)
179. Morales, W. and Buckley, D. H., "Concentrated Contact Sliding Friction and Wear Behaviour of Several Ceramics Lubricated with a Perfluoropolyalkylether at 25°C," Wear, 123, pp 345-354 (1988)
180. Morgan, P. E., "The α/β -Si₃N₄ Question," J. Mat. Sc. Lett., 15, pp 741-793 (1980)
181. Morgan, Peter E. D. and Pugar, Eloise A., "Synthesis of Si₃N₄ with Emphasis on Si-S-N Chemistry," J. Am. Ceram. Soc., 68, 12, pp 699-703 (1985)
182. Mori, M., Sasaki, T., and Takahasi, T., "Adsorption of Lubricants in Sliding surfaces of Ceramics," The 31st JULE Annual Meeting, Nagoya, pp 89-92 (1986)
183. Mori, S., and Imaizumi, Y., "Adsorption of Model Compounds of Lubricant on Nascent Surfaces of Mild and Stainless Steels Under Dynamic Conditions," STLE Tribology Transactions, 31, 4, pp 449-453 (1987)
184. Morrison, J. A., Thakker, A. B., and Armini, A. J., "Ion Implantation of Silicon Nitride for Rolling Element Bearing Applications," Ceram. Eng. Sci. Proc., 9, pp 1265-1276 (1988)

185. Mukerji, J. and Rakshit, J., "Dependence of Strength and Toughness of Reaction Bonded Silicon Nitride and Composites on Fabrication Routes," *Ceramics International* 14, 181-189 (1988)
186. Munro, R. G., "Temperature Considerations in the Study of Surfaces Using a Four-Ball Wear Apparatus," *J. Appl. Phys.* 57, 11, pp 4950-4953 (1985)
187. Myers, D., Surfactant Science and Technology, VCH Publishers, New York (1988)
188. Nilsen, K. J., Riman, R. E., and Danforth, S. C., "The Effect of Moisture on the Surface Chemistry and Dispersion Properties of Silicon Nitride in Imidazoline-Hexane Solutions," *Ceramic Transactions*, 1, Part A, pp 469-475 (1988)
189. O'Brien, J. A., "Lubricating Oil Additives," CRC Handbook of Lubrication, Vol. II, CRC Press, Boca Raton (1986)
190. Page, T. F., "Ion Implantation into Ceramics," pp 247-252 from Encyclopedia of Materials Science and Engineering, Pergammon Press, New York (1986)
191. Page, T. F., Sawyer, G. R., Adewoye, O. O., and Wert, J. J., "Hardness and Wear Behaviour of SiC and Si₃N₄ Ceramics," *Proc. Br. Cer. Soc.*, 26, pp 193-208 (1987)
192. Pallini, R. A. and Wedeven, L. D., "Traction Characteristics of Graphite Lubricants at High Temperature," *STLE, Tribology Transactions*, 31, 2, pp 289-295 (1987)
193. Park Jr., Y., Kim, J. R., and Kim, C. H., "Effects of Free Silicon on the α to β Phase Transformation in Silicon Nitride," *J. Am. Ceram. Soc.*, 70, 10, pp C-240-C-242 (1987)
194. Pasto, Arvid E., "Causes and Effects of Fe-Bearing Inclusions in Sintered Si₃N₄," *J. Am. Ceram. Soc.*, 67, pp C240-C242 (1984)
- 194a. Patent, Farberfabriken Bayer, "Mixed Condensates of Polyanhydride Structure," British Patent # 706,781, April 7, 1954
195. Perry, R. H., and Chilton, C. E., editors: "Chemical Engineers Handbook," Fifth Edition, McGraw-Hill, New York (1973)
196. Plagge, A., "Reduction of Friction and Wear on Ceramic Materials by Use of Solid Lubricants," *Proceedings of JITC, Nagoya*, pp 673-676 (1990)
197. Plueddemann, E.P., Silane Coupling Agents, Plenum Press, New York (1982)

198. Polivanov, A. N., Bernadskii, A. A., Silkina, N. N., Klimentov, B. N., and Bochkarev, V. N., "Mass Spectrometry Study of Alkoxy- and Chloro- Silanes," *Zhurnal Obshchei Khimii*, 50, 8, pp 1780-1783 (1980)
199. Prakash, B., Wani, M. F., Mukerji, J., and Das, P. K., "Tribological Studies of Hot Pressed Silicon Nitride and Composites," *Proceedings of JITC, Nagoya*, pp 1383-1388 (1990)
200. Pulker, H. K., Coatings on Glass, John Wiley and Sons, New York (1973)
201. Quinn, T. F. J., "The Role of Oxidation in the Mild Wear of Steel," *B. J. Appl. Phys*, 13, pp 33-37 (1962)
202. Quinn, T. F. J. and Winer, W. O., "Thermal Aspects of Oxidational Wear," *Wear*, 102, pp 67-80 (1985)
203. Rahaman, M. N., Boiteux, Y., and De Jonghe, L. C., "Surface Characterization of Silicon Nitride and Silicon Carbide Powders," *American Ceramic Society Bulletin*, 65, 8, pp 1171-1176 (1986)
204. Raider, S. I., Flitsch, R., Aboaf, J. A., and Pliskin, W. A., "Surface Oxidation of Silicon Nitride Films," *J. Electrochem. Soc. : Solid State Science and Technology*, 123, 4, pp 560-565 (1976)
205. Ramis, G., Busca, G., Lorenzelli, V., Baraton, M., Merle-Mejean, T., and Quintard, P., "FT-IR Characterization of High Surface Area Silicon Nitride and Carbide," pp 173-184, Surfaces and Interfaces of Ceramics, Kluwer Academic Publishers, Boston, (1989)
206. Ramsey, P. M. and Page, T. F., "A New Approach to Predicting the Wear Behaviour of Ceramic Surfaces," *Br. Ceram. Trans. J.*, 87, pp 74-80 (1988)
207. Ranney, M. W., Lubricant Additives, Noyes Data Corporation, Park Ridge (1973)
208. Ranney, M. W., Lubricant Additives : Recent Developements, Noyes Data Corporation, Park Ridge (1978)
209. Ranney, M. W., Synthetic Oils and Additives for Lubricants: Advances Since 1977, Noyes Data Corporation, Park Ridge (1980)
210. Richerson, D. W., Modern Ceramic Engineering Properties, Processing and Use in Design, 2nd Ed., Marcel Dekker, New York (1992)

211. Rimstidt, J. D. and Barnes, H. L., "The Kinetics of Silica-Water Reactions," *Geochemica et Cosmochem. Acta*, 44, pp 1684-1699 (1980)
212. Rossi, C., Munari, S., and Cengarle, L., "Reazioni di Superficie fra Silice e Alcoli," *La Chimica E L'Industria*, 41, pp 1067-1072 (1959) [In Italian]
- 212a. Rounds, F. G., "Effects of Additives on the Friction of Steel on Steel I. Surface Topography and Film Composition Studies," *ASLE Transactions*, 7, pp. 11-23 (1964)
213. Rowe, C. N., "Some Aspects of the Heat of Adsorption in the Function of a Boundary Lubricant," *ASLE Transactions*, 9, pp 100-111 (1966)
214. Rowe, C. N., "Role of Additive Adsorption in the Mitigation of Wear," *ASLE Transactions*, 13, pp 179-188 (1970)
215. Ruff, A. W., and Jahanmir, S., "Measurements of Tribological Behavior of Advanced Materials: Summary of U.S. Results on VAMAS Round-Robin No. 2," *NISTIR* 89-4170 (1989)
216. Saito, S., Fine Ceramics, Elsevier, New York (1988)
217. Sakurai, Toshio, "Role of Chemistry in the Lubrication of Concentrated Contacts," *Journal of Lubrication Technology*, 103, October, pp 473-485 (1981)
218. Sasaki, S., "The Effects of Surrounding Atmosphere on the Friction and Wear of Alumina, Zirconia, Silicon Carbide, and Silicon Nitride," *Wear of Materials*, pp 409-417 (1989)
219. Sato, Y. and Motoi, S., "Studies of the State of Iron Contained in α - and β -Silicon Nitride by Mossbauer and Raman Effects," *J. Phys. Chem. Solids*, 40, No. 1-A, pp 1-7 (1979)
220. Sato, Tsugio, Kanno, Yoshimi, Endo, Tadashi, and Shimada, Masahiko, "Corrosion of Si_3N_4 in Molten Alkali Sulfate and Carbonate," *Advanced Ceramic Materials*, 2 3A, pp 228-31 (1987)
221. Shaw, T. M. and Pethica B. A., "Preparation and Sintering of Homogeneous Silicon Nitride Green Compacts," *J. Am. Ceram. Soc.* 69, 2, pp 88-93 (1986)
222. Shimada, M., Sato, T., Koike, Y., and Endo, T., "Strength Degradation of Silicon Nitride Based Ceramics by Hot Corrosion in Alkalai Sulfate and Carbonate Melts," pp 831-840, *Proceedings of the Third International Symposium on Ceramic Materials and Components for Engines*, Las Vegas, 1988

- 223. Singhal, S. C., "Thermodynamics and Kinetics of Oxidation of Hot-Pressed Silicon Nitride," *Journal of Material Science*, 11, pp 500-509 (1976)
- 224. Singhal, S. C., "Effect of Water Vapor on the Oxidation of Hot-Pressed Silicon Nitride and Silicon Carbide," *Journal of the American Ceramic Society-Discussions and Notes*, 59, 1-2, pp 81-82 (1976)
- 224a. Sinitsyn, V. V., Kunina, E. A., Linnikova, O. P., and Aleshina, T. S., "Decomposition of Tricresyl Phosphate in Lubricating Greases at Elevated Temperatures," *Chemistry and Technology of Fuels and Oils*, vol. 10, pp. 485-487 (1987)
- 225. Smith, A. L., The Analytical Chemistry of Silicones, John Wiley & Sons, New York (1991)
- 226. Somiya, S., Mitomo, M., and Yoshimura, M., Silicon Nitride - 1, Elsevier, London, (1990)
- 227. Spikes, H. A., "Additive-Additive and Additive-Surface Interactions in Lubrication," *Lub. Sci.* 1, 2, pp 3-23 (1989)
- 228. Stöber, von W., "Adsorptionseigenschaften und Oberflächenstruktur von Quarzpulvern," *Kolloid Zeitschrift*, 145, 1, pp 17-46 (1956) [In German]
- 229. Studt, P., "Influence of Lubricating Oil Additives on Friction of Ceramics Under Conditions of Boundary Lubrication," *Wear*, 115, pp 185-191 (1987)
- 230. Sugita, T., Ueda, K., and Kanemura, Y., "Material Removal Mechanism of Silicon Nitride During Rubbing in Water," *Wear*, 97, pp 1-8 (1984)
- 231. Sullivan, J. L., "The Role of Oxides in the Protection of Tribological Surfaces - Part 1," Proceedings of the Institute of Mechanical Engineers International Conference Tribology - Friction, Lubrication and Wear Fifty Years On, pp 283-291 (1987)
- 232. Sullivan, J. L., "The Role of Oxides in the Protection of Tribological Surfaces - Part 2," Proceedings of the Institute of Mechanical Engineers International Conference Tribology - Friction, Lubrication and Wear Fifty Years On, pp 293-302 (1987)
- 233. Sutor, P., "Tribology of Silicon Nitride and Silicon Nitride-Stel Sliding Pairs," *Proceedings of the 9th Annual Conference on Composites and Advanced Materials*, Cocoa Beach FL, Jan 20-23, pp 460-469 (1985)

234. Takase, A., Umebayashi, S., and Kishi, K., "Infra-Red Absorption Spectroscopic Study of β -Sialons in the System $\text{Si}_3\text{N}_4\text{-Al}_2\text{O}_3\text{-AlN}$," Japanese Journal of Applied Physics, 21, 10, pp 1447-1450 (1982)
235. Takase, A., Umebayashi, S., and Kishi, K., "Infrared Spectroscopic Study of β -Sialons in the System $\text{Si}_3\text{N}_4\text{-SiO}_2\text{-AlN}$," Journal of Materials Science Letters 1, pp 529-532 (1982)
- 235a. Tien, T.-Y. and Hummel, F. A., "The System $\text{SiO}_2\text{-P}_2\text{O}_5$," J. Am. Ceram. Soc., 45 (9) 422-424, September 1962
236. Tomizawa, H. and Fischer, T. E., "Friction and Wear of Silicon Nitride at 150°C to 800°C ," ASLE Transactions, 29, 4, pp 481-488 (1985)
237. Tomizawa, H. and Fischer, T. E., "Friction and Wear of Silicon Nitride and Silicon Carbide in Water: Hydrodynamic Lubrication at Low Sliding Speed Obtained by Tribochemical Wear," ASLE Transactions, 30, 1, pp 41-46, (1986)
238. Tribology of Ceramics, Vol 1 Fundamentals, STLE SP-23 (1987)
239. Tribology of Ceramics, Vol 2 Applications, STLE SP-24 (1987)
- 239a. Tricaud, C., Hipeaux, J. C., and Lemerle, J., "Micellar Structure of Alkaline Earth Metal Alkylarylsulphonate Detergents," Lub. Sci. (1) pp. 207-218
240. Tsunai, Y., and Enomoto, Y., "Tribochemistry of Silicon Based Ceramics in Alcohols," Proceedings of the VIII International Symposium on Alcohol Fuels, Tokyo, pp 715-720, Oct. (1988)
241. Tsunai, Y. and Enomoto, Y., "Tribochemical Wear of Silicon Nitride in Water, n-Alcohols and Their Mixtures," Wear of Materials, pp 369-374 (1989)
242. Tsutsumi, "Reaction of 1-Butanol with Silicas," Nippon Kagaku Kaishi, 10, pp 180 (1972)
243. Tsuya, Y., "Tribology of Ceramics," Proceedings of the JSLE International Tribology Conference, July 8-10, Tokyo, Japan, (1985)
244. Tsuya, Y., Sakuta, Y., Akanuma, M., Murakami, T., Shimauchi, T., Chikugo, K., Kiuchi, Y., Takatsu, S., Katsumura, Y., Fukuhara, M., Umeda, K., Yaguchi, G., Enomoto, Y., and Yamanaka, K., "Compatibility of Ceramics with Oils," Proceedings of the JSLE International Tribology Conference, July 8-10, Tokyo, Japan, pp 167-172 (1985)

245. Unger, K. K., Porous Silica - Its Properties and Use as Support in Column Liquid Chromatography, Journal of Chromatography Library, Vol. 16, Elsevier, New York (1979)
246. Ura, A., Nakashima, A., and Moritaka, H., "The Effect of the Atmosphere on Wear and Friction of Engineering Ceramics," Proceedings of JITC, Nagoya, pp 1377-1382 (1990)
247. Utsugi, H., and Nishimura, S., "Studies on the Surface Properties of the Organophilic Silica Gels through the Adsorption of Various Kinds of Vapors and the Heats of Immersion," Zairo (Materials), 21, 225, pp 534-539 (1972) [in Japanese]
248. Utsugi, H., Nishimura, S., and Kano, T., "Preparation of Organophilic Silica Gels by the Surface-Treatment Through the Solutions of Various Kinds of Alcohols in Hydrocarbon, and Their Physicochemical Properties," (Sic) Zairo (Materials), 21, 225, pp 528-533 (1972) [in Japanese]
249. Utsugi, H., and Nishimura, S., "Studies on the Surface Properties of the Surface-Treated Silica Gels by the n-Pentanol Through the Adsorption of Various Kinds of Vapours and the Heats of Immersion," (Sic) Zairo (Materials), 22, 238, pp 680-683 (1973) [in Japanese]
250. Utsugi, H., Nishimura, S., and Horikoshi, H., "Surface Treatment of Silica Gels with Acetone- or Hexane- Solution of Alcohols or Phenols with Some Functional Groups and the Chemical Nature of their Surface Groups," (Sic) Zairo (Materials), 22, 238, pp 673-679 (1973) [in Japanese]
251. Utsugi, H., Matsuzawa, T., and Akoshima, A., "Dehydration and Surface- Treatment of Silica Gels with Alcohols in Hydrocarbons with High Boiling Point by Reflux Method," Zairo (Materials), 24, 262, pp 638-642 (1975) [in Japanese]
252. Utsugi, H., Matsuzawa, T., and Akoshima, A., "Surface Properties of Silica Gels Treated with Alcohols in Long Chain Hydrocarbons by Reflux Method," Zairo (Materials), 24, 262, pp 643-648 (1975) [in Japanese]
253. Utsugi, H., "The Identification of Surface Groups on the Surface-Treated Silica Gels Through Infrared Spectra," Journal of the Chemical Society of Japan, 12, pp 2237-2244 (1972) [in Japanese]
254. Utsugi, H., and Horikoshi, H., "Studies on the Surface Groups of the Surface-Treated Silica Gels by Means of the Differential Thermal and Thermogravimetric Analysis," Journal of the Chemical Society of Japan, 12, pp 2244-2255 (1972) [in Japanese]

- 255. Wada, N., Solin, S. A., Wong, J., and Prochazka, S., "Raman and IR Absorption Spectroscopic Studies on α , β , and Amorphous Si_3N_4 ," *Journal of Non-Crystalline Solids*, 43, pp 7-15 (1981)
- 256. Walsh, R., "Bond Energies of Silicon Compounds," *Acc. Chem. Res.*, pp 142-146 (1981)
- 257. Wang, H., Kimura, Y., and Okada, K., "Sliding Friction and Wear of Ceramics at Elevated Temperatures up to 1000°C," *Proceedings of JITC, Nagoya*, pp 1389-1394 (1990)
- 257a. Wang, F. X., Lacey, P. I., Gates, R. S., and Hsu, S. M., "A Study of the Relative Surface Conformity Between Two Surfaces in Sliding Contact," *ASME Journal of Tribology*, 113, October, pp 755-761 (1991)
- 258. Wang, P. S., Hsu, S. M., Malghan, S. G., and Wittberg, T. N., "Surface Oxidation kinetics of Si_3N_4 -4% Y_2O_3 Powders by Bremsstrahlung-Excited Auger Spectroscopy," *Journal of Material Science*, 26, pp 3249-3252 (1991)
- 259. Watson, G. K., Moore, T. J., and Millard, M. L., "Effect of Hot Isostatic Pressing on Reaction-Bonded Silicon Nitride," *Communications of the American Ceramic Society*, Oct. , pp C-208-C210 (1984)
- 260. Wayne, S. F. and Buljan, S. T., "The Role of Thermal Shock on Wear Resistance of Selected Ceramic Cutting Tool Materials," *Ceram. Eng. Sci. Proc.*, 9, pp 1395-1408 (1988)
- 261. Weast, R. C., editor: "CRC Handbook of Chemistry and Physics," 56th Edition, CRC Press, Cleveland (1975)
- 262. Wedeven, L. D., Pallini, R. A., and Miller, N. C., "Tribological Examination of Unlubricated and Graphite-Lubricated Silicon Nitride Under Traction Stress," *Wear*, 122, pp 183-205 (1988)
- 263. Wei, D., Han, X., and Wang, R., "The Influence of Chemical Structure of Certain Nitrogen-Containing Organic Compounds on Their Antiwear Effectiveness: The Critical Role of Hydroxy Group," *Lub. Sci.*, 1, 2, pp 63-87 (1989)
- 264. Willermet, P., "An Evaluation of Several Metals and Ceramics in Lubricated Sliding," *ASLE Transactions*, 30, 1, pp 128-130 (1987)
- 265. Winer, W. O., "A Review of Temperature Measurements in EHD Contacts," *Proceedings of the 5th Leeds-Lyons Symposium on Tribology*, University of Leeds, England, Sept. 19-22, pp 125-130 (1978)

266. Wright, M. S., Jain, V. K., and Saba, C. S., "Wear Rate Calculation in the Four-Ball Wear Test," *Wear*, 134, pp 321-334 (1989)
267. Ying, T. N., and Hsu, S. M., "Asperity-Asperity Contact Mechanisms Simulated by a Two-Ball Collision Apparatus," *Proceedings of the 1st International Workshop on Microtribology*, October 12-13, Morioka, Japan, pp 298-318 (1992)
268. Yust, C. S., "Wear of Advanced Ceramics: An Overview," *Proceedings of JITC*, Nagoya, pp 657-662 (1990)
269. Yust, C. S. and Carignan, F. J., "Observations on the Sliding Wear of Ceramics," *STLE Sp-23 Tribology of Ceramics*, vol 1, pp 213-220 (1987)
270. Zhang, S., and Cannon, W., "Preparation of Silicon Nitride from Silica," *J. Am. Ceram. Soc.*, 67, 10, pp 691-695 (1984)
271. Zutshi, A., "Effect of Microstructure on the Wear Resistance of Silicon Nitride," *PHD Thesis*, Rutgers University, 1992

Appendix A

AN ESTIMATE OF THE HERTZIAN CONTACT DIAMETER FOR THE FOUR-BALL CONTACT GEOMETRY

The Hertz¹¹⁸ equation for the four-ball contact geometry can be derived from the equation for a Hertzian elastic contact between two convex (ball) surfaces. For two balls simply labeled 1 and 2, the Hertz equation is:

$$\text{Contact Radius (mm)} = a = (10^3) \left[\frac{3 \pi P_1 (K_1 + K_2) R_1 R_2}{4 (R_1 + R_2)} \right]^{\frac{1}{3}}$$

Where P_1 = Normal force on surface of 1 ball (N)
 $= 0.408 * P * (9.8 \text{ N/kg}_f)$, where P is the applied load in kg_f

R_i = Radius of ball i (for our case both balls are the same radius $= 6.35 \times 10^{-3} \text{m}$)

K_i = Material constants involving Young's Modulus (E) and Poisson's Ratio (ν) such that

$$K = \frac{(1 - \nu^2)(10^{-9} \text{ GPa/Pa})}{\pi E}$$

Thus for the four-ball configuration with identical materials for the upper and lower specimens the equation reduces to:

$$d = 0.534 \left[\frac{P(1 - \nu^2)}{E} \right]^{\frac{1}{3}}$$

where d = diameter of the contact in mm
 P = Applied machine load in kg_f
 ν = Poisson's Ratio
 E = Young's Modulus in GPa

Calculated Hertzian Wear Scar Diameter and Pressure
for the Four-Ball configuration with Silicon Nitride Specimens

Applied Load (kg)	Hertzian W.S.Dia (mm)	Estimated Hertzian Pressure			
		Mean		Maximum*	
		(MPa)	(kpsi)	(MPa)	(kpsi)
1	0.077	857	124.2	1,285	186.4
2	0.097	1,079	156.5	1,619	234.8
3	0.111	1,235	179.2	1,853	268.8
4	0.122	1,360	197.2	2,040	295.8
5	0.132	1,465	212.4	2,197	318.7
6	0.140	1,557	225.8	2,335	338.6
8	0.154	1,713	248.5	2,570	372.7
10	0.166	1,846	267.7	2,768	401.5
12	0.176	1,961	284.4	2,942	426.7
14	0.186	2,065	299.4	3,097	449.2
16	0.194	2,159	313.1	3,238	469.6
18	0.202	2,245	325.6	3,368	488.4
20	0.209	2,325	337.2	3,488	505.9
25	0.225	2,505	363.3	3,757	544.9
30	0.240	2,662	386.0	3,993	579.1
35	0.252	2,802	406.4	4,203	609.6
40	0.264	2,930	424.9	4,395	637.4
45	0.274	3,047	441.9	4,571	662.9
50	0.284	3,156	457.7	4,734	686.6
60	0.302	3,354	486.4	5,031	729.6
70	0.318	3,531	512.0	5,296	768.1
80	0.332	3,691	535.3	5,537	803.0
90	0.345	3,839	556.8	5,759	835.2
100	0.358	3,976	576.7	5,964	865.0
120	0.380	4,225	612.8	6,338	919.2
150	0.410	4,552	660.1	6,827	990.2
180	0.435	4,837	701.5	7,255	1,052.3
210	0.458	5,092	738.5	7,638	1,107.7
240	0.479	5,324	772.1	7,986	1,158.2
270	0.498	5,537	803.0	8,305	1,204.5

* Maximum pressure = 1.5 x mean pressure for hemispherical pressure distribution.

Poissons ratio = 0.26
Young's Modulus = 310 GPa

Data supplied for Norton Noralide Silicon Nitride at 21°C

Appendix B

AN ESTIMATE OF THE HERTZIAN CONTACT DIAMETER FOR THE BALL-ON-THREE-FLAT CONTACT GEOMETRY

The Hertz equation for the ball-on-three-flat contact geometry is merely the limiting case of the convex on convex (ie four-ball type) geometry where the radius of the lower ball (R_1) $\rightarrow \infty$, which gives

$$\text{Contact Radius (mm)} = a = (10^3) \left[\frac{3 \pi P_1 (K_1 + K_2) R_2}{4} \right]^{\frac{1}{3}}$$

Where P_1 = Normal force on surface of 1 specimen (N)
 = $0.408 P$ (9.8 N/kg_f), where P is the applied load in kg_f

R_2 = Radius of ball (for our case = 6.35×10^{-3} m)

K_i = Material constants (for material i) involving Young's Modulus (E) and Poisson's Ratio (ν) such that

$$K = \frac{(1 - \nu^2)(10^{-9} \text{GPa/Pa})}{\pi E}$$

Thus for the ball-on-three-flat configuration, with similar materials for the upper and lower specimens, the equation reduces to

$$d = 0.673 \left[\frac{P(1 - \nu^2)}{E} \right]^{\frac{1}{3}}$$

where d = diameter of the contact in mm
 P = Applied load in kg_f
 ν = Poisson's Ratio
 E = Young's Modulus in GPa

Calculated Hertzian Wear Scar Diameter and Pressure
for the Ball-on-Three-Flat configuration with Silicon Nitride Specimens

Applied Load (kg)	Hertzian W.S.Dia (mm)	Estimated Hertzian Pressure			
		Mean		Maximum*	
		(MPa)	(kpsi)	(MPa)	(kpsi)
1	0.097	539	78.2	809	117.3
2	0.122	679	98.5	1,019	147.8
3	0.140	778	112.8	1,167	169.2
4	0.154	856	124.2	1,284	186.2
5	0.166	922	133.8	1,383	200.6
6	0.177	980	142.1	1,470	213.2
8	0.194	1,079	156.4	1,618	234.7
10	0.209	1,162	168.5	1,743	252.8
12	0.222	1,235	179.1	1,852	268.6
14	0.234	1,300	188.5	1,950	282.8
16	0.245	1,359	197.1	2,039	295.7
18	0.255	1,413	205.0	2,120	307.5
20	0.264	1,464	212.3	2,196	318.5
25	0.284	1,577	228.7	2,366	343.1
30	0.302	1,676	243.0	2,514	364.6
35	0.318	1,764	255.9	2,646	383.8
40	0.332	1,844	267.5	2,767	401.3
45	0.346	1,918	278.2	2,878	417.3
50	0.358	1,987	288.2	2,980	432.3
60	0.380	2,111	306.2	3,167	459.3
70	0.400	2,223	322.4	3,334	483.6
80	0.419	2,324	337.0	3,486	505.6
90	0.435	2,417	350.5	3,625	525.8
100	0.451	2,503	363.1	3,755	544.6
120	0.479	2,660	385.8	3,990	578.7
150	0.516	2,866	415.6	4,298	623.4
180	0.549	3,045	441.7	4,568	662.5
210	0.577	3,206	464.9	4,809	697.4
240	0.604	3,352	486.1	5,028	729.2
270	0.628	3,486	505.6	5,229	758.4

* Maximum pressure = 1.5 x mean pressure for hemispherical pressure distribution.

Poissons ratio = 0.26
Young's Modulus = 310 GPa

Data supplied for Norton Noralide Silicon Nitride at 21°C

Appendix C

AN ESTIMATE OF THE HERTZIAN CONTACT DIAMETER FOR THE PIN-ON-DISK CONTACT GEOMETRY

The Hertz equation for the pin-on-disk contact geometry is similar to the ball-on-three-flat case since they are both convex on flat configurations. The only real difference is the applied load is the same as the normal load; therefore, no geometric load factor need be applied. The equation is:

$$\text{Contact Radius (mm)} = a = (10^3) \left[\frac{3 \pi P_1 (K_1 + K_2) R_2}{4} \right]^{\frac{1}{3}}$$

Where P = Applied load (N)

R = Radius of pin (for our case the radius = $3.175 \times 10^{-3}\text{m}$)

K_i = Material constants (for material i) involving Young's Modulus (E) and Poisson's Ratio (ν) such that

$$K = \frac{(1 - \nu^2)(10^{-9} \text{ GPa/Pa})}{\pi E}$$

Thus for the pin-on-disk configuration, with similar materials for the upper and lower specimens, the equation reduces to

$$d = 0.336 \left[\frac{P(1 - \nu^2)}{E} \right]^{\frac{1}{3}}$$

where d = diameter of the contact in mm
 P = Applied load in Newtons
 ν = Poisson's Ratio
 E = Young's Modulus in GPa

Calculated Hertzian Wear Scar Diameter and Pressure
for the Pin-on-Disk configuration with Silicon Nitride Specimens

Applied Load (N)	Hertzian W.S.Dia (mm)	Estimated Hertzian Pressure			
		Mean		Maximum*	
		(MPa)	(kpsi)	(MPa)	(kpsi)
0.5	0.038	429	62.3	644	93.4
1	0.049	541	78.5	812	117.7
2	0.061	682	98.9	1,023	148.3
3	0.070	780	113.2	1,171	169.8
4	0.077	859	124.6	1,289	186.9
5	0.083	925	134.2	1,388	201.3
6	0.088	983	142.6	1,475	213.9
8	0.097	1,082	157.0	1,623	235.5
10	0.104	1,166	169.1	1,749	253.6
12	0.111	1,239	179.7	1,858	269.5
14	0.117	1,304	189.2	1,956	283.7
16	0.122	1,364	197.8	2,045	296.6
18	0.127	1,418	205.7	2,127	308.5
20	0.132	1,469	213.0	2,203	319.6
25	0.142	1,582	229.5	2,373	344.2
30	0.151	1,681	243.9	2,522	365.8
35	0.159	1,770	256.7	2,655	385.1
40	0.166	1,851	268.4	2,776	402.6
45	0.173	1,925	279.2	2,887	418.7
50	0.179	1,994	289.1	2,990	433.7
55	0.184	2,058	298.5	3,087	447.7
60	0.190	2,119	307.3	3,178	460.9
70	0.200	2,230	323.5	3,345	485.2
80	0.209	2,332	338.2	3,498	507.3
90	0.217	2,425	351.7	3,638	527.6
100	0.225	2,512	364.3	3,768	546.4

* Maximum pressure = 1.5 x mean pressure for hemispherical pressure distribution.

Poissons ratio = 0.26

Young's Modulus = 310 GPa

Data supplied for Norton Noralide Silicon Nitride at 21 °C

Diameter of pin hemisphere = 6.35 mm (0.25")

Appendix D

SILICON NITRIDE FLAT SPECIMEN PREPARATION PROCEDURE

The following procedure is used to prepare flat wear test specimens for the ball-on-three-flat test. The final goal is to produce flats that are 6.35 mm (0.25 inch) diameter, 1.59 mm (1/16 inch) thick, with a mirror surface finish on one side. It is not critical that the specimens end up exactly 1.59 mm thick. Tests have been successfully run on specimens from 1.4 mm to 1.8 mm thick. It is important however, that the three specimens of a single test be within 0.02 mm of each other in thickness. The grinding and polishing steps are summarized in Table D.1.

- 1) Check the diameter of the 6.35 mm (0.250 inch) rod stock. If it is not 6.35 ± 0.025 mm (0.250 ± 0.001 inch) then it must be ground to these dimensions.
- 2) Cut 1.70 mm thick flats from the rod stock using a diamond saw. The extra thickness is to accomodate material loss during the grinding stages.
- 3) Remove any burrs from at least one side of each flat. Diamond grinding and water cooling is appropriate for this operation.
- 4) Mount the flats (deburred side down) to a grinding plate using a melt adhesive such as AREMCO Crystalbond 509. Press the flats firmly onto the plate as it cools (the adhesive is setting) to ensure proper alignment of the specimens.
- 5) Grind the specimens manually until and burrs on the exposed surface are removed using a coarse fixed diamond grinding disc such as a LECO 240 grit DIMAR disc. Speed of rotation should be approximately 200 rpm with water lubrication/cooling.
- 6) Transfer the grinding plate to an autopolisher and continue grinding on the coarse diamond wheel at 200 rpm and apply a load of 0.5 lb_f per flat. Check the flat thickness periodically to ensure that the flats are not becoming too thin (1.60 mm minimum). Continue grinding until the surface of all of the specimens have been ground flat and parallel. Repeat grinding at the same conditions using a fine diamond disc such as LECO 11-14 μ m DIMAR disc.
- 7) Change the grinding disc to a fixed 120 grit SiC attached to the wheel with Pressure Sensitive Adhesive (PSA). Use this PSA backed disc at a holder for other (plain backed) SiC grinding discs. Place a 120 grit plain backed SiC

Table D.1
Summary Si₃N₄ Flat Preparation Procedure

Step	Media	Speed (rpm)	Duration (min)	Repeat (#)
Grinding	Coarse Diamond	200	2	*
	Fine Diamond	200	2	*
	120 grit SiC	200	1	6
	240 grit SiC	200	1	6
	320 grit SiC	200	1	6
	400 grit SiC	200	1	6
	600 grit SiC	200	1	6
Polishing	6 μ m diamond	100	30	*
	1 μ m diamond	100	30	*

* Indicates that judgement must be used to determine the number of times this step must be repeated to achieved the proper results.

In all cases the desire is to have each step remove the surface damage caused by the previous step.

It is imperative that the samples be cleaned properly after the 6 μ m polishing step to avoid contaminating the 1 μ m polishing wheel with 6 μ m diamond.

disc on the wheel. Grind at 200 rpm and 0.5 lb_f per flat with water coolant for between 30 seconds and 1 minute. Discard the SiC disc and repeat this procedure five times with new discs. Change to the next smaller grit size SiC and repeat the grinding procedure. The following grit sizes should be used in order: 120,240,320,400,600.

- 8) Dry the specimens and holder thoroughly. Polish the specimens using 6 μ m free diamond on polishing cloth such as LECO Technotron cloth. Rotating speed of the wheel should be 100 rpm (VP150 polisher) and lapping oil should be used as the lubricant/coolant. Pressure on the autopolisher should be set at 0.5 lb_f per flat. Polish for 30 minutes. Specimens should be checked occasionally to avoid overheating of the samples and possible melting of the melt adhesive holding the flats. Check the surface to see if the grinding damage has been removed using an optical microscope if necessary. If damage still remains, continue polishing for another 30 minutes. Note some small pits may remain at this stage. This type of damage will be removed by the next polishing step.

- 9) Thoroughly clean the specimens and holder with detergent (MICRO) then water to remove polishing contaminants (6 μm diamond particles). A final cleaning in the ultrasonic bath is a good assurance against contaminating the next polishing step.
- 10) Repeat steps 8) and 9) using 1 μm diamond paste on another polishing cloth.
- 11) Heat the plate to remove the polished specimens. Soak them in acetone to dissolve the residual adhesive. Pour off the acetone, rinse the specimens a few times in fresh acetone then dry the specimens.
- 12) Size the specimens to the nearest 0.01 mm and package in groups of three. The specimens in any one group should not differ in thickness by more than 0.02 mm. Label the bag with the thickness of the flats that they contain. The specimens are now ready for solvent cleaning prior to testing.

Appendix E

CLEANING PROCEDURE FOR Si_3N_4 WEAR TESTING

The following cleaning procedure has been developed for removing contaminants and organic impurities from the surfaces of Si_3N_4 prior to testing. It is based on a previous study* conducted on another ceramic (alumina) which found the most effective cleaning used a series of organic solvents (hexane, acetone) followed by either a detergent solution then deionized water or a high temperature bakeout in air to remove residual organics. High temperature (700°C) bakeout is feasible for alumina since it is already in its most oxidized state (Al_2O_3); however, Si_3N_4 cannot be subjected to such high temperatures since its surface will easily oxidize to form thick layers of SiO_2 at these temperatures. For this reason, the detergent/DI water cleaning procedure was adopted. The following procedure is used to prepare both ball and flat specimens immediately prior to wear testing. Tweezers should be used to handle all specimens to eliminate contamination by skin oils:

- 1) Place ball and flat specimens in a beaker and cover with hexane. Place in an ultrasonic bath and ultrasonically agitate for ≈ 5 seconds. Let soak for at least one minute.
- 2) Pour off the hexane, and repeat this procedure using acetone.
- 3) Pour off the acetone and rinse the specimens with 18 M Ω deionized (DI) water.
- 4) Cover specimens with a solution of non residue forming laboratory detergent in DI water. A 5% solution of "Micro" has been found to be satisfactory. Place in an ultrasonic bath and treat for ≈ 5 seconds. Let soak for at least one minute. Pour off the detergent solution and rinse four times with DI water. Cover specimens with DI water, ultrasonically treat for 5 seconds, pour off the water. Rinse two more times with DI water, transfer the specimens to a clean dry lintless tissue and dry by blotting then with a stream of nitrogen gas.
- 5) Immediately place the flats, polished side up, in their receptacles in the test cup. Cover with 1.5 ml of the desired lubricant. Snap the ball into place in the top ball chuck and insert and lock into machine.
- 6) Apply a slight load (< 2 kg) until the test cup rises and the specimens contact. At this point, both the ball and the flats will be covered in the lubricant and will not be susceptible to picking up contamination from the laboratory environment. The test can now be conducted.

APPENDIX F

CALCULATION OF WEAR SCAR DEPTH & WEAR VOLUMES FOR
THE BTF, POD, & FOUR-BALL WEAR TEST GEOMETRIES

Wear scar volumes for flats from ball-on-three-flat tests can be calculated using geometric considerations and a few assumptions. The basic geometry for this test is sphere on a flat surface (Figure F.1). If wear rates are relatively low, then wear of the upper specimen (sphere) will have a negligible effect on the geometry (curvature) of the upper surface. One can then calculate the volume of material removed from the flat surface by knowing only the diameter of the wear scar. The following assumptions are inherent in this calculation :

- 1) Wear of the upper rotating specimen (ball) is low enough that negligible changes take place in the curvature.
- 2) Elastic contributions are minor (ie. elastic deformation does not change the shape of the wear scar or the curvature of the upper specimen).

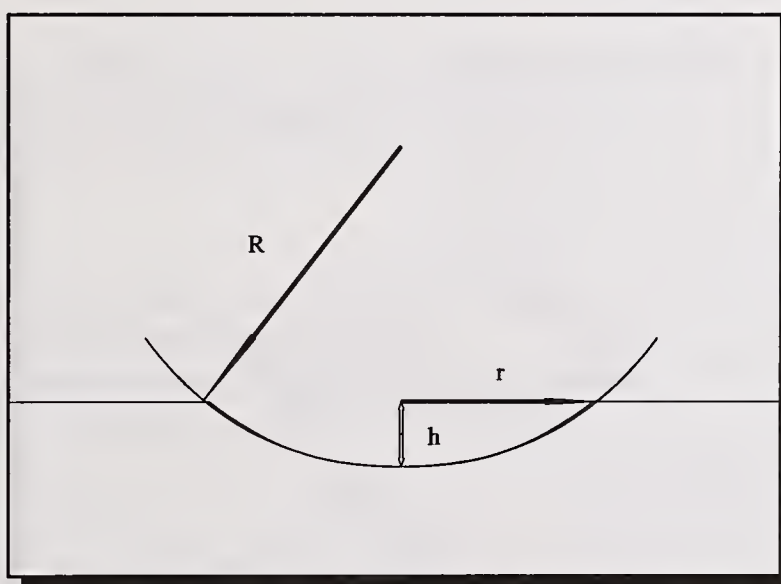


Figure F.1 Ball-on-Three-Flat Wear Geometry

Where: h = depth of the wear scar (mm)
 r = radius of the wear scar (mm)
 R = radius of the upper ball (mm)

The calculation of height and volume of a spherical segment can be found in any number of handbooks such as Perry¹⁹⁵.

$$h = R - [R^2 - r^2]^{1/2} = \frac{D}{2} - \frac{1}{2}[D^2 - d^2]^{1/2}$$

Where $d = 2r =$ diameter of the wear scar
 $D = 2R =$ diameter of the upper ball

The resulting volume (V) of wear on a single flat is:

$$V_{BTF} = \frac{\pi h}{6} [3r^2 + h^2] = \frac{\pi h}{6} \left[\frac{3}{4} d^2 + h^2 \right]$$

In the case of the POD test, the calculations are identical; however, the material is removed from the curved specimen (pin) instead of the flat specimen (Disk).

In the case of the Four-Ball contact geometry, for any given wear scar diameter, the depth and volume segment removed from the ball during wear is merely twice that of the BTF case (see figure F.2).

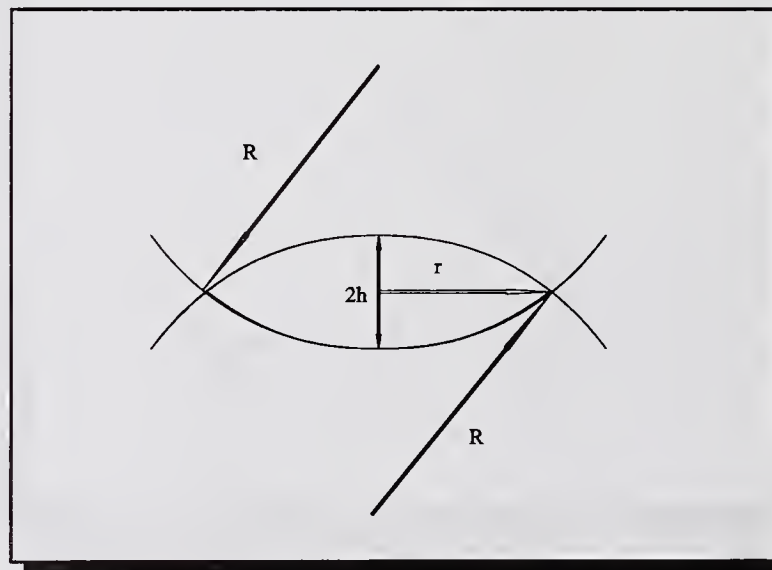


Figure F.2 Four-Ball Wear Geometry

The equation for the BTF wear volume case is modified accordingly.

$$V_{FB} = \frac{\pi h}{3} [3r^2 + h^2] = \frac{\pi h}{3} \left[\frac{3}{4} d^2 + h^2 \right]$$

where h (defined previously) represents 1/2 the four-ball wear scar depth.

Wear rates can be calculated from these wear volumes

$$\text{Normalized Wear Rate} = \frac{\text{Volume}}{(\text{Normal Load})(\text{Linear Sliding Distance})}$$

for the Roxana Ball-on-Three-Flat and Four-Ball configuration this becomes :

$$WR_N = \frac{V}{(0.408)(9.8)(P)(\Omega)(0.023)(t)} = \frac{(10.87)*V}{(P)(\Omega)(t)}$$

where :
 WR_N = normalized wear rate ($\text{mm}^3/\text{N m}$)
 P = applied machine load (kg_f)
 Ω = rotating speed of upper specimen (rpm)
 t = test duration (minutes)

Appendix G

DESCRIPTION OF ANALYTICAL TECHNIQUES

A wide variety of analytical techniques were used in the course of this investigation. The specific instruments and their capabilities are described below. Except where noted, all measurements have been made by the author.

G.1. Optical Microscopy

Optical microscopy was performed using an Olympus SZH Stereozoom microscope fitted with a calibrated graduated eyepiece reticle and a polaroid camera. This instrument has the capability of providing a zoom range of from 8.4x to 144x using a combination of a continuous zoom lens and two different objective lenses. The eyepiece reticle was calibrated at the highest zoom setting using a stage reticle. All wear measurements were taken using this highest zoom setting since the mechanical stop of the zoom knob provided the most repeatable magnification setting. For most cases the 1.5x objective lens (144x total magnification at highest zoom) was used because it allowed the greatest measurement accuracy (0.004 mm). In some cases, if the wear scar was over 0.8 mm, the 0.75 x objective was used and the accuracy of measurement dropped to 0.008 mm. If the wear scar was over 1.6 mm, a lower, less accurate, zoom setting was used. In these rare cases the accuracy was estimated to be on the order of 0.02 mm.

Polaroid photographs were taken of each wear scar of each test to provide a record of the wear scar morphology and reaction film formation.

G.2. Scanning Electron Microscopy (SEM/EDX)

Scanning electron microscopy was performed using a Hitachi S-530 SEM with a resolution of 5 nm (50 Å). Si_3N_4 is not electrically conductive, therefore specimens were coated with gold (15 nm), or carbon if Energy Dispersive X-ray (EDX) analysis was required. EDX was performed within the SEM using a KEVEX detector equipped with a QUANTUM™ window capable of detecting elements as low as boron. It should be noted however that it is very difficult to accurately detect the lighter elements of boron, carbon, nitrogen, and oxygen, because the characteristic x-ray energies of these elements are so low that they are easily absorbed by carbon coatings, and even trace vacuum pump oil adsorbed on the detector window.

G.3. Thermogravimetric Analysis (TGA)

Thermogravimetric analysis was performed using a Perkin Elmer TGS-2 TGA connected to a data station computer capable of storing and analysing the collected data. The sensitivity of the balance used in this TGA was better than 0.1 μg . In most cases, less than 50 mg of sample were used. The heating chamber was designed to allow a gas to flow over the sample during heating. A flowrate of 40 ml/min were used for all TGA analyses. Temperatures ranged from 50°C to 700°C during the course of a run.

G.4. Fourier Transform Infrared (FTIR)

FTIR analysis was performed using a Nicolet 5sx optical system with integrated minicomputer capable of storing and analysing the resulting data. Two different optical benches were used. A micro-FTIR system was used that allowed for spectra to be taken from $\approx 100 \mu\text{m}$ diameter spots in either transmission or reflectance mode. A mercury-cadmium telluride detector allowed for a resolution of 4 cm^{-1} and was capable of taking data from 4,000 cm^{-1} to 700 cm^{-1} . A second optical bench allowed for the same resolution with a wider spectrum (4,000 cm^{-1} to 400 cm^{-1}), but required a larger sample size. This system was used when diffuse reflectance infrared transmission analysis (DRIFT) was required, or it was necessary to gather data from the low wavenumber, "fingerprint," region of the spectrum.

G.5. Gel Permeation Chromatography - Graphite Furnace Atomic Absorption (GPC-GFAA)

GPC-GFAA is an analytical technique, developed at NIST, which combines gel permeation chromatography with atomic absorption spectroscopy to selectively monitor the concentration of metal associated with specific molecular weights of organic compounds. The technique is described in greater detail in the paper by Gates et al.⁹² For the purposes of this study, the element of interest was silicon, which ideally can be measured down to concentrations of 0.2 ppb. Calibration of the atomic absorption spectrometer was performed using oil soluble standards. Calibration of the molecular weight scale was performed using a series of polystyrene and hydrocarbon standards dissolved in tetrahydrofuran (THF). Since the samples injected into the GPC are not pure hydrocarbons or polystyrene, the molecular weight calibration scale is only an "approximation."

G.6. Secondary Ion Mass Spectrometry (SIMS)

Secondary Ion Mass Spectrometry was performed by Joe Bennett of the Chemical Microanalysis group at NIST using a Kratos 401 LS time-of-flight "static" SIMS. The "static" refers to the gentle nature of the ion bombardment, which results in little disturbance to either the surface, or the analyte of interest. This ensures that the system is measuring

compounds that represent the true surface chemical composition. The bombarding ion used was isotopically enriched (99.6%) gallium 69. This instrument was capable of unit resolution through 500 AMU. Since Si_3N_4 is not electrically conductive, a pulsed low energy electron charge compensation system was used to neutralize charge buildup during the analysis.

G.7. X-Ray Diffraction (XRD)

X-ray diffraction was performed on samples of Si_3N_4 to identify specific crystalline phases present. Data was acquired using a Norelco goniometer with 0.02° (2θ) step size coupled to a $\text{Cu}_{K\alpha}$ x-ray source. Data was acquired and analyzed on a micro-Vax II minicomputer running under a Siemens Diffrac 500 x-ray diffraction software package. Spectral search and match was performed on the computer against the Joint Committee on Powder Diffraction Standards (JCPDS) reference library.

G.8. Electron Spectroscopy for Chemical Analysis (ESCA) and Auger Electron Spectroscopy (AES or Auger)

ESCA and Auger analyses provide compositional information about surfaces of samples. ESCA also provides some additional information about bonding. Auger has the ability to focus down to small spot size. Both techniques can be coupled with argon ion etching to provide depth profiling capabilities. Both ESCA and Auger analyses were performed under contract by Tom Whittberg of the University of Dayton Research Institute. Auger analysis was performed on a Varian model 981-2707 Auger spectrometer at a base pressure of 10^{-10} Torr. Data were acquired using a 3 keV electron beam of 0.1 mm diameter. Additional interpretation of the results was provided by Pu-Sen Wang of NIST.

G.9. Raman Spectroscopy

Raman spectroscopy provides information on the (surface and near surface) chemical structure of samples. Analysis was performed by Bruce Heggemann of NIST using a custom-made system. This system consisted of a Nd-YAG laser, Spex triple spectrometer, and a diode-array detector capable of resolution of 4 cm^{-1} . Data were collected and analyzed using a dedicated personal computer.

G.10. Interferometry

Interferometry was performed with a Zeiss interference microscope using thallium ($\lambda/2=0.27\mu\text{m}$) illumination. The EHL example interferogram photograph was kindly provided by Zhu Dong of Alcoa.

G.11. Neutron Activation Analysis (NAA)

Neutron Activation Analysis (NAA) is an analytical technique used to quantify the concentrations of a wide range of elements in a bulk material. The analysis is performed by activating a sample (subjecting to a neutron flux such as found in a nuclear reactor), and analyzing the gamma ray spectrum of the resulting radionuclides over a period of time. Since each radionuclide (element) will generate gamma rays of different energies, approximately 40 elements can be simultaneously measured. The sensitivity will vary from element to element, depending on the half-life of the radionuclide formed; however, part per million (ppm) capability is common. The results in this study were provided under contract by GSI Spectroscopy Division, Oxnard, California.

Appendix H

PPO WEAR TEST DATA ON OTHER Si_3N_4 BATCHES

In the course of this project, the major stock of NC132 Si_3N_4 (CER019 balls and CER024 flats) became depleted and it became necessary to switch testing to a second manufacturing batch of NC132 Si_3N_4 (CER037 balls and CER038 flats). Table H.1 summarizes the results of four PPO lubricated wear tests conducted on this second batch of NC132 material. It would appear that this second batch of NC132 Si_3N_4 has a slightly smaller wear scar diameter under the same conditions. Since the repeatability of the entire wear test procedure has already been established, the difference in performance is attributed to a difference in Si_3N_4 processing by the manufacturer. Only a small number of wear tests

Table H.1
Repeatability Data on PPO Lubricated Si_3N_4
CER038 Batch of NC132 Flats

	WSD	WSD	COF ²	Run	Polishing
	(mm)	Incr ¹ (mm)	—	#	Batch
	0.625	0.245	0.110	2940R	A
	0.623	0.243	0.122	2943R	A
	0.617	0.237	0.106	2946R	A
	<u>0.621</u>	<u>0.241</u>	<u>0.105</u>	2947R	A
AVERAGE	0.622	0.242	0.111		
Std Deviation	0.003	0.003	0.008		

1 Wear Scar Diameter Increase above the Hertzian Contact Diameter (0.380 mm)

2 Measured at the end of the test

All BTF tests conducted on CER037 (Ball) on CER038 (Flat) NC132 hot pressed Si_3N_4 at 0.23 m/s (600 rpm), 60 kg, 30 minutes, 1.5 ml PPO, 21°C.

were conducted with this material.

Some of the wear tests were conducted on a second type of Si_3N_4 known as NBD100 (HIP'd). This Si_3N_4 had a slightly higher wear scar diameter and final coefficient of friction than either of the NC132 Si_3N_4 materials, as shown in Table H.2. The repeatability is also poorer than for the previous materials. The PPO wear test results on all three batches of Si_3N_4 flats are compared graphically in Figure H.1. The figure indicates that the wear scar

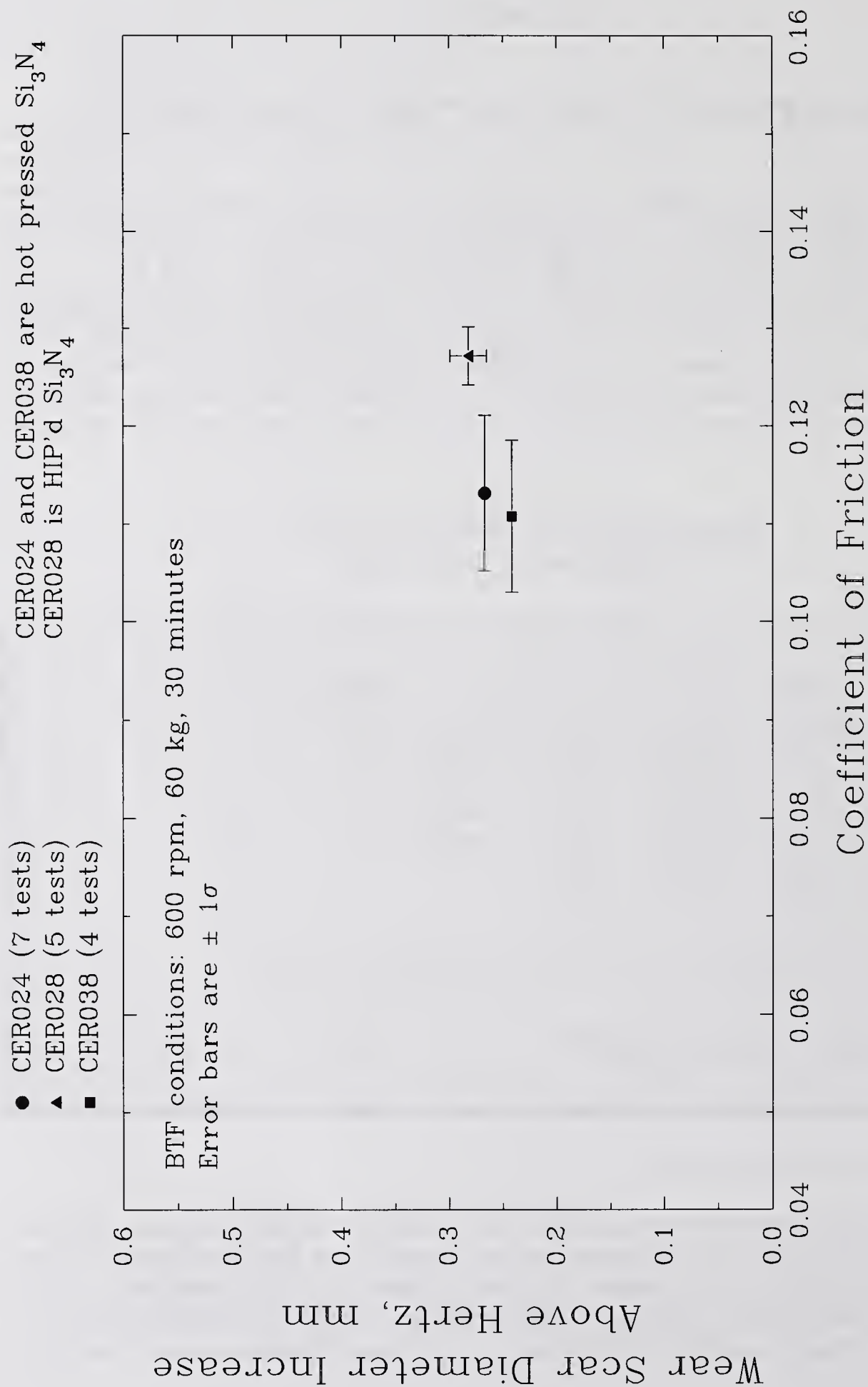


Figure H.1 Graphical Comparison of PPO Lubricated Friction and Wear Data for the Three Commercial Si_3N_4 's used in this Thesis

Table H.2
Repeatability Data on PPO Lubricated Si_3N_4
CER028 Batch of NBD100 Flats

	WSD		Run #	Polishing Batch
	WSD (mm)	Incr ¹ (mm)		
	0.650	0.270	0.132	2869R A
	0.646	0.266	0.128	2870R A
	0.689	0.309	0.126	2964R A
	0.658	0.278	0.125	3065R E
	<u>0.667</u>	<u>0.287</u>	<u>0.125</u>	3110R G
AVERAGE	0.662	0.282	0.127	
Std Deviation	0.017	0.017	0.003	

1 Wear Scar Diameter Increase above the Hertzian contact diameter (0.380 mm)

2 Measured at the end of the test

All Tests conducted on CER030 (Ball) on CER028 (Flat) NBD100 HIPPED Si_3N_4 at 600 rpm, 60 kg, 30 minutes, 1.5 ml PPO, 21°C.

diameter of the CER028 NBD100 Si_3N_4 is statistically similar (within one standard deviation) to the first (CER024) batch of NC132. The friction coefficient at the end of the test is significantly higher for CER028 (NBD100) than either NC132 batches of Si_3N_4 material. In any case, the variation in wear scar diameter among the different materials is not significant enough to change the antiwear and prowear criteria stated earlier. The average of all 16 PPO lubricated wear tests on all three batches of Si_3N_4 material were used as the benchmark to determine whether there was an effect of chemistry. These average values were: a wear scar diameter of 0.645 ± 0.018 mm and coefficient of friction of 0.117 ± 0.010 . This is shown graphically in figure H.2. The tabulated data included in this report indicate which specific material was used for each particular test in case a more accurate direct comparison is desired.

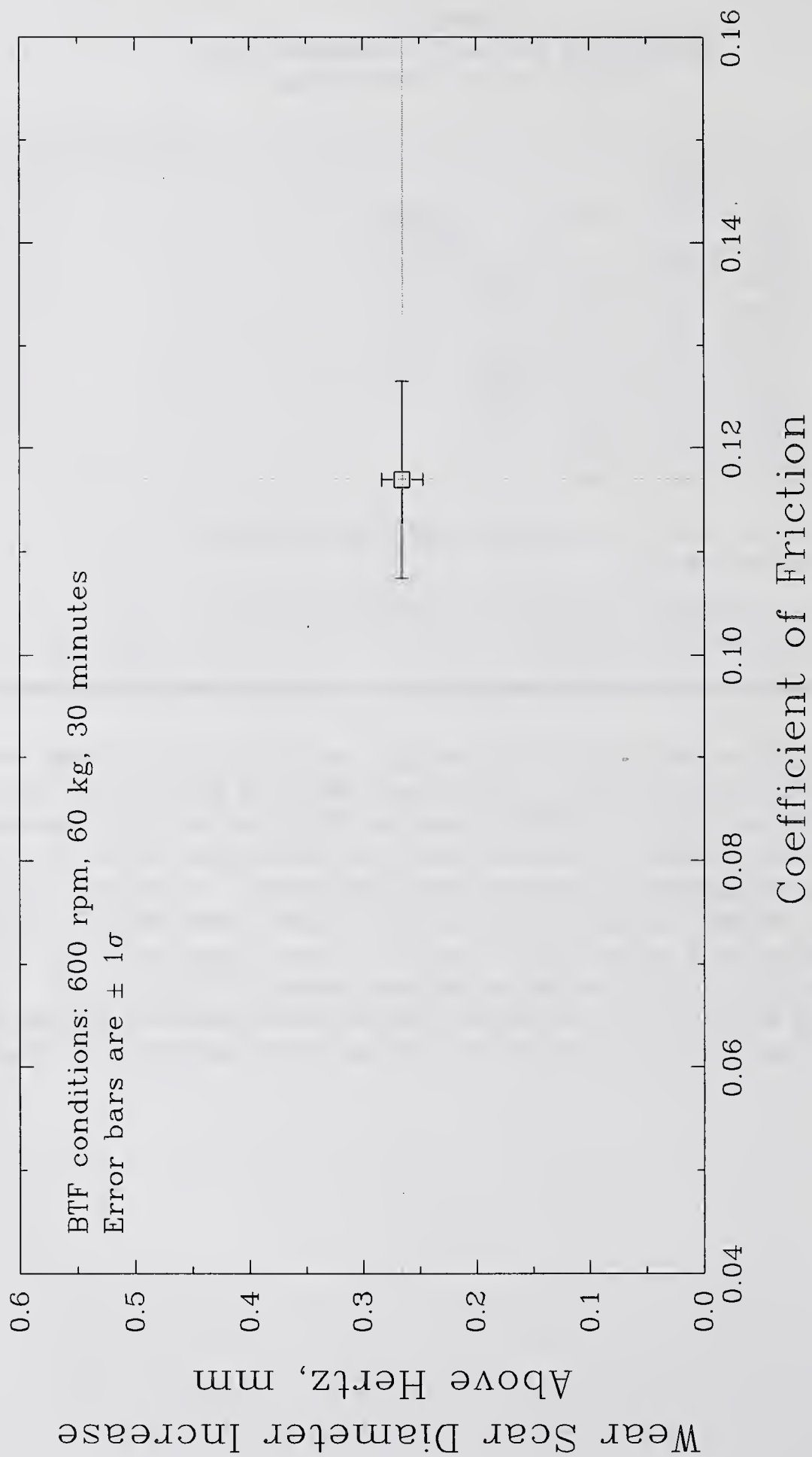


Figure H.2 Average PPO Lubricated Friction and Wear Data Used for the Wear versus Friction Plots

Appendix I

TEMPERATURE CALCULATIONS FOR THE BALL-ON-THREE-FLAT CONTACT GEOMETRY

The maximum flash temperature for a rubbing contact can be roughly approximated using Archard's¹¹ method. Unfortunately, this method is really only applicable to metal systems because a key assumption implicit in this method is that for the maximum flash temperature the load is entirely supported by the asperities undergoing plastic deformation. This requires knowing the yield or flow pressure for the material. In metals, this is a common measurement. For ceramics, there is considerable controversy about the prevalence of plastic deformation, and the yield pressure is not known. It is approximated in this case by the hardness value for the ceramic (Si_3N_4). It does not include any effect of cooling from a lubricating fluid.

For a circular point contact, the maximum flash temperature is estimated as:

$$\theta_{\max} = 0.25 \beta N L$$

where β is a correction for the effect of sliding speed. β ranges from 0.95 at $L=0.1$ to approximately 0.5 at $L=5$. N is a proportionality constant based on coefficient of friction and material parameters, and L is a dimensionless parameter that is essentially the ratio of sliding velocity to the thermal diffusivity. This is a relative measure of the balance between the movement of the heat source (the contact) and the ability of the thermal energy to dissipate into the material, and is a measure of the depth of penetration of the heat into the surface. The equations defining N and L are:

$$N = \frac{\mu \pi H}{\rho C_p} \cdot 10^6$$

$$L = \frac{W^{1/2} V}{2 D (\pi H)^{1/2}} \cdot 10^4$$

where the values used for octanol lubricated Si_3N_4 were:

f	=	0.050	Coefficient of friction
H	=	310 GPa	Hardness
ρ	=	3.2 g/cm ³	Density
C_p	=	810 J/kg ^o K	Heat capacity
W	=	240 N	Normal load (60 kg applied load)
V	=	0.23 m/s	Sliding speed (600 rpm)
D	=	0.123 cm ² /s	Thermal Diffusivity

Using these values, the flash temperature for octanol lubricated Si_3N_4 is estimated at 120°C. If a coefficient of friction of 0.080 is used (typical for well lubricated), the temperature estimate jumps to 180°C. A poorly (PPO) lubricated system (coefficient of friction = 0.120), results in an estimate of 250°C.

APPENDIX J

AUGER ANALYSIS DATA FOR ALCOHOL-LUBRICATED BTF TEST FLATS

Auger depth profiling was performed on a flat from an octanol-lubricated BTF test. A region away from the wear scar (Figure J.1) indicated a thick carbon-containing film covered the surface. The thickness of the film was estimated at 500 Å and was thought to be organic in nature. A second location, on the wedge-shaped feature within the wear scar (Figure J.2), contained a similar but thinner carbon-containing film. The thickness of this film was estimated to be 260 Å. Profilometry indicated that the wedge-shaped feature is 2 μm thick when compared to the expected wear morphology. The Auger depth profiling shows that 30 nm (15 minutes sputter time) into the sample, the surface is Si₃N₄. No strong oxygen signal is detected. This demonstrates that the wedge-shaped feature is merely unworn Si₃N₄ and not a silica or a compacted wear debris layer.

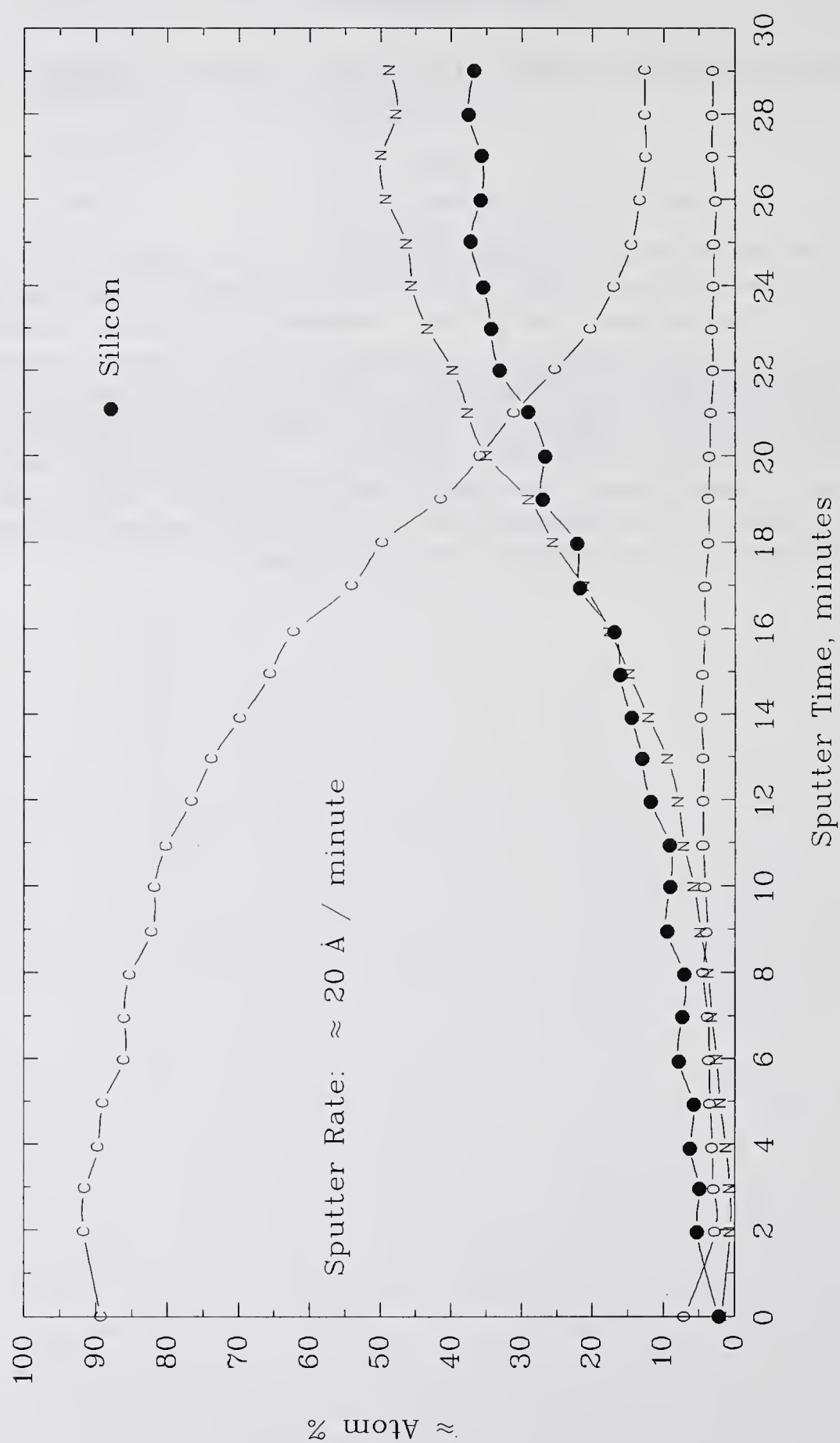


Figure J.1 Auger Depth Profile of Deposit Region Outside the Wear Scar for 6 μl Neat Octanol Lubricated Si_3N_4 BTF Test

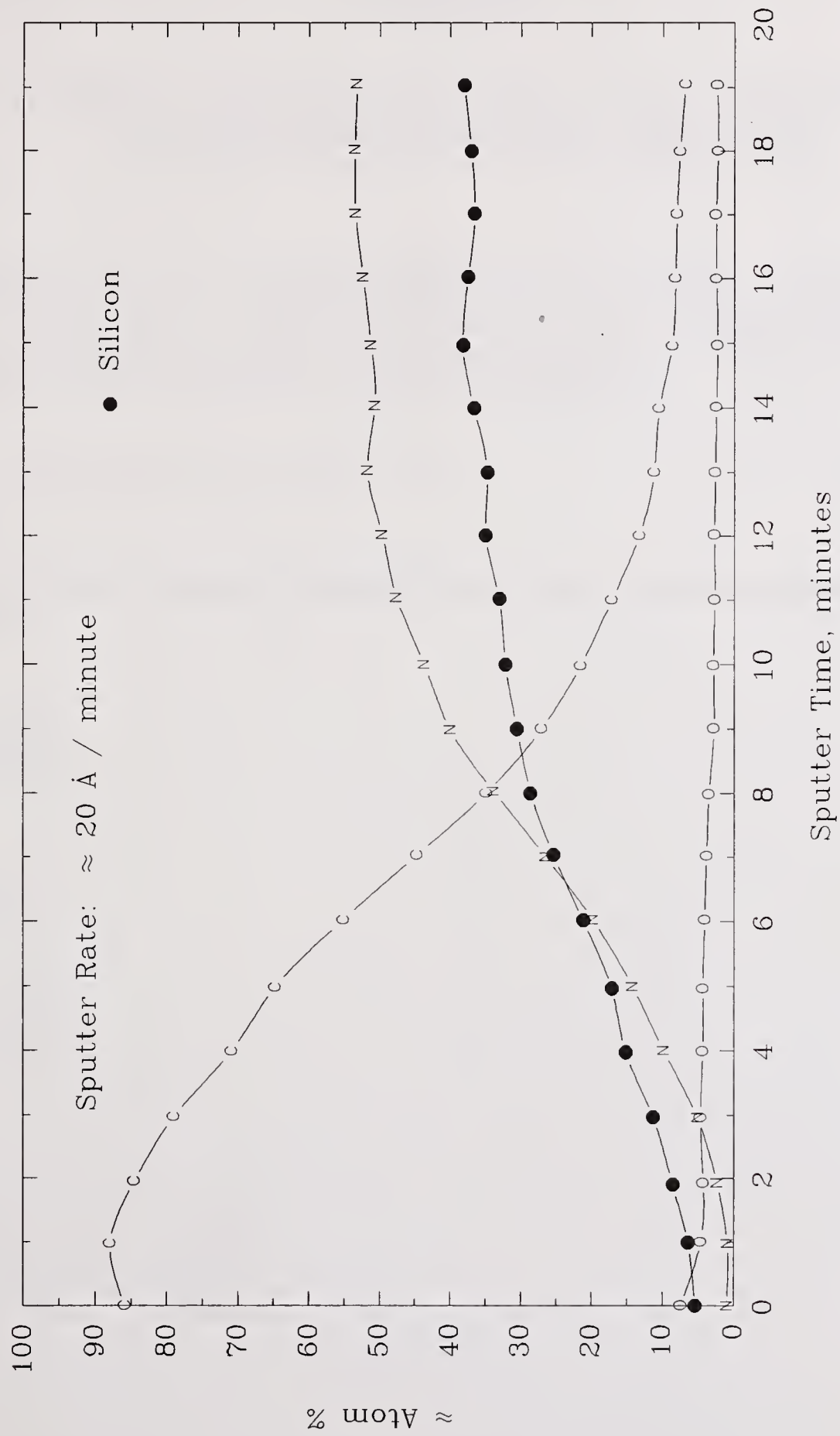


Figure J.2 Auger Depth Profile of Triangular-Shaped Region within the Wear Scar for $6 \mu\text{l}$ Neat Octanol Lubricated Si_3N_4 BTF Test

Appendix K

HAMROCK AND DOWSON MINIMUM FILM THICKNESS CALCULATION FOR BTF EHL CONTACTS

Hamrock and Dowson¹⁰⁹ have developed an empirical expression to estimate the minimum film thickness for a fully flooded EHL point contact. It assumes an ideal (perfectly smooth) surface, and does not accommodate temperature increases due to friction. The formula used for dimensionless minimum film thickness is:

$$H_{\min} = 3.63 U^{0.68} G^{0.49} W^{-0.073} (1 - e^{-0.68k})$$

Where U , G , and W represent dimensionless speed, material, and load parameters respectively.

$$U = \frac{\mu u}{E' R_x}$$

$$G = \alpha E'$$

$$W = \frac{F}{E' R_x^2}$$

Where:

$$E' = \frac{2}{\left(\frac{1 - \nu_A^2}{E_A} + \frac{1 - \nu_B^2}{E_B} \right)}$$

The values used for an octanol lubricated BTF test on Si_3N_4 under the standard test conditions (600 rpm, 60 kg applied load) were:

E_A, E_B	=	$3.10 \times 10^{11} \text{ Pa}$	Young's modulus
ν_A, ν_B	=	0.26	Poisson's ratio
μ	=	$0.006 \text{ Pa s}^{\text{Dean}}$	Viscosity at ambient T, P
R_x	=	$6.35 \times 10^{-3} \text{ m}$	Effective radius of curvature
α	=	$0.74 \times 10^{-8} \text{ Pa}^{-1}$ Eng. Sci. Data	Pressure-viscosity coefficient
u	=	0.23 m s^{-1}	Sliding speed
F	=	240 N	Normal force
k	=	1	Ellipticity parameter

Using these values, a minimum film thickness of 4 nm was estimated for octanol lubricated silicon nitride.

Appendix L

GLOSSARY

BTF	ball-on-three-flat
ESCA	electron spectroscopy for chemical analysis
DI	deionized
DSC	differential scanning calorimetry
EHD	elastohydrodynamic
EHL	elastohydrodynamic lubrication
FB	four-ball
FTIR	Fourier transform infrared
GC	gas chromatography
GFAA	graphite furnace atomic absorption
GPC	gel permeation chromatography
HIP	hot isostatic pressing
HMW	high molecular weight
IR	infrared
MS	mass spectrometry
MW	molecular weight
NAA	neutron activation analysis
PDSC	pressurized differential scanning calorimetry
POD	pin-on-disc
PPO	purified paraffin oil
RI	refractive index
SEM	scanning electron microscopy
SIMS	secondary ion mass spectrometry
TCP	tricresyl phosphate
TGA	thermogravimetric analysis
THF	tetrahydrofuran
TLC	thin layer chromatography
UV	ultraviolet
WI	water insoluble
WS	water soluble
XRD	x-ray diffraction
ZDP	zinc dithiophosphate

NIST Technical Publications

Periodical

Journal of Research of the National Institute of Standards and Technology—Reports NIST research and development in those disciplines of the physical and engineering sciences in which the Institute is active. These include physics, chemistry, engineering, mathematics, and computer sciences. Papers cover a broad range of subjects, with major emphasis on measurement methodology and the basic technology underlying standardization. Also included from time to time are survey articles on topics closely related to the Institute's technical and scientific programs. Issued six times a year.

Nonperiodicals

Monographs—Major contributions to the technical literature on various subjects related to the Institute's scientific and technical activities.

Handbooks—Recommended codes of engineering and industrial practice (including safety codes) developed in cooperation with interested industries, professional organizations, and regulatory bodies.

Special Publications—Include proceedings of conferences sponsored by NIST, NIST annual reports, and other special publications appropriate to this grouping such as wall charts, pocket cards, and bibliographies.

National Standard Reference Data Series—Provides quantitative data on the physical and chemical properties of materials, compiled from the world's literature and critically evaluated. Developed under a worldwide program coordinated by NIST under the authority of the National Standard Data Act (Public Law 90-396). NOTE: The Journal of Physical and Chemical Reference Data (JPCRD) is published bimonthly for NIST by the American Chemical Society (ACS) and the American Institute of Physics (AIP). Subscriptions, reprints, and supplements are available from ACS, 1155 Sixteenth St., NW, Washington, DC 20056.

Building Science Series—Disseminates technical information developed at the Institute on building materials, components, systems, and whole structures. The series presents research results, test methods, and performance criteria related to the structural and environmental functions and the durability and safety characteristics of building elements and systems.

Technical Notes—Studies or reports which are complete in themselves but restrictive in their treatment of a subject. Analogous to monographs but not so comprehensive in scope or definitive in treatment of the subject area. Often serve as a vehicle for final reports of work performed at NIST under the sponsorship of other government agencies.

Voluntary Product Standards—Developed under procedures published by the Department of Commerce in Part 10, Title 15, of the Code of Federal Regulations. The standards establish nationally recognized requirements for products, and provide all concerned interests with a basis for common understanding of the characteristics of the products. NIST administers this program in support of the efforts of private-sector standardizing organizations.

Order the following NIST publications—FIPS and NISTIRs—from the National Technical Information Service, Springfield, VA 22161.

Federal Information Processing Standards Publications (FIPS PUB)—Publications in this series collectively constitute the Federal Information Processing Standards Register. The Register serves as the official source of information in the Federal Government regarding standards issued by NIST pursuant to the Federal Property and Administrative Services Act of 1949 as amended, Public Law 89-306 (79 Stat. 1127), and as implemented by Executive Order 11717 (38 FR 12315, dated May 11, 1973) and Part 6 of Title 15 CFR (Code of Federal Regulations).

NIST Interagency Reports (NISTIR)—A special series of interim or final reports on work performed by NIST for outside sponsors (both government and nongovernment). In general, initial distribution is handled by the sponsor; public distribution is by the National Technical Information Service, Springfield, VA 22161, in paper copy or microfiche form.

U.S. Department of Commerce
National Institute of Standards and Technology
Gaithersburg, MD 20899-0001

Official Business
Penalty for Private Use \$300